

VOLUME 76 FEBRUARY 17, 1972 NUMBER 4

JPCA_x

THE JOURNAL OF

PHYSICAL

CHEMISTRY

PUBLISHED BIWEEKLY BY THE AMERICAN CHEMICAL SOCIETY

THE JOURNAL OF PHYSICAL CHEMISTRY

BRYCE CRAWFORD, Jr., *Editor*

STEPHEN PRAGER, *Associate Editor*

ROBERT W. CARR, Jr., FREDERIC A. VAN-CATLEDGE, *Assistant Editors*

EDITORIAL BOARD: A. O. ALLEN (1970-1974), J. R. BOLTON (1971-1975),
F. S. DAINTON (1972-1976), M. FIXMAN (1970-1974),
H. S. FRANK (1970-1974), R. R. HENTZ (1972-1976), J. R. HUIZENGA (1969-1973),
W. J. KAUZMANN (1969-1973), R. L. KAY (1972-1976), W. R. KRIGBAUM (1969-1973),
R. A. MARCUS (1968-1972), W. J. MOORE (1969-1973), J. A. POPLE (1971-1975),
B. S. RABINOVITCH (1971-1975), H. REISS (1970-1974), S. A. RICE (1969-1975),
F. S. ROWLAND (1968-1972), R. L. SCOTT (1968-1972),
R. SEIFERT (1968-1972), W. A. ZISMAN (1972-1976)

CHARLES R. BERTSCH, *Manager, Editorial Production*

AMERICAN CHEMICAL SOCIETY, 1155 Sixteenth St., N.W., Washington, D. C. 20036

FREDERICK T. WALL, *Executive Director*

Books and Journals Division

JOHN K. CRUM, *Director*

JOSEPH H. KUNEY, *Head, Business Operations Department*

RUTH REYNARD, *Assistant to the Director*

©Copyright, 1972, by the American Chemical Society. Published biweekly by the American Chemical Society at 20th and Northampton Sts., Easton, Pa. 18042. Second-class postage paid at Washington, D. C., and at additional mailing offices.

All manuscripts should be sent to *The Journal of Physical Chemistry*, Department of Chemistry, University of Minnesota, Minneapolis, Minn. 55455.

Additions and Corrections are published once yearly in the final issue. See Volume 75, Number 26 for the proper form.

Extensive or unusual alterations in an article after it has been set in type are made at the author's expense, and it is understood that by requesting such alterations the author agrees to defray the cost thereof.

The American Chemical Society and the Editor of *The Journal of Physical Chemistry* assume no responsibility for the statements and opinions advanced by contributors.

Correspondence regarding accepted copy, proofs, and reprints should be directed to Editorial Production Office, American Chemical Society, 20th and Northampton Sts., Easton, Pa. 18042. Manager: CHARLES R. BERTSCH. Assistant Editor: EDWARD A. BORGER. Editorial Assistant: WILLIAM T. BOYD.

Advertising Office: Century Communications Corporation, 142 East Avenue, Norwalk, Conn. 06851.

Business and Subscription Information

Remittances and orders for subscriptions and for single copies,

notices of changes of address and new professional connections and claims for missing numbers should be sent to the Subscription Service Department, American Chemical Society, 1155 Sixteenth St., N.W., Washington, D. C. 20036. Allow 4 weeks for changes of address. Please include an old address label with the notification.

Claims for missing numbers will not be allowed (1) if received more than sixty days from date of issue, (2) if loss was due to failure of notice of change of address to be received before the date specified in the preceding paragraph, or (3) if the reason for the claim is "missing from files."

Subscription rates (1972): members of the American Chemical Society, \$20.00 for 1 year; to nonmembers, \$60.00 for 1 year. Those interested in becoming members should write to the Admissions Department, American Chemical Society, 1155 Sixteenth St., N.W., Washington, D. C. 20036. Postage to Canada and countries in the Pan-American Union, \$5.00; all other countries, \$6.00. Single copies for current year: \$3.00. Rates for back issues from Volume 56 to date are available from the Special Issues Sales Department, 1155 Sixteenth St., N.W., Washington, D. C. 20036.

This publication and the other ACS periodical publications are now available on microfilm. For information write to: MICROFILM, Special Issues Sales Department, 1155 Sixteenth St., N.W., Washington, D. C. 20036.

THE JOURNAL OF
PHYSICAL CHEMISTRY

Volume 76, Number 4 February 17, 1972

JPCHAx 76(4) 459-614 (1972)

- A Kinetic Study of the Reaction of Methylene Radicals with Dimethylsilane. The Decomposition of Chemically Activated Trimethylsilane and Methylethylsilane **W. L. Hase, W. G. Breiland, P. W. McGrath, and J. W. Simons*** 459
- The Electron-Transfer Mechanism of Fluorescence Quenching in Polar Solvents. I. Dicyanobenzene as Quencher **K. H. Grellmann, A. R. Watkins, and A. Weller*** 469
- Photodissociation of Nitrogen Dioxide by Pulsed Laser Light at 6943 Å **John W. Gerstmayr, Paul Harteck,* and Robert R. Reeves** 474
- The Path of Triplet Excitation Energy in Simple Carbonyl-Monoolefins System in the Liquid Phase **S. M. Japar, J. A. Davidson, and E. W. Abrahamson*** 478
- The Reaction of Trifluoromethyl Radicals with Hexafluoroacetone Imine **D. W. Follmer, S. Toby, and G. O. Pritchard*** 487
- Photoreactions in Aqueous Solutions of Thymine, pH 12 **D. W. Whillans and H. E. Johns*** 489
- The Thermal Growth of the Formyl Radical at 87°K in a 50% Methanol-Water Matrix **Cornelius U. Morgan** 494
- Photolysis of Solid Dimethylnitramine: Nitrogen-15 Study and Evidence for Nitrosamine Rearrangement **K. Suryanarayanan and Suryanarayana Bulusu*** 496
- Influence of Rotational Conformation on the Stereochemical Course of Hot Halogen for Halogen Substitution in Liquid 2,3-Dichlorobutane. **L. Vasáros, H.-J. Machulla, and G. Stöcklin*** 501
- Electronic Spectral Study of the Ionizations of the Naphthalene Monosulfonic Acids **G. J. Yakatan and S. G. Schulman*** 508
- Magnetic Circular Dichroism of Ferrocene and Substituted Ferrocenes: the d-d Transitions **Dennis Nielson, Daniel Boone, and Henry Eyring*** 511
- High-Resolution Carbon-13 Nuclear Magnetic Resonance Spectra and Substituent Effects for Monohalobenzenes **A. R. Tarpley, Jr., and J. H. Goldstein*** 515
- Dielectric Relaxation of (a) *p*-Benzoquinones and (b) Me_{4-n}C(OMe)_n and Me_{4-n}Si(OMe)_n (*n* = 1-4) in Benzene Solution. **C. W. N. Cumper* and R. F. Rossiter** 525
- Ultrasonic Absorption Mechanisms in Aqueous Solutions of Bovine Hemoglobin **W. D. O'Brien, Jr., and F. Dunn*** 528
- The Role of Orientation Constraints and Rotational Diffusion in Biomolecular Solution Kinetics **Kenneth S. Schmitz and J. Michael Schurr*** 534
- Quantum Mechanical Tunneling in Hydrogen Atom Abstraction from Solid Acetonitrile at 77-87°K **Robert J. Le Roy,* Estel D. Sprague, and Ffrancon Williams** 546
- The Role of Nonbonded Intramolecular Forces in Barriers to Internal Rotation in Molecules with Two Equivalent Methyl Groups. **Kenneth C. Ingham** 551
- A Theoretical Study of Hyperfine Coupling Constants of Some σ Radicals Based on the INDO Method **M. F. Chiu, B. C. Gilbert,* and B. T. Sutcliffe** 553
- The Size Distribution of Small and Large Micelles: a Multiple Equilibrium Analysis **Pasupati Mukerjee** 565
- An Infrared Study of Surface Properties of α -Chromia. IV. Pyridine and Heavy Water Adsorption on Oxygen-Covered Surface **A. Zecchina, E. Guglielminotti, L. Cerruti, and S. Coluccia** 571

Proton Magnetic Resonance Studies of the Structure of Water in Dowex 50W Darryl G. Howery,* Lawrence Shore, and Barry H. Kohn	578
The Kinetics of the Hydrolysis of the Dichromate Ion. VI. Environmental Influences on the Acid-Catalyzed Reaction Ruth Koren and Berta Perlmutter-Hayman*	582
Hydrogen Bonding Interactions of <i>p</i> -Chlorophenol with Aliphatic Amines Mei-Lan Lin and Ronald M. Scott*	587
The Interaction of Leghemoglobin with Nitrogen and with Xenon Gordon J. Ewing* and Lavinel G. Ionescu	591
Activity Coefficient of <i>n</i> -Heptane in 4,4'-Dihexyloxyazoxybenzene Liquid Crystal Henry T. Peterson, Daniel E. Martire,* and Wolfgang Lindner	596
Solubilities of Gases in Liquids at Elevated Temperatures. Henry's Constants for Hydrogen, Methane, and Ethane in Hexadecane, Bicyclohexyl, and Diphenylmethane P. M. Cukor and J. M. Prausnitz*	598
Gas Solubilities from a Perturbed Hard-Sphere Equation of State P. M. Cukor and J. M. Prausnitz*	601
Solvent Dependence of Charge-Transfer Spectra of 1-(<i>p</i> -Substituted benzyl)-4-carbomethoxypyridinium Iodides Raymond A. Mackay, Edward J. Poziomek,* and David W. Reger	603
Kinetics of Vibrationally Hot Propane Produced by Methylene Insertion into Ethane F. B. Growcock, W. L. Hase, and J. W. Simons*	607

AUTHOR INDEX

Abrahamson, E. W., 478	Follmer, D. W., 487	Kohn, B. H., 578	Perlmutter-Hayman, B., 582	Simons, J. W., 459, 607
Boone, D., 511	Gerstmayr, J. W., 474	Koren, R., 582	Peterson, H. T., 596	Sprague, E. D., 546
Breiland, W. G., 459	Gilbert, B. C., 553	Le Roy, R. J., 546	Poziomek, E. J., 603	Stöcklin, G., 501
Bulusu, S., 496	Goldstein, J. H., 515	Lin, M.-L., 587	Prausnitz, J. M., 598, 601	Suryanarayanan, K., 496
Cerruti, L., 571	Grellmann, K. H., 469	Lindner, W., 596	Pritchard, G. O., 487	Sutcliffe, B. T., 553
Chiu, M. F., 553	Growcock, F. B., 607	Machulla, H.-J., 501	Reeves, R. R., 474	Tarpley, A. R., Jr., 515
Coluccia, S., 571	Guglielminotti, E., 571	Mackay, R. A., 603	Reger, D. W., 603	Toby, S., 487
Cukor, P. M., 598, 601	Harteck, P., 474	Martire, D. E., 596	Rossiter, R. F., 525	Vasáros, L., 501
Cumper, C. W. N., 525	Hase, W. L., 459, 607	McGrath, P. W., 459	Schmitz, K. S., 534	Watkins, A. R., 469
Davidson, J. A., 478	Howery, D. G., 578	Morgan, C. U., 494	Schulman, S. G., 508	Weller, A., 469
Dunn, F., 528	Ingham, K. C., 551	Mukerjee, P., 565	Schurr, J. M., 534	Whillans, D. W., 489
Ewing, G. J., 591	Ionescu, L. G., 591	Nielson, D., 511	Scott, R. M., 587	Williams, F., 546
Eyring, H., 511	Japar, S. M., 478	O'Brien, W. D., Jr., 528	Shore, L., 578	Yakatan, G. J., 508
	Johns, H. E., 489			Zecchina, A., 571

In papers with more than one author the name of the author to whom inquiries about the paper should be addressed is marked with an asterisk in the by-line.

ANNOUNCEMENT

On the last two pages of this issue you will find reproduced the table of contents of the January 1972 issue of the *Journal of Chemical and Engineering Data*.

A Kinetic Study of the Reaction of Methylene Radicals with Dimethylsilane.

The Decomposition of Chemically Activated Trimethylsilane

and Methyleneethylsilane^{1a}by W. L. Hase,^{1b} W. G. Breiland,^{1c} P. W. McGrath,^{1d} and J. W. Simons*

Chemistry Department, New Mexico State University, Las Cruces, New Mexico 88001 (Received August 6, 1971)

Publication costs borne completely by The Journal of Physical Chemistry

A study of the decomposition of chemically activated trimethylsilane and methyleneethylsilane is reported. Chemical activation was by the insertion of singlet methylene, from the photolysis of diazomethane at 3660 Å and 24°, into the C-H and Si-H bonds of dimethylsilane. The total rate constants for trimethylsilane, k_{TMS} , and methyleneethylsilane, k_{MES} , unimolecular decomposition were found to be $2.93 \times 10^7 \text{ sec}^{-1}$ and $3.30 \times 10^7 \text{ sec}^{-1}$, respectively. H_2 , CH_4 , and C_2H_6 were formed as decomposition products in the presence of the radical scavengers, oxygen and 1,3-butadiene, indicating they are formed by molecular elimination processes. The experimental results combined with RRKM calculations infer that Si-C bond rupture and methane elimination are the major primary decomposition paths for chemically activated trimethylsilane, and Si-C bond rupture and molecular hydrogen elimination are the major primary decomposition paths for chemically activated methyleneethylsilane. The rate constant for methyl rupture from the chemically activated trimethylsilane, $2.2 \pm 0.8 \times 10^7 \text{ sec}^{-1}$, yields an A factor for Si-C bond rupture in trimethylsilane, via RRKM theoretical calculations, equal to $10^{16.6 \pm 0.6} \text{ sec}^{-1}$.

Introduction

Although alkanes thermally decompose by unimolecular C-C bond fissions,² recent pyrolysis studies suggest that some silanes and alkylsilanes decompose at least in part by direct molecular elimination.³⁻¹⁰ It has been pointed out^{11,12} that a fine balance exists between the radical and molecular elimination modes of decomposition in silicon compounds, and care must be taken in evaluating the relative importance of the two paths for different silicon compounds. For example, it has been proposed that the pyrolysis of Si_2H_6 ^{3a,5-8} yields SiH_2 and SiH_4 as the primary decomposition products, but $(\text{CH}_3)_3\text{SiH}$ ¹³ appears to decompose by Si-H and Si-C bond rupture at 1000°K. Both decomposition modes are operative during the pyrolysis of CH_3SiH_3 ,^{3b,4b,12} where H_2 molecular elimination and Si-C bond rupture seem to occur with comparable importance.

Pyrolysis studies suffer frequently from heterogeneous effects and complicating secondary reactions, which lead to complex chain mechanisms, and obscure the

(1) (a) The National Science Foundation is gratefully acknowledged for financial support; (b) Chemistry Department, University of California, Irvine, Calif.; (c) NSF Undergraduate Research participant during the summer of 1968; (d) Undergraduate Research Assistant.

(2) H. M. Frey and R. Walsh, *Chem. Rev.*, **69**, 103 (1969).

(3) (a) E. M. Tebben and M. A. Ring, *J. Inorg. Chem.*, **8**, 1787 (1969); (b) J. J. Kohanek, P. Estacio, and M. A. Ring, *ibid.*, **8**, 2516 (1969).

(4) (a) J. H. Purnell and R. Walsh, *Proc. Roy. Soc. Ser. A*, **293**, 543 (1966); (b) M. A. Ring, M. J. Puentes, and H. E. O'Neal, *J. Amer. Chem. Soc.*, **92**, 4845 (1970).

(5) M. A. Ring, R. B. Baird, and P. Estacio, *J. Inorg. Chem.*, **9**, 1004 (1970).

(6) P. Estacio, M. D. Sefcik, E. K. Chan, and M. A. Ring, *J. Inorg. Chem.*, **9**, 1068 (1970).

(7) R. B. Baird, M. D. Sefcik, and M. A. Ring, *ibid.*, **10**, 883 (1971).

primary rates. Considerable effort has been spent in determining the Arrhenius parameters for the initiation reactions of alkane decompositions, but there is still a major question as to the order of magnitude of the A factors for C–C bond rupture.^{2,14} Using a chemical activation technique¹⁵ one can minimize the problems that plague thermal studies, and a comparison of the data for the two types of studies is of interest.

In this paper we present the results of a low-pressure study of diazomethane–dimethylsilane photolyses at 3660 Å. An internal standard, tetramethylsilane, was used to determine the unimolecular decomposition rate constants for the chemically activated trimethylsilane and methylethylsilane. Product analyses, with and without radical scavengers added to the reaction mixtures, were used to establish the probable decomposition paths of the energized trimethylsilane and methylethylsilane. We reported the high pressure results for this system previously.^{16a}

Experimental Section

Apparatus and Materials. All gas handling was performed with standard high vacuum equipment. A Toepler pump was used to transfer noncondensables. The volume used to measure out the reactants was isolated by greaseless valves. In all other phases of the gas handling process the pressures were low enough to ensure that no measurable absorption in stopcock grease with subsequent contamination occurred. The source of photolysis radiation was a Hanovia 673A medium-pressure mercury arc lamp. The 3660 Å line was isolated either by Hanovia filter 16223B or Esco Products No. 5860 filter. The photolyses were carried out in seasoned Pyrex vessels, varying in volume from 1 to 12,710 cm³. An Aerograph 90-P3 gas chromatograph and a Hitachi, Model RMU-6E, mass spectrometer were used for product analyses.

Baker lecture bottle 1,3-butadiene (99.5% pure) contained no interfering impurities and was used without further purification. The remaining materials used in this study were the same as those described previously.¹⁶

Procedure. Dimethylsilane–diazomethane and dimethylsilane–tetramethylsilane–diazomethane mixtures with and without added oxygen or 1,3-butadiene were photolyzed from 2 to 20 hr depending on the total pressure. All of the photolyses were performed at room temperature ($\sim 24^\circ$). No surface effects were observed by varying reactor volumes for experiments at the same pressure.

A slow dark reaction occurred between dimethylsilane and oxygen to produce hydrogen and methane. No other products of interest were formed from the dark reaction. The dark reaction was slow enough, less than 1% of the dimethylsilane was destroyed during 24 hr, to ensure that the alkylsilane products of interest were not destroyed by the oxygen. In all experiments oxygen was removed upon completion of the photolysis.

There was no ethane or propane formed from photolysis of diazomethane in the presence of only oxygen or 1,3-butadiene. The measurable products were hydrogen, ethylene, acetylene, and propylene. Products formed from methylene + 1,3-butadiene were not measured. A correction for the small amount of methane formed by the photolysis of diazomethane and 1,3-butadiene mixtures was applied to the dimethylsilane–diazomethane–1,3-butadiene photolyses at each pressure. The maximum correction was 15%.

Analysis. Upon completion of the photolyses, a sample of an argon–neohexane calibration mixture was added to the photolyzed reaction mixture. The noncondensables (H₂, CH₄, N₂, O₂, Ar) at -196° were removed by means of a Toepler pump. The condensable components were trapped in a U-tube at -196° . H₂ and CH₄ were analyzed on the mass spectrometer and measured relative to Ar. The condensable components were analyzed by glpc and measured relative to neohexane. The glpc column was packed with 25 ft 30% dibutyl phthalate on Chromasorb and operated at room temperature. A known mixture of H₂, CH₄, and Ar was run on the mass spectrometer after each H₂ and CH₄ analysis in order to quantitatively calibrate the mass spectrometer for H₂, CH₄, and Ar. Mixtures similar to the reaction mixtures were used to calibrate the glpc column for the measured products.

Since ethane and ethylene had the same retention time on the DBP column, the ethane analyses were performed by trapping the ethane and ethylene peak and the neohexane peak as they eluted from the DBP column and then analyzing this trapped portion on a 30-ft AgNO₃–butanediol (sol.) + 25-ft dinonyl phthalate column.

Results and Interpretation of the Data

Products. The major condensable products of the reaction system were trimethylsilane (TMS) and methylethylsilane (MES). When tetramethylsilane (TEMS) was added to the reaction mixtures, ethyltrimethylsilane (ETMS) was a major product. In the

(8) M. Bowery and J. H. Purnell, *J. Amer. Chem. Soc.*, **92**, 2594 (1970).

(9) H. Sakurai, A. Hosemi, and M. Kumada, *Chem. Commun.*, **4** (1969).

(10) W. H. Atwell and D. R. Weyenberg, *J. Amer. Chem. Soc.*, **90**, 3438 (1968); W. A. Atwell, L. G. Mahone, S. F. Hayes, and J. G. Uhlmann, *J. Organometal. Chem.*, **18**, 69 (1969).

(11) R. A. Jackson, *Advan. Free-Radical Chem.*, **3**, 231 (1969).

(12) I. M. T. Davidson, *J. Organometal. Chem.*, **24**, 97 (1970).

(13) I. M. T. Davidson and C. A. Lambert, *Chem. Commun.*, 1276 (1969); I. M. T. Davidson and C. A. Lambert, *J. Chem. Soc. A*, 882 (1971).

(14) E. V. Waage and B. S. Rabinovitch, *Int. J. Chem. Kinet.*, **3**, 105 (1971).

(15) B. A. Rabinovitch and M. C. Flowers, *Quart. Rev. Chem. Soc.*, **18**, 122 (1964).

(16) (a) W. L. Hase, W. G. Breiland, and J. W. Simons, *J. Phys. Chem.*, **73**, 4401 (1969); (b) W. L. Hase and J. W. Simons, *J. Chem. Phys.*, **54**, 1277 (1971).

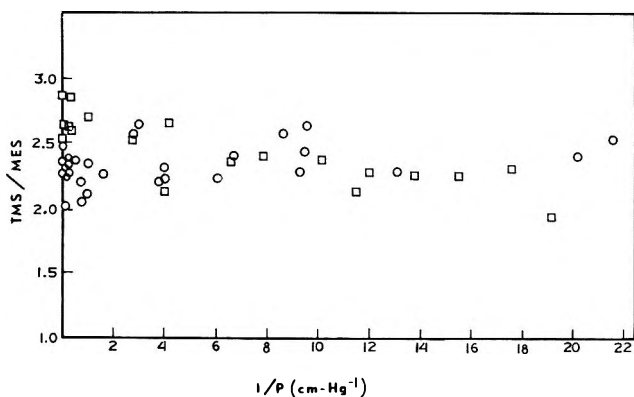


Figure 1. Plot of TMS/MES vs. $1/P$ (cm^{-1}) for CH_2N_2 -DMS photolyses at 3660 \AA : \square , no scavenger added; \circ , oxygen added. The collision frequency, w , is equal to $2.09 \times 10^8 \text{ sec}^{-1} \text{ cm}^{-1}$ for points with no scavenger added, $2.12 \times 10^8 \text{ sec}^{-1} \text{ cm}^{-1}$ for points with 1,3-butadiene added, and $2.05 \times 10^8 \text{ sec}^{-1} \text{ cm}^{-1}$ for points with oxygen added. These w 's were calculated using the following collision diameters: TEMS, 8.6 \AA ; TMS, 7.2 \AA ; MES, 7.2 \AA ; DMS, 6.6 \AA ; DM, 5.5 \AA ; Bd, 6.6 \AA ; and O_2 , 3.6 \AA . These values are the Lennard-Jones collision diameters multiplied by the square root of the collision integral $\Omega^{2,2*}(kT/\epsilon)$ (S. C. Chan, B. S. Rabinovitch, J. T. Bryant, L. D. Spicer, T. Fujimoto, Y. N. Lin, and S. P. Pavlou, *J. Phys. Chem.*, **74**, 3169 (1970)). The collision diameters for the alkylsilanes were determined by assuming that a Si atom contributes as much to the collision diameter of a molecule as two carbon atoms in an alkane. The deactivation efficiency of oxygen was taken as 0.25 in accordance with the results of G. H. Kohlmaier and B. S. Rabinovitch, *J. Chem. Phys.*, **38**, 1709 (1963).

absence of any radical scavenger H_2 , CH_4 , C_2H_6 , C_3H_8 , and ethyldimethylsilane (EDMS) were also formed. Upon addition of O_2 or 1,3-butadiene (Bd) to the reaction mixtures the formation of C_3H_8 and EDMS was completely suppressed. The presence of either O_2 or Bd should eliminate radical recombination reactions since O_2 scavenges ground triplet state methylenes¹⁷ as well as other triplet or doublet radicals¹⁸ which are formed in the system. H-atom, alkyl radical and triplet methylene additions to 1,3-butadiene are fast.¹⁹ No attempt was made to measure ethylene, acetylene, and propylene, which are formed by pure diazomethane photolyses.

DMS-DM. In Figure 1 the ratios of TMS/MES vs. $1/P$ are given for DMS-DM photolyses at 3660 \AA in the presence and absence of O_2 . For $1/P$ from 2 to 22 cm^{-1} there appears to be no detectable difference between the two sets of points. But an average of the high pressure points, $1/P < 2$, gives a value for TMS/MES = 2.30 in the presence of O_2 and 2.69 in the absence of any scavenger.

Propane and ethyldimethylsilane (EDMS) formation were completely suppressed upon addition of O_2 or 1,3-butadiene to the reaction mixtures, indicating they probably are formed by radical recombination processes. The high pressure ratios of EDMS/MES and $\text{C}_3\text{H}_8/\text{MES}$ in the absence of a scavenger were 0.24 and

0.03, respectively. The formation of C_3H_8 and EDMS indicate that ethyl radicals are produced in this reaction system.

The product ratios, H_2/MES , CH_4/TMS , and $\text{C}_2\text{H}_6/\text{TMS}$, are presented in Table I. It was found that H_2 was formed from photolyses of pure CH_2N_2 . The H_2 possibly is formed by molecular elimination from chemically activated C_2H_4 , formed by methylene recombination or the reaction of methylene with diazomethane.²⁰ The addition of 1,3-butadiene did not eliminate H_2 formation. It was found that this source of H_2 could be minimized by decreasing the fraction of CH_2N_2 in the reaction mixtures with DMS. A ratio of DMS/DM equal to 8.5 gave no H_2 at a relatively high pressure of 14.7 cm and ratios of DMS/DM in the range of 10-20 gave a linear relationship for H_2/MES vs. $1/P$ (Figure 2). These results indicate that the H_2 formation from CH_2N_2 photolyses is eliminated by using a ratio of DMS/DM ≈ 10 -20.

The data in Table I and Figure 3 show that within experimental error the CH_4/TMS ratios are invariant upon addition of Bd to the reaction mixtures, indicating that CH_4 probably is formed entirely by a molecular elimination process. It should be noted that at the higher pressures CH_4 formation in the absence of a scavenger is negligible.

The $\text{C}_2\text{H}_6/\text{TMS}$ ratios in Table I are greatly reduced when Bd or O_2 is added to the system, but C_2H_6 forma-

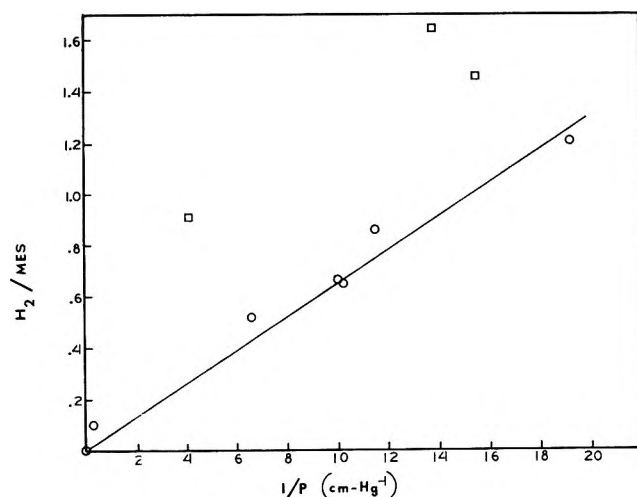


Figure 2. Plot of H_2/MES vs. $1/P$ (cm^{-1}) for CH_2N_2 -DMS photolyses at 3660 \AA : \square , DMS/ $\text{CH}_2\text{N}_2 = 5$; \circ , DMS/ $\text{CH}_2\text{N}_2 = 10$ -20. The line was determined by the method of least-squares with the intercept forced to zero.

(17) P. S. T. Lee, R. L. Russell, and F. S. Rowland, *Chem. Commun.*, 18 (1970).

(18) See ref 8-15 in ref 16.

(19) R. J. Cvetanovic and R. S. Irwin, *J. Chem. Phys.*, **46**, 1694 (1967); G. R. Woolley and R. J. Cvetanovic, *ibid.*, **50**, 4697 (1969); R. J. Cvetanovic and L. C. Doyle, *ibid.*, **50**, 4705 (1969); S. Krzyzanowski and R. J. Cvetanovic, *Can. J. Chem.*, **45**, 665 (1967).

(20) W. Braun, A. M. Bass, and M. Pilling, *J. Chem. Phys.*, **52**, 5131 (1970).

Table I: Product Ratios from Photolysis of Diazomethane-Dimethylsilane Mixtures of 3660 Å

Total pressure ^a	Bd/DMS	% O ₂	(Bd + DMS)/DM	TMS/MES	H ₂ /MES	CH ₄ /TMS	C ₂ H ₆ /TMS
14.69	0.00	0	8.5	...	0.00
3.41	0.00	0	23.4	2.60	0.10	0.09	...
2.90	0.00	0	5.1	2.85	0.19
2.35	1.90	0	5.8	0.04	0.03
0.374	0.00	0	5.1	2.53	0.40
0.360	0.00	17	3.6	2.58	0.03
0.281	3.25	0	5.6	0.22	0.07
0.239	0.00	0	5.5	2.66	0.91	0.36	...
0.212	0.00	0	18.8	...	0.68	0.34	...
0.165	0.00	16	3.4	2.23	0.05
0.152	0.00	0	19.6	2.36	0.52	0.36	...
0.132	3.11	0	5.5	0.33	0.16
0.127	0.00	0	4.0	2.40	0.54
0.100	0.00	0	8.3	...	0.66	0.31	...
0.104	0.00	22	3.6	2.64	0.09
0.0989	3.80	0	10.0	0.08
0.0977	0.00	0	9.0	2.37	0.65	0.37	...
0.0973	3.22	0	8.1	0.32	...
0.0956	2.95	0	4.4	0.47	0.15
0.0869	0.00	0	16.4	2.12	0.87	0.52	...
0.0767	2.44	0	2.7	0.58	...
0.0764	0.00	11	2.8	2.28	0.08
0.0745	1.91	0	2.8	0.42	0.09
0.0725	0.00	0	6.6	2.26	1.64	0.68	...
0.0648	4.60	0	5.6	0.20
0.0645	0.00	0	6.2	2.25	1.45	0.71	...
0.0614	3.36	0	3.2	0.52	0.14
0.0612	1.05	0	5.2	0.24
0.0569	0.00	0	3.9	2.30	0.77
0.0520	0.00	0	11.3	1.94	1.20	0.76	...
0.0507	0.00	20	3.1	2.40	0.12
0.0472	2.52	0	2.7	0.70	0.34
0.0465	3.11	0	3.7	0.26
0.0464	0.00	18	3.5	2.53	0.16
0.0451	5.19	0	3.6	0.44
0.0427	3.12	0	6.1	0.92	0.15
0.0404	1.00	0	7.4	0.78	...
0.0357	2.08	0	2.6	1.09	...
0.0352	2.87	0	2.8	0.99	...

^a The pressures are expressed in cm.

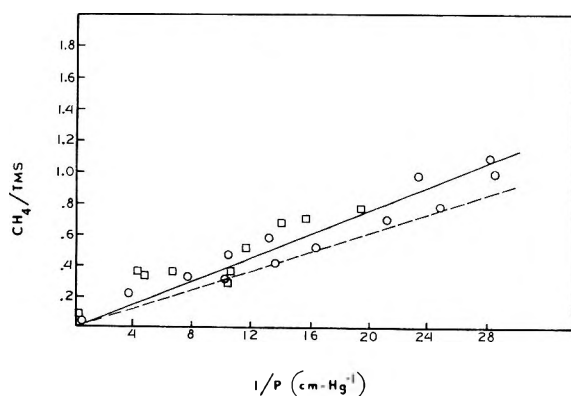


Figure 3. Plot of CH₄/TMS vs. 1/P (cm⁻¹) for DMS-CH₂N₂ photolyses at 3660 Å: □, no scavenger added; ○, Bd added. The line through the CH₄/TMS points with Bd added was determined by the method of least squares with the intercept forced to zero. The dashed line is the CH₄/TMS plot that would result if $k_{24} = 0.36 \times 10^7 \text{ sec}^{-1}$.

tion is not completely suppressed. The C₂H₆/TMS ratios with O₂ as a scavenger were more reproducible than the ratios with Bd as a scavenger; however, the agreement is satisfactory and the data reveal that C₂H₆ probably is formed in part by a molecular elimination process. The MES peak was not measured in the experiments with Bd added, since Bd and MES had identical glpc retention times.

TEMES-DMS-DM. The ETMS/TMS ratios for the photolysis of tetramethylsilane-dimethylsilane-diazomethane mixtures at 3660 Å with and without O₂ added are presented in Table II. MES was not measured in this system since in the glpc analyses the tail of the large tetramethylsilane peak swamped the MES peak. The high pressure ETMS/TMS ratio is increased upon O₂ addition. At the lower pressures the difference between the ratios in the presence and absence of O₂ is less significant. Also, the ETMS/TMS

Table II: ETMS/TMS Product Ratios

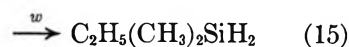
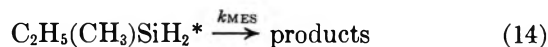
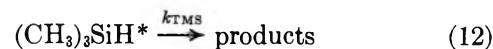
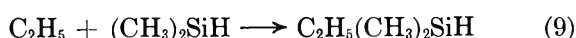
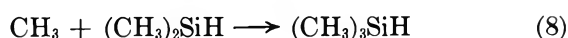
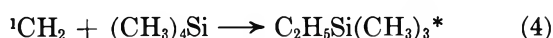
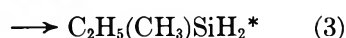
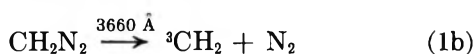
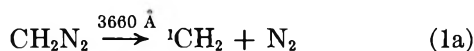
Total pressure ^a	(DMS + TEMS)/CH ₂ N ₂	% O ₂	ETMS/TMS
67.8	6.8	0	0.86
19.3	10.4	0	0.98
12.2	6.2	0	1.16
10.4	11.4	0	0.61
4.48	7.6	0	1.08
1.05	7.9	0	1.32
0.231	7.6	0	1.85
129.0	7.9	31	1.26
117.2	6.1	48	1.17
99.9	7.2	18	1.06
19.6	6.3	30	1.30
19.1	8.2	10	1.23
9.01	6.5	12	1.16
8.13	5.8	30	1.34
4.72	6.5	11	1.33
1.87	6.4	28	1.62
1.04	6.2	27	1.41
0.479	6.7	28	1.74
0.379	6.6	12	1.97
0.290	6.3	27	2.16
0.258	7.6	10	2.04
0.144	6.0	34	2.81
0.143	6.1	13	2.67
0.116	6.3	27	2.84
0.093	4.9	27	3.72

^a All pressures are expressed in cm.

ratios are independent of the percent O₂ added to the reaction mixture in the range of 10–50%.

Discussion

Mechanism. The following reaction scheme, which is consistent with previous work,^{16,21} satisfactorily explains the observed products and their variations in the present system.



Reactions 12 and 14 represent sums of several paths which will be discussed in a subsequent section. An asterisk represents a species with internal energy in excess of that required for a decomposition reaction, and w is the collisional stabilization rate constant. M denotes any bath molecule. All of the ETMS* was assumed to be collisionally stabilized, since at the lowest pressure used in this study less than 2% of the ETMS* decomposed.²²

Singlet methylenes are formed by the initial photodissociation process (1a) and triplet methylenes also may be formed during the initial photodissociation (1b) and by singlet to triplet methylene intersystem crossing.^{20,23}

Reactions 2–4 represent the primary insertion reactions of the singlet methylenes. The quantities k_2/k_3 and $k_4/(k_2 + k_3)$ have been determined previously and are 2.3 and 0.86, respectively.¹⁶ The quantity k_4/k_2 is equal to the high pressure ETMS/TMS ratio. The value of $k_4/k_2 = 1.28$ from the intercept of Figure 4 is nearly identical with the value 1.23 which was reported earlier.^{16b}

Reaction 6 is the abstraction of an H-atom from the silicon atom of DMS by CH₂. Experimental studies show that it is the ³CH₂ which abstracts H atoms from carbon.^{20,23–25} It has not been determined that some

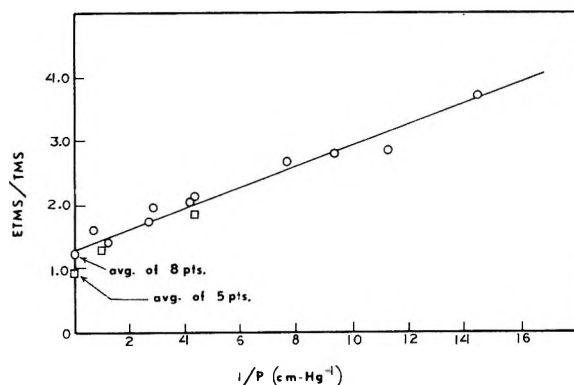


Figure 4. Plot of ETMS/TMS vs. $1/P$ (cm^{-1}) for TEMS–DMS–CH₂N₂ photolyses at 3660 Å: □, no scavenger added; ○, oxygen added. The line through the ETMS/TMS points with oxygen added was determined by the method of least squares.

(21) C. J. Mazac and J. W. Simons, *J. Amer. Chem. Soc.*, **90**, 2484 (1968).

(22) W. L. Hase and J. W. Simons, *J. Chem. Phys.*, **52**, 4004 (1970).

(23) J. A. Bell, *J. Phys. Chem.*, **75**, 1537 (1971).

(24) D. F. Ring and B. S. Rabinovitch, *Int. J. Chem. Kinet.*, **1**, 11 (1969).

abstraction from silicon is not due to singlet methylenes;²¹ therefore the abstracting methylene is designated CH₂. C-H abstraction by triplet methylenes is not included in the mechanism since there was no methylpropylsilane formed. This compound would be formed by C₂H₅ + CH₂SiH₂CH₃ recombination. The presence of ethyldimethylsilane in this system and no methylpropylsilane implies that C-H abstraction is unimportant. In addition, at 300°K methyl radicals abstract H atoms 3.6 × 10⁵ times faster from SiH₄ than from CH₄,²⁶ and assuming a similar trend for CH₂ it is reasonable that C-H relative to Si-H abstraction by methylene radicals would be of minor importance in this system.

Reaction 7, which has been proposed previously,²⁷ was included to account for the formation of ethyl radicals at the higher pressures in this system.

Reaction 8 accounts for the higher TMS/MES and lower ETMS/TMS ratios for 1/P < 2 in the absence of O₂. The equivalence of the TMS/MES ratios (Figure 1) in the presence and absence of O₂ for 1/P > 2 indicates that reaction 8 becomes relatively less important at lower pressures. The same conclusion can be made from the ETMS/TMS ratios (Figure 3), where the difference between the ETMS/TMS ratios in the presence and absence of O₂ decreases for the experiments performed at the lower pressures. This could be a result of higher concentrations of other radicals at the lower pressures in this system competing with reaction 8 for CH₃ and (CH₃)₂SiH radicals.

Reactions 9 and 10 account for the formation of EDMS and C₃H₈ in this reaction system. Reaction 11 is included to allow for the formation of the large amount of C₂H₆ in the absence of a scavenger (Table I).

Si-H abstraction by methyl radicals was not included in the mechanism since the CH₄/TMS ratios remained unchanged when Bd was added to the reaction mixtures.

Applying the steady state approximation to the (CH₃)₂SiH radical yields at high pressures the following equation

$$\frac{\text{TMS}^{\text{abs}} + \text{EDMS}}{\text{MES} + \text{TMS}^{\text{ins}}} = \frac{k_6[\text{CH}_2]}{[k_3 + k_2][^1\text{CH}_2]} \quad (\text{I})$$

where TMS^{abs} and TMS^{ins} signify the TMS formed by abstraction-recombination and insertion, respectively. Inserting the appropriate product ratios into eq I gives

$$\frac{k_6[\text{CH}_2]}{(k_3 + k_2)[^1\text{CH}_2]} = \frac{2.69 - 2.30 + 0.24}{1.00 + 2.30} = 0.19$$

Thus 16% of reaction of methylene radicals with DMS under these conditions is abstraction of an H atom from silicon. This value is slightly smaller than the value of 27% found by Mazac and Simons for reaction with methylsilane.

Unimolecular Decomposition of TMS and MES*.*

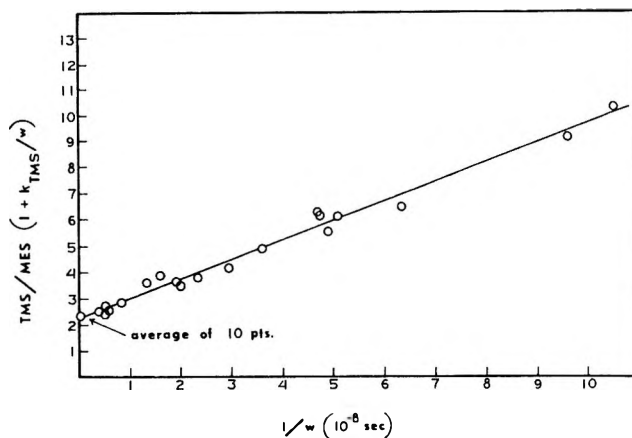


Figure 5. Plot of TMS/MES (1 + k_{TMS}/w) vs. 1/w (10⁻⁸ sec) for DMS-CH₂N₂-O₂ photolyses at 3660 Å. The line was determined by the method of least squares.

Application of the steady state approximation to TMS* and MES* gives the following two equations for reactions in the presence of a scavenger

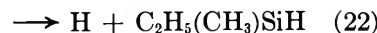
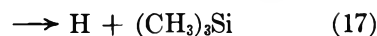
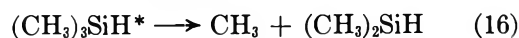
$$\frac{\text{ETMS}}{\text{TMS}} = \frac{k_4}{k_2} + \frac{k_{\text{TMS}}}{w} \frac{k_4}{k_2} \quad (\text{II})$$

$$\frac{\text{TMS}}{\text{MES}} \left(1 + \frac{k_{\text{TMS}}}{w} \right) = \frac{k_2}{k_3} + \frac{k_{\text{MES}}}{w} \frac{k_3}{k_2} \quad (\text{III})$$

where the ETMS/TMS product ratio has been normalized to a DMS/ETMS reactant ratio of 1.

A plot of the data according to eq II is shown in Figure 4 and the value derived for k_{TMS} is 2.93 ± 0.47 × 10⁷ sec⁻¹. A plot of the data according to eq III is presented in Figure 5 from which a value of k_{MES} = 3.30 ± 0.43 × 10⁷ sec⁻¹ is derived.

The following reactions represent possible unimolecular decomposition paths for TMS* and MES*



(25) D. F. Ring and B. S. Rabinovitch, *J. Phys. Chem.*, **72**, 191 (1968).

(26) O. P. Strausz, E. Jakubowski, H. S. Sandhu, and H. E. Gunning, *J. Chem. Phys.*, **57**, 552 (1971).

(27) (a) G. Z. Whitten and B. S. Rabinovitch, *J. Phys. Chem.*, **69**, 4348 (1965); (b) B. M. Herzog and R. W. Carr, Jr., *ibid.*, **71**, 2688 (1967); (c) D. F. Ring and B. S. Rabinovitch, *Can. J. Chem.*, **46**, 2435 (1968).

Molecular elimination of C_3H_8 from MES^* is not included in the mechanism since C_3H_8 was not formed in the presence of a scavenger.

A steady-state treatment of the above mechanism leads to the following equations for the molecular elimination processes

$$\frac{CH_4^{(TMS)}}{TMS} = \frac{k_{18}}{w} \quad (IV)$$

$$\frac{C_2H_6^{(TMS)}}{TMS} = \frac{k_{19}}{w} \quad (V)$$

$$\frac{H_2}{MES} = \frac{k_{23}}{w} \quad (VI)$$

$$\frac{CH_4^{(MES)}}{MES} = \frac{k_{24}}{w} \quad (VII)$$

$$\frac{C_2H_6^{(MES)}}{MES} = \frac{k_{25}}{w} \quad (VIII)$$

where the superscripts (TMS) and (MES) indicate the product is formed by TMS^* and MES^* decomposition, respectively.

CH_4 could be formed by either reaction 18 or 24, and C_2H_6 could be formed by either reaction 19 or 25. Reaction 18 is the more likely source of CH_4 since: (a) 2.3 times as much TMS^* is formed as MES^* , (b) the ratio of the reaction path degeneracy of reaction 18 to that of reaction 24 is 1.5, (c) TMS^* contains ~ 7 kcal/mol more excess energy than MES^* (the difference in the energies of TMS^* and MES^* will be discussed in the subsequent section) and (d) the critical energies and A factors per path for reactions 18 and 24 should be similar. A plot of CH_4/TMS vs. $1/P$ is presented in Figure 3, and a least-squares line with the intercept forced through zero gives $k_{18} = 0.80 \pm 0.09 \times 10^7 \text{ sec}^{-1}$. This procedure assumes k_{24} equals zero.

The lack of C_3H_8 formation in the presence of a scavenger suggests that molecular elimination reactions involving two alkyl groups are unimportant for these alkylsilanes relative to the other decomposition paths. Intuitively one would expect these processes to be slow due to tight complex structures. Thus, one would expect reaction 25 to be the major source of C_2H_6 in the presence of a scavenger and not reaction 19. k_{19} will be taken as zero. Making this assumption, the C_2H_6/MES ratios are plotted vs. $1/P$ in Figure 6. The least-squares lines give k_{25} equal to $0.36 \pm 0.04 \times 10^7 \text{ sec}^{-1}$ and $0.61 \pm 0.10 \times 10^7 \text{ sec}^{-1}$ for the experiments with O_2 and Bd added, respectively. Comparison of the two sets of data shows that $0.36 \times 10^7 \text{ sec}^{-1}$ probably is the more correct value for k_{25} , since the data with O_2 present is more reproducible and the C_2H_6/MES ratios are smaller with added O_2 , indicating that O_2 is the more efficient scavenger.

A possible assumption would be that $k_{24} \simeq k_{25} = 0.36 \times 10^7 \text{ sec}^{-1}$. Equating k_{24} with this value for k_{25} would

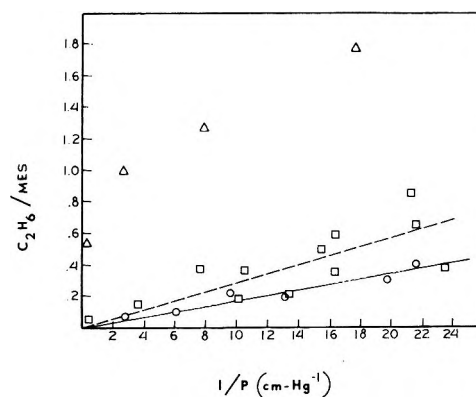


Figure 6. Plot of C_2H_6/MES vs. $1/P$ (cm^{-1}) for $DMS-CH_2N_2$ photolyses at 3660 \AA : Δ , no scavenger added; \square , Bd added; and \circ , oxygen added. The solid line is a least-squares line through the open circles with the intercept forced to zero and the dashed line is a least-squares line through the squares with the intercept forced to zero.

yield $k_{18} = 0.65 \times 10^7 \text{ sec}^{-1}$. The plot of CH_4/TMS that would result if $k_{18} = 0.65 \times 10^7 \text{ sec}^{-1}$ is indicated by the dashed line in Figure 3.

Since H_2 formation was not measured with a scavenger present in the reaction mixtures, H_2 could be formed by $Si-H$ abstraction by H atoms. The source of H atoms being reactions 17 and 22. The large excess of methyl radicals in this system relative to H atoms and the lack of evidence for $Si-H$ abstraction by CH_3 radicals suggests that $Si-H$ abstraction by H atoms is unimportant. Also, it has been found²⁸ in this laboratory that chemically activated methylsilane and dimethylsilane produced by silane-diazomethane and methylsilane-diazomethane photolyses at 3660 \AA decompose almost entirely by molecular elimination, with H_2 elimination being the primary decomposition path in each case. No evidence for $Si-H$ bond rupture was found in these systems. Therefore, the formation of CH_4 and C_2H_6 by molecular elimination reactions in this system suggests that H_2 is also formed by molecular elimination. Assuming H_2 is formed by reaction 23, a plot of H_2/MES vs. $1/P$ is given in Figure 2. The least-squares line gives a value for $k_{23} = 1.37 \pm 0.07 \times 10^7 \text{ sec}^{-1}$. This represents the maximum value for k_{23} . If the H_2 were formed entirely by reaction 17, k_{17} would equal $0.55 \times 10^7 \text{ sec}^{-1}$.

A summary of the experimental rate constants is presented in Table III.

Theoretical Calculations

RRKM calculations were performed to determine the A factor for methyl rupture from trimethylsilane and to place some restrictions on the relative importance of the possible decomposition paths for TMS^* and MES^* . The RRKM theory expression for k_{E^*} ,^{29,30} the specific dissociation rate at the energy E^* , is

(28) Unpublished results.

Table III: Trimethylsilane and Methyleneethylsilane Unimolecular Rate Constants^a

Process	Rate constant, sec ⁻¹	
	Exptl ^b	Calcd ^c
(CH ₃) ₃ SiH* → products	$k_{TMS} = 2.93 \pm 0.47 \times 10^7$	$k_{TMS} = 2.93 \times 10^7$
→ CH ₃ + (CH ₃) ₂ SiH	$1.44 \leq k_{16} \leq 2.93 \times 10^7$ [$k_{16} = 2.28 \times 10^7$]	$k_{16} = 2.00 \times 10^7$
→ H + (CH ₃) ₃ Si	$k_{17} \leq 0.55 \times 10^7$ [$k_{17} = 0.00$]	$k_{17} = 0.20 \times 10^7$
→ CH ₄ + (CH ₃) ₂ Si	$k_{18} \leq 0.80 \times 10^7$ [$k_{18} = 0.65 \times 10^7$]	$k_{18} = 0.74 \times 10^7$
→ C ₂ H ₆ + CH ₃ SiH	$k_{19} \leq 0.14 \times 10^7$ [$k_{19} = 0.00$]	$k_{19} = 0.00$
C ₂ H ₅ (CH ₃)SiH ₂ * → products	$k_{MES} = 3.30 \pm 0.43 \times 10^7$	$k_{MES} = 3.30 \times 10^7$
→ CH ₃ + C ₂ H ₅ SiH ₂	$0 \leq (k_{20} + k_{21}) \leq 3.30 \times 10^7$	$k_{20} = 0.21 \times 10^7$
→ C ₂ H ₅ + CH ₃ SiH ₂	[($k_{20} + k_{21}$) = 1.2×10^7]	$k_{21} = 1.09 \times 10^7$ [$k_{21} = 1.71 \times 10^7$]
→ H + C ₂ H ₅ (CH ₃)SiH	$(k_{22} + k_{23}) \leq 1.37 \times 10^7$ [$k_{22} = 0.00$]	$k_{22} = 0.12 \times 10^7$ $k_{23} = 1.37 \times 10^7$
→ H ₂ + C ₂ H ₅ SiCH ₃	[$k_{23} = 1.37 \times 10^7$]	[$k_{23} = 0.75 \times 10^7$]
→ CH ₄ + C ₂ H ₅ SiH	$k_{24} \leq 2.00 \times 10^7$ [$k_{24} = 0.36 \times 10^7$]	$k_{24} = 0.15 \times 10^7$
→ C ₂ H ₆ + CH ₃ SiH	$k_{25} \leq 0.36 \times 10^7$ [$k_{25} = 0.36 \times 10^7$]	$k_{25} = 0.36 \times 10^7$

^a The error limits listed are those for a 90% confidence interval. ^b The experimental rate constants given within the brackets are those which result if C₂H₆ and H₂ are formed only by reactions 25 and 23, respectively. CH₄ is formed by reactions 18 and 24, and $k_{24} = k_{25}$. ^c RRKM theory calculations in which ($k_{16} + k_{17} + k_{18}$) was set equal to k_{TMS} and ($k_{20} + k_{21} + k_{22} + k_{23} + k_{24} + k_{25}$) was set equal to k_{MES} . $k_{19} = 0$ was assumed. The rate constants in brackets are those which result when it is assumed that the H₂ is formed by reactions 17, 22, and 23.

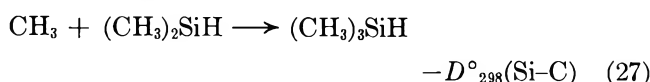
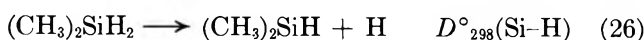
$$k_{E^*} = dI_r \sum P(E_{vr}^+) / hN(E_{vr}^*) \quad (\text{IX})$$

where d is the reaction path degeneracy, I_r is the adiabatic partition function ratio, $\sum P(E_{vr}^+)$ is the sum of all vibrational-internal rotational energy eigenstates for the activated complex up to the energy E^+ ($E^+ = E^* - E_0$), h is Planck's constant, and $N(E_{vr}^*)$ is the density of the vibrational-internal rotational eigenstates for the activated molecule. A more recent treatment of adiabatic overall rotations gives results identical with the expression above for this particular calculation.³¹

The energy, E^* , of TMS* is defined by the equation

$$-E^* = \Delta H_f^\circ(\text{TMS}) - \Delta H_f^\circ(\text{DMS}) - [\Delta H_f^\circ(^1\text{CH}_2) + E^*(^1\text{CH}_2)] - E_{th} \quad (\text{X})$$

$E^*(^1\text{CH}_2)$ is the excess energy carried by ¹CH₂ from the photolysis reaction into TMS* and E_{th} is the average thermal energy of the formed TMS*. The value for [$\Delta H_f^\circ(^1\text{CH}_2) + E^*(^1\text{CH}_2)$] is 116.1 kcal/mol,^{24,32} and E_{th} , calculated from statistical thermodynamics, is 3.3 kcal/mol. The difference in the heats of formation of TMS and DMS was determined by the following procedure. Combining reactions 26 and 27



leads to the following equation

$$D^\circ_{298}(\text{Si-H}) - D^\circ_{298}(\text{Si-C}) = \Delta H_f^\circ(\text{H}) - \Delta H_f^\circ(\text{CH}_3) + [\Delta H_f^\circ(\text{TMS}) - \Delta H_f^\circ(\text{DMS})] \quad (\text{XI})$$

From a survey of the literature³³⁻³⁵ we derive a value of 6 ± 2 kcal/mol as the most likely difference between the Si-H bond dissociation energy of DMS and the Si-C bond dissociation energy of TMS. Using $\Delta H_f^\circ(\text{H}) = 52.0$ kcal/mol and $\Delta H_f^\circ(\text{CH}_3) = 34.0$ kcal/mol,³⁶ the difference in the heats of formation of TMS and DMS at 298°K is -12 ± 3 kcal/mol. This is in agreement with the most recent bond additivity determination of this quantity, -11.3 kcal/mol, by Potzinger and Lampe.³⁷ At 0°K this difference between

(29) (a) R. A. Marcus, *J. Chem. Phys.*, **20**, 359 (1952); (b) G. M. Wieder and R. A. Marcus, *ibid.*, **37**, 1835 (1962).

(30) B. S. Rabinovitch and D. W. Setser, *Advan. Photochem.*, **3**, 1 (1964).

(31) (a) R. A. Marcus, *J. Chem. Phys.*, **43**, 2658 (1965); (b) E. V. Waage and B. S. Rabinovitch, *Chem. Rev.*, **70**, 377 (1970).

(32) J. W. Simons and G. W. Taylor, *J. Phys. Chem.*, **73**, 1274 (1969); G. W. Taylor and J. W. Simons, *ibid.*, **74**, 464 (1970).

(33) W. C. Steele, L. D. Nichols, and F. G. A. Stone, *J. Amer. Chem. Soc.*, **84**, 4441 (1962).

(34) S. J. Band, I. M. T. Davidson, and C. A. Lambert, *J. Chem. Soc. A*, 2068 (1968).

(35) M. Ya. Agarunov and S. N. Hadzhiev, *Dokl. Akad. Nauk SSSR*, **185**, 577 (1969).

(36) J. A. Kerr, *Chem. Rev.*, **66**, 465 (1966).

(37) P. Potzinger and F. W. Lampe, *J. Phys. Chem.*, **74**, 719 (1970).

the heats of formation of TMS and DMS is -10.5 ± 3.0 kcal/mol. The value for E^* , the energy of TMS*, is 130 ± 3 kcal/mol.

The critical energy, E_0 , for Si-C bond rupture in trimethylsilane is probably equivalent to the Si-C bond dissociation energy. Steele and coworkers³³ determined a value of 86 kcal/mol for the Si-C bond dissociation energy in methylsilane. Recent electron impact studies by Davidson and coworkers³⁴ and Lappert, *et al.*,³⁸ place the Si-C bond dissociation energy in tetramethylsilane at approximately 76 and 74.5 kcal/mol, respectively. More recently, Davidson and Lampert¹³ have measured an activation energy of 76.5 kcal/mol for Si-C bond rupture in trimethylsilane. A value of 78 ± 2 kcal/mol was used for the critical energy in the calculations presented here.

Three activated complex structures were derived to fit the median value for k_{16} , $2.2 \pm 0.8 \times 10^7 \text{ sec}^{-1}$, with a theoretical rate constant at $E^* = 130$ kcal/mol and $E_0 = 76, 78,$ and 80 kcal/mol. In each complex a Si-C stretching vibration was taken as the reaction coordinate and two rocking and two bending motions were each lowered by constant factors until the calculated rate was identical to $k_{16} = 2.2 \times 10^7 \text{ sec}^{-1}$. These adjustments are consistent with previous complexes for alkane and alkylsilane decompositions.^{22,24} The adjusted vibrational frequencies for the four complex models are given in Table IV. In the calculations all internal rotations in the molecule and activated complexes were treated as free rotors, since the barrier to internal rotation about a C-Si bond is low.³⁹

Table IV: Activated Complex Models for Si-C Bond Rupture in Trimethylsilane^{a,b,c}

Motion	Mole- cule	Complex model		
		I	II	III
Si-C stretch	714	R.C. ^c	R.C.	R.C.
Si-CH ₃ rock	874	404	344	289
Si-CH ₃ rock	835	386	329	276
C-Si-C bend	244	113	96	81
C-Si-C bend	225	104	89	75
log A^d		15.3	15.6	15.9

^a $I_r = 1.6$ for each complex model, ref 22. ^b The reaction path degeneracy is 3 for each complex. ^c R.C. = reaction coordinate. ^d Theoretical Arrhenius A factors at 1000°K. For calculational procedure see S. Glasstone, K. J. Laidler, and H. E. Eyring, "The Theory of Rate Processes," McGraw-Hill Book Co., New York, N. Y., 1941. ^e The vibrational frequencies used for trimethylsilane are by I. F. Kovalev, *Opt. Spectrosc. (USSR)*, 8, 166 (1960).

The calculational results are presented in Table V. Complexes I, II, and III give calculated rates that fit the experimental rate at $E_0 = 76, 78,$ and 80 kcal/mol, respectively. The A factors for complexes I-III lie in the range $10^{15.6 \pm 0.3} \text{ sec}^{-1}$ (Table IV). If the uncer-

Table V: Calculated k_{E^*} (sec^{-1}) Values for Methyl Rupture from Trimethylsilane

E_0	Complex models		
	I	II $E^* = 130 \text{ kcal/mol}$	III
76	2.2×10^7	4.3×10^7	8.5×10^7
78	1.1×10^7	2.2×10^7	4.4×10^7
80	0.6×10^7	1.0×10^7	2.2×10^7

$$k_{16} = 2.2 \pm 0.8 \times 10^7 \text{ sec}^{-1}$$

Calculated Values of k_{E^*} (sec^{-1}) vs. E^*
For Complex II and $E_0 = 78$ kcal/mol

E^*	k_{E^*}, sec^{-1}
123	6.80×10^6
124	8.13×10^6
125	9.68×10^6
126	1.15×10^7
127	1.36×10^7
128	1.60×10^7
129	1.88×10^7
130	2.20×10^7
131	2.57×10^7
132	3.00×10^7
133	3.48×10^7

tainties in E^* and the experimental rate constant were included in the calculations, complex structures giving A factors in the range of $10^{15.0}$ - $10^{16.2} \text{ sec}^{-1}$ would fit these chemical activation results, in agreement with $10^{15.9 \pm 0.7} \text{ sec}^{-1}$, reported by Davidson and Lambert.¹³ This A factor also agrees with those which have been calculated for methyl rupture in tetramethylsilane^{16b} and ethyltrimethylsilane,⁴⁰ $10^{15.0 \pm 0.6} \text{ sec}^{-1}$ and $10^{15.8 \pm 0.6} \text{ sec}^{-1}$, respectively.

The relative importance of reactions 16-25 depends in part on the difference in the energies of TMS* and MES*. The energy of MES* is defined by an equation identical with eq X except $\Delta H_f^\circ(\text{MES})$ replaces $\Delta H_f^\circ(\text{TMS})$. The difference in the heats of formation of DMS and MES was determined by the following procedure. The difference in the heats of formation of twenty related compounds, $\Delta H_f^\circ(\text{CH}_3\text{X}) - \Delta H_f^\circ(\text{C}_2\text{H}_5\text{X})$, gave an average value of 3.5 ± 0.5 kcal/mol, the substituent group varied from alkyl, alkenyl, and alkynyl to NH_2 and $\text{O}=\text{COH}$. Using this value, the energy of MES* is 122.9 kcal/mol. Thus TMS* contains ~ 7 kcal/mol more internal energy than MES*. The data in Table V show that a change in E^* of 7 kcal/mol lowers the rate constant for methyl rupture from trimethylsilane by a factor of 3.2.

In order to make a qualitative comparison of calculated rate constants for reactions 16-25, which fit the

(38) M. F. Lappert, J. Simpson, and T. R. Spalding, *J. Organometal. Chem.*, 17, 1 (1969).

(39) J. R. Durig, S. M. Craven, and J. Bragin, *J. Chem. Phys.*, 52, 2046 (1970); 53, 38 (1970).

(40) W. L. Hase and J. W. Simons, *J. Organometal. Chem.*, 32, 47 (1971).

experimental results presented in this study, the following two approximations were made: (1) that similar decomposition paths for TMS* and MES* have rate constants which differ by a factor of 3.2 per path, and (2) the ratio, k_{16}/k_{17} , can be derived from the Arrhenius parameters determined by Davidson and Lambert¹³ for Si-C and Si-H bond rupture in trimethylsilane. The first approximation assumes identical critical energies and A factors per path for similar decomposition modes. The validity of the second approximation depends on the validity of Davidson and Lambert's data. The agreement between our calculated A factor and theirs

for Si-C bond rupture in trimethylsilane supports the second approximation. The first approximation gives $k_{18}/k_{24} = 4.8$, $k_{16}/k_{20} = 9.6$ and $k_{17}/k_{26} = 1.6$. To satisfy the second approximation, complex models were chosen that fit Davidson and Lambert's¹³ Arrhenius A factors and are given in Table VI. The calculated values of k_{16} and k_{17} are presented in Table VI and $k_{16}/k_{17} = 10.00$. Rate constants which result from making these two approximations are given in Table III. The calculated rate constants in brackets for reactions 21 and 23 are those which result when it is assumed that the H_2 measured in these experiments is formed by reactions 17, 22, and 23 instead of only 23.

We are not suggesting that these various rate constants are correct as to absolute values but their relative sizes do indicate which paths are the important decomposition paths for TMS* and MES*. The results show that CH_3 rupture is the most probable decomposition path for TMS* and H_2 molecular elimination and C_2H_5 rupture are the most probable decomposition paths for MES*.

The formation of CH_4 by molecular elimination from TMS*, as the data implies, does not contradict the proposal of Davidson and Lambert that at 1000°K trimethylsilane decomposes entirely by Si-C and Si-H bond rupture. If the A factor and critical energy for reaction 16 are assumed to equal $10^{15.6} \text{ sec}^{-1}$, and 78 kcal/mol, respectively (Tables IV and V), the following sets of A factors and critical energies for reaction 18 yield the minimum value of k_{16}/k_{18} 3.0 (Table III): $10^{15.7} \text{ sec}^{-1}$, 82 kcal/mol; $10^{15.4} \text{ sec}^{-1}$, 80 kcal/mol; $10^{15.1} \text{ sec}^{-1}$, 78 kcal/mol; $10^{14.8} \text{ sec}^{-1}$, 76 kcal/mol; and $10^{14.5} \text{ sec}^{-1}$, 74 kcal/mol. None of these sets of A factors and activation energies agree exactly with that measured by Davidson and Lambert¹³ for CH_4 formation and indicate that they were probably correct in associating their Arrhenius parameters with Si-C bond rupture.

Table VI: Complex Models for Si-C and Si-H Bond Rupture in Trimethylsilane Derived from Experimental A factors^a

Motion	Si-C Bond Rupture ^b	
	Molecule	Complex
Si-C stretch	714	R.C.
Si-CH ₃ rock	874	282
Si-CH ₃ rock	835	269
C-Si-C bend	244	79
C-Si-C bend	225	73
	$\log A^d = 15.9$	$E_a = 76.5$ kcal/mol
	$k_{E^*}(130 \text{ kcal/mol}) = 7.2 \times 10^7 \text{ sec}^{-1}$	
Motion	Si-H Bond Rupture ^c	
	Molecule	Complex
Si-H stretch	2118	R.C.
H-Si-C bend	914(2)	92(2)
	$\log A^d = 15.6$	$E_a = 80.3$ kcal/mol
	$k_{E^*}(130 \text{ kcal/mol}) = 7.2 \times 10^6 \text{ sec}^{-1}$	

^a For these calculations E_a was assumed to equal E_0 . ^b $I_r = 1.6$. ^c $I_r = 1.0$. ^d The complex structures were determined using this A factor at a temperature of 1000°K, the median of Davidson and Lambert's study.¹³

The Electron-Transfer Mechanism of Fluorescence Quenching in

Polar Solvents. I. Dicyanobenzene as Quencher

by K. H. Grellmann, A. R. Watkins, and A. Weller*

Max Planck Institut für Biophysikalische Chemie, Karl Friedrich Bonhoeffer Institut, D-3400 Göttingen, Germany
(Received August 2, 1971)

Publication costs assisted by Max Planck Institut für Biophysikalische Chemie

The transient absorption spectra for the systems naphthalene, phenanthrene, coronene, pyrene, 1,2-benzanthracene, anthracene, perylene, tetracene with dicyanobenzene as quencher have been obtained (using acetonitrile as the solvent) by conventional flash photolytic methods. From these spectra it can be concluded that not only the ions but also the triplet states of the fluorescing hydrocarbons are intermediates in the quenching process. The question as to which mechanism could lead to the appearance of hydrocarbon triplets in the course of the quenching reaction is discussed.

Baur¹ and Weiss and Fischgold² were the first authors to propose a fluorescence quenching mechanism proceeding by way of an electron transfer between fluorescer and quencher. In this scheme the electronic energy of the excited molecule is dissipated, in the course of the electron transfer and reverse electron transfer steps, as vibrational energy to the solvent sink. One might expect, from this mechanism, a correlation between quenching efficiency and the oxidation-reduction properties of the molecules involved, and such a correlation has in fact been found for a considerable number of systems.³

Fluorescence quenching in nonpolar solvents is accompanied by the appearance of a new fluorescence emission at longer wavelengths⁴ attributed to an excited charge transfer complex (heteroexcimer) which is formed from the initial collision complex (encounter complex)



This supposition has been confirmed by four types of experimental observation. (i) The species emitting the fluorescence has a large dipole moment.⁵ (ii) The wavelength of the new emission shows a marked and very general correlation with the oxidation-reduction properties of the fluorescer and quencher.⁶ (iii) The absorption spectrum of the species emitting the new fluorescence shows a strong resemblance to the absorption spectra of the ions constituting the ${}^1(D^+A^-)$ complex.⁷ (iv) The enthalpy of formation of the new species can be correlated with the oxidation-reduction properties of the fluorescer and quencher.⁸

As the polarity of the solvent increases, the fluorescence intensity and fluorescence lifetime of the heteroexcimer decrease,⁹ and in polar solvents the new fluorescence emission can no longer be detected. The quenching efficiency still depends on the oxidation and

reduction potentials (or ionization potential and electron affinity) of donor and acceptor,^{10,11} however, and

- (1) E. Baur, *Z. Phys. Chem., Abt. B*, **16**, 465 (1932).
- (2) J. Weiss and H. Fischgold, *Z. Phys. Chem. Abt. B*, **32**, 135 (1936).
- (3) A. Weller, *Progr. React. Kinet.*, **1**, 187 (1961); H. Leonhardt and A. Weller in "Luminescence of Organic and Inorganic Materials," Kallmann and Spruch, Ed., Wiley, New York, N. Y., 1962; A. Nakajima and H. Akamatu, *Bull. Chem. Soc. Jap.*, **41**, 1961 (1968); D. Schulte-Frohlinde and R. Pfefferkorn, *Ber. Bunsenges. Phys. Chem.*, **72**, 330 (1968); B. S. Solomon, C. Steel, and A. Weller, *Chem. Commun.*, 927 (1969).
- (4) H. Leonhardt and A. Weller, *Ber. Bunsenges. Phys. Chem.*, **67**, 791 (1963); N. Mataga, K. Ezumi, and K. Takahashi, *Z. Phys. Chem. (Frankfurt am Main)*, **44**, 250 (1965); N. Mataga, T. Okada, and H. Oohari, *Bull. Chem. Soc. Jap.*, **39**, 2563 (1966); H. Knibbe and A. Weller, *Z. Phys. Chem.*, **56**, 99 (1967); M. S. Walker, T. W. Bednar, and R. Lumry, *J. Chem. Phys.*, **45**, 3455 (1966); N. Mataga and K. Ezumi, *Bull. Chem. Soc. Jap.*, **40**, 1355 (1967); N. Mataga, K. Ezumi, and T. Okada, *Mol. Phys.*, **10**, 201 (1966); W. R. Ware and H. P. Richter, *J. Chem. Phys.*, **48**, 1595 (1968); T. Okada, H. Matsui, H. Oohari, and H. Matsomoto, *ibid.*, **49**, 4717 (1968); D. Cros and P. Viallet, *J. Chim. Phys.*, **67**, 794 (1970); K. Mutai, *Chem. Commun.*, 1209 (1973); I. G. Lopp, R. W. Hendren, P. D. Wildes, and D. G. Whitten, *J. Amer. Chem. Soc.*, **92**, 6440 (1970).
- (5) H. Beens, E. Knibbe, and A. Weller, *J. Chem. Phys.*, **47**, 1183 (1967); M. G. Kuzmin and L. N. Guseva, *Chem. Phys. Lett.*, **3**, 71 (1969).
- (6) H. Knibbe, D. Rehm, and A. Weller, *Z. Phys. Chem. (Frankfurt am Main)*, **56**, 95 (1967); E. A. Chandross and J. Ferguson, *J. Chem. Phys.*, **47**, 2557 (1967); H. Beens and A. Weller, *Acta Phys. Pol.*, **34**, 593 (1968); D. Rehm and A. Weller, *Z. Phys. Chem.*, **69**, 183 (1970); M. A. F. Tavares, *Trans. Faraday Soc.*, **66**, 2431 (1970); D. Rehm, *Z. Naturforsch. A*, **25**, 1442 (1970); D. W. Ellis, R. G. Hamel, and B. S. Solomon, *Chem. Commun.*, 1697 (1970).
- (7) C. R. Goldschmidt and M. Ottolenghi, *Chem. Phys. Lett.*, **4**, 570 (1970); R. Potashnik and M. Ottolenghi, *ibid.*, **6**, 525 (1970); H. Masuhara and N. Mataga, *ibid.*, **6**, 608 (1970).
- (8) H. Knibbe, D. Rehm, and A. Weller, *Ber. Bunsenges. Phys. Chem.*, **73**, 839 (1969).
- (9) N. Mataga, T. Okada, and N. Yamamoto, *Bull. Chem. Soc. Jap.*, **39**, 2562 (1966); N. Mataga, T. Okada, and K. Ezumi, *Mol. Phys.*, **10**, 203 (1966); H. Knibbe, K. Röllig, F. P. Schäfer, and A. Weller, *J. Chem. Phys.*, **47**, 1184 (1967); N. Mataga, T. Okada, and N. Yamamoto, *Chem. Phys. Lett.*, **1**, 119 (1967); K. Kaneta and M. Koisumi, *Bull. Chem. Soc. Jap.*, **40**, 2254 (1967); S. Murata, H. Kokubun, and M. Koizumi, *Z. Phys. Chem. (Frankfurt am Main)*, **70**, 47 (1970).
- (10) K. Kaneta and M. Koizumi, *Bull. Chem. Soc. Jap.*, **40**, 2254 (1967); D. Rehm and A. Weller, *Ber. Bunsenges. Phys. Chem.*, **73**, 834 (1969).

fluorescence quenching still seems to take place by electron transfer, leading, this time, to solvated ions



Flash studies¹²⁻¹⁴ have shown that in fact ions are produced in quenched systems in acetonitrile and dimethylformamide; however, triplet states are also observed, which, at the high quencher concentrations used, cannot be formed by intersystem crossing from the excited molecule. The present investigation was made in order to gain more information about what part these intermediates play in the quenching process.

Experimental Section

The following compounds were recrystallized and zone-refined: pyrene, 1,2-benzanthracene, perylene, anthracene, and naphthalene. Coronene was recrystallized and zone-sublimed. Phenanthrene was freed from anthracene by the method of Bachmann,¹⁵ recrystallized twice from ethanol, chromatographed on an Al_2O_3 column and zone-refined. In subsequent experiments with phenanthrene purified in this way no trace of anthracene could be detected. Tetracene was purified by recrystallization and sublimation; commercial *p*-dicyanobenzene (hereafter DCB) was recrystallized, sublimed and then zone-melted under 3-4 atm of nitrogen. The solvent used in most experiments, acetonitrile, was prepared from uv grade acetonitrile (Merck UVASOL) by refluxing over P_2O_5 followed by fractional distillation. This product proved to be 100% transparent to 200 nm.

Flash experiments were carried out with an apparatus having a stored electrical energy of 150 J available for the flash, which had a half-life of 5 μ sec. A photoelectric recording system with a 1P28 photomultiplier and a Tektronix 549 Oscilloscope was used. The transient spectra were obtained by varying the monochromator wavelength of the detection system through the entire wavelength range (300-730 nm) at 5-nm intervals, flashing at each of these wavelengths and recording the transient absorption immediately after the flash had ceased (about 25 μ sec after firing). The maximum sensitivity of the transient absorption measurements was about 0.001 optical density units, the detection system becoming less sensitive (as a result of the photomultiplier and monitoring light source characteristics) at the extremes of the wavelength range.

The flash cell used consisted of a cylindrical quartz cell, 10 cm long, to which two reservoirs were attached. Using these reservoirs, the solutions to be investigated (fluorescer and quencher) were degassed separately by repeated freeze-pump-thaw cycles, and then mixed prior to flashing, in order to avoid the occurrence of any light induced reaction between the two in the presence of air. A 0.1 M solution of DCB in 1-cm filter cells inserted between the flash lamps and the cell ensured that only the donor molecule (in all cases the

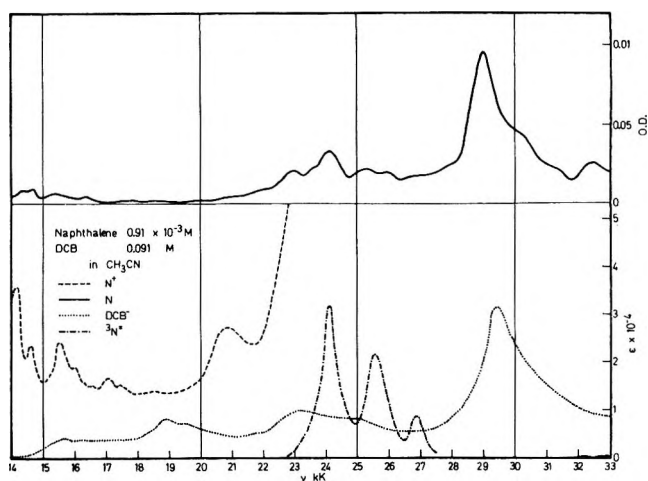


Figure 1. The transient absorption spectrum (upper half) and corresponding literature spectra (lower half) for the system naphthalene-DCB. N^+ spectrum from ref 16, DCB^- from ref 17, ${}^3N^*$ from ref 18.

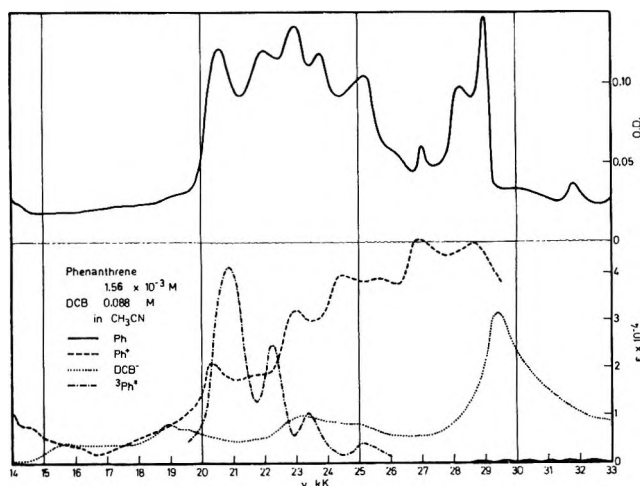


Figure 2. The transient absorption spectrum (upper half) and corresponding literature spectra (lower half) for the system phenanthrene-DCB. Ph^+ spectrum from ref 16, ${}^3Ph^*$ from ref 18.

aromatic hydrocarbon) was excited by the flash light. In no case was there any evidence of irreversible photochemical changes occurring during the flash experiments, and no complex formation in the ground state between fluorescer and DCB could be detected.

Fluorescence quenching measurements were carried out with a Perkin-Elmer Fluorescence Spectrophotometer MPF2A in conjunction with a Phillips Digital Multimeter PM1412, by means of which the observed

- (11) D. Rehm and A. Weller, *Israel J. Chem.*, **8**, 259 (1970).
- (12) H. Leonhardt and A. Weller, *Z. Phys. Chem. (Frankfurt am Main)*, **29**, 277 (1961); *Ber. Bunsenges. Phys. Chem.*, **67**, 791 (1963).
- (13) H. Knibbe, D. Rehm, and A. Weller, *Ber. Bunsenges. Phys. Chem.*, **72**, 257 (1968).
- (14) K. H. Grellmann, A. R. Watkins, and A. Weller, *J. Lumin.*, **1**, 2, 678 (1970).
- (15) W. E. Bachmann, *J. Amer. Chem. Soc.*, **57**, 555 (1935).

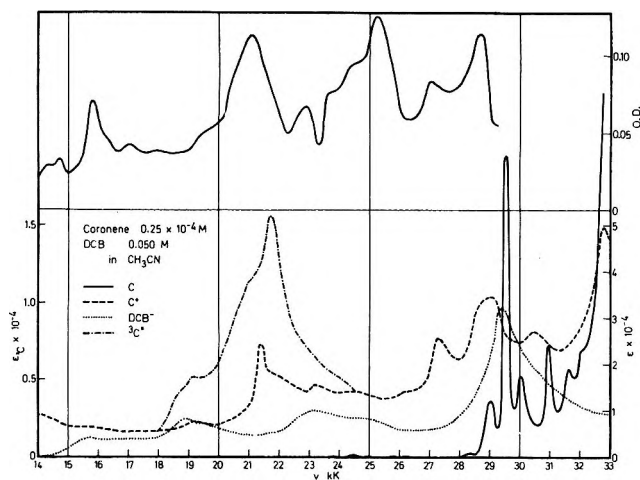


Figure 3. The transient absorption spectrum (upper half) and corresponding literature spectra (lower half) for the system coronene-DCB. C^+ spectrum from ref 19, ${}^3C^*$ from ref 18.

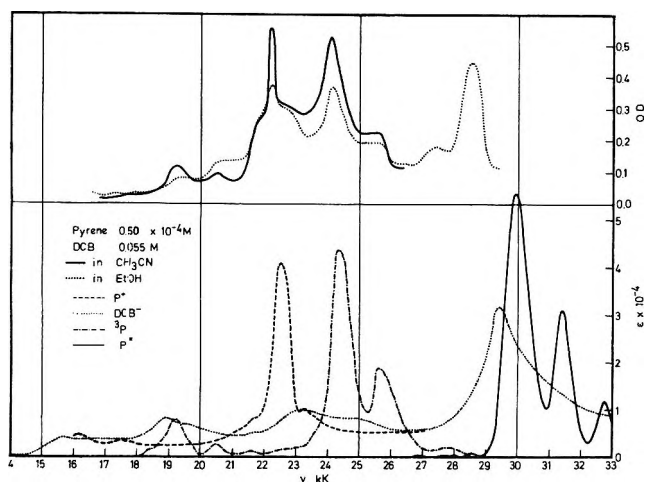


Figure 4. The transient absorption spectra (upper half) and corresponding literature spectra (lower half) of the system pyrene-DCB in ethanol and acetonitrile. P^+ spectrum from ref 20, ${}^3P^*$ from ref 21.

fluorescence intensity at a fixed wavelength could be read off accurately. A solution of the fluorescing substance without added quencher served as a standard, by means of which fluctuations in the exciting light intensity could be corrected for. Both the flash and fluorescence quenching experiments were carried out at room temperature.

Results and Discussion

The transient absorption spectra obtained in the flash experiments described above, together with the relevant spectra from the literature, are presented in Figures 1-8.¹⁶⁻²³ Extinction coefficients for triplet states were taken from ref 24. Extinction coefficients for the following species were not available in the literature: the triplet states of perylene and tetracene, DCB radical anion, and the radical cations of coronene, phenanthrene and naphthalene. The corresponding

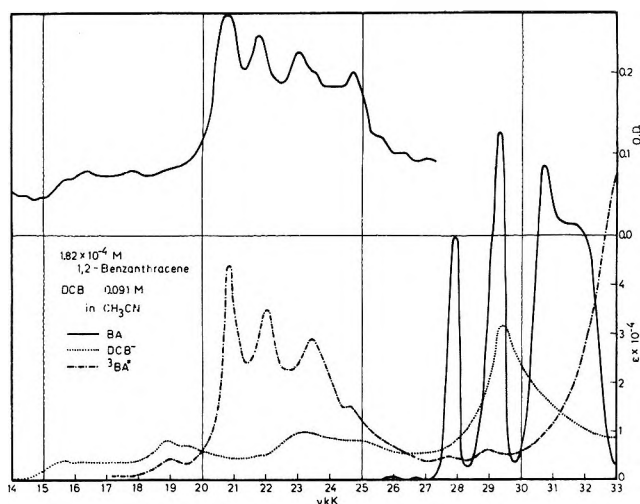


Figure 5. The transient absorption spectrum (upper half) and corresponding literature spectra (lower half) for the system 1,2-benzanthracene-DCB. ${}^3BA^*$ spectrum from ref 21.

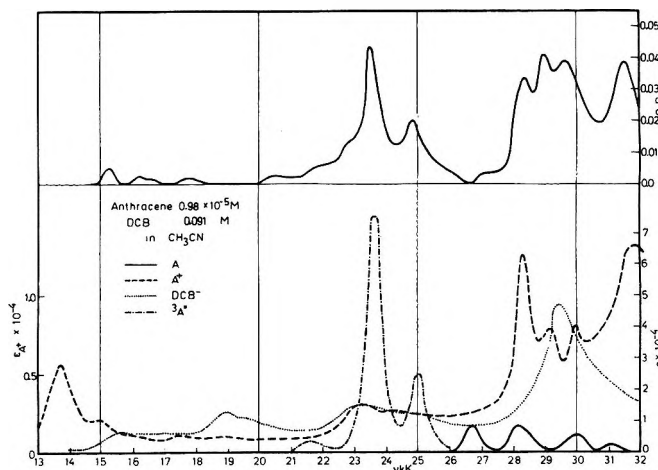


Figure 6. The transient absorption spectrum (upper half) and corresponding literature spectra (lower half) for the system anthracene-DCB. A^+ spectrum from ref 20, ${}^3A^*$ from ref 18.

spectra have therefore been drawn in arbitrary units.

Comparison of the flash spectra with the literature spectra shows that the radical cation and the triplet state of the excited molecule (in these systems the elec-

- (16) T. Shida and W. H. Hamill, *J. Chem. Phys.*, **44**, 2375 (1966).
- (17) A. Ishitani and S. Nagakura, *Theor. Chim. Acta*, **4**, 236 (1966).
- (18) G. Porter and M. W. Windsor, *Proc. Roy. Soc. Ser. A*, **245**, 238 (1958).
- (19) P. Bennema, G. J. Hoijtink, J. H. Lupinski, L. J. Oosterhoff, P. Selier, and J. D. W. van Voorst, *Mol. Phys.*, **2**, 431 (1959).
- (20) W. I. Aalbersberg, G. J. Hoijtink, E. L. Mackor, and W. P. Weijland, *J. Chem. Soc.*, 3049 (1959).
- (21) W. Heinzelmann and H. Labhart, *Chem. Phys. Lett.*, **4**, 20 (1969).
- (22) "DMS UV Atlas of Organic Compounds," Butterworths, London, 1966.
- (23) H. Staerk, private communication.
- (24) J. S. Brinen, in "Molecular Luminescence," W. A. Benjamin, New York, N. Y., 1969, p 333.

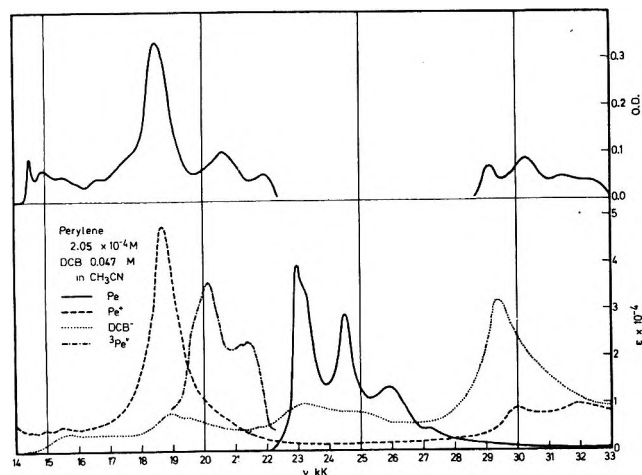


Figure 7. The transient absorption spectrum (upper half) and corresponding literature spectra (lower half) for the system perylene-DCB. Pe^+ spectrum from ref 22, $^3Pe^*$ from ref 23.

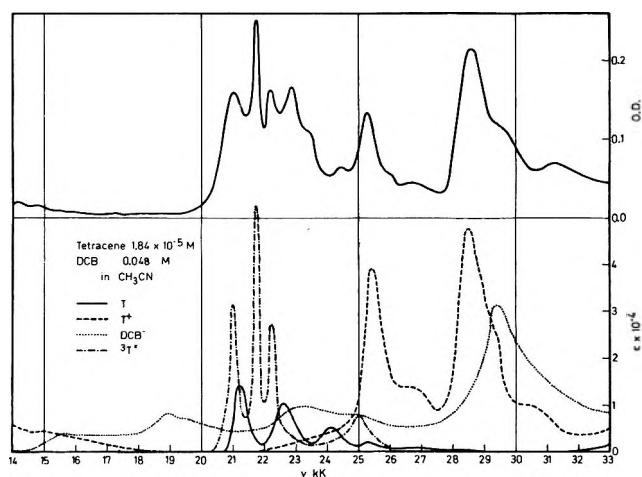


Figure 8. The transient absorption spectrum (upper half) and corresponding literature spectra (lower half) for the system tetracene-DCB. T^+ spectrum from ref 22, $^3T^*$ from ref 18.

tron donor) together with the radical anion of DCB, are formed in the systems phenanthrene-DCB in acetonitrile, pyrene-DCB in ethanol, and anthracene-DCB and perylene-DCB in acetonitrile. The spectrum of the radical cation of 1,2-benzanthracene has to date not been reported, and the unfavorable position of the ground state absorption of 1,2-benzanthracene prevented identification of the DCB^- absorption at 29 kK in this system; however, the triplet spectrum can be clearly identified in the experimentally obtained flash spectrum. The system coronene-DCB shows a peak at 21 kK which is probably due to both the coronene triplet and the coronene radical cation; the peak between 28 and 29 kK is probably made up of the coronene radical cation and DCB^- . No explanation has yet been found for the peaks at 25 and 16 kK. The transient absorption spectrum of the system naphthalene-DCB is made up of the DCB^- absorption at 29

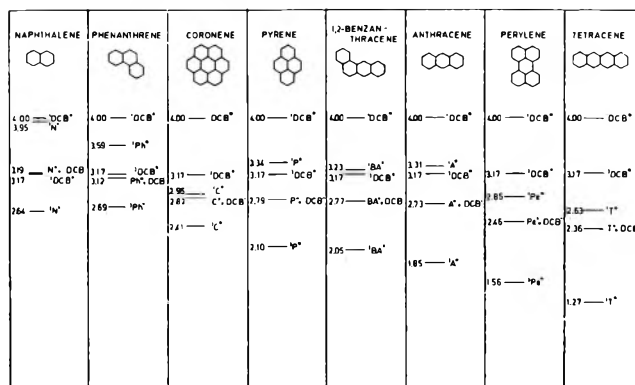


Figure 9. Schematic representation of the energy levels of the intermediates involved in the quenching process.

kK and a weaker absorption centered at 24 kK, presumably due to the triplet and radical cation of naphthalene, although the published spectrum of the latter species extends to only 23 kK, making a definite assignment impossible. In no case can it be concluded from the observed transient spectra that the triplet of the fluorescing molecule is absent; it is either clearly recognizable or overlapped by the absorption of some other species.

Figure 9 shows the energies, calculated from published spectral and electrochemical data, of the singlet, triplet, and ionic states involved in the quenching reaction. It can be seen that in all cases the quenching reaction leading to the free ions is thermodynamically favored, although only slightly in the case of coronene-DCB. The favorable free energy changes are reflected in the quenching data given in Table I, where the measured quenching constants K are given. The extent to which the donor fluorescence was quenched in the systems investigated in the flash experiments is also included. Also included in Table I are the quantum yields of the donor triplet (ϕ_T) and of the donor cation (ϕ_c). The quantum yield of DCB^- , ϕ_A , was assumed to be equal to ϕ_c . These quantum yields were obtained by flashing the donor molecule twice under the same conditions, once with acceptor and once without. The quantum efficiency of transient formation in the quenched system is given by

$$\phi = \frac{A}{T_0} \frac{\epsilon_T \phi_{T_0}}{\epsilon} \quad (3)$$

where ϵ_T and ϵ are the extinction coefficients, at the wavelengths of maximum absorption, of the donor triplet and of the transient, A and T_0 are the observed maximum optical densities (at these wavelengths) of the transient formed in the presence of acceptor, and of the donor triplet in the absence of acceptor, respectively, and ϕ_{T_0} is the quantum efficiency of triplet formation for the donor when no acceptor is present.

This method presupposes well-separated spectra of the transient species involved, and a knowledge of the

relevant extinction coefficients and of the quantum yield of donor triplet formation in the absence of acceptor. In fact, these requirements were difficult to meet, and in most cases only the quantum yield of triplet formation in the quenched system could be obtained.

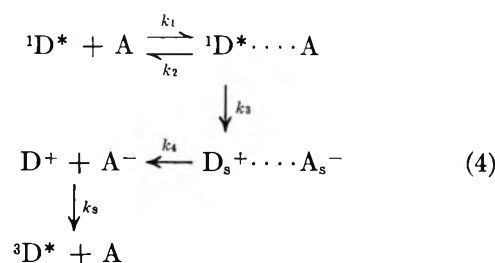
Table I: Data on the Quenching of Fluorescence and the Transient Quantum Yields for the Systems Studied

Donor	K, M^{-1}	Extent of quenching at quencher concn used	ϕ_T^b	ϕ_0^b
Naphthalene	175 ^a	94.1%	0.39	...
Phenanthrene	2800	99.6%	0.53	...
Coronene	280 ^a	93.3%
Pyrene	5000 ^a	99.6%	0.46	0.51
1,2-Benzanthracene	590 ^a	98.2%	0.45	...
Anthracene	77.3	78.6%	0.69	...
Perylene	93.3	81.6%	0.05	0.05 ^c
Tetracene	30.5	59.1%

^a From ref 11. ^b The intersystem crossing quantum yields used in calculating these quantities were taken from the collection in J. B. Birks, "Photophysics of Aromatic Molecules," Wiley-Interscience, New York, N. Y., 1970. ^c Calculated from eq 3 using the value of the perylene triplet-triplet extinction coefficient reported by R. Bensasson and E. J. Land, *Trans. Faraday Soc.*, **67**, 1904 (1971).

Comparison of the data of Figures 1-9 and of Table I leads to some interesting conclusions. Firstly, the flash data confirm the generality of the charge transfer mechanism of fluorescence quenching, since in nearly all cases radical ions of the fluorescer and/or quencher could be identified in the flash spectra. Secondly, the triplet, in most cases, also appears to be an intermediate in the quenching reaction. Since quenching is substantially complete in most cases, intersystem crossing from unquenched donor molecules cannot account for the appearance of the donor triplets in the flash spectra, with the possible exception of the systems anthracene-DCB, perylene-DCB, and tetracene-DCB. It is difficult to assess the origin of the triplets observed in these experiments. In the cases investigated here the triplet level of the donor lies below the energy level of the free ions (which is 0.06 eV higher than the corresponding ion pair energy) and a process, whereby triplets are produced from a recombination reaction of the free radical ions produced by the initial flash,¹¹ is clearly energetically possible. It has been established from chemiluminescence experiments²⁵ that ion recombination can lead to triplet formation, and the diffusion controlled nature of this process could, with the ion concentrations produced in these flash experiments, lead to a substantial formation of donor triplets

within the lifetime of the flash. This quenching reaction may be represented as



where formation of the ion pair (k_3) is decisive in determining the energy gain and, therefore, the rate constant, of the overall quenching reaction. However, other possible explanations of triplet formation, that the donor triplets are formed from the encounter complex ${}^1D^* \cdots A$,²⁶ or from the solvated ion pair $D_s^+ \cdots A_s^-$,¹³ cannot be discounted. The common intermediate in both cases could be a contact ion pair (D^+, A^-) which differs from the heteroexcimer insofar as the doublet character of the radical ions is still preserved, and from the solvated ion pair by having no solvent molecules in between the ions. It is not at all impossible that the charge transfer interaction in this ion pair results in such strong spin-orbit coupling that the correspondingly enhanced intersystem crossing rate can effectively compete with the dissociation rate of the contact ion pair.

The triplet quantum yields reported in Table I are complex quantities involving a number of steps; for example, in the reaction scheme 4 above, the steps corresponding to radical ion formation from the excited molecule ${}^1D^*$, and to triplet formation from the radical ions. It is remarkable, however, that, in the case of pyrene, such a high proportion of excited molecules are converted into triplets and radical cations, only 3% of the originally excited molecules reaching the ground state directly, whereas, in the case of perylene, this figure reaches 90%.²⁷

Acknowledgments. The authors are grateful for the assistance of Mrs. S. Reiche, who carried out much of the experimental work, and to Dr. B. Nickel, who provided considerable help with the zone-refining of the chemicals used. A. R. W. wishes to thank the Alexander von Humboldt-Stiftung for the award of a fellowship, during the tenure of which this work was carried out. Thanks are also due to Dr. W. Kühnle, who purified the solvents used in this work.

(25) A. Weller and K. Zachariasse, *J. Chem. Phys.*, **46**, 4984 (1967).

(26) C. R. G. G. Schmidt, R. Potashnik, and M. Ottolenghi, *J. Phys. Chem.*, **75**, 1025 (1971).

(27) NOTE ADDED IN PROOF. An analysis of the kinetics of formation and decay of both ions and triplets shows that the initial increase in triplet concentration expected from the reaction scheme 4 will occur in a time too short to be observed using the flash apparatus described here.²²

Photodissociation of Nitrogen Dioxide by Pulsed Laser Light at 6943 Å

by John W. Gerstmayr, Paul Harteck,* and Robert R. Reeves

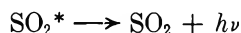
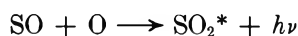
Chemistry Department, Rensselaer Polytechnic Institute, Troy, New York 12181 (Received September 20, 1971)

Publication costs assisted by the National Aeronautics and Space Administration

Nitrogen dioxide was photodissociated using a pulsed ruby laser at 6943 Å. The energy of a single photon at this wavelength was equivalent to only 57% of the dissociation energy. The mechanism proposed to account for the results was the consecutive absorption of two photons, the first resulting in a short-lived excited state. The second photon is then absorbed by the excited species resulting in dissociation.

Introduction

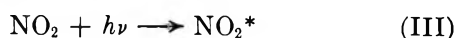
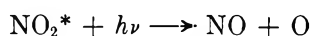
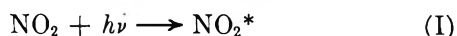
In work done previously in this laboratory it was demonstrated that two-photon emission was present in the reaction



The time delay between the two emissions was found to be of the order of 30 nsec.¹ (Smith observed emission corresponding to a lifetime of SO_2^* of 12 nsec in pulse electron beam studies.²)

The purpose of the present work has been to investigate the possibility of a reverse mechanism of this type occurring in the dissociation of NO_2 . Photodissociation becomes energetically possible at wavelengths below about 3945 Å.³ Some dissociation still occurs around 4070 Å due to the availability of the vibrational and rotational energy of the molecule. At 4358 Å, however, no dissociation is found.⁴

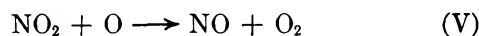
At higher wavelengths, up to approximately 7900 Å, the combined energy of two photons would once again make the dissociation reaction possible. The following three mechanisms are considered for discussion



A fourth possible mechanism would be



The reaction of ground state molecules is 26 kcal endothermic or for the excited molecule it would need the equivalent energy absorbed from photons at wavelengths of about 10,000 Å or less. However, such a reaction has not been observed as noted above. The net result of any of these mechanisms is the production of oxygen when the fast reaction of NO_2 with O atoms is included



The simultaneous absorption of two photons has been observed by several investigators. Pao and Rentzepis were the first to report a multiphoton process terminating in a specific chemical reaction: the photoinitiation of the polymerization of styrene and of *p*-isopropylstyrene.⁵ Porter has reported the initiation of the explosive reaction of H_2 and Cl_2 by a two photon absorption at 6943 Å leading to dissociation of the Cl_2 .⁶ Speiser has used a Q-switched ruby laser to achieve a two photon absorption in iodoform, followed by the liberation of iodine.⁷

The absorption in some cases may have been, at least in part, consecutive rather than simultaneous, with a short-lived excited intermediate absorbing the second photon. Porter has observed this consecutive two-photon absorption in the photodissociation of phthalocyanine.⁸

Experimental Section

A Korad K-1QP laser system was used in these experiments. The 9/16-in. ruby rod was operated with a passive Q-switch containing cryptocyanine dye to obtain single pulses of 1–2 J energy and 10 nsec duration at 6943 Å. The energy of the laser output was verified using a Korad KJ-2 calorimeter.

The gases used were obtained from the Matheson Co., East Rutherford, N. J. The argon was supplied at 99.995% purity and was used without further purification. The nitrogen dioxide was further purified until it was better than 99.99% purity. Several mix-

(1) J. A. Emerson, Ph.D. Dissertation, Rensselaer Polytechnic Institute, Troy, N. Y., 1969.

(2) W. H. Smith, *J. Chem. Phys.*, **51**, 3410 (1969).

(3) J. G. Calvert and J. M. Pitts, Jr., "Photochemistry," Wiley, New York, N. Y., 1966, pp 217, 219.

(4) P. A. Leighton, "Photochemistry of Air Pollution," Academic Press, New York, N. Y., 1961, p 47.

(5) Y. H. Pao and P. M. Rentzepis, *Appl. Phys. Lett.*, **6**, 93 (1965).

(6) G. Porter, *Nature (London)*, **215**, 502 (1967).

(7) S. Speiser and S. Kimel, *J. Chem. Phys.*, **51**, 5614 (1969).

(8) G. Porter and J. I. Steinfeld, *ibid.*, **45**, 3456 (1966).

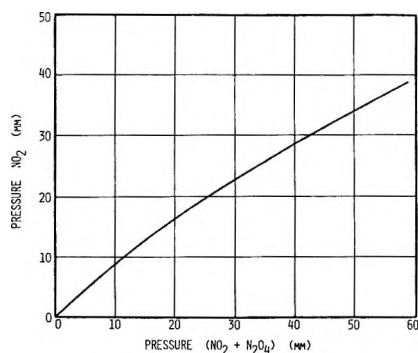


Figure 1. Partial pressure of NO₂ vs. pressure of (NO₂ + N₂O₄) equilibrium mixture at 20°.

tures of NO₂ and argon were prepared and gas analyses were performed on a CEC 21-130 mass spectrometer.

The fluorescent lights in the laboratory were found to cause some dissociation of the NO₂; therefore, the storage vessels containing the gas mixtures were covered with black cloth and the laboratory was in virtually total darkness at all times.

A cylindrical quartz cell of 9.5-cm path length was filled to the desired pressure with the mixture to be irradiated and placed in the path of the laser beam. The laser was fired five times at 2-min intervals. Each flash was monitored to ensure that the laser had produced only a single pulse, using a RCA-1P21 photomultiplier. The output signal of the phototube was recorded on film by a Tektronix 545-A oscilloscope fitted with a camera. The NO₂ was frozen out of the sample and the amount of O₂ present was measured against the argon standard on the mass spectrometer. Each set of experiments was run in one time span so that effects of variables related to laser operation, room temperature, etc. would be minimized.

Samples of NO₂ were repeatedly exposed to only the light from the xenon flash lamp of the laser under normal experimental conditions to ensure that no oxygen was being produced in this way. The results consistently showed no detectable formation of oxygen (*i.e.*, <0.01%).

The dimerization which occurs in NO₂ (2NO₂ ⇌ N₂O₄) had to be considered in these experiments. The true pressures of NO₂ were calculated for a series of gas pressures at 20° using the equilibrium constants of Harris and Churney.⁹ The results are shown in Figure 1. All pressures of NO₂ cited in this paper refer to true pressures of NO₂ in the equilibrium mixtures.

The absorption coefficient of NO₂ was measured in the region of 6943 Å using a Beckman DK-2 spectrophotometer. The experimental value of $\alpha = 0.15 \text{ cm}^{-1} \text{ atm}^{-1}$ was in good agreement with the value found by Dixon in this region of the spectrum.¹⁰ Dixon also reports that Beer's law is valid in the pressure region of these experiments. Due to the fine structure of the NO₂ bands, the actual absorption coefficient for the very narrow laser line may be somewhat different.

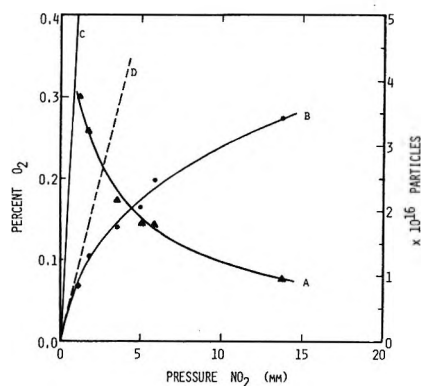


Figure 2. O₂ formed by five pulses in a mixture of 53% NO₂ and 47% argon: (A) as percent of total gas pressure and (B) as number of particles vs. pressure of NO₂; (C) number of NO₂* formed by five pulses vs. pressure of NO₂; (D) tangent drawn to production curve at lowest pressures of NO₂.

Results

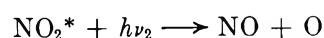
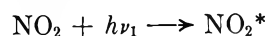
Using various pressures of NO₂ in the cell, oxygen was produced by firing the laser five times for each data point. Figure 2 depicts the O₂ production curve in a mixture of 47% argon and 53% (NO₂ + N₂O₄), which is representative of our observations below 15 mm of NO₂. Both O₂ as a percentage of total gas pressure and the number of O₂ molecules formed are plotted against the pressure of NO₂.

In order to have sufficient amounts of O₂ produced for purposes of gas analysis it was desirable to irradiate each sample 5 times. Calculations showed that the fractional loss of O₂ *via* the back reaction: 2NO + O₂ → 2NO₂, was negligible during the 20 min interval between the first laser pulse and the analysis.

Discussion

The formation of oxygen as shown in Figure 2 cannot be explained by ordinary photochemical mechanisms. As mentioned earlier, the absorption of light above ~4300 Å does not result in dissociation, but rather the formation of an excited state which eventually fluoresces or is quenched by collision. The dissociation energy of NO₂ into NO and an O atom is put at 71.8 kcal/mol, while an einstein of light quanta at the laser wavelength was calculated to supply only 41 kcal. The results suggest that the energies of two photons are combining to cause dissociation of the molecule. Several mechanisms are possible: the simultaneous absorption of two photons, the consecutive absorption of two photons, and the collisional interaction of two singly excited species.

The results appear to be consistent with the consecutive absorption mechanism represented by



(9) L. Harris and K. L. Churney, *J. Chem. Phys.*, **47**, 1703 (1967).

(10) J. K. Dixon, *ibid.*, **8**, 157 (1940).

(followed by $\text{NO}_2 + \text{O} \rightarrow \text{NO} + \text{O}_2$). From the known absorption coefficient at 6943 Å, and expected radiative and collisional lifetimes, a significant amount of oxygen should be formed, assuming a reasonable coefficient for the second absorption to the continuum, resulting in dissociation of the NO_2 .

The simultaneous process is expected to produce only small amounts of product such as mentioned by Porter in the initiation of the $\text{H}_2\text{-Cl}_2$ reaction,⁶ much less than those observed. These would also follow a different reaction pattern because the results of Porter should be independent of quenching. The amounts of O_2 observed are also far in excess of those permitted by the low probability of the collision of two excited species before collisional deactivation occurs.

A primary consideration in discussing the dissociation of NO_2 by the consecutive absorption process is the production of the NO_2^* state by the laser light. Calculations made from Beer's law using an average photon flux of 5×10^{18} photons/pulse (calculated from pulse energy measurements) showed that the number of excited molecules created during each pulse

$$\text{NO}_2^* = 1 \times 10^{16} \text{ (particles/mm)} P(\text{NO}_2)$$

or for the five pulses

$$\text{NO}_2^* = 5 \times 10^{16} \text{ (particles/mm)} P(\text{NO}_2)$$

where $P(\text{NO}_2)$ is the pressure of NO_2 in millimeters. This relationship is plotted along with the O_2 production curve in Figure 2. Collisional deactivation at very low pressures becomes negligible during the pulse time of 10^{-8} sec, and a comparison with a tangent drawn to the experimental O_2 production curve at the lowest pressures suggests that about one in five of the NO_2^* produced eventually absorbs a second photon leading to dissociation.

We believe that the consecutive absorption process can be described by three rate equations

$$+ \frac{d[\text{NO}_2^*]}{dt} = \gamma_1[\text{NO}_2] \quad (1)$$

$$- \frac{d[\text{NO}_2^*]}{dt} = \gamma_2[\text{NO}_2^*] = + \frac{d[\text{O}_2]}{dt} \quad (2)$$

$$- \frac{d[\text{NO}_2^*]}{dt} = (\lambda_1 + \lambda_2 + \dots)[\text{NO}_2^*] \quad (3)$$

where eq 1 governs the production of the singly excited species; eq 2 governs the loss of the NO_2^* via the absorption of the second photon; hence, also the production of O_2 . Equation 3 governs the loss of the NO_2^* due to collisional deactivation with λ_1, λ_2 , etc. relating to the quenching effects of the various components of the gas mixture. Since the duration of the laser pulse is much shorter than the radiative lifetime of 4×10^{-5} sec,¹¹ loss by fluorescence is considered to be negligible. The coefficients $\gamma_1, \gamma_2, \lambda_1, \lambda_2$, all have dimensions of re-

iprocal time. The rate coefficient for production of the NO_2^* was calculated from Beer's law as $\gamma_1 = 2.0 \times 10^6 \text{ sec}^{-1}$.¹² The general form of λ_1, λ_2 , etc. is $\lambda = Qk(M)$, where Q is the quenching efficiency of a gas component, $k \cong 2 \times 10^{-10} \text{ particles}^{-1} \text{ sec}^{-1}$ and (M) is the number of particles of that particular gas component in the reaction volume. The only approximation which has been made is the assumption of a constant light intensity for the duration of the pulse. Solving these equations for the net O_2 production during the laser pulse time ($T = 10^{-8}$ sec) yields the expression

$$[\text{O}_2] = \frac{\gamma_2 \gamma_1 [\text{NO}_2] T}{(\gamma_2 + \lambda_1 + \lambda_2 + \dots)} \times \left[1 + \frac{1}{(\gamma_2 + \lambda_1 + \lambda_2 + \dots) T} \times (e^{-(\gamma_2 + \lambda_1 + \lambda_2 + \dots) T} - 1) \right] \quad (4)$$

If collisional quenching of the reaction is set equal to zero, the fraction of the NO_2^* which eventually absorbs a second photon and dissociates, is given by

$$\frac{\text{NO}_2^* \rightarrow \text{O}_2}{\text{NO}_2^*} = \frac{\text{O}_2}{\gamma_1(\text{NO}_2) T} = \left[1 + \frac{1}{\gamma_2 T} (e^{-\gamma_2 T} - 1) \right] \quad (5)$$

This expression was calculated for several values of γ_2 . Graphical analysis showed that our experimental observation of the dissociation of one in five singly excited molecules corresponds to $\gamma_2 = 4.6 \times 10^7 \text{ sec}^{-1}$. Calculating again from Beer's law (using the reaction volume, $V_R = 15 \text{ cm}^3$) yields the coefficient for the second absorption, $\alpha_2 = 3.5 \text{ atm}^{-1} \text{ cm}^{-1}$. The value of expression 5 is plotted against different values of the second absorption coefficient in Figure 3.

In order to test the validity of the theory presented, O_2 production curves were calculated for a mixture containing 50% ($\text{NO}_2 + \text{N}_2\text{O}_4$) and 50% argon (a mixture similar to the experimental mixture of 53% ($\text{NO}_2 + \text{N}_2\text{O}_4$) and 47% argon which is reported). The coefficient for the second absorption, α_2 , was taken as $3.5 \text{ atm}^{-1} \text{ cm}^{-1}$ and quenching efficiencies were estimated from the results of Myers as 0.5 for NO_2 , 0.1

(11) D. Neuberger and A. B. F. Duncan, *J. Chem. Phys.*, **22**, 1693 (1954).

(12) Applying the approximation that, for small values of y , $e^{-y} = 1 - y$ to Beer's law results in the expression

$$\Delta I = \text{no. of NO}_2^* = \left[\frac{I_0 \alpha_1 X}{\left(\frac{\text{No. particles}}{\text{cm}^3 \text{ mm}} \right) \cdot V_R} \right] (\text{NO}_2)$$

where I_0 is the average photon flux, α is the coefficient for the first absorption, X is the path length of the cell, V_R is the volume of gas exposed to the laser light ($V_R = 15 \text{ cm}^3$), and $(\text{No. particles}/\text{cm}^3 \text{ mm})$ is a conversion factor from pressure to particles. The term in brackets is equal to γ_1 .

for Ar, and 1.0 for N_2O_4 .¹³ If the dimerization is ignored, oxygen production levels off at higher pressures. When the quenching of the N_2O_4 molecule is taken into account, oxygen production reaches a maximum and begins to diminish. These calculated curves are shown in Figure 4.

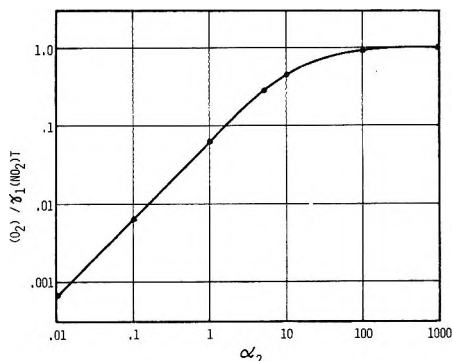


Figure 3. Fraction of NO_2^* which absorbs a second photon with zero quenching *vs.* the second absorption coefficient, α_2 .

Preliminary experiments have verified this diminishing oxygen yield at higher pressures and have suggested a possible quenching efficiency for the N_2O_4 molecule that exceeds gas kinetic expectations. We are continuing our investigations in the higher pressure region where the deactivation processes dominate and are

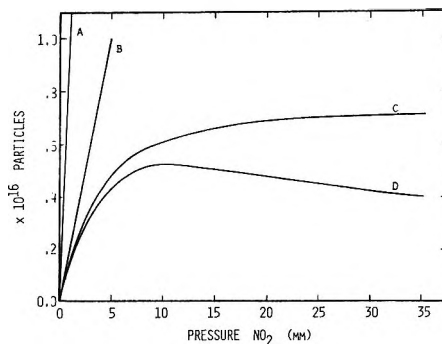


Figure 4. Calculated values for a mixture of 50% ($\text{NO}_2 + \text{N}_2\text{O}_4$) and 50% argon: (A) total number of NO_2^* formed per pulse *vs.* pressure of NO_2 ; (B) O_2 production curves for (B) zero quenching, (C) quenching but no dimerization, (D) quenching and dimerization of NO_2 as shown in Figure 1.

studying the effects of various other gases, such as CO_2 , on the overall reaction.

Acknowledgment. This work was supported by a grant from the National Aeronautics and Space Administration, NGL 33-018-007. Presented in part at the Second International Laser Workshop dealing with "Laser Interaction and Related Plasma Phenomena," held on Aug 30–Sept 3, 1971, at the Rensselaer Polytechnic Institute Graduate Center in Hartford, Conn.

(13) G. H. Myers, D. M. Silver, and F. Kaufman, *J. Chem. Phys.*, **44**, 718 (1966).

The Path of Triplet Excitation Energy in Simple Carbonyl-Monoolefins System in the Liquid Phase

by S. M. Japar,¹ J. A. Davidson,² and E. W. Abrahamson*

Department of Chemistry, Case Western Reserve University, Cleveland, Ohio 44106 (Received October 2, 1969)

Publication costs assisted by Case Western Reserve University

A study of the photochemical reactions of the systems acetone-*d*₆-tetramethylethylene and acetaldehyde-*d*₄-*cis*-2-butene reveal three types of processes arising from the ³(n,π*) states of the carbonyls; transfer of triplet excitation energy to the olefin acceptor, methylene exchange between the carbonyl and olefin, and, to a small extent in the latter system, ground state oxetane formation. Although the yields of these processes vary markedly, they have about the same activation energy which suggests that a ³(n,σ*) oxetane mediates all three processes.

The problem of the intermolecular transfer of triplet excitation energy has been extensively studied since the discovery of the low-temperature photosensitized phosphorescence of organic materials almost two decades ago.³ The studies have been extended to the liquid⁴ and gas phases⁵ and the scope of the reactions investigated has been extended most notably to photosensitized *cis*-*trans* isomerizations.^{6,7}

The mechanism of this process has generally been interpreted as a physical one based on a weak exchange interaction between the involved states of the two molecules⁸ which comes into play when the intermolecular distance is about 10–15 Å. This concept can qualitatively account for a considerable amount of the data which has been obtained on the subject particularly when donor and acceptor are rigidly fixed in the solid state. However, a number of systems in liquid solution and the gaseous state have been studied that are not readily explained by this mechanism. For example, Hammond and his coworkers⁷ have demonstrated what is apparently the transfer of triplet excitation energy from a donor to an acceptor of higher energy. Since the exchange mechanism requires that the (vibronic) excited states involved in the transition be isoenergetic,⁸ the observation of the so-called "endothermic" transfer of triplet excitation energy was explained in terms of a physical "non-Franck-Condon" excitation of the acceptor molecule.⁷

More recently another mainstay of the exchange mechanism has come under attack. As the weak exchange interaction depends on the overlap of the wave functions of the two molecules⁸ transfer of triplet excitation energy by this mechanism requires molecular collision, in which case the process should be largely diffusion-controlled⁹ providing the collision lifetime is sufficiently long (>10⁻⁹ sec). In solution the "cage effect" should ensure this condition. Recent studies, however, have shown that diffusion control operates

only in the more viscous solvents while in most cases the rate of energy transfer is less, by a factor of 3–5, than the rate of diffusion in the solvent.⁹

The fact that the triplet energy transfer distance is of the order of molecular diameters suggests other more chemical possibilities for transferring the energy in the liquid and gaseous states. In this regard Schenck¹⁰ has proposed a biradical intermediate in the case of the photosensitized cyclodimerization of certain olefins. Comparable arguments have also recently been employed to explain the observed efficiencies of energy transfer from aryl carbonyl compounds to olefins.¹¹ In a previous paper¹² the present authors through an investigation of possible parallel reactions accompanying energy transfer, examined the possibility of another type of chemical intermediate in the triplet energy transfer process, specifically a triplet donor-acceptor complex. The present paper extends this earlier work and further elaborates the nature of the proposed triplet donor-acceptor complex and its role in the transfer

(1) NSF Trainee, 1965–1966; NASA Trainee, 1966–1969.

(2) NSF Trainee 1967–1970.

(3) A. Terenin and V. Ermolaev, *Dokl. Akad. Nauk USSR*, **85**, 547 (1952).

(4) (a) H. Backstrom and K. Sandros, *Acta Chem. Scand.*, **14**, 49 (1960); (b) K. Sandros and H. Backstrom, *ibid.*, **16**, 958 (1962).

(5) (a) J. Heicklen and W. A. Noyes, Jr., *J. Amer. Chem. Soc.*, **81**, 3858 (1959); (b) R. Rebbert and P. Ausloos, *ibid.*, **87**, 5569 (1965).

(6) R. B. Cundall and P. A. Griffiths, *Trans. Faraday Soc.*, **61**, 1968 (1965).

(7) G. S. Hammond, *et al.*, *J. Amer. Chem. Soc.*, **86**, 3197 (1964).

(8) D. L. Dexter, *J. Chem. Phys.*, **21**, 836 (1953).

(9) P. J. Wagner and I. Kochevar, *J. Amer. Chem. Soc.*, **90**, 2232 (1968).

(10) G. O. Schenck and R. Steinmetz, *Bull. Soc. Chem. Belg.*, **71**, 781 (1962).

(11) N. C. Yang, J. L. Cohen, and A. Shani, *J. Amer. Chem. Soc.*, **90**, 3264 (1968).

(12) S. M. Japar, M. Pomerantz, and E. W. Abrahamson, *Chem. Phys. Lett.*, **2**, 137 (1968).

of triplet excitation energy as well as in parallel chemical processes.

Experimental Section

Materials. The acetone- d_6 and acetaldehyde- d_4 were obtained from Merck, Sharp, and Dohme, Ltd., of Canada and were guaranteed 99% isotopically pure. They were used as received.

2,3-Dimethyl-2-butene (hereafter TME) was obtained from Aldrich Chemical Co. and was fractionally distilled until a purity of >99.5% was obtained. *cis*-2-Butene was obtained from Matheson Gas Co. and was found to contain 0.98% of the trans isomer. The material was used as received.

Research grade methylcyclohexane and isopentane were purified by washing with concentrated sulfuric acid and water and passage twice through a 2 ft basic alumina column. Both solvents were dried over calcium oxide and distilled, with the middle fraction being collected. Neither of the purified solvents showed any near ultraviolet absorption.

Sample Preparation. Acetone- d_6 -TME samples were prepared by pipetting the appropriate amounts of material directly into the sample cell, which was then attached to the vacuum system by a greaseless insert joint. The solution was degassed on a grease-free, mercury-free vacuum line by a series of freeze-thaw cycles until the pressure over the frozen solution was below 5×10^{-6} Torr for three successive cycles. The sample cell was then sealed and removed from the line. Isopentane solutions were typically 0.5 *M* in acetone and 1.2 *M* in TME.

With acetaldehyde- d_4 -*cis*-2-butene samples the components were degassed individually and then combined in the sample cell. This was necessary because acetaldehyde polymerizes when cooled to temperatures approaching its freezing point.¹³ To avoid this, degassing of the acetaldehyde was carried out by first chilling the sample in a Dry Ice-isopropyl alcohol bath and further cooling the bath until it was solidified by adding of small amounts of liquid nitrogen. The chilled acetaldehyde was degassed directly under vacuum for a total of 30 min, and then distilled into the sample cell for use.

cis-2-Butene and the solvent were degassed by the usual freeze-thaw method. Both the *cis*-2-butene and the acetaldehyde- d_4 were degassed in calibrated tubes attached to the vacuum system. This allowed the recording of their final volumes before they were distilled into the sample cell. Absolute calibration of the sample volumes was made in terms of the weight of material used. Methylcyclohexane solutions were 0.5 *M* in acetaldehyde and 2.0 *M* in *cis*-2-butene while solutions containing only donor and acceptor were approximately 1.0 *M* in acetaldehyde and 10 *M* in *cis*-2-butene.

Irradiations. Irradiations were carried out with a 450-W high-pressure xenon arc enclosed in a lamp

housing equipped with a spherical reflector and a quartz focusing lens. Generally the light filter consisted of two Corning 0-53 (cutoff) filters, which passed less than 1% of the light below 283 nm. Absolute quantum yield determination utilized a solution filter for the 313-nm region.¹⁴

Temperature Control and Measurement. An Aminco constant temperature bath capable of refrigeration as well as heating was used to control the temperature of the sample cell within $\pm 0.2^\circ$. Temperature measurement was carried out with a calibrated Fenwall thermistor inserted into the opened sample cell.

Sample Analysis. Nmr spectra were measured on a Varian A-60 instrument and mass spectrometric analyses for the exchange reactions were carried out on a Varian M-66 mass spectrometer equipped with variable slits.

Analysis of *cis*-trans isomerization of 2-butene was done gas chromatographically using a 26 ft 25% AgNO₃-benzyl cyanide column. Analysis for oxetanes was carried out on a 15 ft 15% TCEP (tetracyano ethylated pentaerythritol) on Chromosorb P, mesh 45/60, nonacid washed column.

Reaction Yields. With the exception of measurements of the absolute quantum yields of the reactions at room temperature, all studies were carried out in terms of relative yields of the products. This procedure is valid as long as the initial reactant concentrations and the output of the light source are constant. Samples were prepared so that the former restriction was observed. Corrections for light output variations were obtained by measuring the light output by potassium ferrioxalate actinometry¹⁵ before and after each irradiation through a narrow band-pass filter. Knowing the variation in light output and the initial concentrations, the number of molecules converted per unit time was calculated and taken as a measure of the relative quantum yield of the reaction under the experimental conditions. In all cases the light was completely absorbed.

Treatment of Temperature Data. By plotting the relative quantum yields for the three processes at various temperatures *vs.* the reciprocal of the absolute temperature relative activation energies for these processes were obtained (Figure 2), but these relative activation energies may not be the true activation energies as the quantum yield is defined in terms the reaction rates according to eq 1

$$\phi_i = \frac{k_i}{k_i + k_j + k_l + \dots} \quad (1)$$

where the denominator is the sum of the rates of all the processes leading from a particular (excited state or

(13) P. D. Zemaný and M. Burton, *J. Phys. Chem.*, **55**, 949 (1951).

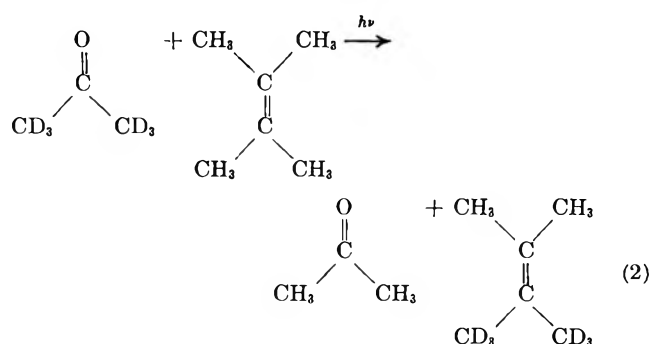
(14) J. G. Calvert and J. N. Pitts, Jr., "Photochemistry," Wiley, New York, N. Y., 1967, p. 732.

(15) C. G. Hatchard and C. A. Parker, *Proc. Roy. Soc., Ser. A*, **235**, 518 (1956).

intermediate) chemical species. For the quantum yield activation energy to approximate the true activation energy for the reaction ($k_j + k_1 + \dots$) would have to be large relative to k_i and temperature insensitive. These conditions should be satisfied when the relatively temperature insensitive rate constant for intersystem crossing of the triplet carbonyl to its ground state dominates the denominator of 1.

Results

Acetone- d_6 -TME System. In our previous study it was shown¹² that the irradiation of degassed equimolar solutions of acetone- d_6 and TME with 313-nm radiation leads to the formation of acetone and TME- d_6 , as in (2). The quantum yield of (2) was found to be $0.05 \pm$



0.005 at 16°, and the presence of oxygen at concentrations provided by air saturation of the reaction mixture completely quenched the reaction.¹² In the present study 5% 1,3-pentadiene (relative to the molarity of TME) was found to quench the exchange reaction by greater than 90%. The temperature dependence of the exchange reaction in isopentane solutions is indicated in Figure 1. Identical results were obtained in neat acetone- d_6 -TME solutions, where the molar ratio of TME:acetone- d_6 was 10:1.

As the bandpass of the filter combination was shifted to higher energies ($\lambda > 283$ nm) a second product was detected in small amounts by gas chromatography. The nmr spectrum of this product showed two singlets with τ 1.19 and 1.11 (external TMS standard), and integration of the signals yielded $(\tau = 1.11)/(\tau 1.19) = 11/10$. The low energy mass spectrum of the compound is given in Table I. As can be seen from the assignments in Table I the most probable structural assignment of the product is that of the oxetane (I) which is the product expected in the Paterno-Buchi reaction.¹⁶ This structure is in agreement with the observed nmr spectra. The yield of the oxetane, however, was too small to obtain an accurate measure of its variation with temperature. As the extent of photolysis at the shorter wavelength ($\lambda > 250$ nm) was at least an order of magnitude larger than at 313 nm, it is quite possible extended photolysis at 313 nm would have also yielded detectable amounts of (I).

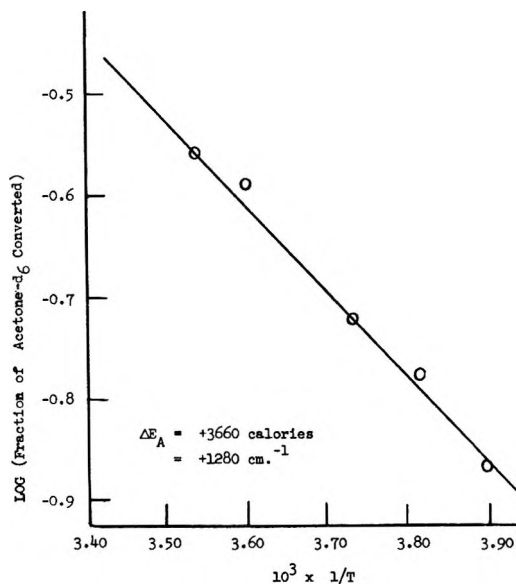
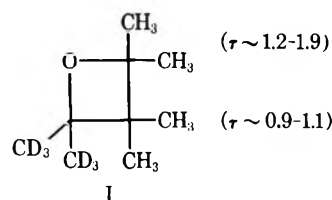


Figure 1. Calculation of the quantum yield activation energy for methylene exchange in the acetone- d_6 -TME system from relative yield data in isopentane solutions.

Table I: 20 MeV Mass Spectrum of the Unknown Product formed during Irradiation of Acetone- d_6 -TME Solutions

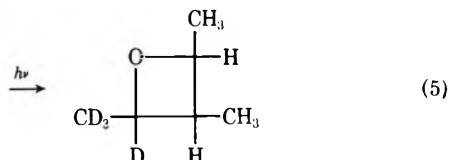
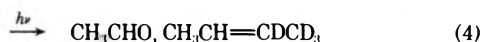
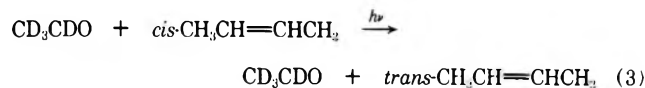
m/e	Strength	Assignment
148	w (weak)	Parent
133	m (medium)	Parent-(CH_3)
107	vw	Parent-($\text{CH}_3 + \text{CD}_3$)
105	vw	
90	s (strong)	TME- d_6
88	s	TME- d_6 -(D)
84	s	TME
83	m	TME-(H)
75	m	TME- d_6 -(CH_3)
72	m	TME- d_6 -(CD_2)
69	vs	TME-(CH_3)
64	m	Acetone- d_6
60	m	
59	m	
58	m	Acetone
55	m	
46	w	Acetone- d_6 -(CD_3)
43	w	Acetone-(CH_3)



Acetaldehyde- d_4 -*cis*-2-Butene. In contrast to acetone- d_6 , irradiation of degassed solutions of acetaldehyde- d_4 and *cis*-2-butene at wavelengths longer than 283 nm yields three distinct products, *trans*-2-butene

(16) D. R. Arnold, *Advan. Photochem.*, **6**, 30 (1968).

formed through photosensitized *cis*-*trans* isomerization, 2-butene-*d*₄, and 2,3-dimethyl-4-deuteriomethyl-4-deuterio-*d*₄-oxetane.



Gas chromatographic analysis indicates the presence of no other products after approximately 5% conversion of the 2-butene through isomerization. The oxetane of reaction 5 was identified by mass spectrometry as in the acetone-*d*₆ system. The presence of oxygen in air saturated solutions quenched reactions 3 and 5 by greater than 90%. Analysis for (4) relative to O₂ quenching was not attempted. A number of new products, however, were formed under these conditions due, presumably, to photooxidation reactions. The presence of 5% 1,3-pentadiene (relative to the molarity of *cis*-3-butene) quenched > 90% of (4) > 92% of (3) and > 98% of (5), without the appearance of new products.

Temperature dependences of the quantum yields of the three reactions are given in Figure 2 for methylcyclopentane solutions. Results identical within experimental error were obtained for a 10:1 molar ratio of *cis*-2-butene to acetaldehyde-*d*₄. The quantum yields were obtained from the relative yield data and a determination of the absolute quantum yield of reaction 3 by potassium ferrioxalate actinometry. At 14.8° the quantum yield of *trans*-2-butene formation by (3) is 0.023 ± 0.002. Although absolute yields of isomerization were not obtained for the concentrated samples, comparison of the relative yields under otherwise identical reaction conditions indicate that the absolute yields were not significantly different. The yields of reactions 3 and 4 are given in Table II in terms of the % conversion of the initial 2-butene present. From Table II it can be seen that the ratio of yields is approximately constant (0.39 ± 0.03). On this basis the

Table II: Yields of Reactions 3 and 4 at Different Temperatures

Temp. °C	% Conversion by (3)	% Conversion by (4)	Ratio % (4):(3)
+19.8	0.760	0.296	0.389
+10.6	0.665	0.266	0.400
+0.4	0.628	0.282	0.449
-17.6	0.360	0.120	0.333
			0.393 ± 0.032

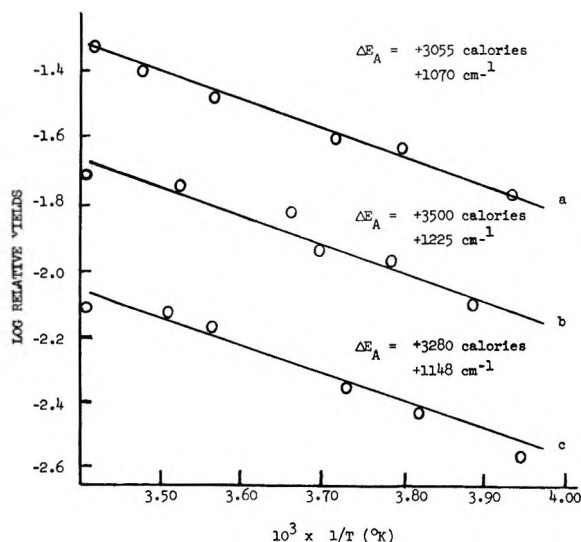


Figure 2. Determination of the relative quantum yield activation energies, ΔE_A , for the products resulting from irradiation of acetaldehyde-*d*₄ + *cis*-2-butene in methylcyclopentane. (a) *cis*-*trans* isomerization. The ordinate is milliliters of *cis*-2-butene converted. (b) Methylene exchange. The ordinate is milliliters of *cis*-2-butene converted. (c) Oxetane formation. The ordinate is milliliters of acetaldehyde-*d* converted.

quantum yield of exchange represented by (4) is 0.009 ± 0.002.

Table III shows a similar correlation for the yields of reactions 3 and 5 in terms of % conversion of *cis*-2-butene. It is seen that the ratios of the two yields are essentially constant (0.156 ± 0.011). On this basis the quantum yield of oxetane formation is 0.0035 ± 0.0007.

Table III: Yields of Reactions 3 and 5 at Different Temperatures

Temp °C	% Conversion (3)	% Conversion (5)	Ratio (5):(3)
-18.9	0.408	0.0548	0.134
-5.6	0.538	0.0882	0.164
+8.3	0.700	0.117	0.167
+20.3	0.924	0.146	0.158
			0.156 ± 0.011

The gas chromatographic data were not corrected for the thermal conductivities of the various products. This presented no particular problem with the analysis of *cis*-*trans* isomerization of the 2-butenes but may have been significant in the calculation of the amount of oxetane formed as the percentage changes in this case were derived from the peak areas of the acetaldehyde-*d*₄ and the oxetane. With this consideration the value of the quantum yield of oxetane formation may be in error by as much as 50%. On the other hand, this problem should not have affected the calculation of the relative quantum yield activation energy of the reaction since

relative yields, which cancel out the constant correction factor involved, were used for that determination.

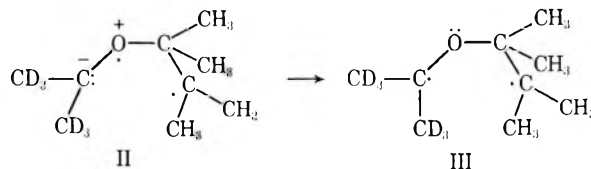
Discussion

The Nature of the Methylene Exchange Reaction and Oxetane Formation. As indicated in reactions 2 and 4 both the acetone- d_6 -TME and acetaldehyde- d_4 -*cis*-2-butene systems undergo methylene exchange. Concomitant formation of ground state oxetane has also been observed as shown in equation 5. The complete absence of TME- d_4 and lower mass isomers of TME in irradiated acetone- d_6 solutions¹² eliminates acetone photochemistry characteristic of the gas phase,¹⁷ *i.e.*, production of methyl radicals, as being responsible for the observed products in the exchange reaction. This agrees with the report of the very low quantum yield of acetone photodecomposition in the liquid phase.¹⁸ The lack of products in the acetaldehyde- d_4 irradiations, other than those indicated in reactions 3-5, leads to similar conclusions. Furthermore, photosensitized decomposition of stable oxetanes under the experimental conditions cannot account for the observed exchange products, as we have shown previously.¹²

The spin multiplicity of the excited states involved in the reactions has been identified by quenching of both oxetane formation and the exchange reactions by oxygen and 1,3-pentadiene. These studies clearly point to a triplet state intermediate in both reaction sequences.¹⁹⁻²² In all likelihood the lowest excited triplet states of acetone and acetaldehyde are $^3(n, \pi^*)$ and presumably it is this $^3(n, \pi^*)$ state of the carbonyl that is responsible for both processes. Such a result is not unexpected since gas phase studies have indicated that the quantum yield of formation of triplet acetone using 300 nm irradiation is 1.0 while that of acetaldehyde is 0.4.²³ In both cases the gas-phase photochemistry appears to arise solely from the triplet state.

The above discussion points to oxetane formation (4) and the methylene exchange reaction (5) as arising from a molecular complex formed between the $^3(n, \pi^*)$ state of the carbonyl compounds and the ground state of the olefin. One such possibility is a two-center biradical intermediate analogous to that proposed by Schenck.¹⁰ But such an intermediate would be expected to form a triplet oxetane as there seems to be no feasible way of effecting the clean exchange reaction without first forming a structure like (I). If the reaction results directly from a triplet biradical, the intermediate should form as (II) and revert to the presumably more stable form (III). Decomposition of the triplet biradical (III) to yield the methylene exchange reaction would necessarily involve the formation of a triplet oxetane intermediate. If (III) were quenched to a singlet biradical then ground state oxetane would result but the exchange portion could occur only by its subsequent thermal decomposition. This we have already demonstrated does not happen.¹² Therefore, although the

formation of ground state oxetane can feasibly occur *via* a biradical intermediate, the methylene exchange reaction cannot.



Evidence of a theoretical nature against the participation of biradicals in ground state oxetane formation is provided by a recent treatment of the photocycloaddition of formaldehyde to ethylene within the framework of a perturbation molecular orbital approach²⁴ carried out by Herndon and Giles.²⁵ They concluded that the concerted addition of either $^1(n, \pi^*)$ or $^3(n, \pi^*)$ formaldehyde to ethylene has a significantly lower energy barrier than does any mechanism involving intermediate biradical formation. They unfortunately assumed that in the cycloaddition of $^3(n, \pi^*)$ formaldehyde to ethylene the rate controlling step is a slow intersystem crossing process favoring a biradical path. Our molecular orbital treatment given further on, however, quite clearly shows that it is the surmounting of the energy barrier in the concerted photocyclo addition which is rate controlling and hence the concerted process is the more favored one for $^3(n, \pi^*)$ formaldehyde and alkyl substituted aldehydes and ketones.

A further point against the participation of biradicals in either process is that no photoproducts of the type expected in radical reactions, *i.e.*, higher molecular weight compounds, were observed. This evidence coupled with the fact that the activation energies of the two processes are essentially the same points to these reactions as proceeding *via* the concerted formation of a 4-center triplet oxetane intermediate (I) which can decompose in the same manner indicated in Figure 3.

(17) R. B. Cundall and A. S. Davies, *Proc. Roy. Soc., Ser. A*, **290**, 563 (1966).

(18) R. Pieck and E. W. R. Steacie, *Can. J. Chem.*, **33**, 1304 (1955).

(19) It has been shown that large amounts of olefins also quench singlet state reactions.²⁰ However, in systems similar to those studied here marked deviations from Stern-Volmer quenching of the triplet states usually occurs only when the concentrations of the diolefin approaches 50% of that of the monoolefin.²¹ Even at these concentrations the effect is minor and insignificant compared to the total quenching observed. Significantly, a recent study of the singlet excited acetone photosensitized decomposition of 1,4-dichlorobutane in the liquid phase shows no quenching of the reaction by simple olefins.²² Therefore, the quenching effect reported here is most reasonably assigned to a triplet excited state reaction.

(20) L. M. Stephenson and G. S. Hammond, *Pure Appl. Chem.*, **16**, 125 (1968).

(21) A. Morikawa and R. J. Cvetanovic, *Can. J. Chem.*, **46**, 1813 (1968).

(22) M. A. Golub, *J. Amer. Chem. Soc.*, **91**, 4925 (1969).

(23) R. B. Cundall and A. S. Davies, *Progr. React. Kinet.*, **4**, 149 (1967).

(24) M. J. S. Dewar, "The M. O. Theory of Organic Chemistry," McGraw-Hill, New York, N. Y., (1969), Chapter 6.

(25) W. C. Herndon and W. B. Giles, *Mol. Photochem.*, **2**, 277 (1970).

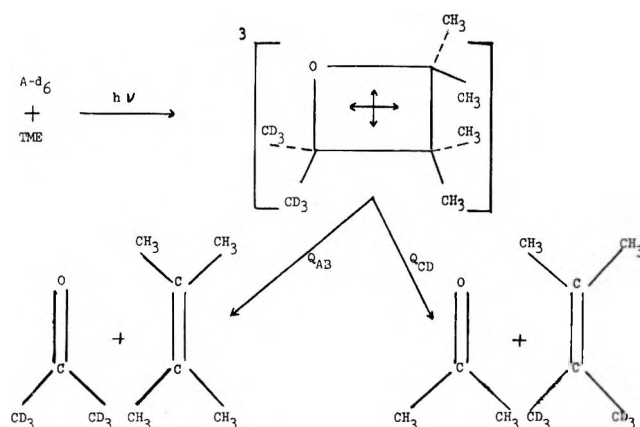


Figure 3. Methylene exchange *via* a triplet oxetane intermediate in the acetone- d_6 -TME system.

In view of the proposed concerted mechanism for oxetane formation one would expect to observe stereospecific products.¹⁶ We were, however, not able to resolve such stereospecific isomers on our GLC column so that this point remains to be settled.

If the intermediate is indeed an excited state of an oxetane, the assignment of the multiplicity of the state as triplet is upheld. The observed activation energy of only 3.3 kcal would hardly be sufficient to populate significantly an excited singlet state of an oxetane as the lowest spectroscopically apparent state of trimethylene oxide is found at wavelengths shorter than 230 nm.²⁶ For irradiation at 300 nm therefore, an activation energy of at least 30 kcal would be necessary for the population of such an excited state.

Direct 4-center reaction of $^3(n, \pi^*)$ acetone and ground state TME should produce a $^3(n, \sigma^*)$ state but should a $^3(\sigma, \sigma^*)$ state lie lower in energy then one can expect internal conversion to this state. In any event, however, the lower lying of these two triplet states cannot exceed the energy of the $^3(n, \pi^*)$ state of the carbonyl compound plus the activation energy for the reaction. Unfortunately, reliable calculations for the energies of either of these states have not been published but it is not unreasonable to expect them to be close to the $^3(n, \pi^*)$ state of the parent carbonyl.

Mechanism of Triplet Excitation Transfer in Simple Carbonyl-Olefin Systems. As it seems reasonable to involve a triplet oxetane intermediate in the methylene exchange reaction as well as ground state oxetane formation, the question is raised as to whether this same intermediate might participate in the triplet energy transfer process occurring in the same and similar systems. For example, it has been shown that TME and many other olefins quench the phosphorescence of both acetone and acetone- d_6 in the gas phase.⁵ Similarly, photosensitized *cis-trans* isomerization of 2-pentene has been shown to occur *via* triplet excitation transfer from acetone in the liquid state.²⁷

As has been mentioned above, triplet excitation trans-

fer has been inferred in the acetaldehyde- d_4 -*cis*-2-butene system from the photosensitized formation of *trans*-2-butene. The quantum yield of *trans*-2-butene formation by our measurements is 0.023 ± 0.002 at 15°. *Cis-trans* isomerization of both isomers is considered to proceed *via* a common excited 2-butene molecule²⁸ which would relax to either a *cis*- or *trans*-2-butene ground-state molecule. In the gas phase 48.1% of such excited molecules relax to *trans*-2-butene while 51.9% relax to *cis*-2-butene.²⁹ On this basis the overall quantum yield of excitation transfer is equal to 0.048 ± 0.004 .

It is seen from Figure 2 that the relative quantum yield activation energies of the three reactions resulting from the irradiation of acetaldehyde- d_4 in the presence of *cis*-2-butene, reactions 3-5, fall in the range 3.25 ± 0.25 kcal. The oxygen and 1,3-pentadiene quenching of all three processes indicates that they involve triplet excited states. This coupled with the close correspondence of the activation energies suggests that they either all proceed *via* a common intermediate, or, as one might infer from the magnitude of the activation energies, that all three processes are diffusion controlled. But this latter point can be eliminated as the quantum yields and activation energies for all three processes in the case of a 1:10 *M* mixture of acetaldehyde- d_4 in *cis*-2-butene are quite the same as when the two are present in a relatively dilute solution of methylcyclopentane. Furthermore the activation energies, calculated for diffusion based on the viscosities, are lower than those obtained experimentally for the three processes.

Although the acetone- d_6 -TME system cannot show the effects of triplet excitation transfer, *i.e.*, *cis-trans* isomerization, some insight into this process is possible if the acetone photosensitized *cis-trans* isomerization of 2-pentene is considered. In this case an activation energy of 4.2 kcal is associated with the transfer of triplet excitation to 2-pentene,²⁷ which is in good agreement with the present observation of a 3.7 kcal activation energy associated with the methylene exchange reaction in the acetone- d_6 -TME system. That energy transfer in this system appears to involve an activation energy is in agreement with gas phase observations^{5b} which indicate that the triplet state of acetone is quenched by only one in fifty collisions with conjugated diene molecules, in a reaction which should be markedly exothermic. The tenfold higher yield of energy transfer in the acetone-2-pentene system as opposed to the acetaldehyde- d_4 -*cis*-2-butene, can be accounted for by assuming that

(26) J. D. Margerum, J. N. Pitts, J. G. Rutgers, and S. Searles, *J. Amer. Chem. Soc.*, **81**, 1549 (1959).

(27) R. F. Borkman and D. R. Kearns, *J. Amer. Chem. Soc.*, **88**, 3467 (1966).

(28) J. Saltiel and G. S. Hammond, *ibid.*, **85**, 2515 (1963).

(29) E. K. C. Lee, H. O. Denshlag, and G. A. Haniger, Jr., *J. Chem. Phys.*, **48**, 4547 (1968).

the triplet quantum yield of ${}^3(n,\pi^*)$ acetaldehyde is smaller than that of acetone. As we have already pointed out the yield of ${}^3(n,\pi^*)$ state in acetaldehyde is 0.4 as compared with 1.0 for acetone. The lifetime of the ${}^3(n,\pi^*)$ state in acetone has been reported to be of the order of 10^{-6} sec,^{27,30,31} but no comparable data exists for acetaldehyde. This difference could also be accounted for if the ${}^3(n,\pi^*)$ state of acetaldehyde was in equilibrium with an eximeric species much less reactive in the three processes than the monomeric ${}^3(n,\pi^*)$ state.

Triplet Oxetane as an Intermediate. It is instructive to consider the nature of the triplet state of the oxetane formed from the concerted addition of the ${}^3(n,\pi^*)$ of the carbonyl donor and the olefinic acceptor. A simple molecular orbital treatment shows that the planar, symmetrical oxetane formed by the concerted 4-center overlap of the π orbitals of the carbonyl and olefin yields, through its C_{2v} symmetry, bonding and antibonding fourfold degenerate sets of molecular orbitals (Figure 4). Moving along the reaction coordinate, Q , from the symmetrical oxetane in the direction of the initially separated triplet carbonyl and ground state olefin, the C_{2v} symmetry is lost. This permits mixing of the oxetane orbital wave functions $\psi_{A_1'}$, $\psi_{B_1'}$, $\psi_{A_1^*}$, and $\psi_{B_2^*}$ so that they correlate with ψ_3 , ψ_4 , ψ_5 , and ψ_6 of the separated carbonyl and olefin, as shown. A qualitative consideration of the behavior of the orbital energies on displacement along Q from the point of the symmetrical oxetane toward the initial separated carbonyl and olefin predicts little change in the energies of the four-center molecular orbitals ψ_{A_1} and ψ_{B_1} , as the energy increase accompanying the stretching of the horizontal pair of σ bonds would be largely compensated by the energy decrease accompanying the initial compression of the vertical pair of σ bonds coupled with the onset of π bonding. The energies of $\psi_{A_1'}$ and $\psi_{B_1'}$ would be increased relative to ψ_{A_1} and ψ_{B_1} as the vertical π orbitals being formed in this case are initially antibonding. Similar considerations lead to an increase of the energies of ψ_3 and ψ_4 over ψ_1 and ψ_2 when the separated carbonyl and olefin are displaced along Q toward the symmetrical oxetane. A corresponding lowering in energy will occur for $\psi_{A_1^*}$, $\psi_{B_1^*}$, ψ_5 and ψ_6 under the same operations. On this basis one can expect a pair of energy barriers bounding a region of metastability in proceeding along Q from the separated ${}^3(n,\pi^*)$ carbonyl and ground state olefin in the initial and methylene exchanged forms to the planar symmetrical ${}^3(n,\pi^*)$ oxetane. The barriers would be further enhanced by the accompanying nuclear displacements.

The complete reaction coordinate Q is shown in Figure 5. If one proceeds from the initial state along Q the energy barrier is surmounted in order to reach the symmetrical oxetane at the minimum, which will probably be somewhat higher in energy than the initial state. Proceeding further, a second equal energy barrier is

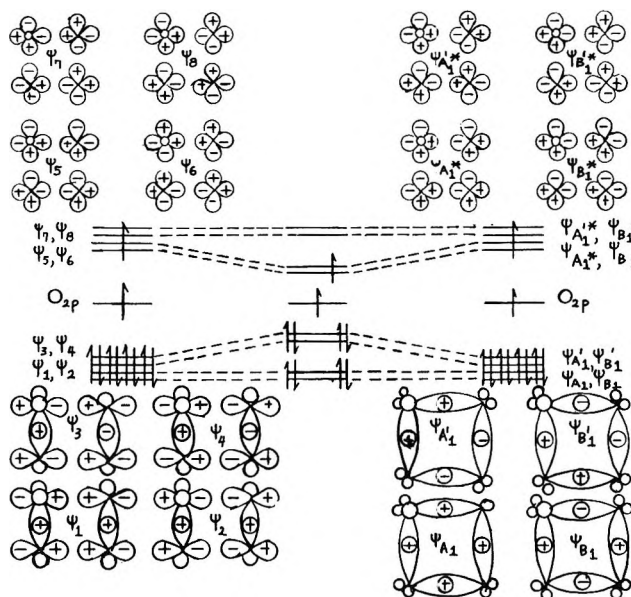


Figure 4. Correlation of the symmetry orbitals of the planar oxetane intermediate with those of the separated olefin and carbonyl.

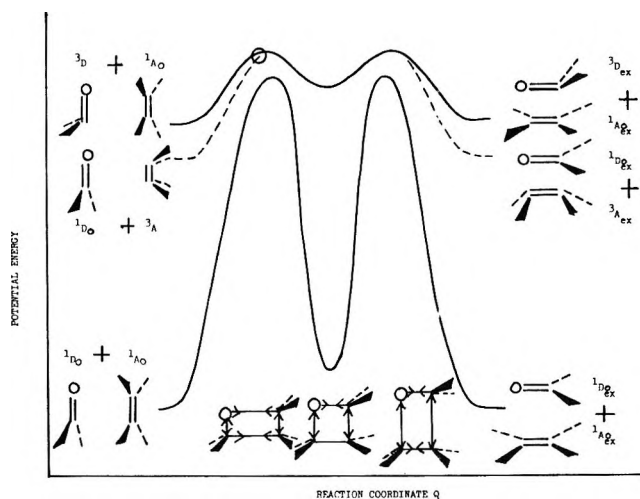


Figure 5. Potential energy curves for the formation of the oxetane from a simple carbonyl-olefin system along a coordinate Q leading to exchange products.

surmounted yielding the methylene exchange products. Should the excited oxetane be collisionally quenched to a lower energy while traversing this minimum the ${}^3(n,\pi^*)$ oxetane would be stabilized in this metastable region in which case it could then undergo intersystem crossing to yield a stable ground state oxetane molecule. Alternatively the path to ground state oxetane could be *via* transfer of triplet excitation energy from the triplet oxetane to either the olefin or carbonyl but because of the much less favorable orbital overlap this should be much less efficient than the carbonyl-olefin excitation energy transfer.

(30) F. Wilkinson and J. T. Dubois, *J. Chem. Phys.*, **39**, 377 (1963).

(31) P. J. Wagner, *J. Am. Chem. Soc.*, **88**, 5672 (1966).

The reaction coordinate in Figure 5 does not indicate the possibility of an internal conversion from the ${}^3(n, \sigma^*)$ to lower lying ${}^3(\sigma, \sigma^*)$ should one exist. However, if this does, in fact, occur it should not change the qualitative pattern of the coordinate. Similarly it has been reported that ground state oxetanes, although planar, have a small inversion barrier in the out-of-plane bending mode.³² This barrier may also be manifest in the ${}^3(n, \sigma^*)$ oxetane but it should not be of a magnitude as to effect the reaction coordinate, Q , in any significant way.

In contrast to the methylene exchange process and ground state oxetane formation the triplet energy transfer reaction is quite likely effected outside the region of metastability of the triplet oxetane before the initial energy barrier is surmounted. Logically this should occur somewhere near the top of the barrier because of the small energy separation of the ${}^3D + {}^1A_0$ and ${}^1D_0 + {}^3A$ pairs. The closer the energy of these two systems the greater should be the interaction of the potential surfaces along Q and the lower the ascent of the energy barrier necessary to effect energy transfer. The fact that the experimental activation energy for triplet energy transfer is slightly less than those for the other two processes would indicate, by this mechanism, that the barrier need not be completely surmounted. Strictly speaking, therefore, by the mechanism shown in Figure 5, the transfer of triplet excitation energy is not mediated by a truly *metastable* triplet oxetane as is ground state oxetane formation and methylene exchange. But as the same reaction coordinate is involved and the carbonyl-olefin distance is less than Van der Waals radii the transfer process can be viewed as involving an (unstable) triplet oxetane.

The potential surfaces as drawn in Figure 5 point to the triplet energy transfer process as being exothermic while work of Evans³³ suggests that the ${}^3(\pi, \pi^*)$ state of the olefin is about 3–4 kcal higher in energy than the ${}^3(n, \pi^*)$ state of acetone, and most likely also for acetaldehyde. This assignment, however, is based on absorption to essentially planar olefin, while the true 0-0 band corresponding to absorption to nonplanar olefins may lie at much lower energies. This is borne out by a recent calculation of Ross³⁴ in this laboratory. Using a modification of the CNDO method of Del Bene and Jaffe³⁵ he finds that the lowest ${}^3(\pi, \pi^*)$ state of ethylene in the "boat" form is more stable than the planar form by 2 eV. This calculation may not be quantitatively significant but one would expect even on qualitative principles that a triplet olefin in the boat form would have a substantially lower energy than the planar form. On this basis the transfer of triplet excitation energy would be expected to be exothermic in the systems discussed.

The above discussion relating to the common triplet oxetane intermediate can be summarized in terms of Figure 5. Energy transfer is favored over exchange by

the somewhat lower activation energy for the former arising from the strong interaction of the two potential surfaces outside the region of metastability of triplet oxetane below the barrier maximum. In the acetaldehyde-*d*₄-*cis*-2-butene system the comparatively low yield of ground state oxetane formation can be explained by the high probability of continuing over the second barrier to yield exchange once the first barrier has been surpassed. This can be understood in terms of the probability of a deactivating collision taking place along Q in the metastable region of triplet oxetane. Since the energy necessary to surmount the second barrier is present when the first barrier has been crossed, the molecule can traverse Q and yield exchange in the time of one vibration, $\sim 10^{-12}$ sec. As this is also approximately the time between collisions of molecules in solution, one would expect of the order of 50% of the molecules crossing the first barrier to be quenched to a metastable triplet oxetane eventually reaching ground state by intersystem crossing. The observed ratio oxetane yield:exchange yield of 0.39 in the acetaldehyde-*d*₄-*cis*-2-butene system is consistent with this line of reasoning.

Comparison of Mechanisms. It is instructive to compare the mechanism of triplet excitation transfer as proposed for the systems studied here with the more generally accepted mechanism based on the weak exchange interaction treatment of Dexter.⁸ Actually the principal perturbation interaction is the same in both mechanisms, *i.e.*, exchange repulsion as given by

$$\int \psi_D'(1)\psi_A(2) \frac{1}{r_{12}} \psi_A'(1)\psi_D(2) d\tau_{12} \quad (5)$$

The difference between the two cases is one of the strength of the interaction. Dexter treats the weak coupling interaction occurring at intermolecular distances somewhat greater than the sum of Van der Waals radii for essentially stationary molecules; in which case the probability of the transfer is given by the square of the product of (5) and the spectral overlap integral (6)

$$\int_0^\infty E_D(\bar{\nu})A_A(\bar{\nu})d\bar{\nu} \quad (6)$$

where ψ_D and ψ_D' are the spin-orbital wave functions before and after excitation for the carbonyl donor, ψ_A and ψ_A' the corresponding functions for the olefin acceptor, in which ψ_D' and ψ_A have the same total spin as do the pair ψ_A' and ψ_D . $E_D(\bar{\nu})$ and $A_A(\bar{\nu})$ are the phosphorescence emission spectrum of the donor and the singlet-triplet absorption spectrum of the acceptor each normalized to unity.

(32) S. I. Chan, T. R. Borges, J. W. Russell, H. L. Strauss, and W. D. Gwinn, *J. Chem. Phys.*, **44**, 1103 (1966).

(33) D. F. Evans, *J. Chem. Soc., London*, 1351 (1957).

(34) R. T. Ross, private communication (1969).

(35) J. Del Bene and H. H. Jaffe, *J. Chem. Phys.*, **48**, 4050 (1968).

For the model presented in this paper the exchange repulsion interaction is several orders of magnitude stronger by virtue of the fact that the collision of donor and acceptor brings them somewhat closer together than the sum of their Van der Waals radii. The probability (rate) of transfer in this case depends again on the square of (5) but is independent of the overlap integral.³⁶ One would also expect the rate to be roughly inversely proportional to the difference in the slopes of the two interacting potential curves^{37,38} in Figure 5. This condition would generally favor a small difference in energy between the triplet states of donor and acceptor for the transfer process in contrast to the weak coupling case where a large energy difference leads to a large spectral overlap integral.

The cases studied here, in Hammond terminology, are endothermic, non-Franck-Condon processes.⁷ They can be visualized as involving a long-lived donor-acceptor solution cage complex in which the acceptor molecule is excited in a particular vibrational mode to a level where its singlet-triplet energy separation is isoenergetic with that of the donor. The activation energy for this process is associated with vibrational excitation of the acceptor in contrast to the triplet oxetane mechanism in which the activation energy is associated with the ascent of the barrier along the reaction coordinate, Q to a point where the interaction energy and the velocity, dQ/dt are such that the radiationless transition from ${}^3D + {}^1A_0 \rightarrow {}^1D_0 + {}^3A$ can readily occur.

In addition to the formal equivalence of the type of interaction energy in both mechanisms there is another point of similarity for the cases studied, namely, that the overlap integral (6) will be maximal along Q . This coupled with the fact that no data exist at the present time for a quantitative evaluation of the activation energies of the two processes make it difficult to predict just which mechanism is operative. There is, however, one point which clearly favors the triplet oxetane mechanism in solution and gases where collisions are involved, namely that the region of weak interaction along Q is traversed rapidly, *i.e.*, large dQ/dt , relative to the region of strong interaction. If the dwell time in the region of weak interaction is too short, *i.e.*, $< h/2\beta$ where β is the interaction energy, then the transfer can occur only in the strong interaction region.

Gas-phase studies by Schmidt and Lee cite a number of cases where benzene is the sensitizer in which the transfer rate roughly increases with the donor-acceptor triplet energy difference but this trend is not apparent for cases where acetone is the sensitizer.³⁹

The above considerations also apply to the "exothermic" triplet transfer processes. Here one might expect that dependence of the transfer probability (or lack of it) on the overlap integral (6) would allow one to distinguish between the strong and weak coupling mechanism. An examination of the existing literature,

however, has not disclosed any data which would permit this distinction.

The question naturally arises as to whether and to what degree the reaction mechanism as pictured in Figure 5 can be generalized to other carbonyl donor-olefin acceptor systems. If the oxetane intermediate is not symmetrical with respect to attached groups, the reaction coordinate, Q , will not be symmetrical. Variation in the depth of the potential minimum and differences in energy of the triplet transfer and exchange products can be expected and in some cases the minimum in Q may disappear altogether. This could clearly change the character and relationship of the three processes. Thus, for example, in the aforementioned case of the acetone-photosensitized isomerization of 2-pentene²⁷ the exchange process might be largely ruled out because of a higher energy barrier in the exchange portion of Q .

In the majority of carbonyl-olefin systems studied by other investigators^{7,10,11,16,40-42} aromatic or unsaturated groups were conjugated with the carbonyl and/or olefin linkage in an unsymmetrical manner with respect to their oxetane. This could change the picture presented in Figure 5 even more drastically. With such systems there also may be triplet states of the oxetane lying lower in energy than the ${}^3(n,\sigma^*)$ in which the excitation energy can eventually become localized in the attached groups resulting in stabilization of the oxetane ring.

It is also possible that there will be cases where the exchange repulsion interaction will be greater along reaction coordinates other than that associated with concerted oxetane formation. Thus it may be that in certain cases a biradical mechanism such as proposed by Schenck¹⁰ for the C_4 cyclomerization might be operative in the triplet excitation transfer process, although it has also been suggested that the Schenck intermediate is an alternative to, rather than a part of the triplet pathway.³⁷

One might advance other mechanisms linking the three processes. For example one might invoke a vibrationally excited (hot) ground state oxetane as a common intermediate. But this molecule would have to be initially formed with energy in excess of that sufficient for the decomposition of the ground state, otherwise ground state oxetane would be the predominant product. According to this picture exchange and triplet transfer should have equal yields. This is not ob-

(36) G. W. Robinson and R. P. Frosch, *J. Chem. Phys.*, **38**, 1187 (1963).

(37) C. Zener, *Proc. Roy. Soc. Ser. A*, **137**, 696 (1932).

(38) C. Zener, *ibid.*, *Ser. A*, **140**, 660 (1933).

(39) M. W. Schmidt and E. K. C. Lee, *J. Amer. Chem. Soc.*, **92**, 3579 (1970).

(40) J. Saltiel, private communication.

(41) N. Turro and P. A. Wriede, *J. Amer. Chem. Soc.*, **90**, 6863 (1968).

(42) J. Saltiel, R. M. Coates, and W. G. Dauben, *J. Amer. Chem. Soc.*, **88**, 2745 (1966).

served experimentally. Another possibility might involve a thermal pumping of the ³(n,π*) carbonyl to the ¹(n,π*) state and subsequent reaction from this state⁴⁰ but certainly in the case of the acetone/TME this possibility may be rejected as the observed activation energies are only one half as large as the minimum figure of 2000 cm⁻¹ reported for the separation of the ³(n,π*) and ¹(n,π*) states of acetone. The same considerations, no doubt, apply to acetaldehyde although no explicit measurements of the ¹(n,π*)-³(n,π*) separation has been reported for this molecule.

Summation

A study of the photochemistry of two carbonyl-olefin systems, acetone-*d*₆/tetramethylethylene and acetaldehyde-*d*₄/*cis*-2-butene, reveals three types of reactions derivable from the ³(n,π*) state of the carbonyl: (1) a transfer of triplet excitation energy as manifest in the *cis*-*trans* isomerization of the olefin, (2) an exchange of substituted methylenic groups between carbonyl and olefin and (3) the formation of the ground state oxetane complex of the two. The similarity in activation energies, the demonstration of the lack of diffusion control, and the quenching by oxygen and 1,3-pentadiene of all three processes point to a triplet oxetane as a common intermediate. This is further supported by a theoretic

calculation²⁵ showing a more favorable energy path for oxetane formation *via* a 4-center as opposed to 2-center photocycloaddition.

Molecular orbital correlation along a 4-center coordinate, *Q*, linking the symmetrical oxetane with the separated carbonyl and olefin in both the initial and methylene exchanged forms reveals a region of metastability having a minimum at the configuration of the symmetrical oxetane. The proposed triplet oxetane mechanism requires methylene exchange and ground state oxetane formation to have sufficient energy to surmount the barriers bounding the region of metastability. The radiationless transfer of triplet excitation energy, however, does not require that the barrier be surmounted. Its energy of activation suggests that it occurs in a region near the top of the barrier but at intermolecular distances less than the sum of van der Waals radii of the carbonyl and olefin where strong exchange repulsion interaction can effect the transfer.

Acknowledgments. Support of this work by the Atomic Energy Commission, Contract No. AT-11-1-904 is gratefully acknowledged. The authors wish to thank Dr. Lester Friedman for the AgNO₃ column used in the investigation and Dr. Martin Pomerantz for helpful discussions concerning the problem.

The Reaction of Trifluoromethyl Radicals with Hexafluoroacetone Imine

by D. W. Follmer, S. Toby, and G. O. Pritchard*

Department of Chemistry, University of California, Santa Barbara, California 93106
(Received September 13, 1971)

Publication costs borne completely by The Journal of Physical Chemistry

By photolyzing hexafluoroacetone the addition reaction between CF₃ radicals and hexafluoroacetone imine has been studied. The reaction is rapid, with an *A* factor of 5.2×10^{10} cm³ mol⁻¹ sec⁻¹ and an activation energy of 3900 cal mol⁻¹. Hydrogen atom abstraction occurs much less readily, with *A* = 1.6×10^9 cm³ mol⁻¹ sec⁻¹ and *E* = 4500 cal mol⁻¹.

We have recently investigated the photochemistry of hexafluoroacetone imine at 2537 Å.^{1,2} CF₃CN was the only major volatile product, while CF₃H was a minor product, and C₂F₆ could not be positively identified.² It was anticipated that the photochemical cleavage of the imine would generate CF₃ radicals, but the absence of C₂F₆ indicated that this may not be so. However, due to the very low quantum yields found for the photodecomposition,² the stationary concentration of the CF₃ radicals could be extremely low, and if

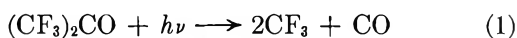
they further reacted facily with the imine source, detectable amounts of C₂F₆ may not have been produced. To examine this possibility we have used hexafluoroacetone (HFA) as a photolytic source of CF₃ radicals to investigate their reaction with hexafluoroacetone imine. The experiments were carried out at

(1) S. Toby and G. O. Pritchard, *J. Phys. Chem.*, **75**, 1326 (1971).

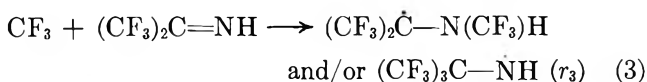
(2) F. S. Toby, S. Toby, and G. O. Pritchard, Abstracts 162nd National Meeting of the American Chemical Society, Washington, D. C., Sept 1971, Phys 034.

3130 Å, at which wavelength the imine does not absorb.^{1,2}

The photolysis of HFA at 3130 Å has been extensively investigated, and it is well established that $R_{C_2F_6} = R_{CO}$,



in the temperature range of interest.³ In preliminary experiments at 150°, using 20 Torr of HFA in the presence of 20 Torr of added imine, C_2F_6 formation was almost completely suppressed; it was found that $R_{C_2F_6} \simeq 0.01R_{CO}$. A small quantity of CF_3H was also produced. This indicates that CF_3 radicals must enter into a very rapid addition reaction with the imine



The rapid addition of CF_3 radicals to the $-N=N-$ double bond in hexafluoroazomethane is well docu-



mented.³ CF_3H can only arise *via* the abstraction reaction

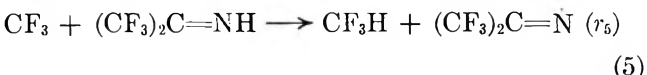


Table I: Photolysis of HFA in the Presence of Hexafluoroacetone Imine

Temp, °C	Time, min	Initial pressure, cm		Products, mol × 10 ⁶			Ratio C ₂ F ₆ /CO
		HFA	Imine	CO	C ₂ F ₆	CF ₃ H	
154	10	2.0	0.0	7.85	7.83		1.00
154	10	2.0	0.0	11.2	11.4		1.02
155	10	2.0	2.0	8.90	0.11	0.13	0.01
154	10	2.0	1.0	6.88	0.14	0.06	0.02
137	10	5.0	1.0	7.36	0.55	0.11	0.08
137	20	5.0	1.0	23.7	2.30	0.29	0.10
132	5	5.0	1.0	3.86	0.30	0.05	0.08
112	12.5	5.4	1.2	10.8	1.10	0.12	0.10
111	16.5	5.0	1.0	13.6	1.52	0.20	0.11
75	25	5.0	1.0	14.3	2.14	0.10	0.15
75	25	5.0	1.0	14.4	1.97	0.15	0.14
75 ^a	10	5.0	0.9	13.0	3.63	0.14	0.28
75 ^a	10	5.0	1.0	14.1	2.91	0.12	0.21
27	50	5.0	1.0	13.1	4.71	0.12	0.36
27	55	5.0	1.0	17.2	6.18	0.11	0.36
27.5 ^a	60	5.0	1.0	48.2	21.5	0.15	0.45
27.5 ^a	30	5.0	1.0	24.8	9.66	0.10	0.39
0.5 ^a	60	5.0	1.2	25.6	10.2	0.21	0.40
0.5 ^a	20	5.0	1.0	10.8	5.08	~0.1	0.47
-30 ^a	30	5.0	1.2	12.8	8.40	None	0.66

^a Reaction volume 188.2 ml. A double-walled vessel was used and temperatures were maintained *via* circulating fluids through the outer chamber. The other reactor was 152.6 ml. Both vessels were approximately 5-cm diameter × 10-cm long cylindrical quartz cells.

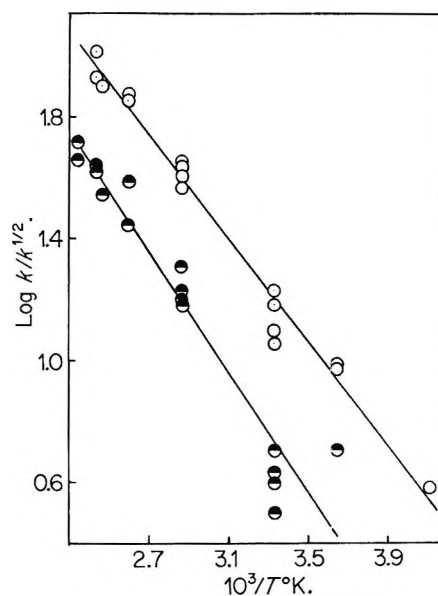
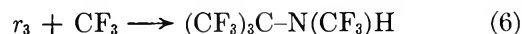


Figure 1. Arrhenius plots for $k_3/k_2^{1/2}$ and $k_5/k_2^{1/2}$, units $cm^{3/2} mol^{-1/2} sec^{-1/2}$: $k_2/k_3^{1/2}$ plot, O; $k_5/k_2^{1/2}$ plot, ●. The ordinate has been increased by 1.5 log units for $k_5/k_2^{1/2}$ plot.

The complete data are recorded in Table I; conditions were chosen so that the competition between reactions 2 and 3 could be most effectively studied.

Our basic kinetic assumptions are that reaction 3 is rate determining, and that the radicals produced (r_3) react rapidly with a further CF_3 radical



to give the final addition product. Thus the rate of formation of the addition product is equal to $(R_{CO} - R_{C_2F_6})$,⁴ and the rate constant for the addition reaction is given by⁵

$$k_3/k_2^{1/2} = (R_{CO} - R_{C_2F_6})/R_{C_2F_6}^{1/2}[\text{imine}] \quad (7)$$

The original data⁶ on reaction 4 were treated in this manner, and a steady-state treatment leads to an identical result.³ An Arrhenius plot of expression 7 is given in Figure 1, which yields $k_3/k_2^{1/2} = 1.1 \times 10^4 \exp(-3900/RT) cm^{3/2} mol^{-1/2} sec^{-1/2}$ by the method of least squares. The estimated error is ± 100 cal. The imine concentration used was an averaged value based on the initial concentration less $1/2\{[CO] - [C_2F_6]\}$. The correction varied between 1 and 10% for all experiments, except for two higher conversion runs at 27.5 and 137°, respectively, where it amounted to about

(3) S.-L. Chong and S. Toby, *J. Phys. Chem.*, **74**, 2801 (1970), and references contained therein.

(4) This expression ignores CF_3H formation in the radical balance; however its significance is negligible relative to this difference, at all temperatures. Only data up to 137° are considered, where $R_{C_2F_6} \simeq 0.1R_{CO}$.

(5) Alternatively, assuming the rapid removal of r_3 and r_5 by CF_3 radicals, expression 7 is simply derived from a steady-state treatment, when $k_3 \gg k_5$.

(6) G. O. Pritchard, H. O. Pritchard, H. I. Schiff, and A. F. Trotman-Dickenson, *Trans. Faraday Soc.*, **52**, 849 (1956).

15%. The ketone conversion was generally about 3%. Adopting⁷ $k_2 = 2.3 \times 10^{13} \text{ cm}^3 \text{ mol}^{-1} \text{ sec}^{-1}$, we obtain $k_3 = 5.2 \times 10^{10} \exp(-3900/RT) \text{ cm}^3 \text{ mol}^{-1} \text{ sec}^{-1}$, which may be compared³ to $k_1 = 3.9 \times 10^{10} \exp(-3900/RT) \text{ cm}^3 \text{ mol}^{-1} \text{ sec}^{-1}$. The similarity in the Arrhenius parameters suggests that reaction 3 occurs predominantly by addition to the N atom.⁸

Because of the rapid addition reaction, the competition between abstraction and combination (reactions 5 and 2) is not easily studied. However, for the small yields of CF_3H obtained, we may write

$$k_5/k_2^{1/2} = R_{\text{CF}_3\text{H}}/R_{\text{C}_2\text{F}_6}^{1/2}[\text{imine}] \quad (8)$$

The Arrhenius plot for expression 8 is shown graphically in Figure 1, from which a value of $k_5 = 1.6 \times 10^9 \exp(-4500/RT) \text{ cm}^3 \text{ mol}^{-1} \text{ sec}^{-1}$ is obtained. The low activation energy is compatible with similar studies involving >N-H groups,⁹ but the *A* factor appears to be somewhat lower than that for comparable systems. However the agreement between k_3/k_5 obtained in this work and that obtained in the direct photolysis of the imine² lends credence to our value.

The data are consistent with the production of CF_3 radicals in the direct photolysis of the imine. At low stationary CF_3 radical concentrations C_2F_6 production would not occur due to the highly efficient addition reaction. The formation of CF_3H in the direct photolysis may be attributed, in part, to H-atom abstraction by CF_3 radicals as well as to an intramolecular elimination from the photoexcited imine. The primary processes are discussed in detail elsewhere.²

Acknowledgment. D. W. F. and G. O. P. thank the Clapp Foundation, Milford, Conn., for generous support, and S. T. thanks Rutgers University for a Faculty Fellowship. The partial support of the National Science Foundation is also acknowledged.

(7) P. B. Ayscough, *J. Chem. Phys.*, **24**, 944 (1956).

(8) The data at 154° give $\log k_2/k_3^{1/2}$ values of 2.07 and 2.25, respectively, which lie close to the line in Figure 1. However, they are omitted due to the low C_2F_6 yields and some interference by about equivalent amounts of CO_2 in the analysis. A trace (~0.025%) of CO_2 was present in the HFA, but its formation in the reactor at 154° could occur to a slight extent. See ref 3.

(9) P. Gray, A. A. Herod, and A. Jones, *Chem. Rev.*, **71**, 247 (1971).

Photoreactions in Aqueous Solutions of Thymine, pH 12

by D. W. Whillans¹ and H. E. Johns*

Department of Medical Biophysics, University of Toronto, and The Ontario Cancer Institute, Toronto, Ontario, Canada

Publication costs assisted by The Ontario Cancer Institute

Aqueous solutions of thymine at pH 12 have been studied by flash photolysis. Under these conditions we see a transient species due to the hydrated electron which arises from excitation of OH^- . This electron absorption is quenched by N_2O , by O_2 at a rate of $1.6 \times 10^{10} \text{ M}^{-1} \text{ sec}^{-1}$ and by the thymine anion at a rate of $3.0 \times 10^9 \text{ M}^{-1} \text{ sec}^{-1}$. In addition two species which we attribute to absorption by thymine alone are observed. One of these is short-lived and quenched by O_2 ; it is also quenched by ground-state thymine at a rate of $7.3 \times 10^8 \text{ M}^{-1} \text{ sec}^{-1}$ and is almost certainly the triplet state. The spectrum of this species is red-shifted 60 nm compared to that of the neutral triplet seen at pH 7. The other species produced in thymine alone has a lifetime of at least 1 msec and may in fact be a stable product. This species is not quenched by O_2 . Its nature is unclear.

Introduction

When neutral aqueous solutions of thymine are irradiated with ultraviolet (uv) light, permanent photodimers identical with those which cause biological inactivation of DNA are produced.² These dimers have been shown to result from the bimolecular reaction of a thymine ground state and an excited triplet state. The triplet state has been detected by flash photolysis techniques and has been characterized by its spectrum. Rate constants for reactions with ground-state thymine and O_2 have been determined.³

Our interest in the excited states of thymine led us to examine species produced in solutions of thymine above the *pK* for ring ionization which occurs about pH 9.9.⁴ Changes in properties of the excited states at high pH are not unexpected since one tautomeric

(1) Research Fellow, National Cancer Institute of Canada.

(2) G. J. Fisher and H. E. Johns, *Photochem. Photobiol.*, **11**, 429 (1970).

(3) D. W. Whillans and H. E. Johns, *J. Amer. Chem. Soc.*, **93**, 1358 (1971).

(4) D. Shugar and J. J. Fox, *Biophys. Biochem. Acta*, **9**, 199 (1952).

form of thymine has been shown to fluoresce strongly in such solutions whereas thymine fluoresces only very weakly at neutral pH.⁵ We also expect that bimolecular reactions between the triplet and ground states should be inhibited by mutual repulsion of the negative species. Indeed, dimer photoproducts have not been detected in alkali solutions, although their instability in such solutions may have made their detection impossible.⁶

At high pH, however, other photolytic reactions occur in aqueous solution. Hart⁷ and others^{8,9} have shown that large yields of e_{aq}^- and $\cdot OH$ are produced by reaction 1. The subsequent reactions of these prod-



uct species with thymine, which have so far been studied solely by pulse radiolysis techniques,^{10,11} are expected in flash systems. The purpose of this paper is to describe these reactions and to characterize the species resulting from the excitation of thymine.

Experimental Section

Materials and Methods. Our flash photolysis techniques have already been described,¹² and a more detailed account is in preparation.¹³ Briefly, the flash results from the discharge of 250 J through two lamps in series, each of which is a hollow quartz cylinder nearly filled by a solid quartz rod at an air pressure of 10 Torr. These lamps are placed on either side of the reaction cell and enclosed in a polished double-elliptical cavity. The uv flux below 320 nm through the cell is about 1μ -einstein, as determined by MGL calibration.¹⁴ The spectrum of the flash is limited to about 200 nm by the transmission of the quartz lamps (G.E. Type 204 fused quartz). This is 20 nm below the limit of our detection system. The width of the discharge at half-height is 1.3 μ sec and the output falls below 0.2% of the peak value within 5 μ sec.

Thymine solutions were prepared using Calbiochem A grade thymine in triply quartz-distilled water and concentrations were calculated using an extinction coefficient of $7.9 \times 10^3 M^{-1} cm^{-1}$ at λ 264 nm and pH 7.⁴ Spectra of such solutions at pH 8 and pH 12 are shown in Figure 1. No transients are detectable at neutral pH in this water alone. Sodium hydroxide solutions were prepared fresh using Analar Reagent Grade NaOH and water prebubbled with N_2 . pH adjustments were then made into prebubbled solutions by the addition of this freshly prepared material. Nitrogen and oxygen used in bubbling were Prepurified Grade from Canadian Anaesthetic Gases, Ltd. Various oxygen concentrations were obtained by bubbling O_2 - N_2 mixtures prior to photolysis and concentrations were calculated assuming the solubility of O_2 in water as $1.3 \times 10^{-3} M$ at 25°, and the per cent oxygen in the mixture. Nitrous oxide of similar quality was also obtained from this supplier. Tertiary bu-

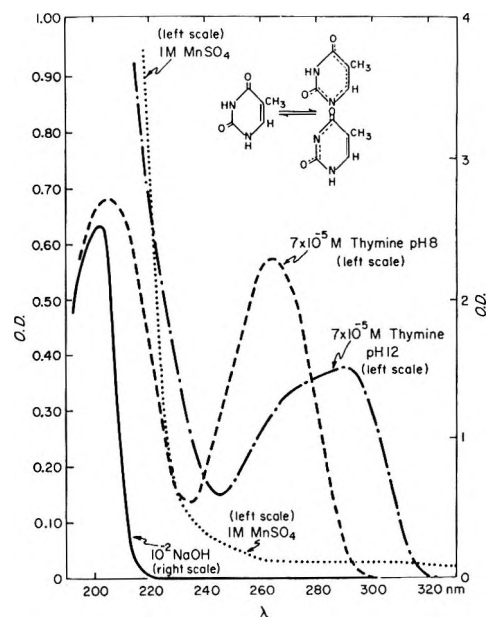


Figure 1. Ground-state absorption spectra of materials used in these experiments including the $10^{-2} M$ sodium hydroxide matrix, the $1 M$ $MnSO_4$ filter and the neutral and ionized forms of thymine, $7 \times 10^{-6} M$. Path lengths are 1 cm. Also indicated are the two tautomeric forms of the anion described by Wierzchowski, *et al.*¹⁹

tanol and manganous sulfate were of reagent grade quality.

All spectra were obtained through the point-by-point method with a reference wavelength using two monochromators and a Tektronix 556 dual beam oscilloscope. After passing through the cell the analyzing beam was split so that about 10% passed to a Bausch and Lomb High Intensity monochromator set to a fixed wavelength as reference. The main portion of the beam passed on through a preprism to a Spex monochromator. Detection by both systems was made using either an R136 or R196 photomultiplier tube (Hamamatsu TV Company). The incident analyzing light level at both wavelengths was sampled immediately before the flash and the absorptions of the species

(5) (a) K. Berens and K. L. Wierzchowski, *Photochem. Photobiol.*, **9**, 433 (1969); (b) W. Hauswirth and M. Daniels, *ibid.*, **13**, 157 (1971).

(6) M. A. Herbert, J. C. LeBlanc, D. Weinblum, and H. E. Johns, *ibid.*, **9**, 33 (1969).

(7) K. Schmidt and E. J. Hart, *Advan. Chem. Ser.*, **81**, 267 (1968).

(8) J. W. Boyle, J. A. Ghormley, C. J. Hochenadel, and J. F. Riley, *J. Phys. Chem.*, **73**, 2886 (1969).

(9) J. Rabani, W. A. Mulac, and M. J. Matheson, *ibid.*, **64**, 53 (1965).

(10) C. L. Greenstock, M. Ng, and J. W. Hunt, *Advan. Chem. Ser.*, **No. 81**, 397 (1968).

(11) C. L. Greenstock, J. W. Hunt, and M. Ng, *Trans. Faraday Soc.*, **65**, 3279 (1969).

(12) D. W. Whillans, M. A. Herbert, J. W. Hunt, and H. E. Johns, *Biochem. Biophys. Res. Commun.*, **36**, 912 (1969).

(13) J. C. LeBlanc, M. Herbert, D. W. Whillans, W. B. Taylor, and H. E. Johns, unpublished results.

(14) G. J. Fisher, J. C. LeBlanc, and H. E. Johns, *Photochem. Photobiol.*, **7**, 757 (1967).

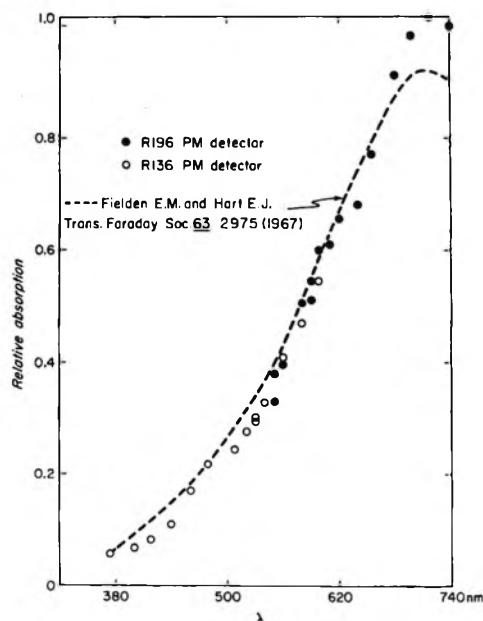


Figure 2. Absorption spectrum of strongly absorbing transient produced in the flash photolysis of $10^{-2} M$ NaOH. Also shown is the spectrum of the hydrated electron obtained by Fielden, *et al.*, by pulse radiolysis.¹⁵

were determined from the transient levels and these incident values. All absorptions were then normalized to the reference level to correct for variations in flash intensity. The analyzing beam itself was produced by pulsing an Osram XBO 150 W/1 xenon lamp to 15 times its continuous level from a current source for a 20-msec period surrounding the flash. This beam then passed three times through the 15-cm cell and to the monochromators. The noise level on the beam corresponds to an average absorbance of 0.0003 over a period of 100 μsec .

Rate constants for decays were obtained from oscillographs using an analogue to digital converter and a computer regression analysis for the exponential decays. Most points represent the result of several traces. The second-order plots were analyzed by hand.

Results and Discussion

Species in Alkaline Water. When $10^{-2} M$ solutions of NaOH are flashed in our system, two very weak and one strongly absorbing species are observed. These transients all disappear when the exciting light is filtered by a 1 M MnSO_4 solution placed in a 0.5-cm concentric jacket around the cell. From Figure 1 it is clear that the transients are due to excitation of the NaOH.

Figure 2 shows the spectrum of the strongly absorbing transient, which peaks at ~ 720 nm and which is completely quenched by N_2O . Also shown by the dashed line is a spectrum obtained by Fielden and Hart for the aqueous electron in the pulse radiolysis of water.¹⁵ It has a half-life of ~ 70 μsec or more in carefully degassed solutions, and its decay is nonexponential, as observed by others,¹⁶ and varies with flash

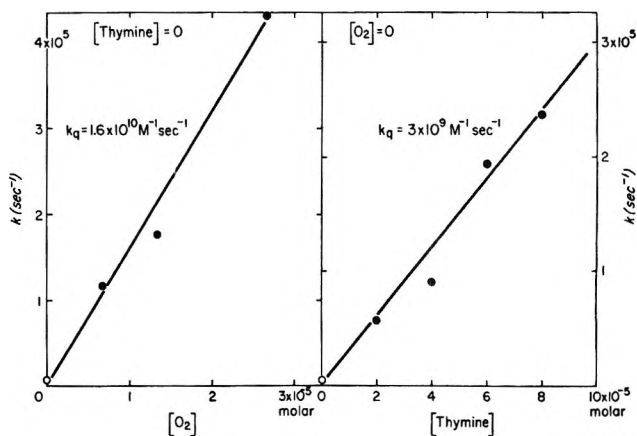


Figure 3. Quenching of the hydrated electron signal by (a) O_2 in the absence of thymine, and (b) thymine in the absence of oxygen. For both cases the initial points represent poor exponentials, as explained in the text.

intensity. This species is efficiently quenched by O_2 in a pseudo-first-order reaction, as shown in Figure 3a. The value for the bimolecular quenching rate of $1.6 \times 10^{10} M^{-1} \text{sec}^{-1}$ agrees well with the published value of $1.9 \times 10^{10} M^{-1} \text{sec}^{-1}$.¹⁶ From this evidence the species has been identified as the aqueous electron.

One of the weakly absorbing species whose yield is just above noise level is observed at wavelengths below 300 nm. This species is longer-lived than e_{aq}^- and not quenched by N_2O , but is removed by the addition of $10^{-2} M$ tertiary butanol. On this basis it is the hydroxyl radical, $\cdot\text{OH}$, which is produced along with e_{aq}^- according to eq 1. A second weakly absorbing species is observed in the region 350–450 nm in solutions which have not been carefully deoxygenated. The species builds in over 50 μsec or more at low O_2 concentrations and is observed only when $\cdot\text{OH}$ is present. From this evidence it is the ozonide ion, O_3^- , which is formed at this pH from interactions between $\text{O}^-(\cdot\text{OH} \rightleftharpoons \text{O}^- + \text{H}^+ pK \sim 11.9)$ and O_2 .¹⁷

When $10^{-2} M$ NaOH solutions are prepared containing small concentrations of thymine, the principal absorbing transient remains e_{aq}^- , but its rate of decay is increased by thymine as illustrated in Figure 3b where the exponential decay rate of e_{aq}^- , observed at 550 nm, is plotted against thymine concentration. A linear relationship is observed with a quenching rate constant of $3.0 \times 10^9 M^{-1} \text{sec}^{-1}$. Since very few thymine molecules are excited under these conditions the reaction is between e_{aq}^- and the ground state thymine anion. The rate constant agrees well with that

(15) E. M. Fielden and E. J. Hart, *Trans. Faraday Soc.*, **63**, 2975 (1967).

(16) S. Gordon, E. J. Hart, M. S. Matheson, J. Rabani, and J. K. Thomas, *Discuss. Faraday Soc.*, **36**, 193 (1963).

(17) G. E. Adams, J. W. Boag, J. Currant, and B. D. Michael, in "Pulse Radiolysis." M. Ebert, J. P. Keene, A. J. Swallow, and J. H. Baxendale, Ed., Academic Press, New York, N. Y., 1965, Chapter 9.

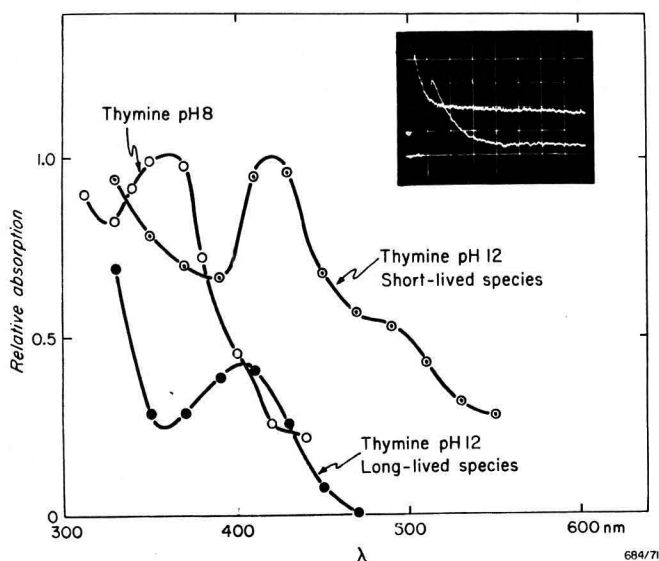


Figure 4. Transient absorption spectra of species due to thymine at pH 8 and 12. Although the pH 12 spectra are in the correct proportion no absolute comparison with the pH 8 species is intended. (In fact the peak neutral signal is several-fold smaller than that of the anion.) Because we have no measure of concentration of these species no extinctions can be given. The insert shows a typical photograph of these transients, observed at (a) 350 nm and 50 μsec /division, and (b) 470 nm and 20 μsec /division. The vertical gains are 0.02 and 0.01 V/division, respectively.

of $2.7 \times 10^9 \text{ M}^{-1} \text{ sec}^{-1}$ obtained by Hart, *et al.*, for the thymine anion at pH 12 by pulse techniques.¹⁸

Excited Species Produced in Thymine. If one eliminates the transient absorptions observed in the NaOH matrix by filtering the exciting light with MnSO_4 or by rapid quenching with high concentrations of N_2O and tertiary butanol, two new species are observed in thymine solutions at pH 12. One is a short-lived species ($\tau < 70 \mu\text{sec}$) and the other a much longer-lived one which in fact may be a stable product. The former is completely quenched by O_2 , whereas the latter is not. A typical transient is shown in Figure 4 together with the spectra of these species. Figure 4 also gives the spectrum of the thymine triplet at neutral pH, as previously reported.³ The spectrum of the short-lived species at pH 12, which we believe to be the triplet state, has a similar structure to that at neutral pH, although the peak is red-shifted by 60 nm. In comparison the peak of the ground state spectrum of thymine shown in Figure 1 is red-shifted by 25 nm at pH 12. It is also evident that the shape of the ground state spectrum is considerably altered at high pH. The effect is almost certainly due to the presence of two tautomeric forms indicated as I and II in Figure 1 and discussed by Wierzchowski, *et al.*¹⁹ No similar change of structure with pH is evident for the excited species suggesting that only one tautomer may contribute to its spectrum at pH 12.

The two species also react differently with thymine as shown in Figure 5. The short-lived species is

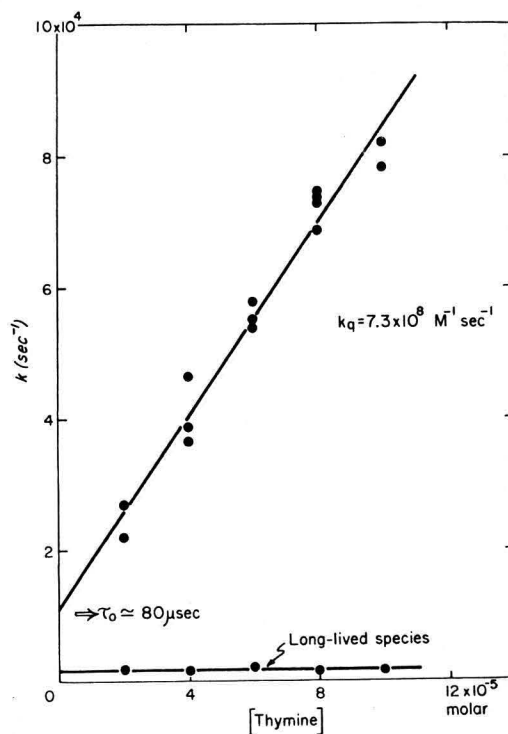


Figure 5. Ground-state thymine quenching of the transient absorption species produced from thymine at pH 12. The upper line represents the species which we believe to be the anion triplet. The lower species has not been identified, and its decay rate may be zero.

quenched with a bimolecular rate constant of $7.3 \times 10^8 \text{ M}^{-1} \text{ sec}^{-1}$ whereas the longer-lived one is not quenched up to a detectable level of $10^7 \text{ M}^{-1} \text{ sec}^{-1}$. In fact, the long-lived species may be a permanent product since our detecting system cannot distinguish between a permanent product and one which has a half-life greater than $\sim 1 \text{ msec}$. The quenching rate for the anion triplet is one-third of that observed for the neutral triplet ($2.3 \times 10^9 \text{ M}^{-1} \text{ sec}^{-1}$). This reduction in rate is nearly the value to be expected on the basis of charge repulsion for the interaction of the ground-state anion and a singly charged triplet anion.

Effect of pH. The pK of the ground state of thymine can be obtained by spectrophotometric titration²⁰ at 291 nm where neutral thymine has no absorbance. Such a titration is shown as curve A in Figure 6, and yields a pK of 9.98 ± 0.07 in close agreement with the published value.^{3,19} Since the spectrum of the thymine triplet at high pH is red-shifted with respect to the spectrum at neutral pH (see Figure 4), a similar plot of the transient triplet absorption at 440 nm against pH can be used to obtain an estimate of the pK^* for

(18) E. J. Hart, S. Gordon, and J. K. Thomas, *J. Phys. Chem.*, **68**, 1271 (1964).

(19) K. L. Wierzchowski, E. Litonska, and D. Shugar, *J. Amer. Chem. Soc.*, **87**, 4621 (1965).

(20) A. Albert and E. P. Sargeant, "Ionization Constants of Acids and Bases," Wiley, New York, N. Y., 1962.

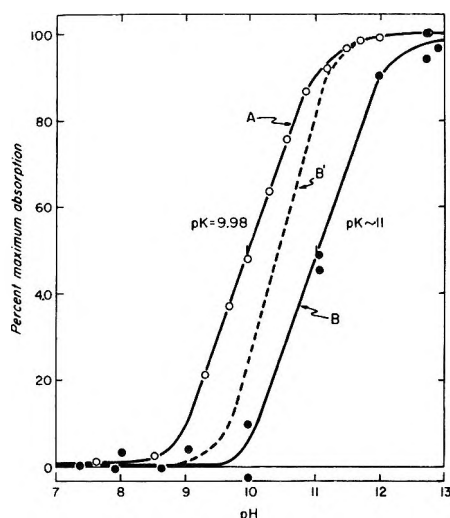
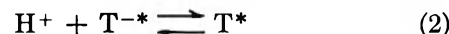


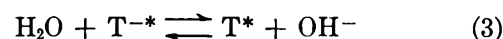
Figure 6. Absorption yields in thymine as a function of pH. Curve A is the ground-state absorption at 291 nm; curve B is the yield of transient triplet absorption at 440 nm; curve B' is calculated assuming an excited state pK of 10 and a 100-fold increase in total triplet yield from the ground-state anion over that from the neutral molecule.

the excited triplet state. Such a plot is shown as curve B in Figure 6, and suggests a pK^* of ~ 11 . However, in contrast to the case of ground-state titration, we do not know whether the total yield of triplet changes with pH. If there is no change in yield then our conclusion about pK^* is valid. If the triplet yield does change with pH the most reasonable assumption is of one yield from the neutral ground state and a different yield from the ground-state anion, so that the total yield of triplet will follow curve A. If we assume that the excited state pK is 10 and that the yield of triplets from the anion ground state is 100 times the yield from the neutral molecule then we obtain curve B'. Note that B' is shifted slightly from A. (Assuming any other increase in yield results in a curve which lies no farther from A than B'.) Similarly, if we assume the pK of the excited state is 11 and as before that the yield from the anion is 100 times that from the neutral molecule then we obtain a curve which exactly coincides with B. Clearly including a possible increase in yield with increase in pH can alter the titration curve and shifts the apparent pK up to about 0.4 unit. We conclude then that curve B could hardly be in error by more than about 0.4 unit and that the pK of the excited state is close to 11, about 1 pH unit above that of the ground state.

A change in the charge of the excited state within our 5 μ sec resolution cannot occur at this pH according to the formal equation



since the concentration of H^+ is very low. Because we see no evidence that equilibrium is not established within this time, we conclude that a more likely mechanism is the following



Such a mechanism has been discussed in detail by Adams, *et al.*,¹⁷ in dealing with the pK of the hydroxyl radical.

Summary

In the flash photolysis of thymine solutions at pH 12, the following observations have been made. (1) Three species are observed in the NaOH matrix alone. The major absorption is due to the hydrated electron. Its spectrum peaks at ~ 720 nm and it is quenched by N_2O , and by O_2 with a rate constant of $1.6 \times 10^{10} M^{-1} sec^{-1}$. One much weaker species is observed whose spectrum lies below 300 nm. It is not quenched by O_2 , but by tertiary butanol. This absorption is almost certainly due to the hydroxyl radical. A second weak species is observed in the presence of O_2 and is attributed to O_3^- . (2) The hydrated electron reacts with the thymine anion with a bimolecular rate constant of $3.0 \times 10^9 M^{-1} sec^{-1}$. (3) Excitation of thymine alone at pH 12 gives rise to a strongly absorbing transient due to the anion triplet. It is quenched by O_2 and reacts with the anion ground state with a rate constant of $7.3 \times 10^8 M^{-1} sec^{-1}$. Its spectrum is very similar to that of the neutral triplet, though red-shifted by 60 nm. (4) Excitation of thymine at pH 12 also gives rise to a weakly absorbing species which has a lifetime > 1 msec and may be a permanent product. It does not react with O_2 or with thymine. Its identity is not known. (5) The pK^* for the excited triplet state is about 11 and one unit above the pK of the ground state.

Acknowledgment. The authors take pleasure in acknowledging the financial support of the Medical Research Council of Canada and the National Cancer Institute of Canada. We are indebted to Mr. Morley Herbert, Dr. T. Penner, and Dr. J. W. Hunt for helpful discussions.

The Thermal Growth of the Formyl Radical at 87°K in a 50% Methanol-Water Matrix

by Cornelius U. Morgan

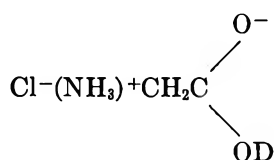
U. S. Army Ballistic Research Laboratories, Aberdeen Proving Ground, Maryland 21005 (Received August 27, 1971)

Publication costs assisted by the Ballistic Research Laboratories

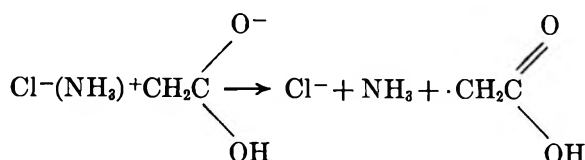
Investigations were carried out on radicals produced by ultraviolet irradiation of 50% methanol-water matrices. Among the radicals generated the formyl radical (HCO) exhibited somewhat unusual temperature characteristics. The electron spin resonance (esr) signal of the formyl radical was stable at 77°K. However, at 87°K the formyl radical concentration increased markedly with time. The following are proposed as possible explanations: hydrogen atoms escape from traps and diffuse through the matrix and (1) react with carbon monoxide molecules at 87°K to form formyl radicals or (2) abstract a hydrogen atom from formaldehyde to form formyl radicals and molecular hydrogen. The carbon monoxide and formaldehyde in the matrix are produced by the initial uv irradiation. Other mechanisms that were given consideration but eliminated as less likely possibilities were the rearrangement of a $\cdot\dot{\text{C}}\text{OH}$ radical and multiple abstractions from $\cdot\text{CH}_2\text{OH}$ and methanol to form HCO.

Introduction

The subject of reaction mechanisms of radicals in frozen matrices has been investigated with considerable interest. Ayscough and Thomson¹ observed, over a period of 27 days, the thermal conversion at 77°K of isobutyl radicals to *tert*-butyl radicals. Sullivan and Koski,^{2,3} as well as Morgan,⁴ observed the decay of methyl radicals at liquid nitrogen temperature in frozen methanol matrices and postulated mechanisms for this decay. These mechanisms involved both hydrogen abstraction by radicals from the matrix and radical-radical recombinations. Box, Budzinski, and Freund⁵ X-irradiated single crystals of glycine hydrochloride and deuterated crystals of this compound at 4.2°K. The deuteration occurred at all positions but the methylene group. The intermediates formed in each radiolysis were observed by esr spectroscopy at 4.2°K. When the deuterated crystal was allowed to warm from 4.2 to 110°K, they observed the decay of the



anion radical and the formation of the neutral $\cdot\text{CH}_2\text{COOD}$ radical. They postulate the following reaction for the undeuterated molecule



Tsuji and Okamura⁶ irradiated at 77°K a glassy matrix of 3-methylpentane-isobutylene using γ radiation. They observed an esr spectrum consisting of an alkyl radical and trapped electrons. Irradiating the sample with visible light enabled them to bleach out the line due to the trapped electrons leaving only the alkyl spectrum. After maintaining the sample at 77°K for 7 days, they again observed the esr spectrum and noticed that the alkyl radical had been converted to an allylic radical. They attribute this formation to hydrogen abstraction from isobutylene by the alkyl radical.

In this investigation the radicals produced by ultraviolet irradiation of a 50% methanol-water matrix at 77°K and 87°K were examined. The behavior of the methyl radical at 77°K was reported in an earlier report.⁴ Here we examine the increase with time of the formyl radical at 87°K in this matrix.

Experimental Section

The samples of 50% methanol-water were prepared by adding at room temperature 20 ml of either Mallinckrodt ACS or Matheson Coleman and Bell spectroquality methanol to a 100-ml graduated cylinder and then adding distilled water until the volume of solution was 40 ml. This solution was then used to fill 5.0-mm o.d. quartz sample tubes of 0.5-mm wall thickness.

(1) P. B. Ayscough and C. Thomson, *Trans. Faraday Soc.*, **58**, 1477 (1962).

(2) P. J. Sullivan and W. S. Koski, *J. Amer. Chem. Soc.*, **85**, 384 (1963).

(3) P. J. Sullivan and W. S. Koski, *ibid.*, **84**, 1 (1962).

(4) C. U. Morgan, *ibid.*, **91**, 1599 (1969).

(5) H. C. Box, E. E. Budzinski, and H. G. Freund, *J. Chem. Phys.*, **50**, 2880 (1969).

(6) K. Tsuji and S. Okamura, *Bull. Chem. Soc. Jap.*, **42**, 2827 (1969).

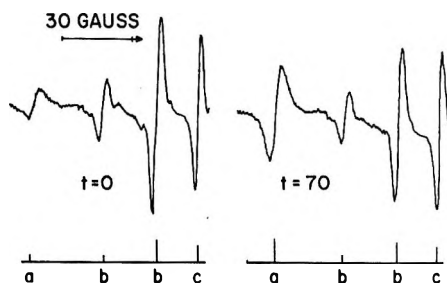


Figure 1. Spectra showing increase of formyl radical concentration *vs.* time in a 50% methanol-water matrix at 87°K. In the stick diagram (a) represents one of the two formyl lines, (b) two of the four methyl lines, and (c) line from internal standard. The time *t* is in minutes.

These samples which froze to a glassy solid in liquid nitrogen were irradiated at 77°K with a high pressure mercury lamp (General Electric BH-6) using a spherical reflector behind the lamp to concentrate the light on a small spot on the sample. After each sample was irradiated for periods of 0.5 to 4 hr, it was transferred from the irradiation dewar to the sample dewar in the Varian V-4531 X-band cavity of the Varian V-4500 esr spectrometer. Using 100-kHz field modulation, the formyl concentration in the sample was monitored first at 77°K and then at 87°K. The latter temperature was attained by using liquid argon as the coolant. An esr standard⁷ was used to monitor the stability of the spectrometer during some of the runs. This standard, which consisted of a small chip cut from a polyethylene sheet having phosphorus-doped silicon imbedded in it, was frozen to the inner wall of the sample dewar. The esr signal from this standard was constant at a fixed temperature but decreased slightly when the temperature was raised from 77°K to 87°K. A single line resonance was produced by the standard at a *g* value of 1.99875 ± 0.0001 with a line width of 1.8 G at 87°K.

Results and Discussion

The concentration of $\dot{\text{HCO}}$ in the samples remained constant at 77°K but at 87°K the concentration increased with time as shown in Figure 1. Only half of the spectrum is shown. In the stick diagram *a* represents one of the two formyl lines, *b* two of the four methyl lines, and *c* is the resonance from the esr standard. The nearly isotropic hyperfine splitting of the formyl radical was 130.6 ± 1 G with measured *g* values g_{\parallel}, g_{\perp} of 1.997 and 2.004 ± 0.001 . The concentration of $\dot{\text{HCO}}$ is plotted as a function of time in Figure 2 for this run. In all these runs the initial concentration of $\dot{\text{HCO}}$ was approximately 5×10^{15} spins/cm³.

The concentration of methyl radical in the spectra was nearly constant at 77°K as shown from a previous report.⁴ The decay half-life was 183 hr. At 87°K the methyl radical did decay but power saturation of the methyl lines prevented a quantitative correlation between the decay of $\cdot\text{CH}_3$ and the increase in $\dot{\text{HCO}}$ concentration.

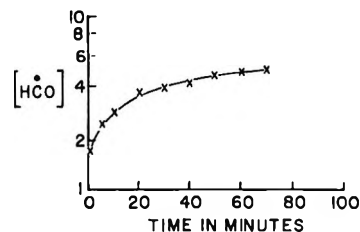
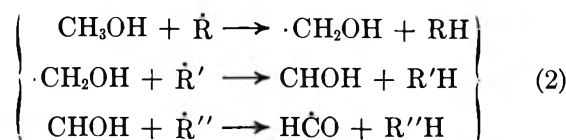


Figure 2. Plot of the concentration of the formyl radical in arbitrary units *vs.* time at 87°K.

The following are four possible mechanisms that could explain the thermal increase in formyl radicals at 87°K in a 50% methanol-water matrix



where the R's represent any of the radicals in the system.

Since no esr signal from $:\dot{\text{C}}\text{OH}$ was observed,³ the probability of its being present is diminished but not eliminated. The esr lines of such a species could be broad and masked by stronger resonances. Multiple abstractions from $\cdot\text{CH}_2\text{OH}$ or methanol are unlikely because of concentration considerations. The concentration of methanol in the matrix is from four to five orders of magnitude in excess of all other components with the exception of water. For this reason an abstraction reaction would probably involve a single abstraction from methanol to give the $\cdot\text{CH}_2\text{OH}$ radical. Formyl radicals could be formed from a single abstraction⁸ from formaldehyde which is believed to be one of the major products of the initial uv irradiation. Since the increase in $\dot{\text{HCO}}$ at 87°K does not follow a simple zero, first, or second-order kinetic mechanism, reactions 1, 3, and 4 are simultaneously possible. However, there is some question about the activation energy of reaction 4 which has not been resolved.^{9,10}

Since the H atom spectrum is observed in these runs, its concentration should decrease as the $\dot{\text{HCO}}$ concentration increases if reaction 4 contributes markedly to the overall reaction. In order to check this the H atom concentration should be monitored simultaneously with the $\dot{\text{HCO}}$ concentration. However, there are several

(7) E. A. Gere, Bell Laboratories, Inc., Murray Hill, N. J., personal communication, 1966.

(8) E. D. Sprague and F. Williams, *J. Amer. Chem. Soc.*, **93**, 787 (1971).

(9) D. E. Milligan and M. E. Jacox, *J. Chem. Phys.*, **41**, 3032 (1964).

(10) D. E. Milligan and M. E. Jacox, *ibid.*, **51**, 277 (1969).

difficulties in making H atom concentration measurements. The hydrogen atoms are probably trapped in multiple sites with different relaxation times at the different sites.¹¹ Since some of these sites are saturated, intensity measurements using our present apparatus are unreliable. When the microwave power is reduced to a low level, the HCO signal is reduced below the threshold detection level without completely alleviating the H atom saturation.

Although other mechanisms cannot be ruled out, it is postulated that reaction mechanisms 3 and 4, the H

atom abstraction from formaldehyde and the recombination of H atoms and CO molecules, are the most probable mechanisms for the increase of formyl radicals at 87°K.

Acknowledgment. The author wishes to acknowledge with thanks the many suggestions that were rendered to him by Dr. Kevin White in the preparation of this report.

(11) C. J. Ultee and C. R. Kepford, *J. Chem. Phys.*, **52**, 3462 (1970).

Photolysis of Solid Dimethylnitramine: Nitrogen-15 Study and Evidence for Nitrosamine Rearrangement

by K. Suryanarayanan and Suryanarayana Bulusu*

*Explosives Laboratory, Feltman Research Laboratories, Picatinny Arsenal, Dover, New Jersey 07801
(Received August 27, 1971)*

Publication costs assisted by the Feltman Research Laboratories, Picatinny Arsenal

The photolysis of solid dimethylnitramine with 2537-Å light results in the formation of dimethylnitrosamine as a major product. The mechanism of bond-breaking in this photolytic reaction has been investigated *via* a ¹⁵N tracer technique. Photolysis of a *ca.* 1:1 mixture of doubly ¹⁵N-labeled and unlabeled dimethylnitramine followed by mass spectrometric analysis gave the following isotopic distribution in product dimethylnitrosamine: *m/e* 74:75:76 = 1:2:1. While the product showed efficient isotopic mixing, the unconverted dimethylnitramine in the photolyzed sample showed *no* mixing. A 1:1 mixture of doubly ¹⁵N-labeled dimethylnitramine and unlabeled dimethylnitrosamine gave efficient (almost 100%) light-induced isotopic equilibration. The results show that (a) dimethylnitrosamine arises from dimethylnitramine as a result of N-O bond breakage and (b) dimethylnitrosamine after being formed undergoes almost 100% light-induced rearrangement involving the bond between the two nitrogen atoms.

Introduction

Nitramines, compounds that contain the >N-NO₂ function, are important as explosives. Dimethylnitramine (I) is the simplest member of the secondary nitramines.

In this paper photolysis of dimethylnitramine in the solid state with 2537-Å uv light from a low-pressure mercury lamp is shown to result in the formation of dimethylnitrosamine (II) as a major product. The mechanism of bond breaking in this photolytic step has been investigated with the aid of ¹⁵N in both nitrogen positions of dimethylnitramine and the results of this study form the principal subject of this paper.

Thermal decomposition of dimethylnitramine in the gas phase is reported¹ to give dimethylnitrosamine by a process involving radicals produced by breakage of the N-N bond. In the only previously reported² photo-

chemical study of nitramines, *N*-methyl-*N*-nitro-1-naphthylamine was photolyzed in solution with uv light of wavelength greater than 3600 Å and found to yield the rearranged products, 2- and 4-nitro-*N*-methyl-1-naphthylamines. It was proposed that the photodecomposition, by analogy with thermal decomposition,² proceeded *via* heterolytic fission of the N-N bond followed by an intramolecular migration of NO₂. However, the primary photochemical processes in nitramines are not as well characterized as in the case of C-nitro compounds.³

(1) (a) J. M. Flournoy, *J. Chem. Phys.*, **36**, 1106 (1962); (b) B. L. Korsunskii, F. I. Dubovitskii, and G. V. Sitonina, *Dokl. Akad. Nauk SSSR*, **174**, 1126 (1967).

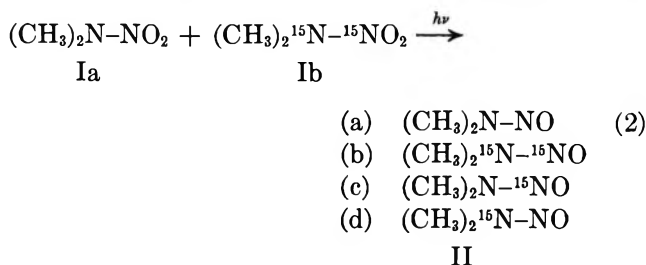
(2) D. V. Banthorpe and J. A. Thomas, *J. Chem. Soc.*, 7158 (1958).

(3) H. A. Morrison, "The Chemistry of Nitro and Nitroso Groups," Part 1, H. Feuer, Ed., Wiley-Interscience, New York, N. Y., 1969, Chapter 4.

The present ^{15}N -isotope tracer experiments are designed to determine if the chief photolysis product dimethylnitrosamine is formed by the breakage of the N-N bond, as in thermal decomposition of the vapor, or by the rupture of an N-O bond. The latter may be an obvious one-step process



The doubly ^{15}N -labeled, Ib, and the unlabeled, Ia, dimethylnitramine are mixed in *ca.* 1:1 ratio and subjected to photolysis followed by a mass spectrometric analysis. Of the four possible isotopic species of the nitrosamine, IIa-d, strictly a and b would be formed in the event of reaction without N-N fission. Contribution of c and d would indicate the degree of partici-



pation of the N-N fission process.

Experimental Section

Materials. Dimethylnitramine obtained from K and K Laboratories was sublimed before use. Dimethylnitrosamine (Puriss grade) from Aldrich Chemical Co. was used without further purification.

Dimethyl- ^{16}N -nitro- ^{15}N -amine. The ^{16}N -labeled compound was synthesized starting with dimethylamine- ^{15}N (99% enriched, Isomet Corp., Palisades, N. J.) and K^{15}NO_3 (99% enriched, Prochem Ltd., Lincoln Park, N. J.). K^{15}NO_3 was first treated with concentrated H_2SO_4 on a vacuum line to generate H^{15}NO_3 which was later distilled *in vacuo* into a stoichiometric amount of dimethylamine- ^{15}N held at low temperature in a receiver. The mixture thus obtained was thawed gradually to allow salt formation. The doubly labeled dimethylammonium nitrate was then dehydrated by treatment with anhydrous acetic anhydride and zinc chloride⁴ at 35° for 15 hr.

Irradiation Procedure. For convenience in mass spectrometric determination of isotopic distribution among products, the irradiations were carried out with samples (5 to 10 mg) contained in quartz capillaries (1 mm i.d. \times 4-5 cm long) sealed at both ends. Air was not removed by pumping prior to irradiation. Each capillary with sample was irradiated for 120 min at the center of a helical (4.5 cm diameter \times 5 cm high and consisting of six turns; 90 W output) low-pressure mercury lamp (chiefly 2537-Å wavelength).

Mass Spectrometric Analysis. The spectra were obtained by introducing the samples into the mass spectrometer (Consolidated 21-104, single focusing) *via*

the gas inlet system rather than the solid probe since the vapor pressure of the samples was found to be inconveniently high. The capillary containing the sample was placed in a demountable tube which was then attached to the inlet system. The tube containing the sample was flushed with nitrogen, cooled to 77°K, and then pumped down. The 3-l. expansion volume was filled to approximately 300 μ with sample vapor.

The different experimental runs consisted of (i) pure dimethylnitramine, (ii) *ca.* 1:1 mixture of doubly ^{15}N -labeled and unlabeled *dimethylnitramine* (prepared by intimate mixing in a mortar as well as by coprecipitation from ether), and (iii) *ca.* 1:1 mixture of the labeled dimethylnitramine (Ib) (24.0 mg) and unlabeled *dimethylnitrosamine* (20.3 mg). The last mentioned mixture was a pale yellow solution but still for the sake of uniformity, the above capillary sampling procedure was used. The 10- μ l samples were transferred to the quartz capillaries using a Hamilton syringe and then handled in the same way as the solid samples.

Results

When dimethylnitramine (I) was irradiated in the solid form (as a thin layer or in a "capillary") the white solid turned into a viscous yellow liquid. The latter was analyzed by gas chromatography using a P.E. Model 154D instrument equipped with a flame-ionization detector. A 6 ft \times 1/4 in. S.S. column containing firebrick coated with Ucon polyglycol (P.E. LB-550x) was operated at 140° and 10 psig helium pressure. Under these conditions dimethylnitrosamine (II) could be readily separated from (I) and identified by elution times (II, 9 min; I, 20 min). The conversion to nitrosamine was of the order of 35%. No other products were detectable by the above method or by an nmr analysis (Varian T-60). The nmr spectrum of (I) in acetone- d_6 showed a triplet at δ 3.4 (measured from TMS). The nitrosamine (II), however, gave two peaks, δ 3.0 and δ 3.8 corresponding to the trans and the cis methyl groups, respectively. The nitramine (I) after a 110-min irradiation clearly showed strong absorptions at δ 3.0, 3.4, and 3.8. An ir spectrum of the neat yellow liquid obtained after irradiation was consistent with dimethylnitrosamine since it showed peaks at 842 (m), 682 (m), and 1048 (vs) cm^{-1} . The uv absorption spectrum had a maximum at 345 nm corresponding to the nitrosamine band in addition to the short wavelength band around 240 nm which appeared in the spectra of both nitramines and the nitrosamines. The mass spectral data discussed in detail here provide additional confirmation for the nitrosamine as the main photoproduct.

Tables I and II show the mass spectral data pertinent to the molecular ions of the dimethylnitramine and the nitrosamine. The isotopic distribution derived

(4) W. J. Chute, K. G. Herring, L. E. Toombs, and G. F. Wright, *Can. J. Chem., Sect. B*, **26**, 89 (1948).

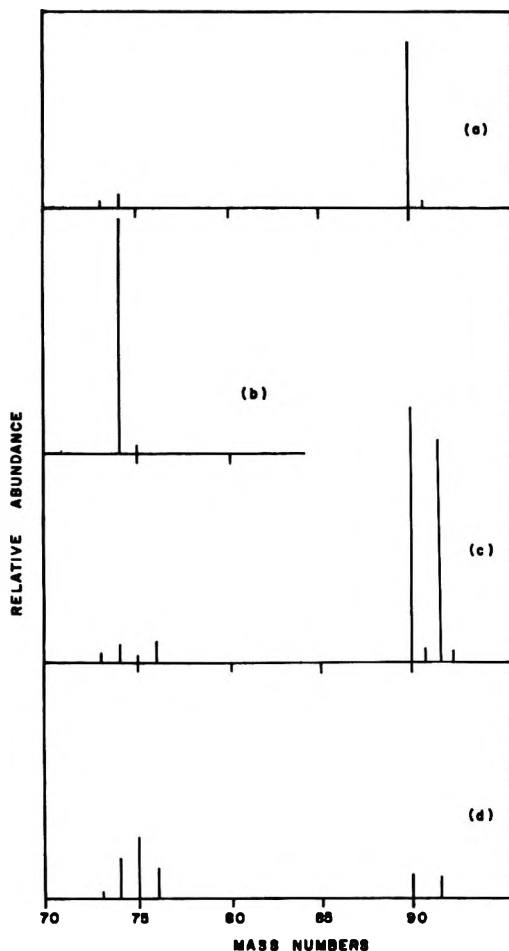


Figure 1. Observed mass spectra: (a), $(\text{CH}_3)_2\text{N}-\text{NO}_2$; (b), $(\text{CH}_3)_2\text{N}-\text{NO}$; (c), ca. 1:1 mixture of $(\text{CH}_3)_2\text{N}-\text{NO}_2$ and $(\text{CH}_3)_2\text{N}^{15}\text{-N}^{16}\text{O}_2$ —unirradiated; (d), mixture in (c)—after irradiation. Relative sensitivity: $\times 10$ for (a), (b), (c) and $\times 1$ for (d).

from these data is shown in Table III. Figure 1 shows the corresponding mass spectra of the above and those of irradiated and unirradiated mixtures (ca. 1:1) of dimethylnitramine and its doubly tagged analog.

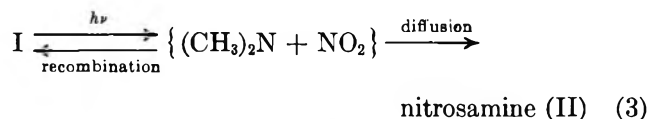
In the mass spectrum of dimethylnitramine the relative abundance of the ion (this ion has been previously postulated⁵ to be $(\text{CH}_3)_2\text{N}-\text{N}^+=\text{O}$) at m/e

74 is about 6% while in the nitrosamine the molecular ion at m/e 74 has a relative abundance of 96%. The formation of nitrosamine in the dimethylnitramine is therefore readily followed by a measurement of m/e 74. The ^{15}N isotopic isomers would then move to m/e 75 and 76, respectively.

In using the data of Tables I and II to get isotopic distribution some corrections have to be applied. In the spectrum of dimethylnitramine (Ia) (Table I, lines 1 and 2) the m/e 91 arises from the natural ^{13}C content and likewise the m/e 93 in the spectrum of Ib (Table II) is due to natural carbon-13. Of the m/e 91 values shown in Table II about 2% of each is due to the ^{14}N impurity in the doubly tagged dimethylnitramine (1% at each position) and the remainder is due to the ^{13}C . The ratios of m/e 90 and 92 in the spectra of the unirradiated mixtures of Ia and Ib (Table II, lines 1 and 2 in Batch 1 and line 1 in Batch 2) give the ratios of the unlabeled and doubly ^{15}N -labeled species actually present in the mixture used for photolysis. These ratios were used to determine the statistical distribution to be expected of m/e 74, 75, and 76 if complete isotopic equilibration took place. For an equimolar mixture of Ia and Ib the ratio would be 1:2:1. The observed and the "calculated" ratios are summarized in Table III.

Discussion

The data presented in Table II reveal that there is extensive contribution of m/e 75 in addition to the normal increase in m/e 74 and 76 subsequent to photolysis. Prior to photolysis m/e 75 appeared to be less than 2% which indicated that no isotope exchange was caused by electron impact. Furthermore, the ratio of 74:75:76 was nearly statistical as shown in Table III. One obvious conclusion which may be drawn from this excellent agreement with statistical distribution would be that the photolysis involves an initial N-N bond fission. However, the spectra failed to show any increase in m/e 91 above the initial levels. This indicated no isotopic exchange between Ia and Ib. The conclusion that the N-N bond undergoes a cleavage in the photolysis is inconsistent with no isotope exchange taking place in the nitramine itself. For, in order to account for the rather high conversion to nitrosamine (35% as determined by nmr analysis)



the radicals formed on N-N fission have to *escape*, by *diffusion*, the highly favored geminate recombination in the solid state and also not lead to bulk recombination and isotopic exchange in (I). It seemed likely, there-

Table I: Relative Abundance^a of Selected Ions in the Mass Spectra of Dimethylnitramine before and after Uv Irradiation (Irradiation Time: 120 min)

Sample no.		Relative abundance						
		(m/e)	74	75	76	90	91	92
1	Unirradiated		5.8	0.3	0.2	100	3.6	0.5
2			3.2	0.3	0.2	100	3.2	0.5
1	Irradiated		179	4.6	0.7	100	3.1	0.7
2			148	4.6	0.3	100	3.0	0.6
3			129	3.5	0.3	100	3.3	0.6

^a Each set is average of two mass scans.

(5) S. Bulusu, T. Axenrod, and G. W. A. Milne, *Org. Mass. Spectrom.*, 3, 13 (1970).

Table II: Relative Abundance^a of Selected Ions in the Mass Spectra: 1:1 Mixture of (CH₃)₂N-NO₂ (Ia) and (CH₃)₂¹⁵N-¹⁵NO₂ (Ib) before and after Irradiation (Irradiation Time: 120 min)

Sample no.	(m/e)	Relative abundance						
		74	75	76	90	91	92	93
Batch 1								
1	Unirradiated	5.0	1.8	5.3	100	4.3	84	2.2
2		4.0	1.7	4.6	100	4.1	95	2.1
1	Irradiated	134	221	84	100	7.0	70	2.3
2		164	279	133	100	4.8	81	1.9
Batch 2								
1	Unirradiated	8	2	8	100	7	78	3.7
1	Irradiated	208	345	155	100	6	82	4.3
2		232	390	179	100	7	88	3.7
3		357	528	249	100	7	87	4.3
4		299	522	243	100	7	90	3.5

^a Each set is an average of two mass scans. Batch 1: sample mixture prepared by intimate mixing in a mortar. Batch 2: sample mixture prepared by coprecipitation from ether.

Table III: Isotopic (¹⁴N/¹⁵N) Distribution in the Nitramine and Nitrosamine after Photolysis, Derived from Table II

(m/e)		Nitrosamine (II)			Nitramine (I)	
		74	75	76	90	92
Batch 1						
Sample 1	Relative abundance	129	219	79	100	70
	Observed ratio	1.00	1.70	0.61		
	Calculated ratio	1.00	1.70	0.70		
Sample 2	Relative abundance	160	275	128	100	81
	Observed ratio	1.00	1.72	0.82		
	Calculated ratio	1.00	1.81	0.81		
Batch 2						
Sample 1	Relative abundance	200	343	147	100	82
	Observed ratio	1.00	1.72	0.74		
	Calculated ratio	1.00	1.82	0.82		
Sample 2	Relative abundance	224	388	171	100	88
	Observed ratio	1.00	1.73	0.76		
	Calculated ratio	1.00	1.88	0.88		
Sample 3	Relative abundance	349	526	241	100	87
	Observed ratio	1.00	1.51	0.69		
	Calculated ratio	1.00	1.87	0.87		
Sample 4	Relative abundance	291	520	215	100	90
	Observed ratio	1.00	1.79	0.74		
	Calculated ratio	1.00	1.90	0.90		

fore, that the isotope crossover in the photoproduct, nitrosamine, had occurred in a secondary light-induced process *after* its initial formation from the nitramine (I).

In order to test the possibility of a nitrosamine photorearrangement, a 1:1 mixture of (CH₃)₂¹⁵N-¹⁵NO₂ (Ib) and unlabeled nitrosamine was irradiated. The results which are shown in Table IV established clearly that nitrosamine had undergone an efficient light-induced isotopic equilibration. In fact, the 75:76 ratio was higher than 2.4 presumably due to the fact that in the initial stages of the photolysis experiment the concentration of the unlabeled nitrosamine was overwhelmingly large.

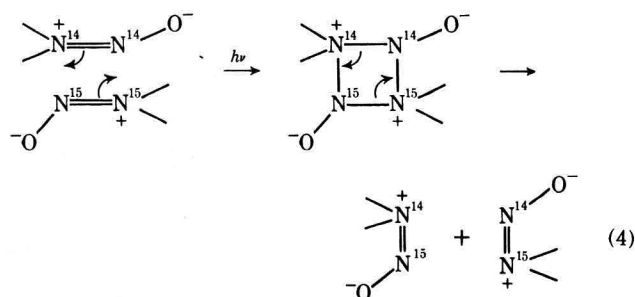
Mechanism of Nitrosamine Photorearrangement. The

Table IV: Relative Abundance of Selected Ions in the Mass Spectra: Mixture (ca. 1:1) of (CH₃)₂¹⁵N-¹⁵NO₂ and (CH₃)₂N-NO Before and After Irradiation (Irradiation time: 120 min)

Sample no.	(m/e)	Relative abundance				
		74	75	76	92	75:76 ^a
1	Unirradiated	393	12.6	8.5	100	
2		409	13.0	8.6	100	
1	Irradiated	441	306	125	100	2.52
2		717	417	176	100	2.36
3		533	335	130	100	2.59

^a The m/e 75 and 76 were corrected for background shown in the control run before 75:76 ratio was computed.

above isotope crossover in nitrosamine may or may not proceed from an initial N–N bond cleavage. However, the extent of the crossover (nearly 100%) is inconsistent with the favored geminate recombination in the condensed phase if the $(\text{CH}_3)_2\text{N}$ and NO radicals are indeed formed first. The following mechanism (4) is now proposed which is consistent with the major experimental observations, *viz.*, a very efficient isotopic crossover in the nitrosamine and almost total preclusion of exchange in the parent nitramine.



Nitrosamines reportedly are resistant to photodecomposition.⁶ Very early studies⁷ of the photolysis of dimethylnitrosamine itself in the gas phase showed dimethylamine and uncharacterized polymeric material as products. Later work on nitrosamines dealt with studies of photolysis in solution.^{6,8} Photodecomposition of dibenzyl nitrosamine in presence of oxygen was observed to yield dibenzylamine, *N*-benzylidene benzylamine, and dibenzylammonium nitrate.⁸ The reported conversion to nitrate is about 0.3% per hour of photolysis. The products were interpreted to arise from radicals generated by breakage of the N–N bond. In solution, breakage of the N–N bond would be favored since the resulting radicals could be stabilized by solvation. To our knowledge, a photorearrangement of nitrosamines such as the one proposed here to explain the present results was never considered. However, this reaction is reminiscent of a recent study⁹ of C-nitroso compounds describing a light-induced shift of the equilibrium, dimer \rightleftharpoons monomer, toward the monomer.

Mechanism of Formation of Nitrosamine from Dimethylnitramine Photolysis in Solid State. From the absence of mass 91 in our experiments with doubly labeled (¹⁵N) dimethylnitramine we conclude that the

N–N bond does not break in the solid-phase photolysis. However, since nitrosamine is formed in large yield, it has to result by a one-step process involving cleavage of the N–O bond.

Thermolysis of dimethylnitramine in the gas phase to give nitrosamine was proposed¹ to take place with prior formation of the radicals $(\text{CH}_3)_2\text{N}$ and NO₂. While in the gas phase and in solution one can visualize formation of these radicals, the mechanism of solid phase photolysis seems to involve preferential breakage of the N–O bond analogous to the case of aromatic C-nitro compounds.³ The stability of the N–N bond is also in line with the observed short N–N bond length (1.26 Å)¹⁰ in solid dimethylnitramine and the attributed double bond character in virtue of it. Detailed crystal structure data¹¹ are, however, lacking to see if the lattice orientation of adjacent molecules of dimethylnitramine is such as to promote the nitrosamine photorearrangement.

Summary and Conclusion

Photolysis of dimethylnitramine carried out in the solid state yields dimethylnitrosamine as the major product. Isotope crossover experiments using mixtures of doubly ¹⁵N-labeled dimethylnitramine with unlabeled dimethylnitramine and dimethylnitrosamine, respectively, lead to the conclusion that nitramine converts to nitrosamine as a photoproduct by an N–O bond cleavage. Labeled and unlabeled nitrosamines also undergo a light-induced rearrangement resulting in an efficient isotope crossover.

Acknowledgment. The authors wish to thank Professor B. S. Thyagarajan of the University of Idaho for helpful discussions and Mr. J. R. Autera for much technical assistance.

(6) E. M. Burgess and J. M. Lavinish, *Tetrahedron Lett.*, 1221 (1964).

(7) C. H. Bamford, *J. Chem. Soc.*, 12 (1939).

(8) T. Axenrod and G. W. A. Milne, *Tetrahedron*, **24**, 5775 (1968).

(9) A. L. Bluhm and J. Weinstein, *Nature (London)*, **215**, 1478 (1967).

(10) W. Costain and E. G. Cox, *ibid.*, **160**, 826 (1947).

(11) In answer to a point raised by one of the referees, it may be said that space group *P2₁/m* given in ref 10 indicates that the more probable orientation of adjacent molecules in the unit cell is head-to-tail which is consistent with the rearrangement mechanism given in eq 4.

Influence of Rotational Conformation on the Stereochemical Course of Hot Halogen for Halogen Substitution in Liquid 2,3-Dichlorobutane

by L. Vasáros,¹ H.-J. Machulla,² and G. Stöcklin*

Institut für Radiochemie der Kernforschungsanlage Jülich GmbH, Jülich, West Germany (Received May 17, 1971)

Publication costs assisted by Kernforschungsanlage Jülich GmbH

The mechanistically important question of retention *vs.* inversion of configuration in hot halogen for halogen replacement at asymmetric carbon atoms has been reinvestigated in the light of conformational analysis. Substitution of chlorine in liquid 2,3-dichlorobutane by recoil halogen can lead to both retention and inversion, depending on the conformation of the molecule and the mode of impact. The observed conformational effect provides evidence that true hot replacement reactions in the liquid phase can also proceed with inversion of configuration. The possible contribution from thermal cage combination processes to the product formation is also discussed.

Introduction

Energetic substitution reactions by hot nucleogenic atoms with translational energies in the eV range exhibit some characteristic features, particularly with respect to their stereochemical course (for review *cf.* ref 3–5). Results obtained on the substitution of recoil tritium for hydrogen^{6–10} and recoil halogen for halogen^{11–15} at asymmetric carbon atoms have shown that the replacement occurs predominantly with retention of configuration. Whereas in gas phase experiments^{8–15} substitution proceeds with almost complete retention, less stereospecificity is generally observed in the condensed phases, a fact which has been ascribed to a contribution from radical–radical cage combination reactions, allowing a racemization of the intermediate radical. The almost complete retention of configuration in the gaseous phase has been explained on the basis of the impact model,¹⁶ assuming a direct replacement process on a time scale comparable to molecular transit times for the hot tritium and chlorine atoms, estimated to be about 10^{-13} – 10^{-14} sec. The collision time during which the energetic atom is available for bond formation should be smaller than the time required for the motion of the substituent groups during the inversion process, or these rapid motions involve so much vibrational excitation energy that the molecules thus formed undergo secondary decomposition within about 10^{-10} sec,¹³ and hence are not experimentally observed in the gaseous phase.

Trajectory studies of the hot reaction of tritium with methane^{17,18} show that T-for-H substitution is a “concerted” process involving at least four atoms, and there are indications that it may proceed with inversion of configuration. It remains questionable, however, whether a substantial fraction of inversion can occur (*cf.* also ref 11). Experimental studies on the excitation decomposition following ¹⁸F-for-F substitution

in gaseous CH₃CF₃¹⁹ also indicate a “concerted” mechanism. Hot substitution with inversion of configuration is most likely to be observed in the liquid phase; however, the question still remains open, since essentially nothing is known about a contribution from caged radical reactions. Furthermore, a possible influence of rotational conformation, when using diastereomeric alkyl halides, has been so far completely neglected. Drastic steric effects, however, can be expected when considering the degree of steric hindrance for different modes of attack at the various conformers. Such con-

(1) Visiting Chemist from Central Research Institute of Physics, Budapest, Hungary.

(2) In partial fulfillment of the requirements for a Ph.D. degree.

(3) A. P. Wolf, *Advan. Phys. Org. Chem.*, **2**, 201 (1964).

(4) R. Wolfgang, *Progr. React. Kinet.*, **3**, 97 (1965).

(5) G. Stöcklin, “Chemie heisser Atome,” Verlag Chemie, Weinheim, 1969.

(6) H. Keller and F. S. Rowland, *J. Phys. Chem.*, **62**, 1373 (1958).

(7) J. G. Kay, R. P. Malsan, and F. S. Rowland, *J. Amer. Chem. Soc.*, **81**, 5050 (1959).

(8) M. Henchman and R. Wolfgang, *ibid.*, **83**, 2991 (1961).

(9) Yi-N. Tang, C. T. Ting, and F. S. Rowland, *J. Phys. Chem.*, **74**, 675 (1970).

(10) G. F. Palino and F. S. Rowland, *J. Phys. Chem.*, **75**, 1299 (1971).

(11) C. M. Wai, C. T. Ting, and F. S. Rowland, *J. Amer. Chem. Soc.*, **86**, 2525 (1964).

(12) F. S. Rowland, C. M. Wai, C. T. Ting, and G. Miller, in “Chemical Effects of Nuclear Transformations,” Vol. 1, IAEA, Vienna, 1965, p 333.

(13) C. M. Wai and F. S. Rowland, *J. Phys. Chem.*, **71**, 2752 (1967).

(14) C. M. Wai and F. S. Rowland, *ibid.*, **74**, 434 (1970).

(15) G. F. Palino and F. S. Rowland, *Radiochim. Acta*, **15**, 57 (1971).

(16) M. Henchman, D. Urch, and R. Wolfgang, *Can. J. Chem.*, **38**, 1722 (1960); *cf.* also ref 4.

(17) D. L. Bunker and M. Pattengill, *Chem. Phys. Lett.*, **4**, 315 (1969).

(18) D. L. Bunker and M. Pattengill, *J. Chem. Phys.*, **53**, 3041 (1970).

(19) C. F. McKnight, N. J. Parks, and J. W. Root, *J. Phys. Chem.*, **74**, 217 (1970).

formational effects, if observed, would provide evidence for true hot one-step substitution reactions, since two-step radical processes should not be affected by the conformation of the original substrate molecule. Thus, a possible influence of rotational conformation might also provide information on the question whether direct hot substitution can also occur with inversion of configuration.

Experimental Section

Sample Preparation and Irradiation. The meso and racemic forms of 2,3-dichlorobutane (DCB) were prepared by stereospecific addition of Cl_2 to *trans*- and *cis*-2-butene, respectively.²⁰ The products (purity >95%) were then purified by gas chromatography. A purity >99% was achieved when using a 4-m glass column (8 mm i.d.) with 20% Igepal CO-880 on Chromosorb W-AW 60-80 mesh at 70° and 100 cc He/min. Similarly, *threo*- and *erythro*-2-chloro-3-fluorobutane (CFB), 2-bromo-3-chlorobutane (BCB) and 2-chloro-3-iodobutane (CIB), which were used as carriers in small amounts for radio gas chromatographic purposes (*vide infra*), were also prepared by stereospecific addition reactions analogous to procedures described in the literature.²¹⁻²³ The solvents (methanol, *n*-pentane and cyclopentane) were obtained from Merck AG, Darmstadt, in high purity (Uvasol for spectroscopy), and were used without further purification. The bromine and iodine were reagent grade (Merck).

Samples of about 400 μl (substrate + additives) were placed in micro-quartz ampoules, which were outgassed on a vacuum line by freezing and melting cycles and then sealed and stored in dark until irradiation. For the *in situ* production of recoil chlorine the $^{37}\text{Cl}(n,\gamma)\text{-}^{38}\text{Cl}(T_{1/2} = 37.3 \text{ min})$ process was used. Neutron irradiations were carried out in a bismuth shielded thermal column facility of the FRJ-1 at a thermal neutron flux density of $7 \times 10^9 \text{ cm}^{-2} \text{ sec}^{-1}$ for a period of 90 min. The accompanying γ -exposure rate was $\leq 10^{-4}$ R/hr. Recoil fluorine, bromine, and iodine were produced *via* the $^{19}\text{F}(n,2n)^{18}\text{F}(T_{1/2} = 110 \text{ min})$, the $^{81}\text{Br}(n,2n)^{80\text{m}}\text{Br}(T_{1/2} = 4.4 \text{ hr})$ and the $^{127}\text{I}(n,2n)^{126}\text{I}(T_{1/2} = 12.8 \text{ days})$ processes, respectively, by irradiation with 14-MeV neutrons from a (d-t) Neutron Generator (Dynagen 300, Radiation Dynamics). The neutron flux density was about $5 \times 10^9 \text{ cm}^{-2} \text{ sec}^{-1}$, and the irradiation time varied from 15 to 30 minutes. For the determination of dose effects (*vide infra*) irradiation time and flux density (position) were varied over a wide range. For this purpose high flux irradiations were also carried out in the FRJ-1 at a neutron flux density of $5 \times 10^{12} \text{ cm}^{-2} \text{ sec}^{-1}$ for a period of 10 min in the case of ^{38}Cl .

Analytical Procedure. The details of our experimental technique for the analysis of products have been described elsewhere.²⁴ Yields of the individual prod-

ucts are expressed in % of the total induced radiohalogen activity (radiochemical yield). For the separation of the inorganic products (HX^* and XX^*) and for the determination of the total induced activity, the irradiated ampoules were crushed under the surface of 5 ml of a 1:1 mixture of Na_2SO_3 and Na_2CO_3 solution (10%) and the organic products extracted with 2 ml of CCl_4 or pentane. After washing and drying, aliquots of the phases were submitted to radioactivity determination (*vide infra*) and, in the case of the organic phase, to gas chromatographic analysis. The relatively low radioactivity made it necessary to use a discontinuous radio gas chromatographic technique.²⁴ Each fraction under a peak, as indicated by the thermal conductivity of the added carrier or the parent compound itself, was adsorbed in a charcoal tube and submitted to radioactivity measurement.

Gas Chromatographic Separation of the Diastereomers. The gas chromatographic separation of the diastereomeric 2,3-dihalobutanes had to be fast because of the relatively short half-life (37 min in the case ^{38}Cl). Furthermore, a 100% separation was necessary to guarantee radiochemical purity of the fractions, particularly when small activities of the opposite diastereomer had to be separated from relatively large activities of the parent isomer and *vice versa*. Thus, conditions were chosen which allowed a 4-6 min interval between the tail of the first and the front of the second peak. Three types of columns (8 m, 4 mm i.d.) were used: (1) 20% Igepal CO-880 on Chromosorb W-AW, 60-80 mesh (I), (2) 30% β,β' -oxidipropionitril on Chromosorb P-NAW, 60-80 mesh (II), (3) 15% SF-96 on Chromosorb W-AW DMCS, 60-80 mesh (III).

Separation as specified above could be achieved under the following conditions: (a) *rac*- and *meso*-2,3-DCB on column I, 80-100°, 80 cc of He/min; (b) *threo*- and *erythro*-2,3-CFB on column II, 60°, 80 cc of He/min; (c) *threo*- and *erythro*-2,3-BCB on column II, 100°, 80 cc of He/min; (d) *threo*- and *erythro*-2,3-CIB on column III, 80°, 100 cc of He/min. Further details on the gas chromatographic separation of several diastereomeric haloalkanes are published elsewhere.²⁵

Radioactivity Measurements. The total induced radioactivity and that of individual organic products, each adsorbed on charcoal and transferred into plastic vials, was measured with a well-type scintillation counter or a Ge(Li)-semiconductor detector under identical

(20) M. C. Lucas and C. W. Gould, Jr., *J. Amer. Chem. Soc.*, **63**, 2541 (1941).

(21) (a) G. A. Olah and J. M. Bollinger, *ibid.*, **89**, 4744 (1967); (b) G. A. Olah and J. M. Bollinger, *ibid.*, **90**, 947 (1968).

(22) M. Delephine and L. Ville, *Bull. Soc. Chim. Fr.*, **23**, 673 (1920).

(23) S. Winstein and E. Grunwald, *J. Amer. Chem. Soc.*, **70**, 836 (1948).

(24) G. Stöcklin and W. Tornau, *Radiochim. Acta*, **6**, 86 (1966); G. Stöcklin and W. Tornau, *ibid.*, **9**, 95 (1968).

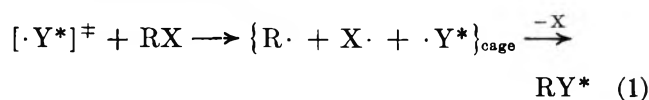
(25) L. Vasáros, H.-J. Machulla, and W. Tornau, *J. Chromatogr.*, **62**, 458 (1971).

conditions, taking into account radioactive decay and self-absorption. Selective γ -spectrometric techniques had to be applied in mixed halogen systems to avoid interference from radiohalogen activities other than that of the recoil halogen of interest, particularly, when ^{38}Cl was counted in the presence of large radiobromine activities.

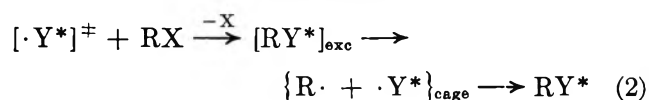
Conformational Analysis. In order to examine the stereochemical course of the reaction as a function of the equilibrium concentration of the rotational isomers in different solvents, it was necessary to carry out conformational analyses. In the case of racemic 2,3-DCB, three conformers exist in which the C-Cl bonds are in trans (RT) or in gauche positions (RG and RG'). They have different dipole moments and can be assigned and quantitatively determined by ir²⁶ or by nmr²⁷ spectroscopy. We have applied the ir-spectroscopic method described by Imura, *et al.*,²⁶ for the determination of the equilibrium concentration of the three conformers in racemic 2,3-DCB as a function of cyclohexane, *n*-pentane, and methanol concentration, respectively. The stretching vibration of the C-Cl bond at 652 cm^{-1} (RT), 596 cm^{-1} (RG), and 703 cm^{-1} (RG') have been used. In the case of bromine as solvent, the concentration of the conformers has been calculated by using the method of Mizushima, *et al.*,²⁸ based on the Onsager reaction field theory.²⁹

Results and Discussion

Cage Effects. For the determination of the stereochemical course of hot halogen for halogen substitution in liquid 2,3-dihalobutanes it is essential to take into account a possible contribution from immediate caged radical-radical combination following either a hot displacement of a halogen atom X by a radioactive recoil atom with excess kinetic energy [$\cdot\text{Y}^*$][‡]



or a hot one-step substitution after excitation decomposition of the first formed product molecule



The time scale for such combination has been estimated (in the case of ^{38}Cl for Cl substitution in liquid 2,3-DCB) as being comparable with the time required for attainment of planarity, *i.e.*, racemization of the intermediate chloro-*sec*-butyl radical.¹² Hence, these thermal caged radical processes can lead to both retention and inversion of configuration, thus obscuring the true stereochemical course of a hot one-step substitution.

For $\text{Y} = \text{F}$ or Cl , one would not necessarily expect a substantial contribution from radical-radical combination processes, since thermal fluorine and chlorine atoms

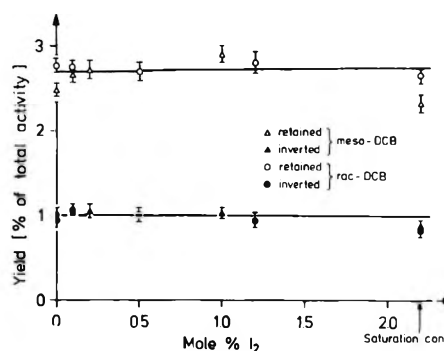


Figure 1. Lack of I_2 scavenger effects on the radiochemical yield of retained and inverted ^{38}Cl for Cl substitution products in *meso*- and *rac*-2,3-DCB.

are readily removed by the exothermic hydrogen abstraction reaction



The activation energy for gas phase hydrogen abstraction of a primary hydrogen by a chlorine atom is about 1 kcal/mol.³⁰ Fluorine and chlorine atoms will only have a small chance for any type of combination reaction, due to the fast competing hydrogen abstraction. For these atoms the alkyl halide system should be self-scavenging.

In order to demonstrate the self-scavenging properties of the substrate, we have measured the absolute yield of the retained and inverted substitution products as a function of iodine scavenger concentration in the system ^{38}Cl -2,3-DCB. Figure 1 shows that the yields remain unaffected by iodine scavenger over the entire concentration range studied, up to saturation. While this experiment does not give any answer to the possible occurrence of immediate cage combination reactions, it demonstrates the absence of thermal diffusive radical reactions and the self-scavenging properties of the system.

Cage combination reactions can generally be influenced by mass, viscosity, and temperature changes, which affect the rate of out of cage diffusion.^{31,32} Looking for a possible mass effect we have compared the replacement of chlorine by recoil ^{18}F , ^{38}Cl , $^{80\text{m}}\text{Br}$ and ^{126}I , respectively, in liquid, unscavenged racemic 2,3-DCB. It can be seen from Table I that the ratio of

(26) K. Imura, N. Kawakami, and M. Takeda, *Bull. Chem. Soc. Jap., Ind. Chem. Sect.*, **42**, 2091 (1969).

(27) A. A. Bothner-By and C. Naar-Colin, *J. Amer. Chem. Soc.*, **84**, 743 (1962).

(28) I. Watanabe, S. Mizushima and Y. Mashika, *J. Chem. Soc. Jap., Pure Chem. Sect.*, **64**, 962 (1943); I. Watanabe, S. Mizushima, and Y. Morino, *ibid.*, **63**, 1131 (1942).

(29) L. Onsager, *J. Amer. Chem. Soc.*, **58**, 1486 (1936).

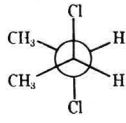
(30) E. S. Huyser, Ed., "Methods in Free Radical Chemistry," Vol. 1, Marcel Dekker, New York 1969, p 86.

(31) L. Herk, M. Feld, and M. Szwarc, *J. Amer. Chem. Soc.*, **83**, 2998 (1961).

(32) J. Smid and M. Szwarc, *J. Amer. Chem. Soc.*, **78**, 3322 (1956).

retention to inversion of configuration is identical, within the experimental error, for the substitution by ^{18}F and ^{38}Cl , but decreases when going to $^{80\text{m}}\text{Br}$ and ^{126}I . For both fluorine and chlorine the substitution of a Cl atom in racemic 2,3-dichlorobutane proceeds with about 75% retention of configuration, leading to ^{18}F -labeled *threo*-2-chloro-3-fluorobutane and ^{38}Cl -labeled racemic 2,3-dichlorobutane, respectively. The smaller retention values obtained in the case of bromine for chlorine (59% retention as $^{80\text{m}}\text{Br}$ -labeled *threo*-2-bromo-3-chlorobutane) and iodine for chlorine substitution (54% retention as 2-chloro-3-iodobutane) can be attributed to an increasing contribution from nonstereospecific radical combination. This can be expected, since hydrogen abstraction by thermalized bromine and iodine is endothermic and the system is no longer self-scavenging.³³

Table I: Cl Replacement in Liquid *rac*-2,3-Dichlorobutane by Recoil ^{18}F , ^{38}Cl , $^{80\text{m}}\text{Br}$, and ^{126}I , Respectively, at 20°

	Parent yield (% of total activity)		Ratio, $\left(\frac{\text{retention}}{\text{inversion}}\right)$
	Retained	Inverted	
$[^{18}\text{F}]^\ddagger$ for Cl	2.14 ± 0.25	0.78 ± 0.08	3.0 ± 0.3
$[^{38}\text{Cl}]^\ddagger$ for Cl	2.78 ± 0.03	0.95 ± 0.01	2.9 ± 0.1
$[^{80\text{m}}\text{Br}]^\ddagger$ for Cl	2.70 ± 0.15	1.93 ± 0.13	1.4 ± 0.1
$[^{126}\text{I}]^\ddagger$ for Cl	2.53 ± 0.19	2.15 ± 0.08	1.2 ± 0.1

The fact that there is essentially no difference between the ratio of retention to inversion for recoil fluorine and chlorine indicates the absence of a mass effect. It should be pointed out, however, that this argument is not valid, when the cage effect is occurring after excitation decomposition (eq 2). In this case, the caged atom would be chlorine for both 2-chloro-3-fluorobutane and 2,3-dichlorobutane, provided excitation decomposition proceeds *via* C-Cl bond rupture. Thus a mass effect should not be observed in ^{18}F for Cl and ^{38}Cl for Cl substitution, while $^{80\text{m}}\text{Br}$ for Cl and ^{126}I for Cl replacement should give different results since these product molecules would most likely involve C-Br and C-I bond rupture. In fact, Table I shows the predicted sequence in loss of stereospecificity. In the case of ^{18}F for Cl and ^{38}Cl for Cl replacement, however, the major path for excitation decomposition is expected to proceed *via* HF or HCl elimination. Even in liquid 2,3-DCB we find a yield of 0.56% for the HCl-elimination product 2-chlorobutene-2 (cis + trans). This is about 15% of the substitution product yield (*meso*- and *rac*-2,3-DCB = 100%).

Further support against a substantial contribution from cage reactions comes from the lack of a viscosity effect, when comparing cyclohexane (1.02 cP) and *n*-pentane (0.24 cP) solutions. For both *meso*- and *rac*-2,3-DCB the ratio retention/inversion is identical for both solvents, up to the highest dilution (see Figure 4).

We have also looked for a temperature effect. In view of the solvent effects (see below) we have irradiated iodine scavenged *rac*-2,3-DCB samples containing 0.9 mol fraction of cyclohexane at 0° and 100°. The ratio retention/inversion remained unchanged within the experimental error (0.38 ± 0.02 for 0° and 0.36 ± 0.02 for 100°). It should be pointed out that Rowland, *et al.*,¹² have reported a temperature effect on the stereochemical course in undiluted DPPH-scavenged *rac*-2,3-DCB, when irradiating at 20° and -56°. This might, however, also be due to a conformational effect (see below) which, in our above mentioned cyclohexane solution is small and does not affect the stereochemical course within the experimental error. It is interesting to note that the temperature change did not lead to an appreciable change in the product yield,¹² while such a change might be expected on the basis of a cage effect.

It is also pertinent to point out that photohalogenation of gaseous and liquid 2-halobutanes occurs with a significant preference (60 to 70%) of the erythro and *meso* forms, respectively, increasing with the size of the substituting halogen,^{34,35} while only about 25% of the erythro and *meso* form, respectively, is observed after recoil fluorination and chlorination of liquid *rac*-2,3-DCB.

While a possible contribution from caged radical processes cannot completely be ruled out, even for recoil fluorine and chlorine, the above mentioned arguments indicate that in our system this contribution is not substantial. It is also significant to point out that the density effects, studied in the ^{18}F - CH_2F system by Richardson and Wolfgang,³⁶ clearly demonstrate that caging of ^{18}F becomes important only when mean intermolecular distances shrink to about half the diameter of the fluorine atom, *i.e.*, at high densities of the liquid caused by lower temperatures. The relatively small importance of cage reactions in our diluted ^{38}Cl -2,3-DCB systems is also demonstrated by the observation of strong conformational effects, which will be discussed

(33) Reactions of $^{80\text{m}}\text{Br}$ and ^{38}Cl with 2,3-DCB in the liquid phase have been reported previously by Rowland and coworkers.^{11,12,14} While the ^{38}Cl results are in reasonable agreement, Rowland¹² observes less inversion in $^{80\text{m}}\text{Br}$ for Cl replacement, when using a Br_2 -scavenged system (Br_2 concentration unspecified). This is to be expected, since in our unscavenged system the substrate should not be a good scavenger for Br-atoms and hence more radical reactions leading to inversion will occur in our case. Furthermore, the presence of molecular bromine changes the equilibrium concentration of the conformers, thus also giving rise to an increase of the ratio retention/inversion (see Figure 5).

(34) P. S. Fredericks and J. M. Tedder, *J. Chem. Soc.*, 3520 (1961).

(35) W. Thaler, *J. Amer. Chem. Soc.*, **85**, 2607 (1963).

(36) A. E. Richardson and R. Wolfgang, *J. Amer. Chem. Soc.*, **92**, 3480 (1970).

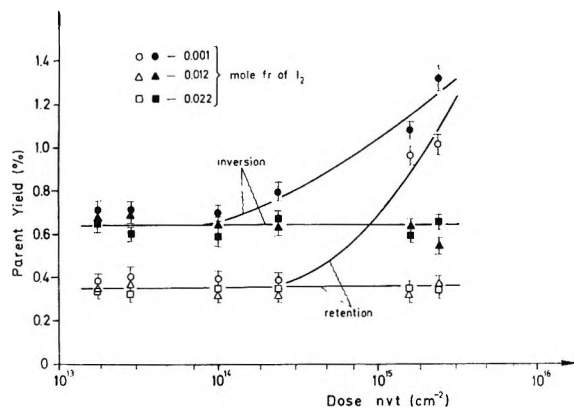


Figure 2. Effects of dose and I_2 scavenger on the radiochemical yields of retained and inverted ^{38}Cl for Cl substitution products in the system racemic 2,3-DCB-cyclohexane (1:9).

below. These effects can only be observed if the major substitution process is a hot one-step replacement.

Dose Effect. Chemical reactions initiated by the ionizing radiation accompanying the neutron bombardment can also conceivably perturb the original product distribution from hot reactions. Even though irradiations have been carried out under relatively mild conditions (*vide supra*), and the above mentioned lack of I_2 -scavenger effect in the ^{38}Cl -2,3-DCB system indicates the absence of thermal diffusive radical reactions at least in this system, it seemed necessary to study the effect of irradiation time and/or flux on the product distribution with particular reference to the stereochemical course of the substitution reaction of interest. In view of the solvent effects to be studied (*vide infra*) we carried out these experiments in the ^{38}Cl -rac-2,3-DCB system, containing 90 mol % of cyclohexane in the presence of small amounts of I_2 scavenger. In Figure 2 we have plotted the absolute yields of the retained and inverted substitution product as a function of thermal neutron dose (nvt), which is proportional to the accompanying ionizing radiation dose absorbed. It can be seen that, in the presence of 10^{-3} mol fraction of iodine, the yields remain constant up to a neutron dose of about $5 \times 10^{14} \text{ cm}^{-2}$. At higher doses, the yields start increasing with different rates. In the presence of larger I_2 scavenger concentrations ($\geq 10^{-2}$ mol fraction) no dose effect is observed up to the highest dose studied ($3 \times 10^{15} \text{ n/cm}^2$). Our typical irradiations were carried out in the dose range of about 3×10^{13} – 10^{14} n/cm^2 in the presence of 10^{-3} mol fraction of iodine; hence the yields were unperturbed by a contribution from radiation chemical reactions. For methanolic solutions similar tests were made to confirm the absence of dose effects.

Figure 2 represents a typical example of the dose effect and of the protection against it. The increase of the labeled substitution product can be explained by thermal diffusive reactions between radiolytically produced chloro-*sec*-butyl radicals and inorganic recoil

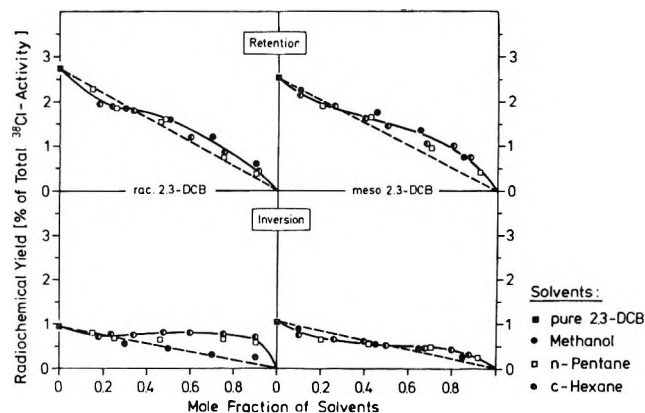


Figure 3. Solvent effect on the radiochemical yield of the inverted and the retained ^{38}Cl for Cl substitution products in *rac*- and *meso*-2,3-DCB.

products such as $^{38}ClCl$ and $H^{38}Cl$. In the presence of iodine scavenger, the radicals can be removed by a competing reaction with iodine. The dose at which radiation chemical reactions interfere is a function of iodine scavenger concentration, which is used up at higher doses.

Conformational Effects. In view of the changes of rotational isomer concentration in 2,3-DCB which can be caused by solvents, we expected solvent effects on the stereochemical course of hot halogen for halogen substitution. We have therefore determined the radiochemical yields of the inverted and retained ^{38}Cl for Cl substitution product in *meso*- and *rac*-2,3-DCB as a function of solvent concentration (in the presence of 10^{-3} mol fraction of iodine scavenger). The results shown in Figure 3 indicate considerable solvent effects as indicated by the deviation from the linear dilution curves (dashed line). The effect becomes more obvious when plotting the ratio retention/inversion against the mole fraction of solvents (Figure 4). Figure 4 demonstrates that the stereochemical course of the substitution can be varied over a wide range (from about 35 to 85% retention) by changing the type and the concentration of the solvent. The magnitude of the effects is quite different for *meso* and *rac*emic 2,3-DCB. Both decrease and increase of retention are more pronounced in the case of *rac*-2,3-DCB as parent. The different behavior of the two diastereomers cannot be explained by secondary effects, such as different contribution from thermal radical reactions and/or different moderating behavior. In fact, this lack of similarity again indicates the absence of such effects. The most likely explanation of the solvent effect is a changing stereochemical influence caused by the changing rotational isomer concentration.

The influence of the solvent on the relative equilibrium concentration ($RT + RG + RG' = 100$) of the three rotational isomers is shown in Figure 5 for *rac*-2,3-DCB. As expected from the Mizushima treatment²⁸ of the Onsager theory, the equilibrium is changed

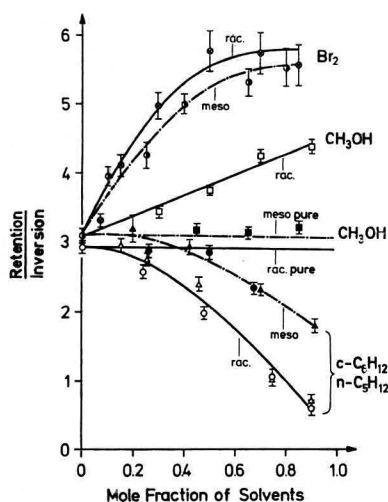


Figure 4. Solvent effect on the stereochemical course (ratio retention/inversion) of ^{38}Cl for Cl substitution in *rac*- and *meso*-2,3-DCB. Key: \otimes , *rac*-DCB- Br_2 ; \square , *rac*-DCB- CH_3OH ; Δ , *rac*-DCB-*n*- C_6H_{12} ; \circ , *rac*-DCB-*c*- C_6H_{12} ; \bullet , *meso*-DCB- Br_2 ; \blacksquare , *meso*-DCB- CH_3OH ; \blacktriangle , *meso*-DCB-*n*- C_6H_{12} ; \bullet , *meso*-DCB-*c*- C_6H_{12} .

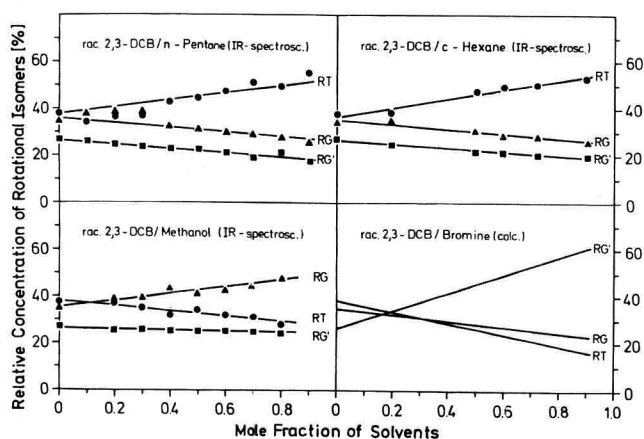


Figure 5. Solvent effect on the relative equilibrium concentration of the rotational isomers in racemic 2,3-DCB.

by the reaction field of the solvent molecules. In the nonpolar solvents, cyclohexane and *n*-pentane, the nonpolar RT form is stabilized, while the polar RG and RG' forms are destabilized. The opposite effect is observed in methanol, a polar solvent. The effect caused by bromine is somewhat different, but also follows the theoretical prediction. The large volume of the Br_2 -molecule overcompensates the small dielectric constant; thus the relative concentration of the RT form decreases, and only that of the most polar RG' form is seen to increase with increasing Br_2 concentration.

In order to find a correlation between the stereochemical course of Cl for Cl substitution and the equilibrium concentration of the conformers it is necessary to compare the conformers under the aspect of steric suitability for the reaction. From the Stuart models of Figure 6, it can easily be seen that an "invertive" at-

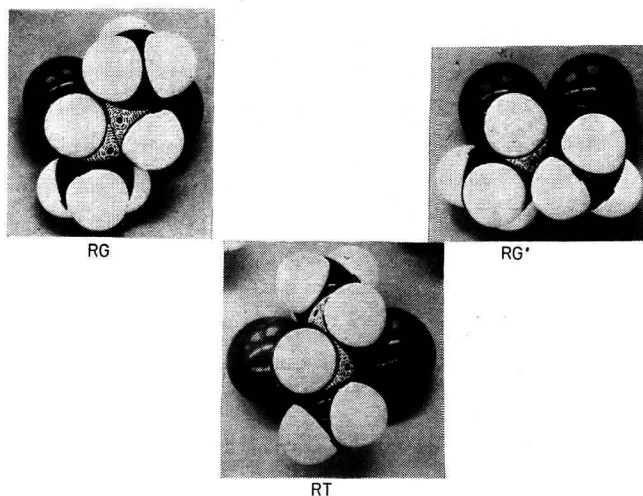


Figure 6. Models of rotational isomers in racemic 2,3-DCB.

tack from the opposite side of the halogen to be replaced can only be successful at the RT and especially at the RG form, where the asymmetric carbon atoms are relatively free (see marked target areas in Figure 6). In the case of the RG' form, however, the carbon atoms are obscured by the methyl groups. Formation of a carbon-halogen bond can hardly take place, and the interaction will mainly occur with hydrogen atoms of the methyl groups. On the other hand, direct halogen for halogen replacement with retention of configuration can occur with all three forms. If we treat the kinetics of the substitution as a simple bimolecular process with different relative reaction cross sections for retention (σ) and inversion (σ') for each of the three conformers, the following expression is obtained for the ratio [retention]/[inversion]

$$\frac{[\text{retention}]}{[\text{inversion}]} = \frac{\sigma_1[\text{RT}] + \sigma_2[\text{RG}] + \sigma_3[\text{RG}']}{\sigma_1'[\text{RT}] + \sigma_2'[\text{RG}] + \sigma_3'[\text{RG}']} + K \quad (4)$$

The constant K stands for a contribution from processes other than direct hot substitution (*e.g.*, cage combination reactions), which would give rise to a different stereochemical course, and hence to changes in the ratio retention/inversion. Processes with low stereospecificity like radical combinations will lead to a decrease of the ratio, *i.e.*, the constant should have a negative value. As we have seen from the above steric consideration (Figure 6) the relative reaction cross section σ_3' for an attack with inversion at the RG' form should be essentially zero. The remaining constants have been determined by "trial and error." In Figure 7 we have then plotted the experimental values *vs.* those obtained by calculation from eq 4, using the following constants $\sigma_1 = 0.4$, $\sigma_2 = 4.6$, $\sigma_3 = 4.6$, $\sigma_1' = 1.0$, $\sigma_2' = 0.4$, $\sigma_3' = 0$ and $K = -2.5$. While the 45° straight line obtained is no proof for our kinetic assumption, it demonstrates the existence of a direct relation between

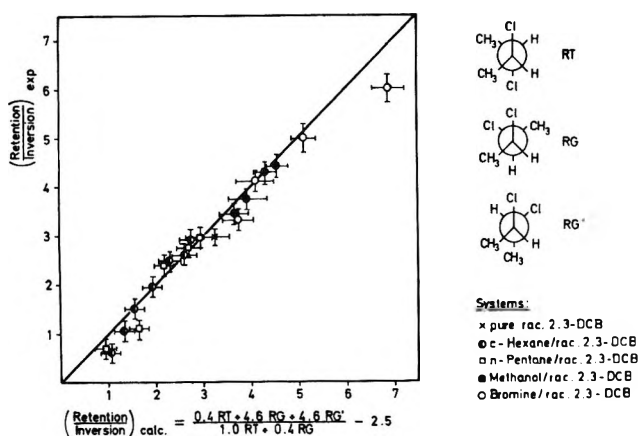


Figure 7. Error and trial fitting of the kinetic treatment (see text).

the concentration of the individual conformers and the stereochemical course of the substitution. The relative cross sections obtained are qualitatively meaningful. From a steric standpoint there is practically no difference between the RG and the RG' form with respect to a direct halogen replacement with retention ($\sigma_2 = \sigma_3$). In comparison, the cross section for the identical process at the RT form is smaller ($\sigma_2 = 12 \sigma_1$), possibly indicating the importance of competing processes (C-C bond scission, H abstraction and H substitution), when the incoming hot halogen attacks the trans form of the molecule. At the two gauche forms, on the other hand, an attack from the side of the two cis positioned halogens should have a much greater chance for a halogen substitution, since there is practically no interference from the methyl group. For a substitution from the back-side, however, the cross section is higher for the trans than for the gauche form ($\sigma_1' = 2.5 \sigma_2'$). An attack at the RG form leading to inversion might be more favorable for a competing C-C bond scission than at the RT form.

"Chemical" influences, such as electron density and electronegativity effects may also play a role. In fact, it has been demonstrated by Rowland and coworkers^{37,38} that in the case of hot tritium reactions "chemical" influences are more important than steric effects. The small energetic differences, however, between the individual conformers (about 0.04–0.05 eV) can be neglected in view of the hot atom energy range (about 1 to 20 eV). A change of conformation during the impact and before bond formation also seems unlikely, since the transient time during which bond formation takes place (about 10^{-13} sec) is several orders of magnitude smaller than the time required for rotational changes of conformation (10^{-9} – 10^{-8} sec).

The strong conformational effects observed can only be attributed to hot one-step replacement reactions and not to two-step radical combination processes. Even though thermal cage reactions may also be occurring, the conformational effect provides new evidence that true hot substitution reactions can also proceed with inversion of configuration, at least for recoil chlorine in liquid systems.

Conclusion

In the liquid phase, hot halogen for halogen substitution at asymmetric carbon atoms in 2,3-DCB can lead to both retention and inversion of configuration, depending on the conformation of the substrate and the mode of impact. The conformational effect observed seems to exhibit a new and an additional characteristic feature of hot one-step substitution processes. Despite a possible small contribution from radical-radical combinations, there is obviously a true hot substitution with inversion, possibly proceeding *via* a collision complex with a life time longer than the time for molecular vibration. The fact that in the gas phase reactions substitution almost exclusively proceeds with retention of configuration does not necessarily indicate the absence of the inversion mechanism in the gaseous phase. As has been pointed out by Rowland and coworkers,¹⁴ hot substitution with inversion may involve so much vibrational excitation energy that the molecules formed will undergo secondary decomposition within 10^{-10} sec. The reason for a more pronounced inversion in the liquid phase could then simply be attributed to a more efficient collisional deexcitation. The present results can only be interpreted by assuming two channels for hot substitution: (i) a direct replacement without a change in configuration, leaving the product molecule with little excitation energy; (ii) a back side attack with inversion giving rise to a highly excited product molecule.

Extensive gas phase studies on the pressure dependence of the stereochemical course of hot substitution by tritium and halogens are therefore presently being carried out on diastereomeric haloethanes in this laboratory.

Acknowledgment. The authors wish to thank Mr. M. Schüller for his extremely valuable experimental assistance. They are also indebted to Dr. W. Porschen and his crew for carrying out the Neutron Generator irradiations.

(37) F. S. Rowland, E. K. C. Lee, and Y. N. Tang, *J. Phys. Chem.*, **73**, 4024 (1969).

(38) Y. N. Tang, E. K. C. Lee, E. Tachikawa, and F. S. Rowland, *J. Phys. Chem.*, **75**, 1290 (1971).

Electronic Spectral Study of the Ionizations of the Naphthalene

Monosulfonic Acids

by G. J. Yakatan and S. G. Schulman*

College of Pharmacy, University of Florida, Gainesville, Florida 32601 (Received July 16, 1971)

Publication costs borne completely by The Journal of Physical Chemistry

Failure of the protonation of the 1- and 2-naphthalenesulfonates to shift their absorption and fluorescence spectra is attributed to negligible conjugation between the site of protonation and the aromatic system. Protonation of the neutral naphthalenesulfonic acids, however, apparently occurs at a site strongly coupled to the aromatic system as both fluorescence and absorption spectra are affected. The fluorescences of all species studied arise from the 1L_b state of naphthalene except for the 1-naphthalenesulfonic acidium ion fluorescence, which may originate from the 1La state.

Introduction

There is, at present, a paucity of quantitative information about the chemical properties and electronic structures of sulfonic acids. Early electrometric determinations of the dissociation constants of the naphthalenesulfonic acids yielded pK_a values of 0.74 and 0.60 for the 1 and 2 isomers, respectively.¹ Indicator methods have been employed to determine a pK_a of 0 for methanesulfonic acid.² These values appear reasonable by comparison with the pK_a values of -3 and $+2.0$ for sulfuric acid³ and suggest that OH is a weaker electron donor, while $-O^-$ is a stronger electron donor than an alkyl or aryl group attached to the $-SO_3H$ moiety.

In a recent study of the solvent dependence of anthracene monosulfonate fluorescence⁴ it was found that changes in acidity had no effect on the absorption spectra and only a very small effect on the fluorescence spectra of these compounds.

The deactivating and meta directing properties of the sulfonic acid group, with respect to aromatic electrophilic substitution, have long been attributed to the ability of the hexavalent sulfur atom to expand its valence shell by d orbital participation, thereby withdrawing electrons from the aromatic ring. It would then be apparent that the sulfonic acid group would be essentially a part of the aromatic system, so that a change in the electronic distribution at the sulfonic acid group, such as that produced by protonation of the sulfonate anion, would perturb the entire aromatic system. Moreover, due to the dipole nature of electronic transitions, the electronic distributions of the aryl sulfonic acids are expected to be different in the lower electronically excited singlet states than in the ground state. Consequently, the protonation energies in ground and excited states should be different, as a result of which the neutral sulfonic acid and the sulfonate anion should absorb or fluoresce at different frequencies.⁵ Obviously

this is not the case for the anthracene monosulfonates. Studies in this laboratory indicate that it is also not the case for the naphthalene monosulfonates. Since this phenomenon obviously is related to the nature of the electronic structure of arylsulfonic acids, it was decided to undertake the present study of the acidity dependence of the electronic transitions in the naphthalenesulfonic acids.

Experimental Section

1-Naphthalenesulfonic acid and 2-naphthalenesulfonic acid were purchased from Eastman Organic Chemicals, Inc., Rochester, N. Y., and were recrystallized from chloroform. Mallinckrodt reagent grade sulfuric acid and distilled deionized water were employed as the solvents in these studies.

Absorption spectra were taken on a Beckman DB-GT spectrophotometer. Fluorescence measurements were performed on a Perkin-Elmer MPF-2A fluorescence spectrophotometer whose monochromators were calibrated against the xenon line emission spectrum and whose output was corrected for instrumental response by means of a rhodamine-B quantum counter.

Results and Discussion

In the region pH 14 to $H_0 - 2$ there is no change in either the absorption or fluorescence spectra of the naphthalenesulfonic acids. At acidities greater than $H_0 - 2$ the fluorescence of 1-naphthalenesulfonic acid diminishes in intensity and shifts to the red (Figure 1). No vibrational structure is apparent for the 1-isomer in any solution. A corresponding change in the fluores-

(1) H. E. Fierz and P. Weissenbach, *Helv. Chim. Acta*, **3**, 305 (1920).

(2) K. N. Bascombe and R. P. Bell, *J. Chem. Soc.*, 1096 (1959).

(3) A. Albert and E. P. Serjeant, "Ionization Constants of Acids and Bases," Wiley, New York, N. Y., 1962, p 151.

(4) K. K. Rohatgi and B. P. Singh, *J. Phys. Chem.*, **75**, 595 (1971).

(5) T. Förster, *Z. Elektrochem.*, **54**, 42 (1950).

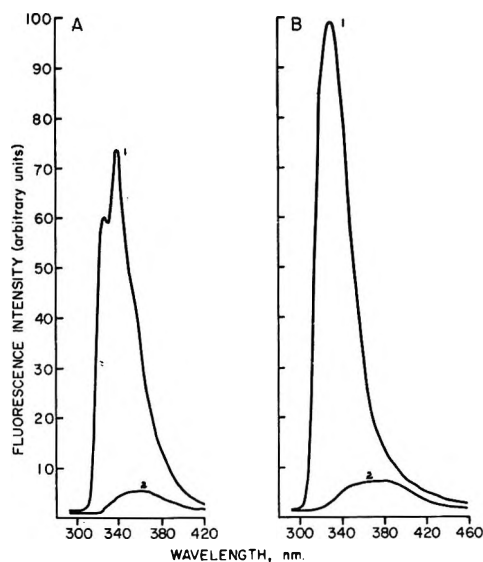


Figure 1. A. Fluorescence spectra of 2-naphthalenesulfonic acid: 1, at pH 7 and $H_0 - 2$; 2, at $H_0 - 10$. B. Fluorescence spectra of 1-naphthalenesulfonic acid: 1, at pH 7 and $H_0 - 2$; 2, at $H_0 - 10$. The naphthalenesulfonic acid concentration in each case was $1.0 \times 10^{-6} M$.

cence of 2-naphthalenesulfonic acid occurs beginning at $H_0 < -3$ (Figure 1). The fluorimetric titration of the 1-isomer reaches a minimum and constant fluorescence intensity at $H_0 \sim -6$ with a total red shift of 3300 cm^{-1} while that for the 2-isomer reaches a minimum at $H_0 \sim -8$, and exhibits a red shift of 1500 cm^{-1} and a loss of vibrational structure present in the fluorescence at low acidities. The absorption spectra of the 1-isomer do not begin to change appreciably until $H_0 - 6$ is attained whereupon the 1L_a band begins to red shift and overlaps the 1L_b band envelope (Figure 2). The absorption spectra of the 2-isomer do not change until an acidity of $H_0 - 7$ is reached (Figure 2). Appreciable shifting of neither the 1L_a or 1L_b band is observed for the 2-isomer but an increase in absorbance with increasing acidity occurs. For neither isomer is the absorptiometric titration complete by the time the most acidic sulfuric acid solution ($H_0 - 10$) is employed. The spectral features of the naphthalenesulfonic acids in some representative solutions along with those of naphthalene are presented in Table I.

The failure of the absorption spectra to change with acidity in the same region where the fluorescence spectra change indicates that the quantum yields of fluorescence of the naphthalenesulfonic acids are acidity dependent and thus the fluorimetric titrations correspond to ionizations of the sulfonic acids in an electronically excited state. The pK_a^* values, estimated from the midpoints of the fluorimetric titration curves, are found to be -3.7 for the 1-isomer and -5.1 for the 2-isomer. That the fluorescence spectra of both isomers shift to longer wavelengths with increasing acidity suggests that these molecules become more basic in the fluores-

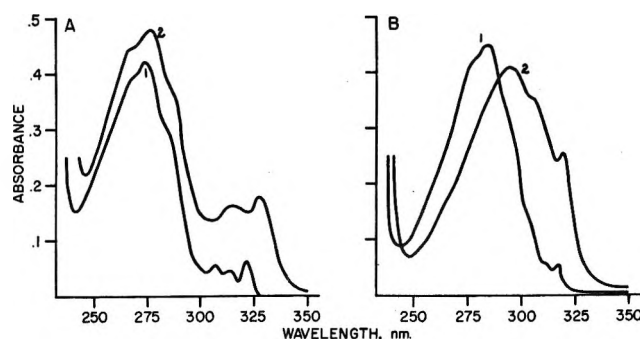


Figure 2. A. Absorption spectra of 2-naphthalenesulfonic acid: 1, at pH 7 and $H_0 - 2$; 2, at $H_0 - 10$. B. Absorption spectra of 1-naphthalenesulfonic acid: 1, at pH 7 and $H_0 - 2$; 2, at $H_0 - 10$. The naphthalenesulfonic acid concentration in each case was $1.0 \times 10^{-4} M$.

Table I: Absorption ($\bar{\nu}_a$) and Fluorescence ($\bar{\nu}_f$) Frequencies of Naphthalene and the Naphthalenesulfonic Acids in the Anion (pH 4), Neutral ($H_0 - 2$), and Protonated ($H_0 - 9$) Forms (Frequencies Are Given in $\text{cm}^{-1} \times 10^{-4}$)

	$\bar{\nu}_a({}^1L_b)^a$	$\log \epsilon$	$\bar{\nu}_a({}^1L_a)^a$	$\log \epsilon$	$\bar{\nu}_f^a$
Naphthalene (in 10% aqueous methanol)					
	3.20	2.40	3.62	3.62	2.99
1-Naphthalenesulfonic Acid					
Anion	3.15	2.65	3.50	3.61	3.02
Neutral	3.15	2.65	3.50	3.61	3.02
Cation	3.15 ^b	3.34 ^b	3.31 ^b	3.56 ^b	2.69
2-Naphthalenesulfonic Acid					
Anion	3.10	2.83	3.62	3.62	2.95
Neutral	3.10	2.83	3.62	3.62	2.95
Cation	3.06 ^b	3.22 ^b	3.62 ^b	3.19 ^b	2.80

^a $\bar{\nu}_a({}^1L_b)$ was taken at the 0-0 band of the 1L_b absorption. Due to the lack of distinct structure in the 1L_a absorption and in some of the fluorescence spectra $\bar{\nu}_a({}^1L_a)$ and $\bar{\nu}_f$ were taken at the band maxima. This corresponds to the second vibronic feature in the structured fluorescence spectra. ^b These are approximate values, as the cation absorptions are not isolated at this acidity.

cent state. It is possible, employing the shifts in the fluorescence spectra and the excited state dissociation constants in conjunction with the Förster cycle,⁵ to estimate the ground state pK_a values for the corresponding equilibria. The ground state pK_a value of the 1-isomer is found to be -10.6 , while that for the 2-isomer is estimated to be -8.3 . These results are in accord with the partial absorptiometric titration data obtained and are far more acidic than the pK_a values obtained for the equilibria between the neutral sulfonic acids and the sulfonate anions. It is suggested that the pK_a values of -10.6 and -8.3 correspond to prototropic equilibria, in the ground state, between the neutral sulfonic acids and the corresponding sulfonic acidium ions: $\text{RSO}_3\text{H} + \text{H}^+ \rightleftharpoons \text{RSO}_3\text{H}_2^+$.

That the protonations of the naphthalenesulfonates are reflected neither in the absorption nor in the fluorescence spectra while the protonations of the neutral sulfonic acids are apparent in both types of spectra, leads to the conclusion that the site of protonation (oxygen atom) in the sulfonate anion is essentially uncoupled, electronically, to the aromatic system while the oxygen atom protonated in the neutral sulfonic acid is strongly coupled to the aromatic system. Thus the three oxygen atoms in each sulfonate anion are not equivalent to one another. That the excited state pK_a^* values of the protonated sulfonic acids are less acidic than the ground state pK_a values indicated that in the fluorescent state, charge transfer from the naphthyl moieties to the sulfonic acid group occurs to a greater extent than in the ground state.

The absorption spectra of the naphthalenesulfonic acids are similar in appearance to those of naphthalene, the ratios of the molar absorptivities of the 1L_b bands to those of the 1L_a bands being about the same as that for naphthalene (~ 0.1). This fact suggests that the transitions in the anions and neutral acids are localized on the naphthalene rings. The weakness of the 1L_b transition is due to its symmetry forbiddenness. However, substituents on or in the naphthyl ring, as in quinoline, isoquinoline and the naphthylamines, which couple with the aromatic system, tend to reduce the symmetry of the naphthalene ring and thereby reduce the forbiddenness of the 1L_b transition.⁶ Consequently, in quinoline, isoquinoline, and the naphthylamines $\epsilon^1L_b/\epsilon^1L_a \sim 1$. Since enhancement of the 1L_b transition is small for the naphthalenesulfonates, it can be concluded that sulfonate or sulfonic acid substitution does not substantially affect the symmetry of the π -electron system of naphthalene. However, in the sulfonic acidium ions, charge transfer to the exocyclic groups, in the excited state, reduces the symmetry of the π -systems, removing the forbiddenness of the 1L_b transitions.

Relative to the 1L_b and 1L_a absorption bands of naphthalene, substitution of a sulfonate anion or sulfonic acid group in the 2-position of naphthalene produces a greater shift of the 1L_b band than does substitution in the 1-position of naphthalene. The opposite is true for the 1L_a band. This is in accord with the longitudinal (long axis) polarization of the ${}^1L_b \leftarrow {}^1A$ transition and with the transverse (short axis) polarization of the ${}^1L_a \leftarrow {}^1A$ transition in naphthalene. The fluorescences of the 2-substituted naphthalene sulfonate and sulfonic acid are shifted relative to the fluorescence of naphthalene to a greater extent than are the fluorescences of the

corresponding 1-substituted compounds. This suggests that the fluorescences of these compounds arise from the 1L_b state since the 1L_b state is lowest in the absorption spectrum. The electronic transition is localized on the naphthalene so that no dramatic excited state thermal relaxation processes which may alter the ordering of electronic states should occur. The fluorescences show approximate mirror image relationships with the 1L_b absorption bands, and substituent orientation and transition polarization correlate approximately the same for fluorescence as for absorptive transitions between the same states. However, it is obvious that protonation of the 1-sulfonic acid produces a much greater fluorescence shift than protonation of the 2-isomer. The opposite is to be expected if the fluorescent states in both protonated isomers are 1L_b . As a result of the greater shifting of the fluorescence of the 1-naphthalene sulfonic acid upon protonation, which parallels (approximately) the shifting of the 1L_a absorption band of the 1-isomer upon protonation, and the greater sensitivity of the 1L_a band of naphthalene to 1-substitution, it is proposed that while fluorescence of the protonated 2-naphthalenesulfonic acid occurs from the 1L_b state, in the protonated 1-naphthalenesulfonic acid fluorescence occurs from the 1L_a state. This is a result of the red shift of the 1L_a state relative to the 1L_b state, in the 1-isomer, upon protonation, which probably leaves the long wavelength end of the 1L_a band at lower energy than the O-O band of the 1L_b band. Thus the 1L_a state would be the lowest excited singlet state in the protonated 1-isomer.

If the neutral 1-naphthalenesulfonic acid does, in fact, fluoresce from the 1L_b state while the protonated 1-isomer fluoresces from the 1L_a state, it is possible that the application of the Förster cycle to equilibria involving these species is not, strictly speaking, valid since interconversion between the two excited conjugate species entails a change in electronic configuration along with the chemical reaction,⁷ a process which violates the assumption of equal protonation entropies in ground and electronically excited states, upon which the validity of the Förster cycle rests. However, that there is good agreement between the Förster cycle calculation for the 1-isomer and the fluorimetric and absorptiometric titrations suggests that the entropy error due to fluorescence from noncorresponding states may be too small to affect the general conclusions, at least in this case, obtained from Förster cycle calculations.

(6) H. H. Jaffé and M. Orchin, "Theory and Applications of Ultraviolet Spectroscopy," Wiley, New York, N. Y., 1962.

(7) H. H. Jaffé and H. L. Jones, *J. Org. Chem.*, **30**, 964 (1965).

Magnetic Circular Dichroism of Ferrocene and Substituted Ferrocenes: the d-d Transitions

by Dennis Nielson,¹ Daniel Boone,² and Henry Eyring*¹

Departments of Chemistry, University of Utah, Salt Lake City, Utah 84112
and University of Pittsburgh, Pittsburgh, Pennsylvania (Received September 1, 1971)

Publication costs assisted by the National Institutes of Health

The MCD spectra of the d-d transitions of ferrocene and some substituted ferrocenes are measured and found to fall into two distinct categories: one group of compounds giving absorption-like peaks and the other giving S shaped curves. It is found that the lowering of symmetry of the molecule is responsible for the difference.

Introduction

Due to its unique structure, ferrocene has been of great interest to theoreticians, and there have been various attempts made to describe its electronic structure and explain its spectrum, but all have fallen short of being completely satisfactory. In recent years, magnetic circular dichroism has come to be recognized as a useful tool in the study of electronic structure, and it has been previously used to study the d-d transitions in ferrocene.³ However, the results of a preliminary investigation of the MCD spectrum of ferrocene in this laboratory were in direct conflict with this earlier work, leading to further study of the problem.

An excellent discussion of MCD theory can be found in the review article by Buckingham and Stephens,⁴ or in more recent work.⁵ For the discussions to follow here, it is sufficient to know that there are three types of peaks possible in MCD spectra: an S shaped curve and two absorption-like curves, both of which may be either positive or negative in sign, and one of which is temperature dependent. The S shaped curve may occur when a given transition has a ground or excited state that is degenerate, and the point at which this type of curve crosses the base line corresponds to the absorption maximum. The first of the gaussian-shaped peaks is due to a mixing of states and is the only contribution to magnetic circular dichroism for a transition in which both the ground and excited states are nondegenerate, but which may occur for any transition. The temperature-dependent peak arises only when the ground state is degenerate, and it is due to the population difference in the states resulting from the degenerate ground state being split by the magnetic field. These three types of peaks have been called A, B, and C, respectively. The equations derived by Buckingham and Stephens⁴ for magnetic circular dichroism are

$$\theta(a \rightarrow j) = \frac{4\pi}{hc} N_a^{(0)} \times \left\{ \frac{4\omega_{ja}^{(0)} \omega^3 \Gamma_{ja} A(a \rightarrow j) (\omega_{ja}^{(0)2} - \omega^2)}{h [(\omega_{ja}^{(0)2} - \omega^2)^2 + \omega^2 \Gamma_{ja}^2]} + \right.$$

$$\left. \frac{\omega^3 \Gamma_{ja}}{(\omega_{ja}^{(0)2} - \omega^2)^2 + \omega^2 \Gamma_{ja}^2} \times [B(a \rightarrow j) + (C(a \rightarrow j)/kT)] \right\} H_z \quad (1)$$

$$A(a \rightarrow j) = \frac{1}{6} [\langle j | \hat{\mu} | j \rangle - \langle a | \hat{\mu} | a \rangle] \cdot 1m \{ \langle a | \hat{m} | j \rangle \times \langle j | \hat{m} | a \rangle \} \quad (2)$$

$$B(a \rightarrow j) = \frac{1}{3} 1m \sum_{k \neq a} \frac{\langle k | \hat{\mu} | a \rangle}{h\omega_{ka}^{(0)}} \cdot \langle a | \hat{m} | j \rangle \times \langle j | \hat{m} | k \rangle \quad (3)$$

$$C(a \rightarrow j) = \frac{1}{6} \langle a | \hat{\mu} | a \rangle \cdot 1m \{ \langle a | \hat{m} | j \rangle + \langle j | \hat{m} | a \rangle \} \quad (4)$$

where $\theta(a \rightarrow j)$ is the ellipticity through the $a \rightarrow j$ transition, and A, B, and C are the various contributions to the spectrum. Any number of the three terms may contribute for a given transition, although many times one term dominates. Ferrocene has a nondegenerate ground state, which eliminates the possibility of a contribution from $C(a \rightarrow j)$, but its excited state for the forbidden d-d transition is thought to be degenerate. Thus, both $A(a \rightarrow j)$ and $B(a \rightarrow j)$ may contribute to the MCD spectrum for ferrocene for this transition.

One method for extracting parameters from experimental data uses the damped oscillator model.⁶ If $[\theta]_{m1}$ and $[\theta]_{m2}$ are the maximum values, including sign, of the molar ellipticity of the S shaped curve for the peaks at longer wavelength (λ_1) and shorter wavelength

(1) University of Utah.

(2) University of Pittsburgh.

(3) H. Falk, *Monatsh. Chem.*, **100**, 411 (1969).

(4) A. D. Buckingham and P. J. Stephens, *Annu. Rev. Phys. Chem.*, **17**, 399 (1966).

(5) P. N. Schatz and A. J. McCaffery, *Quart. Rev., Chem. Soc.*, **23**, 4, 552 (1969); (b) D. J. Caldwell and H. Eyring, "The Theory of Optical Activity," Wiley-Interscience, New York, N. Y., 1971; (c) D. J. Caldwell, J. Thorne, and H. Eyring, *Annu. Rev. Phys. Chem.*, **22** (1971).

(6) B. Briat, et al., *J. Amer. Chem. Soc.*, **89**, 26, 7062 (1967).

Table I: Data for the d-d Transitions for Those Compounds Exhibiting Spectra of the Kind Shown in Figure 1

Compound	Solvent	Band I				Band II			
		Absorption		MCD		Absorption		MCD	
		λ_{\max}^a	ϵ_{\max}	λ_{\max}^a	$B/D \times 10^3$	λ_{\max}^a	ϵ_{\max}	λ_{\max}^a	$B/D \times 10^3$
Ferrocene	Cyclohexane	440	94	470	7.62	324	54	334	-8.7
<i>n</i> -Butyl ferrocene	Cyclohexane	435	97	462	4.43	324	53	334	-6.3
Hydroxymethylferrocene	Methanol	435	101	470	2.79	323	63	333	-11.2
1,1'-Dihydroxymethylferrocene	Methanol	435	143	470	2.15	323	68	333	-10.4

^a All wavelengths are in units of $m\mu$.

(λ_2) and S and Dif stand for their sum and difference, respectively, it is found that

$$A \simeq -\frac{1}{55.4} \frac{\Delta}{\lambda} (\text{Dif})/\epsilon_m \quad (5)$$

$$[B + (C/kT)]/D = -\frac{1}{32} \frac{\Delta}{\lambda} S \quad (6)$$

where Δ (band width) and λ_0 (wavelength of maximum absorption) are expressed in the same units (here nanometers) and Γ (width of half-maximum of the absorption peak) is expressed in cm^{-1} . The dipole strength may be estimated from the formula $D \simeq 9.2 \times 10^{-3} \epsilon_m/\lambda_0$ where ϵ_m is the maximum molar extinction coefficient, and the ratios A/D and $[B + (C/kT)]/D$ can be expressed as

$$A/D \simeq -1.97 \Gamma (\text{Dif})/\epsilon_m \quad (7)$$

$$[B + (C/kT)]/D \simeq -3.47 (S/\epsilon_m) \quad (8)$$

However, in ferrocene itself the d-d transitions display no evidence of being S shaped, so that the equation to be used in such a case is

$$[B + (C/kT)]/D \simeq -5.12[\theta]_{\text{mmax}}/\epsilon_m$$

where $[\theta]_{\text{mmax}}$ is the maximum value of the molar ellipticity. This is the equation used to calculate the values of B/D in Table I (Figure 1).

Experimental Section

Samples of ferrocene and the various substituted ferrocenes listed in Tables I and II were obtained from Aldrich Chemical Co. and Research Organic/Inorganic Chemical Corp. (Sun Valley, Calif.). Solutions were made using spectral grade cyclohexane and methanol obtained from Matheson Coleman and Bell. Sample solutions ranged in concentration from approximately 8–200 mg of ferrocene or substituted ferrocene in 25 ml of solution. Measurements were made using 1.00-mm, 5.00-mm, and 1.00-cm cells. The spectra were measured on a Cary 14 spectrophotometer (uv and visible absorption) and a Cary 60 spectropolarimeter with CD attachment and super conducting solenoid capable of approximately 50,000 G, both supplied and installed by the Cary Co. All measurements were made using a field strength of 45,000 G, with one exception which is discussed below.

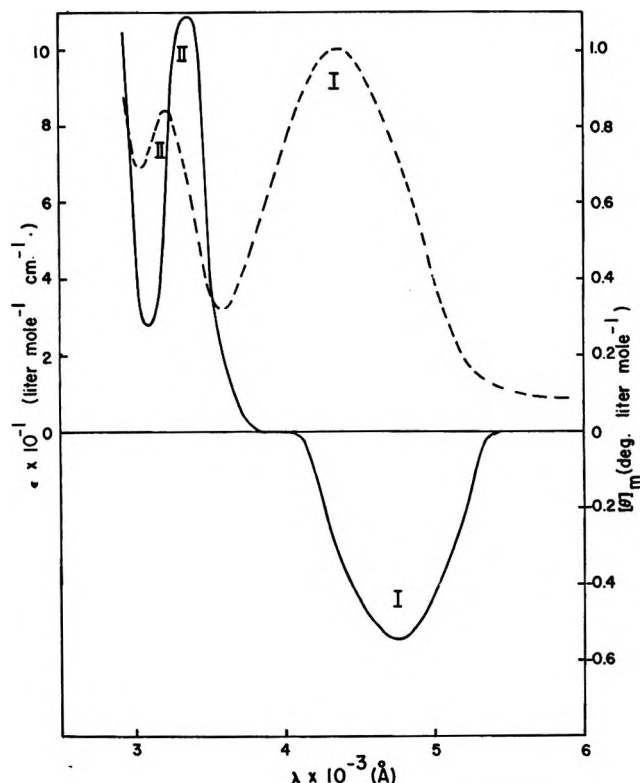


Figure 1. Absorption (---) and MCD (—) spectra of hydroxymethyl ferrocene.

Results and Discussion

Falk,³ using a Jouan-Roussel micrograph with a magnet attached, reported the MCD spectra of the 4400-Å transition of ferrocene and some substituted ferrocenes to be dominated in all cases by $A(a \rightarrow j)$. His work was done using a field strength of only 2830 G, which necessitated measuring the spectrum of the forbidden d-d transition of ferrocene with a highly concentrated solution. In the Cary 60, solutions whose optical density ($\log I_0/I_{\text{transmitted}}$) is greater than 2 give rise to artifacts which may appear to be part of the MCD spectrum. As it happens, in ferrocene one of these artifacts appears in the d-d transition, and, if the proper concentration and cell path length are used, an S shaped curve can be "created." For example, with a 172 mg/25 ml solution of ferrocene in cyclohexane and using a 1.00-cm cell, the peak appears to be a perfect example of an $A(a \rightarrow j)$ dominated spectrum. However, the same so-

Table II: Data for the d-d Transitions for Those Compounds Exhibiting Spectra of the Kind Shown in Figure 2

Compound	Solvent	Absorption		Band I			Band II		
		λ_{\max}^a	ϵ_{\max}	λ_1^a	λ_2^a	λ_{cross}^a	λ_{\max}^a	ϵ_{\max}	λ_{\max}^a
Acetylferrocene	Cyclohexane	447	301	485	415	440	358	148	364
1,1'-Diacetylferrocene	Cyclohexane	463	417	505	435	457			360
Carboxylic acid ferrocene	MeOH	443	278	480	410	435	355		353
1,1'-Dicarboxylic acid ferrocene	MeOH	447	313	485	417	440			357
Benzoyl ferrocene	Cyclohexane	462	613	502	433	455			387
1,1'-Dibenzoyl ferrocene	Cyclohexane	471	747	520	443	467			400
Ferrocene aldehyde	Cyclohexane	452	151	490	418	447			368
Chlorocarbonyl ferrocene	Cyclohexane	455	401	495	425	455			374
1,1'-Dichlorocarbonyl ferrocene	Cyclohexane	462	533	502	433	460			375
Methyl ferrocenoate	Cyclohexane	438	224	475	410	434			355
1,1'-Dimethyl ferrocenedioate	Cyclohexane	445	275	480	415	440			355

^a All wavelengths are in units of $m\mu$. ^b See ref 7, p 522.

lution placed in a 5.00-mm cell now has an optical density through the transition less than 2 and yields a perfect gaussian curve. It is possible that Falk observed a similar artifact with his equipment. It might be argued that, for some reason, at a lower field strength an S shaped curve might be observed. However, the MCD spectrum of a solution of ferrocene with an optical density less than 2 and measured at a field strength of 3.38×10^3 G, which is close to that used by Falk, continues to yield an absorption-like curve of negative sign. It should be pointed out that the spectra obtained by Falk for compounds other than ferrocene itself are in basic agreement with our own results, but the possibility of their containing artifacts is still very real. In the S-shaped curves obtained in this laboratory the appearance of the artifacts in the highly concentrated solutions are such that they alter position and peak height, without changing the essential form of the curves.

Figures 1 and 2 are typical examples of the two types of MCD spectra observed, corresponding to the data of Tables I and II, respectively. Of the compounds studied, those whose cyclopentadienyl rings are substituted with a carbonyl containing group give S shaped curves (see Figure 2 and Table II). In these same compounds, *i.e.*, those containing C=O, a peak at $\sim 3550 \text{ \AA}$ partially overlaps the S shaped curve of the d-d transition, making the calculations of A/D and B/D questionable at best. The other compounds, including ferrocene, give the absorption-like curves of Figure 1, all of which are negative in sign for the 4400 \AA transition. In Table II the wavelengths for ϵ_{\max} or $[\theta]_m$ for band II are listed where values can be conveniently assigned. Often the wavelength for $[\theta]_m$ was easily discernible while that for ϵ_{\max} was not.

The data reviewed by Scott and Becker⁷ and some later work by Armstrong, Carroll, and McGlynn⁸ are typical of the various attempts which have been made to describe the electronic structure of ferrocene. In most of the work discussed by Scott and Becker the bonding in ferrocene is considered to be the result of the

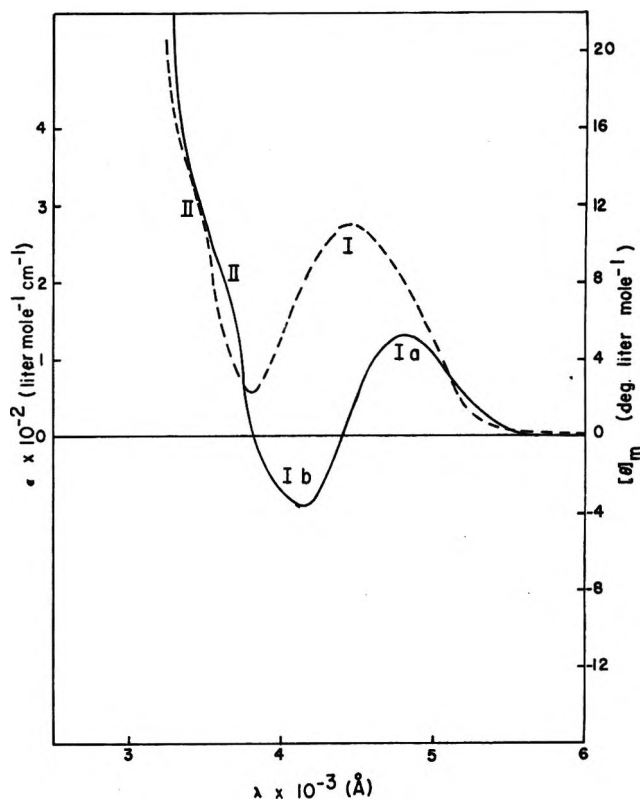


Figure 2 Absorption (---) and MCD (—) spectra of 1,1'-dimethyl ferrocenedioate.

overlap of the π orbitals of the cyclopentadienyl rings with the orbitals of the central metal. In this same discussion, however, the mixing of metal orbitals is taken into account in Moffitt's and Dunitz and Orgel's works. In the paper by Armstrong, *et al.*, the σ bond structure of the cyclopentadienyl rings is taken into account in describing the bonding of ferrocene. Although all of these treatments suffer from an excess of predicted tran-

(7) D. R. Scott and R. S. Becker, *J. Chem. Phys.*, **35**, 2, 516 (1961).

(8) A. T. Armstrong, D. G. Carroll, and S. P. McGlynn, *ibid.*, **47**, 3, 1104 (1967).

sitions, there is general agreement that the 4400-Å band is a d-d metal transition with some ring character, gaining its intensity mainly through vibronic stealing. The 3240-Å band (II) in ferrocene is thought to be a d-d transition containing substantial ring character. Assuming D_{5d} symmetry for ferrocene and considering only spin allowed transitions, there are three possible d-d transitions. These consist of one transition to a ${}^1E_{2g}$ excited state and two to ${}^1E_{1g}$ excited states from a ${}^1A_{1g}$ ground state. A recent paper by Sohn, Hendrickson, and Gray⁹ has shown the 4400-Å transition to consist of two overlapping transitions by an investigation of the single crystal absorption spectrum of ferrocene at liquid helium temperature. Using ligand field theory and including configuration interactions in their calculations they obtained excellent agreement with experimental results for the d-d transitions. Assuming their results to be correct, band II in ferrocene is due to a ${}^1A_{1g} \rightarrow {}^1E_{1g}$ transition arising from a change in electronic configuration of $e_{2g}{}^2a_{1g}{}^2 \rightarrow e_{2g}a_{1g}{}^2e_{1g}$. Band I consists of a ${}^1A_{1g} \rightarrow {}^1E_{1g}$ transition at 4580 Å due to the change of $e_{2g}{}^2a_{1g}{}^2 \rightarrow e_{2g}{}^2a_{1g}e_{1g}$, and a transition of ${}^1A_{1g} \rightarrow {}^1E_{2g}$ type at 4170 Å arising from the same change in electronic configuration as band II. Configuration interaction must account for the energy difference between band II and Ib.

In the absorption spectra of substituted ferrocenes there is a distinct increase in ϵ_{\max} over that of ferrocene. For the compounds in Table I the small increases in ϵ_{\max} are accounted for by the heavy atom effect, and, although quantum mechanical calculations will give nonzero, but very small, oscillator strengths for such compounds,⁸ these transitions still gain their intensity mainly through vibronic stealing. Thus, the symmetry of the orbitals responsible for binding the molecule together must be essentially unperturbed for these compounds. The compounds of Table II show a generally marked increase in ϵ_{\max} , which cannot be accounted for by the heavy atom effect. In these compounds the possibility of some overlap between the π orbitals of the carbonyl group with those of the ring in certain conformations constitutes a perturbation of molecular symmetry, and it is this which accounts for much of the increase in the extinction coefficients. Also in these carbonyl substituted ferrocenes band II is shifted to ~ 3550 Å.

The interesting and useful character of MCD spectroscopy is manifest in the results listed in Tables I and II. For ferrocene and the other compounds of Table I, bands Ia and Ib appear as one peak (as in the absorption spectra) which is negative in sign while band II is positive. For the compounds of Table II the d-d transitions now appear as three peaks of alternating sign, so that while absorption spectroscopy shows little significant change and yields no new information in going from the first to the second set of compounds, magnetic circular dichroism measurements do. The appearance

of the two types of curves observed may be explained by considering eq 3 which consists of a sum of terms where the magnitude of each term depends upon the coupling between the ground and excited state with other states of the system. It has been found that if states which are strongly coupled have transition moments or components of transition moments at right angles, the signs of their B terms will be opposite.¹⁰ This rule does not determine absolute but only relative signs, and applies only to electronically allowed transitions or, as in the present case, an electronically forbidden transition which is allowed by a single vibration and where the absorption bands consists of a totally symmetric vibrational progression superimposed on a single electronic transition in this vibration.¹⁰ Assuming these conditions to be fulfilled in ferrocene, for which there is some evidence,⁹ the argument may proceed. States of symmetry E_{1g} transform like xz and yz while E_{2g} transforms like $x^2 - y^2$ and xy , thus E_{1g} and E_{2g} have components at right angles, so that strongly coupled states having these two symmetries will give B terms of opposite sign. Band II and Ib must be strongly coupled due to their common origin, and experimentally band II (${}^1A_{1g} \rightarrow {}^1E_{1g}$) is positive while band Ib (${}^1A_{1g} \rightarrow {}^1E_{2g}$) is negative. Band Ia (${}^1A_{1g} \rightarrow {}^1E_{1g}$) is negative for the compounds in Table I, indicating that it is coupling to a greater extent with a state or states other than ${}^1E_{2g}$, probably the higher energy states for which transitions are symmetry allowed. For the compounds in Table II the II and Ib bands are more allowed than for those in Table I so that Ia and Ib will increase their coupling. Because of the proximity of Ia and Ib the denominator of their mixing term in the $B(a \rightarrow j)$ is small, so that a small increase in their coupling will produce a large effect and thus may dominate the sum and change the sign of the B term. Therefore, band Ia is seen in solution at room temperature in the MCD spectra of the carbonyl substituted compounds of Table II and should also be seen in other substituted ferrocenes not investigated here where the perturbation of the system is sufficient. It should be noted as a supporting argument that the symmetry of the molecular orbitals of the carbonyl substituted ferrocenes binding the molecule together is not destroyed, for if it were, 4-6 peaks would appear in the MCD spectra of their d-d transitions where only three are observed. Also, the width of band I in the ferrocene-like spectrum of Figure 1 is approximately equal to the width of the band obtained by the summation of bands Ia and Ib of Figure 2.

Thus the MCD spectra of the compounds studied support the contention of Sohn, Hendrickson, and Gray in their assignments of the d-d transitions of ferrocene and show the usefulness of magnetic circular

(9) Y. S. Sohn, D. N. Hendrickson, and H. B. Gray, *J. Amer. Chem. Soc.*, **93**, 15, 3603 (1971).

(10) B. Briat, *ibid.*, **90**, 17, 3691 (1968).

dichroism measurements in easily revealing information which must be sought at great lengths by other means.

Conclusions

1. In the measurement of MCD spectra it should be reiterated that caution must be exercised in avoiding the very real danger of the appearance of artifacts in experimental curves. In the Cary 60, samples should have an optical density less than two through regions of absorption.

2. The 4400-Å band of ferrocene consists of two overlapping peaks due to d-d transitions in the metal.

3. The symmetry assignments for the excited states made by Sohn, Hendrickson, and Gray⁹ can be used as the basis of a reasonable interpretation of the signs of the observed bands in the MCD spectra of the compounds studied.

Acknowledgment. The authors wish to thank the National Science Foundation, Grant GP-28631X, National Institute of Health, Grant GMI2862-07, U. S. Army, Grant DA ARO-D-31-1240G1110, and the American Chemical Society, Grant PRF 753-C, for support of this work.

High-Resolution Carbon-13 Nuclear Magnetic Resonance Spectra and Substituent Effects for Monohalobenzenes

by A. R. Tarpley, Jr.,¹ and J. H. Goldstein*

Chemistry Department, Emory University, Atlanta, Georgia 30322 (Received July 29, 1971)

Publication costs borne completely by The Journal of Physical Chemistry

Analysis of high-resolution ¹³C nmr spectra has provided all long-range ¹³CH coupling constants and their relative signs in chloro-, bromo-, and iodobenzene. Also, all directly bonded ¹³CH coupling constants and ¹³C chemical shifts for these compounds and for fluorobenzene are reported. These ¹³CH coupling constants are compared with coupling values in the vinyl halides and are shown to be related to halogen substituent electronegativity. In all cases, three-bond ¹³CH coupling constants are found to be larger in magnitude than the two-bond coupling values. Substituent contributions to the ¹³CH coupling constants and ¹³C chemical shifts for the monohalobenzenes are calculated relative to benzene which, assuming additivity of substituent effects, account for 63 previously determined long-range ¹³CH coupling constants in symmetrical *o*- and *m*-dihalobenzenes to within an average deviation of only 0.18 Hz. The assumption of additivity of monohalobenzene substituent effects also accounts very well for the previously determined directly bonded ¹³CH coupling constants and ¹³C chemical shifts in these same dihalobenzenes. However, due to the uniform experimental conditions employed throughout and the relatively small estimated errors in the parameters, significance is attached to a relatively small number of observed anomalous deviations from additivity predictions.

Introduction

Despite the well-known inherent difficulties with the ¹³C nucleus, the use of very stable field-frequency locked ¹³C spectrometers has allowed for time averaging of complete ¹³C spectra at natural isotopic abundance for relatively long periods, yielding resolution of 1 Hz or better in some cases.²⁻¹¹ This in turn has made possible complete analyses of high-resolution ¹³C spectra including relative signs of the coupling constants, at least in the more favorable instances. Recent studies^{10,11} have demonstrated the applicability of systematic, iterative, high-resolution analysis and substituent effect studies from the ¹³C-nmr spectra of molecules of up to five-spin complexity.

¹³C chemical shifts for the monohalobenzenes have been previously reported.¹² Also, Roberts and

(1) NDEA Fellow, 1967-1970; Tennessee Eastman Fellow, 1970-1971.

(2) (a) F. J. Weigert and J. D. Roberts, *J. Amer. Chem. Soc.*, **89**, 2967 (1967); (b) F. J. Weigert and J. D. Roberts, *ibid.*, **90**, 3543 (1968).

(3) F. J. Weigert, Ph.D. Dissertation, California Institute of Technology, Pasadena, Calif., 1968.

(4) F. J. Weigert and J. D. Roberts, *J. Phys. Chem.*, **73**, 449 (1969).

(5) G. Miyazima, Y. Utsumi, and K. Takahashi, *ibid.*, **73**, 1370 (1969).

(6) K. M. Creceley, R. W. Creceley, and J. H. Goldstein, *ibid.*, **74**, 2680 (1970).

(7) K. Takahashi, T. Sone, and K. Fujieda, *ibid.*, **74**, 2765 (1970).

(8) K. M. Creceley, R. W. Creceley, and J. H. Goldstein, *J. Mol. Spectrosc.*, **37**, 252 (1971).

Weigert,^{2a} with the aid of selective deuteration, have obtained long-range ^{13}C coupling constants which account very nicely for the observed high-resolution ^{13}C spectrum of benzene. However, since the benzene molecule poses a seven-spin problem for ^{13}C analysis, rigorous iterative computer techniques were not employed. In no case as yet, however, have long-range ^{13}C coupling constants been previously reported for the monohalobenzenes.

In the present study, high-resolution ^{13}C spectra have been obtained under very uniform experimental conditions and completely analyzed, yielding the long-range ^{13}C coupling constants with their relative signs for the parent molecule, benzene, and for chloro-, bromo-, and iodobenzene. Also, the directly bonded ^{13}C coupling constants and ^{13}C chemical shifts for the above compounds and for fluorobenzene are reported. The long-range ^{13}C coupling constants from these analyses are compared to ^{13}C coupling constants observed for the vinyl halides. In addition, both the directly bonded and long-range ^{13}C coupling constants are related to substituent electronegativity, E_x . In all cases it is observed that three-bond ^{13}C coupling constants are larger in magnitude than are the two-bond couplings. Also, substituent effects are calculated and reported for the monohalobenzenes relative to the benzene parameters determined from iterative analysis. By the assumption of additivity of these substituent effects, long-range ^{13}C coupling constants, directly bonded ^{13}C coupling constants, and ^{13}C chemical shifts are calculated which account quite well for the corresponding couplings and shifts previously reported for *o*- and *m*-dihalobenzenes.^{10,11} Several deviations from the additivity rule are clearly outside the limits of experimental error. Of these relatively few cases the most prominent are believed to reflect the effects of steric interaction.

Experimental Section

All compounds used in this study were the commercially available materials requiring no further purification as indicated by their physical properties and proton nmr spectra. Acetone was used as a solvent and also conveniently allowed for internal proton stabilization on its methyl resonance. Samples were prepared as approximately 50 mol % solutions and sealed in 13-mm nmr tubes. A small part of these solutions was withdrawn for proton analysis at 90 MHz.

All ^{13}C -nmr (cmr) spectra were obtained in the frequency sweep mode with a Bruker Scientific HFX-90 spectrometer operating at 22.62 MHz. Since proton noise decoupling was not employed and the complete ^{13}C spectrum was obtained in all cases, it was necessary to accumulate narrow-range spectra for up to 10 hr with a Fabri-Tek 1074 signal averaging system. The most narrow sweep width available (12 Hz) and a sweep rate of 0.3 Hz/sec were used throughout. Under these

conditions, it is estimated that the absolute chemical shifts are good to approximately 2.0 Hz or 0.1 ppm. However, the uniform experimental conditions employed make the relative chemical shifts internally very consistent, to at least 0.5 Hz or 0.025 ppm. The long-range coupling constants are estimated to be reliable to within about 0.1 Hz.

All ^{13}C spectra were analyzed using the iterative program LAOCOON-III¹³ on a Digital Equipment Co. PDP-10 computer. The monohalobenzenes of this series were treated as ABB'CC'X (X = ^{13}C) spin systems with each monohalobenzene molecule consisting of four separate six-spin problems. (Trial calculations using an ABCDEX model and reasonable isotopic shift differences showed no advantage over the ABB'CC'X results for C_o and C_m ^{13}C patterns.) Benzene, itself, was analyzed rigorously as a seven-spin system. Trial parameters for these analyses were taken from the ^{13}C work of Weigert and Roberts on benzene^{2a} and from previous papers on the ^{13}C spectra of symmetrical *o*- and *m*-dihalobenzenes.^{10,11}

The quality of the spectral fitting is indicated by the low root-mean-square deviations obtained between calculated and observed frequencies, in all cases less than 0.1 Hz. Visual comparisons of observed spectra with theoretical Lorentz-shape patterns indicated that the computed intensities were satisfactory in each case. However, some allowance was made for diminished intensities in a few cases where multiple resonance lines were closely spaced, since slow passage conditions were not employed in obtaining the spectra.

Results

Shown in Table I are the ^{13}C chemical shifts and ^{13}C coupling constants for benzene and the monohalobenzenes of this series. For comparison, the ^{13}C coupling constants determined by Roberts and Weigert^{2b} for benzene are given in parentheses after the values for benzene found in the present study from iterative analysis. The substituent effects determined for the ^{13}C couplings in the monohalobenzenes are given in brackets after the observed values. All coupling constants are given in Hz while the ^{13}C chemical shifts are given in ppm relative to benzene. Therefore, the ^{13}C chemical shifts reported for the monohalobenzenes in ppm relative to benzene are also the substituent effects on the shifts, by definition. C_s refers to the carbon directly bonded to the substituent while C_o refers to the carbon two bonds removed from the substituent. C_m refers to the carbon three bonds re-

(9) K. M. Creceley, Ph.D. Dissertation, Emory University, Atlanta, Ga., 1970.

(10) A. R. Tarpley, Jr., and J. H. Goldstein, *J. Mol. Spectrosc.*, **37**, 432 (1971).

(11) A. R. Tarpley, Jr., and J. H. Goldstein, *ibid.*, **39**, 275 (1971).

(12) H. Spiesscke and W. G. Schneider, *J. Chem. Phys.*, **35**, 731 (1961).

(13) S. Castellano and A. A. Bothner-By, *ibid.*, **37**, 1891 (1962).

Table I: ^{13}C Chemical Shifts,^a ^{13}CH Coupling Constants,^b and Substituent Effects^c for Monohalobenzenes^d

Com- pound (X=)	δ (^{13}C)	^{13}CH Coupling Constants				
		A				
	C_8	J_{12}	J_{13}	J_{14}	J_{15}	J_{16}
H	0.0	+1.11 (+1.0) ^e	+7.58 (+7.4)	-1.20 (-1.1)	+7.58 (+7.4)	+1.11 (+1.0)
F	-34.40
Cl	-5.63	-3.39 [-4.50]	+11.10 [+3.52]	-2.02 [-0.82]	+11.10 [+3.52]	-3.39 [-4.50]
Br	+6.02	-3.34 [-4.45]	+11.22 [+3.64]	-1.88 [-0.68]	+11.22 [+3.64]	-3.34 [-4.45]
I	+33.54	-2.41 [-3.52]	+10.73 [+3.15]	-1.85 [-0.65]	+10.73 [+3.15]	-2.41 [-3.52]
B						
	C_0	J_{12}	J_{13}	J_{14}	J_{15}	J_{16}
H	0.0	+158.77 (+157.5)	+1.11 (+1.0)	+7.58 (+7.4)	-1.20 (-1.1)	+7.58 (+7.4)
F	+13.41	+163.14 [+4.37]
Cl	-0.05	+164.84 [+6.07]	+1.41 [+0.30]	+7.85 [+0.27]	-1.24 [-0.04]	+4.95 [-2.63]
Br	-3.07	+165.77 [+7.00]	+1.44 [+0.33]	+7.91 [+0.33]	-1.24 [-0.04]	+5.32 [-2.26]
I	-9.15	+165.65 [+6.88]	+1.55 [+0.44]	+7.78 [+0.20]	-1.27 [-0.07]	+5.98 [-1.60]
C						
	C_m	J_{12}	J_{13}	J_{14}	J_{15}	J_{16}
H	0.0	+1.11 (+1.0)	+158.77 (+157.5)	+1.11 (+1.0)	+7.58 (+7.4)	-1.20 (-1.1)
F	-1.53	...	+162.00 [+3.23]
Cl	-1.43	+0.29 [-0.82]	+161.22 [+2.45]	+1.55 [+0.44]	+8.18 [+0.60]	-0.91 [+0.29]
Br	-1.86	+0.46 [-0.65]	+161.90 [+3.13]	+1.60 [+0.49]	+8.23 [+0.65]	-1.05 [+0.15]
I	-2.14	+0.74 [-0.37]	+161.43 [+2.66]	+1.44 [+0.33]	+8.15 [+0.57]	-1.25 [-0.05]
D						
	C_p	J_{12}	J_{13}	J_{14}	J_{15}	J_{16}
H	0.0	+7.58 (+7.4)	+1.11 (+1.0)	+158.77 (+157.5)	+1.11 (+1.0)	+7.58 (+7.4)
F	+4.43	+162.16 [+3.39]
Cl	+1.86	+7.37 [-0.21]	+0.87 [-0.24]	+161.30 [+2.53]	+0.87 [-0.24]	+7.37 [-0.21]
Br	+1.36	+7.39 [-0.19]	+0.86 [-0.25]	+161.55 [+2.7]	+0.86 [-0.25]	+7.39 [-0.19]
I	+0.68	+7.39 [-0.19]	+0.82 [-0.29]	+160.97 [+2.20]	+0.82 [-0.29]	+7.39 [-0.19]

^a All ^{13}C chemical shifts are given in ppm relative to benzene, and thus are the substituent effects. Positive values indicate higher field than benzene. ^b All coupling constants are in Hz. ^c Substituent effects on the ^{13}CH coupling constants, that is, the observed coupling minus the corresponding coupling in benzene, are given in brackets after the observed coupling constants. ^d The numbering is as shown in all cases. ^e The coupling constants in parentheses for X=H are from reference 1. ^f $^1J_{^{13}\text{C}-\text{F}} = 246.34$ Hz.

moved from the halogen substituent and C_p denotes the carbon four bonds from the halogen. In all cases, the numbering and subsequent chemical shift and coupling designations are in accord with the structures shown. The ^{13}C shifts and directly bonded ^{13}CH coupling constants reported in Table I for fluorobenzene were not obtained from a complete iterative analysis but were measured very carefully on a first-order basis using the narrow sweep range indicated earlier.

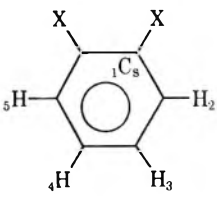
Tables II and III compare the ^{13}C chemical shifts

and ^{13}CH coupling constants observed in the *o*- and *m*-dihalobenzenes, respectively, with the corresponding values calculated by the assumption of additivity of the substituent effects in the monohalobenzenes. These additivity calculations were made in the standard manner.^{14,15} In all cases the numbering scheme

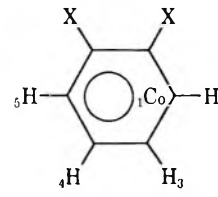
(14) R. W. Creely, J. M. Read, Jr., R. S. Butler, and J. H. Goldstein, *Spectrochim. Acta, Part A*, **24**, 685 (1968).

(15) H. B. Evans, Jr., A. R. Tarpley, and J. H. Goldstein, *J. Phys. Chem.*, **72**, 2552 (1968).

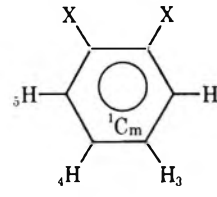
Table II: Observed and Calculated^a ¹³C Chemical Shifts and ¹³CH Coupling Constants in Symmetrical *o*-Dihalobenzenes^b



A



B



C

Compound (X=)	δ (¹³ C)	¹³ CH Coupling Constants			
		A			
	C _s	J ₁₂	J ₁₃	J ₁₄	J ₁₅
F	-21.80 (-20.99)
Cl	-3.61 (-5.68)	-3.53 (-3.09)	+11.57 (+11.37)	-1.85 (-2.06)	+7.92 (+8.47)
Br	+3.97 (+2.95)	-3.24 (-3.01)	+11.52 (+11.55)	-2.00 (-1.92)	+8.36 (+8.96)
I	+19.90 (+24.39)	-1.80 (-1.97)	+10.91 (+10.93)	-1.77 (-1.92)	+8.44 (+9.13)
	B				
	C _o	J ₁₂	J ₁₃	J ₁₄	J ₁₅
F	+11.51 (+11.88)	+164.56 (+166.37)
Cl	-1.90 (-1.48)	+166.53 (+167.29)	+1.89 (+1.85)	+8.41 (+8.45)	-1.23 (-0.95)
Br	-5.23 (-4.93)	+167.63 (+168.90)	+2.05 (+1.93)	+8.33 (+8.56)	-1.11 (-1.09)
I	-11.03 (-11.29)	+167.21 (+168.31)	+1.98 (+1.88)	+8.30 (+8.35)	-1.17 (-1.32)
	C				
	C _m	J ₁₂	J ₁₃	J ₁₄	J ₁₅
F	+3.91 (+2.90)	...	+165.25 (+165.39)
Cl	+0.62 (+0.43)	-0.02 (+0.05)	+164.04 (+163.75)	+1.11 (+1.31)	+8.63 (+7.97)
Br	-0.30 (-0.50)	+0.30 (+0.21)	+163.94 (+164.68)	+1.10 (+1.35)	+8.47 (+8.04)
I	-1.07 (-1.46)	+0.50 (+0.45)	+163.04 (+163.63)	+1.23 (+1.15)	+8.09 (+7.96)

^a The values given in parentheses below the observed values are calculated assuming additivity of the substituent effects reported for the monohalobenzenes in Table I. ^b The numbering scheme and designations are as indicated and are the same as in ref 10.

and designations are as indicated in the structure diagrams and are the same as in previous work.^{10,11}

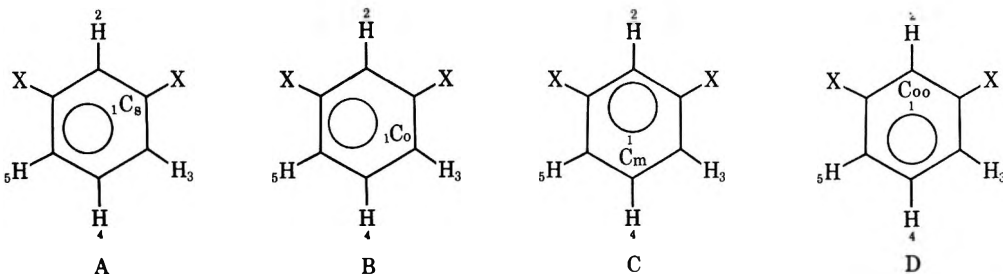
Shown in Table IV is a comparison of the differences in some long-range ¹³CH coupling constants for some symmetrical *p*-dihalobenzenes determined from ¹³CH satellite spectra¹⁶ and those predicted from additivity of the substituent effects given in Table I. The additivity predicted values are given in parentheses just below the observed values. The numbering employed is as shown in the structure diagram in Table IV.

Discussion

Shown in Figure 1 is a wide-range ¹³C natural abun-

dance spectrum of bromobenzene showing all carbons. A portion of the upfield C_p pattern and the C_s pattern appear to overlap in this spectrum but on a more narrow range these patterns are in fact separate. It is indeed fortunate that for this series of compounds only minimal problems with overlap of spectral patterns were encountered, none of which had any effect on the quality of the analyses. Spectra taken on more narrow ranges are shown for portions of the ¹³C spectral patterns arising from C_s, C_o, C_m, and C_p carbons in

(16) J. M. Read, Jr., R. W. Creely, and J. H. Goldstein, *J. Mol. Spectrosc.*, 25, 107 (1968).

Table III: Observed and Calculated^a ¹³C Chemical Shifts and ¹³CH Coupling Constants in Symmetrical *m*-Dihalobenzenes^b


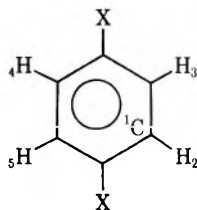
Compound (X=)	δ (¹³ C)	¹³ CH Coupling Constants			
		A			
	C ₈	J ₁₂	J ₁₃	J ₁₄	J ₁₅
F	-34.59 (-35.93)
Cl	-6.41 (-7.06)	-4.25 (-4.21)	-3.18 (-2.95)	+12.47 (+11.70)	-1.81 (-1.73)
Br	+5.40 (+4.16)	-3.91 (-3.99)	-2.94 (-2.85)	+12.30 (+11.87)	-1.75 (-1.73)
I	+32.77 (+31.40)	-2.94 (-2.78)	-2.14 (-2.08)	+11.45 (+11.30)	-1.75 (-1.90)
B					
	C ₀	J ₁₂	J ₁₃	J ₁₄	J ₁₅
F	+17.66 (+17.84)	...	+165.20 (+166.53)
Cl	+1.60 (+1.81)	+5.14 (+4.74)	+167.54 (+167.37)	+1.32 (+1.17)	+7.72 (+7.64)
Br	-1.91 (-1.71)	+5.37 (+5.13)	+168.43 (+168.55)	+1.36 (+1.19)	+7.74 (+7.72)
I	-8.43 (-8.47)	+6.06 (+5.79)	+168.27 (+167.85)	+0.99 (+1.26)	+7.78 (+7.59)
C					
	C _m	J ₁₂	J ₁₃	J ₁₄	J ₁₅
F	-2.13 (-3.06)	+165.60 (+165.23)	...
Cl	-2.28 (-2.86)	-0.53 (-0.62)	+0.67 (+0.73)	+164.39 (+163.67)	+0.67 (+0.73)
Br	-2.99 (-3.72)	-0.65 (-0.90)	+0.78 (+0.95)	+164.28 (+165.03)	+0.78 (+0.95)
I	-3.72 (-4.28)	-0.89 (-1.30)	+0.95 (+1.07)	+163.95 (+164.09)	+0.95 (+1.07)
D					
	C ₀₀	J ₁₂	J ₁₃	J ₁₄	J ₁₅
F	+25.25 (+26.82)	+165.50 (+167.51)
Cl	+0.01 (-0.10)	+170.14 (+170.91)	+5.42 (+5.22)	-1.47 (-1.28)	+5.42 (+5.22)
Br	-5.53 (-6.14)	+171.92 (+172.77)	+5.70 (+5.65)	-1.31 (-1.28)	+5.70 (+5.67)
I	-16.53 (-18.30)	+171.97 (+172.53)	+6.46 (+6.18)	-1.27 (-1.34)	+6.46 (+6.18)

^a The values given in parentheses below the observed values are calculated assuming additivity of the substituent effects reported for the monohalobenzenes in Table I. ^b The numbering scheme and designations are as indicated in all cases.

Figures 2, 3, 4, and 5, respectively. These second-order spectra were typically very sensitive to the rela-

tive signs of the couplings and in most cases dramatic differences were observed between the downfield and

Table IV: Observed^a and Predicted^b Differences in Some Long-Range ¹³CH Coupling Constants in Symmetrical *p*-Dihalobenzenes^c



Compound (X=)	$J_{14} - J_{13}$	$J_{16} - J_{13}$
Cl	-1.77 (-1.54)	+5.29 (+4.96)
Br	-1.93 (-1.88)	+5.48 (+5.18)
I	-2.28 (-2.50)	+5.65 (+5.37)

^a The observed values are given in Hz and were obtained by the analysis of ¹³CH satellite spectra in ref 16. ^b The predicted values given in parentheses are the differences in the long-range ¹³CH coupling constants determined by the assumption of additivity of the substituent effects for the monohalobenzenes given in Table I. ^c The numbering and designations are as shown in all cases.

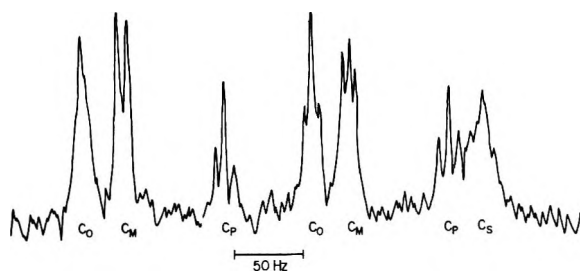


Figure 1. Wide-range natural abundance ¹³C nmr spectrum of bromobenzene with the carbons designated as in Table I. The spectrum was time-averaged for 32 scans using a 600-Hz sweep range and a sweep rate of 15 Hz/sec.

upfield portions of the spectrum arising from each carbon as is shown for instance in Figures 3 and 4 for C₀ and C_m carbons, respectively.

These ¹³C spectral patterns for the monohalobenzenes were found to be dependent on the order and relative differences between the proton chemical shifts. Therefore, as has been noted before,^{6,8-11} it was necessary to analyze the proton patterns for these compounds using the same sample and experimental conditions employed for the ¹³C measurements. Due to the large number of low intensity second-order lines available in most cases, only one spectral fit was obtained for the spectral pattern arising from each carbon, yielding the relative signs of the ¹³CH coupling constants. Therefore, the values given for the coupling constants and their relative signs are probably unique.

It is quite remarkable that all the substituent effects on the ¹³C chemical shifts reported in Table I agree to

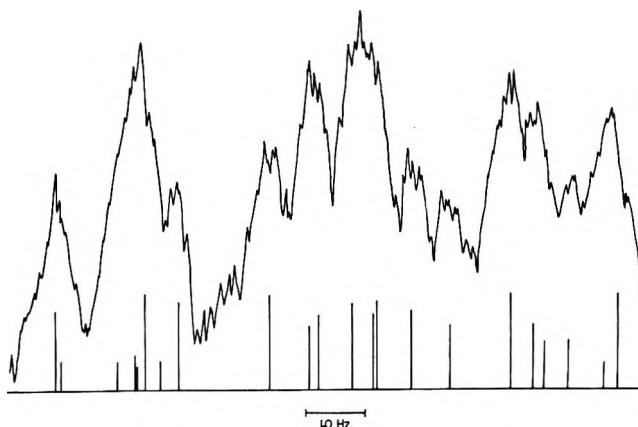


Figure 2. A portion of the observed ¹³C-nmr spectrum of C₀ in bromobenzene with calculated line plot. Time-averaged for 512 scans at 0.2 Hz/cm (12 Hz sweep width) and 0.3 Hz/sec.

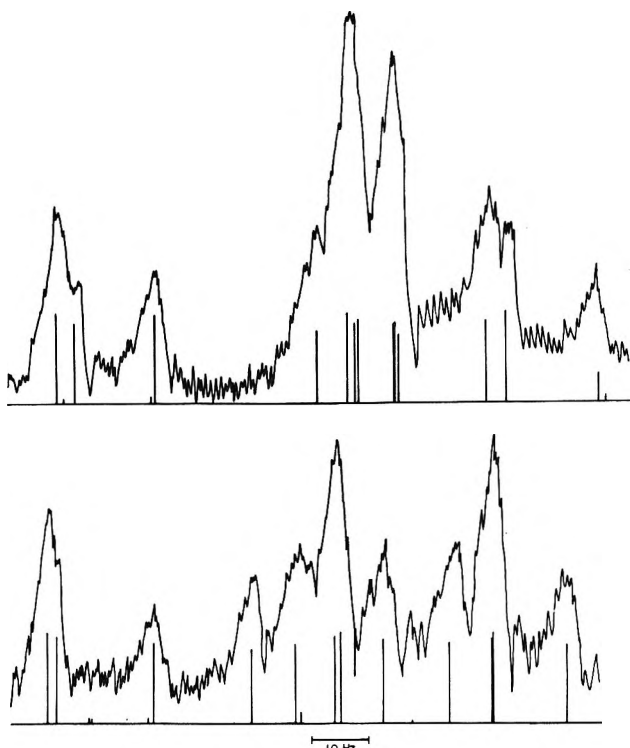


Figure 3. Observed portions of the upfield (upper) and downfield (lower) ¹³C nmr spectra of C₀ in bromobenzene with calculated line plots. Time-averaged for 256 scans at 0.2 Hz/cm and 0.3 Hz/sec.

within 1 ppm with those reported by Spiesecke and Schneider in 1961,¹² considering that the latter values were determined from 5 mol % cyclohexane solutions. In fact, in most cases these two sets of ¹³C chemical shift substituent effects are identical to within the experimental error reported for the values of Spiesecke and Schneider. Also, the observed trends for the ¹³C chemical shifts with substituent electronegativity, E_x ,¹⁷

(17) Halogen electronegativity values are taken from B. P. Dailey and J. N. Shoolery, *J. Amer. Chem. Soc.*, **77**, 3977 (1955).

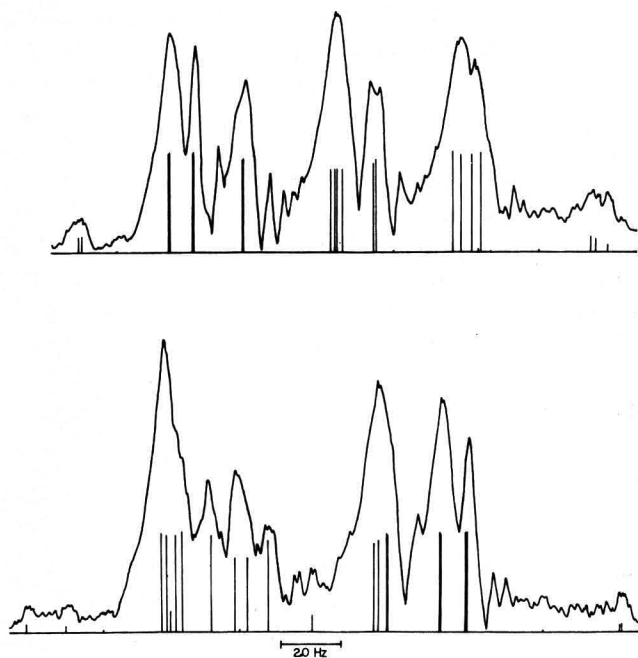


Figure 4. Observed upfield (upper) and downfield (lower) ^{13}C -NMR spectra of C_m in bromobenzene with calculated line plots. Time-averaged at 0.4 Hz/cm and 0.6 Hz/sec.

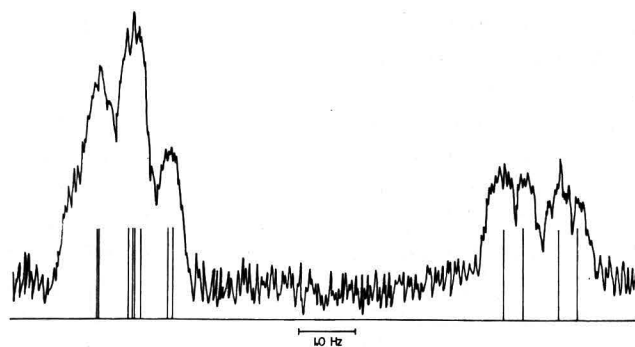


Figure 5. A portion of the observed upfield ^{13}C -NMR spectrum of C_p in bromobenzene with calculated line plot. Time-averaged at 0.2 Hz/cm and 0.15 Hz/sec.

are identical with those discussed previously by Sp. - secke and Schneider.

As shown in Table I, the largest substituent effects on long-range ^{13}C H coupling constants are noted for protons coupling with C_s . J_{12} , a two-bond coupling involving C_s , is about 4.6 Hz more negative than the two-bond ^{13}C H coupling in benzene. This effect is not unreasonable since the comparable couplings in monohaloethylenes, $J_{C\alpha H\beta}$, are negative^{4,6,8,18,19} and are more negative by approximately 5 Hz than is the two-bond ^{13}C H coupling in ethylene itself.²⁰ Also, J_{12} becomes more negative with increasing E_x . It has been predicted from molecular orbital theory that a comparable ^{13}C H coupling in the monohaloethylenes should increase with increasing E_x .²¹ Experimentally, however, this coupling in the monohaloethylenes⁸ is found to decrease with increasing E_x , in accord with the trend

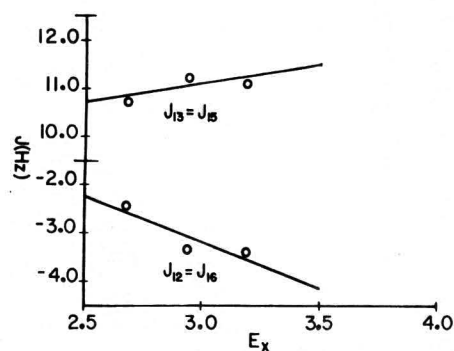


Figure 6. Plots of ^{13}C H coupling constants involving C_s vs. substituent electronegativity, E_x , in monohalobenzenes.

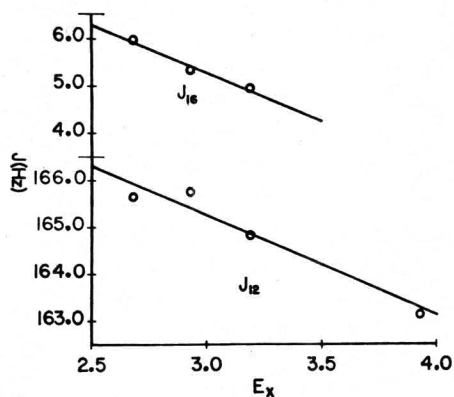


Figure 7. Plots of ^{13}C H coupling constants involving C_o vs. substituent electronegativity, E_x , in monohalobenzenes.

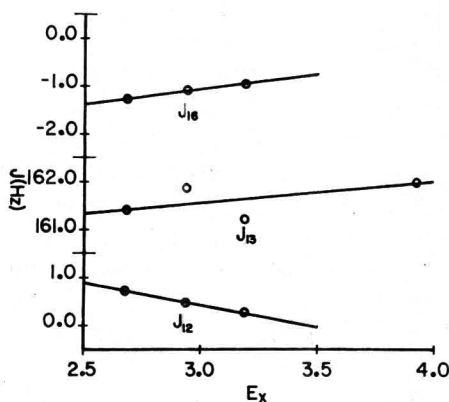


Figure 8. Plots of ^{13}C H coupling constants involving C_m vs. substituent electronegativity, E_x , in monohalobenzenes.

observed in the present study for J_{12} involving C_s . The substituent effect on the three-bond ^{13}C H coupling involving C_s , J_{13} , is to increase this coupling by ~ 3.5 Hz over the value in benzene. For the four-bond

(18) R. M. Lynden-Bell, *Mol. Phys.*, **6**, 537 (1963).

(19) L. Lunazzi and F. Taddei, *Spectrochim. Acta, Part A*, **25**, 553 (1969).

(20) R. M. Lynden-Bell and N. Sheppard, *Proc. Roy. Soc. Ser. A*, **269**, 385 (1962).

(21) V. M. S. Gil and S. J. S. Formosino-Simoes, *Mol. Phys.*, **15**, 639 (1968).

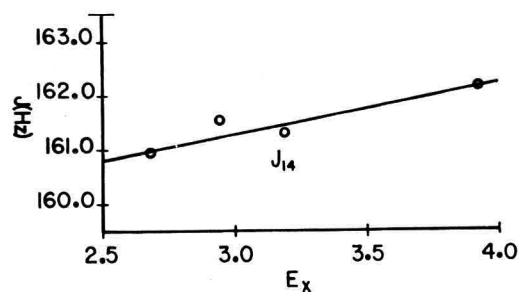


Figure 9. Plot of the directly bonded ^{13}CH coupling constant involving C_p vs. substituent electronegativity, E_x , in monohalobenzenes.

coupling involving C_s , J_{14} , the substituent effect is -0.8 Hz. Therefore the magnitude of the substituent effect falls off rapidly as the distance between the C_s carbon and the proton involved in the coupling increases. Also, the variation in the ^{13}CH coupling constant with variation in halogen substituent is smaller for J_{13} than for J_{12} while for J_{14} the variation is only 0.15 Hz, barely outside the experimental uncertainty in the coupling itself. As shown in Figure 6, the trends observed when the ^{13}CH coupling constants involving C_s are plotted against substituent electronegativity, E_x ,¹⁷ are opposite for J_{12} and J_{13} . J_{12} decreases with increasing E_x while J_{13} increases with increasing E_x . Also, as pointed out above, the substituent effects are negative for J_{12} but are positive for J_{13} . Some kind of polarization of charge in the molecular framework by electronegative halogen would seem to be a reasonable explanation for the above observations.

Plots of the ^{13}CH coupling constants involving the other types of carbon atoms, C_o , C_m , and C_p against E_x are given in Figures 7, 8, and 9, respectively. Only those coupling constants showing experimentally significant variations with halogen substituent are plotted. In each case, for the ^{13}CH coupling constants plotted, the correlation appears reasonably monotonic and has been assumed to be linear. The magnitudes of the variation in the couplings with E_x become progressively smaller on going from C_o to C_p , that is, upon increasing the distance between the carbon involved in the coupling and the substituent. In fact, at C_p the long-range ^{13}CH coupling constants observed for the monohalobenzenes are essentially constant even when the proton involved is ortho to the substituent. In the case of C_o and C_m the long-range couplings show significant variation only when the proton involved is ortho to the substituent. Also, the magnitudes of the observed substituent effects decrease in going from C_o to C_p and again at C_p the substituent effects are not experimentally significant. It appears, then, that the distances from the substituent of both the carbon and the proton involved in the ^{13}CH coupling constants are important factors in determining the magnitude and the variations of the substituent effects.

In all cases, for long-range ^{13}CH coupling constants in the monohalobenzenes of the present series, coupling constants over three bonds are observed to be larger in magnitude than coupling constants over two bonds. This observation is in agreement with most previous work (2a,2b,7,9,22-25) although a limited number of exceptions have been noted.⁷ This important phenomenon, which is quite unlike the behavior observed for proton-proton coupling constants and ^{13}CF coupling constants, will have to be accounted for in any acceptable theory of ^{13}CH coupling constants.

Additivity of proton chemical shifts in substituted benzenes has been studied extensively.²⁶ Very little work has been done concerning additivity of the ^{13}C chemical shifts, however, with the exception of a study carried out by Savitsky²⁷ for symmetrical *p*-dihalobenzenes. With the substituent effects presented in Table I, it is now possible to test additivity of substituent effects on ^{13}C chemical shifts for all substituted benzenes for which ^{13}C data are available. Tables II and III present this comparison between the observed ^{13}C chemical shifts and the calculated additivity values for symmetrical *o*- and *m*-dihalobenzenes. These same data are also presented graphically in Figure 10 where the line of 45° slope represents exact correspondence between the calculated and observed shifts.

For all twenty-eight ^{13}C chemical shifts in the symmetrical *o*- and *m*-dihalobenzenes, the average deviation from the 45° line in Figure 10 is 0.84 ppm. There are only seven cases in which the deviation between observed and calculated values is significantly greater than 1 ppm. The two of these cases where the deviation is largest occur for C_s in the *o*-dihalobenzenes. For C_s in *o*-diiodobenzene the deviation is 4.5 ppm, which is more than twice as great in magnitude as the next largest deviation, probably reflecting a large halogen-halogen steric interaction in this case. Likewise, C_s chemical shifts in the *m*-dihalobenzenes show relatively large deviations and account for three more of the seven cases where deviations are greater than 1 ppm. The fact that C_s , the carbon attached to the halogen substituent, consistently shows relatively large deviations suggests that there are interactions involving the halogens, whatever their origin. For the meta compounds halogen-hydrogen interactions are perhaps more likely than the halogen-halogen type since there is a proton ortho to both substituents. The

(22) G. J. Karabatsos, *J. Amer. Chem. Soc.*, **83**, 1230 (1961).

(23) G. J. Karabatsos, J. D. Graham, and F. Vane, *ibid.*, **83**, 1657 (1961).

(24) G. J. Karabatsos, J. D. Graham, and F. Vane, *ibid.*, **84**, 37 (1962).

(25) A. R. Tarpley, Jr., and J. H. Goldstein, *ibid.*, **93**, 3573 (1971).

(26) For example, H. B. Evans, Jr., A. R. Tarpley, and J. H. Goldstein, *J. Phys. Chem.*, **72**, 2552 (1968); J. M. Read, Jr., Ph.D. Dissertation, Emory University, Atlanta, Ga., 1967.

(27) G. B. Savitsky, *J. Phys. Chem.*, **67**, 2723 (1963).

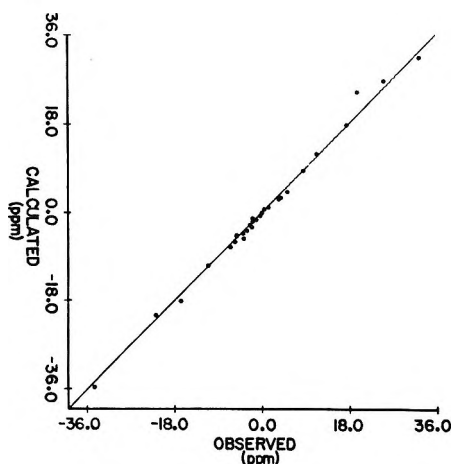


Figure 10. The ^{13}C chemical shifts calculated by additivity of monohalobenzene substituent effects vs. the ^{13}C chemical shifts observed in *o*- and *m*-dihalobenzenes.

remaining two deviations greater than 1 ppm occur for C_{oo} in *m*-dihalobenzenes, the only case available here where the directly bonded proton is ortho to both substituents. It is perhaps reasonable that the deviations at C_{oo} are also indicative of halogen-hydrogen interactions. It is interesting to note that significant deviations at C_{oo} are for cases involving the highly electronegative -F or very large -I. Excluding the seven cases above for C_s and C_{oo} , the other twenty-one ^{13}C chemical shifts are accounted for quite well by the assumption of additivity. For these 21 shifts, an average deviation from additivity of only 0.45 ppm is noted which is quite close to the estimated cumulative uncertainties in the calculated values. Certainly, ^{13}C chemical shift assignments in substituted benzenes made on the basis of additivity predictions should be quite unambiguous, considering the size of these deviations in relation to the total range of ^{13}C shifts normally observed as was evident for symmetrical *o*- and *m*-dihalobenzenes.^{10,11}

Malinowski²⁸ and Gutowsky and Juan²⁹ have discussed the additivity of substituent effects in the calculation of ^{13}CH directly bonded coupling constants in substituted methanes. Also, Malinowski, *et al.*,³⁰ have demonstrated that the additivity of ring substituent effects holds for the sp^2 systems, pyridine and pyrimidine. However, with the exception of a ^{13}CH satellite study of dihalobenzenes,¹⁴ additive substituent effects on directly bonded ^{13}CH coupling constants in substituted benzenes have not been reported. This latter study was hindered considerably by the lack of experimentally determined substituent effects for the monohalobenzenes.

Therefore, these monohalobenzene substituent effects which have now been experimentally determined and are given in Table I have been used to calculate additivity values for the directly bonded ^{13}CH coupling constants in the *o*- and *m*-dihalobenzenes. The

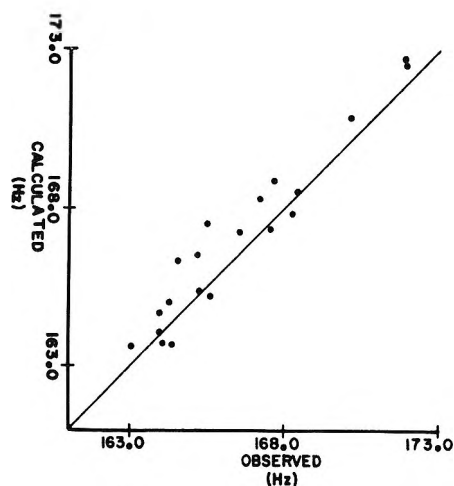


Figure 11. The directly bonded ^{13}CH coupling constants calculated by additivity of monohalobenzene substituent effects vs. the corresponding couplings observed in *o*- and *m*-dihalobenzenes.

individual calculated values are given in Tables II and III while the calculated and observed values are compared graphically in Figure 11. As before, the line of 45° slope represents exact correspondence between the calculated and observed coupling constants. Of the total of twenty observations, there are five observations which show deviations from additivity of more than 1 Hz. In each of these five cases the carbon involved in the coupling is either a C_o carbon or a C_{oo} carbon, both of which have directly bonded protons that are ortho to the halogen substituent. In the three of these five cases where the deviations are the largest, the halogen involved is fluorine. As has been pointed out earlier, the ^{13}CH directly bonded coupling constants for the difluorobenzenes¹¹ and for fluorobenzene were measured carefully on a first-order basis but were not obtained from iterative analysis. Therefore, the possibly larger error in these couplings for fluoro compounds than for the other halogens is perhaps partly responsible for the larger deviations in the case where $\text{X} = \text{F}$. However, it should be noted that for C_m in both the *o*- and *m*-difluorobenzene, the directly bonded ^{13}CH coupling constants are accounted for quite well by the assumption of additivity of substituent effects.

It is difficult to estimate the accuracy of the reported directly bonded ^{13}CH coupling constants. However, if the five cases above where the deviation from additivity is greater than 1 Hz are excluded, the average deviation from the 45° line for the other fifteen observations is less than 0.5 Hz which seems to be a reasonable indication that additivity relationships are holding. It is interesting to note, as shown in Figure 11,

(28) E. R. Malinowski, *J. Amer. Chem. Soc.*, **81**, 1471 (1959).

(29) C. Juan and H. S. Gutowsky, *J. Chem. Phys.*, **37**, 2198 (1962).

(30) E. R. Malinowski, L. F. Pollara, and J. P. Larmann, *J. Amer. Chem. Soc.*, **84**, 2649 (1962).

that all of the observed deviations from additivity of greater than 1 Hz are negative, that is, the observed coupling is less than that calculated. Since in all cases the observed substituent effects in the monohalobenzenes are positive, the effect of interactions on ^{13}C H directly bonded coupling constants in dihalobenzenes, then, is a reduction in the magnitude of the monohalobenzene substituent effect.

The assumption of additivity of substituent effects on nmr parameters has been quite useful in predicting H-H coupling constants in substituted benzenes.³¹ Also, Weigert and Roberts⁴ have found that geminal ^{13}C H couplings in bromo- and chloroethylenes can be predicted to within 1 Hz of the observed values using additivity relationships. In addition, the CCH couplings in maleic acid, diethyl maleate and diethyl fumarate are adequately calculated from the substituent effects observed in acrylic acid. Crecey⁹ has recently tested the validity of additivity for long-range ^{13}C H coupling constants in some nitrogen heterocycles using assorted data from the literature. In this latter study, deviations from additivity as large as 2-3 Hz were noted which were attributed to the relatively large error limits for some of the observed couplings and, of course, the wide variability in experimental conditions employed for obtaining the data. Therefore, although additivity relationships have been referred to in the treatment of long-range ^{13}C H coupling constants, additivity and deviations from additivity in these coupling constants have not been adequately demonstrated for a systematic collection of uniform data.

Therefore, the monohalobenzene substituent effects in Table I have been used to calculate additivity values for the 63 two-, three-, and four-bond ^{13}C -H coupling constants in the *o*- and *m*-dihalobenzenes, that is, all possible different long-range ^{13}C H couplings in the above dihalobenzenes except the fluoro derivatives for which no data are yet available. These calculated and observed values are compared in Figure 12. As before, the solid line of 45° slope in Figure 12 represents exact correspondence between the calculated and observed values. Because the uncertainties in the long-range coupling constants are conservatively estimated at 0.1 Hz and since the additivity calculated values involve this uncertainty three times, deviations from additivity greater than 0.4 Hz are believed to be experimentally significant. The dashed lines in Figure 12 represent this limit of ± 0.4 Hz.

As shown in Figure 12, there are only five observations which fall outside these dashed lines, the largest deviation being 0.77 Hz. Three of these deviations belong to J_{15} for C_5 in the *o*-dihalobenzenes, the deviation from the 45° line being about 0.6 Hz in each of the three cases. For this particular coupling the proton involved is ortho to the substituent and, in addition, the most likely pathway for transmission of the coupling is through that portion of the bonding

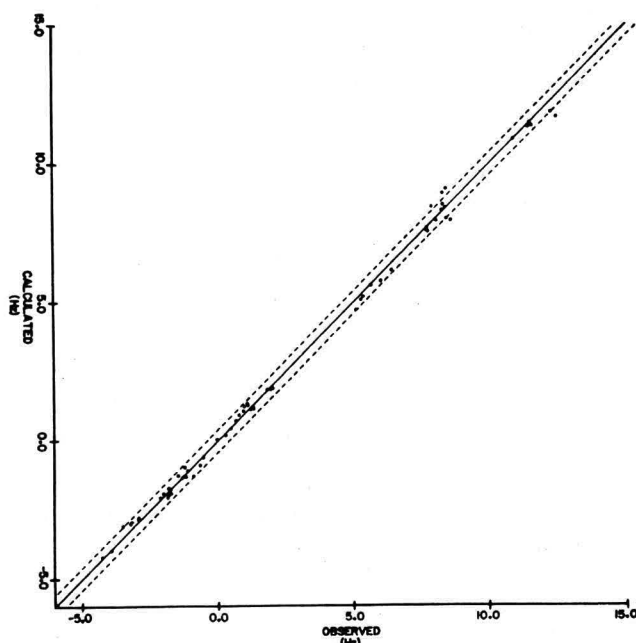


Figure 12. The long-range ^{13}C H coupling constants calculated by additivity of monohalobenzene substituent effects vs. the corresponding couplings observed in *o*- and *m*-dihalobenzenes.

framework to which both ortho substituents are attached. It appears reasonable, then, that this coupling might be likely to reflect any existing steric or other interactions between the halogen substituents in the disubstituted compounds. Another of the five significant deviations observed also corresponds to a coupling involving C_s , J_{14} in *m*-dichlorobenzene. The remaining deviation from additivity is for J_{15} involving C_m in *o*-dichlorobenzene where the proton involved is ortho to one of the two ortho halogen substituents. It is interesting to note that all of the five deviations are for three-bond ^{13}C H couplings rather than for two-bond couplings. Perhaps three-bond ^{13}C H couplings are more sensitive to interactions resulting from multiple substitution than are two-bond couplings for the same reason that three-bond couplings have been observed to be larger in magnitude than two-bond couplings in all cases thus far encountered in substituted benzenes.

Despite these deviations from additivity which are believed to be experimentally significant, the assumption of additivity of substituent effects generally accounts quite well for the observed long-range ^{13}C H coupling constants as the average deviation from the 45° line for all sixty-three couplings is only 0.18 Hz. In addition, excluding the five significant deviations above, the average deviation from additivity for the remaining 58 couplings is only 0.14 Hz which is barely

(31) For example, J. M. Read, Jr., R. W. Crecey, R. S. Butler, J. E. Loemker, and J. H. Goldstein, *Tetrahedron*, **10**, 1215 (1968).

larger than the estimated uncertainty in the coupling constants themselves. The value of uniform experimental conditions in substituent effect studies of this kind was evident here. The long-range coupling constants for benzene reported in Table I which were determined from iterative analysis using spectra taken under the same experimental conditions as for the monohalobenzenes and dihalobenzenes differ only slightly from the values of Roberts and Weigert^{2a} determined under somewhat different conditions. However, the use of these latter values for determination of monohalobenzene substituent effects increases the average deviation between observed and additivity calculated values for all 63 long-range coupling constants in the dihalobenzenes by more than 10%.

The data presented in Table IV lend even further support to the validity of additivity of substituent effects in disubstituted benzenes and also further indicate the quality and uniformity of the substituent effects given for the monohalobenzenes. Read, *et al.*,¹⁶ have previously analyzed the ^{13}C satellite spectra of symmetrical p -dihalobenzenes and have thus determined quite accurate differences in long-range

^{13}C coupling constants. For comparison with these observed differences additivity values have been calculated for the corresponding ^{13}C coupling constants in $para$ -dihalobenzenes which give, therefore, the calculated differences. As shown in Table IV, these calculated differences agree with the observed differences to within 0.3 Hz in all cases. This result is really quite remarkable and certainly demonstrates the consistency which is characteristic of systematic substituent effect studies.

In summary, the ^{13}C substituent effects presented here for monohalobenzenes provide a basis for meaningful investigations of additivity relationships in disubstituted benzenes. Results thus far obtained indicate that these substituent effects can be of great value in predicting ^{13}C nmr parameters for analysis purposes in further investigations of the spectra of substituted benzenes.

Acknowledgments. This study was supported in part by a grant from the National Institutes of Health. We also wish to acknowledge assistance provided by a Biomedical Sciences Support Grant.

Dielectric Relaxation of (a) p -Benzoquinones and (b) $\text{Me}_{4-n}\text{C}(\text{OMe})_n$ and

$\text{Me}_{4-n}\text{Si}(\text{OMe})_n$ ($n = 1-4$) in Benzene Solution

by C. W. N. Cumper* and R. F. Rossiter

School of Chemistry, Thames Polytechnic, London, S.E.18, England (Received August 2, 1971)

Publication costs borne completely by The Journal of Physical Chemistry

Dielectric relaxation times and electric dipole moments have been determined at two microwave frequencies for twelve compounds in benzene solution at 25.0°. The results are discussed in terms of (a) the flexibility of the benzoquinone ring and (b) the internal rotation of methoxy groups in the alkoxy compounds of carbon and silicon.

Measurements at microwave frequencies might provide information about the apparent dipole moments of centrosymmetric p -benzoquinones; DiCarlo and Smyth¹ reported that for p -benzoquinone itself, at a wavelength of 3.22 cm, the dielectric loss was only a tenth of the expected value. Further evidence might also be obtained from measurements at these frequencies about the greater freedom of rotation of methoxy groups in the $\text{Me}_{4-n}\text{Si}(\text{OMe})_n$ series of compounds compared to those of the $\text{Me}_{4-n}\text{C}(\text{OMe})_n$ series.

Experimental Section and Results

Preparation and Purification of Compounds. The physical measurements were made immediately after the final purification of each compound. p -Benzoquinone: a commercial sample was recrystallized from petroleum ether (bp 40–60°) to a constant mp of 115°. 2,5-Dimethyl- p -benzoquinone, prepared by oxidizing

(1) E. N. DiCarlo and C. P. Smyth, *J. Amer. Chem. Soc.*, **84**, 1128 (1962).

Table I: Polarization Data and Electric Dipole Moments (μ) of *p*-Benzoquinones in Benzene Solution at 25.0°

Compound	Max wt fraction $\times 10^4$	α	β	γ	P_2, cm^3	R_D, cm^3	μ, D
<i>p</i> -Benzoquinone	362	0.454	-0.306	0.091	36.24	28.43	0.62
2,5-Dimethyl- <i>p</i> -benzoquinone	646	0.443	-0.233	0.045	48.35	37.54	0.73
2,5-Diisopropyl- <i>p</i> -benzoquinone	1120	0.343	-0.148	0.007	69.59	56.42	0.80
2,5-Di- <i>tert</i> -butyl- <i>p</i> -benzoquinone	956	0.263	-0.121	-0.008	78.06	65.75	0.78

Table II: Electric Dipole Moments (μ) and Relaxation Times (τ) of *p*-Benzoquinones in Benzene Solution at 25.0°

Compound	Frequency, GHz	Max wt fraction $\times 10^4$	α'	α''	μ, D	τ, psec
<i>p</i> -Benzoquinone	9.86	714	0.519	0.011	0.65	0.05
	20.02	714	0.503	0.030	0.65	0.06
2,5-Dimethyl- <i>p</i> -benzoquinone	9.86	1170	0.428	0.005	0.70	0.5
	25.17	1170	0.422	0.053	0.69	0.6
2,5-Diisopropyl- <i>p</i> -benzoquinone	9.86	960	0.272	0.017	0.69	1.0
	25.18	2310	0.225	0.022	0.63	0.7
2,5-Di- <i>tert</i> -butyl- <i>p</i> -benzoquinone	9.87	703	0.241	0.028	0.73	1.7
	25.19	1680	0.261	0.046	0.74	1.5

Table III: Electric Dipole Moments and Relaxation Times in Benzene Solution at 25.0°

Compound	Frequency, GHz	Max wt fraction $\times 10^4$	α'	α''	μ, D	τ, psec	μ radio-frequency
$\text{Me}_3\text{CO Me}$	9.86	209	1.795	0.490	1.37	3.5	1.36
	25.30	209	1.296	0.825	1.33	3.3	
$\text{Me}_2\text{C}(\text{OMe})_2$	9.86	2220	-0.071	0.028	0.53	1.5	0.59
	25.29	2220	-0.086	0.051	0.52	1.3	
$\text{MeC}(\text{OMe})_3$	9.86	291	1.399	0.597	1.46	5.6	1.53
	24.88	310	0.713	0.800	1.40	5.3	
$\text{C}(\text{OMe})_4$	9.84	954	0.158	0.023	0.78	0.8	0.82
	25.29	954	0.155	0.014	0.77	0.9	
Me_3SiOMe	9.87	495	1.002	0.174	1.18	1.9	1.19
	25.27	1890	0.830	0.392	1.16	1.9	
$\text{Me}_2\text{Si}(\text{OMe})_2$	9.86	494	1.214	0.178	1.31	1.4	1.29
	24.86	670	1.055	0.288	1.30	1.3	
$\text{MeSi}(\text{OMe})_3$	9.86	490	1.878	0.192	1.69	1.3	1.68
	25.26	1200	1.740	0.492	1.67	1.2	
$\text{Si}(\text{OMe})_4$	9.86	503	1.885	0.105	1.74	0.8	1.78
	25.29	503	1.784	0.299	1.74	0.9	

p-xylenol with peracetic acid,² was recrystallized from glacial acetic acid to a constant mp of 125°. 2,5-Diisopropyl- and 2,5-di-*tert*-butyl-*p*-benzoquinones were made by oxidizing the corresponding hydroquinone in acetic acid solution with CrO_3 at 5°, the products precipitated with water and recrystallized from acetic acid; mp 43 and 150°, respectively. The preparation of the remaining compounds has been described previously.³

Experimental measurements at radio and microwave frequencies, and the methods of evaluating the electric dipole moments and relaxation times, have been described.⁴ Seven solutions were studied for each compound and all measurements were made at 25.0°.

Table I summarizes the polarization data and electric dipole moments obtained at radiofrequency for the *p*-benzoquinones; α , β , and γ are, respectively, the slopes of the graphs of electric permittivities, specific volumes, and refractive indices squared against weight fraction, P_2 is the total molar polarization of the solute,

(2) D. Bryce-Smith and A. Gilbert, *J. Chem. Soc.*, 873 (1964).

(3) C. W. N. Cumper, A. Melnikoff, and A. I. Vogel, *J. Chem. Soc. A*, 246, 323 (1966).

(4) (a) C. W. N. Cumper, A. A. Foxton, J. F. Read, and A. I. Vogel, *J. Chem. Soc.*, 430 (1964); (b) C. W. N. Cumper, A. Melnikoff, and R. F. Rossiter, *Trans. Faraday Soc.*, 65, 2892 (1969); (c) C. W. N. Cumper and J. W. M. Wood, *J. Chem. Soc. B*, 1811, (1971).

and *R_D* its molar refraction to Na(D) light. Corresponding results for the other compounds have been published.³ Tables II and III contain the slopes against weight fraction of the real (α') and imaginary (α'') parts of the electric permittivities at microwave frequencies, together with the dipole moments (μ) and relaxation times (τ).

Discussion

(a) *p*-Benzoquinone and 2,5-Dialkyl-*p*-Benzoquinones. Although the *p*-benzoquinone molecule is planar in the crystalline state⁶ its apparent dipole moment, and those of symmetrically substituted 2,5-*p*-benzoquinones, in solution are about 0.7 D. Coop and Sutton's claim⁶ that this is due to an inadequate allowance for atom polarization has been denied.⁷ A finite moment has been attributed to collision between the solute and solvent molecules⁸ but this would result in a lower polarity of the symmetrically substituted molecules which is not observed. Another explanation, that the applied electric field deforms the oxygen lone-pair electrons,⁹ is not substantiated by birefringence studies¹⁰ which indicate a high atom polarization.

The induced atomic polarization is particularly large in flexible molecules with high opposing bond moments. In the present case this would arise from those bending vibrations of the molecule which affect the linearity of the two carbonyl groups. If the vibrations are of sufficiently low frequency, solution in nonpolar solvents would result in the broad absorption bands, characteristic of such vibrations, tailing into the microwave region. We consider this to be the situation in *p*-benzoquinone and also in cyclohexane-1,4-dione.¹¹ The greater flexibility of cyclohexane-1,4-dione compared to *p*-benzoquinone would produce a lower vibration frequency and greater loss in the microwave region, thereby causing its greater relaxation time (0.7 compared to 0.05 psec).

In 2,5-dialkyl-*p*-benzoquinones it seems reasonable to predict that the alkyl groups increase the reduced mass for the bending vibrations with a consequent decrease in their frequencies and increase in the overall relaxation times. The results in Table II show that τ is 10–20 times greater in 2,5-dialkyl-*p*-benzoquinones than in the unsubstituted molecule and increases with the size of the alkyl group.

If the apparent dipole moment of these molecules is attributed to the large atom polarization the two bulky alkyl groups should reinforce its value; their apparent moments substantiate this. The underestimate of atom polarization causes the dipole moments and relaxation times in Table II to be too high (*cf.* eq 11, ref 4b).

It would seem desirable to make spectroscopic measurements on these compounds in the far-infrared and short microwave regions. It is interesting to note that

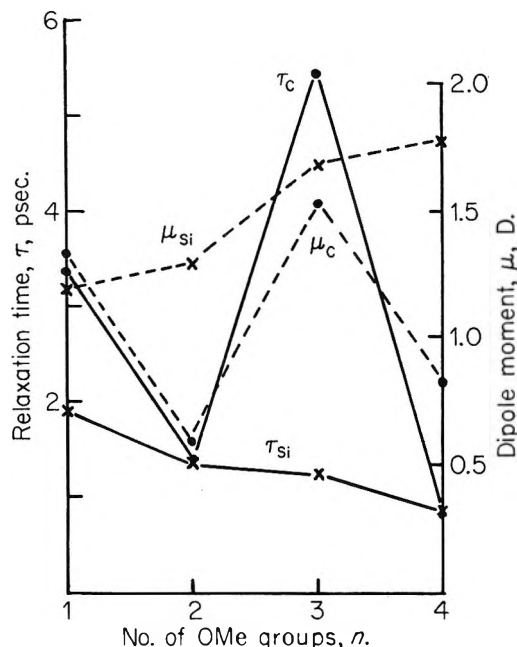


Figure 1. Relaxation times (—) and electric dipole moments (---) of Me_{4-n}C(OMe)_n and Me_{4-n}Si(OMe)_n.

the band at 120 cm⁻¹ observed for *p*-benzoquinone¹² corresponds to a relaxation time of 0.03 psec.

(b) Me_{4-n}C(OMe)_n and Me_{4-n}Si(OMe)_n. The electric dipole moments³ and ultraviolet¹³ and nmr¹⁴ spectra of these molecules have been reported. It was concluded that in the carbon series only hindered rotation of the methoxy groups occurred but that in the silicon compounds these groups rotated relatively freely. This difference between the two series of compounds should be reflected in their relaxation times.

From the results in Table III and in Figure 1 it is seen that in spite of the increases in molecular size and dipole moment the relaxation times of the silicon compounds decrease as the number of methoxy groups is increased.

The relaxation time of Me₃COME is greater than that of Me₃SiOME but both are consistent with the presence

- (5) J. M. Robertson, *Nature (London)*, **134**, 138 (1934); *Proc. Roy. Soc. Ser. A*, **150**, 106 (1935).
- (6) I. E. Coop and L. E. Sutton, *J. Chem. Soc.*, 1269 (1938).
- (7) C. C. Meridith, L. Westland and G. F. Wright, *J. Amer. Chem. Soc.*, **79**, 2385 (1957); K. H. Illinger and C. P. Smyth, *J. Chem. Phys.*, **35**, 392 (1961); H. Huber and C. F. Wright, *Can. J. Chem.*, **42**, 1446 (1964).
- (8) D. L. Hammick, G. C. Hampson, and G. I. Jenkins, *J. Chem. Soc.*, 1263 (1938).
- (9) L. Poaloni, *J. Amer. Chem. Soc.*, **80**, 3879 (1958).
- (10) E. Charney, *ibid.*, **83**, 578 (1961).
- (11) C. W. N. Cumper and R. F. Rossiter, *Trans. Faraday Soc.*, **65**, 2900 (1969).
- (12) C. H. Cartwright and J. Errera, *Proc. Roy. Soc. Ser. A*, **154**, 138 (1936).
- (13) C. W. N. Cumper, A. Melnikoff and A. I. Vogel, *J. Chem. Soc. A'* **242** (1966).
- (14) C. W. N. Cumper, A. Melnikoff, E. F. Mooney and A. I. Vogel, *ibid.*, **B**, 874 (1966).

of an internal rotation; the greater time for the carbon compound indicates some frictional resistance to rotation. Both dimethoxy compounds have similar relaxation times, as also have the tetramethoxy compounds. The greater size and substantially higher dipole moments of the silicon compounds, however, should produce a proportionately greater contribution from the molecular tumbling motion. The relaxation time for end-over-end rotation is approximately proportional to the molar volume and, when several relaxation mechanisms occur, the relative weighting of each depends

upon the square of its orientating dipole moment.¹⁵ Consequently, these results are only explicable if the internal dielectric relaxation by rotation of the methoxy groups occurs more readily in the silicon compounds. With three methoxy groups the carbon and silicon compounds have similar dipole moments but the four and a half-fold difference between their τ values again demonstrates the greater freedom of rotation in the silicon compound.

(15) E. Fischer, *Z. Phys.*, **127**, 49 (1949); A. Budo, *ibid.*, **39**, 706 (1938).

Ultrasonic Absorption Mechanisms in Aqueous Solutions of Bovine Hemoglobin¹

by W. D. O'Brien, Jr., and F. Dunn*

Bioacoustics Research Laboratory, University of Illinois, Urbana, Illinois 61801 (Received June 21, 1971)

Publication costs assisted by the Institute of General Medical Sciences, National Institutes of Health

In order to study further the principal loss mechanisms of ultrasonic energy in biological media, the absorption and velocity were determined in aqueous solutions of hemoglobin, largely at 10°, over the frequency range 1–50 MHz. A distribution of relaxation processes is necessary to characterize the absorption spectra. Interaction of the acoustic wave with the hydration layer of the macromolecule, and not direct interaction with macromolecular configuration, appears as a dominant mechanism. The ultrasonic absorption titration curves exhibit maxima around pH 2–4 and pH 11–13, in addition to possessing a broad peak in the pH range 5–9. The peaks in the absorption titration and the similar ones observed for bovine serum albumin (*J. Phys. Chem.*, **73**, 4256 (1969)), are attributed to the proton-transfer reaction occurring between particular amino acid side chain groups and the solvent. The broad peak is partially attributed to the proton transfer resulting from the imidazolium function of the histidine residue.

Introduction

Although ultrasonic spectroscopy has been available, in principle, for at least two decades, to date only a few biological macromolecules have been examined. Probably the most extensively studied biopolymer is the globular protein hemoglobin, the oxygen carrier in the red blood cells of vertebrates.^{2–4} The earliest work of importance is that of Carstensen, *et al.*,⁵ who investigated the ultrasonic absorption and velocity in the blood, plasma and solutions of albumin, and hemoglobin, and concluded that the acoustical properties of blood are largely determined by the protein concentration. In addition they showed that the absorption coefficient of hemoglobin is approximately the same as that of serum albumin within the frequency range 0.8–3 MHz in the temperature range 10–40°.

Within the neutral pH region, aqueous solutions of hemoglobin have now been examined over the extended frequency range 35–1000 MHz^{2,3} and it has been shown that it is possible to approximate the entire spectrum

with four appropriately selected discrete relaxation processes.

More recently other globular proteins have been examined. Kessler and Dunn⁶ studied aqueous solutions of bovine serum albumin and attributed the ultrasonic absorption in the neutral pH region to solvent-solute interactions. Outside of the neutral pH range,

(1) (a) Portions of this work were extracted from the Thesis submitted by W. D. O'Brien, Jr., in partial fulfillment of the requirement for the Ph.D. degree in electrical engineering, University of Illinois. (b) A preliminary report of this work was presented at the 78th meeting of the Acoustical Society of America in San Diego, Calif., Nov 1969 [*J. Acoust. Soc. Amer.*, **47**, 98 (1970)].

(2) F. Dunn, P. D. Edmonds, and W. J. Fry, in "Biological Engineering," H. P. Schwan, Ed., McGraw Hill, New York, N. Y., 1969, Chapter 3, p 205.

(3) F. Schneider, F. Muller-Landay, and A. Mayer, *Biopolymers*, **8**, 537 (1969).

(4) P. D. Edmonds, T. J. Bauld, J. F. Dyro, and M. Hussey, *Biochem. Biophys. Acta*, **200**, 174 (1970).

(5) E. L. Carstensen, K. Li, and H. P. Schwan, *J. Acoust. Soc. Amer.*, **25**, 286 (1953).

(6) L. W. Kessler and F. Dunn, *J. Phys. Chem.*, **73**, 4256 (1969).

the absorption behavior was thought to correlate with conformation changes. Wada, *et al.*,⁷ investigated the ultrasonic absorption of gelatin at 3 MHz as a function of pH which had a peak in the absorption spectrum around pH 4 and was interpreted to be a dissociation type reaction of the protein side chains. Also it has been reported that the absorption magnitude of gelatin solutions within the frequency range 0.7–10 MHz is approximately half that in hemoglobin and albumin solutions.⁸ For each of these protein solutions the ultrasonic absorption spectra exhibit a distribution of relaxation times.

Two synthetic polyamino acids have been examined under varying environmental conditions with respect to their ultrasonic absorption. The primary mechanism proposed to explain the excess ultrasonic absorption in poly-L-glutamic acid solutions⁹ is that of the solvent-solute interaction whereas Schwarz¹⁰ attributes the excess absorption to the helix-coil transition. The examination by Wada, *et al.*,⁷ revealed that at 50 kHz the absorption mechanism is that of helix-coil transition while at 3 MHz the absorption is attributed to side chain dissociation. It has been shown¹¹ that the observed ultrasonic absorption behavior in aqueous poly-L-lysine solutions can be associated with the helix-coil transition.

The carbohydrate, dextran, a linear α (1-6) anhydroglucose polysaccharide, assumes a random coil conformation in solution whereas most proteins exist as a compact, rigid molecule. The ultrasonic absorption spectra of dextran, in the frequency range 3 to 69 MHz, can be represented by a distribution of relaxation times.¹² The absorption magnitude is considerably less than that exhibited by proteins, and has been attributed to the proteins possessing a secondary and tertiary structure while dextran does not. In addition, the protein gelatin, which does not possess a tertiary structure, also exhibits a lesser absorption magnitude than those proteins with higher ordered structure. Thus the suggestion that the tertiary structure may be responsible for some of the excess ultrasonic absorption observed in protein solutions appears to have received attention.^{13,14}

It is apparent from above that the mechanisms mainly responsible for the ultrasonic absorption are unsettled. The present study was undertaken to provide additional data from observations at extreme pH values.

Experimental Techniques

Two distinct systems, described in detail elsewhere,^{15,16} were utilized. The high frequency system, an automated version of that of Pellam and Galt,¹⁷ utilizes a transmitting and a receiving transducer and has a lower frequency limit of approximately 9 MHz because of the apparent attenuation due to diffraction effects. The upper frequency limit is well beyond the

50 MHz employed here. At the lower frequencies, a comparison method is used which minimizes the difficulties due to diffraction,^{5,18} and is capable of measuring ultrasonic absorption and velocity over the frequency range 0.3–20 MHz. Both systems employ the standard pulse techniques. These measurement techniques assume the absorption behavior of the fluid under investigation to be exponential in nature, *viz.*

$$p = p_0 e^{-\alpha x} \quad (1)$$

where p_0 is the pressure amplitude at $x = 0$, x is the acoustic path length over which the acoustic pulse travels, and α is the amplitude absorption coefficient per unit length. Speed of sound measurements are accomplished by adding algebraically the received signal to a reference signal and recording the time required to change the acoustic path length by 100 wavelengths.¹⁶ The temperature of the liquid under investigation was maintained to $\pm 0.05^\circ$.

Two grades of methemoglobin (Hb), obtained from Nutritional Biochemicals Corp., Cleveland, Ohio, were investigated, *viz.*, uncrystallized Bovine Hemoglobin (Hb-OX), control no. 3099, and Hemoglobin Bovine 2X Crystalline (Hb-2X), control no. 1480, 8647, and 8995. Singly deionized and distilled water, testing to at most 0.15 ppm impurities¹⁹ was used throughout. The protein solutions were prepared by placing the proper amount on top of a measured volume of water and refrigerating until mixing was complete, usually 2–5 hr. The uncrystallized hemoglobin solution, which contained some red blood cell structures, was centrifuged at 20,000*g* for 2 hr to remove heavier particles. This supernatant, as well as other protein solutions, were filtered twice through type A glass fiber filters (Gellman Inst. Co., Ann Arbor, Mich.) to remove particles larger than 0.3 μ in diameter and stored at 7° until used, usually not more than a few hours. The weight concentrations of the acoustically measured solutions were determined, to an accuracy of better

(7) Y. Wada, H. Sasaba, and M. Tomono, *Biopolymers*, **5**, 887 (1967).

(8) H. P. Schwan and H. Pauly, *J. Acoust. Soc. Amer.*, **50**, 692 (1971).

(9) J. J. Burke, G. G. Hammes, and T. B. Lewis, *J. Chem. Phys.*, **42**, 3520 (1965).

(10) G. Schwarz, *J. Mol. Biol.*, **11**, 64 (1965).

(11) R. C. Parker, L. J. Slutsky, and K. R. Applegate, *J. Phys. Chem.*, **72**, 1968 (1968).

(12) S. A. Hawley and F. Dunn, *J. Chem. Phys.*, **52**, 5497 (1970).

(13) S. A. Hawley, L. W. Kessler, and F. Dunn, *J. Acoust. Soc. Amer.*, **38**, 521 (1965).

(14) W. D. O'Brien, Jr., and F. Dunn, *J. Acoust. Soc. Amer.*, **50**, 1213 (1971).

(15) W. D. O'Brien, Jr., Ph.D. Thesis, University of Illinois, Urbana, Ill., 1970.

(16) L. W. Kessler, S. A. Hawley, and F. Dunn, *Acustica*, **23**, 105 (1971).

(17) J. R. Pellam and J. K. Galt, *J. Chem. Phys.*, **14**, 608 (1946).

(18) E. L. Carstensen, *J. Acoust. Soc. Amer.*, **26**, 858 (1954).

(19) Tested at the Illinois State Water Survey, Champaign, Ill.

than $\pm 0.3\%$ at room temperature, by evaporating 15 ml in a tared beaker over air until dry and placing in a vacuum desiccator for 24 hr.

The pH of the hemoglobin solution was altered by the addition of standard volumetric solutions of either 1.0 N HCl or KOH. The acid or base was introduced slowly, to minimize pH gradients, into the circulating fluid within the acoustic chamber in steps to produce changes ranging from 0.1 to 1.5 pH units. The pH readings were obtained to within a relative accuracy of ± 0.01 pH unit with a Beckman Century SS pH Meter using a Beckman pH combination electrode (39013) which fitted directly into the acoustic chamber. The pH meter was standardized at pH 2.01, 4.01, 7.00, 9.18, and 12.45.

In order to obtain the entire ultrasonic titration spectrogram, two measurement procedures were performed, each starting at neutral pH. A single procedure took from 8 to 20 hr, depending upon the number of points to be determined. Typically, the test liquid remained at a fixed pH for 1 hr, of which 15–20 min was allowed for the test liquid to equilibrate and the balance of time devoted to determining the ultrasonic absorption and velocity at the desired frequencies. Two complete titration spectrograms were obtained for each grade of hemoglobin in order to verify the results, the data being available in ref 15. The solutions, at the terminal pH values, were stored for several days at 7°, following the measurement procedure, with no observable precipitation occurring.

Results

The ultrasonic absorption of the two grades of hemoglobin was examined as a function of solute concentration to determine the onset of finite concentration effects. Deviation from linearity of Hb-OX solutions occurs around 0.10 g/cm³ while that for the purer Hb-2X deviates around 0.16 g/cm³, the latter agreeing with earlier reports.²⁰ Such deviation from linearity is commonly attributed to interactions among the solute molecules. Thus equating the volume of an assumed spherical particle and the volume per molecule, $4/3\pi R^3 = cN_A/M$, where M is the molecular weight of the biopolymer and N_A is Avogadro's number, yields a molecular radius $R = 54 \text{ \AA}$ at the concentration, c , of 0.16 g/cm³, *i.e.*, where the ultrasonic absorption begins to deviate from linearity. This value is in substantial agreement with that determined from X-ray diffraction techniques wherein the Hb molecule was found to be roughly spherical with overall dimensions of 64 Å by 55 Å by 50 Å.²¹ In all the work reported herein, the concentration was maintained well below 0.16 g/cm³.

The ultrasonic absorption data are presented in terms of the excess frequency-free absorption per unit concentration parameter

$$A = \Delta\alpha/cf^2 \quad (2)$$

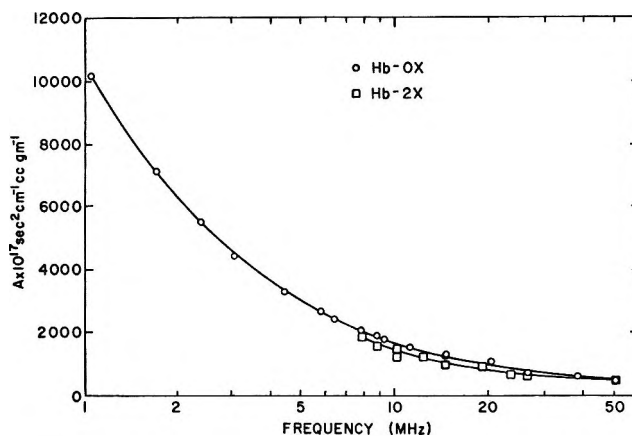


Figure 1. Ultrasonic absorption spectrogram in aqueous solutions of bovine hemoglobin ($T = 10^\circ$).

where $\Delta\alpha$ is the difference between the absorption of the solution and that of the solvent, c is the biopolymer concentration in grams per cubic centimeter, and f is the ultrasonic frequency. The absorption parameter is shown in Figure 1 as a function of frequency for aqueous solutions of Hb-OX and Hb-2X at their isoelectric point, at 10.0°. The excess absorption exhibited by the uncrystallized Hb over the purer grade (about 10%) possibly reflects impurities contained in the former, and not present in the latter, which may also possess relaxational behavior. A similar situation has been reported for bovine serum albumin.²²

The composite ultrasonic absorption titration curve is shown in Figure 2 for the frequency range 8.9–50.5 MHz and over the pH range 1.5–12.3. Similar shaped curves were also determined for Hb-OX down to 2.4 MHz.¹⁵ The titration curves are similar in shape and magnitude to those for aqueous solutions for bovine serum albumin,⁶ where the increase in A below pH 4.3 was associated with the intermediate N–F' transition of Foster.²³ Hemoglobin, however, does not exhibit this transition. Similarly, in the alkaline pH region, both BSA and Hb show excess absorption peaking beyond pH 10.5.

The ultrasonic absorption coefficient and velocity were determined as functions of temperature over the range 10–37° in a neutral aqueous solution of Hb-2X at a concentration of 0.0349 g/cm³ in order to provide information on apparent activation energies, shown in Table I with that of water. In all cases ΔF is less than that of water though it increases with increasing frequency. A similar experiment reported for BSA⁶ indicates no frequency dependence within the neutral

(20) E. L. Carstensen and H. P. Schwan, *J. Acoust. Soc. Amer.*, **31**, 185 (1959).

(21) M. F. Perutz, M. G. Rossmann, A. F. Cullis, H. Muirhead, G. Will, and A. C. T. North, *Nature (London)*, **185**, 416 (1960).

(22) L. W. Kessler, private communication, 1968.

(23) J. F. Foster, in "Plasma Proteins," F. W. Putnam, Ed., Academic Press, New York, N. Y., 1960, Chapter 6.

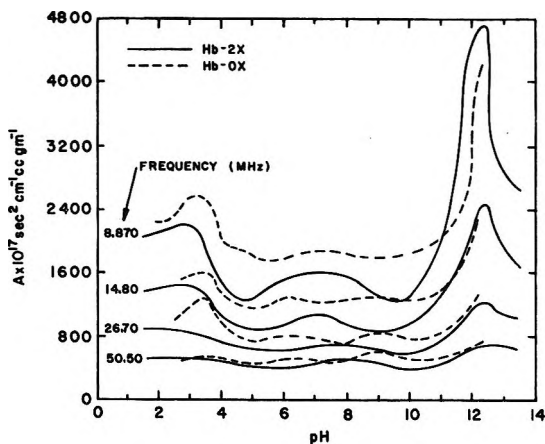


Figure 2. Composite ultrasonic absorption titration curve in aqueous solutions of bovine hemoglobin ($T = 10^\circ$).

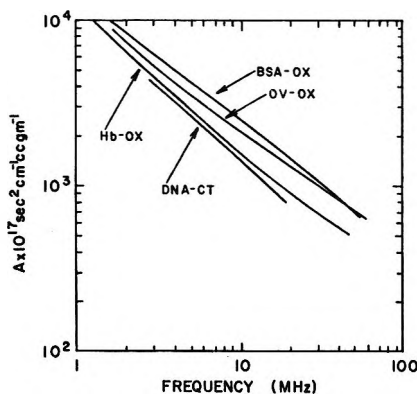


Figure 3. Composite ultrasonic absorption spectrogram, 10° : Hb-OX, uncrystallized bovine hemoglobin; BSA-OX, uncrystallized bovine serum albumin; OV-OX, uncrystallized ovalbumin; DNA-CT, calf thymus deoxyribose nucleic acid.

pH region and strong frequency dependence at pH 2.9, which was attributed to additional relaxation processes occurring in the acidic region. Such processes, resulting in strong frequency dependence of the activation energy, could be proton-transfer reactions occurring at neutral pH values in Hb and at pH 2.9 in BSA aqueous solutions which are absent in neutral pH BSA solutions.

Discussion

Figure 3 shows the absorption parameter A for aqueous solutions of Hb-OX, BSA, ovalbumin-uncrystal-

lized,²⁴ and calf thymus DNA²⁵ at 10° . All four curves possess approximately the same frequency dependence although differences in magnitude are apparent. The former suggests that the mechanism(s) of ultrasonic absorption, for these four solutions, at their isoelectric point, may be the same. One universal feature of aqueous solutions of globular proteins and nucleic acids is the existence of the ubiquitous structuring of water about the macromolecule. It thus seems reasonable to speculate that the magnitude differences result from differing degrees of hydration, depending upon detailed molecular differences. Interaction of the solvent and solute has already been invoked to describe the excess ultrasonic absorption in aqueous solutions of biological molecules.^{6,9} The present consideration is that the mechanism is the perturbation of the hydration layer, which is essential for maintaining the integrity of the biopolymer, by the acoustic wave process.

Hemoglobin is a globular protein composed of four subunits, two α polypeptide chains and two β polypeptide chains, with each consisting of approximately 144 amino acid residues and conjugated to a heme moiety (an iron-containing porphyrin derivative). No disulfide cross-links exist which would prevent each of the polypeptide chains from assuming a completely extended or helical configuration and each chain possesses approximately 65% helix content.²⁶ Under normal conditions approximately 6% of the human hemoglobin molecules in aqueous solution (pH 7; no denaturing agents present) are dissociated in half without loss of tertiary structure of the individual polypeptide chains.²⁷ This indicates the unique nature of the hemoglobin molecule to dissociate into its half subunits under very mild conditions without hydrolysis or pigment denaturation occurring. The nature of the bonds, or noncovalent links, which connect the individual polypeptide chains is unknown although it is assumed that the contacts are between α and β chains resulting in $\alpha\beta$ half molecules upon dissociation rather than α and β half molecules.²⁸ All forms of hemoglobin undergo major conformational changes when exposed to low pH. As the pH is lowered from the isoelectric point to 4.5, the hemoglobin molecule dissociates in half without appreciable change in the conformation of the resulting $\alpha\beta$ polypeptide chains.²⁹ As the pH is lowered from 7 to 3.5 to 2.9, the intrinsic viscosity increases from $3.5 \text{ cm}^3/\text{g}$ ³⁰ to $13.55 \text{ cm}^3/\text{g}$ ³⁰ to $17 \text{ cm}^3/$

Table I: Apparent Activation Energy of Aqueous Solution of Hb-2X (Concentration = 0.0349 g/cm^3)

pH	f , MHz	ΔF , kcal/mol
6.9	8.870	1.2
6.9	14.80	2.0
6.9	26.70	2.6
6.9	50.50	3.4
Water	All	4.48

(24) W. D. O'Brien, Jr., and F. Dunn, unpublished results.

(25) W. D. O'Brien, Jr., and F. Dunn, unpublished results.

(26) C. Tanford, "Physical Chemistry of Macromolecules," Wiley, New York, N. Y., 1961.

(27) K. Kawahara, A. G. Kirschner, and C. Tanford, *Biochemistry*, **4**, 1203 (1965).

(28) A. F. Cullis, H. Muirhead, M. F. Perutz, M. G. Grossman, and A. C. T. North, *Proc. Roy. Soc. Ser. A*, **265**, 161 (1962).

(29) E. C. Field, and J. R. P. O'Brien, *Biochem. J.*, **60**, 656 (1955).

(30) D. Tanford, *J. Amer. Chem. Soc.*, **79**, 3931 (1957).

g,³¹ respectively. Thus at pH values less than 4, the Hb molecule clearly shows a marked expansion. Within the pH range 4.0–2.2, Polet and Steinhardt³² reported that the heme is expelled from the apoprotein and the globin is unfolded, but the specific pH at which these two events occur is still unknown. Finally, Reichmann and Colvin³³ determined that around pH 2.0–1.8, the Hb molecule splits into four fragments of nearly equal size.

The hemoglobin molecule also dissociates at alkaline pH, *viz.*, the sedimentation coefficient decreases above pH 10, where it is 4.2×10^{-13} sec, reaching a value of 2.55×10^{-13} sec at pH 11.³⁴ Within the pH range 7–11, the diffusion coefficient remains relatively constant, indicating that the hemoglobin molecule dissociates in half as the pH is increased from 10 to 11, while the individual polypeptide chains retain their tertiary structure. As the pH is increased from 11, the sedimentation coefficient, along with the diffusion coefficient, decreases showing that the two subunits are expanding but not necessarily dissociating further.

Repulsion of like charges has been discounted as a mechanism of dissociation since at pH 6 the molecule possesses a charge of +5 whereas at pH 10 it is –30.³⁴ Thus the denaturation of Hb must be attributed to different mechanisms in the acidic and alkaline pH regions.

The effect of pH on the ultrasonic absorption characteristics of a number of aqueous solutions of amino acids have been investigated, *viz.*, serine and threonine,³⁵ glycine,^{36,37} glutamic acid, aspartic acid and alanine,³⁶ and arginine and lysine,³⁸ and absorption maxima were observed in the acidic and alkaline pH regions. This absorption peaking, as a function of pH, has been described quantitatively for the above amino acids, assuming the proton-transfer reaction dominates the absorption process. However, the task of dealing with the similar peaking for macromolecules such as proteins which contain a large number of side chains able to participate in such reactions is far more difficult since detail of reaction coupling among sub-chain groups is not currently available. Thus a more qualitative discussion of the proton-transfer reaction for proteins must suffice for the present. For this reaction, which is a chemical relaxation mechanism, it is considered that the propagating acoustic wave disturbance perturbs the proton from the solvent (water) to the solute, an amino acid side chain, and *vice versa*. The energy necessary to drive the reaction is extracted from the acoustic field. The pH values at which the peaks in Figure 2 are maximum can be correlated with the pK values of the individual amino acid side chains which participate, both in the acidic and alkaline pH regions, *viz.*

$$\text{pH}_{\text{acid}} = \frac{1}{2}(\text{pK} + \text{pC}) \quad (3)$$

and

$$\text{pH}_{\text{base}} = \frac{1}{2}(14 + \text{pK} - \text{pC}) \quad (4)$$

where *C* is the molar concentration of the particular side chain group. Table II lists the amino acid side chains for Hb, along with their quantity in moles per 100,000 g of protein which can participate in the proton transfer reaction. Within the acidic pH range, the μ -carboxyl group (pK range on protein of 3.0–4.7) of aspartic acid (ASP) and glutamic acid (GLU) is primarily responsible for absorption peak. At the alkaline pH values, the ϵ -amino group (pK range 9.4–10.6) of lysine (LYS), the guanidinium group (pK range 9.8–10.4) of tyrosine (TYR), and the sulfhydryl group (pK range 9.4–10.8) of cysteine (CYS) contribute primarily to the absorption maximum. The diffuse peak, in Figure 2, occurs within the same pH range (5–9) in which about one-third, or 22, of the histidine groups (HIS) per Hb molecule titrate³⁹ suggesting that the broad peak around neutral pH may be a result of the imidazolium group (pK range 5.6–7.0), although the majority of the excess absorption still results from the

Table II: Proton-Transfer Side-Chain Groups (in mol/100,000 g of Protein)

Amino acid side chain	Human Hb ^a	Bovine Hb ^b	BSA ^c
ASP/GLU (ω -carboxyl)	162	194	152
LYS (ϵ -amino)	133	133	88
HIS (Imidazolium)	115	103	24.6
ARG (Guanidinium)	36.4	42.4	33.8
TYR (Phenolic hydroxyl)	36.4	36.4	29.3
CYS (Sulfhydryl)	18.2	6.1	0
α -Carboxyl	12.1	12.1	1.54
α -Amino	12.1	12.1	1.54

^a G. Braunitzer, K. Hilse, V. Rudloff, and N. Hilshmann, *Advan. Protein Chem.*, **19**, 1 (1964). ^b W. B. Gratzer and A. C. Allison, *Biol. Rev. Cambridge Phil. Soc.*, **35**, 459 (1960). ^c See ref 23.

(31) D. Tanford, *Advan. Protein Chem.*, **23**, 121 (1968).

(32) H. Polet and J. Steinhardt, *Biochemistry*, **8**, 857 (1969).

(33) M. E. Reichmann and J. E. Colvin, *Can. J. Chem.*, **34**, 411 (1956).

(34) U. Hasseroth and J. Vinograd, *Proc. Nat. Acad. Sci. U. S.*, **45**, 12 (1959).

(35) R. D. White, L. J. Slutsky, and S. Pattison, *J. Phys. Chem.*, **75**, 161 (1971).

(36) K. Applegate, L. J. Slutsky, and R. C. Parker, *J. Amer. Chem. Soc.*, **90**, 6909 (1968).

(37) M. Hussey and P. D. Edmonds, *J. Acoust. Soc. Amer.*, **49**, 1309 (1971).

(38) M. Hussey and P. D. Edmonds, *ibid.*, **49**, 1907 (1971).

(39) C. Tanford and Y. Nozaki, *J. Biol. Chem.*, **241**, 2832 (1966).

interaction of the hydration layer with the acoustic wave.

Bovine serum albumin consists of a single polypeptide chain with molecular weight of about 68,000. The conformation of the molecule remains unchanged at pH values between 4.3 and 10.5 and sedimentation coefficients decrease, with their ratios remaining constant,⁴⁰ implying that the molecule expands but does not dissociate. The intrinsic viscosity of the BSA molecule expands in steps, from 3.6 to 4.5 cm³/g around pH 4 and from 4.5 to 8.4 cm³/g around pH 3.⁴¹ At $[\eta] = 8.4$ cm³/g, the BSA molecule is not highly expanded, and this can be attributed to the large number of disulfide bonds the molecule possesses. Tanford, *et al.*,⁴¹ and Weber⁴² have speculated that the alkaline expansion of the BSA molecule is similar to that in the acid pH region but this has neither been confirmed nor denied²³ by experiment.

The effect of the protonation reaction of the imidazolium group of the histidine amino acid to the results of serum albumin⁶ appears to be minimal on the ultrasonic absorption within the pH range 5–9, possibly because of the small number of histidine amino acids in serum albumin (Table II). For both Hb and BSA, there is approximately the same ratio of amino acid groups which can partake in the proton transfer reaction between the alkaline (LYS, ARG, TYR, CYS) and

acidic (ASP, GLU) pH region and as shown in Table II, these concentration ratios are 217/194 for Hb and 151/152 for BSA. The similarity of these ratios is considered to lend support to the view that the similar ultrasonic absorption magnitude of the peaks of these two globular proteins results from the same mechanism. Previously⁶ the peaks in the BSA spectrogram were discussed in terms of conformational changes such as Foster's²³ N–F' transition. It now appears that a more acceptable explanation for such peaks in the ultrasonic absorption titration curves of Hb and BSA may be the proton-transfer reaction. However, the role of conformation cannot be completely discounted at this time as the evidence for each mechanism (1) is less convincing than one would like and (2) does not exclude the other from being present, simultaneously, to some degree of effectiveness.

Acknowledgment. The authors acknowledge gratefully the support of this research by a grant from the Institute of General Medical Sciences, National Institutes of Health.

(40) W. F. Harrington, P. Johnson, and R. H. Ottewill, *Biochem. J.*, **62**, 569 (1956).

(41) C. Tanford, J. G. Buzzel, D. G. Rands, and S. A. Swanson, *J. Amer. Chem. Soc.*, **77**, 6421 (1955).

(42) G. Weber, *Biochem. J.*, **51**, 155 (1952).

The Role of Orientation Constraints and Rotational Diffusion in Bimolecular Solution Kinetics

by Kenneth S. Schmitz and J. Michael Schurr*

Department of Chemistry, University of Washington, Seattle, Washington 98105 (Received September 1, 1971)

Publication costs borne completely by The Journal of Physical Chemistry

A theoretical investigation of the reaction between mobile orientable spheres, bearing single reactive sites, with localized stationary sites on a plane leads to general expressions for the rate constants for association and dissociation steps. The requirement for reaction is that the center of the reactive sphere must lie on a hemisphere above the site on the plane and the orientation vector must lie within a suitable angular range. Numerical computations show that moderate angular constraints produce rather drastic reductions in the maximum diffusion-controlled rate constant, when the spherical molecules orient by classical rotational diffusion. An attempt to fit the data of Farwell and Ackermann for the viscosity dependence of the rate of association of the H_2O_2 -horseradish peroxidase complex with cytochrome c met with only fair success. The data of Wetmur and Davidson for the rate of renaturation of DNA as a function of solvent viscosity is reinterpreted here in terms of a diffusion-controlled reaction with a fairly stringent orientation constraint for the bimolecular step.

I. Introduction

The classical theory of diffusion in bimolecular solution kinetics, as formulated by Smoluchowski,¹ Debye,² Collins and Kimball,³ Noyes,⁴ and Schurr,^{5a} is strictly applicable only to spherical particles that are uniformly reactive over their entire surface. For this special case the theory is now fairly complete in the sense that the steady-state forward and reverse rate constants are known, even in the presence of spherically symmetric interparticle potentials, and moreover the frequency-response spectrum of such a reaction has also been obtained.^{5a} Logically, the next step in the development of the theory is the introduction of orientation constraints for the occurrence of chemical reaction between the two species involved. Proper treatment of such angular constraints naturally necessitates the inclusion of rotational diffusion in the equations of motion of the diffusing particles. Although the general case of two freely diffusing species reacting subject to a mutual orientation constraint appeared to be intractable, a simpler model, retaining still an orientation constraint, but with the active site of one reactant localized on a stationary plane, proved to be susceptible to solution. Recently Solc and Stockmayer^{6b} have achieved a formal solution for the general problem, but as yet they have presented no numerical results.

Of special interest is the effect of orientation constraints on the maximum diffusion-controlled bimolecular rate constant. A fairly large number of enzyme-substrate association rate constants are known⁶ to lie in a range 10^6 – $5 \times 10^8 \text{ M}^{-1} \text{ sec}^{-1}$, which is sufficiently far below the value of 8×10^9 predicted by the Smoluchowski formula that the possibility of diffusion-control has generally been dismissed. At least for some of these

enzyme-substrate pairs the substrate is sufficiently large that its orientation probably proceeds by a process closely akin to classical rotational diffusion. Such pairs certainly include Old Yellow Enzyme with flavine mononucleotide,⁷ and the H_2O_2 -horseradish peroxidase complex with cytochrome c,⁸ and may also include β -amylase with amylose,⁹ and liver alcohol dehydrogenase with diphosphopyridine nucleotide.¹⁰ It is the main thesis of this communication that moderate angular constraints imposed on reactants that orient by rotational diffusion produce rather drastic decreases in the maximum diffusion-controlled rate constant. Thus, it is entirely possible that reactions previously thought to be far from the diffusion-controlled range in fact are strongly viscosity dependent. Furthermore a knowledge of the maximum diffusion-controlled rate constant may permit a rational estimate of the allowed angular tolerance for the chemical reaction.

The theory and computational data obtained here are applied to the experimental data for the horseradish peroxidase- H_2O_2 + cytochrome c reaction⁹ in section VII, and to the data for the rate of renaturation

- (1) M. V. Smoluchowski, *Z. Phys. Chem.*, **92**, 129 (1917).
- (2) P. Debye, *Trans. Electrochem. Soc.*, **82**, 265 (1942).
- (3) F. C. Collins and G. E. Kimball, *J. Colloid Sci.*, **4**, 425 (1949).
- (4) R. M. Noyes, in *Progr. React. Kinet.*, **1**, 131 (1961).
- (5) (a) J. M. Schurr, *Biophys. J.*, **10**, 700 (1970); (b) K. Solc and W. H. Stockmayer, *J. Chem. Phys.*, **54**, 2981 (1971).
- (6) M. Eigen and G. G. Hammes, *Advan. Enzymol. Relat. Areas Mol. Biol.*, **25**, 1 (1963).
- (7) H. Theorell and A. Nygaard, *Acta Chem. Scand.*, **8**, 1649 (1954).
- (8) R. W. Farwell and E. Ackermann, *Biophys. J.*, **3**, 479 (1963).
- (9) L. Peller and R. A. Alberty, *J. Amer. Chem. Soc.*, **81**, 5907 (1959).
- (10) (a) V. Bloomfield, L. Peller, and R. A. Alberty, *J. Amer. Chem. Soc.*, **84**, 4375 (1962); (b) H. Theorell and J. S. M. McKee, *Acta Chem. Scand.*, **15**, 1797, 1811, 1834 (1961).

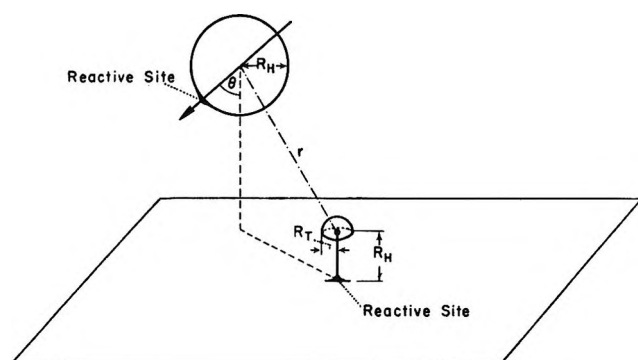


Figure 1. Schematic diagram of the model for reaction between a mobile, orientable sphere bearing a reactive site and a localized, stationary site on the plane. In order for reaction to occur the center of the sphere must lie on the small hemisphere, and θ must be less than or equal to some θ_0 .

of DNA¹¹ in section VIII, both reactions having been shown to be viscosity dependent.

II. The Model

The microscopic process treated here is the reaction of orientable spheres suspended in an infinite half-space of solution with a localized site on the bounding plane as depicted in Figure 1. Such a model is perhaps appropriate for the reaction of globular enzymes with small substrates that are rigidly attached to very large, flat surfaces, or platelets. A requirement for chemical reaction is that the center of the sphere must lie on a small hemisphere of (target) radius R_T centered at a distance R_H directly above the reactive site, R_H being the (hydrodynamic) radius of the sphere itself. It is also required that the orientation vector associated with the sphere must lie within an angle θ_0 of some suitable axis, here taken to be the normal directed down into the plane. One may imagine that the orientation vector indicates the position of a reactive patch, or site, on the sphere, and that reaction can occur only when the reactive sites of the sphere and plane are in close proximity. Although physically more appealing reaction conditions can easily be found, we have yet to discover one that provides anywhere near the same degree of mathematical simplicity.

Points in the solution half-space (containing the spheres) are located relative to an origin taken at the center of the hemisphere above the reactive site on the plane. Let r, α, β be the radius, polar angle with respect to the normal directed down into the plane, and azimuthal angle with respect to any arbitrary vector in the plane, respectively, of a point in the solution half-space. It will be observed that $0 \leq r \leq \infty$; $\pi/2 \leq \alpha \leq \pi$; $0 \leq \beta \leq 2\pi$. Let θ, ϕ denote the polar angle with respect to the downward normal into the plane, and the azimuthal angle with respect to an arbitrary vector in the plane, respectively, of the orientation vector associated with a sphere.

Suppose, now, that a number of very large identical plate-like surfaces bearing single (or a few widely separated) reactive sites are present in a unit volume of the sample along with a much larger number of reactive spheres. As long as the dimensions of the plates and the distances between sites are large compared to the extents of the diffusion gradients⁵ at the sites, the basic process may still be viewed as the reaction of spheres in microscopically infinite half-spaces with stationary reactive sites on the bounding planes. The average concentration of spheres at a particular point in the vicinity of any reactive site may be defined by the procedure described in a previous communication^{5a} hereinafter referred to as paper I. The extension required to define average concentrations of spheres with particular orientations is trivial.

The concentration of spheres at $r = \infty$ is maintained at a constant value c_0 , and all orientations at $r = \infty$ are equally probable. From the symmetry of the problem it is apparent that the concentration of spheres at the point r, α, β with orientation θ, ϕ is independent of α, β and ϕ . Let

$$c(r, \theta) 2\pi r^2 dr \frac{\sin \theta d\theta}{2}$$

be the number of spheres between r and $r + dr$ with orientations in the range θ to $\theta + d\theta$. The 2π occurs in place of the usual 4π owing to the restricted range of α . The continuity equation for spheres in the steady state is

$$\frac{\partial c(r, \theta)}{\partial t} = 0 = D \nabla_r^2 c(r, \theta) + \Theta \nabla_\theta^2 c(r, \theta) \quad (1)$$

where D and Θ are translational and rotational diffusion coefficients, respectively, ∇_r^2 is the usual spatial Laplacian operator, and ∇_θ^2 is the Laplacian on the surface of a unit sphere. The first term on the r.h.s. gives the divergence of the translational diffusion current density for spheres of a fixed θ , while the second term gives the divergence of rotational diffusion current density for spheres at constant r . The boundary conditions arise from the constant concentration at $r = \infty$, and the requirement that the total inward current equal the net rate of reaction. That is, respectively

$$\lim_{r \rightarrow \infty} c(r) \equiv \lim_{r \rightarrow \infty} \int_0^\pi c(r, \theta) \frac{\sin \theta d\theta}{2} = c_0 \quad (i)$$

where $c(r)$ is the total concentration of spheres of all orientations, and

$$2\pi R_T^2 D \left. \frac{\partial c(r, \theta)}{\partial r} \right|_{R_T} = k_a^0 X(\theta) c(R_T, \theta) - k_d^0 X(\theta) \frac{N_f}{N_0} \quad (ii)$$

(11) J. G. Wetmur and N. Davidson, *J. Mol. Biol.*, **31**, 349 (1968).

where N_f is the concentration of sites containing bound spheres and N_e is the concentration of empty or reactive sites; k_a^0 and k_d^0 are the intrinsic association and dissociation rate constants, and $X(\theta)$ is a step function

$$X(\theta) = \begin{cases} 1 & 0 \leq \theta \leq \theta_0 \\ 0 & \theta_0 \leq \theta \leq \pi \end{cases} \quad (2)$$

that defines the range of θ over which reaction may occur. The overall rate in (ii) refers to one site and is evidently the total rate per empty site for spheres of a particular orientation.

Finally, we shall make use of the auxiliary condition for the total rate of reaction of spheres of all orientations per empty site

$$\phi = 2\pi R_T^2 D \int_0^\pi \frac{\partial c(r, \theta)}{\partial r} \Big|_{R_T} \frac{\sin \theta d\theta}{2} \quad (iii)$$

This equation introduces an additional unknown ϕ , but also provides an independent equation.

III. The Formal Solution

Since the distribution of orientation vectors at any given r may be expanded in Legendre polynomials $P_l(\cos \theta)$ one may write in general

$$c(r, \theta) = \sum_l b_l(r) P_l(\cos \theta) \quad (3)$$

where the $b_l(r)$ are functions of r yet to be determined from the differential equation 1 together with the boundary conditions (i) and (ii) and the auxiliary condition (iii). After substituting eq 3 into eq 1, carrying out the angular Laplacian operation, multiplying by $P_m(\cos \theta) \sin \theta d\theta/2$, and integrating over θ one obtains

$$D \frac{1}{r^2} \frac{\partial}{\partial r} r^2 \frac{\partial}{\partial r} b_m(r) - \Theta m(m+1) b_m(r) = 0 \quad (4)$$

Thus, when $m = 0$

$$b_0(r) = A + \frac{B}{r} \quad (5)$$

and when $m \geq 1$

$$b_m(r) = C_m \frac{e^{-\kappa_m r}}{r} \quad (\kappa_m = \sqrt{m(m+1)\Theta/D}) \quad (6)$$

where A , B , and C_m are constants still to be determined. The corresponding positive exponential solution for $m > 1$ is, of course, eliminated by boundary condition (i). Furthermore, condition (i) also implies that

$$A = c_0 \quad (7)$$

The auxiliary condition (iii) gives directly

$$B = -\frac{\phi}{2\pi D} \quad (8)$$

After substituting equation 3 into boundary condition

(ii), multiplying by $P_m(\cos \theta) \sin \theta d\theta/2$, $m \geq 1$, and integrating over θ , one finds

$$\begin{aligned} & -2\pi R_T D C_m e^{-\kappa_m R_T} \left(\kappa_m + \frac{1}{R_T} \right) \frac{1}{2m+1} = \\ & \left(k_a^0 \left(A + \frac{B}{R_T} \right) - k_d^0 \frac{N_f}{N_e} \right) \int_0^\pi P_m(\cos \theta) X(\theta) \frac{\sin \theta d\theta}{2} + \\ & k_a^0 \sum_{n=1}^\infty C_n \frac{e^{-\kappa_n R_T}}{R_T} \int_0^\pi P_m(\cos \theta) X(\theta) P_n(\cos \theta) \frac{\sin \theta d\theta}{2} \end{aligned} \quad (9)$$

where $m = 1, 2, 3, \dots, \infty$.

Equation 9 comprises a set of simultaneous equations for the C_m . If one first defines

$$X_{mn} \equiv \int_0^\pi P_m(\cos \theta) X(\theta) P_n(\cos \theta) \frac{\sin \theta d\theta}{2} \quad (10)$$

$$Q \equiv k_a^0 / 2\pi R_T D \quad (11)$$

$$P \equiv k_d^0 (N_f / N_e) / 2\pi R_T D \quad (12)$$

then eq 9 may be written in the form

$$\mathbf{GC} = \mathbf{L}_0 \quad (13)$$

where the elements of the column vector \mathbf{C} are just the coefficients C_m

$$(\mathbf{C})_m = C_m \quad (14)$$

and the vector \mathbf{L}_0 is defined by

$$(\mathbf{L}_0)_m = \left\{ Q \left(A + \frac{B}{R_T} \right) - P \right\} X_{m0} \quad (15)$$

The matrix \mathbf{G} is defined by

$$G_{mn} = -Q \frac{e^{-\kappa_n R_T}}{R_T} X_{mn} - e^{-\kappa_m R_T} \left(\kappa_m + \frac{1}{R_T} \right) \frac{\delta_{m,n}}{2m+1} \quad (16)$$

and $\delta_{m,n}$ is the Kronecker delta. For computational purposes it is convenient to symmetrize the matrix \mathbf{G} . This can be achieved by defining

$$(\xi^{1/2})_{mn} = e^{-\kappa_m R_T / 2} \delta_{m,n} \quad (17)$$

$$(\xi^{-1/2})_{mn} = e^{+\kappa_m R_T / 2} \delta_{m,n} \quad (18)$$

which can be seen to be inverses of one another by inspection. Now for $i \neq l$

$$\begin{aligned} (\xi^{1/2} \mathbf{G} \xi^{-1/2})_{il} &= \sum_{j,k} (\xi^{1/2})_{ij} G_{jk} (\xi^{-1/2})_{kl} \\ &= -Q e^{-[(\kappa_i + \kappa_l) R_T] / 2} X_{il} \end{aligned} \quad (19)$$

which is symmetric.

Transforming eq 12 we have

$$(\xi^{1/2} \mathbf{G} \xi^{-1/2}) (\xi^{1/2} \mathbf{C}) = (\xi^{1/2} \mathbf{L}_0) \quad (20)$$

Direct matrix inversion and multiplication by $\xi^{-1/2}$ gives

$$C = \xi^{-1/2}(\xi^{1/2}G\xi^{-1/2})^{-1}\xi^{-1/2}L_0 \quad (21)$$

which enables one to determine the C_m in terms of D , Θ , R_T , k_a^0 , k_d^0 , N_t , N_e , c_0 , and ϕ . Since ϕ remains an unknown, we are not yet finished. Fortunately the ϕ occurs only in a constant factor of L_0 (cf. eq 15). If one defines a vector \mathbf{d} with elements d_m such that

$$C_m \equiv \left\{ Q \left(A + \frac{B}{R_T} \right) - P \right\} d_m \quad (m = 1, 2, \dots, \infty) \quad (22)$$

then from eq 21 and 15 one has

$$\mathbf{d} = \xi^{-1/2}(\xi^{1/2}G\xi^{-1/2})^{-1}\xi^{1/2}X_0 \quad (23)$$

where $(X_0)_m = X_{m0}$. The d_m can now be found in terms of D , Θ , R_T , k_a^0 , k_d^0 , N_t , and N_e to any desired accuracy by including a sufficiently large number of Legendre polynomials in the set. One more independent equation is needed to determine ϕ . This equation is obtained by multiplying boundary condition (ii) by $P_0(\cos \theta) \sin \theta d\theta/2$ and integrating over θ , thus obtaining

$$\phi = \int_0^\pi k_a^0 \left(c(R_T, \theta) - \frac{k_d^0 N_t}{k_a^0 N_e} \right) X(\theta) \frac{\sin \theta d\theta}{2} \quad (24)$$

Upon substituting eq 23 into eq 22, 6, and 3, which are in turn put into eq 24, one finds

$$\phi = \left\{ k_a^0 \left(c_0 - \frac{\phi}{2\pi D R_T} \right) - k_d^0 \frac{N_t}{N_e} \right\} X_{00} + k_a^0 \left\{ Q \left(c_0 - \frac{\phi}{2\pi R_T D} \right) - P \right\} \sum_{m=1}^{\infty} d_m \frac{e^{-\kappa_m R_T}}{R_T} X_{m0} \quad (25)$$

Rearrangement of eq 25 and multiplication by N_e leads finally to the total reaction rate

$$\Phi \equiv N_e \phi = \frac{k_a^0 (2\pi R_T D) c_0 N_e - k_d^0 (2\pi R_T D) N_t}{\left(\frac{2\pi R_T D}{\text{sum}} \right) + k_a^0} \quad (26)$$

where

$$\text{sum} = X_{00} + \frac{k_a^0}{2\pi R_T D} \sum_{m=1}^{\infty} d_m \frac{e^{-\kappa_m R_T}}{R_T} X_{m0} \quad (27)$$

The effective association rate constant is

$$\bar{k} = \frac{k_a^0 2\pi R_T D}{\left(\frac{2\pi R_T D}{\text{sum}} \right) + k_a^0} \quad \left(\frac{\text{cm}^3}{\text{molecule sec}} \right) \quad (28)$$

and expressed in molar units it is

$$\bar{k}_M = \frac{N_A}{1000} \bar{k} \quad \left(\frac{\text{l.}}{\text{mol sec}} \right) \quad (29)$$

where N_A is Avogadro's number.

The effective unimolecular constant is

$$\bar{k} = \frac{k_d^0 2\pi R_T D}{\left(\frac{2\pi R_T D}{\text{sum}} \right) + k_a^0} \quad (\text{sec}^{-1}) \quad (30)$$

These formulae, apart from the sum factor in the denominator, are equivalent to those for spheres that are uniformly reactive over their entire surface,^{5a} provided that only half the allowed solid angle is accessible.

Complete solution of the problem is effected by solving eq 23 for the d_m , and then substituting these values into sum (cf. eq 27), which may then be utilized directly in eq 26, 28, 29, or 30. This completes the formal solution of the problem.

IV. The Numerical Solution

Numerical values for the d_m were obtained by considering a finite number of successive Legendre polynomials from $m = 1$ up to some suitable $m = n$, computing the X_{mn} by numerical integration, constructing the G matrix and symmetrizing it by matrix multiplication with the $\xi^{1/2}$ and $\xi^{-1/2}$ matrices, and applying eq 23 directly. The numerical integrations required to determine all the X_{mn} consumed the bulk of the computing time, while the matrix inversion constituted the major memory capacity requirement. Actually, the X_{mn} could have been determined by analytic integrations in this case, in which $X(\theta)$ is given by the step function in eq 2, but the program was written so as to permit inclusion of arbitrary $X(\theta)$ functions in future calculations. The integration on θ needs to be carried out only over the region for which $X(\theta)$ is nonvanishing, and typically 200 points interior to this region were used.

If Stokes laws are employed for the friction factors associated with translational and rotational motions of the spheres, then the diffusion coefficients may be written as^{12, 13}

$$D = kT/6\pi\eta R_H \quad (31)$$

$$\Theta = kT/8\pi\eta R_H^3 \quad (32)$$

where η is the solvent viscosity, T the absolute temperature, and k is Boltzmann's constant. It is now apparent that the quantity $\kappa_m R_T = (m(m+1)\Theta/D)^{1/2} R_T$ is proportional to R_T/R_H . Similarly, $2\pi R_T D$ is also proportional to R_T/R_H . Furthermore, every element G_{mn} may be written as the product of $(R_T)^{-1}$ and a function of R_T/R_H ; consequently d_m is a product of R_T and a function of R_T/R_H . It is clear from eq 27, then, that sum is a function simply of the ratio R_T/R_H . Indeed, the effective rate constants are also functions simply of R_T/R_H . Thus, at constant η and T the only variables are R_T/R_H , and θ_0 the allowed angular reaction range. In the calculations reported here the temperature was always taken to be 300°K.

Cost considerations influenced the decision not to use more than the first 140 Legendre polynomials. Since only values of $\theta_0 \geq 0.05$ radian were employed,

(12) A. Einstein, "Investigations on the Theory of Brownian Movement," Dover Publications, New York, N. Y., 1956, p 17.

(13) P. Debye, "Polar Molecules," Dover Publications, New York, N. Y., 1929, p 85.

truncation of the series at 140 appeared to be adequate. The exponential factors act to diminish the contribution of the terms with large m for reasonable values of R_T/R_H . In all cases the result was insensitive to enlargement of the set with additional Legendre polynomials.

Since the main objective here was the investigation of the diffusion-controlled limit for the association reaction, results are presented only for the diffusion-controlled molar forward rate constant

$$k_{\text{eff}} \equiv \bar{k}_M(\text{diffusion-controlled}) \quad (33)$$

where *in every case* the molar intrinsic association rate constant $k_a' = k_a^0 N_A / 1000$ was chosen so that $k_a' \gg k_{\text{eff}}$ (i.e., the *extreme diffusion-controlled limit*).⁵

To facilitate comparison with the corresponding diffusion-controlled rate constant for reaction between *uniformly reactive spheres*, the following procedure was adopted. The diffusion-controlled rate constant for reaction of such spheres *with an identical sphere rigidly attached to the plane at a (bottom) tangent* is easily ascertained to be

$$k_{\text{diff}} = \frac{N_A}{1000} 2\pi(2R_H)D \quad \left(\frac{1}{\text{mol sec}} \right) \quad (34)$$

the target radius being $2R_H$ in this instance, and the available solid angle being still 2π steradians. The quantity k_{diff} is independent of R_H (and R_T), and at $T = 300^\circ\text{K}$, $\eta = 0.008$ poise

$$k_{\text{diff}} = 2.08 \times 10^9 \quad \left(\frac{1}{\text{mol sec}} \right) \quad (35)$$

The ratio $k_{\text{eff}}/k_{\text{diff}}$ provides a direct measure of the effectiveness of the radial and orientation constraints in reducing the maximum theoretical rate constant below that value expected for uniformly reactive spheres, subject still to the condition that one be stationary and that only half the total solid angle be allowed. Computed values of $k_{\text{eff}}/k_{\text{diff}}$ are plotted against the allowed reactive angular range θ_0 for several values of R_H/R_T in Figure 2. The limiting values at $\theta_0 = \pi$ give the effect of the radial constraint alone, as the spheres are uniformly reactive for that value of θ_0 .

There arises the question of what constitutes a reasonable target radius R_T , or radial constraint, for a particular value of θ_0 . At least for small θ_0 the following criterion seemed useful, and it was adopted for the remainder of the calculations. The reaction condition that allows the center of the diffusing sphere to lie anywhere on a hemisphere of radius R_T introduces an uncertainty $\sim 2R_T$ in the horizontal position of any site on the sphere surface, and a vertical uncertainty $\sim R_T$. The allowed angular deviation θ_0 allows an uncertainty $\sim 2\theta_0 R_H$ in the position of any site on the surface. It seems probable that in reality the *reaction tolerance*

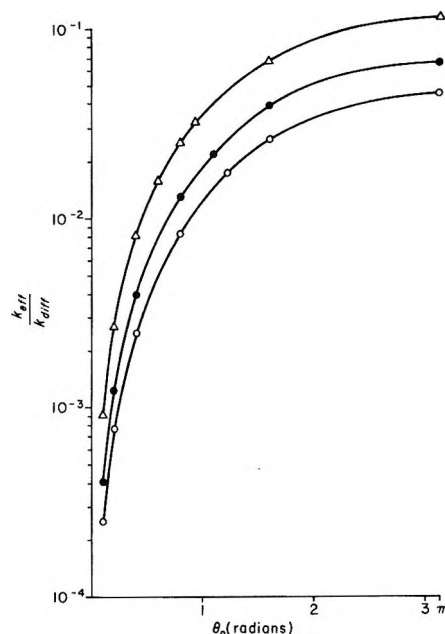


Figure 2. Computed values of $k_{\text{eff}}/k_{\text{diff}} = k_{\text{eff}}/2.08 \times 10^9$ as a function of the allowed angular reaction range θ_0 . For the triangles (Δ) $R_H/R_T = 4.0$, $k_a' = 2.6 \times 10^8 M^{-1} \text{sec}^{-1}$; for the filled circles (\bullet) $R_H/R_T = 7.0$, $k_a' = 1.49 \times 10^8 M^{-1} \text{sec}^{-1}$; for the open circles (\circ) $R_H/R_T = 10$; $k_a' = 1.04 \times 10^8 M^{-1} \text{sec}^{-1}$. For all calculations $T = 300^\circ\text{K}$, $\eta = 0.008$ P.

for spatial deviation of the site on the sphere is the same, whether it originates from translation of the sphere as a whole, or from its rotation. Thus, it was decided to maintain the relation

$$2\theta_0 R_H = 2R_T \quad (36)$$

for the remainder of the calculations. The rotational and translational constraints are thus assumed to be interconnected in this way to guarantee, at least in an approximate way, some element of physical reasonability. Adoption of eq 36 certainly enhances the dependence of the diffusion-controlled rate constant on the allowed angle θ_0 over what one would find using a fixed R_T . However, if the purpose of the orientation constraint is to bring a reactive point on the sphere within some small distance of a reactive point on the plane, then it would be quite unreasonable to employ a very small $\theta_0 R_H$ together with a large R_T . In such a case moving the center of the sphere from one side of the target hemisphere to the other would produce a much greater deflection of the reactive point on the sphere than would a rotation of the sphere through θ_0 . Thus, the acceptable distance for reaction between the reactive sites would depend upon whether the deflection was due to translation or rotation of the sphere, which is clearly unphysical. An alternative that permits one to keep separate radial and angular constraints and also to maintain some physical reasonability is to assume that R_T is proportional to θ_0 . The small target effect noted previously¹⁴ is here seen to be an essential

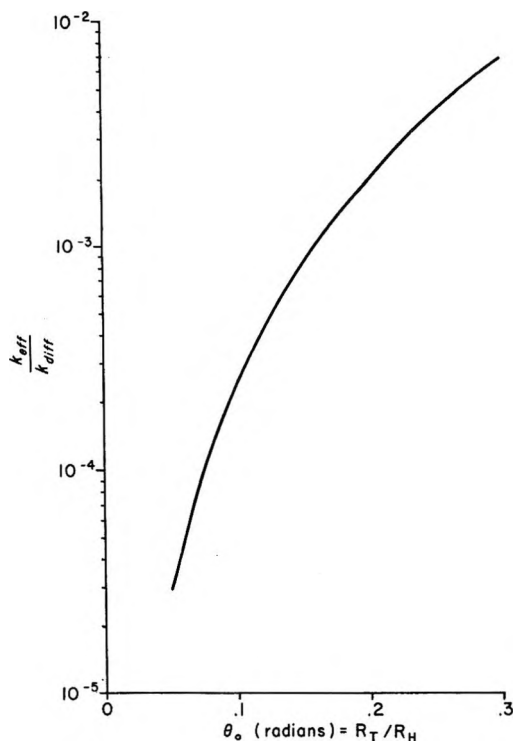


Figure 3. Computed values of $k_{\text{eff}}/k_{\text{diff}}$ as a function of $\theta_0 = R_T/R_H$. The value of k_a^0 was chosen so that $Q = k_a^0/2\pi R_H D = 10.0$ for each point calculated. The range of k_a^0 values was from 5×10^8 to $3 \times 10^9 M^{-1} \text{sec}^{-1}$. For these calculations $T = 300^\circ\text{K}$, $\eta = 0.008$.

prerequisite for any moderately stringent orientation constraint. Since according to eq 36 $\theta_0 = R_T/R_H$, we now find that the rate constants \bar{k} , \bar{k} , and k_{eff} are functions only of R_H/R_T , T , and η .

The quantity $k_{\text{eff}}/k_{\text{diff}}$ is plotted against $\theta_0 = R_T/R_H$ in Figure 3. This is a kind of "universal" relation along which "reasonable" systems at room temperature in aqueous solution may be expected to cluster.

V. Results and Discussion

Perhaps the most interesting feature of Figures 2 and 3 is the extreme smallness of the $k_{\text{eff}}/k_{\text{diff}}$ values at only moderately small allowed angular ranges. The maximum rate constant for a diffusion-controlled reaction in solution is evidently reduced by four and a half orders of magnitude with an angular constraint of only $\theta_0 = 0.05$ radian $= 2.86^\circ$, and without any azimuthal constraint whatsoever. The total angle subtended by the reaction cone is $2\theta_0$, so that such a constraint is in fact not an extremely stringent one. As noted above, the values of $k_{\text{eff}}/k_{\text{diff}}$ at $\theta_0 = \pi$ (cf. Figure 2) exhibit a reduction in rate constant arising from the fact that R_T is used in place of $2R_H$ for the "reaction radius." This *small target effect* results in somewhat more than a factor of 10 reduction in the diffusion-controlled rate constants. The limiting values of $k_{\text{eff}}/k_{\text{diff}}$ at $\theta_0 = \pi$ are not exactly equal to $R_T/2R_H$ owing to the fact that k_a^0 is not infinite, but is in-

stead only about ten times k_{eff} . Thus, the k_{eff} calculated here is actually about 10% below its maximum value at $\theta_0 = \pi$, and this discrepancy disappears with decreasing θ_0 .

It is possible to assess the role of rotational diffusion in the following way. Suppose that the orientation constraint remains, but that there is no rotational diffusion. Clearly, only that fraction $f(\theta_0)$ of the molecules possessing orientation vectors in the proper range needs to be considered. In the absence of rotational diffusion the effective diffusion-controlled rate constant is easily found to be

$$k_{\theta_0} = f(\theta_0)2\pi R_T D \frac{N_A}{1000} \quad (37)$$

where, of course, $f(\theta_0)$ is given by

$$f(\theta_0) = \int_0^{\theta_0} \frac{\sin \theta \, d\theta}{2} = \frac{(1 - \cos \theta_0)}{2}$$

Values of k_{θ_0} are compared with values of k_{eff} computed for the same $\theta_0 \simeq R_T/R_H$ in Table I. It will be observed that for the smaller angles, the effect of rotational diffusion is to enhance the rate by just about a factor of two over the rate prevailing in the absence of rotational diffusion. This observation may be of some benefit in estimating the diffusion-controlled rate constant at somewhat smaller angular constraints than those employed in these calculations.

Table I: Effect of Rotational Diffusion on the Diffusion-Controlled Rate Constant

θ_0 , radians	R_H/R_T	η , P	k_{eff} , $M^{-1} \text{sec}^{-1}$	$k_{\text{eff}}/k_{\theta_0}$
1.04	1	0.008	4.3×10^8	1.65
0.30	3.33	0.008	1.39×10^7	1.975
0.20	5.0	0.008	4.13×10^6	1.988
0.149	6.72	0.008	1.74×10^6	2.04
0.143	7.0	0.008	1.53×10^6	2.06
0.098	10.0	0.008	5.19×10^5	2.12
0.048	20.0	0.008	6.18×10^4	2.23

It has been previously noted that, for the case of uniformly reactive spheres, the reciprocal of the effective forward bimolecular (or reverse unimolecular) rate constant is linear in the viscosity, irrespective of the degree of diffusion control.¹⁴ Although we are at present unable to establish by analytical arguments the same conclusion for a reaction involving orientable spheres capable of rotational diffusion, we have examined this conjecture numerically. Plots of k_M^{-1} vs. η are given for several values of θ_0 in Figure 4. Indeed, there is only a very slight curvature with a change in slope amounting to only a few per cent over two orders of magnitude in η . On the basis of these computa-

(14) J. M. Schurr, *Biophys. J.*, **10**, 717 (1970).

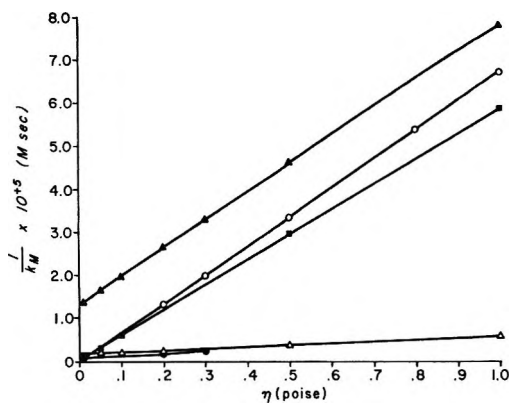


Figure 4. The reciprocal (k_M)⁻¹ of the computed bimolecular rate constant as a function of viscosity η . For the filled triangles (\blacktriangle) $R_T/R_H = \theta_0 = 1/7$, $k_a' = 1.48 \times 10^7$; for the open circles (\circ) $R_T/R_H = 1/555$, $\theta = 3.1416$, $k_a' = 1.48 \times 10^7$; for the filled squares (\blacksquare) $R_T/R_H = \theta = 1/7$, $k_a' = 1.48 \times 10^9$; for the filled circles (\bullet) $R_T/R_H = \theta_0 = 0.37$, $k_a' = 1.53 \times 10^7$; for the open triangles (\triangle) $R_T/R_H = \theta_0 = 1/3$, $k_a' = 3.46 \times 10^7$. The k_a' above are given in units of $M^{-1} \text{sec}^{-1}$. For all of the calculations $T = 300^\circ\text{K}$.

tions we adopt, tentatively, the conclusion that k_M^{-1} is essentially linear with respect to η under all conditions.

A thorough analysis of these results is postponed until Section VIII, where the discussion is pertinent to experimental data for the renaturation rate of DNA as a function of viscosity.

VI. Estimation of Diffusion-Controlled Rate Constants for Bimolecular Reactions with Orientation Constraints

Although the results presented in this paper apply strictly to orientable spheres reacting with stationary sites on a plane, one may readily estimate the *diffusion-controlled bimolecular* rate constant k_G for the reaction between two mobile species of orientable spheres using the rate constants computed here. If one includes a factor $(D_A + D_B)/D_A$ to account for the simultaneous translational diffusion of both species, following Smoluchowski, and if one also includes a factor of two to account for both the simultaneous rotational diffusion of the reactants and the departure from planar geometry, then one has in general

$$k_G \cong 2 \left(\frac{D_A + D_B}{D_A} \right) k_{\text{eff}} \quad (38)$$

where $D_A = kT/(6\pi\eta R_H)$ is the diffusion coefficient that is employed in computing k_{eff} . It is anticipated that k_G estimated in this way will be in error by probably less than a factor of two. Physical reasonability requires that this procedure be applied only for spheres B with sufficiently large radii so that $R_B \gg \theta_0 R_A = R_T$

It is the author's hope that eq 38 employed in conjunction with Figure 3 and eq 34 and 35 will enable reasonable estimates of diffusion-controlled rates to be made for any bimolecular reaction involving large

molecules with a reasonable (known or guessed) orientation constraint, and conversely, that from a knowledge of the experimental diffusion-controlled rate constant the orientation constraint may be estimated for any reaction.

VII. Reaction of the H_2O_2 -Horseradish Peroxidase Complex with Cytochrome c

Farwell and Ackerman⁸ have examined the viscosity dependence of the rate of association of H_2O_2 -horseradishperoxidase with cytochrome c. The bimolecular rate constant for this association was observed to become viscosity dependent when the viscosity was about ten times that of water, and the rate constant had the value $\bar{k}_M \cong 5 \times 10^5 M^{-1} \text{sec}^{-1}$. In water, presumably, the rate constant has its low viscosity limiting value. It is important now to examine the low viscosity limit for \bar{k} in eq 28 and sum in eq 27. It is clear from eq 11 that Q is proportional to the viscosity η so that in the low viscosity limit $Q \rightarrow 0$, and the matrix \mathbf{G} becomes independent of viscosity (*cf.* eq 16). In this limit the d_m are then independent of η (*cf.* eq 23), and we see that

$$\lim_{\eta \rightarrow 0} \text{sum} = X_{00} = \int_0^{\theta_0} \frac{\sin \theta d\theta}{2} = f(\theta_0) \quad (39)$$

and, consequently

$$\lim_{\eta \rightarrow 0} \bar{k} = k_a^0 \frac{(1 - \cos \theta_0)}{2} \quad (40)$$

The problem is to select a k_a^0 and a $\theta_0 = R_T/R_H$ such that the following two conditions are approximately satisfied: (a) $\lim_{\eta \rightarrow 0} \bar{k}_M = k_a^0 (1 - \cos \theta_0)/2 \cong 5 \times 10^5 M^{-1} \text{sec}^{-1}$, where $k_a^0 = (N_A k_a^0 / 1000)$; and (b) the rate constant \bar{k}_M becomes viscosity dependent when $\eta \cong 0.05 \text{ P}$. Inspection of the expressions for \mathbf{G} and sum indicates that increasing the viscosity will begin to affect the rate constant when $k_a^0 \approx (0.25) (2\pi R_T D N_A / 1000) = (kT N_A / 3000\eta) (0.25) \theta_0$. If we now specify that this relation shall obtain when $\eta \cong 0.05$, then we find $k_a^0 \approx 4.2 \times 10^7 \theta_0$, which together with (a) above permits determination of both k_a^0 and θ_0 . There results

$$\theta_0 \approx 0.37 \text{ radian} \quad (41)$$

$$k_a^0 \approx 1.5 \times 10^7 M^{-1} \text{sec}^{-1} \quad (42)$$

Values of \bar{k}_M computed using eq 41, 42 are plotted against the inverse viscosity in Figure 5. The experimental data of Farwell and Ackerman are also shown for comparison. A curve computed using $\theta_0 = 0.143$ radian and $k_a^0 = 1.48 \times 10^7 M^{-1} \text{sec}^{-1}$ is also shown to indicate the sensitivity of the result to choice of angular constraint. Perhaps it is not too optimistic to anticipate that more precise data will enable a fairly accurate estimate of the angular constraint θ_0 for this reaction.

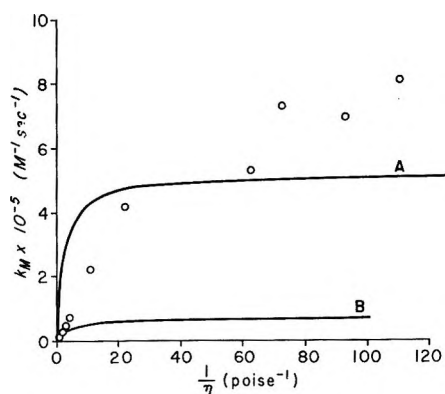


Figure 5. The bimolecular rate constant k_M for the association of the H_2O_2 -horseradish peroxidase complex with cytochrome *c* as a function of the reciprocal viscosity $1/\eta$. The open circles (O) represent the data of Farwell and Ackerman (*cf.* ref 8). Solid line A is the theoretical curve computed with $R_T/R_H = \theta_0 = 0.37$, $k_a' = 1.5 \times 10^7 M^{-1} \text{sec}^{-1}$. Solid line B is a theoretical curve computed with $R_T/R_H = \theta_0 = 0.143$, $k_a' = 1.48 \times 10^7 M^{-1} \text{sec}^{-1}$.

VIII. The Effect of Viscosity on the Rate of Renaturation of DNA

Wetmur and Davidson¹¹ have presented a thorough study of the renaturation rate of various DNA's as a function of complexity, chain length, temperature, and viscosity. The observed complexity and chain-length dependence were summarized concisely in their eq 20 as

$$k_2 = 3.5 \times 10^5 L^{0.5} / N \quad (43)$$

where k_2 is the second-order rate constant calculated from $v_2 = k_2 P^2 / 4$, v_2 being the molar rate of base pair formation and P the denatured DNA phosphorus concentration; L is the average number of bases per single-stranded DNA molecule; and N is the complexity, or number of base pairs in nonrepeating sequences for a given biological species. The rate constant k_2 applies at temperature $(T_m - 25)^\circ$, and $[Na^+] = 1.0 M$ in aqueous solution in the neutral pH range. Furthermore, the rate constant was strongly viscosity dependent. Although Wetmur and Davidson concluded that k_2 was "inversely proportional" to the viscosity, we wish to consider the strong possibility that this is not strictly the case. This point will subsequently be discussed further. The constant k_2 also exhibited a moderately broad maximum as a function of $(T_m - T)$ with the maximum occurring some 20–30° below T_m .

The linearity of the second-order rate plots of the optical density over 75% of the renaturation range certainly argues that the bimolecular step is rate-limiting. Furthermore, the $L^{0.5}$ dependence of k_2 and its sharp viscosity dependence strongly suggest that this bimolecular step is diffusion-controlled. On the basis of general theoretical arguments (neglecting diffusion-control) Wetmur and Davidson showed that k_2 should be proportional to L , since this is the number of base-

pairs formed in the rapid zippering reaction immediately following each bimolecular recognition, or nucleation, step. Since the diffusion coefficient for a nondraining random coil has the form $D \sim TL^{-0.5} \eta^{-1}$, it is apparent that, if the reaction were diffusion-controlled, one might expect to find $k_2 \sim L^{0.5}$ as was observed. All of these considerations were carefully made by Wetmur and Davidson, who nonetheless *rejected* diffusion-control of the bimolecular step primarily on the grounds that the absolute rate constant calculated according to the formula of Smoluchowski $k_2 = 4\pi(2D)R_T$ would be far too large for any reasonable choice of reaction radius R_T . From our calculations it is easily shown that a cylindrically symmetrical orientation constraint of $\theta_0 = 0.05$ radian (or an allowed fraction of total solid angle $f(0.05) = 6.3 \times 10^{-4}$) will reduce the diffusion-controlled rate by three orders of magnitude, quite apart from the small target effect (*i.e.*, $R_T < \text{twice the effective hydrodynamic radius} = 2kT/6\pi\eta D$) already considered by Wetmur and Davidson. Removal of cylindrical symmetry by including an azimuthal constraint will reduce the diffusion-controlled rate constant even further below the value predicted by the Smoluchowski equation. Such constraints for the alignment of strands during the nucleation step are not unreasonable. Presumably a number of base-pairs must be nearly aligned so that they can react almost simultaneously. A single hydrogen bond could not hold such large particles against their Brownian motion. If the polar axis from which θ_0 is measured is taken *parallel to one* of the strands, then a reaction cone constraint of $\theta_0 = 3^\circ$ for the axis of the complementary strand is not unreasonable. Furthermore, it is difficult to see how more than a quarter of the azimuthal angular range of the other strand could permit reaction to occur, since the bases of the two parallel chains must be pointing toward one another. If it is assumed that our calculated rate reduction factors due to orientation constraints $(2R_H/R_T)(k_{\text{eff}}/k_{\text{diff}})$ can be transferred directly to the DNA problem, then we may employ an orientation rate constant

$$k_\theta = (3 \times 10^{-4}) 4\pi R_T D; \theta_0 = 0.05 \text{ radian} \quad (44)$$

which is simply the Smoluchowski constant, including the small target effect, multiplied by a factor (3×10^{-4}) that pertains to the polar angle constraint $\theta_0 = 0.05$ and contains an additional (and arbitrary) reduction by a factor of four to account for both the azimuthal constraint and the reduced solid angle available for reaction. If our eq 44 is used in place of their eq 22, then Wetmur and Davidson's eq 23 becomes

$$R_T \approx 2 \times 10^{-8} \beta^{-3} \text{ cm} \quad (45)$$

where β is the fraction of base pairs that may serve as nucleation sites. Now, when $\beta = 1$, $R_T = 2 \times 10^{-8}$ cm, which is not at all an unreasonable value.

Wang and Davidson¹⁵ have argued that segment diffusion will increase the reaction rate by a factor of 100 above that due to translational diffusion alone. Their estimate hinges in a crucial way on the value of the segmental diffusion coefficient and the interpretation of its role in determining the encounter frequency. The segmental diffusion coefficient was estimated from the shortest relaxation time in the electric birefringence spectrum and used in Smoluchowski's formula to compute the segment encounter rate. Although this procedure may give a crude estimate of the dynamics of segments engaged in low-amplitude, small-displacement motions, it is hardly adequate to describe diffusion along a steep and extensive diffusion gradient varying as R_T/r , where $r \geq R_T$ can be as large as the dimensions of the entire polymer molecule. Surely the effective segmental diffusion coefficient for diffusion into a sink is very much smaller than that applicable to the relaxation of small distortions of the radial distribution function. For this reason the conjectured rate enhancement by a factor of 100 due to segmental diffusion appears to be a very gross overestimate. Furthermore, the coulombic repulsion of the strands will act to reduce the rate constant below the value predicted by Smoluchowski's formula.

In view of these considerations it is felt that the primary argument of Wetmur and Davidson against diffusion-control of the bimolecular step has been essentially nullified.

In any event the mechanism advanced by Wetmur and Davidson to account for the $L^{0.5}$ dependence of the bimolecular rate constant, the excluded volume effect, is inconsistent with their contention that the bimolecular step is not diffusion-controlled. It simply is not possible for the imposition of any large-scale (*i.e.*, excluded volume) geometrical constraint to reduce the rate of reaction of these flexible, freely-diffusing, single-strand molecules without introducing a concomitant "diffusion control" of that reaction. Only if these polymers were highly branched, or formed metastable bonds so as to inhibit free diffusion, would such a conclusion require modification. As shown in paper I, the extent of diffusion-control depends upon a relative competition between the *intrinsic rate constant* and the *diffusion rate constant*. The imposition of a large-scale geometrical constraint is capable only of reducing the diffusion rate constant. This will either leave the rate unchanged or decrease it, and any decrease necessarily implies an onset of diffusion-control. Clearly an excluded volume effect of such a magnitude as to make itself felt in the rate constant implies a large degree of diffusion-control of the reaction.

Finally, it must be noted that since the dependence of sum upon D (or L) is not known, we have not offered an explanation for the $L^{0.5}$ dependence of the bimolecular rate constant. Indeed, the excluded volume effect *may* be responsible for this length dependence *pro-*

vided that the overall reaction is largely diffusion-controlled. Detailed arguments in support of our belief that the reaction is to a considerable extent diffusion-controlled are given below.

A feature of the renaturation reaction that is difficult to reconcile with *complete* diffusion-control is the bell-shaped temperature dependence of the bimolecular rate constant k_2 . It is possible to examine the question of the *degree of diffusion-control* by plotting the reciprocal $(k_2)^{-1}$ vs. η/T . As is apparent from the calculations presented in Figure 3, one expects to obtain a nearly straight line for any reaction, irrespective of the degree of diffusion-control. However, the relative magnitudes of \bar{k}_M and its low viscosity limit k_M^0 provide a measure of the degree of diffusion-control as shown below. According to eq 28 and 29

$$(1/\bar{k}_M) = \frac{1000}{N_A} \left\{ \frac{1}{2\pi R_T D} + \frac{1}{k_a^0 \cdot \text{sum}} \right\} \quad (46)$$

An expression for the zero-viscosity intercept $1/k_M^0$ is found from eq 40

$$1/k_M^0 \equiv \lim_{\eta \rightarrow 0} 1/k_M = 2000/N_A k_a^0 (1 - \cos \theta_0) \quad (47)$$

and together with an estimate of θ_0 permits an estimate of k_a^0 , the intrinsic rate constant for properly aligned reactants. The existence of a nearly straight line for the calculated values in Figure 3 implies that

$$\frac{1}{\text{sum}} \cong A\eta + B \quad (48)$$

where from equation 39 $B = 2/(1 - \cos \theta_0)$, and A is an empirically determined constant. Equation 46 may be rewritten to display the explicit linearity in η

$$(1/\bar{k}_M) \cong \eta \left\{ \frac{3000}{N_A k T} \frac{R_H}{R_T} + \frac{A}{k_a'} \right\} + \frac{2}{k_a' (1 - \cos \theta_0)} \quad (49)$$

where $k_a' = (1000/N_A)k_a^0$ is the molar intrinsic rate constant. Now, the degree of diffusion-control d may be defined by

$$d \equiv 1 - \bar{k}_M/k_M^0; \quad 0 \leq d \leq 1 \quad (50)$$

Thus, any reciprocal plot of $1/\bar{k}_M$ vs. η for which the intercept $1/k_M^0$ is significantly different from zero cannot represent a completely diffusion-controlled reaction (*i.e.*, $d < 1$). A modification of the reciprocal plot that may be employed when the temperature is not held constant is to graph $1/\bar{k}_M$ vs. (η/T) . We have not investigated the linearity of such plots by direct calculation, but feel confident that deviations from linearity will be small so long as k_a' is only weakly temperature dependent over the same interval. Such plots for the data of Wetmur and Davidson are given in Figures 6 and 7, in which also the $\Delta T = T_m - T$ values associated with each point are presented. Examining

(15) J. C. Wang and N. Davidson, *J. Mol. Biol.*, **19**, 469 (1966).

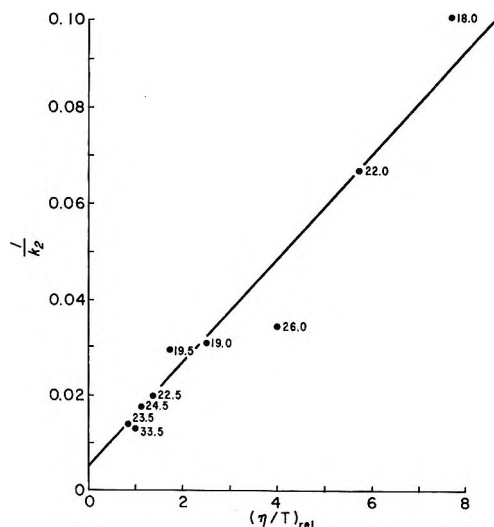


Figure 6. Reciprocal plot of $1/k_2$ vs. $(\eta/T)_{rel}$ for the renaturation of mechanically sheared T4 DNA in 0.4 M sodium ion in phosphate buffer, pH 7, containing ethylene glycol to enhance the viscosity. These data were reported by Wetmur and Davidson (ref 11). The values of $(T_m - T_r)$ associated with each measurement are indicated in the figure. T_m is the melting point of DNA in a solution of the given composition, and T_r is the temperature at which the kinetics of the reaction were observed.

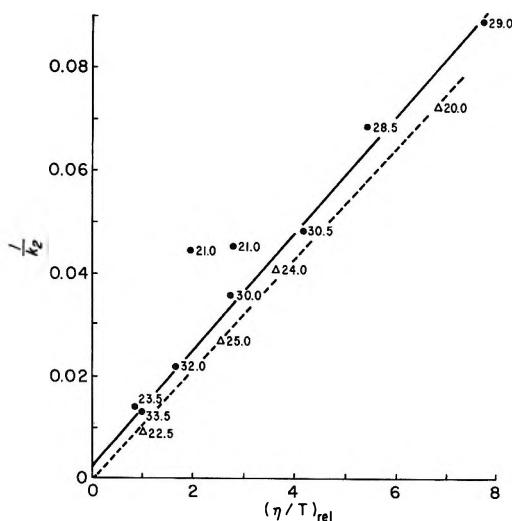


Figure 7. Reciprocal plot of $1/k_2$ vs. $(\eta/T)_{rel}$ for the renaturation of mechanically sheared T4 DNA in 0.4 M sodium ion (the filled circles ●), and in 1.0 M sodium ion (the triangles Δ), in phosphate buffer, pH 7.0, containing sucrose to enhance the viscosity. These data were reported by Wetmur and Davidson (see ref 11). The values of $(T_m - T_r)$ associated with each measurement are indicated in the figure; see legend of Figure 6 for explanation.

Figure 6 for the ethylene glycol data first, it is observed that the data taken in the range $\Delta T = 19$ – 23.5° give a good straight line with a significant positive intercept. Furthermore, the $\Delta T = 18^\circ$ point lies above this line while the 26 and 33.5° points lie below this line. If the intrinsic molar rate constant k_a' increases with de-

creasing temperature, then one would expect points of smaller ΔT to lie above, and the points of larger ΔT to lie below the line characterizing the "main" group of ΔT values, as observed. Taking the intercept in Figure 6 to be $1/k_M^0 = 0.005$ one finds at $\Delta T \approx 21^\circ$ and $[Na^+] = 0.4 M$ a degree of diffusion control for $(\eta/T)_{rel} = 1$ of approximately

$$d = 1 - 50(0.005) = 0.75 \quad (51)$$

The corresponding data for the sucrose solutions in 0.4 M and 1.0 M Na^+ ion are plotted in Figure 7. The data for the 1.0 M Na^+ solutions apparently have an intercept that is not significantly different from zero. The data for the 0.4 M Na^+ solutions appear to have an intercept somewhat different from zero, but its significance is more open to question than it was for the ethylene glycol data. However, if one specifies that only points in the range $\Delta T = 29$ – 33.5° are to be considered, then a reasonable straight line and intercept are obtained. Again, points with ΔT less than the "main" range of values lie above the line drawn, as expected if k_a' increases with decreasing temperature below T_m . Although rather less accuracy can be claimed in this instance, the degree of diffusion control at $\Delta T \approx 31^\circ$ and $[Na^+] = 0.4 M$ for $(\eta/T)_{rel} = 1$ is found to be (taking $1/k_M^0 = 0.0022$)

$$d \cong 1 - (45.6)(.0022) = 0.90 \quad (52)$$

The degree of diffusion control at $\Delta T \approx 25^\circ$ and $[Na^+] = 1.0 M$ is evidently $d \cong 1$ for all values of $(\eta/T)_{rel}$ for which data were obtained. The implication is that the intrinsic rate constant k_a' is simply enough faster in the presence of the extra salt so that the rate constant is essentially completely diffusion-controlled in aqueous solution. A reciprocal plot of the $NaClO_4$ data of Wetmur and Davidson produced a negative intercept. It is felt that this is probably a consequence of the effect of the salt either on k_a' directly, or on the intermolecular potential. It certainly would not be surprising to discover that the intrinsic rate constant k_a' was in general enhanced by increased salt. It may well prove possible by working at lower ionic strengths to obtain rate constants with smaller degrees of diffusion control than those found by Wetmur and Davidson.

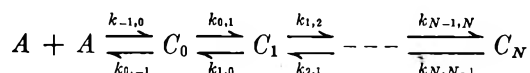
If it may be assumed that the intrinsic rate constants and orientation constraints at the nucleation sites are unaffected by the solutes used to enhance the viscosity, whether sucrose or ethylene glycol, then the estimated values of the intercepts may be employed to obtain the ratio of the intrinsic rate constants at the two values of ΔT

$$k_a'(31)/k_a'(21) \approx 455/200 \approx 2.3 \quad (53)$$

There now arises the interesting possibility that k_a' does not have a bell-shaped temperature dependence at all, at least in this region, and that instead it is a

monotonically increasing function of ΔT , and that the observed decline in the value of k_2 (or \bar{k}_M) with decreasing T arises from the onset of diffusion-control of the overall rate constant in the plateau region.

Although we are skeptical of the mechanism adopted by Wetmur and Davidson to account for the bell-shaped temperature dependence of k_2 , and, in fact, have already noted that there is no reason to believe that the intrinsic rate constant k_a' possesses a bell-shaped temperature profile in this range, there is still an important point to be made in connection with it. Our skepticism stems from the assumption of a steady state for all of the intermediates over 75% of the total reaction, when the rate-limiting step is the bimolecular step. It is difficult to see how a "pre-equilibrium" of a bimolecular step with all of the intermediate steps is compatible with that step being "rate-determining." In any event it is desirable at this point to give the rate expression for the process



where now

$$k_{-1,0} = \bar{k}_M \text{ (cf. eq 28 and 29)} \quad (54a)$$

$$k_{0,-1} = \bar{k} \text{ (cf. eq 30)} \quad (54b)$$

and

$$k_{i,i+1} = k_f; \quad i = 1, \dots, N-1 \quad (55a)$$

$$\bar{k}_{i+1,i} = \frac{k_f}{s}; \quad i = 1, \dots, N-1 \quad (55b)$$

Also

$$k_{0,1} = \sigma_f k_f; \quad k_{1,0} = k_f / s\sigma_b; \quad \sigma_f \sigma_b = \sigma \quad (56)$$

The only change here has been to introduce *intrinsic chemical rate constants* k_a' and k_d^0 in \bar{k}_M and \bar{k} , respectively, for the initial step. The fundamental error made in viewing the reaction as a diffusive bimolecular step proceeding with a Smoluchowski rate constant followed by a unimolecular chemical step was noted in paper I. Even if k_a' and k_d^0 are just the appropriate kinetic theory expressions for the collision rate, they should be included. In this instance the steady-state analysis employed by Wetmur and Davidson leads to

$$-\frac{1}{A^2} \frac{\partial A}{\partial t} = \frac{(\bar{k}_M/\bar{k})\bar{k}_f}{\frac{k_f}{\bar{k}} + \frac{1}{\sigma_f} + \frac{1}{\sigma} \left[\frac{1}{s_1} + \frac{1}{s_1 s_2} + \dots + \frac{1}{s_1 s_2 \dots s_{N-1}} \right]} \quad (57)$$

which may be reduced exactly to

$$-\frac{1}{A^2} \frac{\partial A}{\partial t} = \frac{k_D k_a'}{k_a' + k_D \left\{ \frac{1}{\text{sum}} + \frac{k_d^0}{k_f} \times \left(\frac{1}{\sigma_f} + \frac{1}{s_1} + \frac{1}{s_1 s_2} + \dots + \frac{1}{s_1 s_2 \dots s_{N-1}} \right) \right\}} \quad (58)$$

where $k_D = 2\pi R_T D$ and $s_1' = \sigma s_1$. If now the first term $1/\text{sum}$ is negligible compared to the second term in the curly braces (as in fact would be required in order for the subsequent reactions to affect the rate in the absence of diffusion-control of the bimolecular step), one has

$$-\frac{1}{A^2} \frac{\partial A}{\partial t} = \frac{k_D k_a' / \left\{ k_d^0 / k_f \left(\frac{1}{\sigma_f} + \frac{1}{s_1} + \frac{1}{s_1 s_2} + \dots + \frac{1}{s_1 s_2 \dots s_{N-1}} \right) \right\}}{k_D + k_a' / \left\{ k_d^0 / k_f \left(\frac{1}{\sigma_f} + \frac{1}{s_1} + \frac{1}{s_1 s_2} + \dots + \frac{1}{s_1 s_2 \dots s_{N-1}} \right) \right\}} \quad (59)$$

From eq 59 it is clear that, if $k_f \propto D$ as supposed by Wetmur and Davidson, then $-(1/A^2) \partial A / \partial t$ should be *always inversely proportional to the viscosity*, so that a reciprocal plot would be expected to have a zero-intercept. Although the experimental data of Figures 6 and 7 are hardly unequivocal, they do not appear to substantiate a zero intercept. The mechanism proposed by Wetmur and Davidson to account for the viscosity dependence of the overall bimolecular rate constant is evidently not supported by their data.

Provided that diffusion-control of the bimolecular rate constant is accepted, the mechanism proposed by Wetmur and Davidson might still be employed to account for the increase in the overall rate constant with decreasing T over at least part of the observed range. However, it is our opinion that the steady-state assumption is not formally applicable to those intermediates involved in any of the rapid zippering reactions subsequent to the steps required for nucleation. In order for the steady-state treatment of an intermediate to be valid its logarithmic time derivative must be small (in absolute value) compared to the logarithmic time derivative of the reactants. This condition is clearly not met by intermediates participating in the rapid zippering reaction. In the model discussed above, then, the steady-state assumption is actually applicable only to the intermediate C_0 . A more reasonable model would entail the assignment of a cooperativity parameter to each of the first few steps involved in the slow nucleation process. Such a mechanism can be described by the reaction scheme preceding eq 53 provided the following modifications are incorporated: (i) $N = P$ the number of intermediates involved in slow reactions;

(ii) $k_{i,i+1} = \sigma_{ni}k_i$, $i = 0, \dots, P-1$; (iii) $k_{i+1,i} = k_i/s\sigma_{nb}$, $i = 0, \dots, P-1$; (iv) $\sigma_{nf}\sigma_{nb} = \sigma_n$; (v) $k_{i,i+1}/k_{i+1,i} = s\sigma_n$; (vi) $(\sigma_n)^{P-1} = \sigma$, where σ is the cooperativity parameter for overall helical stability. In this case a steady-state treatment of the states 0 to $(P-1)$ leads to

$$-\frac{1}{A^2} \frac{\partial A}{\partial t} = \frac{k_D k_a'}{k_a' + k_D \left\{ \frac{1}{\text{sum}} + \frac{k_d^0}{k_f \sigma_{nf}} \times \left[1 + \frac{1}{\bar{s}} + \left(\frac{1}{\bar{s}}\right)^2 + \dots + \left(\frac{1}{\bar{s}}\right)^{P-1} \right] \right\}} \quad (60)$$

where $\bar{s} = \sigma_{ns}$. The close resemblance to eq 58 is obvious. It seems likely that the apparent success of eq 58 in predicting the unusual temperature dependence of the overall rate constant is in fact due to its similarity to a valid steady-state expression, such as that given in eq 60. A reciprocal plot of $(- (1/A^2) \partial A / \partial t)^{-1}$ vs. η using eq 60 has an intercept

$$k_M = \left(\frac{2}{k_a'(1 - \cos \theta_0)} + \frac{k_d}{k_f \sigma_{nf}} \left[1 + \frac{1}{\bar{s}} + \dots + \left(\frac{1}{\bar{s}}\right)^{P-1} \right] \right)^{-1} \quad (61)$$

in which the source of the unusual temperature dependence is manifested explicitly.

For the future it is hoped that the clever technique exploited by Wetmur and Davidson of working at constant $T_m - T$ may permit collection of sufficiently precise data to resolve the values of the intercepts of the reciprocal plots.

IX. Summary

Modest angular constraints are capable of producing fairly drastic reductions in the diffusion-controlled bimolecular rate constant. This fact has the important consequence that reactions with interesting (*i.e.*, stringent) orientation requirements should be accessible in the steady-state, stopped-flow, and T -jump time ranges. Major difficulties associated with ultrasonic studies as a function of solvent viscosity may, thus, be circumvented. The high sensitivity of the diffusion-controlled rate constant to the angular constraint offers some promise for determining the orientation requirements for at least some of those chemical reactions involving moderately large, nearly spherical molecules.

Acknowledgment. The authors wish to thank Dr. Mary Dell Chilton for bringing the problem of the viscosity dependence of the rate of renaturation of DNA to their attention.

Quantum Mechanical Tunneling in Hydrogen Atom Abstraction

from Solid Acetonitrile at 77–87°K

by Robert J. Le Roy,*

Department of Physics, University of Toronto, Toronto 181, Ontario, Canada¹

Estel D. Sprague, and Ffrancon Williams

Department of Chemistry, University of Tennessee, Knoxville, Tennessee² 37916 (Received August 2, 1971)

Publication costs assisted by the U. S. Atomic Energy Commission

Recent measurements of the rate of H-atom abstraction from solid acetonitrile at 77–87°K yielded an apparent activation energy of 1.4 ± 0.1 kcal/mol, much smaller than the value 10.0 ± 0.5 kcal/mol reported earlier for the same reaction occurring in the gas phase at 373–573°K. However, exact one-dimensional tunneling calculations for potential energy barriers of different sizes and shapes show that the two sets of results may be quantitatively understood in terms of a single gaussian-shaped potential barrier. This means that at 77–87°K the reaction proceeds almost totally *via* quantum-mechanical tunneling.

1. Introduction

In certain theories of chemical reaction rates it is customary to treat the reacting system as a mass point moving on a potential energy surface from a region labeled "reagents" to one labeled "products."^{3–5} A widely used simplified version of this approach treats the reaction as the motion of the mass point along a critical one-dimensional "reaction-coordinate" on the potential surface. Although the potential surface is in general multidimensional, this one-dimensional approach has received a great deal of attention, probably largely because of its simplicity. However, it does intuitively seem reasonably appropriate for describing reactions such as the transfer of hydrogenic atoms between relatively massive chemical groups, where steric factors could effectively exclude all but a very limited set of "reaction paths."

It has been evident for some time that studies of hydrogen atom reactions at very low temperatures should provide particularly useful tests of simple theories of chemical reaction rates.^{3–5} However, sundry experimental difficulties have severely restricted the availability of reliable data. Although there have been reports^{6,7} of hydrogen atom abstraction from neutral molecules by free radicals or radical ions at 77°K, the process has usually been inferred only from the final observation of radicals whose origin can be rationalized in this way. Also, the possible intervention of "hot-radical" processes in photochemistry and radiation chemistry can usually provide alternate explanations for the occurrence at low temperatures of reactions whose activation energies (measured at high temperatures) exceed 5 kcal/mol.^{6,7} In contrast, the recent report⁸ of hydrogen atom abstraction by methyl radicals in solid γ -irradiated acetonitrile at low temperatures



is unique in two ways. First, the hydrogen atom abstraction mechanism was established kinetically by showing that the decay of $\cdot\text{CH}_3$ and the appearance of $\cdot\text{CH}_2\text{CN}$ occur with the same rate constant. Moreover, the linear variation of this rate constant with the number of H atoms in partially deuterated acetonitriles demonstrates the expected very large primary kinetic isotope effect. Second, since the methyl radicals are produced by photobleaching γ -irradiated acetonitrile with visible light, their subsequent thermal decay can be followed either in the dark or during continuous photobleaching of the sample. Essentially the same rate constant was obtained in each case, which necessarily eliminates possible contributions from hot-radical reactions.

In the following, these provocative new data will be analyzed in terms of the above one-dimensional

(1) Supported by the National Research Council of Canada. The work was initiated while this author was at the Theoretical Chemistry Institute, University of Wisconsin, Madison, Wisconsin, and was at that time supported by National Science Foundation Grant GB-16665.

(2) Work supported by U. S. Atomic Energy Commission Contract No. AT-(40-1)-2968; this is AEC Document No. ORO-2968-64.

(3) (a) R. P. Bell, *Proc. Roy. Soc. Ser. A*, **148**, 241 (1935); (b) S. Glasstone, K. J. Laidler, and H. Eyring, "The Theory of Rate Processes," McGraw-Hill, New York, N. Y., 1941.

(4) (a) R. P. Bell, *Trans. Faraday Soc.*, **55**, 1 (1959); (b) "The Proton in Chemistry," Cornell University Press, Ithaca, New York, 1959, Chapter 11; (c) H. S. Johnston, "Gas Phase Reaction Rate Theory," Ronald Press, New York, N. Y., 1966.

(5) E. F. Caldin, *Chem. Rev.*, **69**, 135 (1969).

(6) J. E. Willard in "Fundamental Processes in Radiation Chemistry," P. Ausloos, Ed., Wiley-Interscience, New York, N. Y., 1968, p 599.

(7) J. E. Bennett, B. Mile, A. Thomas, and B. Ward, *Advan. Phys. Org. Chem.*, **8**, 1 (1970).

(8) E. D. Sprague and F. Williams, *J. Amer. Chem. Soc.*, **93**, 787 (1971).

model. The basic purpose of this treatment is not really to prove or disprove the validity of an obviously oversimplified model. Rather, it is to determine whether this familiar picture which has proved so useful in interpreting reaction rates in the gaseous and liquid state can also provide a consistent interpretation of low-temperature solid-phase results. If this is true, the new low-temperature acetonitrile rate measurements must be compatible with the earlier⁹ high-temperature (373–573°K) gas-phase data for this reaction. Within the framework of the model, this would mean that at liquid nitrogen temperatures the reaction must proceed mainly by quantum-mechanical tunneling through the potential barrier.

2. Method of Approach

According to the one-dimensional model, the temperature dependence of the rate constant $k(T)$ may be expressed as

$$k(T) = A\Gamma(T)e^{-V_0/RT} \quad (2)$$

In eq 2, V_0 is the height of the potential barrier on the reaction coordinate, R the gas constant, A the approximately temperature-independent frequency of mass-point collisions with the barrier, and $\Gamma(T)$ is the ratio of the quantum mechanical to the classical barrier transmission rate for a Boltzmann distribution of incident mass-point kinetic energies. At high temperatures $\Gamma(T)$ smoothly approaches unity, and hence the apparent activation energy

$$E_{\text{app}} = -R \frac{d \ln [k(T)]}{d(1/T)} = V_0 - R \frac{d \ln [\Gamma(T)]}{d(1/T)} \quad (3)$$

approaches V_0 . On the other hand, as the temperature decreases the tunneling factor $\Gamma(T)$ grows at a monotonically increasing rate, and hence at low T , E_{app} will be significantly less than V_0 . Thus, as Bell^{3a} pointed out in 1935, eq 2 and 3 imply that a significant decrease in E_{app} with decreasing temperature is qualitative evidence of a large contribution from tunneling.

Wijnen's⁹ high-temperature (373–573°K) gas-phase measurements of reaction 1 were carried out with deuterated methyl radicals, and had an $E_{\text{app}} = 10.0 \pm 0.5$ kcal/mol. In the procedure used here for fitting the experimental data to eq 2, it is assumed that this approximates the high-temperature limit of E_{app} , and hence that $V_0 = 10.0 \pm 0.5$ kcal/mol. The validity of this assumption will be verified below. In the following, tunneling factors will be calculated for a number of different trial potential barriers with heights $V_0 = 10.0 \pm 0.5$ kcal/mol in an attempt to find a barrier which will yield both the magnitude and the temperature dependence of the reported⁸ low-temperature 77–87°K rate constants. The experimental temperature dependence is given by⁸

$$E_{\text{app}}(82^\circ\text{K}) = 1.4 \pm 0.1 \text{ kcal/mol} \quad (4)$$

and its value for a given model barrier may be calculated directly from eq 3 using computed values of $\Gamma(T)$ at $T = 77$ and 87°K .

In order to calculate the absolute value of the rate constant from a computed $\Gamma(T)$ for a given potential barrier, one must first estimate a value for the frequency factor A in eq 2. This quantity cannot be obtained experimentally from the low-temperature solid-phase measurements⁸ since it is inextricably coupled to $\Gamma(T)$ in eq 2. Furthermore, use of a gas-kinetic value such as might be suitable in the high-temperature gas-phase case⁹ is obviously inappropriate for describing events in the solid. On the other hand, since the reagents are frozen in a crystalline matrix at 77–87°K, the A factor must be directly related to the frequencies of the motion of the hydrogenic atoms in the acetonitrile. Spectroscopic measurements in the solid phase near 77°K show that both the symmetric and antisymmetric CH stretching frequencies are *ca.* $9 \times 10^{13} \text{ sec}^{-1}$.¹⁰ Allowing for some uncertainties due to the possible inclusion of a degeneracy factor or participation of other normal modes, substitution of this A value and the experimental³ $k(77^\circ\text{K}) = 0.025 \text{ min}^{-1}$ into eq 2 yields

$$\log [\Gamma(T)e^{-V_0/RT}]_{77^\circ\text{K}} = \log [k(77^\circ\text{K})/A] = -17.5 \pm 0.5 \quad (5)$$

The left-hand side of eq 5 may be readily computed for any chosen model barrier. In the following, the size and shape of the appropriate barrier will be determined by performing calculations for a range of barriers until both eq 4 and 5 are satisfied.

3. Determination of Barrier Size and Shape

In the present work three different types of model potential barriers are considered: Eckart barriers¹¹

$$V_E(x) = V_0/\cosh^2(x/a) \quad (6)$$

truncated parabolic barriers

$$V_P(x) = V_0[1 - (x/a)^2] \text{ for } |x| < a \quad (7)$$

$$= 0 \text{ for } |x| > a$$

and gaussian barriers

$$V_G(x) = V_0e^{-(x/a)^2} \quad (8)$$

For a given choice of values of the parameters V_0 and a , all three types of barriers have the same height and curvature at the maximum, although the corresponding full-widths at half maximum increase from parabolic to gaussian to Eckart. As is customary,^{3a,4a,4b,12} the

(9) M. H. J. Wijnen, *J. Chem. Phys.*, **22**, 1074 (1954). In this work, the activation energy of reaction 1 was obtained from an analysis of ratios of rate constants, so the frequency factor A in eq 2 was not an observable.

(10) (a) D. E. Milligan and M. E. Jacox, *J. Mol. Spectrosc.*, **8**, 126 (1962); (b) E. L. Pace and L. J. Noe, *J. Chem. Phys.*, **49**, 5317 (1968).

(11) C. Eckart, *Phys. Rev.*, **35**, 1303 (1930).

(12) R. J. Le Roy, K. A. Quickert, and D. J. Le Roy, *Trans. Faraday Soc.*, **66**, 2997 (1970).

size and width of a given type of barrier will be characterized by V_0 and the dimensionless parameter

$$\beta = \pi a(2\mu V_0)^{1/2}/\hbar = 14.30946a [\text{\AA}] (\mu [\text{amu}] V_0 [\text{kcal/mol}])^{1/2} \quad (9)$$

where μ is the effective reduced mass of the reacting system, and a is the length scaling factor appearing in eq 6-8. In the present case, μ is taken as the mass of the hydrogenic atom being abstracted.

While the exact transmission probability of Eckart barriers as a function of incident particle kinetic energy is known analytically,¹¹ this is not the case for truncated parabolic and gaussian barriers. However, for the latter two, and in fact for any chosen type of one-dimensional barrier, these permeabilities may be readily and accurately computed numerically. Here, this was done using the improved version of the method of ref 12 which is discussed in the Appendix.

For each of $V_0 = 9.5, 10.0,$ and 10.5 kcal/mol, E_{app} (82°K) and $\log \{ \Gamma(T) e^{-V_0/RT} \}_{77^\circ\text{K}}$ were calculated for each of the three types of potentials for a range of barrier sizes (*i.e.*, divers β values). The results are the solid curves on Figures 1-3; in each case the horizontal dashed line represents the corresponding experimental quantity and the shaded region its uncertainty. It is evident that eq 4 and 5 can be simultaneously satisfied only for gaussian barriers (Figure 3). At barrier sizes chosen to satisfy eq 5, truncated parabolas give E_{app} (82°K) values which are much too small (Figure 1), while for Eckart barriers the corresponding values are slightly too large (Figure 2). The properties of the barriers corresponding to the labeled points in Figures 1-3 [$P_1, E_1, G_1,$ and G_2] are given in Table I, while the barriers corresponding to points $P_1, E_1,$ and G_1 are shown in Figure 4.

Table I: Properties of Potential Barriers Satisfying Eq 4 and 5

Barrier	β	V_0 , kcal/mol	a , \AA	$\log \{ \Gamma(T) e^{-V_0/RT} \}_{77^\circ\text{K}}$	E_{app} (82°K), kcal/mol
P_1	42.8	10.5	0.919	-18.0	0.46
E_1	25.6	10.5	0.550	-17.0	1.72
G_1	29.6	10.5	0.636	-17.5	1.40
G_2	29.2	10.0	0.643	-17.2	1.46

Figure 5 shows calculated values of $E_{\text{app}}(T)$ and $\Gamma(T)$ for the H- and D-atom abstractions corresponding to gaussian potential barrier G_1 (of course the D-atom results correspond to $\beta = 41.86$; see eq 9). It is interesting to note that for H-atom abstraction at 373-573°K, $E_{\text{app}} \approx 10.0$ kcal/mol (*cf.* $V_0 = 10.5$ kcal/mol), right in the center of the uncertainty in the experimental high-temperature value,⁹ 10.0 ± 0.5 kcal/mol.

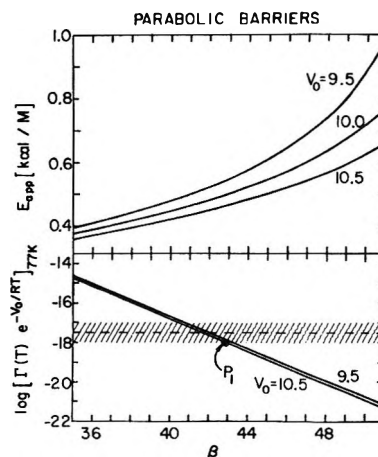


Figure 1. Apparent activation energies E_{app} (82°K) and values of $\log \{ \Gamma(T) e^{-V_0/RT} \}_{77^\circ\text{K}}$ calculated for truncated parabolic barriers (see eq 7) of different sizes (divers β 's). The horizontal dashed lines represent the experimental quantities of eq 4 and 5.

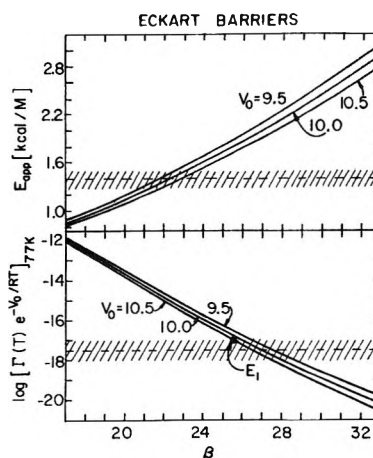


Figure 2. As in Figure 1, for Eckart barriers (see eq 6).

4. Discussion

One apparent inconsistency in the present treatment is the practice of utilizing the quantal vibrational frequencies to estimate the A factor in eq 2, while the tunneling factor calculation assumes a continuous Boltzmann distribution of kinetic energies incident on the potential barrier. Another objection is that the present work has essentially fitted three data:^{12a} the high-temperature E_{app} , low-temperature E_{app} , and a low-temperature rate constant, with three parameters:

(12a) NOTE ADDED IN PROOF. Recently, additional esr studies have been carried out on reaction 1 in Crystal I of acetonitrile between 69 and 112°K (J.-T. Wang and F. Williams, unpublished work). The experimental rate constants can be compared with the values predicted by the present model for a gaussian barrier with the parameters $V_0 = 10.5$ kcal/mol, $\beta = 29.6$, and $A = 9 \times 10^{13}$ sec⁻¹. At 69°K, $k_{\text{exp}} = 1.02 \times 10^{-2}$ min⁻¹ ($k_{\text{cal}} = 0.75 \times 10^3$ min⁻¹); at 100°K, $k_{\text{exp}} = 0.225$ min⁻¹ ($k_{\text{cal}} = 0.203$ min⁻¹); and at 112°K, $k_{\text{exp}} = 0.99$ min⁻¹ ($k_{\text{cal}} = 0.89$ min⁻¹). The agreement is very satisfactory considering that $\Gamma(T)$ changes by almost 11 orders of magnitude over this temperature range, and that an uncertainty of a power of 10 in A is allowed by the treatment (see eq 5 and Figure 3).

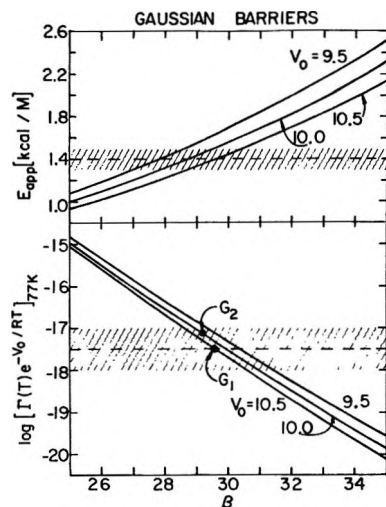


Figure 3. As in Figure 1, for gaussian barriers (see eq 8).

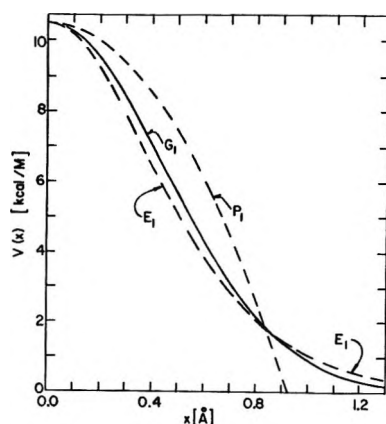


Figure 4. Potential barriers corresponding to points P_1 , E_1 , and G_1 on Figures 1-3, respectively, (see Table I); only positive values of x are shown since all the barriers considered are symmetric about $x = 0$.

V_0 , β (or a), and the barrier shape (parabolic, Eckart, or gaussian). The only additional contributing evidence is the fact that the width scaling parameter of the optimal (gaussian) barrier G_1 , $a = 0.636 \text{ \AA}$, is a plausible result in that it is very similar to values obtained for barriers corresponding to a number of other H-atom transfer reactions (e.g., see Table VII in ref 5).¹³

On the other hand, the present work does demonstrate that the high-temperature gas-phase and low-temperature solid-phase rate constants may be quantitatively explained in terms of a single potential energy surface. This presents a much simpler picture of the reacting system than would arise if one had to try to estimate changes in the potential energy surface between the gas and solid phases. Furthermore, the small differences between the high-temperature gas-, and low-temperature solid-phase values of the diverse vibrational frequencies of acetonitrile¹⁰ strongly suggests that any such changes would be quite small. In addition, the conclusion that the low-temperature re-

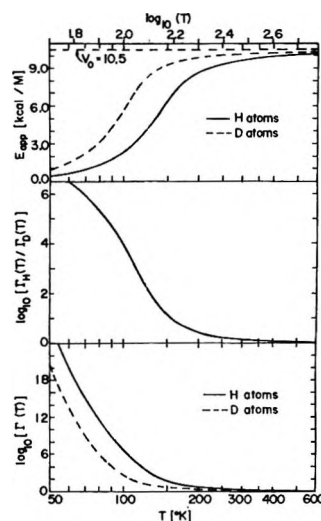


Figure 5. Temperature dependence and tunneling factors for reaction 1 occurring with H or D atoms being transferred; these were calculated for the gaussian potential barrier G_1 (see Table I).

action occurs almost completely *via* quantum-mechanical tunneling suggests that the validity of the present picture may be cleanly tested by comparing the predicted isotope effects (see Figure 5) with experiment. However, such measurements are in practice very difficult to perform because of the very slow rate of the corresponding deuterium abstraction process.

Acknowledgment. We are very grateful to Professor J. E. Willard and Dr. J. R. Miller for making us cognizant of our common interest in this problem.

Appendix

On Calculating the Permeability of One-Dimensional Potential Barriers. Recently a numerical method was presented for calculating exact tunneling probabilities for arbitrary finite one-dimensional potential barriers.^{12,14,15} The purpose of the present discussion is to describe a simple addition to the numerical method of ref 12 (hereafter denoted LQL) which allows a saving in computation time and removes any uncertainty about the convergence of the solution. The procedure is to introduce a WKB "edge-effect" correction to the phases and amplitudes of the numerical wavefunctions at the two boundaries. Throughout, familiarity with LQL¹² and the definitions given therein are assumed,¹⁶ and equation numbers from there are prefixed by LQL.

(13) Although the results in Table VII of ref 5 were obtained using truncated parabola potential barriers [eq 7], the range of values reported, $0.48 \leq a \leq 0.83 \text{ \AA}$, should give a fairly realistic measure of barrier width.

(14) A method similar to that of ref 12 was previously used in a study of the Schottky effect;¹⁵ however, these authors were utilizing semi-infinite potentials and did not consider "edge effect" corrections of the type discussed here.

(15) G. G. Belford, A. Kuppermann, and T. E. Phipps, *Phys. Rev.*, **128**, 524 (1962).

The tunneling probability calculation outlined by eq LQL 1-7 is exact as long as the numerical integration to yield the function $\phi_1(y)$ and $\phi_2(y)$ is performed over the entire interval between the boundary regions where they are exactly described by eq LQL 5 and LQL 6. However, for realistically smooth potentials this interval is infinite, and this requirement cannot be precisely satisfied. In the test calculations of LQL this difficulty was circumvented by assuming the validity of eq LQL 5-7 at the ends of a chosen finite interval, and then increasing the length of the interval until it had no significant further effect on the computed permeability, $\kappa(\bar{E})$. It was found that this condition could be quantitatively expressed as a restriction on the value of the WKB convergence criterion at the chosen boundaries

$$\left| [\alpha(y)]^{-2} \frac{d\alpha(y)}{dy} \right| \leq Z \quad (\text{A1})$$

where $Z \sim 1.0 \times 10^{-6}$. The present treatment presents versions of eq LQL 5-7 which are appropriate when the potential is not identically zero at the ends of the chosen interval. Their utilization allows a weakening of the restriction represented by eq A1 [*i.e.*, an increase in the allowed value of Z], which may save considerable computation time.

Examination of first-order WKB wave functions¹⁷ shows that at large and positive, but finite y (where $\alpha(y) > 0$), the $y \simeq +\infty$ solutions described by eq LQL 5 become

$$\begin{aligned} \phi_1(y) &= A_T \left[\frac{\alpha_+}{\alpha(y)} \right]^{1/2} \cos [\alpha_+ y + \delta_+(y)] \\ \phi_2(y) &= A_T \left[\frac{\alpha_+}{\alpha(y)} \right]^{1/2} \sin [\alpha_+ y + \delta_+(y)] \end{aligned} \quad (\text{A2})$$

where

$$\delta_+(y) = \int_y^\infty [\alpha_+ - \alpha(x)] dx \quad (\text{A3})$$

Similarly, the solutions at large negative y (where $\alpha(y) > 0$), which in the $y \simeq -\infty$ limit become eq LQL 6, are

$$\begin{aligned} \phi_1(y) &= \left[\frac{\alpha_-}{\alpha(y)} \right]^{1/2} \{ C_1 \cos [\alpha_- y + \delta_-(y)] + \\ &\quad D_1 \sin [\alpha_- y + \delta_-(y)] \} \\ \phi_2(y) &= \left[\frac{\alpha_-}{\alpha(y)} \right]^{1/2} \{ C_2 \cos [\alpha_- y + \delta_-(y)] + \\ &\quad D_2 \sin [\alpha_- y + \delta_-(y)] \} \end{aligned} \quad (\text{A4})$$

$$\phi_1(y) = \left[\frac{\alpha_-}{\alpha(y)} \right]^{1/2} \{ C_1 \cos [\alpha_- y + \delta_-(y)] + D_1 \sin [\alpha_- y + \delta_-(y)] \}$$

where

$$\delta_-(y) = - \int_{-\infty}^y [\alpha_- - \alpha(x)] dx \quad (\text{A5})$$

As before, the permeability may be expressed directly in terms of values computed for the solution functions

$\phi_1(y)$ and $\phi_2(y)$ at the integration mesh points y_1 and y_2 (large and negative). However, the inclusion of the phase, $\Delta(y_2, y_1) \equiv \delta_-(y_2) - \delta_-(y_1)$, and amplitude, $A(y) \equiv [\alpha_-/\alpha(y)]^{1/2}$, factors modifies eq LQL 7, yielding

$$\begin{aligned} \kappa(\bar{E}) &= 4(\alpha_+/\alpha_-) \{ A(y_1)A(y_2) \sin [\alpha_-(y_2 - y_1) + \\ &\quad \Delta(y_2, y_1)] \}^2 |A_T|^2 \times \{ [A(y_2)\phi_1(y_1)]^2 + [A(y_2)\phi_2(y_1)]^2 + \\ &\quad [A(y_1)\phi_1(y_2)]^2 + [A(y_1)\phi_2(y_2)]^2 - 2[\phi_1(y_1)\phi_1(y_2) + \\ &\quad \phi_2(y_1)\phi_2(y_2)]A(y_1)A(y_2) \cos [\alpha_-(y_2 - y_1) + \Delta(y_2, y_1)] + \\ &\quad 2[\phi_1(y_1)\phi_2(y_2) - \phi_1(y_2)\phi_2(y_1)]A(y_1)A(y_2) \sin [\alpha_-(y_2 - \\ &\quad y_1) + \Delta(y_2, y_1)] \}^{-1} \quad (\text{A6}) \end{aligned}$$

Another way of expressing the change from eq LQL 7 to eq A6 is to multiply the former by $[A(y_1)A(y_2)]^2$, add $\Delta(y_2, y_1)$ to the arguments of the trigonometric functions, and replace $\phi_i(y_1)$ by $\{A(y_2)\phi_i(y_1)\}$ and $\phi_i(y_2)$ by $\{A(y_1)\phi_i(y_2)\}$ [$i = 1, 2$]. While the amplitude factors $[\alpha_+/\alpha(y)]^{1/2}$ and $[\alpha_-/\alpha(y)]^{1/2}$ are adequately defined as stated, the phase correction factors $\delta_+(y)$ and $\delta_-(y)$ [and hence $\Delta(y_2, y_1)$] depend on the nature of the particular potential barrier $\bar{V}(y)$, and their properties are discussed below. An initial observation is that for barriers symmetric about $y = 0$: $\delta_-(-|y|) = -\delta_+(|y|)$.

The following discussion assumes, without loss of generality, that at each asymptote ($y \simeq +\infty$ or $-\infty$) the zero of energy is chosen such that $V(y) \rightarrow 0$ at these limits. In this case, eq A3 and A5 may be written as

$$\delta_+(|y|) = \alpha_+ \int_{|y|}^\infty [1 - (1 - \bar{V}(x)/\bar{E})^{1/2}] dx \quad (\text{A7})$$

$$\delta_-(-|y|) = -\alpha_- \int_{-\infty}^{-|y|} [1 - (1 - \bar{V}(x)/\bar{E})^{1/2}] dx$$

If $|y|$ is chosen sufficiently large that $|\bar{V}(x)/\bar{E}| \ll 1$ for all $|x| > |y|$, it is clearly valid to expand the integrands of eq A7 as Taylor's series, and retaining only the leading term¹⁸

$$\delta_+(|y|) \approx (\alpha_+/2\bar{E}) \int_{|y|}^\infty \bar{V}(x) dx \quad (\text{A8})$$

$$\delta_-(-|y|) \approx (-\alpha_-/2\bar{E}) \int_{-\infty}^{-|y|} \bar{V}(x) dx$$

For typical analytic potentials eq A8 are readily in-

(16) The LQL¹² quantity of most relevance to the present discussion is $\alpha(y) = (\beta/\pi) [\bar{E} - \bar{V}(y)]^{1/2}$, where $y = x/a$, β is the dimensionless parameter of eq 9 and \bar{E} and $\bar{V}(y)$ are, respectively, the incident particle energy and the potential function, both scaled by the barrier height V_0 . Note that $\alpha(+\infty) \equiv \alpha_+$ and $\alpha(-\infty) \equiv \alpha_-$.

(17) See, *e.g.*, E. Merzbacher, "Quantum Mechanics," Wiley, New York, N. Y., 1961, Chapter 7.

(18) In numerical checks against the exact analytic tunneling probabilities for Eckart barriers it was found that inclusion of the next term in this expression did not significantly improve the results.

(19) M. Abramowitz and I. A. Stegun, "Handbook of Mathematical Functions," National Bureau Standards, Applied Math Series, No. 55, U. S. Dept. of Commerce, 1964, §7.1.

tegrable. For an Eckart function, $\bar{V}(y) = 1/\cosh^2(y)$, it yields

$$\delta_+(|y|) = \alpha_+ / [\bar{E}(e^{2|y|} + 1)] = -\delta_-(-|y|)$$

while for a gaussian barrier, $\bar{V}(y) = e^{-y^2}$, it yields

$$\delta_+(|y|) = \pi^{1/2} \alpha_+ \operatorname{erfc}(y) / 4\bar{E} = -\delta_-(-|y|)$$

where $\operatorname{erfc}(y)$ is the well known error function.¹⁹ Analogously simple expressions for the phase shifts are readily obtained for other model barriers.

Using the above results, the "WKB-improved" permeability calculations would proceed precisely as before except that eq A2 replaces eq LQL 5 as the source of the starting values of the wave function used in initiating the numerical integration, and eq A6 replaces eq LQL 7 as the source of $\kappa(\bar{E})$. Of course a subroutine would have to be added to the computer program to supply the values of $\delta_+(y)$ and $\delta_-(y)$ appropriate to the asymptotic form of the given potential. Testing

this approach with Eckart barriers of different sizes (for which exact $\kappa(\bar{E})$ values are known analytically), it was found that the inclusion of these corrections allows a given accuracy in $\kappa(\bar{E})$ to be achieved using a value of Z [see eq A1] one order of magnitude larger than before. For example, $\kappa(\bar{E})$ could be obtained accurate to 1×10^{-5} using $Z = 1 \times 10^{-4}$, while LQL had found that $Z = 1 \times 10^{-5}$ was required.

One additional improvement in the present computer program over that used by LQL is the addition of a capability for changing the integration mesh in the course of a calculation. Including this and the edge-effect corrections may lead to a considerable saving in computation time. However, this would probably be relatively more important for potentials which die off at long range with an inverse-power form, than for the exponential-tailed potentials considered here. Annotated FORTRAN listings of the computer programs used in the present calculations are available from the first author (R. J. L.)

The Role of Nonbonded Intramolecular Forces in Barriers to Internal Rotation in Molecules with Two Equivalent Methyl Groups

by Kenneth C. Ingham

Department of Biophysics, Michigan State University, East Lansing, Michigan 48823 (Received September 9, 1971)

Publication costs borne completely by The Journal of Physical Chemistry

It is suggested that the often large barrier difference between molecules with two equivalent methyl groups and their corresponding one-top analogs can be readily explained on the basis of a nonbonded repulsion between the methyl groups. The repulsion arises primarily from an interaction between the protons of one methyl group and the carbon atom of the other. This dominance of the $H \cdots C$ interactions offers a simple explanation of the general success of the independent oscillator approximation in most of these two-top molecules.

A recent study of hindered internal rotation in *o*-xylene generated interest in the role of nonbonded (van der Waals) forces in barriers to internal rotation in two-top molecules.^{1,2} A survey of available data revealed that molecules containing two equivalent neighboring methyl groups often have rotational barriers whose magnitudes differ substantially from those of their corresponding one-top analogs, for example, dimethyl ether *vs.* methanol (see Table I). Yet, the independent oscillator approximation, which assumes that each methyl group oscillates in a potential well whose shape is independent of the orientation of the other methyl group, is generally a fairly good approximation in these molecules. These observations could

be made compatible by postulating a strong repulsive interaction between the hydrogen atoms of one methyl group and the carbon atom of the other.

In order to check this hypothesis a variety of nonbonded potential functions were tested for their ability to explain the *difference* in barrier between the two-top molecules and their one-top analogs. The calculation is similar to that used by others^{3,4} to explain the effect

- (1) K. C. Ingham, Ph.D. Thesis, University of Colorado, 1970.
- (2) K. C. Ingham and S. J. Strickler, *J. Chem. Phys.*, **53**, 4313 (1970).
- (3) J. L. DeCoen, G. Elefante, A. M. Liquori, and A. Damiani, *Nature (London)*, **216**, 910 (1967).
- (4) R. Scott and H. Scheraga, *J. Chem. Phys.*, **42**, 2209 (1965).

Table I: Barriers to Internal Rotation in Molecules Containing Two Equivalent Methyl Groups and their One-Top Analogs^a

Compound		V _s		Two-top, (calcd)
One-top	Two-top	One-top	Two-top	
Methanol ^{d,e}	Dimethyl ether ^{f,o}	1.07	2.72	2.84
Methanethiol ^h	Dimethyl sulfide ⁱ	1.24	2.11	2.00
Methylselenol ^j	Dimethyl selenide ^k	0.91	1.50	1.40
Ethane ^{l,m}	Propane ^{n-p}	2.93	3.3-3.5	3.49
Methylsilane ^q	Dimethylsilane ^r	1.70	1.65	1.78
Methylgermane ^o	Dimethylgermane ^t	1.24	1.18	1.27
Methyldiazirine ^u	Dimethyldiazirine ^v	0.77	1.13	1.05
Propylene ^{w,z}	Isobutene ^y	1.98	2.21	2.44
Propylene	<i>cis</i> -Butene ^z	1.98	0.73	0.46 ^b
Methylamine ^{aa}	Dimethylamine ^{bb,cc}	2.0	3.3-3.6	2.80
Acetaldehyde ^{dd}	Acetone ^{ee,ff}	1.15	0.78	1.60
Propylene oxide ^{gg}	<i>cis</i> -2,3-Epoxybutane ^{h,h}	2.56	1.61	1.53
Toluene ⁱⁱ	<i>o</i> -Xylene ^{jj,kk}	0.013	2.0	1.57 ^c

^a All barriers in kcal/mol. ^b Using 127.8° for the C=C-CH₃ bond angles. ^c Using X-ray data for durene taken from J. M. Robertson, *Proc. Roy. Soc. Ser. A*, **141**, 594 (1933). ^d P. Venkateswarlu, H. D. Edwards, and W. Gordy, *J. Chem. Phys.*, **23**, 1195 (1955). ^e P. Venkateswarlu and W. Gordy, *ibid.*, **23**, 1200 (1955). ^f P. H. Kasai and R. J. Myers, *ibid.*, **30**, 1096 (1959). ^g U. Blukis, P. H. Kasai, and R. J. Myers, *ibid.*, **38**, 2753 (1963). ^h T. Kojima, *J. Phys. Soc. Jap.*, **15**, 1284 (1960). ⁱ L. Pierce and M. Hayashi, *J. Chem. Phys.*, **35**, 479 (1961). ^j A. B. Harvey and M. K. Wilson, *ibid.*, **45**, 678 (1966). ^k J. F. Beecher, *J. Mol. Spectrosc.*, **21**, 414 (1966). ^l S. Weiss and G. E. Leroi, *J. Chem. Phys.*, **48**, 962 (1968). ^m L. S. Bartell and H. K. Higginbotham, *ibid.*, **42**, 851 (1965). ⁿ E. Hirota, C. Matsumura, and Y. Morino, *Bull. Chem. Soc. Jap.*, **40**, 1124 (1967). ^o J. R. Hoyland, *J. Chem. Phys.*, **49**, 1908 (1968). ^p D. R. Lide, Jr., *ibid.*, **33**, 1514 (1960). ^q R. W. Kilb and L. Pierce, *ibid.*, **27**, 108 (1957). ^r L. Pierce, *ibid.*, **34**, 498 (1961). ^s V. W. Laurie, *ibid.*, **30**, 1210 (1959). ^t E. C. Thomas and V. W. Laurie, *ibid.*, **50**, 3512 (1969). ^u L. Scharpen, J. Wollrab, D. Ames, and J. Merritt, *ibid.*, **50**, 2063 (1969). ^v J. Wollrab, L. Scharpen, D. Ames, and J. Merritt, *ibid.*, **49**, 2405 (1968). ^w E. Hirota, *ibid.*, **45**, 1984 (1966). ^x D. Lide and D. Christensen, *ibid.*, **35**, 1374 (1961). ^y V. W. Laurie, *ibid.*, **34**, 1516 (1961). ^z T. N. Sarachman, *ibid.*, **49**, 3146 (1968). ^{aa} K. Tamagake, M. Tsuboi, and A. Hirakawa, *ibid.*, **48**, 5536 (1968). ^{bb} W. G. Fateley and F. A. Miller, *Spectrochim. Acta*, **18**, 977 (1962). ^{cc} K. D. Möeller, A. R. Demeo, D. R. Smith, and H. L. London, *J. Chem. Phys.*, **47**, 2609 (1967). ^{dd} R. Kilb, C. C. Lin, and E. B. Wilson, Jr., *ibid.*, **26**, 1965 (1957). ^{ee} J. D. Swalen and C. C. Costain, *ibid.*, **31**, 1562 (1959). ^{ff} R. Nelson and L. Pierce, *J. Mol. Spectrosc.*, **18**, 344 (1965). ^{gg} J. D. Swalen and D. Herschbach, *J. Chem. Phys.*, **27**, 100 (1957). ^{hh} M. L. Sage, *ibid.*, **35**, 142 (1961). ⁱⁱ H. D. Rudolph, H. Dreizler, A. Jaeschke, and P. Wendling, *Z. Naturforsch. A*, **22**, 940 (1967). ^{jj} K. S. Pitzer and D. W. Scott, *J. Amer. Chem. Soc.*, **65**, 803 (1943). ^{kk} J. J. Rush, *J. Chem. Phys.*, **47**, 3936 (1967).

of halogen substitution on the barrier in ethane, and is discussed in detail in ref 1. One first calculates the nonbonded contribution in the one-top molecule. The difference between this and the measured barrier gives the so-called "axial" contribution, which is assumed to be a property of the type of bond and the particular atoms which it joins. This axial component is expected to be the same in the two-top molecules as in the one-top analogue. One then evaluates the nonbonded contribution in the two-top molecule, which when combined with the axial contribution gives the total calculated barrier.

When this method was executed using a variety of nonbonded functions from the literature, the results were uniformly poor. The calculated barrier difference was always less than that observed, reflecting a need for a stronger H···C repulsion. A stronger H···C repulsion makes sense for the following reason. Most of the functions in the literature are evaluated empirically from data on gas viscosity, molecular scattering, and other data pertaining to intermolecular forces. Now, two molecules such as methane approaching each other in the gas phase have unlimited rotational freedom to assume a mutual orientation which minimizes their repulsion. However, two methyl groups rotating in a

molecule have a fixed mutual orientation and thus stronger interaction might be expected.

The H···H and H···C functions used by DeCoen, *et al.*,³ which are of the Buckingham or "6-exp" type, were used as a starting point, $U = a(\exp -bR) - cR^{-6}$. Then the b parameter of the H···C function was adjusted to give the best overall agreement for the pairs of molecules in Table I. The results shown there were obtained using $a = 31,400$, $b = 3.85$, and $c = 121$ for the H···C function and $a = 6600$, $b = 4.08$, and $c = 49.2$ for the H···H function (in units of kcal/mol with R in angstroms).

The general agreement in Table I is encouraging considering the simplicity of the model and in every case except acetone supports the postulation of a strong H···C interaction. Acetone seems to constitute a special case and has been discussed recently by Lowe.⁵ The interatomic distances used in this calculation were determined graphically and have an estimated uncertainty of ± 0.01 Å. This does not include uncertainties in the experimental geometries and equilibrium configurations which were taken from the references in Table I. Also, the methyl groups were as-

(5) J. P. Lowe, *J. Chem. Phys.*, **51**, 832 (1969).

sumed to be tetrahedral with carbon-hydrogen bond lengths of 1.09 Å. Actually, some of the molecules have asymmetric methyl groups while in others the methyl groups rotate about axes which are not collinear with the axial bonds.⁶ All of these effects will lend uncertainty to the calculated results. As more accurate structural and barrier data become available, this ap-

proach should lead to improved *intramolecular* non-bonded potential functions. Such functions are important for predicting the conformations of proteins and other polymers.⁷

(6) J. Wollrab and V. W. Laurie, *J. Chem. Phys.*, **48**, 5058 (1968).

(7) H. A. Scheraga, J. J. Leach, R. A. Scott, G. Nemethy, *Discuss. Faraday Soc.*, **40**, 268 (1965).

A Theoretical Study of Hyperfine Coupling Constants of Some

σ Radicals Based on the INDO Method

by M. F. Chiu, B. C. Gilbert,* and B. T. Sutcliffe

Department of Chemistry, University of York, Heslington, York, United Kingdom YO1 5DD. (Received July 9, 1971)

Publication costs borne completely by The Journal of Physical Chemistry

A study based on the INDO method has been made of a variety of σ radicals. The desirability of minimizing the energy with respect to molecular geometry for a number of small radicals (*e.g.*, $\cdot\text{CONH}_2$, $\text{H}_2\text{C}=\text{N}\cdot$, $\text{H}_2\text{C}=\text{CH}\cdot$) is discussed. INDO calculations have also been performed for a series of iminoxy radicals ($\text{R}_2\text{C}=\text{NO}\cdot$), the appropriate geometry around the radical center being chosen as that which minimizes the energy for the smallest radical in the series. An alternative method of determining the proportionality constants for relating esr hyperfine splittings to spin density matrix elements is suggested. Spin density distributions in the space around some of the radicals studied are expressed in the form of spin density contour maps.

1. Introduction

Organic radicals exhibit a wide variation in their isotropic esr hyperfine splittings, but it is possible, broadly speaking, to divide them into two classes. These are the π radicals, typified by aromatic anions and cations, by semiquinones, and by methyl,¹ and the so-called σ radicals, such as phenyl.²

From a theoretical point of view it is possible to rationalize the observed hyperfine splittings in many π radicals by means of calculations made within the context of the so-called " π -electron approximation," *e.g.*, a Hückel MO³ or a Pariser-Parr-Pople³ MO calculation. In these approaches, certain MO coefficients are related to proton splittings by means of a McConnell-type relationship.⁴

For σ radicals, however, calculations made within the π -electron approximation are inadequate to account for the observed splittings. In a pioneering VB calculation on the vinyl radical,⁵ Karplus and Adrian⁶ were able to obtain good agreement with experiment and were able to interpret their calculations in terms of an unpaired electron in a hybrid orbital in the molecular plane at the radical center. This result suggests that for a calculational method to be successful for σ radicals it must take

into account the electronic "core" of the molecule, which is specifically excluded from consideration in π -electron methods.

With the development of the INDO procedure by Pople, Beveridge, and Dobosh,⁷ a semiempirical method has become available which can, to some extent, allow the presence of an electronic "core." The details of this method are well known and the relevant parts are summarized in the Appendix to this paper. Pople, Beveridge, and Dobosh (PBD)⁸ and Beveridge and Dobosh (BD)⁹ have already carried out calculations

(1) R. W. Fessenden and R. H. Schuler, *J. Chem. Phys.*, **42**, 3670 (1965).

(2) J. E. Bennett, B. Mile, and A. Thomas, *Proc. Roy. Soc. Ser. A*, **293**, 246 (1966).

(3) See, for instance, R. G. Parr, "Quantum Theory of Molecular Electronic Structure," Benjamin, New York, N. Y., 1964.

(4) H. M. McConnell, *J. Chem. Phys.*, **28**, 1188 (1958).

(5) (a) R. W. Fessenden, *J. Phys. Chem.*, **71**, 74 (1967); (b) R. W. Fessenden and R. H. Schuler, *J. Chem. Phys.*, **39**, 2147 (1963).

(6) M. Karplus and F. J. Adrian, *ibid.*, **41**, 56 (1964).

(7) J. A. Pople, D. L. Beveridge, and P. A. Dobosh, *ibid.*, **47**, 2026 (1967).

(8) J. A. Pople, D. L. Beveridge, and P. A. Dobosh, *J. Amer. Chem. Soc.*, **90**, 4201 (1968).

(9) D. L. Beveridge and P. A. Dobosh, *J. Chem. Phys.*, **48**, 5532 (1968).

using the UHF¹⁰ approach within the INDO method and have met with considerable success for a large number of radicals. Essentially, their procedure is to postulate a "reasonable" idealized geometry for the radicals in question (though other investigations^{7,11,12} have found minimum energy geometries for some small radicals and molecules), then to calculate approximate spin densities at various nuclei in the radical, and, by correlating these values with experimental splittings, to derive parameters to relate spin densities and splittings in subsequent calculations.

The radicals employed for parametrization included few σ radicals and in consequence it is perhaps not surprising that, in our pilot calculations on radicals in the iminoxy (σ) series, neither the PBD nor the BD parametrization (the latter being appropriate to spin densities after annihilation of the quartet contaminant) gave good agreement with experiment.

We therefore decided to reinvestigate the parametrization for spin densities in the INDO method in the hope of arriving at values more appropriate for σ radicals and also in an attempt to find some internal criterion within the INDO calculation with which to decide, for a given radical under investigation, whether or not the original PBD (or BD) scheme was appropriate.

2. The Parametrization for σ Radicals

The calculated properties of molecules under study may depend critically on the disposition of the nuclei in space, and to avoid ambiguity, we attempted to refer, wherever possible, to the calculated equilibrium geometry. To do this for some small σ radicals, we proceeded to vary the geometry until the minimum energy configurations were found. For such radicals, it was found that variations in the relative positions of atoms adjacent to the radical center lead to quite sharp variations in the spin densities, in the energy, and in the value of $\langle S^2 \rangle_{av}$. Broadly speaking, however, the value of $\langle S^2 \rangle_{av}$ approached 0.75 (the correct value for a pure doublet), the more closely a minimum energy configuration was achieved.

It was of course not possible to perform such extensive variations of geometry on larger σ radicals but some fairly simple investigations showed that in these cases the energy, $\langle S^2 \rangle_{av}$, and the spin densities were much less sensitive to variations in the positions of atoms remote from the radical center. As a compromise, therefore, we determined the minimum energy configuration of the radical center for the simplest member of the series (*e.g.*, for the iminoxy series, the CNO group in $H_2C=NO\cdot$) and used this conformation, with idealized geometry for other substituents, for other radicals in the series (see "Details of Computation," below).

To calculate the actual parameters for relating spin densities to splittings we did not have enough experimental data to perform an effective correlation like that

possible for π radicals. Instead, we opted for a Direct Parametrization Scheme (DP) the details of which are outlined in the Appendix; this treatment is based essentially on the very good approximation that Slater-type 2s orbitals (which give zero electron density at the nucleus) on first row atoms can be replaced by 2s-like orbitals, orthogonalized to postulated 1s orbitals on the same center (such 2s orbitals have finite, nonzero electron density at the nucleus).

The DP parameters are shown in Table I together with the PBD and BD parameters for comparison. In this kind of approach, one parameter set must be considered appropriate for calculations both involving and not involving annihilation¹³ of the quartet spin component since no correlation with experiment is involved in the parameter determination.

In the PBD and BD work an approximation to the spin density was used (the "diagonal" approximation) for the purposes of parametrization, but in the DP approach it is not necessary to make this approximation and the second term in the expansion [see Appendix, equation A5] may easily be included. We report investigations of the effect of its inclusion in a number of cases.

3. Previous Investigations into σ Radicals

A. Simple Treatments. Several approaches, including many of the "Extended Hückel" type (EH), have been employed.

The calculation of Karplus and Adrian for vinyl⁶ involved an ingenious choice of hybrid orbitals for the α carbon and enabled the authors to obtain a qualitative description of the dependence on the $H_\alpha\hat{C}_\alpha C_\beta$ angle of the two β -proton coupling constants. Using an EH treatment coupled with the theory of spin polarization, Sutcliffe¹⁴ obtained very reasonable agreement with experiment for all three proton splittings when the $H_\alpha\hat{C}_\alpha C_\beta$ angle was chosen to be 140°. A feature of this and all EH methods is that the choice of the Wolfsberg-Helmholz parameter, K ,¹⁵ is arbitrary and therefore "adjustable." Other investigations based on the EH technique were carried out by Drago and Peterson,¹⁶ but as they developed no theory of spin polarization (or some other mechanism for obtaining nonzero values of the 2s function at the nucleus), they were obliged to develop somewhat *ad hoc* rules for correlating experimental results with calculated quantities. The best agreement with experiment from an EH calculation was

(10) J. A. Pople and R. K. Nesbet, *J. Chem. Phys.*, **22**, 571 (1954).

(11) C. Thomson, *Theor. Chim. Acta*, **17**, 320 (1970).

(12) M. S. Gordon and J. A. Pople, *J. Chem. Phys.*, **49**, 4643 (1968).

(13) A. T. Amos and L. Snyder, *ibid.*, **39**, 362 (1963).

(14) B. T. Sutcliffe, International Colloquia of CRNS (Paris), 1966, p 253ff.

(15) M. Wolfsberg and L. Helmholz, *J. Chem. Phys.*, **20**, 837 (1952).

(16) R. S. Drago and H. Peterson, *J. Amer. Chem. Soc.*, **89**, 3978, 5774 (1967).

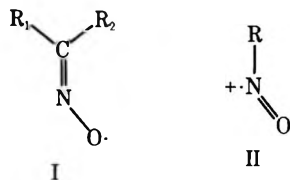
Table I: Values of A^n Obtained by Different Methods (in Gauss)

Atom n	^1H	^{10}B	^{11}B	^{12}C	^{14}N	^{17}O	^{19}F
PBD (before annihilation) ^a	539.86	820.10	379.36	888.69	44829.2
BD (after annihilation) ^a	711.25	828.97	1126.80	2604.37	47884.0
Direct Parametrisation, DP	875.78 ^b	719.25	240.90	1109.8	549.95	-1649.22	17962.74

^a By least-squares regression. ^b Value obtained when $1s_{\text{B}}(r_{\text{B}})$ has exponent 1.2.

that obtained by Petersson and McLachlan¹⁷ who used 2s orbitals orthogonalized to 1s orbitals on the same center. The $\text{H}_\alpha\hat{\text{C}}_\alpha\text{C}_\beta$ angle at which splittings were best reproduced was 146° .

Simple treatments of iminoxy radicals and the nitrosobenzene cation have also appeared. For example, Cramer and Drago, using the methods of ref 16, obtained reasonable agreement with experiment for the iminoxy radicals (I, $\text{R}_1 = \text{H}$, $\text{R}_2 = \text{CH}_3$), (I, $\text{R}_1 = \text{phenyl}$, $\text{R}_2 = \text{H}$), and (I, $\text{R}_1 = \text{H}$, $\text{R}_2 = \text{phenyl}$)¹⁸ and for (II, $\text{R} = \text{phenyl}$)¹⁹. However, to obtain



agreement with the experimental splittings, their calculations required that in the last two radicals the phenyl group is bent out of the CNO plane (the former by 90° , the latter by 70°). For the iminoxy radicals, a value of 120° was employed for $\text{C}\hat{\text{N}}\text{O}$.¹⁸ A number of 1,3-dicarbonyl-2-iminoxy radicals have been studied (EH) by Wold and Lagercrantz²⁰ who found that the calculated minimum energy corresponds to a $\text{C}\hat{\text{N}}\text{O}$ angle of 135° .

Recently, Yonezawa, *et al.*,²¹ reported the results of "extended McLachlan" calculations on vinyl and on $\text{H}_2\text{C}=\text{NO}\cdot$; rather poor agreement with experiment was obtained for the latter while for the former the α -proton coupling constant was predicted to be negative. Although this result is in agreement with the *ab initio* calculation of Claxton,²² most other calculations^{14, 16, 23, 24, 25} and the experimental evidence for $\cdot\text{CH}=\text{CHCO}_2\text{D}$ ²⁶ indicate that this splitting is positive.

B. UHF Calculations. Many of the recent studies of σ radicals have been through the UHF approach, either semiempirically (*e.g.*, CNDO,²⁴ INDO^{8, 11, 12, 27}) or *ab initio*.²² In the former, a general approach has been to start with the EH MO's as an initial guess and then to carry out the UHF iteration procedure until convergence (usually in the energy) is obtained to a specified accuracy.

The first INDO calculations on vinyl were reported by Pople, *et al.*,⁸ for the radical in an "idealized geometry" conformation (see below). A CNDO UHF calculation with quartet spin state annihilation by Ather-

ton and Hinchliffe²⁴ has indicated that qualitative agreement with experiment may be obtained by this method for $120^\circ < \angle \text{H}_\alpha\text{C}_\alpha\text{C}_\beta < 150^\circ$.

Recently, Krusic and Rettig²⁷ have observed the isotropic esr spectrum of the benzoyl radical, $\text{PhCO}\cdot$, and have reported an INDO investigation. For an assumed geometry with fixed bond lengths, the effect on the coupling constants of rotation about the $\text{C}_6\text{H}_5\text{-CO}$ bond was studied and the authors concluded that the equilibrium conformation corresponds to a coplanar structure.

4. Results and Discussion

A. Vinyl. Taking the C-C and C-H bond lengths as 1.40 \AA and 1.08 \AA , respectively, we varied the $\text{H}_\alpha\hat{\text{C}}_\alpha\text{C}_\beta$ angle (θ) between 120° and 180° . An energy minimum was found at $\theta = 145^\circ$, while the total energy barrier to in-plane inversion [$E(180^\circ) - E(145^\circ)$] was 0.0059 au (3.7 kcal/mol), in excellent agreement with Fessenden's estimate of $\sim 3 \text{ kcal/mol}$ from experimental data.⁵ The values of $\langle S^2 \rangle_{\text{av}}$ were not very sensitive to the variation in θ . The coupling constants calculated using the PBD, BD, and DP schemes, and the value of $\langle S^2 \rangle_{\text{av}}$, for $\theta = 145^\circ$ are shown in Table II. Agreement with experiment, especially for $a_{\alpha^{\text{H}}}$, $a_{\beta^{\text{H}}(\text{syn})}$, $a_{\beta^{\text{H}}(\text{anti})}$, is quite encouraging, the values calculated by the DP scheme (after annihilation) being slightly better than the remainder. Here, as elsewhere, our parametrization for H gives somewhat larger splittings than the PBD/BD schemes. The effect on the coupling constants of the additional terms in (A5) is seen to be very small.

B. Some Small Radicals. Table III shows the results of INDO calculations on some small molecules.

(17) G. A. Petersson and A. D. McLachlan, *J. Chem. Phys.*, **45**, 628 (1966).

(18) R. E. Cramer and R. S. Drago, *J. Amer. Chem. Soc.*, **90**, 4790 (1968).

(19) R. E. Cramer and R. S. Drago, *J. Chem. Phys.*, **51**, 464 (1969).

(20) S. Wold and C. Lagercrantz, *Acta Chem. Scand.*, **23**, 1878 (1969).

(21) T. Yonezawa, T. Kawamura, and H. Kato, *Bull. Chem. Soc. Jap.*, **43**, 74 (1970).

(22) T. A. Claxton, *Int. J. Quantum Chem.*, **4**, 337 (1970).

(23) W. T. Dixon, *Mol. Phys.*, **9**, 201 (1965).

(24) N. M. Atherton and A. Hinchliffe, *Mol. Phys.*, **12**, 349 (1967).

(25) A. Hinchliffe, *Theor. Chim. Acta*, **8**, 300 (1967).

(26) M. Iwasaki and B. Eda, *J. Chem. Phys.*, **52**, 3837 (1970).

(27) P. J. Krusic and T. A. Rettig, *J. Amer. Chem. Soc.*, **92**, 722 (1970).

Table II: Coupling Constants in the Vinyl Radical (Gauss)
 $\angle H_\alpha C_\alpha C_\beta = 145^\circ$

	a_β^H (anti)	a_β^H (syn)	a_α^H	a_β^C	a_α^C	$\langle S^2 \rangle_{av}$
Before annihilation						
PBD	64.9	33.9	1.2	-17.9	109.9	0.7721
DP	105.4	55.0	1.9	-24.2	148.7	
Additional terms ^a	-2.3	-1.3	1.0	-0.0	0.4	
After annihilation						
BD	60.3	30.7	13.2	-3.4	96.6	0.7502
DP	74.2	38.8	16.3	-4.5	129.4	
Additional terms ^a	-0.7	-0.4	0.4	0.1	0.3	
Experimental ^b	68.5	34.2	13.3	8.6	107.6	

^a See Appendix, eq A5. ^b Reference 5.

In each case, the geometry chosen is that for minimum energy as found by the previous INDO investigation of Thomson¹¹ (for HBO^- , HCN^- , and $H\dot{C}O$), of Gordon and Pople¹² (for $\dot{N}H_2$), and of Pople, *et al.*,⁷ (for NO_2). For $H_2C=\dot{N}$ we found the following minimum energy geometry: $r_{CH} = 1.10 \text{ \AA}$, $r_{CN} = 1.25 \text{ \AA}$, $\angle HCN = 125^\circ$; for $\cdot CONH_2$ the minimum-energy geometry was $r_{CO} = 1.25 \text{ \AA}$, $r_{CN} = 1.35 \text{ \AA}$, $r_{NH} = 1.07 \text{ \AA}$, $\angle NCO = 125^\circ$, $\angle HNH = 115^\circ$, $\angle HCN = 120^\circ$. A comparison of the calculated coupling constants with experiment shows no outstanding agreement in the case of any single radical, though the DP scheme, both before and after annihilation, appears to account for the ^{14}N splittings in triatomics quite satisfactorily. The DP results for $H\dot{C}O$ are comparable with those found by Hinchliffe and Cook²⁸ in their *ab initio* calculations. The reasons for the somewhat poor agreement between theory and experiment for this species (and probably for HCN^- and HBO^- as well) have been discussed.²⁸ As with vinyl the additional terms in (A5) contribute very little to the calculated splitting.

The agreement here between theory and experiment varies so much from radical to radical that we conclude it is probably unsafe to make generalizations from the results of calculations on so few species.

C. Iminoxy Radicals. In these calculations the PBD/BD parametrization schemes proved to be less satisfactory than the DP scheme and hence the results of the latter only are quoted below.

(i) *The Radical $H_2C=N\dot{O}$.* Since this is the simplest member of the iminoxy series, a theoretical investigation was felt to be desirable. This radical's esr spectrum has not been reported, and although we attempted to prepare the radical from the oxime by oxidation with lead tetraacetate and with cerium(IV), we were unable to detect it. However, the more or less invariant values of a^N and a_β^H (cis and trans) for previously detected aldoxime radicals (*e.g.*, from benzaldoxime²⁹ and trimethylacetaldoxime³⁰) suggest that the following split-

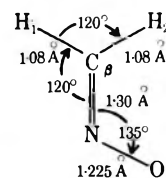


Figure 1.

tings are appropriate: $a^N \simeq 30 \text{ G}$, $a_1^H \simeq 6 \text{ G}$, $a_2^H \simeq 26 \text{ G}$ (see Figure 1). An ^{17}O splitting of $\sim 23 \text{ G}$ would be expected by analogy with that in (I, $R_1 = CH_3$, $R_2 = COCH_3$).³¹

The coupling constants calculated for $H_2C=NO\cdot$ with an idealized geometry ($r_{CN} = 1.35 \text{ \AA}$, $r_{NO} = 1.30 \text{ \AA}$, $r_{CH} = 1.08 \text{ \AA}$, $\angle CNO = 120^\circ$) are poor. Fixing $\angle HCH = \angle HCN = 120^\circ$, $r_{CH} = 1.08 \text{ \AA}$, and varying the geometry of the CNO group, we found the minimum energy geometry to be that shown in Figure 1. The CNO angle of 135° corroborates Symons' estimate³² of 140° (obtained from an analysis of the anisotropy in the nitrogen splitting for iminoxy radicals). The calculated coupling constants for the optimum geometry are shown in Table IV; the large a^N and a_2^H and the small a_1^H are qualitatively well accounted for and confirm the assignments made experimentally.

If considerations of energy and of $\langle S^2 \rangle_{av}$ are ignored, various configurations can be found that reproduce the expected splittings perfectly. However, such geometries prove unsatisfactory when applied to larger radicals.

(ii) *The Radicals $CH_3CH=N\dot{O}$.* Experimental data (obtained *via* one-electron oxidation of acetaldoxime²⁹) are available for one isomer, probably anti³³ (I, $R_1 = H$, $R_2 = CH_3$): $a^N = 32.5 \text{ G}$, $a_\beta^H = 5.2 \text{ G}$; by analogy with the two isomeric iminoxy radicals from benzaldoxime (I, $R_1 = Ph$, $R_2 = H$ and I, $R_1 = H$, $R_2 = Ph$), we would expect $a^N \simeq 30 \text{ G}$ and $a_\beta^H \simeq 26 \text{ G}$ for the syn isomer (I, $R_1 = CH_3$, $R_2 = H$). Methyl proton coupling constants do not appear to be available for either isomer, but the almost unvarying value of $a_{Me^H} = 1.4 \text{ G}$ observed for a large number of iminoxy radicals (I, $R_1 = CH_3$, $R_2 = X$ and I, $R_1 = X$, $R_2 = CH_3$)^{30, 34, 35} suggests that this number would be appropriate here for both isomers. The three methyl-proton conformations chosen for the calculations on each isomer are shown in Figure 2 and the arithmetic mean values of the calculated splittings are given in Table IV. The figures ob-

(28) A. Hinchliffe and D. B. Cook, *Chem. Phys. Lett.*, **1**, 217 (1967).

(29) J. R. Thomas, *J. Amer. Chem. Soc.*, **86**, 1446 (1964).

(30) B. C. Gilbert and R. O. C. Norman, *J. Chem. Soc. B*, 123 (1968).

(31) B. C. Gilbert and W. M. Gulick, *J. Phys. Chem.*, **73**, 2448 (1969).

(32) (a) M. C. R. Symons, *J. Chem. Soc.*, 1189 (1963); (b) W. M. Fox and M. C. R. Symons, *ibid.*, **A**, 1503 (1966).

(33) B. C. Gilbert and R. O. C. Norman, *ibid.*, **B**, 86 (1966).

(34) B. C. Gilbert and R. O. C. Norman, *ibid.*, **B**, 722 (1966).

(35) B. C. Gilbert and R. O. C. Norman, *J. Phys. Chem.*, **71**, 14 (1967).

Table III: Results of Calculations on Some Small Radicals

Radical	$\langle S^2 \rangle_{av}$ before annihilation	$\langle S^2 \rangle_{av}$ after annihilation	Nucleus γ	Coupling constants a^a , G [†]				Experimental a^a	Reference
				(PBD-ba)	(BD-aa)	(DP-ba)	(DP-aa)		
NO ₂	0.7645	0.7501	¹⁴ N	33.36	106.86	48.36	52.15	54.75	<i>a</i>
			¹⁷ O	0.45	2.00	-0.84	-1.26	(-)23	<i>b</i>
NH ₂	0.7547	0.7500	¹⁴ N	12.59	12.77	18.26	6.23	10.3	<i>c</i>
			¹ H	-22.55	-9.74	-36.57	-12.00	23.9	<i>c</i>
HCO	0.7552	0.7500	¹ H	82.82	93.36	134.36	114.96	137	<i>d</i>
			¹³ C	142.22	149.29	192.43	199.86	135	<i>d</i>
			¹⁷ O	4.69	6.21	-8.72	-3.93	...	
HCN ⁻	0.7644	0.7500	¹ H	159.89	184.23	259.38	226.84	137	<i>e</i>
			¹³ C	164.49	170.25	222.57	227.93	75.3	<i>e</i>
			¹⁴ N	2.36	2.56	3.42	1.25	6.5	<i>e</i>
HBO ⁻	0.7563	0.7500	¹ H	77.64	86.58	125.95	106.61	94	<i>f</i>
			¹⁰ B	68.5	70.4	33.5	<i>f</i>
			¹¹ B	204.4	210.2	100	<i>f</i>
			¹⁷ O	3.13	6.29	-5.81	-3.98	...	
H ₂ CN	0.7732	0.7504	¹ H	82.69	77.87	134.14	95.89	87.4/91.2	<i>g, h</i>
			¹³ C	-28.68	-9.52	-38.82	-12.74	...	
			¹⁴ N	8.44	8.50	12.24	4.15	11.4/9.5	<i>g, h</i>
	0.7583	0.7500	¹ H _a	-3.83	-1.30	-6.22	-1.61	1.3	<i>i</i>
			¹ H _b	46.97	41.10	76.20	50.61	30.4	
			¹⁴ N	13.41	40.64	19.44	19.83	21.6	
			¹³ C	136.49	141.04	184.76	188.83	...	
			¹⁷ O	5.49	5.73	-10.19	-3.63	...	

^a Z. Luz, A. Renveni, R. W. Holmberg, and B. L. Silver, *J. Chem. Phys.*, **51**, 4017 (1969). ^b P. D. Foster, J. A. Hodgson, and R. F. Curl, *ibid.*, **45**, 3760 (1966). ^c S. Foner, E. L. Cochran, V. A. Bowers, and C. Jen, *Phys. Rev. Lett.*, **1**, 91 (1958). ^d E. L. Cochran, F. J. Adrian, and V. A. Bowers, *J. Chem. Phys.*, **44**, 4626 (1966). ^e K. D. J. Root, M. C. R. Symons, and B. C. Weatherly, *Mol. Phys.*, **11**, 161 (1966). ^f R. C. Catton, M. C. R. Symons, and H. W. Wardale, *J. Chem. Soc. A*, 2622 (1969). ^g E. L. Cochran, F. J. Adrian, and V. A. Bowers, *J. Chem. Phys.*, **37**, 1938 (1962). ^h J. A. Brivati, K. D. J. Root, M. C. R. Symons, and D. J. A. Tinling, *J. Chem. Soc. A*, 1942 (1969). ⁱ R. Livingston and H. Zeldes, *J. Chem. Phys.*, **47**, 4173 (1967). [†] ba = before annihilation of the quartet. aa = after annihilation of the quartet.

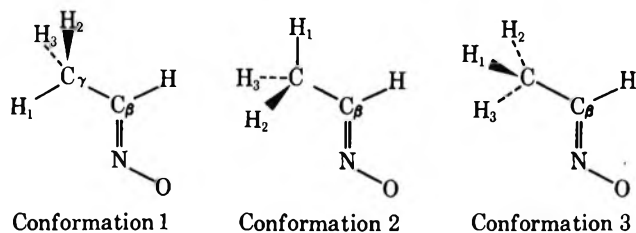


Figure 2.

tained in this way are very similar to those derived by the method of areas in which a_{Me^H} is plotted against ϕ (the angle of rotation about the $C_\beta-CH_3$ bond) and the mean, a_{Me^H} , found by calculus in the usual way. As the maximum difference calculated in rotamer energies for a given isomer (syn or anti) is very low (~ 2.5 kcal/mol), we consider a full statistical analysis involving rotational energy levels to be unnecessary.

The theory accounts quite well for the experimentally observed values of a^N and a_β^H (anti), and for the expected value of a_β^H (syn). For both radicals the calculated methyl proton splittings, after annihilation, are in good agreement with expectation and are predicted to be negative. The variation in a_{Me^H} with ϕ shows a novel effect when compared with calculations of the analogous splitting in a π radical (e.g., ethyl[†]); thus

a_{Me^H} takes its largest positive values when the proton lies in the plane of the CNO system and becomes more negative as the CH bond is rotated out of plane. Hence, for (I, $R_1 = H$, $R_2 = CH_3$), $a_1^H = -5.9$ G in conformation 3 and $a_1^H = +3.1$ G in conformation 1 (see Figure 2). The effect is slightly less marked for (I, $R_1 = CH_3$, $R_2 = H$), where the calculated splittings are -5.7 and 0.0 G, respectively. Detailed experimental evidence on the angular dependence of the splittings is not yet available; we have previously conjectured³³ that the largest proton splitting (~ 4 G) arises from the proton in the plane of the CNO group though recent results for some bicyclic iminoxy radicals³⁶ indicate this splitting to be ~ 2 G. The latter result, together with that for the radical from camphor oxime, where the γ -CH bond makes an angle of 60° with the plane of the CNO group and for which $a_\gamma^H = 2.4$ G, suggests that the absolute value of a_γ^H is not at its maximum in the plane. Our investigations suggest a possible reason for this: the appreciable negative coupling constant predicted for the proton when the γ -CH bond is in the plane perpendicular to the CNO system may be accounted for qualitatively by a "hyperconjugative"

(36) H. Căldărăru, N. Barbulescu, L. Ivan, and V. E. Sahini, *Tetrahedron Lett.* 3039, 1970.

Table IV: Calculated and Experimental Coupling Constants for Some Iminoxy Radicals

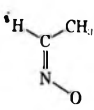
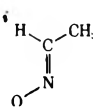
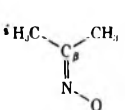
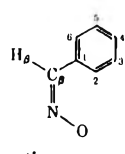
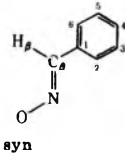
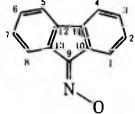
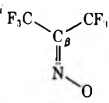
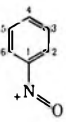
Radical	Atom <i>n</i>	Coupling constants a^n		Exptl
		Calcd b_a	Calcd a_a	
	H ₁	0.92	1.4	6.0 ^a
	H ₂	29.9	18.8	26.8 ^a
	C	4.5	7.7	...
	N	25.6	23.5	30 ^a
	O	-20.0	-6.8	23 ^a
	$\langle S^2 \rangle_{av}$	0.7621	0.7501	
 anti	H _{Me}	-8.2	-2.1	1.4 ^a
	H	3.6	2.8	5.2 ^a
	C _{Me}	5.4	3.2	...
	C	1.8	6.2	...
	N	28.6	26.0	32.5
	O	-19.4	-6.6	23 ^a
$\langle S^2 \rangle_{av}$	0.7734	0.7501		
 syn	H _{Me}	-9.2	-2.9	1.4 ^a
	H	33.6	20.6	26 ^a
	C _{Me}	2.5	1.2	...
	C	5.9	10.5	...
	N	27.4	24.9	30 ^a
	O	-20.1	-6.8	23 ^a
$\langle S^2 \rangle_{av}$	0.7723-0.7734	0.7501		
	H _{Me (syn)}	-10.7	-3.0	1.4 ^b
	H _{Me (anti)}	-11.2	-3.4	1.4
	C _{Me (syn)}	6.7	3.8	...
	C _{Me (anti)}	3.6	1.7	...
	C	2.2	7.2	...
	N	30.9	27.7	30.4
	O	-19.6	-6.7	23 ^a
	$\langle S^2 \rangle_{av}$	0.794-0.799	0.7503	
 anti	C ₁	7.5	4.8	...
	C ₂	-2.0	-0.2	...
	C ₃	2.5	1.0	...
	C ₄	-2.5	-0.8	...
	C ₅	2.4	0.9	...
	C ₆	-0.6	0.7	...
	H ₂	-0.3	1.2	2.8 ^c
	H ₃	-1.0	-0.3	...
	H ₄	2.0	0.7	0.5 ^d
	H ₅	0.0	0.2	...
	H ₆	1.7	0.6	~0
	H _β	4.2	3.0	6.5
	C _β	-3.1	3.1	...
	N	27.5	24.5	32.6
	O	-19.9	-6.7	23 ^a
$\langle S^2 \rangle_{av}$	0.7914	0.7504		
 syn	C ₁	3.3	1.5	...
	C ₂	-3.2	-1.1	...
	C ₃	2.1	0.7	...
	C ₄	-2.6	-0.9	...
	C ₅	2.2	0.7	...
	C ₆	-2.9	-0.9	...
	H ₂	1.9	0.7	...
	H ₃	-1.1	-0.4	...
	H ₄	1.7	0.6	...
	H ₅	-1.2	-0.4	...
	H ₆	1.9	0.6	...
	H _β	35.8	21.7	27.0 ^c
	C _β	1.8	8.3	...
	N	28.3	25.1	30.0
	O	-20.4	-6.9	23 ^a
$\langle S^2 \rangle_{av}$	0.7958	0.7505		

Table IV (Continued)

Radical	Atom α	Coupling constants a^n		Exptl	
		Calcd b_a	Calcd a_a		
	C ₁	-3.1	-1.0	...	
	C ₂	2.3	0.9	...	
	C ₃	-2.5	-0.8	...	
	C ₄	2.0	0.8	...	
	C ₅	1.6	0.5	...	
	C ₆	-2.3	-0.8	...	
	C ₇	1.8	0.6	...	
	C ₈	-2.6	-0.8	...	
	C ₉	-3.0	4.3	9.6 ^{g,j}	
	C ₁₀	9.4	5.7	26.6 ^j	
	C ₁₁	-1.3	-0.1	...	
	C ₁₂	-1.3	-0.2	...	
	C ₁₃	3.2	1.5	...	
	H ₁	2.6	1.3	2.7	
	H ₂	-0.9	-0.3	...	
	H ₃	1.7	0.6	...	
	H ₄	-0.1	0.1	...	
	H ₅	-0.9	-0.3	...	
	H ₆	1.6	0.5	...	
	H ₇	-0.8	0.2	...	
H ₈	1.7	0.6	1.0		
N	29.7	25.9	30.85		
O	-20.1	-6.9	23 ^a		
$\langle S^2 \rangle_{av}$	0.8366	0.7514			
	F (syn)	-1.4	0.6	6.85 ^f	
	F (anti)	-3.6	0.8	0.50	
	C (syn)	7.6	5.3	...	
	C (anti)	0.9	0.8	...	
	C _{β}	5.6	7.9	...	
	N	27.1	25.6	32.6	
	O	-19.7	-6.7	23 ^a	
	$\langle S^2 \rangle_{av}$	0.762	0.750		
		C ₁	3.0	4.6	...
		C ₂	3.2	3.2	...
C ₃		1.4	0.9	...	
C ₄		1.8	-0.6	...	
C ₅		0.9	0.3	...	
C ₆		-0.6	0.5	...	
H ₁		0.4	-0.1	...	
H ₂		2.9	1.8	3.8 ^g	
H ₃		1.3	0.5	...	
H ₄		0.7	-0.2	...	
H ₅		2.8	1.5	...	
H ₆		2.8	1.5	...	
N		22.6	22.8	37.0	
O	-18.1	-6.2	...		
$\langle S^2 \rangle_{av}$	0.7645	0.7501			

^a Reference 29. ^b Reference 35. ^c Reference 34. ^d Reference 37. ^e Reference 33. ^f Reference 35. ^g Reference 41. ^h Estimated value, see text. ⁱ Average values of three conformations. ^j Not assigned.

effect originating from negative π spin density at C _{β} (see section 6).

(iii) *The Radical (CH₃)₂C=NO·*. In contrast to the differing values of a_{β}^H in syn and anti iminoxy radicals from aldoximes, the room temperature spectrum of (CH₃)₂C=NO· in solution shows that cis and trans methyl protons have equal splittings of ~ 1.4 G.³⁵ Calculations were performed on this radical for three rotamers corresponding to the three conformations

shown in Figure 2; in each rotamer, one methyl group was the reflection of the other in the plane containing the CN bond, perpendicular to the C₂CNO plane. The average calculated splittings are shown in Table IV. Agreement with experiment is quite promising and the similar splittings (both negative) for the two sets of methyl protons are accounted for well by the coupling constants calculated after annihilation. As with CH₃CH=NO·, the calculated methyl-proton splittings

before annihilation are far too large, reflecting, perhaps, the extreme sensitivity of these values to the presence of contaminating spin states.

(iv) *The Radicals PhCH=NÖ*. Analysis of the spectra of the anti isomer (I, $R_1 = H$, $R_2 = Ph$) and of some substituted derivatives indicates that the observed triplet ($a^H = 1.4$ G) derives from the ortho protons.³⁴ Further, the results for some mono-ortho substituted radicals in which there appear to be marked conformational preferences suggest that the splittings in the unsubstituted example arise by averaging, due to fast rotation about the C_β -Ph bond, of ortho proton splittings of 2.8 G (when the proton is in the plane of the CNO system and close to the oxygen, cf. the fluorenone iminoxy radical) and ~ 0 G (when the proton is in the CNO plane but removed from the radical center).^{34,35} Calculations were performed for a planar structure, and the calculated value of $\langle S^2 \rangle_{av}$ after annihilation is close enough to $3/4$ for us to have confidence in our deductions; the predicted splittings after annihilation indicate that a_2^H is the largest ring proton splitting, in good agreement with the experimental findings.

Calculations were also performed for the syn isomer; for this radical no ring proton splittings have been resolved, in accord with the assertion that transmission of unpaired electron density in iminoxy radicals is more favorable to groups on the cis rather than the trans side of the NO group.³⁵ Again, $\langle S^2 \rangle_{av}$ after annihilation is close to $3/4$, and the calculations predict that none of the ring proton splittings will be greater than 0.6 G. (The results before annihilation suggest that spin contamination by states of multiplicity greater than the doublet has a profound effect.) Unlike Cramer and Drago¹⁸ we have not had to resort to choosing twisted conformers to obtain reasonable agreement.

The calculations for the syn isomer do show one interesting feature which deserves comment: the largest predicted splittings (~ 0.6 G) are for the ortho and para protons of the aromatic ring and have positive sign. This suggests " π -like" behavior of the unpaired electron density in the ring, with positive splittings from *o*- and *p*-H reflecting negative spin density in the *p* orbitals, derived from negative spin density in the π orbital on C_β . That this is dominant for the ring protons in the syn isomer probably reflects the smaller effect of spin density in the σ system on the trans side of the NO group. There exists experimental evidence to corroborate these suggestions: examination of the iminoxy radicals from benzophenone oxime and some substituted derivatives at low temperature³⁷ reveals not only the characteristic splitting of 1.4 G from the ortho protons in the ring cis to the NO group but also some smaller splittings (probably) from both para protons. Mackor suggests that this provides evidence for spin density in the π system of a σ radical, via a σ - π interaction.³⁷ Confirmation of this refinement to our understanding of delocalization in σ radicals must await the production

of well-resolved spectra from a range of suitably-substituted radicals.

(v) *Fluorenone Iminoxy Radical*. This radical has been investigated experimentally in some detail^{35,38} and the following assignments of hfs have been made: $a_1^H = 2.7$ G, $a_8^H = 1.0$ G, $a^N = 30.85$ G (see Table IV). Two ^{13}C splittings have been observed (26.6 G and 9.6 G) but not assigned.

The observation of splittings from protons (and also halogens³⁵) in close proximity to the NO group led to the suggestion that "through space" interaction might be involved.^{33,35} Assuming the unpaired electron to be associated with the NO system alone and unperturbed by the presence of other nuclei, Malrieu³⁹ obtained estimates for the coupling constants of protons at the 1 and 8 positions in this radical, i.e., for a hydrogen nucleus influenced by an unpaired electron in orbitals on N or O. The values he obtained ($a_1^H = 0.085$ G and $a_2^H = 0.031$ G for $\angle CNO = 140^\circ$) cannot account satisfactorily for the splittings, and we believe that any successful account of these splittings must include the effects of electronic interactions in the regions around the protons.

The results of our calculations are shown in Table IV. To avoid fluctuations due to computer round-off error, the energy convergence criterion was limited to agreement between cycles to 10^{-5} au only. On the whole, the agreement between theory (after quartet annihilation) and experiment is good, and for protons where possible splittings are obscured by the line width (~ 0.5 G) a low value of the coupling constant is calculated. In addition to a_1^H and a_8^H , a_3^H and a_6^H are also predicted to be appreciable, possibly reflecting the " π -like" structure of electron distribution (see above). We note that a similar spin distribution, though of opposite sign, exists in, for instance, the anion radical of fluorenone.⁴⁰ Well-resolved spectra of suitably substituted iminoxy radicals should again clarify this situation. An unsatisfactory result of these calculations is the failure to account satisfactorily for the ^{13}C splittings; our present assignments must therefore be highly tentative.

Interestingly enough, the calculation shows the four highest occupied UHF MO's to be of π symmetry; that the radical can nevertheless be classified as a σ radical (in agreement with the experimental conclusions) we attempt to show in section 5.

(vi) *The Radical (CF₃)₂C=NÖ*. The very large difference between cis and trans fluorine couplings ($a^F = 6.85$ and 0.50 G, respectively) observed for this species appears to be characteristic of trifluoromethyl substituted iminoxy radicals and is generally considered to be

(37) A. Mackor, Thesis, University of Amsterdam (1968).

(38) B. C. Gilbert and R. O. C. Norman, *J. Chem. Soc. B*, 981 (1967).

(39) J. P. Malrieu, *J. Chim. Phys.*, **61**, 1587 (1964).

(40) R. Dehl and G. K. Fraenkel, *J. Chem. Phys.*, **39**, 1793 (1963).

evidence for their being of σ -type (see, *e.g.*, ref 35). This is in contrast with the splittings of *cis* and *trans* methyl protons (*e.g.*, $(\text{CH}_3)_2\text{C}=\text{NO}\cdot$) which are approximately equal (see (iii) above). The calculated coupling constants for $(\text{CF}_3)_2\text{C}=\text{NO}\cdot$ are shown in Table IV; as with $(\text{CH}_3)_2\text{C}=\text{NO}\cdot$, the averages over three conformations of the CF_3 groups are recorded. The comparison of calculated with experimental fluorine couplings is disappointing and suggests that the difference ($a^{\text{F}}(\textit{cis}) - a^{\text{F}}(\textit{trans})$) should be much less than is observed. The calculated maximum difference in total energies between rotamers is 0.0014 au (0.87 kcal/mol), far too small at ordinary temperatures to favor one conformation over another. We also note that whereas the *trans* fluorine splitting varies over a considerable range (from -2.0 G when the CF bond lies in the plane perpendicular to that of the CNO group to $+5.3$ G when the CF bond is coplanar with the CNO group) the parallel range of *cis* fluorine splittings is much smaller (-2.8 G to $+0.8$ G).

In the light of pilot calculations with $\text{H}_2\text{C}=\text{NO}\cdot$ we suggest that possibly a better account of the experimental splittings might be given if the $\text{C}_\beta\text{-CF}_3$ bond lengths were taken to be greater than 1.4 \AA . That such a geometry might also lead to a lower energy of the radical is also plausible on account of the high electronegativity of the CF_3 groups.

D. Nitrosobenzene Cation Radical, (PhNO \cdot +). Cauquis, *et al.*,⁴¹ have measured the following coupling constants for this species: $a^{\text{N}} = 37.0$ G, $a_{\text{meta}}^{\text{H}}(1) = 3.8$ G, and $a^{\text{H}} = 1.3$ G (unassigned). The large a^{N} and asymmetric proton hfs indicate that this is a σ radical with a formal analogy to the iminoxy series and in marked contrast to the (π) nitrosobenzene anion radical. The distribution of proton splittings appears analogous to that in the isoelectronic benzoyl radical [$a_{\text{meta}}^{\text{H}}(2) = 1.16 \text{ G}^{17}$] except that rotation about the Ph-CO bond in benzoyl is fast compared with the difference in frequency of the meta-proton splittings; the rate of the corresponding rotation about the Ph-NO bond is sufficiently slow for the spectrum to show one distinct meta-proton splitting. Cramer and Drago¹⁹ have performed EH calculations on $\text{PhNO}\cdot^+$ and have suggested that the NO bond is twisted from the plane of the phenyl ring (by $\sim 70^\circ$). In the present calculation we have assumed that the NO bond and phenyl ring are coplanar (our results are shown in Table IV). The largest calculated proton splitting, both before and after annihilation, is for the meta proton in the 3 position, the predicted values being in reasonable agreement with observation. The next largest splitting is predicted for a_6^{H} . These results closely resemble the splittings calculated for benzoyl by Krusic and Rettig.²⁷

5. A Theoretical Analogy to the Experimental Differentiation between σ and π Radicals

We have suggested that large π radicals should be

treated by the methods of Pople, *et al.* (*i.e.*, to assume idealized geometry and to adopt the BD and PBD parameters for calculating coupling constants), whereas for large σ radicals we have suggested a slightly different scheme (*i.e.*, the choice of minimum energy geometry for the radical center, idealized geometry for the remainder of the molecule, and the DP parameters to calculate splittings). Examination of our calculations on those radicals which have been clearly established as π or σ on experimental grounds reveals that a theoretical differentiation may be made in terms of the " π spin population," R^π (equation 5.1) for the radical under scrutiny (see Table V and Appendix, equation A3).

$$R^\pi = \sum_i Q_{ii} \quad (5.1)$$

(i over all $2p_\pi$ orbitals on "in-plane atoms"). To evaluate R^π a formal "plane of symmetry" defined by the "in-plane atoms" must be chosen. We have found it convenient to count (a) the atoms of the radical center (or the "nodal" plane for π radicals) and (b) any atoms coplanar with the radical center and connected to it *via* one or more bonds which also lie in the plane of the radical center. Thus, in the iminoxy radical from fluorenone, all carbon atoms, N, and O are included; in $(\text{CF}_3)_2\text{C}=\text{NO}\cdot$, the three carbon atoms, N, O, and any F atoms which may lie in the plane so defined. From Table V we observe that σ radicals have values of R^π close to zero while for π radicals, R^π is nearer unity (*e.g.*, for vinyl and the iminoxy radical from fluorenone oxime, $R^\pi = 0.00$, while for allyl and biacetyl semidione $R^\pi = 1.00$). On the basis of this result we adduce that the forms of vinyl and of $\text{H}_2\text{C}=\text{NO}\cdot$ in which the CCH and CNO systems, respectively, are linear, would still be σ radicals. We suggest that an investigation could profitably be carried out in which it was determined for which values of R^π the DP parametrization scheme would be preferred to the PBD/BD schemes and *vice versa*. We may also consider the value of R^π to give an indication of the σ or π "character" of a radical.

We note that even for radicals described as being of σ type (*e.g.*, the iminoxy radical from fluorenone oxime) the highest occupied UHF MO is not always of σ symmetry. Thus, conclusions about the σ or π nature of the radical cannot be drawn from examination of this orbital alone whereas the value of R^π appears to be a more effective guide.

6. Spin Density Maps

From the spin density matrices and equation A6, spin density maps were calculated by evaluation of $Q(\mathbf{r})$ in regions of space around a selected radical. The basis orbitals chosen were the STO's used elsewhere in the calculation. Two maps for vinyl are shown (Figures 3 and 4), one in the plane of the radical, the other

(41) G. Cauquis, M. Genies, H. Lemaire, A. Rassat, and J. P. Ravet, *J. Chem. Phys.*, **47**, 4642 (1967).

Table V: Values of R^* for Various Radicals (Eq 5.1), before Annihilation

Radical	R^*	Atoms defining plane at symmetry	Radical	R^*	Atoms defining plane of symmetry
Vinyl ($\theta = 145^\circ$)	0.0000	all	HCO	0.0000	all
Vinyl (linear)	0.0000	all	HCN ⁻	0.0000	all
H ₂ C=NO [·]	0.0001	all	HBO ⁻	0.0000	all
H ₂ C=NO [·] (linear)	-0.0001	all	PhNO ^{·+}	0.0000	all
CH ₃ CH=NO [·] (anti) ^a	0.0161	H _{β} C C N O	[·] CONH ₂	0.0000	all
CH ₃ CH=NO [·] (syn) ^a	0.0167	H _{β} C C N O	Methyl	1.0000	all
PhCH=NO [·] (syn)	-0.0001	all	Allyl	1.0000	all
PhCH=NO [·] (anti)	-0.0001	all	Butadiene ^{·-}	1.0000	all
(CH ₃) ₂ C=NO ^{·b}	0.0624	C C C N O	Benzene ^{·-}	0.9998	all
(CF ₃) ₂ C=NO ^{·b}	0.0157	C C F F C N O	Biacetyl semidione ^{·-}	0.9912	C C C C O O
Phenyl	0.0001	all	NH ₂	1.0000	all
NO ₂	0.0001	all			

^a Conformation 3 (see Figure 2). ^b Both CH₃ or CF₃ groups in conformation 2. R^* includes contributions from in-plane F atoms; "all" implies that all the atoms in the radical lie in the plane of symmetry.

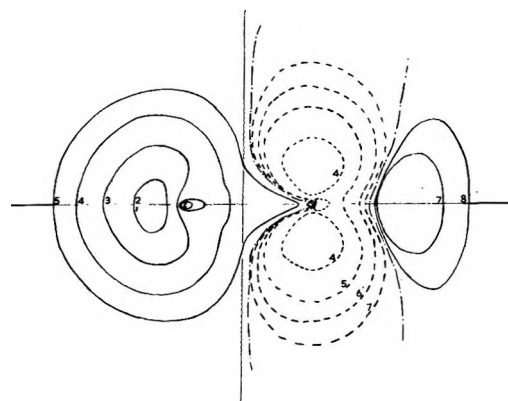
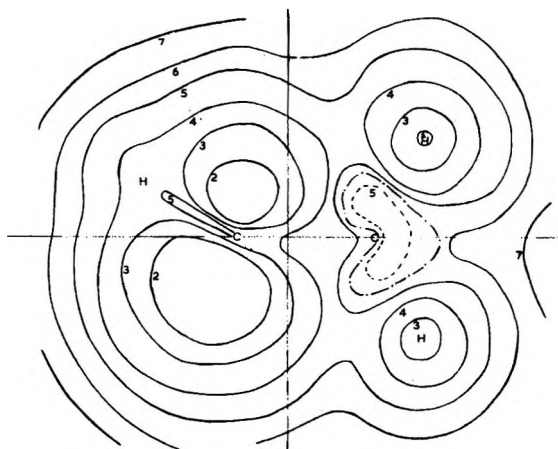


Figure 4. The vinyl radical. Spin density contours in the plane containing the CC bond at right angles to the plane of the radical.

Figure 3. The vinyl radical. Spin density contours (taken from computer output) in the plane of the radical: —, positive spin density; - - - -, negative spin density; - · - · -, surface of zero spin density. The numbers, x , give the minimum magnitude of the spin density within the contour as $10^{-x/2}$ (e.g., 5 implies a spin density of magnitude $10^{-2.5}$ au)

radicals were -0.095 to -0.160 before annihilation and -0.040 to -0.047 after annihilation.

7. Conclusions

We have observed that coupling constants in π radicals are well accounted for by UHF INDO calculations in which each model radical has idealized geometry and the A^n of equation A8 are those of Pople, *et al.*,^{8,9} but that this scheme is less successful for some σ radical splittings. On the other hand, our calculations have shown that a good account of vinyl, iminoxy, and nitrosobenzene cation σ radicals may be given by the following approach: the geometry of the radical center is chosen to be that for minimum energy, as determined by a pilot calculation on the simplest member of the series; the remaining atoms assume positions of idealized geometry (this configuration appears to have an energy close to the overall minimum and to yield good values of $\langle S^2 \rangle_{av}$ and yet economizes on the amount of calculation); the direct parametrization scheme for A^n (discussed in section 2 and in the Appendix) is then

at right angles, containing the CC bond. Figure 3 is not unlike the usual chemical representation in which the unpaired electron "occupies" a lobe on the α carbon; Figure 4 is rather striking in that it shows a volume of negative spin density, ostensibly in a p_x -like "orbital" on C_β . A similar spin density distribution pertains in the case of H₂C=NO[·] (Figures 5 and 6). If the " p_x orbital" on C_β containing negative spin density exists in large σ radicals, it may account in part for the negative π -like behavior of the H and F splittings in the rotamers of radicals with β -CH₃ and CF₃ groups (see, e.g., sections 4. C. (ii), (iii), and (vi)) and for the delocalization of negative spin density to distant ring positions in the iminoxy radicals from benzaldoxime and from fluorenone oxime (see, e.g., sections 4. C. (iv), (v)). Typical values of $Q_{C_\beta C_\beta}$ in these calculations on iminoxy

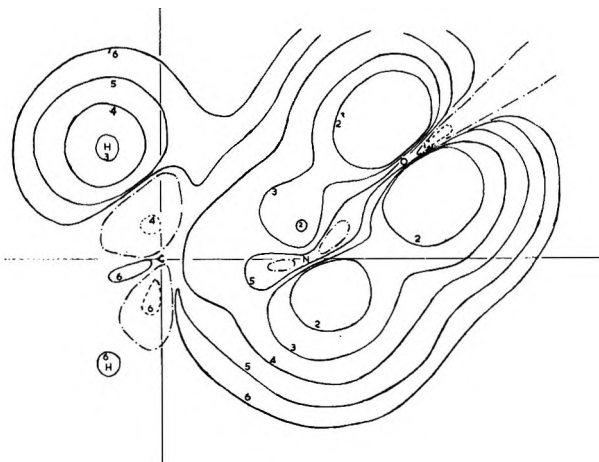


Figure 5. The radical $\text{H}_2\text{C}=\text{NO}\cdot$. Spin density contours in the plane of the radical.

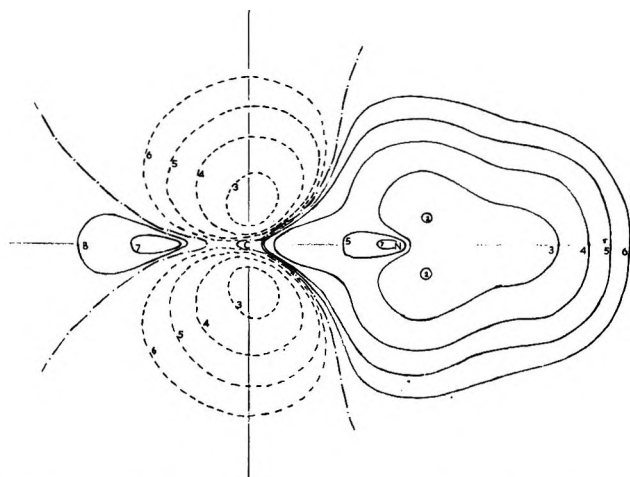


Figure 6. The radical $\text{H}_2\text{C}=\text{NO}\cdot$. Spin density contours in the plane containing the CN bond at right angles to the plane of the radical.

used. A further advantage of the DP scheme is that, unlike schemes depending on least-squares regression to obtain A^N , it can be applied to cases where only a small number of data are available. We have examined the effect of spin projection of the UHF wave function by annihilation of the quartet contaminant and have found that it reproduces experimental spin distributions at positions removed from the radical center more closely than the unprojected function. We tend therefore to prefer the results after annihilation to those before even though in certain cases (see below) the results before annihilation give better absolute agreement with some of the experimental values.

Values of a^N calculated after annihilation are 2–3 G lower than those obtained before annihilation, but still in reasonable agreement with experiment. Proton-coupling constants calculated after annihilation account well for the experimentally observed difference between a_{β}^{H} (cis) and a_{β}^{H} (trans) in iminoxy radicals from al-

doximes and for the similarity between a_{Me}^{H} (cis) and a_{Me}^{H} (trans) in radicals from methyl-substituted oximes. The calculations also account well for the observed distribution and magnitudes of ring proton splittings in iminoxy radicals from aromatic aldoximes (which were assumed to be planar) and in the iminoxy radical from fluorenone oxime. The results for $\text{PhNO}\cdot^+$ show similarities between this radical and $\text{PhCO}\cdot$,²⁷ particularly in the distribution of ring proton splittings. The calculations fail to give unambiguous assignments for the ^{13}C splittings in the iminoxy radical from fluorenone oxime and for the ^{19}F splittings in $(\text{CF}_3)_2\text{C}=\text{NO}\cdot$. ^{17}O splittings calculated after annihilation appear in poor agreement with experiment though before annihilation the agreement is quite good.

Consideration of the spin density maps suggests that positive spin density in the σ system of the radical center may induce some negative spin density in a p_{π} -like "orbital" on C_{β} of vinyl and of some iminoxy radicals. The negative spin density then behaves in a way analogous to positive spin density in a π radical.

We find that a quantitative theoretical distinction between π and σ radicals can be made within the context of our calculational methods in terms of the quantity R^{π} , and suggest that this quantity might be used to determine which of the two parametrization schemes for A^N is appropriate in a given case if a choice is to be made.

Appendix

In order to calculate isotropic hyperfine coupling constants it is necessary to calculate the spin density function $Q(\mathbf{r})$ (defined in ref 42, for example) at the various nuclei involved since the coupling constants a^N are given by (see, e.g., ref 42):

$$a^N = \frac{8\pi g\beta\hbar}{3} \gamma_N Q(\mathbf{r}_N) \quad (\text{A1})$$

The function $Q(\mathbf{r})$ can be calculated as accurately as desired from a configuration interaction expansion of the wave function for the molecule, but it has become the custom to assume that the leading term of this expansion will predominate, if this term is determined by a UHF procedure. This assumption appears to be a good one generally, provided that the leading term is very nearly an eigenfunction of S^2 . If we assume an LCAO form for the MO's ϕ^{α} and ϕ^{β} of the UHF problem, it is easy to show that

$$Q(\mathbf{r}) = \eta(\mathbf{r})Q\eta^{\dagger}(\mathbf{r}) \quad (\text{A2})$$

where $\eta(\mathbf{r})$ is a row matrix of the basis orbitals (AO's) and

$$Q = P^{\alpha} - P^{\beta} \quad (\text{A3})$$

where

(42) R. McWeeny and B. T. Sutcliffe, *Mol. Phys.*, **6**, 493 (1963).

$$P^\alpha = T^\alpha T^{\alpha\dagger}, P^\beta = T^\beta T^{\beta\dagger} \quad (\text{A4})$$

and T^α is the matrix of occupied orbital coefficients for the ϕ^α in terms of the η_i and T^β a similar matrix for the ϕ^β .

In cases where the UHF function is not far from being an eigenfunction of S^2 it is appropriate to use an annihilated form of $Q(\mathbf{r})$ (see ref 13).

In the INDO approach a zero differential overlap approximation is assumed for basis functions (taken to be Slater functions $\eta_i'(\mathbf{r})$) on different centers: *i.e.*

$$\eta_i^*(\mathbf{r})\eta_j(\mathbf{r}) = \delta_{ij}'\eta_i'^*(\mathbf{r})\eta_j'(\mathbf{r})$$

where δ_{ij}' is zero unless η_i and η_j are on the same center. Noting that p_x , p_y , and p_z orbitals give vanishing contributions to the spin density at the nucleus on which they are centered, we can write $Q(\mathbf{r}_n)$ in this approximation as

$$Q(\mathbf{r}_n) = \rho_n |\eta_{n,s}(r_n)|^2 + \sum_{i,j} Q_{ij} \eta_i^*(r_n) \eta_j(r_n) \delta_{ij}' \quad (\text{A5})$$

where $\eta_{n,s}$ denotes the 2s orbital if n is a first row atom or the 1s orbital if n is a hydrogen atom, ρ_n is the appropriate diagonal element of Q . For a general point in the space about the molecule, the spin density is

$$Q(\mathbf{r}) = \sum_{i,j} Q_{ij} \eta_i^*(\mathbf{r}) \eta_j(\mathbf{r}) \delta_{ij}' \quad (\text{A6})$$

In the usual INDO calculation of spin densities the second term in (A5) is ignored and $|\eta_{n,s}(\mathbf{r}_n)|^2$ is treated as a parameter to be assigned by least-squares regression of experimental values of a^n against calculated ρ_n . In our work we chose to use the values of $|\Phi(0)|^2$ of Morton, Rowlands, and Whiffen⁴³ to assign $|\eta_{n,s}(\mathbf{r}_n)|^2$ and the relationship (derivable from (A1)) that

$$A^n = {}^8/3\pi\gamma_n\hbar |\eta_{n,s}(\mathbf{r}_n)|^2 \quad (\text{A7})$$

in order to calculate A^n directly; for points away from the nucleus, the η_i were approximated by Slater orbitals. The values of γ_n were taken from ref 44 or, in the case of γ_B , calculated from nuclear data in ref 45. The re-

sulting parametrization of A^n is the "direct parametrization" (DP) of this paper.

We made a number of trial calculations in which we included the second term in (A5), but except for the α hydrogen in vinyl (as discussed in section 4A), the remaining terms amounted to less than 10% of the first term. Thus, (A1) can for most purposes be written as

$$a^n \simeq A^n \rho_n \quad (\text{A8})$$

Details of Computation. The original version of the INDO was kindly supplied by QCPE.⁴⁶ This was modified for use on a much smaller computer with only 16K of free store. Extra subroutines were written to perform the following: (i) annihilation of the quartet spin state by the method of Amos and Snyder,¹³ (ii) calculation of the additional terms, as given in equation (A5), (iii) calculation of spin density maps (output to the line printer). All results quoted in this paper, except for the iminoxy radical from fluorenone, used a convergence criterion of 6 decimal places in the electronic energy. For the larger radicals, this often required more than the 20 cycles allowed by the original INDO program. If the convergence criterion was reduced to 5 decimal places, usually not a great deal of difference was noted in the coupling constants obtained, though for one or two centers (C_β notably), the alteration in coupling constants was about 1 G.

The "idealized geometry" referred to is similar to that used by Pople, *et al.*,⁸ in which the main interbond angles are taken to be 120° (methyl groups are tetrahedral) and the following bond lengths are assumed: $r_{CH} = 1.08 \text{ \AA}$, $r_{CC} = 1.40 \text{ \AA}$, $r_{CN} = 1.35 \text{ \AA}$, $r_{CO} = 1.36 \text{ \AA}$, $r_{CF} = 1.35 \text{ \AA}$, $r_{NO} = 1.30 \text{ \AA}$.

(43) J. R. Morton, J. R. Rowlands, and D. H. Whiffen, *Nat. Phys. Lab. Pub.*, No. 3PR, 13 (1962).

(44) A. Carrington and A. D. McLachlan, "Introduction to Magnetic Resonance," Harper and Row, New York, N. Y., 1967.

(45) E. R. Andrew, "Nuclear Magnetic Resonance," Cambridge University Press, New York, N. Y., 1955.

(46) Program CNINDO; Quantum Chemistry Program Exchange No. QCPE 141.

The Size Distribution of Small and Large Micelles:

a Multiple Equilibrium Analysis¹

by Pasupati Mukerjee²

Chemistry Department, University of Southern California, Los Angeles, California 90007,
and the School of Pharmacy, University of Wisconsin, Madison, Wisconsin 53706 (Received August 25, 1971)

Publication costs borne completely by The Journal of Physical Chemistry

Some general procedures for dealing with multiple equilibria in step-wise self-association when all species are in rapid association-dissociation equilibrium are extended to and adapted for micellar systems. It is possible by this method to determine the number average degree of association, N_n , from the concentration dependence of the frequently measured weight average value, N_w . The size distribution index, N_w/N_n , is found to be close to unity for many systems, nonionic and ionic, when micelle sizes are small, corresponding to spherical or spheroidal micelles. For large micelles, the size distribution is wide. A step-wise self-association model is derived for such large micelles which predicts an N_w/N_n value of 2 and a linear increase in N_w with the square root of the concentration of micellized surfactant, in agreement with some experimental data for a nonionic and an ionic system in dilute solutions. In concentrated solutions of the large micelles, the nonideality effects become very large. The above self-association model, along with some approximate nonideality corrections, can successfully reproduce the shapes of some observed reduced turbidity data showing minima. Some other consequences of the self-association model are also examined.

Introduction

Polydispersity in micellar systems has been discussed from a theoretical point of view by many investigators³⁻⁷ Experimental measures of the polydispersity have been difficult to obtain, however. While weight average molecular weights of micelles are known for numerous systems from light scattering and equilibrium ultracentrifugation, very few reliable number-average molecular weights have been determined.^{8,9} The first part of this paper deals with a general method and its application for determining the polydispersity of micellar systems first presented several years ago.¹ In this method, the number average degree of association of the micelles, N_n , is determined from the variation of the corresponding weight average value, N_w , with concentration, thus permitting the size distribution index, N_w/N_n , to be determined for many systems for which N_w data are available. The general procedures for handling multiple equilibria in step-wise self-association when all species are in rapid association-dissociation equilibrium have usually been applied to systems showing small numbers of oligomers.¹⁰⁻¹³ The extension and adaptations of these methods to micellar systems, as presented earlier,¹ are different in procedure and details from subsequent publications.^{6,7} The major part of this paper is concerned with the application of these methods to both nonionic and ionic micellar systems, the difficulties arising from nonideality effects due to intermicellar interactions, and the derivation and use of a simple step-wise self-association model for dealing with large micelles, both ionic and nonionic, which are shown to be polydisperse.

The Multiple Equilibrium Model and the Relation between N_n' and N_w' . If the multimer b_q containing q monomers has a molar concentration $[b_q]$ the equilibrium constant for association in an ideal nonionic system, β_q , is given by

$$\beta_q = [b_q]/[b_1]^q \quad (1)$$

where $[b_1]$ is the concentration of monomers. If we now define the quantities S , C , and G as

$$S = \sum [b_q] \quad (2)$$

$$C = \sum q [b_q] \quad (3)$$

$$G = \sum q^2 [b_q] \quad (4)$$

(1) Presented in part at the 152nd National Meeting of the American Chemical Society, New York, N. Y., Sept 1966.

(2) School of Pharmacy, University of Wisconsin, Madison, Wisconsin 53706.

(3) O. Lamm, *Arkiv. Kemi. Mineral Geol.*, **18A**, No. 9 (1944).

(4) M. J. Vold, *J. Colloid Sci.*, **5**, 506 (1950).

(5) D. Stigter and J. Th. G. Overbeek, *Proc. Int. Congr. Surface Activ.*, **2nd**, **1957**, **1**, 311 (1957).

(6) D. G. Hall and B. A. Pethica, in "Nonionic Surfactants," M. J. Shick, Ed., Marcel Dekker, New York, N. Y., 1967.

(7) J. M. Corkill, J. F. Goodman, T. Walker, and J. Wyer, *Proc. Roy. Soc. Ser. A*, **312**, 243 (1969).

(8) H. Coll, *J. Phys. Chem.*, **74**, 520 (1970).

(9) D. Attwood, P. H. Elworthy, and S. B. Kayne, *ibid.*, **74**, 3529 (1970).

(10) R. F. Steiner, *Arch. Biochem. Biophys.*, **39**, 333 (1952); **44**, 120 (1953); **49**, 400 (1954).

(11) F. J. C. Rossotti and H. Rossotti, *J. Phys. Chem.*, **65**, 926, 930, 1376 (1961).

(12) P. Mukerjee, *ibid.*, **69**, 2821 (1965).

(13) A. K. Ghosh and P. Mukerjee, *J. Amer. Chem. Soc.*, **92**, 6408 (1970).

where S is the total molar concentration of all species including the monomer, and C the total equivalent concentration, then the average degrees of association of all species, including the monomer, N_n' and N_w' , at any equivalent concentration C , are given by

$$N_n' = C/S \quad (5)$$

$$N_w' = G/C \quad (6)$$

From the definitions of S , C , and G (eq 2-4), it can be shown by differentiation that irrespective of how many or which multimers form

$$dS/d[b_1] = C/[b_1] \quad (7)$$

$$dC/d[b_1] = G/[b_1] \quad (8)$$

and, therefore

$$d \ln [b_1] = \frac{d \ln C}{N_w'(C)} \quad (9)$$

and

$$dS = \frac{dC}{N_w'(C)} \quad (10)$$

The symbol $N_w'(C)$ indicates that N_w' is a function of C . If this function is known or determined experimentally, $[b_1]$ and S can be determined by graphical integration and N_n' can be determined. The estimate of $[b_1]$ is extremely valuable in any detailed analysis of self-association equilibria, as shown recently for some dye systems.^{13,14}

The above method for determining N_n' from N_w' data is generally applicable. For micellar equilibria, eq 11 below is more suitable.

$$d(S - [b_1]) = \frac{(C - [b_1])}{(G - [b_1])} d(C - [b_1]) \quad (11)$$

$(G - [b_1])/(C - [b_1])$ represents the weight-average degree of association for all associated species, *i.e.*, excluding the monomer. Although the equation is still exact, the use of experimental N_w values in practical cases is facilitated by the use of a slight approximation inherent in the determination of N_w itself. N_w is determined above the critical micelle concentration (cmc) by assuming that the equivalent concentration of micelles is $C - \text{cmc}$, the corresponding approximation being that the monomer concentration above the cmc remains constant, and has the same value as the cmc. The validity of this approximation improves as the value of N_w itself and the ratio $C/[b_1]$ or c/cmc increases in the experimentally accessible region of C . This is implicit in the exact equation

$$d \ln [b_1] = \frac{(C - [b_1])}{(G - [b_1])} d \ln (C - [b_1]) \quad (12)$$

Within the range of the validity of the approximations, therefore, it is possible to write for concentrations above the cmc

$$N_w \approx \frac{G - \text{cmc}}{C - \text{cmc}} \approx \frac{(G - [b_1])}{(C - [b_1])} \quad (13)$$

and, therefore

$$d(S - \text{cmc}) = \frac{d(C - \text{cmc})}{N_w(C)} \quad (14)$$

By graphical integration, it is possible to determine $N_n(C)$ defined as $(C - \text{cmc})/(S - \text{cmc})$. As is to be expected,⁴ N_w cannot decrease with increasing C , because, then $N_n > N_w$, an impossible result. If N_w is approximately constant with C , as is frequently observed, $N_n \approx N_w$, and the micellar size-distribution is narrow. If N_w increases with C as observed in many systems,¹⁵⁻¹⁷ $N_w > N_n$, and there is a distribution in micelle sizes. For approximate purposes, the variation of N_w with C may be put in the form $N_w \propto (C - \text{cmc})^a$. The size distribution index, N_w/N_n , then, from equation 14, has the value $1/(1 - a)$.

Micelles with Narrow Size Distributions

Nonionic Systems. The application of the above analysis to existing literature data suggests that for some nonionic micellar systems, including several zwitterionic ones,¹⁸⁻²⁰ the size-distributions are quite narrow. These systems show characteristically horizontal lines in the usual plots of reduced turbidity against $C - \text{cmc}$, *i.e.*, apparent N_w values which do not change with C , or an apparent reduction in N_w because of excluded volume interactions. Two points of caution must be mentioned, however. As the concentration of micelles increases, intermicellar interactions which lead to positive second or higher virial coefficients may compensate for or mask to some extent the decrease of the reduced turbidity curves with concentration corresponding to an increase in N_w . Thus, the conclusion that size-distributions are narrow when reduced turbidities show small variations with concentration should be made only when nonideality effects are expected to be small. If no pronounced asymmetry of the micelles is expected from the N_w values, *i.e.*, the N_w values are consistent with spherical or spheroidal micelles, and if the absolute concentrations are low, reasonably firm conclusions can be drawn for nonionic systems which do not show long-range intermicellar interactions.

The second point of caution arises from the fact that if highly polydisperse micelles form, N_w increases rapidly with C , as shown later with examples. For such

(14) P. Mukerjee and A. K. Ghosh, *J. Amer. Chem. Soc.*, **92**, 6403 (1970).

(15) P. H. Elworthy and C. B. Macfarlane, *J. Chem. Soc.*, 907 (1963).

(16) R. R. Balmbra, J. S. Clunie, J. M. Corkill, and J. F. Goodman, *Trans. Faraday Soc.*, **60**, 979 (1964).

(17) P. Debye and E. W. Anacker, *J. Phys. Colloid Chem.*, **55**, 644 (1951).

(18) P. Becher, *J. Colloid Sci.*, **16**, 49 (1961).

(19) K. W. Herrmann, *J. Phys. Chem.*, **66**, 295 (1962).

(20) K. W. Herrmann, *J. Colloid Interface Sci.*, **22**, 352 (1966).

systems, the apparent cmc from the turbidity data may be too high.¹⁶ If such high estimates of the cmc are used, spurious horizontal curves of the reduced turbidity *vs.* concentration may be obtained.¹⁷ In general, considerations to be discussed shortly indicate that if N_w is large, requiring highly asymmetric micelles, the size-distribution is probably wide.

Ionic Systems

For ionic micelles, eq 1 is not directly applicable because charge effects are not included. The charge effects can be incorporated in the equilibrium constant either in terms of a physical picture based on the calculated electrostatic free energy of the electrical double layer^{5,21} or in terms of a chemical mass-action picture, using the counterion binding approximation.^{21,22}

At a constant ionic strength and a constant counterion concentration, either approach would lead to a constant value of β_q^* , however, where

$$\beta_q^* = [b_q]/[b_1]^q \quad (15)$$

because the charge effects are constant. Thus all the equations derived above from 2 onward are applicable to ionic micelles as long as the effect of the changing concentration of micelles themselves on the counterion concentration—as also composition since counterions may show specific effects^{22,23}—can be neglected. This assumption is likely to hold true for many systems studied in presence of added salt, with common counterions.

Numerous systems of this kind have been studied.^{24–26} When N_w is not extremely high, they show similar characteristic features in that the reduced turbidity curves in the typical Debye plot are linear and increase with concentration, *i.e.*, the apparent molecular weight, $M_{w(a)}$, decreases with concentration. This is ascribed to repulsive intermicellar interactions leading to positive second virial coefficients. Detailed theories of these virial interactions have been developed²⁵ and the theories give nearly quantitative predictions of the virial coefficients.²⁵ When corrected for these intermicellar interactions, $M_{w(a)}$ shows very little change with concentration in many systems at high salt concentrations. To take a typical example, sodium dodecyl sulfate in 0.1 M NaCl²⁵ shows about a 25% decrease in $M_{w(a)}$ as the micellar concentration $C - \text{cmc}$ changes by a factor of about 30. The theoretically calculated virial coefficient is higher than the experimental value but the difference is less than 20%.²⁵ Thus if there is a decrease in the molecular weight, M_w , it is likely to be about 5% or less over the whole concentration range. The use of equation 14 here leads to a value of less than 1.03 for the size-distribution index N_w/N_n . Similar calculations at a higher NaCl concentration (0.3 M) where the nonideality effects are even smaller show an N_w/N_n ratio even closer to 1.00, the value that characterizes a monodisperse system. It

seems that micelle size-distributions are indeed narrow in many cases and the assumption of monodispersity in many theoretical treatments is well justified.

At low salt concentrations the nonideality effects for ionic micelles are so large that even small uncertainties in the virial coefficients can hide appreciable changes in N_w , and the above method is difficult to apply. It should be stressed that interactions between micelles are likely to be repulsive in most cases so that the nonideality effects in general oppose the trend produced by changes in N_w which can either remain constant or increase with C . An apparently negative second virial coefficient is usually a good indication that the micellar system is polydisperse.

Polydispersity in Systems with Large Micelles

When N_w is very large, the micelles are asymmetric, and are probably rod-like¹⁷ with some flexibility.²⁷ The polydispersity of such micellar systems can be predicted on the basis of a simple model of self-association, assuming ideality, *i.e.*, negligible intermicellar interactions.

In nonionic micellar systems, the step-wise association reaction

$$b_{q-1} + b_1 = b_q \quad (16)$$

is governed by a step-wise association constant, K_q , given by

$$K_q = \frac{[b_q]}{[b_{q-1}][b_1]} \quad (17)$$

Our previously defined β_q then becomes

$$\beta_q = \prod_2^q K_q \quad (18)$$

For ionic micelles, at constant ionic strengths and constant counterion concentration and composition, K_q is still a constant as defined above but is labeled K_q^* , to emphasize the fact that it is not a true equilibrium constant.

If we consider the growth of micelles from small spherical ones to large spherical ones, it is clear that K_q or K_q^* will vary with q . In the case of ionic micelles, the free energy change associated with the introduction of a monomer into a micelle with $q - 1$ monomers is composed in part of a hydrophobic component, ΔG_{HC} , which is primarily responsible for the formation and growth of micelles, and an electrical component, ΔG_{EL} ,

(21) P. Mukerjee, *Advan. Colloid Interface Sci.*, **1**, 241 (1967).

(22) P. Mukerjee, K. J. Mysels, and P. Kapauan, *J. Phys. Chem.*, **71**, 4166 (1967).

(23) E. W. Anaeker and H. M. Ghose, *ibid.*, **67**, 1713 (1963).

(24) K. J. Mysels and L. H. Princen, *ibid.*, **63**, 1696 (1959).

(25) F. Huisman, *Proc. Kon. Ned. Akad. Wetensch., Ser. B*, **67**, 367, 376, 388, 407 (1964).

(26) M. F. Emerson and A. Holtzer, *J. Phys. Chem.*, **71**, 1898, 3320 (1967).

(27) D. Stigter, *ibid.*, **70**, 1323 (1966).

which opposes micelle formation.^{5,28} K_q^* can thus be expressed as

$$-RT \ln K_q^* = \Delta G_{\text{HC}} + \Delta G_{\text{EL}} \quad (19)$$

where R is the molar gas constant and T is the absolute temperature. For nonionic micelles, micelle formation and growth is opposed by the free energy change due to the self-interaction of the hydrophilic head groups of the monomers at the micelle surface.²¹ Thus

$$-RT \ln K_q = \Delta G_{\text{HC}} + \Delta G_{\text{HG}} \quad (20)$$

where ΔG_{HG} is the head group self-interaction contribution. For spherical (or spheroidal) micelles, ΔG_{EL} is known to vary with the radius r , and therefore q .²⁸ Since the addition of a monomer changes the surface density of the head groups and the volume available to each monomeric chain, and therefore its packing characteristics, ΔG_{HG} and ΔG_{HC} are also expected to depend upon q . For sufficiently large rod-like (or disk-like) micelles however, if the end effects can be neglected, and if the radius is assumed to remain constant, the quantities ΔG_{HG} and ΔG_{EL} become independent of q , because the surface group density and geometry do not change on the addition of a monomer, whereas ΔG_{HC} becomes independent of q because the local structure around a micellized monomer and the volume available to it do not change either. For very large micelles, therefore, K_q and K_q^* become independent of q .

The arguments above lead to a schematic diagram of the variation of $\log \beta_q$ or $\log \beta_q^*$ with q (Figure 1). $\log \beta_q$ here is a measure of the free energy of formation of a micelle from the monomers. At low q values, $\log \beta_q$ or $\log \beta_q^*$ is expected to increase with q nonlinearly, reflecting the fact that for small micelles the stability increases with size, and $\log K_q$ or $\log K_q^*$ increases with q . After a transition region close to the fully formed spherical micelle, the details of which are very important for small micelles, asymmetric micelles form. When these become large, at high q values, $\log \beta_q$ or $\log \beta_q^*$ increases linearly with q , with a constant slope, $\log K$.

When q values are very large, well outside of the transition region, the size distribution will be controlled mainly by the linear upper part of the $\log \beta_q$ or $\log \beta_q^*$ vs. q curve (Figure 1). If this linear curve is extended downwards to $q = 2$ to obtain $\log K_2'$ where K_2' is a hypothetical dimerization constant, then the stepwise association scheme, when q is very large, can be represented by a two-parameter model, where

$$K_2 = K_2', K_3 = K_4 = K_q = K \quad (21)$$

This model of stepwise association¹¹ has been previously investigated for the self-association of dyes.¹³ On summing the series for S , C , and G and putting $K[b_1] = X$, we obtain

$$\frac{S - [b_1]}{[b_1]} = \frac{K_2'}{K} \left(\frac{X}{1 - X} \right) \quad (22)$$

$$\frac{C - [b_1]}{[b_1]} = \frac{K_2'}{K} \left\{ \frac{X(2 - X)}{(1 - X)^2} \right\} \quad (23)$$

$$\frac{G - [b_1]}{[b_1]} = \frac{K_2'}{K} \left\{ \frac{2X}{(1 - X)^3} + \frac{X(2 - X)}{(1 - X)^2} \right\} \quad (24)$$

When $K_2' = K$, i.e., all stepwise association constants are the same, the equations above pertain to the well known case of the most probable distribution.

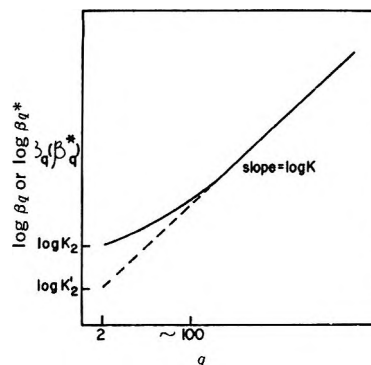


Figure 1. Schematic diagram of the variation of $\log \beta_q$ or $\log \beta_q^*$ with q .

Equations 22–24 can be used to obtain N_n and N_w for micelles in terms of K_2' , K , and $[b_1]$. When N_w is large, $X \approx 1$, so that X can be considered to be unity in all terms excepting $1 - X$. For such a case, we have

$$N_w = 2\sqrt{K/K_2'}\sqrt{(C - [b_1])/[b_1]} \quad (25)$$

If now $C \gg [b_1]$, $[b_1] = \text{cmc}$, and $[b_1]$ is assumed to be constant above the cmc, equation 26 is obtained.

$$N_w = 2\sqrt{K/K_2'}\sqrt{C/\text{cmc}} \quad (26)$$

The association model, therefore, predicts that for large micelles, N_w or M_w should be proportional to $\sqrt{C - [b_1]}$ or \sqrt{C} when $C \gg [b_1]$. The size distribution index N_w/N_n , under these assumptions, is calculated to be 2.0.

For testing the association model, it seems that few systems have been studied for which sufficient data are available at low enough concentrations to make intermicellar interactions in light-scattering studies negligible. Figures 2 and 3 show two suitable examples. The $\text{C}_{16}\text{H}_{33}(\text{EO})_7$ system, where EO stands for an oxyethylene group, was studied by Elworthy and Macfarlane¹⁵ whereas the $\text{C}_{16}\text{H}_{33}\text{N}(\text{CH}_3)_3\text{Br}$ in 0.178 M KBr was studied by Debye and Anacker.^{17,29} The molecular weights have been obtained from the turbidity data at each concentration and are shown in Figures 3 and 4 without any corrections and when corrected for dissymmetry and second virial coefficients. Both were calculated using the rigid-rod model, the parameters used being given in the legends of Figures 2 and 3.

(28) P. Mukerjee, *J. Phys. Chem.*, **73**, 2054 (1969).

(29) E. W. Anacker, private communication.

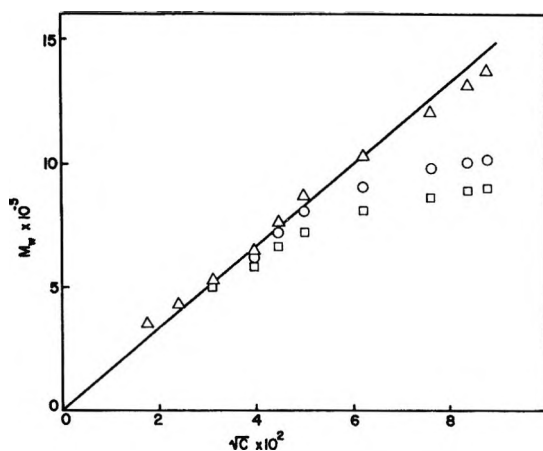


Figure 2. Variation in micellar molecular weights with \sqrt{C} . Molecular weights calculated from turbidity data for $C_{16}H_{33}(OCH_2CH_2)_7OH$ at 25° (C in g/ml). Key: \square , uncorrected molecular weights; \circ , corrected for dissymmetry; Δ , corrected for dissymmetry and second virial coefficients. Micelle dimensions calculated for the rigid cylinder model using a hydrocarbon core density of 0.775, a core radius of 20 Å, and 10 Å for the polyoxyethylene layer thickness.

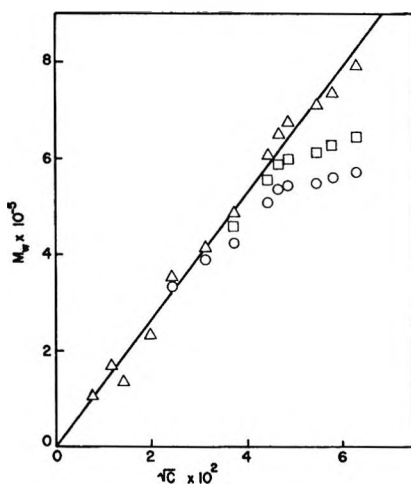


Figure 3. Variation in micellar molecular weights with \sqrt{C} . Molecular weights calculated from turbidity data for $C_{16}H_{33}N(CH_3)_3Br$ in 0.178 M KBr^{17,29} (C in g/ml). Key: \circ , uncorrected molecular weights; \square , corrected for dissymmetry; Δ , corrected for dissymmetry and second virial coefficients. Micelle dimensions calculated for the rigid cylinder model assuming density = 1.00, radius = 24 Å, and 8 Å for the effective thickness of the electrical double layer.

The corrections were applied assuming the micelles are monodisperse and using their weight average molecular weights. The corrections for the second virial coefficient were made using a reiterative procedure in which the apparent molecular weight at any concentration was first corrected for dissymmetry and then fitted to a true molecular weight and the corresponding second virial coefficient correction obtained by using Isihara's equations^{30,31} for rigid cylinders (see later). If the minor axis is the same, the use of Kihara's equation^{31,32} for prolate spherocylinders makes little difference.

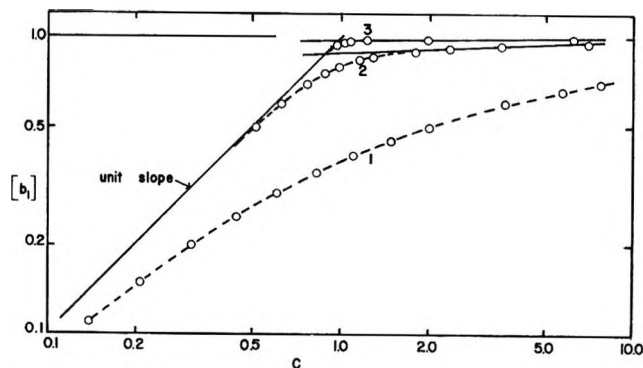


Figure 4. Variation in the monomer concentration, $[b_1]$, with the total concentration C from equation 23 assuming $K = 1$ and $K_2' = 1$ for curve 1, 10^{-2} for curve 2, and 10^{-4} for curve 3.

Prolate ellipsoids of revolution^{31,33} lead to substantially higher corrections. The uncertainties in the corrections are several. For example, the virial coefficient itself should reflect a higher moment of the size distribution than the weight average value,³⁴ and is thus underestimated. On the other hand, the rod-like micelles are probably flexible,²⁷ and thus the correction is over-estimated. However, the corrections are not very large even in the extreme cases, and Figures 2 and 3 show that the predicted linear variation of the molecular weight with \sqrt{C} holds for both systems, even at the lowest concentrations where the corrections are quite small. Thus, the simple self-association model developed for very large micelles fits both nonionic and ionic systems.

Independently of the self-association model discussed above, the fact that the molecular weight varies linearly with \sqrt{C} itself leads to an N_w/N_n value of 2.0 through the use of eq 14. The size distribution is thus wide.

It is interesting to note that whereas the most probable distribution model, where all K 's are the same, leads to a slow increase in the degree of association with concentration, with no sharp change that can be characterized as the cmc, the above distribution model, which can be described as a modified most probable distribution model and in which only the first constant K_2 is allowed to vary, can lead to quite sharp changes characteristic of micellar systems. This is illustrated in Figure 4 in which $\log [b_1]$ is plotted against $\log C$ for an assumed value of $K = 1$ and different values of K_2' , using eq 23. For a K_2'/K ratio of 10^{-4} , the curve already simulates a system with a sharp cmc. Figure 4 illustrates that only a mild cooperativity is needed to produce micellar aggregation, considering that the value of K itself for many nonionic systems is in the range of

(30) A. Isihara and T. Hayasida, *J. Phys. Soc., Jap.*, 6, 40 (1951); T. Kihara, *ibid.*, 8, 686 (1953).

(31) J. O. Hirschfelder, C. F. Curtiss, and R. B. Bird, "Molecular Theory of Gases and Liquids," Wiley, New York, N. Y., 1964.

(32) T. Kihara, *J. Phys. Soc., Jap.*, 6, 289 (1951).

(33) A. Isihara and T. Hayasida, *ibid.*, 6, 46 (1951).

(34) C. Tanford, "Physical Chemistry of Macromolecules," Wiley, New York, N. Y., 1961.

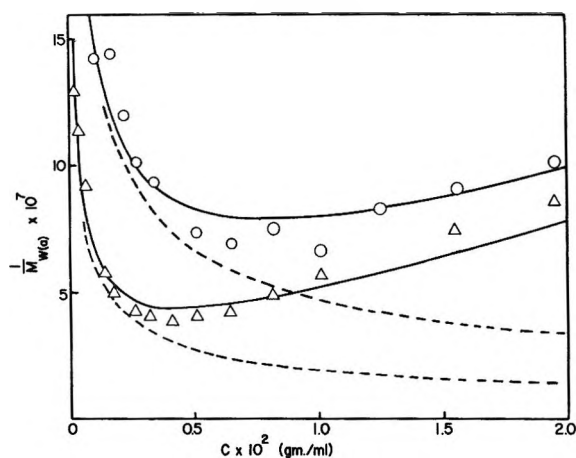


Figure 5. Simulated Debye plots using equation 26. $\text{cmc} = 5 \times 10^{-6}$ g/ml;¹⁶ $K/K_2' = 2.5 \times 10^3$ for upper curves, 1.44×10^4 for lower curves; dashed lines represent uncorrected molecular weights, full lines after correction for second virial coefficients using the rigid cylinder model for micelles, assuming density = 1.00, radius = 25.7 Å. Experimental data for $\text{C}_{14}\text{H}_{29}(\text{OCH}_2\text{CH}_2)_6\text{OH}$ estimated from Balmbra, *et al.*¹⁶ Key: O, 25°, Δ, 30°.

10^4 – 10^6 so that β_{100} , for example, is in the range of 10^{400} – 600 .

When molecular weights are high, and the micelles highly asymmetric, excluded volume interactions alone can be so strong as to completely obliterate the effect of increasing M_w with C . This is illustrated in Figure 5 in which some Debye plots have been simulated by using the self-association model described above (eq 26) to calculate M_w and eq 27 below to calculate the corrections for intermicellar interactions.

$$\frac{H(C - \text{cmc})}{(\tau - \tau_{\text{cmc}})} = \frac{1}{M_{w(s)}} = \frac{1 + 8\phi f}{M_w} \quad (27)$$

H here is the optical constant in light scattering, τ is the turbidity, and ϕ is the volume fraction of micelles. The concentration C and cmc are expressed in g/ml units. f is the shape factor ($f = 1$ for spheres) which was obtained by using Ishihara's equation for rigid cylinders^{30,31}

$$f = \frac{\pi r^2 + (\pi + 3)rl + l^2}{8rl} \quad (28)$$

where l is the length and r is the radius, and the parameters are given in the legend of Figure 5.

The difference between the upper and lower curves is produced by changing only one constant which is truly disposable, namely the ratio K/K_2' . The experimental

points were estimated from the Debye plot given for $\text{C}_{14}\text{H}_{29}(\text{EO})_6$ at 25° and 30°.¹⁶ In view of the numerous sources of uncertainty in the calculations and the use of the turbidity data, exact agreements are not to be expected. The deviations are qualitatively in line with over-estimates of the second virial coefficients on using the rigid-rod model and neglect of the higher order interaction terms. The important points to be made here are that the shapes of the experimental curves are reproduced well as also the positions of the minima. The nonideality corrections can clearly be important enough to change the shapes of the curves. The apparent molecular weights obtained from the minima of experimental curves of the kind shown in Figure 5 should not be used for comparative or theoretical purposes^{16,35} because the true M_w may be very different and may remain a strong function of the concentration.

Experimental molecular weight data of the kind shown in Figures 3 and 5 have sometimes been explained by invoking a reversible aggregation of the micelles themselves.^{15,36} This procedure does not seem to be justified.

For rigid cylinders of constant radius, the shape factor f becomes proportional to M_w when M_w is high. Equation 27, therefore, predicts a constant value of τ when $8\phi f \gg 1$. For $\text{C}_{14}\text{H}_{29}(\text{EO})_6$ micelles, the parameters of Figure 5 lead to a maximum τ value of 6.4×10^2 which appears to be of the right order of magnitude from the data presented by Balmbra, *et al.*¹⁶ Even an approximate agreement here may be fortuitous, particularly because third and higher virial interactions must be important for high concentrations. Qualitatively, however, the introduction of these higher order interaction terms in equation 27 would suggest that τ can go through a maximum. Such maxima have been experimentally observed.^{16,37} Thus, even this apparently unusual behavior is not incompatible with the model of multiple equilibria presented in which M_w continues to increase with C .

Acknowledgment. This work was supported in part by the P.H.S. Research Grant GM 10961-02 from the Division of General Medical Services, U. S. Public Health Service, administered by Karol J. Mysels at the University of Southern California.

(35) D. C. Poland and H. A. Scheraga, *J. Phys. Chem.*, **69**, 2431 (1965).

(36) J. M. Corkill, J. F. Goodman, and T. Walker, *Trans. Faraday Soc.*, **63**, 759 (1967).

(37) J. M. Corkill and K. W. Herrmann, *J. Phys. Chem.*, **67**, 934 (1963).

An Infrared Study of Surface Properties of α -Chromia. IV. Pyridine and Heavy Water Adsorption on Oxygen-Covered Surface

by A. Zecchina, E. Guglielminotti, L. Cerruti, and S. Coluccia

Istituto di Chimica Fisica dell'Università di Torino, Turin, Italy (Received July 26, 1971)

Publication costs assisted by Consiglio Nazionale delle Ricerche (Rome)

It is observed that pyridine (py) is physically adsorbed onto α -chromia surface hydroxyls *via* hydrogen bonds and is strongly chemisorbed onto oxygen-free Cr^{3+} surface sites. py and water also chemisorb on an oxygen-covered surface revealing residual cationic unsaturation. py and water adsorption eliminate $\text{Cr}=\text{O}$ bands typical of sites which still have one coordinative unsaturation. The $\text{Cr}=\text{O}$ stretching frequency as well as the bond order are lowered by adsorption.

Introduction

The nature of active sites on α - Cr_2O_3 surface has been investigated in this laboratory by adsorption of H_2O , CO , CO_2 , and O_2 .¹⁻³ Infrared study of oxygen adsorption at room temperature led to the following main conclusions: (1) Oxygen chemisorbs dissociatively onto Cr^{3+} (cus) ions to form $\text{Cr}=\text{O}$ surface groups. (2) The chromium-oxygen stretching frequency varies with Cr^{3+} coordination number (4 or 5) and with the nature of the ligands attached to it. (3) Cr^{3+} (cus) ions with two vacancies (coordination number 4) chemisorb only one oxygen atom; as a consequence oxygen still leaves cationic vacancies on the surface. In order to investigate the presence of residual surface cationic unsaturations and so confirm previous conclusions, pyridine (py) and water adsorption on an oxygen-covered surface have been studied. The choice of py as a test molecule for residual cationic unsaturation is due to its great ability to form adducts with metal ions. Water is also useful, because it chemisorbs both dissociatively onto chromium-oxygen ion pairs and in a nondissociative form onto isolated and unsaturated cations.¹ In the first paper of this series water chemisorption on an oxygen-free surface was investigated, so that it is possible to compare the two experiments. No infrared data are available for py chemisorption onto oxygen-free α - Cr_2O_3 and this point has also been investigated here.

py is normally used to characterize spectroscopically the Lewis-Brønsted acidity of electron-acceptor molecules of the MX_n type and of surface acidic sites as well.⁴⁻¹⁰ Lewis acidity and surface hydroxyl acidity are usually checked by the shifts of two nuclear frequencies: the 8a (the notation used by Wilmshurst and Bernstein¹¹ and by many others is followed here) at 1583 cm^{-1} and the 19b at 1440 cm^{-1} . Brønsted sites, if present, are deduced from a band at 1540 cm^{-1} that is characteristic of pyridinium ion.⁶

In this work special care has been devoted to the

choice of "analytical" bands of adsorbed py. Due to the wide spectral range in which α - Cr_2O_3 is transparent (4000 – 800 cm^{-1}) we had several py modes from which to choose the one most sensitive to donor-acceptor bonds and hydrogen bonds. According to Filimonov and Bystrov's¹² viewpoint, modes of A_1 symmetry species should be expected to be more affected by the N–M bond formation. Shifts of skeletal modes are also produced when py *N*-oxide is formed.¹³ The breathing mode 1 (992 cm^{-1}) is very sensitive to coordination bond formation; it is shifted upward to 1030 cm^{-1} in strong donor-acceptor complexes like $\text{py} \rightarrow \text{BCl}_3$.⁵ Other skeletal modes of species A_1 might be used as well, the most sensitive being: mode 12, which is at 1033 cm^{-1} in pure py and shifts to 1044 cm^{-1} in py *N*-oxide and to 1050 cm^{-1} in py complexes; mode 8a, which goes from 1588 cm^{-1} to 1602 in py *N*-oxide and 1630 cm^{-1} in complexes of the $\text{py} \rightarrow \text{BX}_3$ type. The use of the breathing mode as the test-band, however, is preferable to mode 8a, in that the latter could give rise to a Fermi resonance effect with a com-

(1) A. Zecchina, S. Coluccia, E. Guglielminotti, and G. Ghiotti, *J. Phys. Chem.*, **75**, 2774 (1971).

(2) A. Zecchina, S. Coluccia, L. Cerruti, and E. Borello, *ibid.*, **75**, 2783 (1971).

(3) A. Zecchina, S. Coluccia, E. Guglielminotti, and G. Ghiotti, *ibid.*, **75**, 2790 (1971).

(4) A. Terenin, W. Filimonov, and D. Bystrov, *Z. Elektrochem.*, **68**, 180 (1958).

(5) N. N. Greenwood and K. Wade, *J. Chem. Soc.*, 1130 (1960).

(6) N. S. Gill, R. H. Nuttali, D. E. Scaife, and D. W. A. Sharp, *J. Inorg. Nucl. Chem.*, **18**, 79 (1961).

(7) N. S. Gill and R. S. Nyholm, *ibid.*, **18**, 88 (1961).

(8) G. S. Rao, *Z. Anorg. Allgem. Chem.*, **304**, 176 (1960).

(9) J. Yarwood, *Trans. Faraday Soc.*, **65**, 934 (1969).

(10) E. P. Parry, *J. Catal.*, **2**, 371 (1963).

(11) J. K. Wilmshurst and H. J. Bernstein, *Can. J. Chem.*, **35**, 1183 (1957).

(12) V. N. Filimonov and D. S. Bystrov, *Opt. Spectrosk.*, **12**, 31 (1962).

(13) P. Mirone, *Atti Accad. Naz. Lincei, Cl. Sci. Fis. Mat. Nat. Rend.*, **35**, 530 (1963).

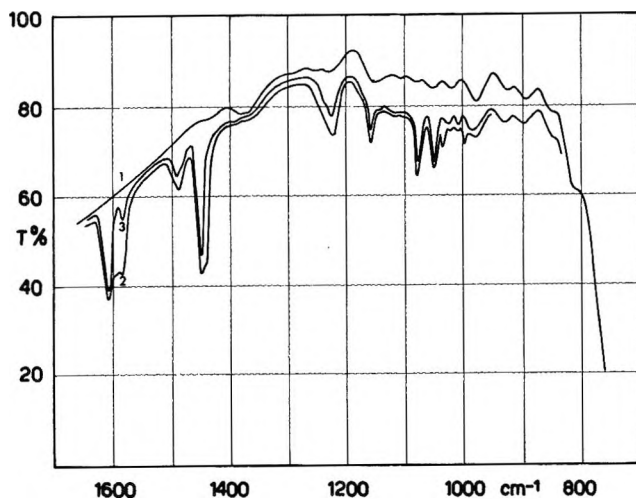


Figure 1. Infrared spectra of py adsorbed onto α -chromia oxygen-free surface (% transmission vs. wavelength in cm^{-1}): curve 1, background; curve 2, after exposure to 15 Torr of py at room temperature (R.T.); curve 3, after 1 hr. evacuation at R.T.

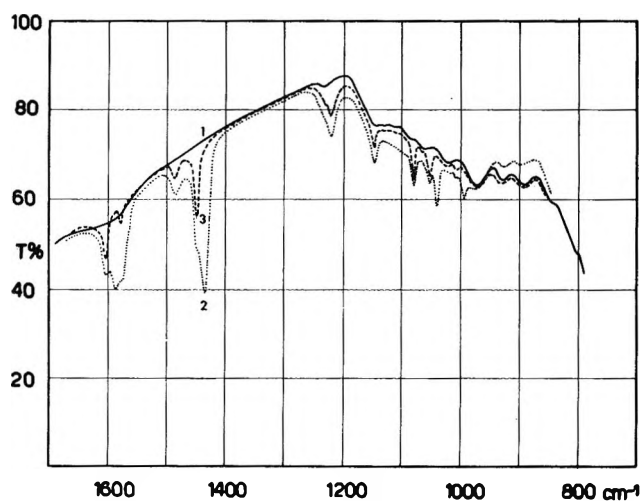


Figure 2. Infrared spectra of py adsorbed into hydrated α -chromia (% transmission vs. wavelength in cm^{-1}): curve 1, background of oxygen-free α -chromia contacted with water vapor ($p = 8$ Torr) 2 hr at 400° and then evacuated for 1 hr at R.T.; curve 2, after exposure to 15 Torr of py at R.T.; curve 3, after 1 hr evacuation at R.T.

combination band at 1597 cm^{-1} ($1 + 6a$), which is of species A_1 and is at 1602 cm^{-1} in the liquid py spectrum. Since the combination band also can be shifted upward due to the increased frequency of both 1 and $6a$ modes upon complex formation, we conclude that the behavior of mode 1 is by far the most representative of the formation of donor-acceptor bonds. Dissociative adsorption of water or heavy water (used instead of water because the latter would give an OH bending mode at $1100\text{--}800 \text{ cm}^{-1}$ where the Cr=O stretching mode is also present) should give rise to bands of surface OH and OD groups, whose stretching frequencies are expected to be sensitive to the oxidation status of

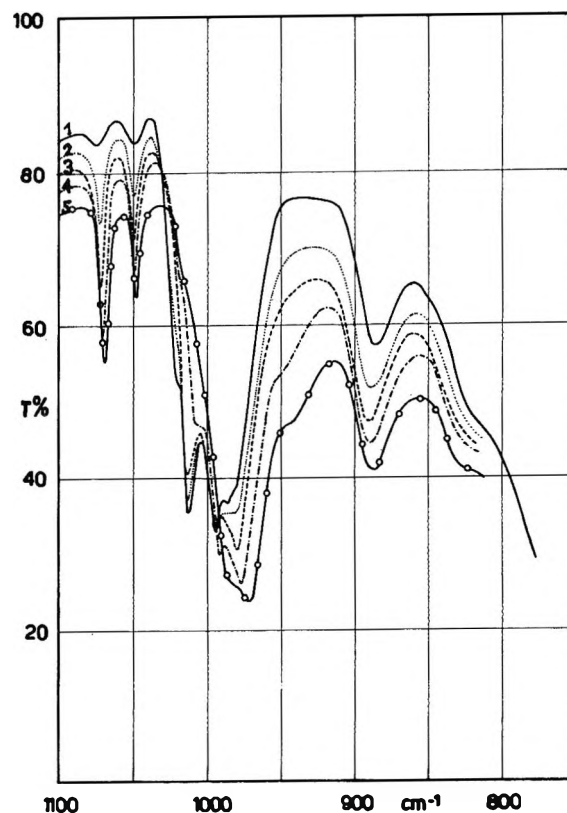


Figure 3. Infrared spectra of py adsorbed into oxygen covered α -chromia (% transmission vs. wavelength in cm^{-1}): curve 1, background of oxygen-free α -chromia contacted with 40 Torr of oxygen at R.T. and then evacuated at R.T. to a final pressure of 10^{-4} Torr; curves 2-4, increasing py coverages; curve 5, py saturation.

the adsorbing chromium ions. In fact OH or OD groups attached to Cr^{3+} ions should be basic or amphoteric while OH or OD groups attached to higher valence ions (Cr^{5+} or Cr^{6+}) should be acidic in nature. On the other hand, H_2O or D_2O adsorption might influence the stretching frequencies of Cr=O surface groups which are present on an oxidized surface.

Experimental Section

All details of the oxygen-free catalyst preparation and characterization have been described elsewhere.¹ Oxygen-covered catalysts are obtained from oxygen free ones by room temperature reaction with oxygen ($p = 40$ Torr). All of our spectra were run on a Beckman ir 12 spectrophotometer. The spectral conditions were those described in the previous papers of this series. Reagent grade pyridine from Carlo Erba—Milano was used after a simple vacuum distillation. Heavy water was ICN reagent grade with 99.75% deuterium.

Curve 2 of Figure 1 shows the ir spectrum of 15 Torr of py in equilibrium at room temperature with an oxygen-free catalyst. A 1 hr evacuation at room tem-

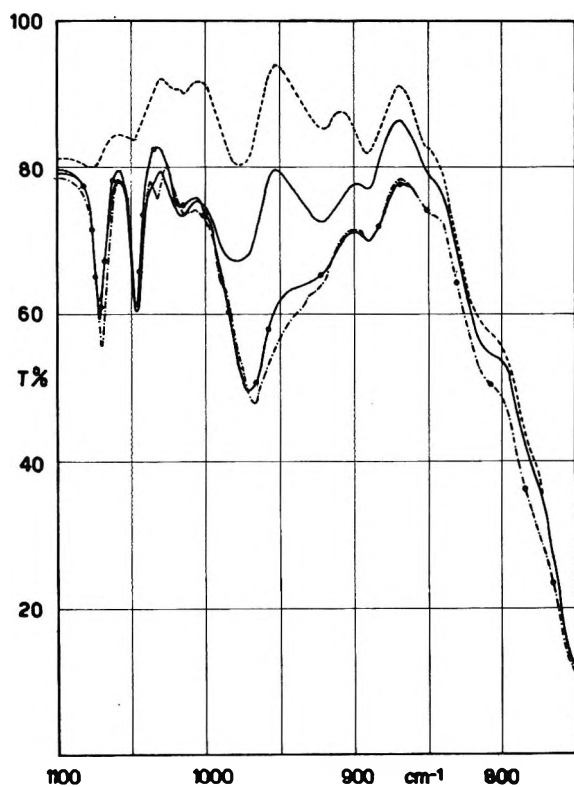


Figure 4. Infrared spectra of O_2 adsorbed onto py covered α -chromia (% transmission vs. wavelength in cm^{-1}): ---, background of α -chromia oxygen-free surface; —, after exposure to 15 Torr of py and evacuation for 1 hr at R.T.; - · - ·, after exposure to 40 Torr of oxygen; ●—, after 1 hr evacuation at R.T.

perature to a final pressure of 10^{-4} to 10^{-5} Torr leads to the situation illustrated by curve 3 of Figure 1.

Figure 2 refers to a hydrated α -chromia sample. In particular, curve 1 is the background spectrum of the oxygen-free catalyst exposed for 2 hr at 400° to water vapor and then pumped down at room temperature for 1 hr. Curves 3 of Figure 1 and 3 of Figure 2 are the spectra of irreversibly adsorbed py that cannot be evacuated at temperatures as high as 400° . A particularly strong chemisorption must be involved in order to account for the high poisoning activity of py on several oxides.

Figure 3 shows the adsorption of py onto a sample which had been allowed to preadsorb oxygen at room temperature. The full-line curve is the spectrum of O_2 chemisorbed onto α - Cr_2O_3 , while other curves refer to increasing py coverages. It is observed that an oxygen-covered catalyst is still capable of adsorbing py and that the spectrum of the chemisorbed oxygen is fairly sensitive to py coverage.

Figure 4 refers to an experiment opposite to the previous: py is allowed to adsorb onto an oxygen-free sample at room temperature and then pumped down to 10^{-4} to 10^{-5} Torr (line spectrum). Oxygen (40

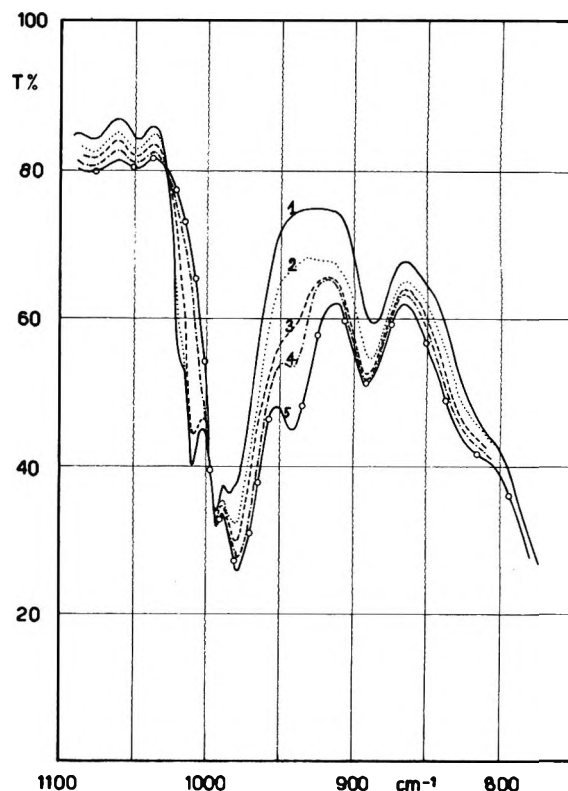


Figure 5. Infrared spectra of D_2O adsorbed onto oxygen covered α -chromia (% transmission vs. wavelength in cm^{-1}): curve 1, background of oxygen-free α -chromia contacted with 40 Torr of oxygen at R.T. and then evacuated at R.T. to a final pressure of 10^{-4} Torr; curves 2-4, increasing D_2O coverages; curve 5, heavy water saturation.

Torr) is then admitted to the cell and the spectrum recorded. Finally, the gaseous phase is evacuated at room temperature to a final pressure of 10^{-5} Torr.

In Figure 5 the effect of heavy water adsorption on the spectrum of oxygen adsorbed at room temperature is reported. The various curves refer to increasing heavy water coverages. The final spectrum was obtained at an equilibrium pressure of 15 Torr.

Figure 6 shows the spectral modifications in the OD stretching region due to exposure of an oxygen-covered sample to heavy water. Only high coverages are considered, for at low coverages no spectral changes are produced and the intensities are very weak. Equilibrium D_2O pressures were 0.15 and 15 Torr, respectively (curves 1 and 2). In the same figure, spectra of D_2O adsorbed on an oxygen-free surface at the same equilibrium pressures are also reported (curves 1' and 2', respectively).

After D_2O saturation, the oxygen-covered sample was pumped down at various temperatures increasing from 25° , and the spectra are shown in Figure 7. Oxygen bands are easily removed, and at 400° they are completely absent. This is quite surprising, for on a well dehydrated sample (see part II²) $Cr=O$ groups are only slowly removed upon evacuation and are still present at 400° .

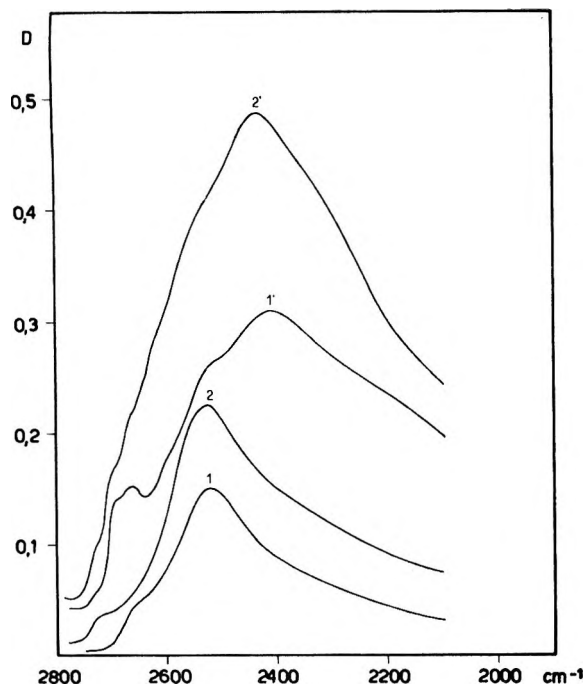


Figure 6. Infrared spectra of OD stretching range of oxygen-free and covered α -chromia surface (optical density vs. wavelength in cm^{-1}): curve 1, after exposure to 0.15 Torr of D_2O at R.T. on an oxygen covered surface; curve 2, after exposure to 15 Torr of D_2O at R.T. on an oxygen covered surface; curve 1', after exposure to 0.15 Torr of D_2O at R.T. on an oxygen-free surface; curve 2', after exposure to 15 Torr of D_2O at R.T. on an oxygen-free surface.

Discussion

(1) *Pyridine Adsorption onto Oxygen-Free α - Cr_2O_3 .* By comparison of curves 2 and 3 of Figures 1 and 2, the spectrum of physically adsorbed py (*i.e.*, removable upon room temperature evacuation) on poorly and highly hydrated samples can be derived. It can be observed that: (a) the bands due to physically adsorbed py are at the same frequencies in both cases, (b) such frequencies do not appreciably differ from those of liquid py (see Table I), (c) equilibrium pressures and other experimental conditions being the same, physically adsorbed py bands are much stronger on the highly hydrated sample. It is therefore concluded that the physical adsorption occurs mainly on surface hydroxyls, which would be engaged in strong hydrogen bonding with the nitrogen. Spectral modification in the OH-stretching and -bending regions (3700 – 3000 and 1100 – 800 cm^{-1} , respectively) seems to confirm the above conclusions. Physical adsorption strongly lowers the OH-stretching frequency (the spectrum is not reported for the sake of brevity) while the OH-bending mode at 800 – 950 cm^{-1} is weakened in intensity and shifted upward to 1000 – 1100 cm^{-1} (see Figure 2) as expected on formation of strong hydrogen bonds. The surface hydroxyl-py interaction does not lead to the formation of observable amounts of pyridinium ions, for no absorption is produced at ap-

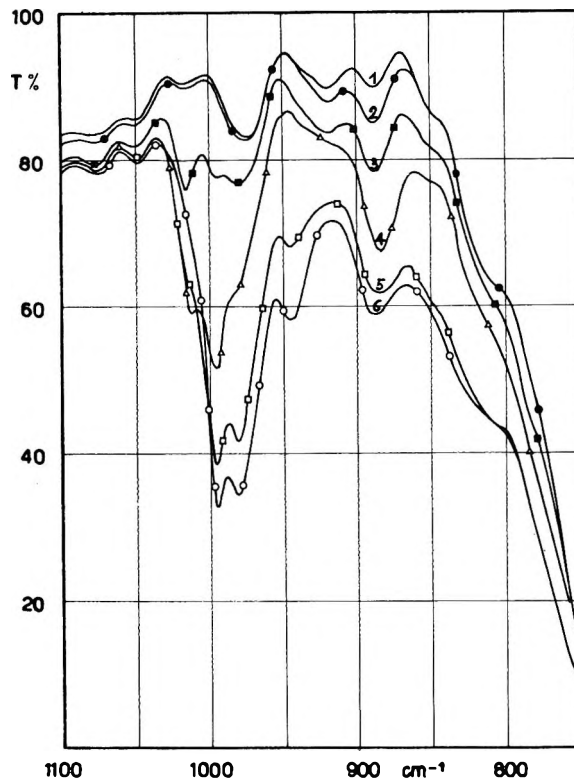


Figure 7. Infrared spectra of oxygen covered and hydrated α -chromia (% transmission vs. wavelength in cm^{-1}): curve 1, background of oxygen-free surface; curve 6, oxygen covered surface contacted with D_2O (15 Torr) at R.T. and then evacuated for 2 hr at R.T.; curves 5–2, after outgassing for 2 hr at 100, 200, 300, and 400°.

Table I: Spectrum of Pyridine in the Phase, cm^{-1}

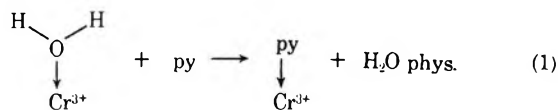
Band no.	Liquid	Physisorbed	Chemisorbed
11	992	922	1010–1020
12	1033	1033	1046
18a	1071	1071	1073
15	1147	1147	1149
9a, 3	1219	{ 1221 1235–1240	{ 1223 1235–1240
19b	1440	1442	1450
19a	1485	1486	1488
8b	1573 sh	1577	1577
8a	{ 1585 1602	1594	1610

proximately 1540 cm^{-1} , where the characteristic N–H⁺ bending mode is commonly observed.⁶ It is therefore concluded that no appreciable amounts of Brønsted sites are available on α - Cr_2O_3 . Curves 3 of Figure 1 and 2 are for irreversibly chemisorbed py and indicate that the frequencies are the same in the two cases but quite different from those of the liquid or physically adsorbed species (see Table I). We think that the observed spectrum could be explained in terms of the formation of a strong σ bond of the donor-acceptor

type between py molecules and surface Cr^{3+} ions which are coordinatively unsaturated. Further observations support our assignment: (a) High resistance to desorption suggests that the py surface interaction must be a strong one in agreement with the "hard" character of both py and Cr^{3+} (cus) ions.¹⁴ (b) No carbon monoxide is chemisorbed onto an α - Cr_2O_3 sample which preadsorbed py: active sites must therefore be the same in the two cases. (c) The ir spectrum of chemisorbed py is very similar to that of complexes involving a dative bond of the $\text{py}\rightarrow\text{M}$ type. In particular, the presence of a shoulder at 1240 cm^{-1} , next to the 1220 cm^{-1} band, has been observed by Gill, *et al.*,⁶ in 24 complexes of the general formula $\text{M}(\text{py})_2\text{X}_2$, and it was justified as due to the formation of the $\text{py}\rightarrow\text{M}$ bond. Also the shifts of a few nuclear bands are typical of the formation of a medium-strong $\text{py}\rightarrow\text{Cr}$ bond. In detail, mode 1 shifts to $\sim 1015\text{ cm}^{-1}$, mode 12 to 1046 cm^{-1} , mode 19b to 1449 cm^{-1} , and mode 8a to 1610 cm^{-1} . According to Filimonov's hypothesis¹² a shift of mode 1 from 992 to 1010 – 1020 cm^{-1} clearly indicates the formation of a medium-strong dative bond of the type formed with SnCl_4 and AlCl_3 . (d) The amount of chemisorbed py is higher on less hydrated samples and this is consistent with the previously proposed theory¹⁴ that it is the dehydration process which creates Cr^{3+} (cus) ions on the surface. It has previously been observed^{1,2} that on the (001) face, five types of Cr^{3+} ions are present which differ in the coordination number (4 or 5) and in the nature of the ligands. They are five different adsorbing sites with different Lewis acid character and thus capable of chemisorbing py. On the other hand, no different bands are observed in the ir spectrum of the coordinate py: this might be ascribed either to slight differences in acidity among the various sites or to a nonselectivity of the py itself. A similar conclusion was drawn by Gill, *et al.*,⁶ on studying py complexes with metals of coordination number 4 and 6. In fact they remarked that "there are few systematic changes in the positions of the bands with changes in mass, electronegativity or valency of the central atom or with changes in the other ligands." As a consequence we conclude that py does not distinguish among different unsaturated surface cations.

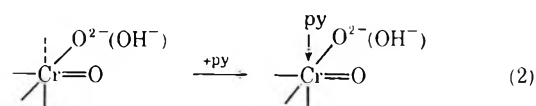
Although the above observations quite clearly indicate that a σ -bond is formed between py molecules and Cr^{3+} (cus) ions, there are a few points in the experiment of Figure 2 that seem to deserve further discussion. In fact it is quite surprising that a thoroughly hydrated sample (*i.e.*, heated with H_2O at 400° and then evacuated at R.T.) still has an appreciable adsorption capacity towards py while no capacity whatever is exhibited towards CO .¹ Spectrum 1 of Figure 2 shows a weak and broad band at $\sim 1590\text{ cm}^{-1}$ that has been assigned to water molecules coordinated to Cr^{3+} (cus) ions.¹ Such a band is no longer detect-

able in spectrum 3 suggesting that coordinated water has been removed, possibly through the exchange mechanism



The above mechanism is consistent with the "harder" nature of py with respect to water; such an exchange process could never occur with CO , which is a "very soft" base. We already observed in a previous paper¹ the presence of coordinated water on a chromia surface that had been rehydrated at 400° , but we could not make any quantitative consideration owing to the weakness of the 1590-cm^{-1} mode. The removal of such coordinated water through the above mechanism, causing the characteristic absorption of coordinated py to appear in the spectrum, indicates that the amounts involved are not negligible.

(2) *Pyridine Adsorption onto Oxygen Covered Surfaces.* Room temperature adsorption of O_2 onto α - Cr_2O_3 has been discussed previously.² Figure 3, full line curve, shows the ir spectrum due to chemisorbed oxygen. Two bands at 1024 and 1016 cm^{-1} have been assigned to the stretching of $\text{Cr}=\text{O}$ groups in which the metal has coordination number five and thus still has one coordinative vacancy. Three bands at 995 – 980 cm^{-1} have been assigned to $\text{Cr}=\text{O}$ groups in which the metal ion has the full coordination number. The results reported in Figure 3 fit the above assignment. The adsorption of py gradually eliminates the two bands at 1024 – 1016 cm^{-1} and produces two new absorptions at lower wave number (~ 980 , $\sim 940\text{ cm}^{-1}$). The following mechanism might account for the observed modifications



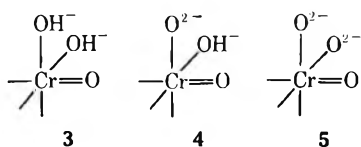
Coordinatively unsaturated $\text{Cr}=\text{O}$ groups would be transformed into saturated ones upon py uptake, thus explaining the disappearance of the two bands at 1024 – 1016 cm^{-1} . The complex absorption produced at lower wave number (980 – 940 cm^{-1}) could be assigned to the new structures (1 and 2) produced by mechanism (2).



The shift to lower frequencies may be easily explained by taking into account the sensitivity of the chromium-oxygen stretching frequency both to the metal coordi-

(14) R. L. Burwell, Jr., G. L. Haller, K. C. Taylor, and J. F. Read, *Advan. Catal. Relat. Subj.*, **19**, 62 (1969).

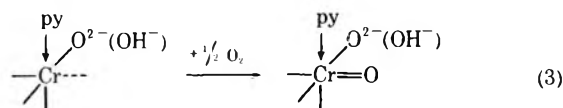
nation number and to the nature of the ligands attached to it. Similar behavior has also been observed in the VO^{2+} group in complexes where electron-donor groups are present.¹⁵ In fact the $\text{M}-\text{O}$ covalent bond has a strong $p\pi \rightarrow d\pi$ back donation from the oxygen to the metal that is sensitive to the presence of electron donors. The formation of py adducts changes the coordination number and increases the electron density of the metal d orbitals and thus decreases the $p\pi \rightarrow d\pi$ back donation. The bond index is expected to decrease, as does the $\text{M}=\text{O}$ stretching frequency. The surface oxo-complexes **1** and **2** differ from the octahedral complexes **3-5** already present on the surface after oxygen adsorption (see part II of this series) only in the presence of a new ligand.



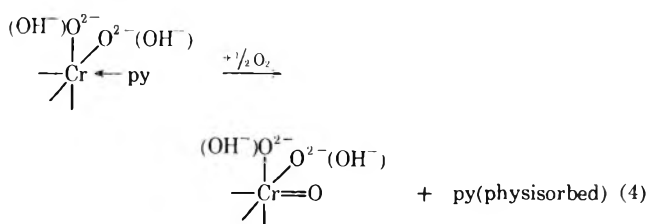
The stretching frequency of $\text{Cr}=\text{O}$ groups in structures **1** and **2** might be either higher or lower than in structures **3-5**, according to the electron-donor ability of py compared to that of OH^- and O^{2-} . It is difficult to decide *a priori*, based only on what is known of similar complexes, because their number is small. In addition, the properties of the O^{2-} ligand are not well known and, finally, it is not clear whether surface OH^- and O^{2-} groups are bonded through covalent, ionic, or mixed bonds. The experimental results reported in Figure 3 show that py adsorption produces two bands at ~ 980 and $\sim 940 \text{ cm}^{-1}$, which should correspond to the newly formed structures **1** and **2**. Nevertheless from our data a more detailed assignment cannot be deduced and, as a consequence, a comparison between the electron-donor ability of the three surface ligands (py, OH^- , and O^{2-} groups) cannot be made. As Figure 3 shows, when py coverages are high the frequencies of all the bands due to adsorbed oxygen are shifted to lower frequencies. This fact is quite normal, as a polar environment commonly lowers the stretching frequency of surface groups. Electronic colligative properties of the solid might be involved as well. In fact the adsorption of a strong electron-donor group directly affects the electronic properties of the adsorbing site but can also be expected to have a minor effect on the properties of all neighboring sites as well. The $\text{Cr}=\text{O}$ bond of all the neighboring surface complexes will thus be weakened by py adsorption.

The spectrum of py adsorbed on an oxidized sample does not really differ from that obtained on an oxygen-free sample. All nuclear bands are nearly at the same frequencies in the two cases and are only slightly shifted with different coverages. Appreciable differences are only observed as regards the relative intensities of some peaks.

(3) *Oxygen Adsorption onto a Sample Pretreated with Pyridine.* The experiment of Figure 4 is in some ways the opposite of that discussed in section 2. py adsorption onto a bare surface does not entirely hinder the surface activity toward oxygen, meaning that not all of the cationic surface vacancies are saturated. We might suppose that chromium sites with one coordinative vacancy are readily saturated by py and chromium sites with two vacancies adsorb only one py molecule, because a cationic site is quite unlikely to form two strong cis acceptive bonds. On the other hand, only few unstable complexes in which two py molecules are coordinated in a cis configuration to the same metal ion are reported in the literature.¹⁶ According to this scheme we might expect py covered surfaces still to have cationic vacancies available for oxygen chemisorption, through the mechanism



The overall result of mechanism 3 is the same described by mechanism 2 with production of structures **1** and **2**. The presence of two bands at ~ 980 and $\sim 940 \text{ cm}^{-1}$ demonstrates that the previous hypothesis is correct. Nevertheless the proposed mechanism seems to be an oversimplification. It accounts for the appearance of the two bands at $980-940 \text{ cm}^{-1}$ due to chemisorption of oxygen onto ions that had already adsorbed py and still had a coordinative vacancy. But it does not explain the appearance of a band at 1033 cm^{-1} upon oxygen chemisorption, which is typical of physically adsorbed py (see Figure 4 and Table I). This fact suggests that other processes might be taking place as well. Among them seems to be likely a ligand displacement reaction of the type



In fact this reaction explains well the production of physically adsorbed py from chemisorbed py.

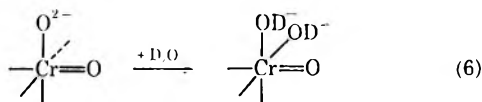
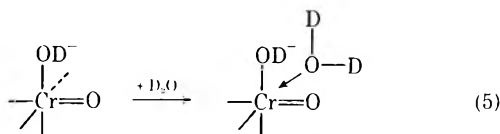
(4) *Heavy Water Adsorption onto Oxygen-Covered Surface.* The experiment of Figure 5 shows that water is still adsorbed onto a sample which preadsorbed oxygen and that the spectrum of adsorbed oxygen is greatly influenced. As in the case of py adsorption, the bands at 1024 and 1016 cm^{-1} are completely eliminated, thus confirming that these bands involve $\text{Cr}=\text{O}$ groups in

(15) J. Selbin, L. M. Holmes, Jr., and S. P. McGlynn, *J. Inorg. Nucl. Chem.*, **25**, 1359 (1963).

(16) C. S. Kraihanzel and F. A. Cotton, *Inorg. Chem.*, **2**, 533 (1963).

which the chromium ion still has one coordinative vacancy.

Two adsorption mechanisms may be proposed



The first one is completely similar to mechanism 2 and involves a coordinative chemisorption of water; in the second one a molecule of water is dissociated onto a Cr^{3+} (cus) O^{2-} (cus) pair. The first resulting structure is analogous to the 2 structure and so we expect it to have a similar spectral behavior. The second structure, involving a CrO group in octahedral coordination with surface OD^- ligands, is one of the three octahedral structures formed upon oxygen adsorption on a partially dehydrated surface (see part II²). Therefore we assign the band at $\sim 940 \text{ cm}^{-1}$ to the product structure of mechanism 5 and the increased absorption at ~ 970 – 980 cm^{-1} to the formation of the structure arising from mechanism 6. It is surprising that in the first structure coordinated water has practically the same effect that py has in decreasing the $\text{Cr}=\text{O}$ stretching frequency, when it is well-known that py is a harder base than water. We think that the large frequency shift induced by water adsorption might be explained by the formation of hydrogen bonds between the OD groups of coordinated water and the $\text{Cr}=\text{O}$ groups on the same sites. Such a hydrogen bond would contribute to the lowering of the $\text{Cr}=\text{O}$ stretching frequency and the overall shift will be larger than is expected. The above considerations definitely indicate that the band at $\sim 940 \text{ cm}^{-1}$ is due to the product of mechanism 5. Nevertheless, the reaction is, as usual, an oversimplification in that it completely disregards the fact that any new ligand enters, at one time, the coordination sphere of more than one unsaturated metal ion. On the other hand, what mainly matters here is that two bands disappear while two more are produced at lower frequencies.

As Figure 6 shows, the amount of heavy water chemi-

sorbed onto an oxygen-covered (curve 1) surface probably is smaller than that adsorbed on the oxygen-free (curve 1') surface at the same equilibrium pressures. The spectrum of OD groups in the 2800 – 2000-cm^{-1} range widely differs in the two cases. In the first one the bands at $\sim 2700 \text{ cm}^{-1}$, characteristic of free OD groups on reduced chromia, are partially absent. This fact might be due to the different acidity of these newly formed OD groups and to the formation of hydrogen bonds favored by the high oxygen coverages. In order to confirm the occurrence of mechanism 5 or 6 we studied the desorption of adsorbed water at increasing temperatures. In fact coordinated water should be desorbed first and, as a consequence, the band at $\sim 940 \text{ cm}^{-1}$ should disappear and bands at 1016 – 1024 cm^{-1} appear again. Figure 7 shows that the band at $\sim 940 \text{ cm}^{-1}$ is completely eliminated at 200° while a band at 1016 – 1024 cm^{-1} is produced. Another surprising result is also obtained: all of the bands due to adsorbed oxygen decrease with increasing desorption temperature and at 400° are completely eliminated. We conclude that oxygen adsorbed on a hydrated sample is less resistant to desorption than oxygen on a well dehydrated one. In paper I¹ we observed that the degree of dehydration of an $\alpha\text{-Cr}_2\text{O}_3$ surface is influenced by the presence of adsorbed oxygen and we think that the two phenomena are not independent, although any explanation would first require more experiments and probably different investigational techniques.

Conclusion

From the above discussion it follows that: (1) py is physically adsorbed onto α -chromia by means of hydrogen bonds to surface hydroxyls. (2) py is adsorbed onto chromium ions through a medium-strong acceptor-donor bond, whose spectral behavior is well characterized. (3) py chemisorbs onto a fully hydrated sample by substitution of coordinated molecular water. (4) py and water adsorption onto an oxygen-covered surface reveal the presence of a residual surface cationic unsaturation. (5) py and water adsorption onto an oxygen-covered surface eliminate the $\text{Cr}=\text{O}$ bands at 1024 – 1016 cm^{-1} confirming that they involve chromium ions with still one coordinative unsaturation.

Acknowledgment. This research has been supported by the Consiglio Nazionale delle Ricerche.

Proton Magnetic Resonance Studies of the Structure of Water in Dowex 50W

by Darryl G. Howery,* Lawrence Shore, and Barry H. Kohn

Department of Chemistry, Brooklyn College of the City University of New York, Brooklyn, New York 11210
(Received July 28, 1971)

Publication costs borne completely by The Journal of Physical Chemistry

Proton magnetic resonance spectra of packed beds of Dowex AG 50W (X4, X8, and X12) in 18 ionic forms are used to determine the effects of counterions on the chemical shifts of the internal water. The counterions studied, with average values of the internal water chemical shifts per unit counterion concentration (Hz/g equiv/kg), are H^+ , -19.5; Li^+ , -1; Na^+ , 1.4; K^+ , 1.9; Rb^+ , 1.3; Ag^+ , -3; NH_4^+ , 0 (assumed); NMe_4^+ , -1; NEt_4^+ , -1; NBu_4^+ , 1.3; $NPhMe_3^+$, 0; Mg^{2+} , -4.5; Ca^{2+} , -2; Sr^{2+} , -1; Ba^{2+} , -1; Zn^{2+} , -5.9; Cd^{2+} , -5.2; and La^{3+} , -4.4. In most cases the chemical shift/g equiv/kg is nearly independent of crosslinkage. The agreement between chemical shifts/g equiv/kg for cations in aqueous solution referred to $NH_4^+(aq)$ and chemical shifts/g equiv/kg for counterions referred to NH_4^+ -form resin is sufficient to substantiate the concentrated-electrolyte model of ion-exchange resins. The widths at half height for both the internal and external water peaks increase with an increase in the difference between the volume magnetic susceptibility of water and the resin bead. A study of Dowex 50W (X4, X8, and X12) equilibrated with solutions containing H^+ and Na^+ indicates that the effects of the counterions on the chemical shift of the internal water are additive.

Introduction

The nature of water within ion-exchange resins can be fruitfully studied using nuclear magnetic resonance.¹⁻¹⁷ Studies of the dependence of internal water proton chemical shifts on counterion concentration^{1,2,4,7,8,10,15} and on temperature^{7,8,15} substantiate the concentrated-electrolyte model of ion exchangers. We present here further studies of the effect of counterion type and concentration on the proton magnetic resonance spectra of packed beds on Dowex 50W.

Experimental

Dowex AG 50W (X4, X8, and X12; 20-50 mesh) was purchased from Bio-Rad Laboratories, Richmond, California. Standard column procedures were used for conversion to the desired ionic forms.¹⁰ Elutions with the salts of NEt_4^+ , NBu_4^+ , and $NPhMe_3^+$ were conducted for at least 2 days to promote complete conversion. The H^+ - Na^+ binary-form resins were prepared at room temperature by elution for at least one day with solutions containing accurately known concentrations of H^+ and Na^+ .⁶ Water contents were determined in duplicate or quadruplicate by the centrifugation technique, with a precision in weight fractions of better than ± 0.015 . Cation-exchange capacities were measured with a precision of ± 0.03 mequiv/g or better by first titrating the protons eluted by NaCl from a H^+ -form sample and then heating to dryness and weighing the resulting Na^+ -form resin.

All pmr spectra were run on a Varian A-60A spectrometer at a probe temperature of $42 \pm 1^\circ$ using 5-mm precision cells supplied by Wilmad Glass Co., Buena, New Jersey. Spectra were taken of at least three samples of each ionic form,¹⁰ except in the H^+ - Na^+

study where only one sample at each equivalent fraction was prepared. The precision of the chemical shifts is ± 0.5 Hz in most cases. A chloroform-tetramethylsilane solution was used to calibrate the frequency scale. The external interstitial water peak served as a convenient primary reference for all chemical shift calculations.

Results and Discussion

Internal Water Chemical Shifts. A major objective of proton chemical shift studies of ion exchangers is the comparison of the effects of a counterion and of the

- (1) J. E. Gordon, *J. Phys. Chem.*, **66**, 1150 (1962).
- (2) D. Reichenberg and I. J. Lawrenson, *Trans. Faraday Soc.*, **59**, 141 (1963).
- (3) R. H. Dinius, M. T. Emerson, and G. R. Choppin, *J. Phys. Chem.*, **67**, 1178 (1963).
- (4) J. P. deVilliers and J. R. Parrish, *J. Polym. Sci., Part A*, **2**, 1331 (1964).
- (5) R. H. Dinius and G. R. Choppin, *J. Phys. Chem.*, **68**, 425 (1964).
- (6) D. G. Howery and B. H. Kohn, *Anal. Lett.*, **3**, 89 (1970).
- (7) T. E. Gough, H. D. Sharma, and N. Subramanian, *Can. J. Chem.*, **48**, 917 (1970).
- (8) R. W. Creekmore and C. N. Reilley, *Anal. Chem.*, **42**, 570 (1970).
- (9) R. W. Creekmore and C. N. Reilley, *ibid.*, **42**, 725 (1970).
- (10) D. G. Howery and M. J. Kittay, *J. Macromol. Sci., Chem.*, **4**, 1003 (1970).
- (11) A. Darickova, D. Doskocilova, S. Sevcik, and J. Stamberg, *J. Polym. Sci., Part B*, **8**, 259 (1970).
- (12) L. S. Frankel, *Can. J. Chem.*, **48**, 2432 (1970).
- (13) D. G. Howery, G. Senum, and L. Madoff, *Anal. Lett.*, **3**, 483 (1970).
- (14) L. S. Frankel, *Anal. Chem.*, **42**, 1638 (1970).
- (15) H. D. Sharma and N. Subramanian, *Can. J. Chem.*, **49**, 457 (1971).
- (16) L. S. Frankel, *J. Phys. Chem.*, **75**, 1211 (1971).
- (17) P. H. Weiner and D. G. Howery, *Can. J. Chem.*, **49**, 2913 (1971).

Table I: Comparison of Chemical Shifts for Cations in Dowex AG 50W and in Aqueous Solution

Cation	Crosslinkage									Aqueous δ/C^c
	X4			X8			X12			
	δ^a	C^b	δ/C	δ	C	δ/C	δ	C	δ/C	
H ⁺	-47.0	2.25	-21.0	-91.5	4.80	-19.0	-124.5	6.70	-18.5	-20.6
Li ⁺ ^d	-3	2.20	-1	-7	4.80	-1	-11	6.65	-1.7	-1.0
Na ⁺	4.5	2.75	1.6	8.0	5.45	1.5	8.5	7.65	1.1	3.0
K ⁺	5.5	2.75	2.0	10.5	5.85	1.8	14.0	7.70	1.8	2.8
Rb ⁺	4.0	2.55	1.6	6.0	5.65	1.1	11.5	8.6	1.3	2.3
Ag ⁺ ^e	-9	3.10	-3	-17	7.15	-2.4	-23	8.0	-2.9	-3.1
NH ₄ ⁺	0.0	2.85	0.0	0.0	5.55	0.0	0.0	7.45	0.0	0.0
NMe ₄ ⁺ ^d	-3	3.00	-1	-7	6.20	-1	-11	9.3	-1	
NEt ₄ ⁺ ^d	-3	3.10	-1	-7	6.65	-1	-11	9.9	-1	
NBu ₄ ⁺	8.5	5.30	1.6	12.5	9.8	1.3	5.0	7.9	0.6	
NPhMe ₃ ⁺	3.0	4.00	0.8	0.5	8.3	0.1	-11 ^d	12	-0.9	
Mg ²⁺	-14.0	3.05	-4.6	-25.0	5.80	-4.3	-32 ^e	7.05	-4.5	-5
Ca ²⁺ ^d	-5 ^f	3.40	-1	-11 ^f	5.95	-1.9	-15 ^f	7.95	-1.9	-1
Sr ²⁺ ^d	-3	4.00	-1	-7	6.20	-1	-11	7.55	-1.5	-1
Ba ²⁺ ^d	-3	7.15	0	-7	7.20	-1	-7 ^f	9.3	-1	1
Zn ²⁺	-18.0	3.15	-5.7	-31.5	5.60	-5.6	-40.0	6.40	-6.3	
Cd ²⁺	-17.0	3.10	-5.5	-28.5	5.45	-5.2	-36.0	7.30	-4.9	
La ³⁺	-21.0	4.90	-4.3	-30.5	6.50	-4.7	-34.0	7.9	-4.3	
R ^{-g}	3.0	2.85	1.1	7.0	5.55	1.3	10.5	7.45	1.4	

^a Chemical shift of internal water (Hz), referred to NH₄⁺ form resin of same crosslinkage, 42°. ^b Counterion concentration in resin bead (g equiv/kg). ^c Chemical shift in aqueous solution (Hz/g equiv/kg), referred to NH₄⁺ in aqueous solution, 25°. Values for monovalent ions from ref 18; values for divalent ions calculated from ref 18 and 21. ^d One peak. ^e Internal peak difficult to resolve. ^f Estimated from chemical shift of overall peak. ^g Chemical shift for resinate in the NH₄⁺ form referred to external water.

same ion in aqueous solution. In Table I are tabulated the proton chemical shifts for the internal water, δ , and the concentrations of the counter ions, C , for 18 ionic forms of Dowex AG 50W at three crosslinkages. Chemical shifts for the internal water are referred to the internal peak of the appropriate NH₄⁺-form resins. This choice of reference, based upon the arguments of Hindman¹⁸ concerning ions in aqueous solutions, has been used in earlier work.^{7,10,15} Chemical shifts upfield to the reference peak are taken as positive. The cation exchange capacity (mequiv/g dry resin) of each resin form was calculated from the measured cec of the Na⁺ form of the same crosslinkage; the counter ion concentration (g equiv/kg internal water) is obtained from the cec and the measured water content of each resin form. The accuracy of the calculated values of the chemical shift for the internal water per unit concentration (δ/C in Table I) is in most cases limited by the uncertainty in δ ; for resins having a relatively low water content, the uncertainty in C is the limiting factor.

The values of δ/C given in Table I are nearly independent of crosslinkage for a given ionic form. Ion-association effects might be the cause of the smaller values for δ/C measured for some of the counterions at higher internal concentrations; however, the constancy of δ/C for each of the polyvalent forms implies to us that ion association plays at most a small role in determining the structure of the internal water.

Qualitatively, the chemical shift patterns are con-

sistent with the views of Shoolery and Alder.¹⁹ Counterions having relatively large charge:volume ratios produce downfield chemical shifts due to polarization of water molecules by counterions. For counterions having a relatively small charge:volume ratio, upfield chemical shifts result if hydrogen bonds are broken. In the tetraalkylammonium-form series, NMe₄⁺ and NEt₄⁺ would appear to be slight net structure makers, NBu₄⁺ may behave as a weak structure breaker (as expected for a large counterion), and NPhMe₃⁺ would appear to change from a structure maker to a structure breaker as the crosslinkage increases. Since the effects of tetraalkylammonium ions on water alone are not yet clearly understood,²⁰ no definitive conclusions concerning the interaction of such counter ions with the internal water can be drawn.

The average value of δ/C for a given counterion agrees qualitatively with the corresponding value for that cation in aqueous solution (last column, Table I). The concentrated-electrolyte model for ion exchange resins is now well substantiated from pmr work.^{1,2,4,6-8,10,15} Values of δ/C for monovalent cations in solution referred to NH₄⁺(aq) are given by Hindman.¹⁸ Molal chemical shifts for salts containing divalent cations²¹

(18) J. C. Hindman, *J. Chem. Phys.*, **36**, 1000 (1962).

(19) J. N. Shoolery and B. J. Alder, *ibid.*, **23**, 805 (1955).

(20) T. S. Sarma, R. K. Mohanty, and J. C. Ahluwalia, *Trans. Faraday Soc.*, **65**, 2333 (1969).

(21) C. Franconi and F. Conti, in "Nuclear Magnetic Resonance in Chemistry," B. Pesce, Ed., Academic Press, New York, N. Y., 1965, p 349.

Table II: Correlation of Widths at Half Height for Dowex AG 50W with Volume Magnetic Susceptibility Differences

Cation	Crosslinkage								
	X4			X8			X12		
	W_e^a	W_i^b	$\Delta\chi^c$	W_e	W_i	$\Delta\chi$	W_e	W_i	$\Delta\chi$
H ⁺	5	8	0.015	6	9	0.025	9	9	0.025
Li ⁺ ^d		4			7			11	
Na ⁺	9	5	0.035	10	6	0.050	13	8	0.075
K ⁺	8	4		11	7		12	8	
Rb ⁺	9	5	0.050	14	10	0.090	17	11	0.100
Ag ⁺ ^d		10			18			24	
NH ₄ ⁺	6	4	0.025	9	5	0.040	10	8	0.050
NMe ₄ ⁺ ^d		6	0.015		10	0.040		9	0.040
NEt ₄ ⁺ ^d		6			9			13	
NBu ₄ ⁺	7	9		9	12		12	11	
NPhMe ₃ ⁺	5	4		6	6			11 ^d	
Mg ²⁺	8	5	0.050	11	11	0.065	14	e	0.085
Ca ²⁺ ^d		5			10			11	
Sr ²⁺ ^d		8			11			15	
Ba ²⁺ ^d		18	0.100		18	0.110		22	0.120
Zn ²⁺	11	5	0.060	14	8	0.085	17	13	0.090
Cd ²⁺	11	6	0.065	15	10	0.090	17	13	0.125
La ³⁺	11	8	0.050	13	12	0.075	16	21	0.100

^a Width at half height of external water peak (Hz). ^b Width at half height of internal water peak (Hz). ^c Difference in volume magnetic susceptibility (ppm), χ_v (water) - χ_v (resin bead). Values from ref 17. ^d One peak. ^e Shoulder.

were used in conjunction with reported anionic molal chemical shifts¹⁸ to calculate the values for δ/C for aqueous divalent cations given in Table I.¹⁰ Additivity of cationic and anionic chemical shifts was assumed. A lower limit for the missing values of δ/C for cations in aqueous solution can be estimated from the counterion values for X4 resin. The nearly constant value of δ/C for the resinate negative framework (bottom entry, Table I) may imply that the sulfonate exchange group is a weak structure breaker, consistent with the rather small charge:volume ratio for the group.

Values of δ/C for the alkali metal counterions determined by Sharma and coworkers⁷ agree moderately well with the values reported in Table I. The small variances probably arise from differences in probe temperature, method for determining water contents, and bead size.

Line Widths. The widths at half height for the external water peak, W_e , and the internal water peak, W_i , are presented in Table II. Except for the broadest peaks, the precision for line widths is ± 1 Hz. Line widths generally increase with an increase in crosslinkage and in atomic mass of the counterion. Gordon¹ stated that the line width of the external water peak should increase with an increase in the difference in volume magnetic susceptibility of the wet resin bead and water. Frankel¹⁶ concluded that the line width of the internal water peak also is dependent upon the difference in susceptibility of the two phases. Differences in volume susceptibility, $\Delta\chi$ for 10 ionic forms measured by a spinning coaxial cell technique,¹⁷ are included in Table II. Qualitatively, the trends in

W_e , W_i , and $\Delta\chi$ are similar, indicating that changes in line widths are indeed controlled by susceptibility effects.

The external peak is broader than the internal peak in most cases. Protons in the voids of the packed bed (especially those near the beads) do experience a magnetic field which is not as spherically symmetrical as the field experienced by the average proton within a bead.

Binary Counterion System. The proton chemical shifts of binary mixtures of aqueous electrolytes have been shown to be simple additive functions even for total molalities as large as the internal ionic concentrations of ion-exchange resins.^{21,22} Preliminary pmr studies on the H⁺-Na⁺-Dowex AG 50W system⁶ indicated that counterion effects on the internal water chemical shift are also additive.

The internal water chemical shift can be related to the counterion composition, assuming rapid proton exchange and constant internal molality, by

$$\nu = \nu_H \bar{X}_H + \nu_{Na} \bar{X}_{Na} \quad (1)$$

where ν is the observed chemical shift for the internal water relative to the convenient reference, external water; ν_H and ν_{Na} are the chemical shifts for the internal water in the H⁺ and Na⁺ forms; and \bar{X}_H and \bar{X}_{Na} are the equivalent fractions of H⁺ and Na⁺ on the resin. Since the water content (and therefore the counterion concentration) varies with conversion, ν can be more accurately expressed by⁶

(22) J. E. Gordon and R. L. Thorne, *J. Phys. Chem.*, **73**, 3643 (1969).

$$\nu = \frac{\nu_H \bar{X}_H w_H + \nu_{Na} \bar{X}_{Na} w_{Na}}{\bar{X}_H w_H + \bar{X}_{Na} w_{Na}} \quad (2)$$

where w_H and w_{Na} are the measured weight fractions of water in the H^+ and Na^+ forms.

Counterion uptakes were estimated from published isotherms. For samples equilibrated with solutions of known molarities of H^+ and Na^+ , the equivalent-fraction composition of the ion exchanger can be estimated if the isotherm for the exchange is known. The thorough isotherms of Bonner and Rhett were used,^{23,24} where the compositions for the X12 system were obtained by interpolation of the isotherms for X8 and X16 resins.

A comparison of observed ν 's and those predicted using equation 2 is given in Table III. The agreement is adequate considering the uncertainties introduced (especially for the X12 system) when using isotherms to calculate resin-phase compositions. Counterion effects are clearly additive. These results furnish additional evidence that ion-exchange resins behave like concentrated electrolytes. If equation 1 is used, the agreement is poorer by about 3, 4, and 6 Hz on the average for the X4, X8, and X12 systems, respectively.

Measuring the chemical shift of ion exchange resins containing two counterions offers a convenient and nondestructive method for determining counterion equivalent fraction. Unfortunately, the chemical shifts for most binary counterion systems (refer to Table I) span rather small frequency differences; the pmr

Table III: Comparison of Observed and Predicted Chemical Shifts for H^+ - Na^+ Dowex AG 50W Systems

Crosslinkage								
X4			X8			X12		
x_{Na}^a	$-\delta_o^b$	$-\delta_p^c$	x_{Na}	$-\delta_o$	$-\delta_p$	x_{Na}	$-\delta_o$	$-\delta_p$
0.14	42	38	0.06	76	80	0.10	104	104
0.28	36	33	0.12	67	68	0.21	96	91
0.40	28	27	0.27	61	63	0.36	78	73
0.51	23	22	0.39	50	52	0.48	64	58
0.61	18	17	0.49	41	41	0.58	50	45
0.70	12	11	0.59	34	32	0.66	39	33
0.79	7	6	0.68	21	23	0.74	28	22
0.86	3	2	0.75	14	14	0.81	15	12
0.92	-2	-3	0.86	0	3	0.85	1	5
			0.96	-8	-9	0.92	-2	-7

^a Equivalent fraction of Na^+ in external solution, total cationic molarity = 0.02. ^b Observed chemical shift for internal water (Hz), referred to external water. ^c Predicted chemical shift using eq 2 for internal water (Hz), referred to external water.

method can be useful if the chemical shifts of the single ion forms differ by at least 20 Hz.

Acknowledgment. This work was supported in part through a National Science Foundation Undergraduate Research Participation Program Grant. We are grateful to Mike Kittay and Jack Emert for assistance in procuring spectra.

(23) O. D. Bonner, *J. Phys. Chem.*, **58**, 318 (1954).

(24) O. D. Bonner and V. Rhett, *ibid.*, **57**, 254 (1953).

The Kinetics of the Hydrolysis of the Dichromate Ion. VI. Environmental Influences on the Acid-Catalyzed Reaction¹

by Ruth Koren and Berta Perlmutter-Hayman*

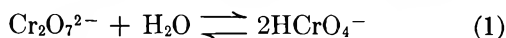
Department of Physical Chemistry, The Hebrew University, Jerusalem, Israel (Received September 20, 1971)

Publication costs assisted by the Department of Physical Chemistry, The Hebrew University

The influence of electrolytes, of dioxane, and of temperature on the rate of the acid-catalyzed hydrolysis of the dichromate ion has been investigated by the T-jump method. Where comparison is possible, the results are in excellent agreement with those reported earlier. The effect of sodium salts shows only a slight deviation from "classical" behavior. The apparent energy of activation is 8.92 ± 0.34 and 8.26 ± 0.44 kcal mol⁻¹ at an ionic strength of 0.05 and 0.20, respectively. The influence of dioxane is less pronounced than would be expected from its influence on the dielectric constant. Tetramethylammonium chloride has a stronger decelerating influence than the sodium salts, at the same time, however, decreasing the apparent energy of activation, especially when temperatures up to 29° are considered. The influence of water structure is discussed as a possible explanation for the effects of dioxane and of tetramethylammonium chloride.

Introduction

In a previous paper of this series,² the activation energy of the hydrolysis of the dichromate ion, *viz.*



was found to decrease with increasing temperature. Furthermore, the addition of electrolytes was found to enhance the rate of reaction, whereas the addition of dioxane or of tetraethylammoniumbromide was found to decrease the rate. It was suggested that these phenomena might be explained by the reaction taking place more rapidly the more the hydrogen-bonded structure of water has broken down—owing either to an increase in temperature or to the presence of structure-breaking substances.

The present investigation was undertaken in order to find out whether similar effects exist also for the reaction catalyzed by hydrogen ions.

Experimental Section

All our experiments were carried out in a T-jump apparatus.

The stoichiometric concentration of K₂Cr₂O₇ was in the range $4\text{--}12 \times 10^{-4}$ M, and the wavelength used for detection was 385–405 nm; the lower wavelength, where the extinction coefficient of Cr₂O₇²⁻ is higher, was employed for the lower concentrations, and *vice-versa*. The electrolyte necessary to ensure sufficient conductance was either provided by the catalyzing acid itself, or by the electrolyte whose influence was being investigated.

The values of k_{H^+} , the catalytic constant for the reaction in the forward direction (referring, as usual, to the "reaction variable"³ and measured in M⁻¹ sec⁻¹) were obtained from the intercept of plots of 1/τ against five different concentrations of HCrO₄⁻,

calculated from the stoichiometric concentration of K₂Cr₂O₇, together with the equilibrium constant of reaction 1 found spectrophotometrically in the presence of various electrolytes.⁴ Each point on a plot was the mean of two to five experiments, exhibiting a maximum spread of ±10%, but usually much less. The intercepts, calculated by the method of least squares, showed a standard deviation of ~9%. The catalytic constant of the back reaction cannot be obtained from these plots; the reason for this is explained elsewhere,⁵ where further details on the experimental method are also given.

The changes in absorbance were $6\text{--}10 \times 10^{-3}$ unit and enabled a very satisfactory signal to noise ratio to be obtained. This is exemplified in Figure 1 which shows a typical oscilloscope trace.

The relaxation times were evaluated with the aid of a device developed in our department.⁶

Near room temperature, the temperature in the cell before the T-jump was taken as that of the thermostat from which water was circulated, and which was constant to ±0.1°. At other temperatures, the temperature difference between the bath and the T-jump cell had to be taken into account, and was measured with a copper-constantan thermocouple. The extent of the T-jump, Δ*T*, was calculated from the known capacity

(1) This work forms part of a thesis to be submitted by R. Koren to the Senate of the Hebrew University, in partial fulfillment of the requirements for a Ph.D. degree.

(2) B. Perlmutter-Hayman and Y. Weissmann, *J. Phys. Chem.*, **71**, 1409 (1967).

(3) See, *e.g.*, A. A. Frost and R. G. Pearson, "Kinetics and Mechanism," 2nd ed, Wiley, New York, N. Y., 1961, p 9.

(4) B. Perlmutter-Hayman and Y. Weissmann, *Israel J. Chem.*, **6**, 17 (1968).

(5) B. Perlmutter-Hayman and R. Koren, *ibid.*, **8**, 1 (1970).

(6) H. J. G. Hayman, *ibid.*, **8**, 603 (1970).

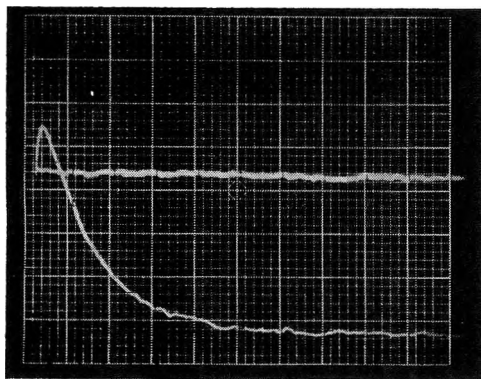


Figure 1. A typical oscillogram; time scale: 5 msec per large scale division; sensitivity of oscilloscope: 5 mV per large scale division. (The horizontal line corresponds to the absorption before the T-jump; the initial rise in the curve has independently been ascertained to follow the time-constant of our high frequency filter and may be ascribed to small changes of the extinction coefficients with temperature.)

and voltage of our condenser and the effective volume of the cell, and was between 3.5 and 4.6°. To minimize uncertainties in ΔT , we used the *same* cell throughout the present investigation. We estimate the error in T to be small in comparison with that in k_{H^+} .

Most of our calculations were carried out with the aid of a CTC 6400 computer.

Results

(a) *Influence of Dioxane.* The influence of dioxane was investigated at 24.6° in the presence of 0.044 *M* perchloric acid at dioxane concentrations up to 30%. Since water takes part in the stoichiometry of our reaction, the rate constants were multiplied by 55.56/[H₂O]. The resulting values of k_{H^+} increased with increasing dioxane concentration. Now, the dielectric constant, D , of the reaction mixture decreases with increasing dioxane concentration; this effect is therefore in the direction expected from classical theory for a reaction between ions of unlike sign. According to this theory, a plot of the logarithm of k^0 , the rate constant at zero ionic strength, against $(1/D)$ should yield a straight line with a slope inversely proportional to a , the distance between the reactants in the activated complex.⁷ Since our experiments were all carried out at the same ionic strength I , it might at first sight seem justified to use the values of k_{H^+} directly for a plot of this kind. However, at different values of the dielectric constant, the rate constants are differently affected by the ionic strength. Unfortunately, measurements at low ionic strength cannot be carried out by our method. Therefore, again basing ourselves on classical electrolyte theory, we added

$$2|z_A z_B| A_{H_2O} (D_{H_2O}/D_{\text{mixture}})^{3/2} \sqrt{I}/(1 + \sqrt{I})$$

(where A_{H_2O} is the constant of the Debye-Hückel equation in water at 25°, and z_A and z_B are the valencies of the reactants) to the logarithm of k_{H^+} in order to

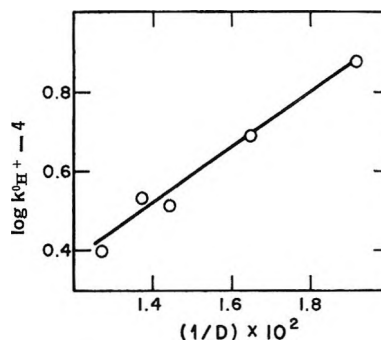


Figure 2. The logarithm of the rate constant, corrected to zero ionic strength, as a function of the reciprocal dielectric constant, in water-dioxane mixtures. (Data for dielectric constant from C. V. King and J. J. Josephs, *J. Amer. Chem. Soc.*, **66**, 767 (1944).)

obtain at least a reasonable approximation to $\log k_{H^+}^0$ (see section b). Obviously, the values of $k_{H^+}^0$ increase with increasing dioxane concentration more strongly than do those of k_{H^+} . Nevertheless, the plot of $\log k_{H^+}^0$ vs. $1/D$, shown in Figure 2, yields a $\sim 7 \text{ \AA}$ which is unreasonably high.⁷ In other words, even after all corrections are applied, dioxane is found to increase the rate less than would be expected from its influence on the dielectric constant. (For a to have a more realistic value, say 3.5 \AA , the rate constant in the presence of 30% dioxane would have to be 3 times higher than our experimental value.)

(b) *Influence of Electrolytes.* Again at 24.6°, we investigated solutions 0.046 *M* in nitric acid, and containing sodium or tetramethylammonium chloride at varying concentrations, up to 0.2 *M*. Experiments at 0.1 *M* sodium nitrate and perchlorate and a similar concentration of nitric acid were also carried out. Following a procedure first suggested by Guggenheim and Prue,⁸ we plotted $\log k_{H^+}^{0'}$ against the concentration of the added electrolyte. (This quantity is defined by

$$\log k_{H^+}^{0'} \equiv \log k_{H^+} + 2.03\sqrt{I}/(1 + \sqrt{I}) \quad (2)$$

where k_{H^+} is the rate constant measured at ionic strength I , and is thus a rate constant which has been partially corrected for the influence of ionic strength.) If the Guggenheim equation⁹ is obeyed, this plot should yield a straight line with a *small* positive slope, corresponding to a suitable combination of the interaction parameters of that equation.⁸ The result is shown in Figure 3. We find that though $k_{H^+}^{0'}$ indeed changes only slightly with ionic strength, the

(7) S. Glasstone, K. J. Laidler, and H. Eyring, "The Theory of Rate Processes," McGraw-Hill, New York, N. Y., 1941, pp 430-438.

(8) E. A. Guggenheim and J. E. Prue, "Physico-Chemical Calculations," North Holland Publishing Co., Amsterdam, 1955, p 466; see also B. Perlmutter-Hayman and Y. Weissmann, *J. Phys. Chem.*, **68**, 3307 (1964); B. Perlmutter-Hayman in *Progr. React. Kinet.*, **6**, 239 (1971).

(9) E. A. Guggenheim, "Thermodynamics," North Holland Publishing Co., Amsterdam, 1949, Chapter 9.

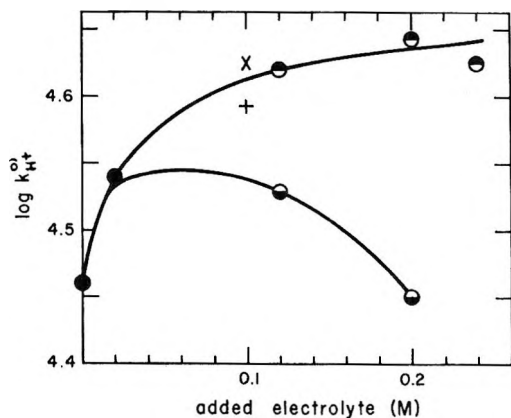


Figure 3. The dependence of $\log k_{H^+}^0$ (as defined by eq 2) on concentration of added electrolyte, in the presence of 0.046 M acid; ●, sodium chloride; X, sodium nitrate; +, sodium perchlorate; ⊖, tetramethylammonium chloride. Straight lines with a small positive slope would correspond to "classical" behavior.

plots are curved instead of straight, especially at low concentrations of added salt. An extrapolation to $I = 0$ was therefore not attempted.

The sodium salts of different anions are seen to fall on or near the same curve which, at the high concentrations, has the expected small positive slope. On the other hand, the points for the tetramethylammonium ion, at concentrations above 0.02 M , begin to diverge in the direction of a stronger decelerating influence, the divergence reaching definite statistical significance at 0.2 M .

(c) *Influence of Temperature.* The influence of temperature was investigated in three series of experiments, in a temperature range from 6.3 (or 8.8) to 45°. In the first series, perchloric acid was $\sim 0.05 M$, with no further substances added. In the second and third series, perchloric acid was $2 \times 10^{-3} M$ and 0.2 M NaClO_4 or tetramethylammonium chloride were added. Arrhenius plots are shown in Figure 4. For the first two series, straight lines were fitted by the method of least squares which yielded activation energies E_A of 8.92 ± 0.34 (standard deviation) and 8.26 ± 0.44 kcal mol $^{-1}$, respectively.

In the presence of tetramethylammonium chloride, however, the result is different. The best straight line through the experimental points yields $E_A = 7.59 \pm 0.81$, but this is not the best representation of the data. Without wishing to attach theoretical significance to any particular mathematical form, we fitted a quadratic equation to our points. This is the line shown in Figure 4. The coefficient of $(1/T)^2$ is 6 times its standard deviation; according to the t -test, this means that the change of activation energy with temperature is significant on a 99% level. When only the temperature range up to 29° is considered, we may say that $E_A \sim 5.9$ kcal mol $^{-1}$.

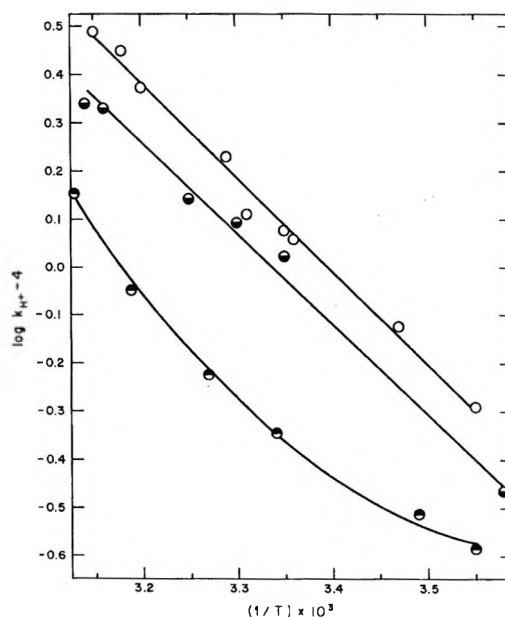


Figure 4. The logarithm of the rate constant as a function of the reciprocal temperature: O, $[\text{HClO}_4] \sim 0.05 M$; ●, $[\text{HClO}_4] = 0.001 M$ plus $[\text{NaClO}_4] = 0.20 M$; ⊖, $[\text{HClO}_4] = 0.001 M$ plus $[\text{Me}_4\text{NCl}] = 0.20 M$.

Discussion

Our present values of $k_{H^+} = 1.14 \times 10^4$ and $1.05 \times 10^4 M^{-1} \text{ sec}^{-1}$ at $I = 0.046$ and 0.2, respectively, are in excellent agreement with our previous results (where a stopped flow apparatus was employed for measurements in the presence of perchloric acid,¹⁰ and ordinary mixing¹⁰ or mixing with a rapid mixing syringe¹¹ for measurements in the presence of suitable buffers).

The influence of sodium salts on the reaction rate, though not exactly following classical behavior—the line in Figure 3 is curved instead of straight—may be considered essentially normal for a reaction of this charge type. This is further emphasized by the fact that the curve in Figure 3 corresponding to the sodium salts continues smoothly to the value calculated from Espenson's result¹² at $I = 1.0$, made up of lithium perchlorate and perchloric acid.

Similarly, the change of 0.66 kcal in activation energy as we pass from $I = 0.05$ to $I = 0.2$, though almost within the limit of experimental error, is in the direction expected from classical theory. (Employing the expression given in the literature¹³ for the dependence of E_A on ionic strength and modifying it for

(10) B. Perlmutter-Hayman, *J. Phys. Chem.*, **69**, 1736 (1965).

(11) R. Baharad, B. Perlmutter-Hayman, and M. A. Wolff, *J. Phys. Chem.*, **73**, 4391 (1969).

(12) J. R. Pladziewicz and J. H. Espenson, *Inorg. Chem.*, **10**, 634 (1971); we should like to thank Professor Espenson for making his manuscript available to us before publication.

(13) E. A. Moelwyn-Hughes, "Kinetics of Reactions in Solution," Oxford University Press, London 1947, Chapter 4. (The expression given for dE_A/dT at nonzero ionic strength is incorrect. Consequently the theoretical value for dE_A/dT is slightly smaller than that predicted on the basis of this reference.)

use at higher ionic strength by dividing through by $(1 + \sqrt{I})$, a slightly smaller change, *viz.* ~ 0.20 kcal mol⁻¹, may be predicted. Both a change of 0.20 and the difference between 0.66 and 0.20 kcal mol⁻¹ are practically within the limit of experimental error.) Furthermore, our value of E_A at $I = 0.2$ lies midway between the two values obtained by Espenson, *et al.*,¹² at $I = 1.0$, on two slightly different assumptions concerning the equilibrium constant.

A specific influence of tetraalkylammonium salts is found in many other reactions involving ions,¹⁴ and may be formally ascribed to the unusual magnitude and often negative sign of the interaction coefficients between these bulky cations and many anions.¹⁵ Although the reason for this behavior is still being discussed,¹⁵ it is agreed to be connected with the interaction of these cations with the solvent water, an interaction which is usually termed "structure making."

The validity of the Born equation, which forms the basis of our treatment of the influence of dioxane, has often been questioned.¹⁶ Factors other than the bulk dielectric constant clearly have to be considered. In our case, the latter factor seems to be partly counterbalanced by another, decelerating one. (This is in contrast with the acetate-catalyzed hydrolysis of dichromate² where the value of a obtained from a plot of the type of our Figure 2 is a very reasonable one.) We suggest that this, again, might be connected with the fact that dioxane profoundly influences the structure of water—according to most criteria (though not all!¹⁷) in the direction of structure promotion.

As far as we are aware, the influence of tetraalkylammonium salts on energies of activation has not been reported. In the present case, in spite of its decelerating effect, the tetramethylammonium ion significantly decreases the activation energy—at least at temperatures up to 29°. Moreover, the activation energy increases with increasing temperature. This effect, although in the direction expected for a reaction between ions of unlike sign,¹³ is much higher than can be accounted for on this basis, and, furthermore, should be more pronounced the lower the ionic strength.

A possible explanation¹⁸ for a positive dE_A/dT is the operation of two different parallel mechanisms, the one with the higher activation energy becoming predominant as the temperature increases. This possibility cannot be ruled out, but is made improbable by the fact that the effect appears only in the presence of tetramethylammonium ion.

The influence of proton tunnelling on the apparent energy of activation has recently been reviewed.¹⁹ This leads to a positive dE_A/dT , the effect becoming noticeable, however, only at temperatures well below those employed by us.

We shall now analyze the possibility that our hydrolysis should indeed be influenced by the structure of water, proceeding at different rates with the hydro-

gen bonded, (1), and the broken-down, unstructured, (2), forms. We have recently developed formulas for the apparent energy of activation, and for dE_A/dT for such a situation,²⁰ and have discussed the applicability of our formulas to the two forms of water.^{20,21} We have shown that

$$E_A = E_{(1)} - \frac{K}{K+1} \Delta H + \frac{Kk_{(2)}/k_{(1)}}{1 + Kk_{(2)}/k_{(1)}} (\Delta H - \delta E) \quad (3)$$

with $\delta E \equiv E_{(1)} - E_{(2)}$, where $E_{(1)}$ and $E_{(2)}$ are the "true" activation energies of the two reaction paths, $k_{(1)}$ and $k_{(2)}$ their rate constants, and K and ΔH refer to the equilibrium between (1) and (2).

There are some difficulties^{21,22} in assigning numerical values to K and to ΔH . If we consider the number of hydrogen bonds broken divided by the number of hydrogen bonds intact as an adequate measure for K , it turns out—according to some modern estimates^{22,23}—that $K > 1$. On the other hand, assuming the tetramethylammonium ion to be structure promoting (*i.e.*, to cause K to decrease), we conclude from its specific decelerating influence that $k_{(2)} > k_{(1)}$, whereas we conclude from its influence on E_A that $\delta E < 0$ (the decelerating influence being due to a decrease in entropy of activation which outweighs the decrease in energy of activation). Now, it can easily be verified from eq 3 that, when the three above inequalities hold simultaneously, then a decrease in K can lead to a decrease in E_A . This is in accordance with our experimental finding.

The dependence of E_A on temperature can also be explained on this basis. Differentiation of eq 3 with respect to temperature shows dE_A/dT to be composed of a negative and a positive term (see eq 9 of reference 20). We have discussed elsewhere²⁰ the conditions which can lead to positive values of dE_A/dT . These conditions are further illustrated in Figure 5 which is designed to emphasize high positive values. In this figure dE_A/dT is shown as a function of $\delta E/RT$, for

(14) A. Indelli, *J. Phys. Chem.*, **65**, 972 (1961); E. S. Halberstadt and J. E. Prue, *J. Chem. Soc.*, 2234 (1952).

(15) J. E. Prue, A. J. Read, and G. Romeo, *Trans. Faraday Soc.*, **62**, 420 (1971); A. D. Pethybridge and J. E. Prue, *Annu. Rep. Progr. Chem. Sect. A*, **65**, 145 (1968).

(16) R. G. Bates in "Hydrogen Bonded Solvent Systems," A. K. Covington and P. Jones, Ed., Taylor and Francis, London, 1968, p 49; D. Feakins and C. M. French, *J. Chem. Soc.*, 2581 (1957).

(17) F. Franks in ref 16, p 34.

(18) J. R. Hulett, *Quart. Rev. Chem. Soc.*, **18**, 227 (1964).

(19) E. Caldin, *Chem. Rev.*, **69**, 130 (1969).

(20) R. Koren and B. Perlmutter-Hayman, *J. Phys. Chem.*, **75**, 2372 (1971).

(21) B. Perlmutter-Hayman, *Israel J. Chem.*, **9**, 377 (1971).

(22) D. Eisenberg and W. Kauzmann, "The Structure and Properties of Water," Oxford University Press, London, 1969, pp 176-179.

(23) G. Némethy and H. A. Scheraga, *J. Chem. Phys.*, **36**, 3382 (1962); K. Arakawa and K. Sasaki, *Bull. Chem. Soc., Jap.*, **42**, 303 (1969).

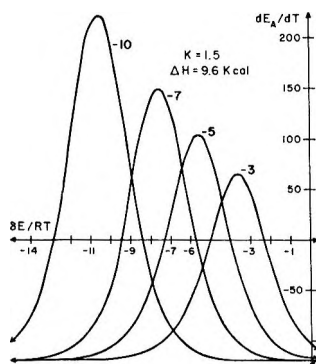


Figure 5. The calculated dependence of dE_A/dT on $\delta E/RT$, for various values of $\delta\Delta S^\ddagger/R$, indicated by a number alongside the appropriate curve (where δE and $\delta\Delta S^\ddagger$ are the differences in activation energy and activation entropy of two reactant forms²⁰).

various values of $\delta\Delta S^\ddagger/R$ (where $\delta\Delta S^\ddagger$ is the difference in activation entropy of the two forms).²⁰ It is seen that a given value of dE_A/dT can be obtained with quite a variety of combinations of δE and $\delta\Delta S^\ddagger$. If we had chosen a different value of ΔH —for instance a lower value, assuming fewer hydrogen bonds to be involved²¹—the same value of dE_A/dT could be explained, but on the basis of higher values of $|\delta E|$ and $|\delta\Delta S^\ddagger|$. Similarly, a shift in K would have shifted the picture without altering it fundamentally. Under the conditions which we believe to obtain in our experiments, a decrease in K will increase the absolute value of the positive term in dE_A/dT more strongly than that of the negative one; this may explain why we found a positive dE_A/dT only in the presence of tetramethylammonium chloride.

Since we are dealing with a hydrolysis reaction, it is very plausible that the structure of water should play some role in the kinetics.²⁴ We have previously suggested¹¹ that the rate determining step in the acid catalysis should be the protonation of the bridging oxygen of the dichromate ion, facilitating the heterolytic fission of a chromium–oxygen bond in a “fast” following reaction. It has further been suggested¹¹ that this fission might be aided by the addition of an OH^- from a neighboring water molecule. The catalyzing acid—which in the present case is H_3O^+ —is thus regenerated. It seems probable that this should occur *via* one or more intervening water molecules. Such a mechanism may well be facilitated when the water molecules involved are hydrogen-bonded and are thus present in just the right spatial configuration. This path may have a lower energy of activation, but at the same time a lower probability factor than a reaction path involving randomly oriented water molecules, both paths thus contributing to the observed rate.

We can thus assign to the structure of water a role which, qualitatively, explains our experimental findings. Too many uncertain parameters are however involved for a quantitative comparison to be possible between experiment and a theory which we consider, at present, to be only tentative.

Acknowledgments. The authors wish to thank Dr. A. Ben-Naim of the Department of Inorganic and Analytical Chemistry for helpful discussions on problems of water structure. The T-jump apparatus is a gift from Professor M. Eigen, to whom we once again express our thanks.

(24) R. E. Robertson, *Progr. Phys. Org. Chem.*, **4**, 213 (1967).

Hydrogen Bonding Interactions of *p*-Chlorophenol with Aliphatic Amines

by Mei-Lan Lin and Ronald M. Scott*

Department of Chemistry, Eastern Michigan University, Ypsilanti, Michigan 48197 (Received June 30, 1971)

Publication costs borne completely by The Journal of Physical Chemistry

The formation of hydrogen bonds between *p*-chlorophenol and a series of aliphatic amines in cyclohexane revealed that tertiary amines react less readily than would be expected from their aqueous *pK*. This was interpreted as reflecting steric hindrance by the alkyl groups of the tertiary amines.

Introduction

The method of spectrophotometric analysis for the study of hydrogen bonding by phenols may first have been utilized by Morton and Stubbs in an investigation of hydroxybenzaldehydes and their methyl ethers.¹ Burawoy, *et al.*,²⁻⁴ made a systematic study of the method to investigate the tautomeric equilibria of phenolic compounds. Other workers⁵⁻¹² employed spectrophotometric methods to study hydrogen bonding by phenols. The thermodynamics of the phenol hydrogen-bond-formation reaction have been measured for several cases.^{5-8, 13-15}

p-Chlorophenol, the phenol selected for this study, is a weak acid (aqueous *pK* = 9.39),¹⁶ with absorbance bands in the ultraviolet region at 283 $m\mu$ and 289 $m\mu$. The previously reported thermodynamic parameters for its hydrogen bond formation are summarized in Table I. Cyclohexane, the solvent in these studies, is a hydrocarbon with a dielectric constant of 2.02 which does not interact either with acidic solutes such as phenols or with basic solutes such as amines.¹⁷

The data reported here were obtained as part of a larger study concerning the types of interaction between phenols and amines. A number of phenols and of amines are being investigated with consideration given to the effects on interaction of the acidity of the phenol, the basicity of the amine, and the dielectric constant of the solvent. The results are interpreted in terms either of formation between phenols and amines of hydrogen bonded complexes or hydrogen bonded ion pairs, or of the complete transfer of the proton to form phenolate and ammonium ions. Some results are published,^{8, 18, 19} and the significance of these results for understanding interactions occurring in biological systems has been considered.^{20, 21}

Experimental Section

p-Chlorophenol and morpholine were Dow Chemical Company reagent grade. *n*-Butylamine, *N*-ethylmorpholine, tri-*n*-butylamine, and triethylamine were Aldrich Chemical Company reagent grade. Di-*n*-butylamine, isopropylamine, and tri-*n*-propylamine were Eastman Organic Chemical reagent grade. 1,4-

Dioxane was Matheson Coleman and Bell Company Spectrograde. Cyclohexane was Baker Analyzed reagent grade. All reagents except dioxane were redistilled before use. Triethylenediamine was obtained from Houdry Process and Chemical Company, and was purified by crystallization in dry ether twice and sublimation in vacuum, and was thereafter stored in a desiccator.

p-Chlorophenol and amine stock solutions were prepared by weighing both solvent and solute. Aliquots were then pipetted into volumetric flasks and diluted with cyclohexane, the flask being reweighed after each addition. In each study the amine concentration was varied while the *p*-chlorophenol concentration was kept constant. The absorption spectra were obtained with

- (1) R. A. Morton and A. L. Stubbs, *J. Chem. Soc.*, 1347 (1940).
- (2) A. Burawoy and I. Markowitsch-Burawoy, *ibid.*, 36 (1936).
- (3) A. Burawoy and J. T. Chamberlain, *ibid.*, 2310 (1952).
- (4) A. Burawoy and J. T. Chamberlain, *ibid.*, 3734 (1952).
- (5) S. Nagakura and H. Bada, *J. Amer. Chem. Soc.*, **74**, 5693 (1952).
- (6) S. Nagakura, *ibid.*, **76**, 3070 (1954).
- (7) L. Bellon, *C. R. Acad. Sci.*, **254**, 3346 (1962).
- (8) R. A. Hudson, R. M. Scott, and S. N. Vinogradov, *Spectrochim. Acta, Part A*, **26**, 337 (1970).
- (9) L. Bellon, *Trav. Inst. Sci. Cherifien Ser. Sci. Phys.*, **6**, (1960).
- (10) M. Bonnet and A. Julg, *J. Chim. Phys.*, **59**, 723 (1962).
- (11) N. S. Coggeshall and E. M. Lang, *J. Amer. Chem. Soc.*, **70**, 3283 (1948).
- (12) S. Nagakura and M. Gouterman, *J. Chem. Phys.*, **26**, 881 (1957).
- (13) R. L. Denyer, A. Gilchrist, J. A. Pegg, J. Smith, T. E. Tomlinson, and L. E. Sutton, *J. Chem. Soc.*, 3889 (1955).
- (14) D. Gurka, R. W. Taft, L. Joris, and P. von R. Schleyer, *J. Amer. Chem. Soc.*, **89**, 5957 (1967).
- (15) E. M. Arnett, T. S. S. R. Murty, P. von R. Schleyer, and L. Joris, *ibid.*, **89**, 5955 (1967).
- (16) I. Avigal, J. Feitelson, and M. Ottolenghi, *J. Chem. Phys.*, **50**, 2615 (1969).
- (17) A. I. Shatenshtein, "Isotopic Exchange and the Replacement of Hydrogen in Organic Compounds," (Translation of 1960 Russian edition by C. N. Turton and T. I. Turton) Consultants Bureau, New York, N. Y., 1962.
- (18) R. Scott, D. De Palma, and S. Vinogradov, *J. Phys. Chem.*, **72**, 3192 (1968).
- (19) R. Scott and S. Vinogradov, *J. Phys. Chem.*, **73**, 1890 (1969).
- (20) R. A. Hudson, R. M. Scott, and S. N. Vinogradov, *Biochim. Biophys. Acta*, **181**, 353 (1969).
- (21) S. N. Vinogradov, R. A. Hudson, and R. M. Scott, *ibid.*, **214**, 6 (1970).

Table I: Previously Reported Thermodynamic Parameters for Hydrogen Bond Formation with *p*-Chlorophenol

Proton acceptor	K	ΔH , kcal/mol	ΔG , kcal/mol	ΔS , eu	Ref
Methyl acetate	16.9, 18.3	-6.7	-1.7	-16.9	6
Piperidine	410 (20°)	-9.0	-4.85	-14.2	7
Triethylamine	89 (20°)	-9.55	-4.0	-18.9	7
Tetrahydropyrene	44 (20°)	-6.4	-3.8	-9.7	7
Trimethylamine	76	-7.4, -8.6	-3.1	-13.0	13
Dioxane			-1.6 (23°)		15

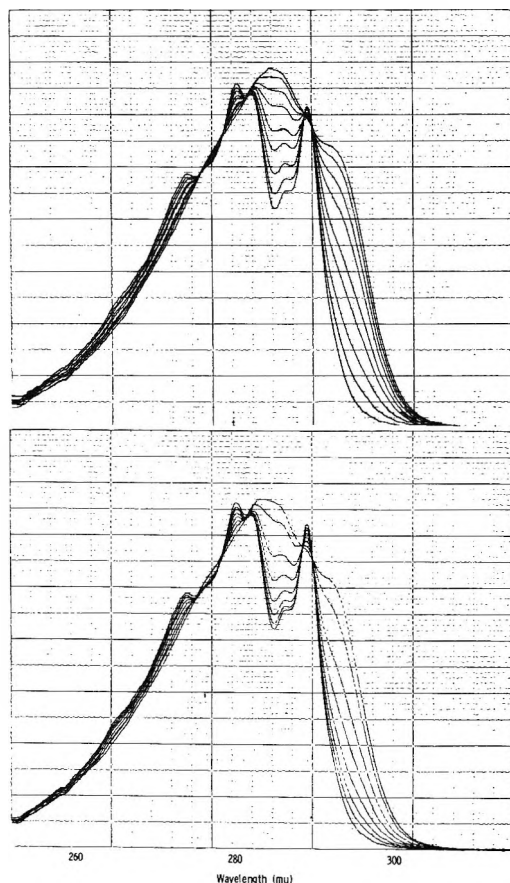


Figure 1. Reproductions of the spectra obtained by scanning cyclohexane solutions of *p*-chlorophenol to which varying concentrations of amine have been added at 25°. Upper represents $2.10 \times 10^{-3} M$ *p*-chlorophenol with additions of morpholine from 0 (lowest absorbance at 285 $m\mu$) to $4.6 \times 10^{-2} M$ (highest absorbance at 285 $m\mu$). Lower represents $2.12 \times 10^{-3} M$ *p*-chlorophenol with additions of *N*-ethylmorpholine from 0 to $4.0 \times 10^{-3} M$ (same order as upper).

a Beckman Model DK-2A spectrophotometer using matched 1-cm silica cells. The temperature of both sample and reference cells was controlled by circulating water from a Lauda K-2/R constant temperature bath through the thermospacers of a brass cell holder similar to that described by Coggeshall and Lang.¹¹ The cells were capped to prevent solvent loss. The spectra of the solutions were recorded from 240 to 315 $m\mu$. Reference cells cancelled the absorbance of both solvent and amine. Each thermodynamic run consisted of at

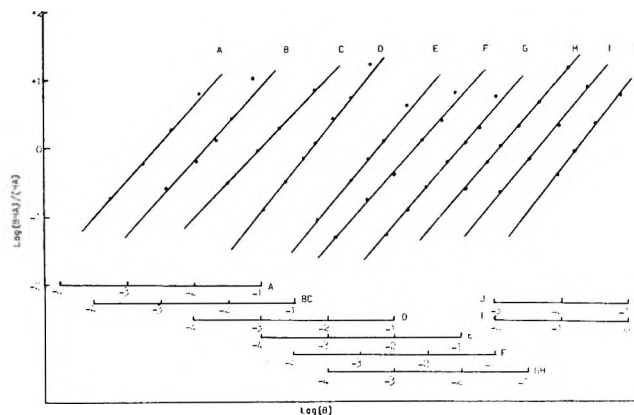


Figure 2. Plots of the log of the ratio of the concentrations of hydrogen bonded to nonhydrogen bonded *p*-chlorophenol ($\log BHA/HA$) vs. log base concentration ($\log B$) calculated from the spectrophotometric data. The bases and the slopes of the lines are: A, dibutylamine 1.1; B, *n*-butylamine 1.0; C, dioxane 1.0; D, morpholine 1.2; E, triethylamine 1.1; F, tributylamine 1.0; G, *N*-ethylmorpholine 1.0; H, *n*-propylamine 1.1; I, isopropylamine 1.2; J, tripropylamine 1.2.

least 5 different *p*-chlorophenol:amine ratios at 5 temperatures ranging from 15 to 55°.

All calculations of equilibrium and thermodynamic parameters were performed on the IBM 1130 digital computer of Eastern Michigan University. Programs were prepared in Fortran IV which convert data in terms of weight and density into molarities, then using these molarities and absorbance readings determine equilibrium constants by the calculation of Rose and Drago.²² Corrections were made for overlapping absorbance bands in the spectra. Final equilibrium constants obtained in this fashion were tested for their statistical validity using the criterion of Chauvenet²³ applying this test twice to the data for each series of amine additions. The remaining constants were averaged.

Thermodynamic parameters were obtained from average $\log K$ values at various temperatures in the usual fashion.²⁴

(22) N. J. Rose and R. S. Drago, *J. Amer. Chem. Soc.*, **81**, 6138 (1959).

(23) H. D. Young, "Statistical Treatment of Experimental Data," McGraw-Hill, New York, N. Y., 1962.

(24) A copy of this program is available from the author on request.

Table II: Experimental Conditions, Equilibrium Constants, and Wavelength Shifts for the Formation of 1:1 Hydrogen Bonded Complexes by *p*-Chlorophenol in Cyclohexane at 25°

Base	Base pK_a^a	Concentration <i>p</i> -chlorophenol $\times 10^3 M$	Concentration range of base $\times 10^3 M$	Equilibrium constant (25°)	Log <i>K</i>	Wavelength shift ($m\mu$) peak
Dioxane	{ -4.3 in HOAc 2.92 in H ₂ SO ₄	2.16	6-18.9	5.42×10	1.72	2.0
<i>N</i> -Ethylmorpholine	7.67	2.12	0.5-40	1.77×10^2	2.15	3.5
Tri- <i>n</i> -butylamine	9.93	2.14	0.2-15	2.45×10^2	2.09	4.0
Tri- <i>n</i> -propylamine	10.26	2.13	2.4-50.6	2.64×10^2	2.42	4.3
Morpholine	8.33	2.10	0.6-46	5.24×10^2	2.65	4.3
Triethylenediamine	8.60 ^b	2.15	0.3-15	7.04×10^2	2.84	4.5
Triethylamine	10.75	2.18	0.3-20	1.55×10^3	3.09	4.7
<i>n</i> -Butylamine	10.68	2.16	0.8-25	1.89×10^3	3.24	4.8
Isopropylamine	10.63	2.17	1.6-16	2.42×10^3	3.38	5.0
Di- <i>n</i> -butylamine	11.25	2.15	0.3-15	2.76×10^3	3.43	5.3

^a D. D. Perrin, "Dissociation Constants of Organic Bases in Aqueous Solution," Butterworths, London, 1965. ^b DABCO, Houdry Process and Chemical Co., Division of Air Products and Chemicals, Inc., Philadelphia, Pa.

Table III: Experimental Conditions, Equilibrium Constants, and Thermodynamic Parameters for the Formation of 1:1 Hydrogen Bonded Complexes of *p*-Chlorophenol in Cyclohexane

Base	<i>p</i> -Chloro-phenol concn $\times 10^3 M$	Base concn $\times 10^3 M$	Wave-length, $m\mu$	$K, l. mol^{-1}$					$-\Delta H,$ kcal/mol	$-\Delta G,$ kcal/mol	$-\Delta S,$ cal/deg
				15°	25°	35°	45°	55°			
Dioxane	2.1-2.2	6.2-190	291.5	82.42	52.72	52.81	44.21	35.07	3.54 ± 0.6	2.44 ± 0.04	3.71
			292.5	75.47	56.46	44.95	41.47	32.45	3.76 ± 0.3	2.41 ± 0.02	4.54
			289	79.11	56.29	48.65	31.87	20.76	3.42 ± 2.4	2.13 ± 0.17	4.33
<i>n</i> -Butylamine	2.1-2.2	0.81-25	285	2156	1728	1603	786.4	426.3	7.50 ± 1.6	4.39 ± 0.11	10.44
			293	2037	2036	1392	722.8	548.9	7.23 ± 1.2	4.37 ± 0.09	9.60
			295	2039	2009	1374	784.4	509.4	6.83 ± 1.2	4.36 ± 0.09	8.30

Results

Spectrophotometric studies of hydrogen bonding were performed in cyclohexane with *p*-chlorophenol and the following amines: *n*-butylamine, morpholine, di-*n*-butylamine, tri-*n*-butylamine, *N*-ethylmorpholine, triethylamine, isopropylamine, triethylenediamine, and tri-*n*-propylamine. Hydrogen bonding with dioxane was also studied for the comparison of an oxygen structure with the nitrogenous bases. Concentrations of *p*-chlorophenol were $2.10-2.18 \times 10^{-3} M$ and 5-8 additions of amine were made in each case ranging in concentration from about 0.1 to 25 times the concentration of the *p*-chlorophenol. All spectra obtained had clear isosbestic points inferring that a simple equilibrium was occurring (Figure 1). The ratio of hydrogen bonded to nonhydrogen bonded form was estimated from the absorbances at 287 and 295 $m\mu$. The information was then plotted using log amine concentration as the *x* axis and log of ratio of hydrogen bonded to nonhydrogen bonded concentration as the *y* axis. The slope of such a plot indicates the number of amines associating with each *p*-chlorophenol, and in each case it provided a clear indication of a 1:1 complex (Figure 2).

The peaks of the *p*-chlorophenol absorption spectrum shift toward the visible range upon the formation of the

hydrogen bond. The magnitude of the shift is not the same for each amine considered. The data obtained for the spectral shift of the 281 $m\mu$ peak are recorded in Table II.

Calculations of the equilibrium constant for the formation of the hydrogen bond were performed on data read at three wavelengths and calculated both as separate and as combined data. The values thus obtained for *K* and log *K* at 25° are reported in Table II.

For the interactions of *p*-chlorophenol with *n*-butylamine and with dioxane the values for log *K* were obtained at several temperatures. ΔH , ΔG , and ΔS were calculated by use of the computer program earlier described, and the results are presented in Table III.

Discussion

The study was restricted to alkyl amines for a practical rather than a theoretical reason. Aromatic amines are not transparent in the region of the spectrum of interest in this investigation.

An interesting pattern emerges as the data are considered. Simple hydrogen bonding is occurring in each case, the conclusion to be drawn from the indication of a 1:1 interaction (slopes of Figure 2) and from the clear isosbestic points (Figure 1). The thermodynamic cal-

culations provide values for ΔH and ΔG that compare well with those obtained previously for other phenol-amine hydrogen-bond formation reactions. The magnitudes of the wavelength shifts (Table II) are seen to correlate with the equilibrium constants of the hydrogen-bond formation reaction. Such shifts should reflect the perturbation of the donor electronic structure given by the formation of the hydrogen bond, hence the bond strength.^{12,25} That these shifts do not correlate with the aqueous pK values of the amines as recorded in the literature is cause for speculation. When a single amine is reacted with a variety of phenols the resulting values for $\log K$ for the reaction were found to be proportional to the aqueous pK of the phenols by Bellon⁹ using triethylamine in cyclohexane, by Denyer, *et al.*,¹³ with the same phenols and trimethylamine, and by Bonnet and Julg¹⁰ using triethylamine, *n*-butylamine, and di-*n*-butylamine in heptane. Gordon²⁶ summarized a linear relationship between infrared stretching frequency shifts and the aqueous pK for bases of similar structure. In our data comparing now a single phenol with various amines the physical characteristics measured by the aqueous pK of the amine did not explain completely the behavior of the system. A plot of $\log K$ for each interaction *vs.* aqueous pK for the particular amine (Figure 3) emphasizes that a linear relationship does in fact exist between these parameters for primary and secondary amines. Conventional tertiary amines (tri-*n*-butylamine, tri-*n*-propylamine, triethylamine) show less tendency to form the hydrogen bond than their aqueous pK would indicate.

We propose that the three alkyl groups of the tertiary amine sterically hinder the interaction of amine and phenol. In support of this proposal we point out that the deviation from the "unhindered" behavior of the primary or secondary amines becomes greater as the length of the alkyl groups becomes greater (butyl > propyl > ethyl). Furthermore in the case of *N*-ethylmorpholine the deviation from "unhindered" behavior is less due to the folding back of two of three alkyl substitutions by ring formation. Finally when we consider the case of a tertiary amine all of whose alkyl substitutions are folded back into rings, triethylenediamine, we find that it falls on the line formed by the primary and secondary amines in the plot.

Coggeshall²⁷ studied the effect steric hindrance by large ortho alkyl groups on the phenol has on self association by hydrogen bonding. The peak at 3.0μ characteristic of the phenol hydroxyl groups shifts toward shorter wavelengths with the formation of the hydrogen bond, and the magnitude of the shift was used as a measure of the strength of the hydrogen bond formed.²⁸ That those phenols having large ortho substituents were hindered in forming hydrogen bonds by self association was indicated by the occurrence of shifts of less than 0.04μ as contrasted with expected shifts of over 0.15μ . This evidence of hindrance correlated with the

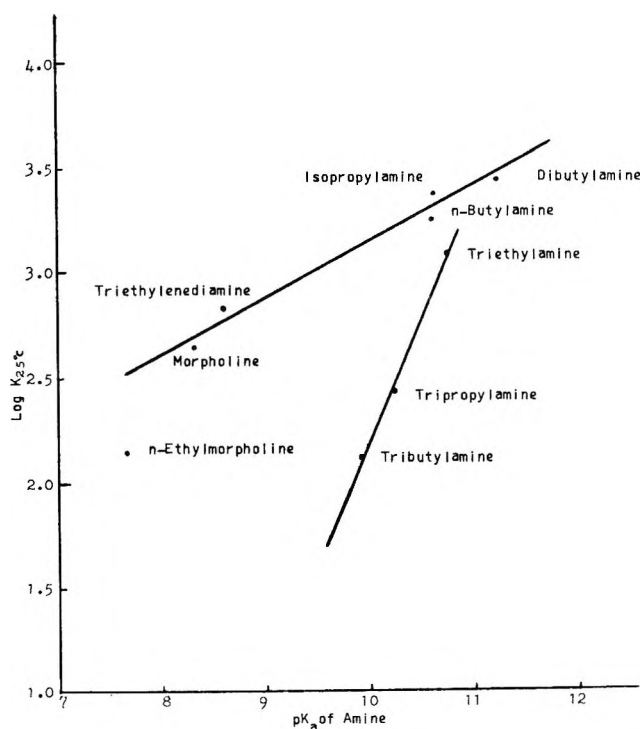


Figure 3. Plot of the log of the equilibrium constant for the formation of the hydrogen bond between *p*-chlorophenol and the indicated amines at 25° *vs.* the aqueous pK_a of the amine.

general loss of phenolic character observed for these compounds exemplified by inability to react with sodium metal in ether solution, insolubility in aqueous alkali, and nonreactivity with alcoholic ferric chloride.²⁹ Parallel work was done later¹¹ with ultraviolet spectroscopy using the same series of hindered and unhindered phenols. A shift of absorbance peaks toward longer wavelengths was observed when comparing the spectra of solutions in the hydrogen bonding solvent ethanol to those taken in isoctane. The spectral shift for hindered phenols was markedly less than for unhindered phenols. In our studies the degree of spectral shift correlated roughly with the log of the equilibrium constant calculated for the formation of the hydrogen bond (Table II).

Studies relating to the steric effects of amine structures in the formation of hydrogen bonds between phenols and amines are not available. Brown^{30,31} has studied the steric characteristics of tertiary amines, however. He noted that in accepting a proton in aqueous solution trimethylamine is a weaker base than tri-

(25) A. Julg and M. Bonnet, *Theoret. Chim. Acta*, **1**, 6 (1962).

(26) J. E. Gordon, *J. Org. Chem.*, **26**, 738 (1961).

(27) N. D. Coggeshall, *J. Amer. Chem. Soc.*, **69**, 1620 (1947).

(28) L. Pauling, *ibid.*, **58**, 94 (1936).

(29) G. H. Stillson, D. W. Sawyer, and C. K. Hunt, *ibid.*, **67**, 303 (1945).

(30) H. C. Brown and M. D. Taylor, *ibid.*, **69**, 1332 (1947).

(31) H. C. Brown and S. Sujiski, *ibid.*, **70**, 2878 (1948).

ethylamine, yet in the vapor state trimethylamine can form a complex with trimethylboron while triethylamine cannot. Support for the interpretation that failure to bond reflects blocking of the binding site on nitrogen was provided when he showed that quinuclidine does form a stable complex with trimethylboron. Earlier³² Perrin and Williams demonstrated that at 80° trimethylamine reacts 61-fold faster than triethylamine with isopropyl iodide. These results all suggest that all three of the alkyl groups of triethylamine are not accommodated to the rear of the molecule and are supportive of our findings.

Dioxane was studied as a nonnitrogenous proton acceptor in the hydrogen bonding interaction for contrast. The results are in general agreement with other such studies performed with phenol and *p*-nitrophenol.^{5,8} It was assumed because of the slope of approximately 1 obtained for the dioxane interaction (Figure 2) and because of the excess of dioxane over *p*-chloro-

phenol in that study that the reaction of two phenols per dioxane reported by Baba and Nagakura³³ was not occurring.

Summary

A detailed study of the hydrogen bonding interactions of *p*-chlorophenol with various nitrogenous proton acceptors and with dioxane was performed. The thermodynamics of the interaction with *n*-butylamine and with dioxane were studied. The relationship between the aqueous *pK* of the amines and the log of the equilibrium constant for the formation of the hydrogen bond was studied. It is proposed that this relationship is linear unless the alkyl groups of the amine hinder the interaction. This occurs with tertiary amines having normal alkyl groups.

(32) M. W. Perrin and E. G. Williams, *Proc. Roy. Soc., Ser. A*, **159**, 162 (1937).

(33) H. Baba and S. Nagakura, *J. Chem. Soc., Jap., Pure Chem. Sect.*, **72**, 3 (1951).

The Interaction of Leghemoglobin with Nitrogen and with Xenon¹

by Gordon J. Ewing* and Lavinel G. Ionescu

Department of Chemistry, New Mexico State University, Las Cruces, New Mexico 88001 (Received July 8, 1971)

Publication costs assisted by the National Science Foundation

The absorption of nitrogen in solutions containing the main components of leguminous hemoglobin has been determined at 5, 15, and 25° in the 0–5 atm pressure range. Nitrogen interacts with both ferri- and ferroleghemoglobin in an approximate 1:1 molar ratio. The thermodynamic quantities for these interactions were determined. For the interaction of nitrogen and ferroleghemoglobin at 15°, $\Delta G^\circ = -4.06 \pm 0.03$ kcal/mol, $\Delta H^\circ = +15.7 \pm 0.1$ kcal/mol, and $\Delta S^\circ = 69 \pm 1$ eu. For the nitrogen ferroleghemoglobin interaction at 15°, $\Delta G^\circ = -3.8 \pm 0.21$ kcal/mol, $\Delta H^\circ = +13 \pm 1$ kcal/mol, and $\Delta S^\circ = 57 \pm 2$ eu. For both interactions ΔC_p was very large, about -1350 cal/(mol deg). The large positive entropy changes, particularly at lower temperatures, suggest a considerable disordering of the leghemoglobin molecule during the absorption of nitrogen. A similar study of the interaction of xenon with leghemoglobin was attempted. While evidence for a weak interaction was obtained, the experimental errors were so large in comparison to the interaction that the stoichiometry could not be determined.

Introduction

Leguminous hemoglobin, legoglobin or leghemoglobin, is the respiratory pigment found in the root nodules of most leguminous plants. The hemoglobin nature of the red pigment was first discovered by Kubo² in 1939 and was confirmed later by the work of Virtanen^{3,4} and of Keilin and Wang.⁵ Leguminous hemoglobin is always found in the interior of nodules growing on the roots and in association with bacteria, usually of the genus *Rhizobium leguminosarum*. Purification of leghemoglobin usually yields two main components of

slightly different molecular weight with values ranging around 16,000–17,000.^{6–8}

(1) This work was partially supported by grant GB 7829 from the National Science Foundation.

(2) H. Kubo, *Acta Phytochim.*, **11**, 195 (1939).

(3) A. I. Virtanen, *Sitzungsber. Finn. Akad. Wiss.*, **12**, 1 (1945).

(4) A. I. Virtanen, *Nature (London)*, **155**, 747 (1945).

(5) D. Keilin and Y. L. Wang, *ibid.*, **155**, 227 (1945).

(6) N. Ellfolk, *Acta Chem. Scand.*, **14**, 609 (1960).

(7) N. Ellfolk, *ibid.*, **14**, 1819 (1960).

(8) N. S. Subba Rao and C. L. Chopra, *J. Sci. Ind. Res.*, **26** (8), 329 (1967); *Chem. Abstr.*, **67**, 113615f (1967).

Virtanen⁹ suggested that nitrogen fixation in legumes is related to the leghemoglobin content in their root nodules. He observed that nitrogen fixation did not take place in nodules not containing the red pigment, and noted that the color of the red active nodules changed to green when the plants cease vegetative growth or were placed in the dark for a few days.¹⁰ This conclusion was supported by Bergersen,¹¹ Keilin and Smith,¹² Proctor and Moustafa,¹³ and many others, all of whom agreed that the capacity of the legume root nodules to fix atmospheric nitrogen is paralleled by the equivalent occurrence of legoglobin in the nodules.

Bauer and coworkers¹⁴⁻¹⁸ proposed some years ago that the leghemoglobin molecule was the site of nitrogen reduction to ammonia. Hanstein¹⁹ gave some support to this theory when he reported that diimide (a possible nitrogen fixation intermediate) formed complexes with respiratory pigments including leghemoglobin. Recent work, however, has indicated that leghemoglobin is only indirectly involved in nitrogen fixation. Bergersen has shown that nitrogen fixation is associated with the bacteroids²⁰ from which two nitrogenase components can be obtained.²¹ Leghemoglobin is found outside the bacteroids and Dilworth²² reports that it is genetically derived from the host legume even though heme synthesis appears to take place in the bacteroid.²³ As this information became known, Bergersen's idea of the role of leghemoglobin evolved from an electron transfer agent,²⁴ to an oxygen scavenger,²⁵ to an oxygen carrier that assists in ventilation of the energy producing sites of the bacteroids.²⁶

While current evidence seems to relegate leghemoglobin to a secondary role in nitrogen fixation, it is interesting to note that Bauer and coworkers reported measuring some interaction between nitrogen molecules and leghemoglobin.¹⁸ Coupling this report with many others that demonstrate that inert gases interact with respiratory pigments^{27,28} has led us to look for interactions between leghemoglobin and N₂ in aqueous solution and between leghemoglobin and xenon. The study involved manometric solubility determinations of the gases in aqueous solutions of both ferri- and ferroleghemoglobin at various temperatures to determine thermodynamic parameters for the process.

Experimental Methods

The solubility of nitrogen in 4-10% aqueous solutions of ferri- and ferroleghemoglobin was determined by a manometric method described in a previous paper²⁸ with one modification: the constant temperature bath was placed in a climatic chamber where the surrounding air temperature was maintained within $\pm 0.5^\circ$ of the bath temperature.

The leguminous hemoglobin employed was prepared from soybean root nodules using a procedure similar to that described by Ellfolk.⁶ The final step in the

procedure was a chromatographic separation on "Cell-ex-D" (a highly purified cellulose powder containing diethylaminoethyl exchange groups that was supplied by Bio-Rad, Richmond, California). The chromatographic method yielded three components. The first two were the major constituents and had, as near as we could tell, identical affinities for nitrogen. A third (minor) component was greenish brown and was discarded. Components 1 and 2 were recombined and the mixture used in most of our determinations. The molecular weights of the leghemoglobin fractions were estimated in two ways. First the iron content of the dry protein was determined using the *o*-phenanthroline method. Assuming one iron atom per molecule we obtained the following molecular weights: component 1, 14,300; component 2, 17,500; and finally for the mixture of the two components used in most of our determinations, 15,600. It should be pointed out that we were unable to crystallize either of the leghemoglobin components. The second method of estimating molecular weight was the gel filtration method described by Andrews.²⁹ Due to a very limited supply of leghemoglobin, this was only tried on a mixture of both components. Using a calibrated Sephadex G-150 column at room temperature, a molecular weight in the vicinity of 17,800 was obtained. These values are in general agreement with the literature values cited above.

In our equilibrium studies the concentration of leghemoglobin was determined by iron analysis coupled with an assigned molecular weight for the molecule. All calculations were carried out using both 16,000 and 17,000 as molecular weights and in every case

(9) A. I. Virtanen, T. Laine, and H. Linkola, *Suom. Kemistilehti, Sect. B*, **18**, 36 (1945).

(10) A. I. Virtanen, J. Jorma, H. Linkola, and A. Linnasalmi, *Acta Chem. Scand.*, **1**, 90 (1947).

(11) F. J. Bergersen, *Biochim. Biophys. Acta*, **50**, 576 (1961).

(12) D. Keilin and J. D. Smith, *Nature (London)*, **159**, 692 (1947).

(13) M. H. Proctor and E. Moustafa, *ibid.*, **197**, 262 (1963).

(14) N. Bauer, *ibid.*, **188**, 471 (1960).

(15) K. Abel and N. Bauer, *Arch. Biochem. Biophys.*, **99**, 8 (1962).

(16) K. Abel, N. Bauer, and J. T. Spence, *ibid.*, **100**, 339 (1963).

(17) K. Abel, *Phytochemistry*, **2**, 429 (1963).

(18) R. G. Mortimer and N. Bauer, *J. Phys. Chem.*, **64**, 387 (1960).

(19) W. G. Hanstein, J. B. Lett, C. E. McKenna, and T. G. Traylor, *Proc. Nat. Acad. Sci.*, **58**, 1314 (1967).

(20) F. J. Bergersen, *Proc. Roy. Soc. Ser. B.*, **172**, 401 (1969).

(21) F. J. Bergersen and G. L. Turner, *Biochim. Biophys. Acta*, **214**, 28 (1970).

(22) M. J. Dilworth, *ibid.*, **184**, 432 (1969).

(23) J. A. Cutting and H. M. Schulman, *ibid.*, **192**, 486 (1969).

(24) F. J. Bergersen, *Bacteriol. Rev.*, **24**, 246 (1960).

(25) F. J. Bergersen, *Nature (London)*, **194**, 1059 (1962).

(26) F. J. Bergersen, *Trans. Int. Congr. Soil Sci.*, **9th**, 1968, **2**, 49 (1968).

(27) A. Wishnia, *Biochemistry*, **8**, 5064 (1969).

(28) S. Maestas and G. J. Ewing, *J. Phys. Chem.*, **74**, 2341 (1970).

(29) P. Andrews, *Biochem. J.*, **91**, 222 (1964).

17,000 gave a somewhat better least-square line in determining equilibrium constants so the results reported below are all based on 17,000 as the effective molecular weight of our leghemoglobin.

Aliquots of 17 ml of the hemoprotein solution were introduced in the reaction vessel, degassed, and then allowed to equilibrate with the reacting gas at the desired temperature. The solution was stirred during the experiments by means of a magnetic bar driven by an immersed stirrer. The average equilibration time required for nitrogen and legoglobin was about 20 hr, but it was dependent on the rate of stirring and the temperature; xenon tended to equilibrate a little faster. Solubility measurements were performed for both ferri- and ferroleghemoglobin at 5°, 15°, and 25° in the 0-5 atm pressure range. Ferroleghemoglobin was obtained by reduction of the oxidized hemoprotein with sodium dithionite, ascorbic acid, and thiourea dioxide.

The amount of gas dissolved in the legoglobin solution was determined by applying the ideal gas law in the form

$$\Delta n = \frac{(\Delta P)(V)}{RT} \quad (1)$$

where Δn = number of moles of gas absorbed, V = volume of gas above solution in ml, R = gas constant 6.24×10^4 mm ml/deg mol, T = temperature in °K, and ΔP = change in pressure in mm. The amount of gas absorbed by the hemoprotein alone was calculated by subtracting the amount dissolved in water at a given pressure and temperature from Δn . This quantity divided by the number of moles of leghemoglobin in the solution (about 10^{-4} mol) gave the amount of gas absorbed per mole of leghemoglobin.

The quantity of nitrogen dissolved in water was calculated for each experimental run from the Henry's law constants determined in this laboratory. The values obtained, *i.e.*, 1070 ± 70 atm/mol (5°), 1410 ± 40 (15°), and 1600 ± 80 (25°), agree well with the results reported by Fox,³⁰ Winkler,³¹ and Pray, *et al.*³² In the xenon experiments, the Henry's law constants determined in this study are 109 ± 10 (5°), 171 ± 8 (15°), and 217 ± 6 (25°) in agreement with the values of Wood and Caputi³³ and Ewing and Maestas.²⁸

Results

The quantity of gas absorbed in various leghemoglobin solutions was measured and corrected by subtracting the amount of that gas calculated to dissolve in the solvent (water).

Nitrogen Legoglobin Interaction. Plots of the number of moles of N₂ absorbed/mole of legoglobin *vs.* the equilibrium pressure at the three temperatures studied are given in Figure 1 for ferrileghemoglobin and in Figure 2 for ferroleghemoglobin obtained by reduction with dithionite. All the curves in Figure 1 exhibit the

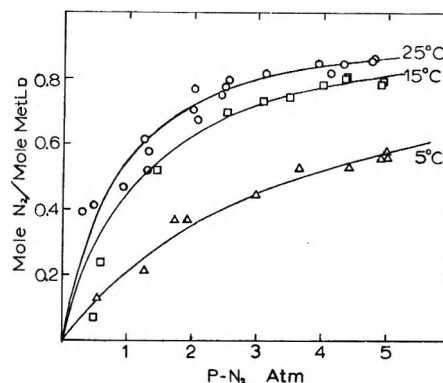


Figure 1. Absorption of N₂ in ferrileghemoglobin. The solid lines represent the theoretical lines for $K_5^\circ = 0.276$, $K_{15}^\circ = 0.859$, $K_{25}^\circ = 1.28 \text{ atm}^{-1}$.

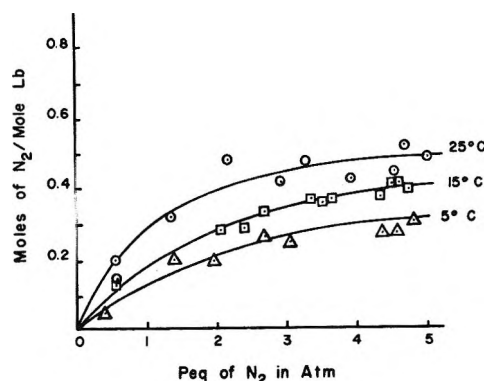


Figure 2. Absorption of N₂ in ferroleghemoglobin. The lines indicate values computed from the equilibrium constants after correction for leghemoglobin denaturation.

leveling off at an approximate molar ratio of 1:1 characteristic of stoichiometric interactions. Figure 3 also includes the results obtained for leghemoglobin reduced with ascorbic acid and thiourea dioxide at 25° along with those for the protein reduced with dithionite. Assuming a 1:1 interaction between nitrogen and ferrileghemoglobin as suggested by the plots in Figure 1, the process can be represented by the following equilibrium

$$K_p = \frac{[N_2 \cdot \text{MetLb}]}{[\text{MetLb}]P_{N_2}} \quad (2)$$

where K_p = equilibrium constant in atm^{-1} , $[N_2 \cdot \text{MetLb}]$ = molal concentration of N₂-MetLb complex, $[\text{MetLb}]$ = molal concentration of unreacted ferrileghemoglobin, and P_{N_2} = equilibrium pressure of nitrogen in atm. A plot of $[N_2 \cdot \text{MetLb}]/[\text{MetLb}]$ *vs.* the equi-

(30) C. J. J. Fox, *Trans. Faraday Soc.*, **5**, 68 (1909); "International Critical Tables," Vol. III, McGraw-Hill, New York, N. Y., 1928, p 256.

(31) L. W. Winkler, *Z. Phys. Chem.*, **9**, 171 (1892).

(32) H. A. Pray, C. E. Schweickert, and B. H. Minnich, *Ind. Eng. Chem.*, **44**, 1146 (1952).

(33) D. Wood and R. Caputi, U. S. Naval Radiological Defense Laboratory, Report TR-988, San Francisco, Calif. 1966.

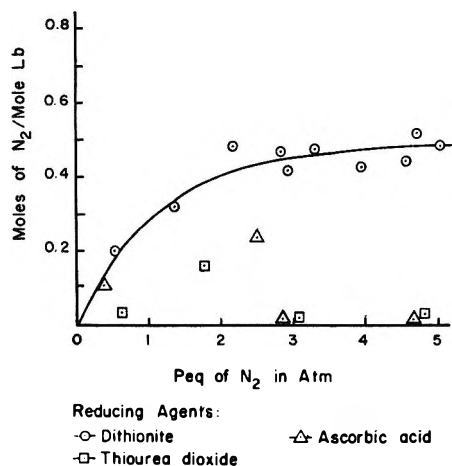


Figure 3. Absorption of N_2 in ferrilegoglobin at 25° showing the effect of various reducing agents. The line is the same curve shown in Figure 3.

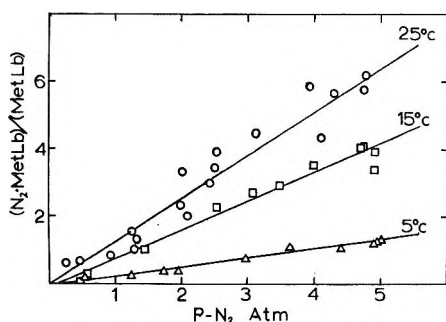


Figure 4. Plots of $(N_2 \cdot \text{MetLb})/(\text{MetLb})$ vs. equilibrium pressure of N_2 assuming a 1-1 interaction. These plots should have K_p for a slope and an intercept of zero. The lines are calculated least-square lines. Values calculated were at 5° , $K_p = 0.276 \pm 0.009 \text{ atm}^{-1}$, intercept = -0.058 ; at 15° , $K_p = 0.859 \pm 0.035 \text{ atm}^{-1}$, intercept = -0.118 ; and at 25° , $K_p = 1.28 \pm 0.05 \text{ atm}^{-1}$, intercept = -0.023 .

Equilibrium pressure of nitrogen should give a straight line with the slope equal to K_p and the intercept equal to zero for good fit of the experimental data.

The concentration ratio $[N_2 \cdot \text{MetLb}]/[\text{MetLb}]$ for ferrilegoglobin was calculated for the interaction at the different temperatures and the equilibrium constants, K_p , were determined by the method of least squares. Plots of these data and their least-squares lines for the ferrilegoglobin- N_2 system are given in Figure 4.

The values of K_p , in units of atm^{-1} , were converted to K_m units of molality $^{-1}$ by multiplying by the experimentally determined Henry's law constants for the solubility of N_2 .

$$K_m = (K_p)(k) \quad (3)$$

This removes the added complication of the solubility of N_2 in water from the thermodynamic calculations. The equilibrium constants obtained for the interaction of nitrogen with ferrilegoglobin in units of atm^{-1} and mol^{-1} are summarized in Table I.

Table I: Equilibrium Constants for N_2 -Legoglobin Interaction

	K_m, mol^{-1}		
	5°	15°	25°
Ferrilegoglobin	295 ± 9	1210 ± 50	2050 ± 80
Ferrilegoglobin	239 ± 46	818 ± 52	1150 ± 160
	K_p, atm^{-1}		
	5°	15°	25°
Ferrilegoglobin	0.276 ± 0.009	0.859 ± 0.035	1.28 ± 0.05
Ferrilegoglobin	0.223 ± 0.043	0.580 ± 0.037	0.716 ± 0.101

As illustrated by the curves in Figures 2 and 3, the interaction between nitrogen and ferrilegoglobin failed to attain an approximate 1:1 ratio, but instead leveled off at approximately 0.5 mol of nitrogen/mole of ferrilegoglobin. This decrease was probably due to the denaturation of the protein by the reducing agents. In fact, the partial denaturation of the reduced samples was confirmed by gel electrophoresis. Whereas an unused solution containing the main components 1 and 2 of ferrilegoglobin and an aliquot exposed to nitrogen gassing gave two distinct bands, the samples of the same solution reduced with dithionite, formamidinesulfonic acid, and ascorbic acid yielded a diffuse band indicative of lack of homogeneity.

Assuming a 1 to 1 interaction the nitrogen-ferrilegoglobin equilibrium is

$$\frac{[N_2 \cdot \text{Lb}]}{[\text{Lb}]P_{N_2}} = K_p \quad (4)$$

where K_p = equilibrium constant in atm^{-1} , $[N_2 \cdot \text{Lb}]$ = concentration of N_2 -Lb complex, $[\text{Lb}]$ = concentration of unreacted ferrilegoglobin, and P_{N_2} = equilibrium pressure of nitrogen in atm.

A system containing some denatured protein should obey the following mass balance equations

$$F_{N_2} = H_{N_2} + B_{N_2} \quad (5)$$

$$F_P = C_{Lb} + C_X \quad (6)$$

where F_{N_2} = total formality of dissolved nitrogen, H_{N_2} = Henry's law solubility of nitrogen in water, B_{N_2} = concentration of nitrogen bound to ferrilegoglobin, F_P = total formality of ferrilegoglobin based on iron analysis, C_{Lb} = concentration of normal ferrilegoglobin, and C_X = concentration of denatured ferrilegoglobin. These expressions transform the equilibrium relationship to

$$\frac{B_{N_2}}{(C_{Lb} - B_{N_2})P_{N_2}} = K_p \quad (7)$$

Substituting for C_{Lb} with the use of equation 6, one obtains

$$\frac{B_{N_2}}{(F_P - C_X - B_{N_2})P_{N_2}} = K_p \quad (8)$$

Equation 8 can also have the form

$$\frac{B_{N_2}}{P_{N_2}} = K_p(F_P - B_{N_2}) - K_p C_X \quad (9)$$

A plot of (B_{N_2}/P_{N_2}) vs. $(F_P - B_{N_2})$ should yield a straight line with the slope equal to K_p in atm^{-1} and the intercept equal to $-K_p C_X$. The terms (B_{N_2}/P_{N_2}) and $(F_P - B_{N_2})$ have been calculated for the interaction of nitrogen with ferrilegoglobin at 5°, 15°, and 25° and the equilibrium constants obtained are listed in Table I together with the results for ferrilegoglobin. The value of C_X obtained from the intercept was not very reliable but at all three temperatures about 40% denaturation ($C_X(100)/F_p$) was obtained.

Plots of $\ln K$ or $1/T$ were not linear indicating that the interaction enthalpy was not a constant. Recognizing that calculations of a curve for which only three points are available is shaky, we present the following thermodynamic calculations. Following a rather common approach of presenting ΔH° as a power series in T , then ΔG° takes the form

$$\Delta G^\circ = A + BT + CT \ln T + DT^2 + ET^3 + \dots \quad (10)$$

In the present study only three temperatures are available so only the first three constants in the ΔG° equation can be determined. Using these first three terms, the other thermodynamic properties of interest can be determined

$$\Delta S = -\frac{d\Delta G}{dT} = -B - C - C \ln T \quad (11)$$

$$\Delta H = \Delta G - T\Delta S = A - CT \quad (12)$$

$$\Delta C_p = d\Delta H/dT = -C \quad (13)$$

Using these equations, the thermodynamic properties given in Table II were obtained.

Xenon Leghemoglobin Interaction. An attempt was made to determine the possible existence of an interaction between leghemoglobin and xenon, since xenon has been reported to interact stoichiometrically with

various respiratory pigments.^{27,28,34-37} The experimental data based on a large number of measurements indicate that the solubility of xenon is higher in leghemoglobin solutions than water. However, the amount of xenon bound to leghemoglobin is of the same order of magnitude as the experimental error making it impossible to determine the stoichiometry of the interaction.

Discussion

The most salient characteristic of the nitrogen-leghemoglobin interaction is that it is of a weak nature, probably similar to the alkane binding sites reported by Wishnia.^{27,38} Also the marked similarity of the thermodynamic parameters for the iron II and iron III legoglobin-N₂ interaction suggest that they are probably identical. Contrary to what one might expect, N₂, which is isoelectronic with CO, does not seem to form an iron-ligand bond in this case. The weak nature of the binding of nitrogen to leghemoglobin is substantiated by the positive (unfavorable) heats of reaction and the absence of spectral shifts between the nitrogenated and nonnitrogenated protein. The standard free energy values obtained for the interaction lie between the more negative free energies for the binding of strong ligands such as CO and O₂ and the more positive values for the Xe-Mb interaction. The standard entropy changes for the interaction were generally large and positive suggesting a considerable disordering of the legoglobin molecule during the absorption of the nitrogen molecule particularly at lower temperatures. The drop in interaction entropies and enthalpies as the temperature increases suggests that temperature increases may have the same disordering effect that nitrogen does. If this were true, it is likely that ΔC_p would also change quite rapidly with temperature. We recalculated the thermodynamic quantities using a power series for the free energy,³⁸ $\Delta G^\circ = A + BT + CT^2$. Here one gets $\Delta C_p = -2CT$ and the value for ΔC_p changes about 7% over the temperature range studied. Measurements at other temperatures are needed to really evaluate the ΔC_p term and its dependence on temperature. The exceptionally large value for ΔC_p also invites further study. Large conformation changes in hemoproteins during the absorption of gases have been observed by Keyes and Lumry³⁹ and have also been suggested by Maestas and Ewing.²⁸ X-Ray studies by Schoenborn⁴⁰ have in-

Table II: Thermodynamic Parameters for the N₂-Legoglobin Interaction Determined from the Temperature Dependence of the Equilibrium Constant, K_m

	T , °C	ΔG° , cal/mol	ΔS , eu	ΔH , kcal/mol	ΔC_p , cal/(mol deg)
Ferrilego- globin	5	-3140 ± 20	116	29.1	-1350
	15	-4060 ± 30	69	15.7	-1350
	25	-4520 ± 20	23	2.2	-1350
Ferrilego- globin	5	-3030 ± 110	106	26.3	-1380
	15	-3840 ± 30	57	12.5	-1380
	25	-4170 ± 60	9	-1.3	-1380

(34) B. P. Schoenborn, *Nature (London)*, **208**, 760 (1965).

(35) B. P. Schoenborn, H. Watson, and J. C. Kendrew, *ibid.*, **207**, 28 (1965).

(36) B. P. Schoenborn and C. L. Nobbs, *Mol. Pharmacol.*, **2**, 491 (1966).

(37) S. Maestas and G. J. Ewing, *Curr. Mod. Biol.*, **1**, 148 (1967).

(38) A. Wishnia, *Biochemistry*, **8**, 5070 (1969).

(39) M. Keyes and R. Lumry, *Fed. Proc. Fed. Amer. Soc. Exp. Biol.*, **27**, 895 (1968).

(40) B. P. Schoenborn, *Nature (London)*, **214**, 1120 (1967).

licated the presence of conformational changes during the binding of cyclopropane by sperm whale myoglobin.

The results of the present study indicating a 1:1 stoichiometric interaction between N_2 and legoglobin exclude the mechanism proposed by Bauer and Abel for nitrogen fixation.¹⁵⁻¹⁷ The N_2 molecule appears to be bonded to one molecule of ferroleoglobin and not to a dimer formed by two ferroleoglobin molecules as suggested by Abel.¹⁷

Also, our attempts to find evidence for a second point of attachment were futile. The present study indicates that the affinity of legoglobin for N_2 is very low, while that for oxygen is known to be very high. In fact, the affinity of ferroleoglobin for O_2 is the highest mea-

sured for any hemoprotein. Appleby has determined spectrophotometrically equilibrium constants ranging from 15 to 25 mm^{-1} for the half-oxygenation of different ferroleoglobin components at 20°. ⁴¹ The value obtained for half-nitrogenation of ferroleoglobin at 25° in the present study was $1.03 \times 10^{-3} mm^{-1}$. This large difference in the affinity for the two gases suggests that legoglobin is probably more concerned with the transport of O_2 than with N_2 and that the new mechanism for nitrogen fixation proposed by Bergersen²⁰ is probably correct. We suggest, however, that leghemoglobin may be an ancillary nitrogen carrier.

(41) C. A. Appleby, *Biochim. Biophys. Acta*, 60, 226 (1962).

Activity Coefficient of *n*-Heptane in 4,4'-Dihexyloxyazoxybenzene Liquid Crystal

by Henry T. Peterson, Daniel E. Martire,* and Wolfgang Lindner

Chemistry Department, Georgetown University, Washington, D. C. 20007 (Received August 23, 1971)

Publication costs assisted by Georgetown University

A McBain-Bakr apparatus, utilizing a Cahn RG electrobalance, has been constructed for the static measurement of activity coefficients. The activity coefficient of *n*-heptane in the nematic phase (90.1°) of 4,4'-dihexyloxyazoxybenzene over a mole fraction range from 0.008 to 0.080 is reported. Good agreement is found between the extrapolated infinite dilution activity coefficient and that obtained by gas-liquid chromatography.

Recently gas-liquid chromatography (glc) was used to study the infinite dilution thermodynamic solution properties of nonmesomorphic solutes in nematogenic liquid crystals.¹ Earlier experiments² had strongly supported the concept of a two phase (bulk gaseous phase and bulk liquid crystal phase) glc partitioning process, and, hence, of negligible surface effects at both the carrier gas-liquid crystal and liquid crystal-solid support interfaces, provided that a liquid crystal film thickness of greater than about 1000 Å was present. This finding produced initial confidence that the thermodynamic solution quantities measured by glc would reflect true bulk liquid crystal behavior. Nevertheless, no independent measurements were available for comparison. Since glc is a particularly advantageous and rapid method for such thermodynamic studies,^{1,3} it was deemed important to confirm the glc activity coefficient results through comparison with values measured by a well-defined static method on bulk liquid crystal.

Accordingly, a vacuum apparatus, based on the McBain-Bakr approach⁴ for obtaining absorption isotherms of volatile solute-nonvolatile solvent systems, and utilizing a Cahn RG electrobalance as the weighing device,⁵ was used to determine the activity coefficients of *n*-heptane over a limited concentration range in the nematogenic liquid crystal 4,4'-dihexyloxyazoxybenzene (DHAB). Measurements were carried out at 90.1° which is in the nematic region of DHAB.²

This system was selected from those previously studied by glc in this laboratory for the following reasons. First, the large vapor pressure of heptane at the maximum allowable temperature of the mercury manom-

- (1) L. C. Chow and D. E. Martire, *J. Phys. Chem.*, **75**, 2005 (1971).
- (2) L. C. Chow and D. E. Martire, *ibid.*, **73**, 1127 (1969).
- (3) D. E. Martire, P. A. Blasco, P. F. Carone, L. C. Chow, and H. Vicini, *ibid.*, **72**, 3489 (1968).
- (4) J. W. McBain and A. M. Bakr, *J. Amer. Chem. Soc.*, **48**, 690 (1926).
- (5) R. L. Pecsok and B. H. Gump, *J. Phys. Chem.*, **71**, 2202 (1967).

eter, 50°, enables accurate measurement of the absolute pressure of heptane over a reasonable pressure range. Second, at temperatures greater than 115°, the "mechanical noise" due to aerodynamic effects increased rapidly with increasing temperature. Thus, the high temperature of the nematic-isotropic liquid transition (128.2°) precluded accurate studies in the isotropic liquid state. The DHAB, obtained from Frinton Laboratories, was purified by oxidation with hydrogen peroxide followed by three recrystallizations from ethanol.⁶ Differential scanning calorimetry measurements utilizing a Perkin-Elmer DSC-1B indicated a minimum purity of 99.4%.² The *n*-heptane (Phillips Petroleum Co., Research Grade, 99.78% pure) was distilled twice under high vacuum to remove any dissolved air and was stored over sodium. The Cahn electrobalance was placed in a sealed glass vessel which was thermostated to prevent condensation of the heptane. The liquid crystal solvent was placed in a sample pan and suspended from the balance arm into a jacketed tube heated to 90.1° by a Haake NBE circulating bath. The temperature was measured to ±0.03° with a calibrated Anschuetz thermometer suspended with its bulb 1 in. from the sample pan. The mole fraction of heptane in solution was determined from the initial weight of the DHAB (210 mg) and the observed weight pickup (measurable to ±2 μg) at the equilibrium vapor pressure. The equilibrium time per datum point was 3–4 hr. The vapor pressure of the system was measured to ±0.03 Torr with a thermostated mercury manometer and a cathetometer (Gaertner Scientific Co.). The usual precautions were taken to minimize systematic errors.

Solute activity coefficients corrected for the non-ideality of the vapor phase were calculated from the well known equation

$$\log \gamma_2 = \log \left(\frac{p}{x_2 p_2^0} \right) - \frac{(B_{22} - V_2^0)(p_2^0 - p)}{2.3RT} \quad (1)$$

where p is the equilibrium vapor pressure of the system, x_2 is the solution mole fraction of heptane, p_2^0 is the saturated vapor pressure of heptane, B_{22} is the second virial coefficient of heptane calculated from the McGlashan-Potter⁷ corresponding states equation, and V_2^0 is the molar volume of heptane determined from the density given by the law of rectilinear diameters. All of the physical properties of heptane needed for the above calculations were taken from Dreisbach.⁸

A least-squares fit of the experimental results to the empirical equation

$$\log \gamma_2 = Ax_1^2 + Bx_1^3 \quad (2)$$

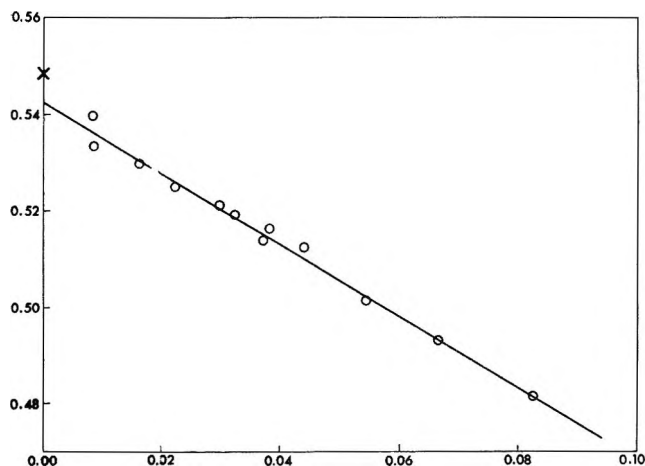


Figure 1. Logarithm of the activity coefficient ($\log \gamma_2$) vs. solution mole fraction (x_2) for *n*-heptane in DHAB at 90.1°. Key: ○, static measurements from this study; ×, gas-liquid chromatography result (ref 1); —, least-squares fit to $\log \gamma_2 = Ax_1^2 + Bx_1^3$, with $A = 0.8995$ and $B = -0.3572$.

which satisfies the Gibbs-Duhem relation, where x_1 is the solvent mole fraction, yielded the results: $A = 0.8995$ and $B = -0.3572$. Figure 1 clearly illustrates the experimental results and the goodness of fit to eq 2. The average standard deviation of $\log \gamma_2$ from the curve is 0.0016. For comparison with the glc results, which are infinite dilution values, we let $x_1 \rightarrow 1$ and find that $\gamma_2^\infty = 3.49$, with an estimated probable error of ±0.02. A glc value of $\gamma_2^\infty = 3.54$ was found,¹ with a quoted probable error of 1.5% or ±0.05. Hence, the values agree within the combined error of the two different measurements. It is important to note that discrepancy between the static and glc values cannot be attributed to a systematic error due to solute adsorption at the carrier gas-liquid crystal interface in the glc experiment, because the observed difference is in the wrong direction.⁹ Therefore, all evidence being considered, it appears that the assumptions made in the glc measurement of thermodynamic solution properties in nematogenic liquid crystals are valid.

Acknowledgment. This work was supported by the U. S. Army Research Office, Durham, N. C.

(6) M. J. S. Dewar and R. S. Goldberg, *Tetrahedron Lett.*, **24**, 2717 (1966).

(7) M. L. McGlashan and D. J. B. Potter, *Proc. Roy. Soc., Ser. A*, **267**, 478 (1962).

(8) R. R. Dreisbach, *Advan. Chem. Ser.*, **22**, 24 (1959).

(9) D. E. Martire, "Progress in Gas Chromatography," J. H. Purnell, Ed., Interscience, New York, N. Y., 1968, pp 93–120.

Solubilities of Gases in Liquids at Elevated Temperatures. Henry's Constants for Hydrogen, Methane, and Ethane in Hexadecane, Bicyclohexyl, and Diphenylmethane

by P. M. Cukor and J. M. Prausnitz*

Department of Chemical Engineering, University of California, Berkeley, California (Received March 5, 1971)

Publication costs assisted by the Petroleum Research Fund

A new gas solubility apparatus has been constructed for studying gas-liquid equilibria at elevated temperatures. Henry's constants for methane, ethane, and hydrogen in *n*-hexadecane, bicyclohexyl, and diphenylmethane are reported for the temperature range 25–200°. In these three solvents, the solubility of hydrogen rises and that of ethane falls with increasing temperature. The solubility of methane goes through a flat minimum in the region near 150°.

Although accurate knowledge of gas solubilities in liquids is of primary importance in many chemical processes, no widely applicable theory exists for their prediction. Further, experimental solubilities at temperatures well removed from 25° are scarce and predictions at elevated temperatures are generally unreliable. In order to build a theory of gas solubility and to understand more fully the effects of temperature on gas-liquid equilibria, an apparatus has been constructed for the determination of gas-liquid equilibria at elevated temperatures.

The experimental technique is based on the method of Dymond and Hildebrand.¹ Solvent is continuously circulated through a vapor space containing a measured quantity of solute. A gas burette is used to determine precisely the number of moles of solute added. The equilibrium total pressure is measured using a fused-quartz Bourdon tube as a null instrument. This tube is mounted in a furnace whose temperature is maintained at 235°. Nitrogen is used to balance exactly the pressure which the system gases exert on the Bourdon tube; the nitrogen pressure is read at 44° on a precision pressure gage. This procedure prevents solvent vapors from distilling into the pressure gage. The pressure-measuring equipment, manufactured by Texas Instruments, Inc., is accurate to within ±0.04 mm Hg over a pressure range of 0–1000 mm Hg. Details of the design and operation of the gas solubility apparatus are given elsewhere.^{2,3}

Data Reduction

The solubility is calculated by determining n' , the number of moles of solute in the vapor phase at equilibrium. This value is subtracted from n° , the number of moles of gas added as calculated from the gas burette readings. The difference is Δn , the number of moles of gas which has dissolved. The number of moles of

solvent, n_s , is calculated from the solvent density and the calibrated volume of the liquid chamber less the quantity of solvent removed due to expansion of the liquid with temperature. The (mole fraction) solubility at the partial pressure of the solute is given by

$$x_2 = \frac{\Delta n}{n_s + \Delta n} \quad (1)$$

Since x_2 is small, Henry's constant for solute 2 dissolved in solvent 1 is calculated from

$$H_{2,1} = \frac{f_2^L}{x_2} \quad (2)$$

To determine n' , the vapor-phase mole fraction y_i was calculated from the equations

$$f_1^L = f_1^V \quad (3)$$

$$f_2^L = f_2^V \quad (4)$$

$$f_1^L = (1 - x_2)P_1^s \quad (5)$$

$$f_1^V = \varphi_1(1 - y_2)P \quad (6)$$

$$f_2^L = H_{2,1}x_2 \quad (7)$$

$$f_2^V = \varphi_2y_2P \quad (8)$$

where f is the fugacity, L and V refer to the liquid and vapor phase respectively, φ is the vapor-phase fugacity coefficient, P_1^s is the solvent vapor pressure at the system temperature, and P is the total pressure. The virial equation, truncated after the second virial coefficient, was used to relate φ_1 and φ_2 to temperature,

(1) J. Dymond and J. H. Hildebrand, *Ind. Eng. Chem., Fundam.*, **6**, 130 (1967).

(2) P. M. Cukor and J. M. Prausnitz, *Ind. Eng. Chem., Fundam.*, **10**, 638 (1971).

(3) P. M. Cukor, Dissertation, University of California, Berkeley, 1971.

pressure, and composition. Virial coefficients were calculated using the correlation of Pitzer and Curl.⁴ Mixing rules suggested by Prausnitz and Chueh⁵ were used to determine the cross coefficient B_{12} .

The solution of equations 1-8 for the compositions x_2 and y_2 is a trial-and-error procedure. Only the temperature and pressure are known. A reasonable first approximation is to assume that $(1 - y_2) = P_1^s/P$.

Since P , T , and V , the volume of the vapor space, are known, n' may be calculated from

$$n' = \frac{y_2 P V}{RT + B_M P} \quad (9)$$

where B_M , the mixture virial coefficient, is given by

$$B_M = (1 - y_2)^2 B_{11} + 2y_2(1 - y_2)B_{12} + y_2^2 B_{22} \quad (10)$$

The liquid phase composition is calculated from equation 1 and Henry's constant is determined from equations 2 and 8. Fugacity coefficients are calculated using the initial values of y . A new approximation for $(1 - y_2)$ is calculated by combining equations 5-8 to obtain

$$1 - y_2 = \frac{\varphi_2 P - H_{2,1}}{\varphi_2 P - \varphi_1 P H_{2,1}/P_1^s} \quad (11)$$

Substitution of the new value of y_2 in eq 9 permits a second approximation to be made for x_2 and $H_{2,1}$. New values of the vapor composition are calculated until the values of the vapor and liquid compositions remain constant.

In reviewing the literature on gas solubilities we found that when calculating solubility many authors assume that the vapor-phase mole fraction of solvent is given by $(1 - y_2) = P_1^s/P$. This assumption can lead to serious error in reported values of x_2 either if the solubility is so low that $n^o \approx n'$ or if the vapor pressure of the solvent is more than about one-tenth of the total pressure at the system temperature. For example, our calculations for the system hydrogen-bicyclohexyl at 475°K ($P \sim 861$ mm, $P_1^s \sim 320$ mm) show that $H_{2,1} = 1197$ atm if we assume that $(1 - y_2) = P_1^s/P = 0.37079$. However, the correct value of $(1 - y_2)$ is 0.38956 which results in a value of $H_{2,1}$ of 964 atm. This represents an error of nearly 24% in the solubility whereas the error in $(1 - y_2)$ is only 4.8%. We expect, therefore, that many solubility data which have been reported previously may be too low.

Results

The experimental values of Henry's constants are shown in Figures 1, 2, and 3. The accuracy of these results is estimated to be at least 2% and probably closer to 1%.⁶ For each gas, the value of H increases (solubility decreases) as the solvent structure changes from (paraffinic) hexadecane to (naphthenic) bicyclohexyl to (aromatic) diphenylmethane. This behavior is in agreement with the trends predicted by Scatchard-

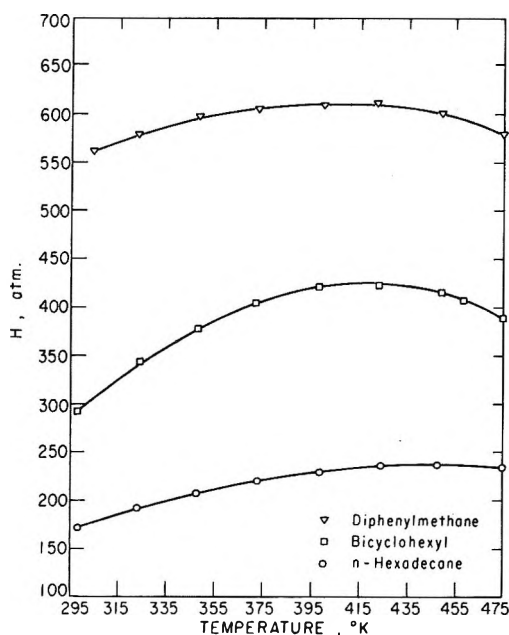


Figure 1. Henry's constants for methane.

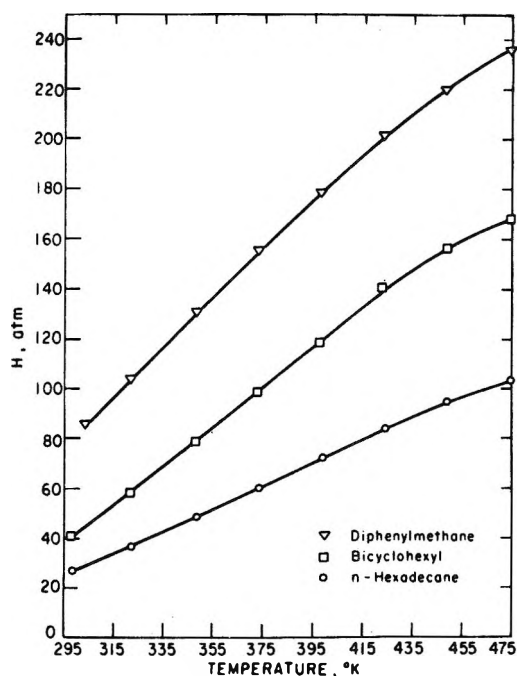


Figure 2. Henry's constants for ethane.

Hildebrand theory: the difference between the solubility parameters (shown in Table IV) of each of the

(4) K. S. Pitzer and R. F. Curl, Jr., *J. Amer. Chem. Soc.*, **79**, 2369 (1957).

(5) J. M. Prausnitz and P. L. Chueh, "Computer Calculations for High-Pressure Vapor-Liquid Equilibria," Prentice-Hall, Englewood Cliffs, N. J., 1968.

(6) Tabulated Henry's constants (Tables I-III) will appear following these pages in the microfilm edition of this volume of the journal. Single copies may be obtained from the Business Operations Office, Books and Journals Division, American Chemical Society, 1155 Sixteenth St., N. W., Washington, D. C. 20036, by referring to author, title of article, volume, and page number. Remit check or money order for \$3.00 for photocopy or \$2.00 for microfiche.

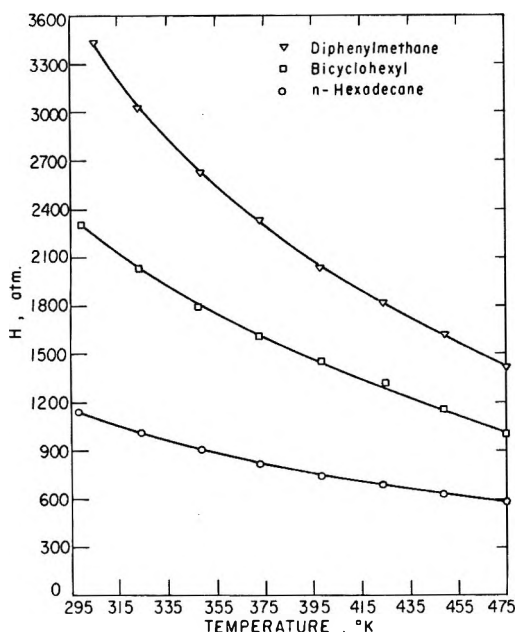


Figure 3. Henry's constants for hydrogen.

Table IV: Solubility Parameters at 25°

Fluid	δ (cal/cm ³) ^{1/2}
H ₂	3.25 ^a
CH ₄	5.68 ^a
C ₂ H ₆	6.60 ^a
<i>n</i> -C ₁₆ H ₃₄	7.46
(<i>c</i> -C ₆ H ₁₁) ₂	8.16
(C ₆ H ₆) ₂ CH ₂	9.08

^a Taken from J. M. Prausnitz and F. H. Shair, *AIChE J.*, 7, 682 (1961).

three gases and a given solvent is smallest in the case of *n*-hexadecane and greatest in the case of diphenylmethane.

The temperature coefficient of Henry's constant is given by

$$\left(\frac{\partial \ln H_{2,1}}{\partial T}\right)_P = -\frac{\Delta \bar{h}_{2,1}^\infty}{RT^2} \quad (12)$$

where

$$\Delta \bar{h}_{2,1}^\infty \equiv \bar{h}_2^{L^\infty} - h_2^G \quad (13)$$

where $\bar{h}_2^{L^\infty}$ is the partial molar enthalpy of solute at infinite dilution in solvent 1 and h_2^G is the enthalpy of ideal gas 2 at the same temperature. The natural logarithms of the experimental Henry's constants were fitted to a second-degree polynomial in temperature and differentiated. Table V summarizes the values of $\Delta \bar{h}_{2,1}^\infty$ for the nine systems at several temperatures.

The temperature dependence of Henry's constant is similar for a given solute in all three solvents. For hydrogen, Henry's constant falls as the temperature increases; for ethane Henry's constant increases with

Table V: Heats of Solution, $\Delta \bar{h}_{2,1}^\infty$ (cal/mol)

<i>T</i> , °K	Methane	Ethane	Hydrogen
in <i>n</i> -Hexadecane			
325	-705	-2389	840
400	-420	-2166	1213
450	14.1	-1514	1484
in Bicyclohexyl			
325	-1002	-2579	792
400	-284	-2140	1608
450	661	-1218	2380
in Diphenylmethane			
325	-304	-1934	1135
400	-0.92	-1691	1575
450	387	-1094	1873

temperature at a decreasing rate as the temperature rises. It appears that at temperatures somewhat higher than 475°K the value of *H* may go through a maximum.

For methane the enthalpy of solution changes sign at about 425°K and Henry's constant goes through a maximum. It is likely that this behavior may be observed for any gas in any nonpolar solvent provided the range of temperature is chosen properly. For example, Prausnitz and Chueh⁵ report values of Henry's constants as a function of temperature for a number of systems. Table VI summarizes the values of *T_m*, the temperature for which a maximum in the Henry's constant is observed, for several gases dissolved in *n*-heptane. As the critical temperature of the solute falls so does *T_m*.

Table VI: Temperature *T_m* Where Henry's Constant Is a Maximum for Solutes in *n*-Heptane

Solute	<i>T_m</i> , °K	Critical temp., °K
N ₂	353	126
CH ₄	411	191
C ₂ H ₆	450	305

The critical temperature of hydrogen is so low that *T_m* for hydrogen is far below the temperatures considered here. For hydrogen, therefore, Henry's constant declines as the temperature increases.

Recently Preston and Funk⁷ have shown that for simple nonpolar systems maxima in Henry's constant do not occur if the data are plotted at constant liquid volume rather than at constant pressure. For (essentially) constant-pressure measurements, Henry's

(7) G. T. Preston, E. W. Funk, and J. M. Prausnitz, *Phys. Chem. Liquids*, 2, 193 (1971).

constant may go through a maximum because the liquid expands with rising temperature, favoring the dissolution of gas molecules.

Acknowledgment. The authors are grateful to the

National Science Foundation, to the donors of the Petroleum Research Fund, and to Gulf Oil Research and Development Company for financial support, and to Cecil Chappelow for assistance in calibrating the apparatus.

Gas Solubilities from a Perturbed Hard-Sphere Equation of State

by P. M. Cukor and J. M. Prausnitz*

Department of Chemical Engineering, University of California, Berkeley, California (Received March 5, 1971)

Publication costs assisted by the Petroleum Research Fund

Solubilities of gases in liquids are correlated using a binary hard-sphere equation of state coupled with a van der Waals attraction term. The correlation is useful for rough estimates of solubilities in nonpolar systems over a wide range of temperature.

Following the work of Longuet-Higgins and Widom,¹ Lebowitz² has proposed that the equation of state of a binary mixture is given by

$$\frac{P}{\rho kT} = \chi_m(\xi_m, x) - \frac{a_m \rho_m}{kT} \quad (1)$$

where P is the pressure, T is the absolute temperature, ρ_m is the number density, k is Boltzmann's constant and

$$\xi_m = \frac{\pi}{6} [x_1 d_1^3 + x_2 d_2^3] \rho_m \quad (2)$$

where x_i is the mole fraction and d_i is the hard-sphere diameter of component i . The constant a_m , characterizing the attractive forces in the mixture, is given by

$$a_m = a_{11}x_1^2 + 2a_{12}x_1x_2 + a_{22}x_2^2 \quad (3)$$

where a_{ij} characterizes attractive forces between molecule i and molecule j . The function χ_m is given by Lebowitz.² Following the work of Pierotti³ and Snider and Herrington,⁴ we have used equation 1 to obtain an expression for Henry's constant. Upon equating the chemical potential of component 2 in the (ideal) gas phase to that in the liquid phase as $x_2 \rightarrow 0$, we obtain

$$\ln \frac{H_{2,1}v_1}{RT} = f\left(\xi_1, \frac{d_2}{d_1}\right) - \frac{2A_{12}}{RTv_1} \quad (4)$$

where $H_{2,1}$ is Henry's constant of solute 2 in solvent 1, R is the gas constant, v_1 is the molar volume of the solvent, and A_{12} is a characteristic binary constant which, to a fair approximation, is independent of temperature. The function f is given by

$$f\left(\xi_1, \frac{d_2}{d_1}\right) = -\ln(1 - \xi_1) + \xi_1 \chi(\xi_1) \left(\frac{d_2}{d_1}\right)^3 + \frac{1}{2} \left(\frac{3\xi_1}{1 - \xi_1}\right)^2 \left(\frac{d_2}{d_1}\right)^2 + \frac{3\xi_1}{1 - \xi_1} \left[\left(\frac{d_2}{d_1}\right)^2 + \frac{d_2}{d_1}\right] \quad (5)$$

where ξ_1 is obtained from equation 2 with $x_2 = 0$.

Experimental Henry's constants⁵⁻⁷ for thirteen gases in sixteen solvents were reduced to obtain values of A_{12} . Hard-sphere diameters for the solvents were obtained from the group contribution method of Bondi⁸ for van der Waals volumes and the equation

$$d_i = 1.47V_{wi}^{1/3} \quad (6)$$

where V_{wi} is the van der Waals volume of molecule i in cm^3/mol and d_i is the hard-sphere diameter in \AA . van der Waals volumes for solute molecules are given in Table I.

From the van der Waals theory of simple, binary mixtures, we expect A_{12} to be related to $(T_c T_{c2}) / (P_{c1} P_{c2})^{1/2}$ where T_c is the critical temperature and P_c is the critical pressure.

(1) H. C. Longuet-Higgins and B. Widom, *Mol. Phys.*, **8**, 549 (1964).

(2) J. L. Lebowitz, *Phys. Rev. A*, **133**, 895 (1964).

(3) R. L. Pierotti, *J. Phys. Chem.*, **67**, 1840 (1963).

(4) N. S. Snider and T. H. Herrington, *J. Chem. Phys.*, **47**, 2248 (1967); see also L. A. K. Staveley, *ibid.*, **53**, 3136 (1970), and R. C. Miller, *ibid.*, **55**, 1613 (1971).

(5) J. M. Prausnitz and P. L. Chueh, "Computer Calculations for High-Pressure Vapor-Liquid Equilibria," Prentice-Hall, Englewood Cliffs, N. J., 1968.

(6) J. H. Hildebrand and R. L. Scott, "Regular Solutions," Prentice-Hall, Englewood Cliffs, N. J., 1962.

(7) P. M. Cukor, Dissertation, University of California, Berkeley, 1971.

(8) A. Bondi, "Physical Properties of Molecular Crystals, Liquids, and Glasses," Wiley, New York, N. Y., 1968.

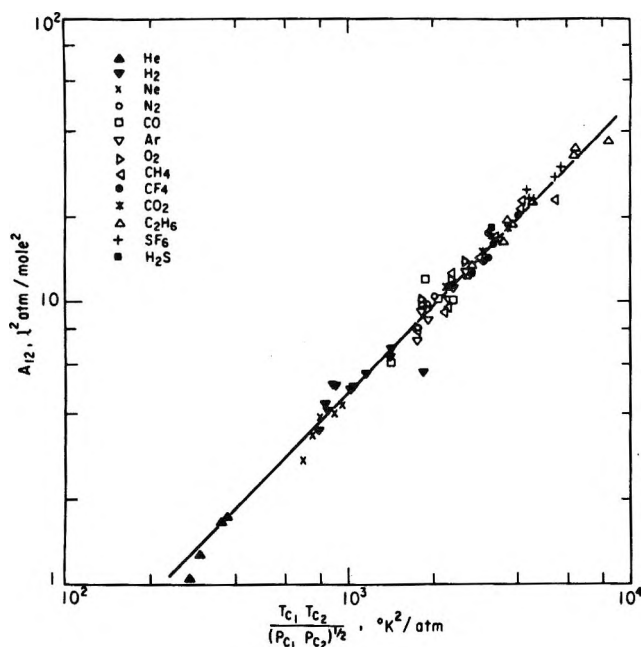


Figure 1. van der Waals interaction constants for liquid (1)-gas (2) systems.

Table I: van der Waals Volumes for Solute Molecules^a

Solute	V_w , cm ³ /mol
H ₂	6.5
He	4.8
Ne	7.5
Ar	12.5
N ₂	15.0
CO	13.0
CO ₂	24.0
O ₂	14.1
CH ₄	17.1
CF ₄	32.0
C ₂ H ₆	29.0
SF ₆	45.0
H ₂ S	24.0

^a V_w values were adjusted so as to minimize scatter in the correlation shown in Figure 1.

The results of data reduction are shown in Figure 1; the data show that the binary constant A_{12} is given by

$$\log A_{12} = \alpha \log \frac{T_{c1} T_{c2}}{(P_{c1} P_{c2})^{1/2}} + \beta \quad (7)$$

with $\alpha = 1.0787$ and $\beta = -5.9081$; T_c is in °K, P_c in atmospheres, and A_{12} in l.² atm/mol². Equation 7 may be used to estimate Henry's constants in non-polar systems over an appreciable range of temperature.

Only pure-component critical properties and the solvent density are required. In data reduction we used the correlation of Bondi and Simkin⁹ to calculate the densities of the pure solvents as a function of temperature.

A statistical comparison of predicted and measured Henry's constants for eight systems is given in Table II. A total of 27 data points over a temperature range of 298–505°K were used in the comparison. Experimental data for the systems included in Table II were *not* used in establishing the constants α and β of equation 7. Table II also reports results calculated by

Table II: Comparison of Predicted and Measured Henry's Constants

	Temp range, °K	Mean dev. ^a %	Max dev. %
This work	298–505	23.1	46
Shair's correlation	298–505	24.4	89

$$^a \text{Mean deviation} = \frac{1}{n} \sum_{i=1}^n |H_i(\text{exp}) - H_i(\text{calcd})|$$

(n is the number of data points.)

Shair's method based on solubility parameters.¹⁰ For the systems considered the two correlations give nearly equal average deviations between calculated and experimental results. Unfortunately, neither the hard-sphere equation nor Shair's correlation gives uniformly accurate estimates of Henry's constants. In some cases the former method is more reliable; in others the latter is better.

However, the individual deviations between calculated and experimental solubilities suggest that:

1. The hard-sphere model tends to give poor results when the solvent molecule is a straight chain of more than seven atoms.
2. For slightly polar solvents (*e.g.*, ethyl ether) the hard-sphere model tends to be superior to Shair's correlation.
3. Shair's correlation gives a temperature dependence on solubility which is stronger than that of the hard-sphere model. Both correlations, however, can predict maxima in plots of Henry's constant *vs.* temperature, consistent with experiment.

Acknowledgment. For financial support the authors are grateful to Gulf Research and Development Company, to the National Science Foundation, and to the donors of the Petroleum Research Fund.

(9) A. Bondi and D. J. Simkin, *AIChE J.*, **6**, 191 (1960).

(10) J. M. Prausnitz and F. H. Shair, *ibid.*, **7**, 682 (1961).

Solvent Dependence of Charge-Transfer Spectra of

1-(*p*-Substituted benzyl)-4-carbomethoxypyridinium Iodides

by Raymond A. Mackay, Edward J. Poziomek,* and David W. Reger

Department of Chemistry, Drexel University, Philadelphia, Pennsylvania 19104
and the Physical Research Laboratory, Edgewood Arsenal, Maryland 21010 (Received May 13, 1971)

Publication costs assisted by Edgewood Arsenal

A study of the first (long wavelength) iodide ion charge-transfer (c-t) band has been performed for a series of 1-(*p*-substituted benzyl)-4-carbomethoxypyridinium iodide salts in a variety of solvents. The methoxy, chloro, nitro, and unsubstituted derivatives were used to examine the effect on the c-t transition of both electron-donating and -withdrawing groups. Spectra were obtained for each salt in chloroform, methylene chloride, acetone, methyl formate, acetonitrile, 2-propanol, and ethanol. These solvents were chosen to cover a wide range of both polarity and ionizing power, and both protic and aprotic media. For these 1-benzylpyridinium ions, interaction is possible between the benzene and pyridinium rings, as has been demonstrated by recent studies of intramolecular c-t bands in various 1-(substituted benzyl)-4-cyanopyridinium salts. The spectral band energies are compared with that of 1-ethyl-4-carbomethoxypyridinium iodide, a similar salt, from which *Z* values are obtained. The dependence of the c-t band energy on the solvent, substituent, and intramolecular interaction is discussed.

Introduction

The first (long wavelength) charge-transfer (c-t) band of 1-ethyl-4-carbomethoxypyridinium iodide is the basis of *Z* values, an empirical measure of solvent polarity.¹ Variations in the alkyl group on the pyridinium nitrogen have been shown to have only small effects on the c-t transition energy.^{2,3} When the 1-substituent is a *p*-substituted benzyl group, a small but significant effect on the c-t energy (E_t) is observed in *cis*-1,2-dichloroethylene.⁴ In addition, E_t is linearly related to the Hammett σ constant of the para substituent.

It has also been shown that 1-benzylpyridinium salts containing strongly electron-donating groups on the benzyl ring exhibit an intramolecular c-t interaction.^{4,5} This band arises from donation of electron density from the benzyl to the pyridinium rings, the intensity being related to the orbital coefficient at the C(1) position of the benzene ring. It was therefore of interest to extend the measurements to a range of solvents for different *p*-benzyl substituents, one of which should possess both inter- and intramolecular c-t bands at comparable frequencies.

Results

The c-t band positions for the *p*-OCH₃, -H, -Cl, and -NO₂ substituted 1-benzyl-4-carbomethoxypyridinium iodide salts in various solvents are given in Table I. The corresponding solvent *Z* values are included for comparison.⁶ Pyridinium iodide salts are susceptible to I₃⁻ formation but no difficulties were experienced except in the hydroxylic solvents. The I₃⁻ has an absorption band at 360 nm with an extinction coefficient of about 30,000 l. mol⁻¹ cm⁻¹; trace amounts interfere

with the determination of the c-t band position. In alcohols, with the pyridinium iodides studied, the ease of triiodide formation was in the order NO₂ ≥ Cl > H > OCH₃. For the methoxy derivative, a freshly recrystallized sample in isopropyl alcohol or ethanol was free of I₃⁻. A few bands are included in Table I for the H and Cl derivatives, but these results are questionable. The addition of thiosulfate did not help; in any event the addition of thiosulfate also gives rise to an absorption band in the region of interest.

The methoxy derivative possesses both inter- and intramolecular c-t bands. The c-t transition energies of 1-(*p*-methoxybenzyl)-4-carbomethoxypyridinium iodide and perchlorate in selected solvents are given in Table II. In methylene chloride, the second iodide to pyridinium c-t band is also observed.⁷ The intramolecular c-t band is not observed due to the low extinction coefficient (~380 l. mol⁻¹ cm⁻¹) as compared with those of iodide c-t bands (~1000 and 1500 for the first and second bands, respectively) in this solvent.

For all solvents except the alcohols and CH₃CN,

- (1) E. M. Kosower, *J. Amer. Chem. Soc.*, **80**, 3253 (1958).
- (2) E. M. Kosower and J. A. Skorcz, *ibid.*, **82**, 2195 (1960).
- (3) J. W. Verhoeven, I. P. Dirx, and Th. J. de Boer, *Tetrahedron*, **25**, 3395 (1969).
- (4) E. M. Kosower, D. Hofmann, and K. Wallenfels, *J. Amer. Chem. Soc.*, **84**, 2755 (1962).
- (5) J. W. Verhoeven, I. P. Dirx, and Th. J. de Boer, *Tetrahedron*, **25**, 4037 (1969).
- (6) E. M. Kosower, "Introduction to Physical Organic Chemistry," Wiley, New York, N. Y., 1968, p 301.
- (7) For a discussion of the nature of the two c-t bands for iodide to pyridinium see R. A. Mackay, J. R. Landolph, and E. J. Poziomek, *J. Amer. Chem. Soc.*, **93**, 5026 (1971).

Table I: First C-t Band Energies of 1-(*p*-Substituted benzyl)-4-carbomethoxy-pyridinium Iodides in Various Solvents^a

Substituent	CHCl ₃ (0.13 M EtOH)	<i>cis</i> -CHCl- CHCl ^b	CH ₂ Cl ₂	CHCl ₃	Acetone	Methyl formate	CH ₃ CN	<i>i</i> -PrOH	EtOH
OCH ₃	65.6	63.3	64.6	64.0	65.7	69.6	<i>c</i>	87.5	89.4
H	64.3	62.8	64.3	63.7	65.4	69.3	71.1	(76.4) ^d	(79.4) ^d
Cl	65.3	62.3	63.9	63.4	65.3	69.0	70.2	<i>e</i>	(78.0) ^d
NO ₂	67.7	60.9	63.0	62.7	65.2	68.5	<i>c</i>	<i>e</i>	<i>e</i>
<i>Z</i> value	63.2	63.3	64.2	65.6	65.7	69.6	71.3	76.3	79.6

^a Band energies in kcal mol⁻¹. *Z* values from ref 6. ^b Reference 4. ^c Poorly defined shoulder. ^d Approximate value since the I₃⁻ interference could not be entirely eliminated. ^e Excessive I₃⁻ interference.

Table II: C-t Spectra of 1-(*p*-Methoxybenzyl)-4-carbomethoxy-pyridinium Iodide and Perchlorate in Various Solvents^a

Solvent	Iodide			Perchlorate ^c
	<i>E</i> ₁₁ (ε) ^b	<i>E</i> ₁₂ (ε) ^c	<i>E</i> ₁₃ (ε) ^d	
CH ₂ Cl ₂	64.6 (1000)	...	92.9 (1500)	84.6 (370)
(CH ₃) ₂ CO	65.7	86.6	...	86.9 (450)
<i>i</i> -PrOH	...	87.5	...	87.5
EtOH	...	89.4 (480)	...	89.0 (450)

^a Energies in kcal mol⁻¹. ^b First I⁻→py⁺ c-t band. ^c Intramolecular c-t band. ^d Second I⁻→py⁺ c-t band.

Table IV: Transition Energies from Nujol Mull Spectra of Iodide Salts^a

<i>p</i> -Benzyl substituent	Whatman No. 1 filter paper	CaF ₂ plates
OCH ₃ ^b	85.4, 98.0	...
OCH ₃	74.2, 103.2	69.2, 95.9
H	70.9, 100.5	63.7, 93.8
Cl	73.7, 100.5	69.1, ^c 94.8
NO ₂	67.8, 104.6	63.2, 94.8

^a Energies in kcal mol⁻¹. ^b Perchlorate salt. ^c Broad band (±0.5 kcal mol⁻¹).

plots of the first iodide c-t band energy (*E*₁) vs. the Hammett σ constant (σ_p) were linear. From these, effective ρ values were calculated using the line slope. A set of dimensionless ρ values, obtained from the slope divided by *RT*, is reported in Table III.

Table III: Effective ρ Values^a

Solvent	ρ (correlation coefficient)	Dielectric constant
<i>cis</i> -CHClCHCl	3.85 (0.997)	9.3
CH ₂ Cl ₂	2.58 (0.997)	9.1
CHCl ₃	2.08 (0.999)	4.8
Methyl formate	1.75 (0.997)	8.5
(CH ₃) ₂ CO	0.73 (0.899)	20.7

^a The ρ are defined here as $\rho = (1/RT)(dE_1/d\sigma_p)$.

Finally, band maxima from Nujol mull spectra of the iodide salts on Whatman No. 1 filter paper and between CaF₂ plates are given in Table IV.

Discussion

The correlation of *E*₁ with σ_p gives rise to negative ρ values with all of the solvents examined for which sufficient data were available. There does not seem to be any specific relationship between the ρ values and the *Z* value or the dielectric constant of the solvent. There may be some trend toward larger ρ values in less polar solvents. This may be rationalized on the basis that

the electrostatic interaction of a polar solvent molecule with a solute substituent will decrease its electron-donating or withdrawing capability.

As was pointed out earlier,⁵ the intramolecular c-t interaction takes place through overlap between orbitals on C₁ of the benzene ring and the pyridinium nitrogen. This requires that the planes of the two rings be 109.5° (the tetrahedral angle) to each other. For the case in which one of the rings is rotated to a dihedral angle of 90°, there should not be intramolecular interaction between the π systems of the donor (*p*-methoxybenzene) and acceptor (4-carbomethoxy-pyridinium ion).

In solution both rings may rotate about the benzyl carbon, creating an equilibrium distribution of rotamers. This is confirmed by the presence of an intramolecular c-t band for the *p*-methoxy derivative (perchlorate salt), as given in Table II. This same band should be present for the other derivatives, but at considerably higher energy since the para substituents are more electron-withdrawing than methoxyl. The intramolecular c-t transitions with expected extinction coefficients of the order of 500 l. mol⁻¹ cm⁻¹ would be buried under the more intense pyridinium and benzene ring absorptions.

A comparison of the solid-state spectra for the *p*-methoxybenzylpyridinium iodide and perchlorate (Table IV) shows that the intramolecular band is present in the perchlorate salt at 85.4 kcal mol⁻¹, while the low energy intermolecular c-t band is at 74.2 kcal mol⁻¹ in

the iodide on Whatman No.1 filter paper. Unless the phenyl rings are rotating in the solid as in solution, which seems unlikely, the presence of the 85.4-kcal mol⁻¹ band implies that the dihedral angle is about 109° in the perchlorate salt. This band is not observed in the iodide salt, which would imply a 90° dihedral angle. However, in solution, the intramolecular c-t band is weaker than the iodide intermolecular c-t band; here also it may be "buried" between the 74.2 and 103.2 kcal mol⁻¹ bands. We have generally observed that in solid-state spectra, band intensities tend to level out, and bands which in solution have extinction coefficients differing by a factor of 30–40 become comparable in intensity. This observation indicates that the band may well be absent rather than buried, but clearly no definite conclusion can be reached with regard to the dihedral angle in the case of the iodide salt.

The rather large difference in E_t for the same mull when placed either on filter paper or between CaF₂ plates (Table IV) for all of the compounds studied indicates that the solid sample is interacting with the filter paper in some manner. The higher E_t observed with filter paper indicates that this matrix is a more polar medium than is the solid.

The *p*-methoxybenzylpyridinium iodide compound possesses two intermolecular c-t bands that arise from the interaction between the iodide ion (donor) and the pyridinium ion (acceptor). One of these bands occurs at lower energy than the intramolecular band, whereas the other one is found at higher energy. It is possible that some interaction between the inter- and intramolecular c-t bands may exist. This will depend on the overlap of the orbitals involved and therefore on the position of the iodide ion.

In all of the nonhydroxylic solvents, the energy of the first iodide c-t band for the *p*-methoxy derivative is about the same as the corresponding solvent Z value (Table I). The intramolecular c-t band is also present, as shown by the data for the same salt in acetone (Table II). The band is not observed in CH₂Cl₂ because of the high extinction coefficients of the two surrounding iodide c-t bands. Thus, in the nonhydroxylic solvents, both the inter- and intramolecular c-t bands are present. They appear to have no appreciable effect on each other; *i.e.*, they do not interact. In the alcohols, however, the first iodide c-t band is apparently absent,⁸ and only the intramolecular c-t band is observed.

A comparison of the spectra of the *p*-methoxy iodide and perchlorate salts in ethanol and 2-propanol shows that the anion has essentially no effect on the intramolecular c-t band with respect to both position and extinction coefficient. Comparison with Z values shows that the iodide c-t band should have been observed at about 76.3 and 79.6 kcal mol⁻¹ in 2-propanol and ethanol, respectively. These are about 10 kcal mol⁻¹ lower than the energy of the intramolecular c-t

band. Although there appears to be no interaction between the iodide and benzene c-t bands, the iodide to pyridinium c-t band is not observed in alcohol, whereas the benzene to pyridinium c-t band remains unaffected.

In dissociating solvents such as acetone and ethanol, the apparent extinction coefficient of the iodide band decreases because of a decrease in the number of pyridinium iodide contact ion pairs. For example, at concentrations of about 10⁻³ *M* in acetone, the effective ϵ of the iodide band is about 350 l. mol⁻¹ cm⁻¹; it is possible that ϵ in ethanol could be somewhat less. It would have to drop considerably below 100, however, to be obscured by a band 10 kcal mol⁻¹ higher in energy with an ϵ of 450. Furthermore, the ϵ in 2-propanol should be greater than in acetone.^{9,10} In 2-propanol the iodide and benzene c-t bands should be of comparable intensity.

Problems with I₃⁻ formation by the other benzyl derivatives in alcohol (Table I) make it difficult to determine whether the "disappearance" of the iodide band occurs with all of the compounds. However, the data suggest that the iodide c-t band is present for all except the methoxy derivative.

An attempt was also made to see if the iodide c-t band could be observed for the methoxy derivative in the presence of an excess of iodide. Tetrahexylammonium iodide was added to 2-propanol solutions of both the *p*-methoxybenzyl iodide and perchlorate salts. Difference spectra were recorded using a solution of the methoxy perchlorate salt (same concentration) as reference. In the presence of a large excess of iodide ion, a very weak band could be observed at about 375 nm (76.3 kcal mol⁻¹). By comparison with the 2-propanol Z value this corresponds to the iodide c-t band. If more iodide salt was added in an attempt to intensify this band, I₃⁻ invariably formed.

Because the iodide c-t band arises only from contact ion pairs (not solvent separated ion pairs) it would seem that the failure to observe the iodide c-t band for the methoxy derivative in alcohols is caused by the lack of an appreciable fraction of contact ion pairs. Thus, a specific combination of the benzyl group, methoxy moiety, and hydroxylic solvent is preventing

(8) The second iodide c-t band would not be observed in alcohol since it would fall under the ring absorptions.

(9) This is illustrated by the calculated values (ref 10) of the dissociation constant (K_D) and extinction coefficient (ϵ) for 1-methyl-4-cyanopyridinium iodide (1) as compared with 1-(*p*-methoxybenzyl)-4-carbomethoxypyridinium iodide (2) in acetone

Compound	Solvent	$K_D (M \times 10^3)$	ϵ (l. mol ⁻¹ cm ⁻¹)
1	2-Propanol	0.31	748
1	Ethanol	2.13	429
1	Acetone	2.64	816
2	Acetone	1.79	639

(10) R. A. Mæckay and E. J. Poziomek, *J. Amer. Chem. Soc.*, **92**, 2432 (1970).

Table V: 1-(*p*-X-Benzyl)-4-carbomethoxypyridinium Iodides

	Mp, °C		Analyses, %					
	Found ^a	Reported	Calcd			Found		
			C	H	N	C	H	N
H	141-143	165-168	47.3	4.0	3.9	47.4	4.1	4.2
Cl	168-170	173-175	43.2	3.4	3.6	43.5	3.5	3.9
NO ₂	153-154	152-154	42.0	3.3	31.7 ^b	42.0	3.5	31.4 ^b
OCH ₃	135-136	136-140
OCH ₃ ^c	136-137	142-144

^a Corrected. Decomposition usually observed. ^b Iodide. ^c Perchlorate.

contact or intimate approach of the iodide and pyridinium ions. Essentially all of the ion pairs present are of the solvent-separated type.

Summary. A study of the c-t spectra of a series of 1-(*p*-substituted benzyl)-4-carbomethoxypyridinium iodide salts in a variety of solvents revealed that a linear correlation exists between electronic transition energy and the σ_p of the *p*-benzyl substituent. In all the nonhydroxylic solvents, the benzyl salts behave with respect to band position and intensity as might be predicted from solvent *Z* values. For the *p*-methoxybenzyl salt, an intramolecular c-t band is present; but it does not interact with the intermolecular iodide to pyridinium transitions. In alcohols, the pyridinium iodide ion pairs are of the solvent-separated type.

Experimental Section

Spectrophotometric Data. Absorption data were obtained on a Cary 14 spectrophotometer; 1-cm quartz cells were used with the solvent as reference. Solid-state spectra were obtained as Nujol mulls, either on Whatman No. 1 filter paper (with Nujol on the paper as reference) or between CaF₂ plates (with air as reference).

Compounds. All of the benzylpyridinium salts were reported previously.⁴ Our procedures of synthesis differed slightly. In general 21 g of the appropriate

benzyl chloride, 11 g of methyl isonicotinate (freshly redistilled), and 50 ml of acetone were heated overnight in a 200-ml capped polymer bottle at 75°. In the case of the *p*-methoxy derivative, the reaction solution was allowed to stand at room temperature for 3 days rather than in the oven at 75°. The mixture was allowed to cool to room temperature. The precipitate was collected and then dissolved in methanol containing 25 ml of methyl iodide. (This procedure of converting chloride pyridinium salts to iodide analogs was reported previously.¹¹) The solution was allowed to stand overnight.

Diethyl ether was added to precipitate the iodide salt. The compound was ground in acetone at room temperature. The final product was obtained by filtration and then dried in a desiccator (protected from light) under vacuum (Table V). All operations were performed in hoods because of the lachrymatory property of the benzyl chlorides. The benzylpyridinium perchlorate was prepared by reaction of the iodide with silver perchlorate in absolute ethanol.

Analyses. Elemental analyses were performed by the Analytical Research Department, Chemical Research Laboratory, Edgewood Arsenal.

(11) E. J. Poziomek, Ph.D. Thesis, University of Delaware, June 1961; *Diss. Abstr.*, 22, 1831 (1962).

Kinetics of Vibrationally Hot Propane Produced by Methylene

Insertion into Ethane¹

by F. B. Growcock, W. L. Hase, and J. W. Simons*

Chemistry Department, New Mexico State University, Las Cruces, New Mexico 88001 (Received September 13, 1971)

Publication costs borne completely by The Journal of Physical Chemistry

The reaction of ethane with excited singlet state methylene radicals produced *via* the photolysis of diazomethane at 4358 Å, yields chemically activated propane with an average energy of 119.4 ± 2.0 kcal/mol. The measured decomposition rate coefficient for the energized propane is $(4.7 \pm 1.2) \times 10^8$ sec⁻¹. This rate is correlated by RRKM and absolute rate theory calculations with thermal *A* factors in the range $10^{16.7}$ – $10^{17.2}$ sec⁻¹ and radical recombination rate coefficients in the range 2.2×10^9 – 5.8×10^9 l. mol⁻¹ sec⁻¹, which are substantially lower than estimates of experimental recombination rates for CH₃ + C₂H₅. A dilemma of possible theoretical significance exists.

Introduction

Pyrolysis studies of propane have shown that the primary reaction in the decomposition of propane is C–C bond rupture giving methyl and ethyl radicals.^{2–4} However, quantitative measurements of rate parameters in the thermal studies have suffered from surface reactions and complicating secondary reactions which accompany the primary process. Chemical activation provides a technique for studying unimolecular reactions at low temperatures, which minimizes these complicating processes. Chemically activated propane may be produced by radical and atom combinations^{5–7} and by singlet methylene insertion.^{7–10}

Recent studies of the decomposition rates of chemically activated alkanes (C₄–C₆) have shown *via* RRKM theory and absolute rate theory that correlations of these decomposition rates with estimated radical recombination rates are barely possible, even though the extremes of high critical energies for decomposition, "tight" radical models, and free-internal-rotor activated complex models are used.^{11,12} In the case of $n\text{-C}_4\text{H}_{10} \rightarrow 2\text{C}_2\text{H}_5$ the correlation was not possible. An extension of these previous studies to the chemically activated propane molecule is of interest. Estimates of the CH₃ + C₂H₅ recombination rate are more reliable than for the larger radicals, and fewer adjustments in complex and radical models are possible.

Diazomethane was photolyzed at 4358 Å to yield excited ¹CH₂, which inserts into the C–H bonds of ethane to yield "hot" propane. The decomposition of excited propane in this system can be measured unambiguously with the aid of oxygen as a triplet and doublet radical scavenger¹³ and an internal standard to monitor total reaction.¹⁴ The excitation energy, *E*^{*}, of the "hot" propane can be determined by addition of *cis*-2-butene and determining *E*^{*} for "hot" *cis*-

1,2-dimethylcyclopropane¹⁵ in a propane bath. The addition of *cis*-2-butene serves as an *E*^{*} monitor.

Experimental Technique

Procedure. Approximately 15% oxygen was added to 2:1:0.6 ethane–*n*-butane–diazomethane mixtures. These were photolyzed at pressures ranging from 0.8 to 107 cm Hg for 2–6 hr, depending on total pressure. A summary of the reactant concentrations is given in Table I.

In the *E*^{*} monitor system ethane–*cis*-2-butene–isobutane–diazomethane mixtures in ratios of 2:0.5:0.5:0.6 with ~15% added oxygen were photolyzed at pressures ranging from 0.2 to 171 cm for 3–14 hr. Several

(1) The National Science Foundation is gratefully acknowledged for financial support.

(2) (a) D. A. Leathard and J. H. Purnell, *Proc. Roy. Soc. Ser. A.*, **305**, 517 (1968); (b) D. A. Leathard and J. H. Purnell, *ibid.*, **306**, 553 (1968).

(3) K. J. Laidler, N. H. Sagert, and B. W. Wojciechowski, *ibid.*, **270**, 242 (1962).

(4) K. J. Laidler, *et al.*, *ibid.*, **270**, 254 (1962).

(5) E. W. R. Steacie and D. S. Dewar, *J. Chem. Phys.*, **8**, 571 (1940).

(6) E. Gorin, W. Kauzman, J. Walter, and H. Eyring, *ibid.*, **7**, 633 (1939).

(7) B. S. Rabinovitch and D. W. Setser, *Advan. Photochem.*, **3**, 1 (1964).

(8) R. L. Johnson, W. L. Hase, and J. W. Simons, *J. Chem. Phys.*, **52**, 3911 (1970).

(9) G. Z. Whitten and B. S. Rabinovitch, *J. Phys. Chem.*, **69**, 4348 (1965).

(10) J. W. Simons, C. J. Mazac, and G. W. Taylor, *ibid.*, **72**, 749 (1968).

(11) W. L. Hase and J. W. Simons, *J. Chem. Phys.*, **54**, 1277 (1971).

(12) W. L. Hase, R. L. Johnson, and J. W. Simons, *Int. J. Chem. Kinet.*, **4**, 1 (1972).

(13) S. G. Lias and P. Ausloos, *J. Chem. Phys.*, **43**, 2748 (1965).

(14) F. H. Dorer and B. S. Rabinovitch, *J. Phys. Chem.*, **69**, 1973 (1965).

(15) J. W. Simons and G. W. Taylor, *ibid.*, **73**, 1274 (1969).

Table I: Ethane-*n*-Butane-Diazomethane-Oxygen System

$P_{C_2H_6}^a$	$P_{n-C_4H_{10}}$	$P_{CH_2N_2}$	$1/4 P_{O_2}$	$\frac{[IP]^b}{[C_3H_8]}$
5.18	2.58	1.35	0.35	2.73
4.65	2.21	1.37	0.384	2.94
4.78	2.32	1.37	0.551	3.36
6.36	2.99	1.81	0.447	2.44
6.61	3.11	1.81	0.532	2.60
7.39	3.49	2.08	0.48	2.41
7.72	3.19	2.09	0.50	2.37
10.14	4.70	2.72	0.74	2.04
15.03	6.78	3.79	0.936	1.71
15.4	7.30	4.50	1.195	1.51
20.9	9.10	5.40	1.34	1.47
33.9	16.6	8.90	2.46	1.20
40.9	20.1	12.7	3.18	1.25
61.5	28.4	22.8	5.05	1.02
93.3	41.9	24.2	9.12	0.831
105.5	47.6	25.3	6.11	0.854
127.1	59.3	36.2	10.15	0.979
260.45	137.3	70.85	17.8	0.786
346.5	156.9	85.5	23.1	0.733
370.0	173.2	94.5	10.43	0.897
709.0	365.0	210.7	44.5	0.788
914.0	449.0	266.0	64.0	0.836

^a All pressures are in units of Torr. ^b Product ratios are molar and are normalized by the reactant ratio.

experiments were performed where ethane:(*cis*-2-butene + isobutane) was 3:1, but the product ratios did not vary with this change. The total product yield was less than 1% in all cases, so that secondary reactions were negligible. The data for this system are reported in Table II.

Materials. Matheson lecture-bottle ethane and *n*-butane were purified by gas chromatography and vacuum distillation at 77°K, and analyses showed them to be relatively free of impurities (less than 1%). Diazomethane was prepared by the reaction of *N*-methyl-*N*-nitroso-*p*-toluenesulfonamide with an anhydrous saturated solution of NaOH in 1,4-butanediol and was stored in di-*n*-butyl phthalate at liquid nitrogen temperature. The nitrogen impurity in commercial-grade Linde oxygen was reduced by distillation at 77°K. Analysis by glpc of the purified O₂ showed only trace impurities.

Isobutane and *cis*-2-butene were Matheson CP grade and were purified by glpc and vacuum distillation.

Apparatus. All gas-handling was performed in a standard high-vacuum system using greaseless stopcocks. Reaction products were analyzed on an Aerograph 90-P3 gas chromatograph which used a thermistor detector. The photolysis radiation was that from a Hanovia No. 673A, 500-W medium-pressure mercury arc lamp which employed No. 7-56(5850) and No. 3-73(3389) Esco Products glass filters to isolate the 4358-Å band.

Analyses. All product amounts were determined by

glpc analyses after the product mixture was vacuum distilled at 77°K to rid the reaction vessel of O₂ and other noncondensables.

The condensables from the ethane + *n*-butane experimental runs were passed through a 25 ft dibutyl phthalate-firebrick column with a 4 ft attachment of didecyl phthalate on firebrick. The oxygenated products did not come off the column; the only products observed with retention times greater than *n*-C₄H₁₀ were isopentane and *n*-pentane. The condensables from the ethane-*cis*-2-butene-isobutane monitor system were first passed through a 25 ft column of AgNO₃ on firebrick to separate C₄ and C₅ olefins from the system, for these species interfered with analyses of *cis*- and *trans*-1,2-dimethylcyclopropane (CDMC and TDMC). The eluents were subsequently trapped and passed through the first column mentioned above.

The dibutyl phthalate column was calibrated periodically to determine the sensitivity of the detector toward reactant and product molecules. The absolute sensitivities of the products cancelled out in the determination of the rate constants, and only their ratio was needed for calculation of the high-pressure intercepts. Samples of the reactants were also checked periodically to reaffirm the absence of impurities. In addition, dark reactions at several pressures for both the propane and *E** monitor systems were run and analyzed to show that no interfering products were present.

The effective pressure of O₂ was taken to be 1/4 its actual value, as the collisional deactivation efficiency of O₂ was taken to be about 0.25.¹⁶ Any error resulting from this choice has a negligible effect on the total collision frequency.

The collision diameters used for all reactant species were those obtained from the application of a Lennard-Jones potential to their transport properties.^{17,18} These lead to collision frequencies of $\omega_{C_2H_6} = (1.95 \times 10^7)P_{C_2H_6}$, $\omega_{n-C_4H_{10}} = (2.12 \times 10^7)P_{n-C_4H_{10}}$, $\omega_{CH_2N_2} = (1.85 \times 10^7)P_{CH_2N_2}$, and $\omega_{O_2} = (1.41 \times 10^7)0.25P_{O_2}$. The collision frequencies for the species present in the *E** monitor system are $\omega_{C_2H_6} = (2.08 \times 10^7)P_{C_2H_6}$, $\omega_{i-C_4H_{10}} = (2.07 \times 10^7)P_{i-C_4H_{10}}$, $\omega_{cis-2-C_4H_8} = (2.14 \times 10^7) \cdot P_{cis-2-C_4H_8}$, $\omega_{CH_2N_2} = (1.92 \times 10^7)P_{CH_2N_2}$, and $\omega_{O_2} = (1.53 \times 10^7)0.25P_{O_2}$.

Experimental Results

Unimolecular Decomposition of C₃H₈* from ¹CH₂ + C₂H₆. The major primary processes in this system are the two insertion reactions given by reactions 1-2'.

(16) G. H. Kohlmaier and B. S. Rabinovitch, *J. Chem. Phys.*, **38**, 1709 (1963); J. D. Rynbrandt and B. S. Rabinovitch, *J. Phys. Chem.*, **74**, 1679 (1970).

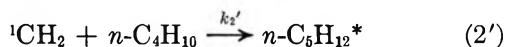
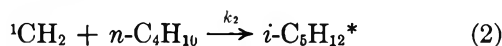
(17) J. O. Hirschfelder, C. F. Curtiss, and R. B. Bird, "Molecular Theory of Gases and Liquids," Wiley, New York, N. Y., 1954.

(18) S. C. Chan, B. S. Rabinovitch, J. T. Bryant, L. D. Spicer, T. Fujimoto, Y. N. Lin, and S. P. Pavlou, *J. Phys. Chem.*, **74**, 3160 (1970).

Table II: Ethane-*cis*-2-Butene-Isobutane-Diazomethane-Oxygen System

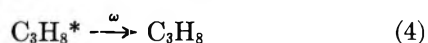
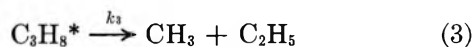
$P_{C_2H_6}^a$	P_{C-2-B}	P_{IB}	$P_{CH_2N_2}$	$1/4 P_{O_2}$	P_{tot}	$\frac{[CDMC]^b}{[TDMC]}$	$\frac{[IP]^{b,c}}{[CDMC] + [TDMC]}$
892	224	234	292	66.2	1708.2	...	1.49
110.2	39.8	13.2	27.7	7.45	198.35	7.66	1.54
99.3	22.7	22.8	29.0	7.63	181.43	...	1.37
84.0	28.8	9.29	21.9	5.68	149.7	5.94	1.68
60.85	14.04	13.81	19.43	4.14	112.3	4.68	...
39.5	10.1	10.1	11.7	2.82	74.22	3.38	...
30.9	7.10	7.30	9.21	2.26	56.77	2.93	1.62
14.79	3.54	3.45	3.98	0.893	26.65	1.82	1.74
14.40	3.47	3.40	4.41	1.192	26.87	1.38	...
4.71	1.17	1.15	1.32	0.36	8.71	0.94	2.42
4.69	1.13	1.09	1.38	0.349	8.639	0.99	2.64
4.09	1.035	1.095	0.74	0.30	7.26	0.94	2.71
3.39	1.23	0.421	0.915	0.248	6.204	...	2.88
2.76	0.516	0.509	0.611	0.155	4.551	0.87	3.65
2.21	0.505	0.534	0.611	0.1794	4.039	0.55	3.64
1.98	0.662	0.287	0.379	0.146	3.454	0.78	3.81
1.71	0.3473	0.3473	0.402	0.1067	2.9133	0.60	4.55
1.54	0.545	0.1734	0.401	0.1006	2.760	0.72	4.26

^a All pressures are in units of Torr. ^b All product ratios are molar. ^c The expression has been normalized by the reactant ratio.



An asterisk denotes a species in the ground electronic state with excess vibrational-internal rotational energy. The pentanes are collisionally stabilized. Isopentane (IP) is formed at an average energy of 121.5 kcal/mol above the ground state¹² and, at the lowest pressure used (0.8 cm), only 1.3% of the excited isopentane decomposed. By utilizing O₂ as a scavenger for triplet and doublet radicals, the large number of radical recombination products that would have been formed were eliminated.

The excited propane formed from (1) can undergo reactions 3 and 4



where k_3 is the average rate constant for decomposition and ω is the collision frequency. H atom split-off from C₃H₈* to form H + *i*-C₃H₇ or H + *n*-C₃H₇ are of minor importance; they occur at a rate of less than 1% compared to CH₃ split-off, as can be derived from the differences in activation energies and *A* factors.^{2a}

A steady-state treatment of reactions 1-4 for C₃H₈* gives

$$\frac{[IP]}{[C_3H_8]} \frac{[C_2H_6]}{[n-C_4H_{10}]} = \frac{k_1 k_3}{k_2 \omega} + \frac{k_2}{k_1} \quad (I)$$

A plot of [IP]/[C₃H₈], normalized to the reactant ratio, vs. 1/ω should be linear from which the average uni-

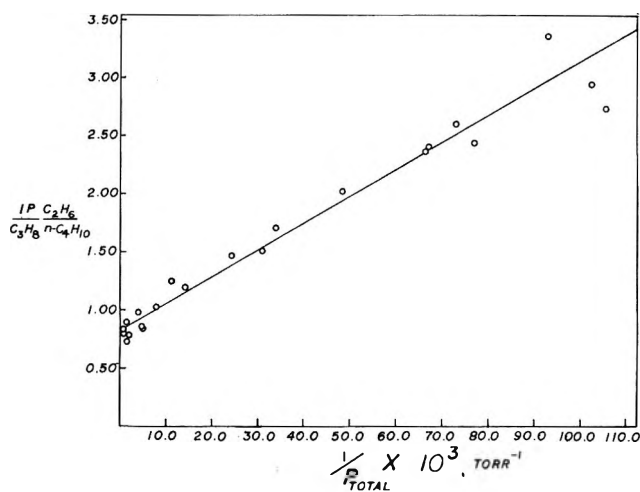


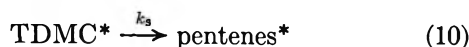
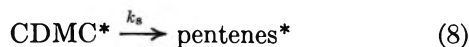
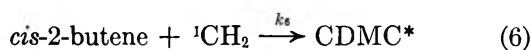
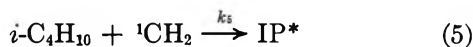
Figure 1. Plot of [IP]/[C₃H₈] vs. 1/*P*_{total} × 10⁴ for the 4358 Å photolysis of CH₂N₂ in the C₂H₆-*n*-C₄H₁₀ systems, where the ratio [IP]/[C₃H₈] has been normalized to a reactant ratio of 1.0 and *P*_{total} is in units of Torr. The collision frequency of C₃H₈* for each experimental point has been calculated with the following collision diameters at 300°K: C₂H₆, 5.23 Å; *n*-C₄H₁₀, 6.73 Å; CH₂N₂, 5.45 Å; and O₂, 3.60 Å. The line through the data points was drawn to give the intercept obtained from a least-squares analysis and an approximate fit to the other points.

molecular rate constant for decomposition, k_3 , can be obtained. Figure 1 depicts a plot of eq I. A least-squares regression analysis of the data points gives $k_3 = (4.7 \pm 0.5) \times 10^8 \text{ sec}^{-1}$, or 26.8 Torr, and the high-pressure intercept $k_2/k_1 = 0.89 \pm 0.07$ for 90% confidence limits. This value for the intercept, combined with $k_2/k_2' = 0.90$ (determined by Simons, *et al.*¹⁰), gives a value for the relative reactivities of ethane and *n*-butane: $(k_2 + k_2')/k_1 = 1.89$. This value is in

excellent agreement with the value of 1.88 determined by Halberstadt and McNesby.¹⁹

*E** Monitor System. The *E** monitor was used to determine the amount of excess energy carried by singlet methylene, $E^*(^1\text{CH}_2)$, into the chemically activated insertion product, C_3H_8^* . This value has been determined for CH_2N_2 -*cis*-2-butene photolyses at 4358 Å, but the average energy of the methylene radical might be expected to be lower in this system which contains ~50% ethane, due to an increased fraction of unreactive collisions.^{9,11} In the monitor system, *cis*-2-butene and isobutane were substituted for *n*-butane to measure the geometric and structural rate constants of chemically activated *cis*-1,2-dimethylcyclopropane. This substitution did not affect the fraction of unreactive collisions, since the intrinsic reactivities of *n*-butane, isobutane, and *cis*-2-butene are nearly the same.¹¹

The reactions of interest in the *E** monitor system are the following



Applying the steady-state assumption to TDMC^* yields¹⁵

$$\frac{[\text{CDMC}]}{[\text{TDMC}]} = \frac{\omega}{k_g} + \frac{k_g' + k_s}{k_g} \quad (\text{II})$$

Application of the steady-state assumption to all activated species gives

$$\frac{[\text{IP}]}{[\text{CDMC}] + [\text{TDMC}]} \frac{[cis\text{-2-butene}]}{[i\text{-C}_4\text{H}_{10}]} = \frac{k_s k_6}{k_6 \omega} + \frac{k_s}{k_6} \quad (\text{III})$$

Data for this *E** monitor system can be found in Table II. Plots of the data for eq II and III are shown in Figures 2 and 3, respectively, where unit collisional deactivation efficiency for ethane is assumed. Least-squares regression analyses on the data in Figures 2 and 3 yield $k_g = (5.74 \pm 0.18) \times 10^8 \text{ sec}^{-1}$ and $k_s = (1.14 \pm 0.11) \times 10^8 \text{ sec}^{-1}$ for 90% confidence limits. This gives a ratio of the geometric to the structural rate constant, k_g/k_s , of 5.03, which is lower than previous values.¹⁵ Simons and Taylor obtained a value for k_g

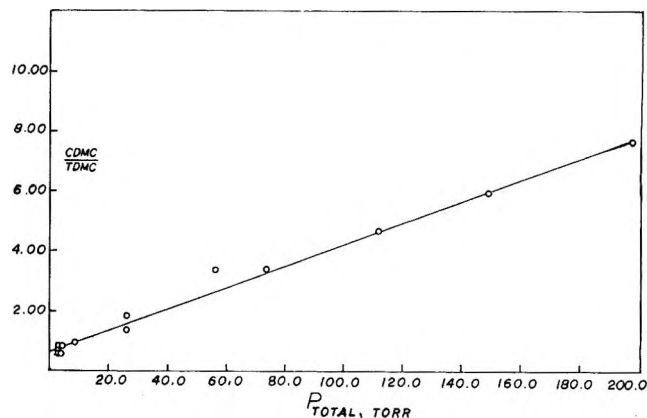


Figure 2. Plot of $[\text{CDMC}]/[\text{TDMC}]$ vs. P_{total} for the 4358 Å photolysis of CH_2N_2 in the *E** monitor system, where P_{total} is in units of Torr. The collision frequency of CDMC^* for each data point was calculated with the following collision diameters at 300° K: *cis*-2- C_4H_8 , 6.69 Å; *i*- C_4H_{10} , 6.56 Å; CH_2N_2 , 5.45 Å; O_2 , 3.60 Å. The line drawn through the data points is an approximate fit which gives the intercept from a least-squares calculation.

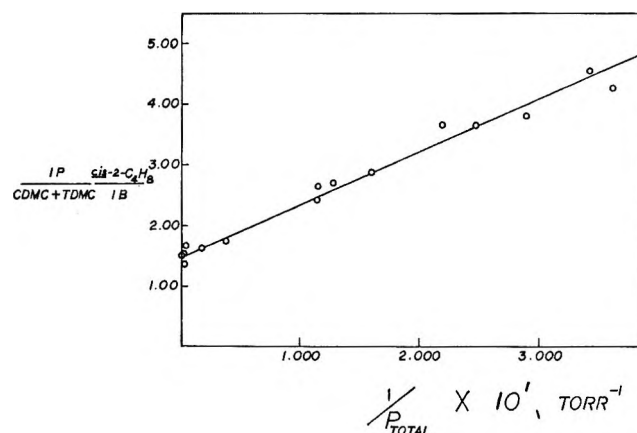


Figure 3. Plot of $[\text{IP}]/([\text{CDMC}] + [\text{TDMC}])$ vs. $1/P_{\text{total}}$ for the 4358 Å photolysis of CH_2N_2 in the *E** monitor system, where the ratio $[\text{IP}]/([\text{CDMC}] + [\text{TDMC}])$ has been normalized to a reactant ratio of 1.0 and P_{total} is in units of Torr. The collision frequency of CDMC^* for each experimental point was calculated with the collision diameters given in the Figure 2 caption. The line drawn through the data points is an approximate fit that gives the intercept calculated by a least-squares analysis.

of $5.5 \times 10^8 \text{ sec}^{-1}$, in good agreement with our own, for diazomethane-*cis*-2-butene photolyses at 4358 Å.¹⁵ Their value for k_s was somewhat lower ($0.68 \times 10^8 \text{ sec}^{-1}$) than ours, but is probably within the experimental uncertainties. These results indicate that methylene does not lose more energy by virtue of unreactive collisions with ethane than with larger hydrocarbons. This conclusion would be altered for a collisional deactivation efficiency of ethane less than one, but an efficiency significantly less than one for

(19) M. L. Halberstadt and J. R. McNesby, *J. Amer. Chem. Soc.*, **89**, 3417 (1967).

ethane is unexpected. An efficiency as low as 0.70¹⁸ would affect E^* and k_3 values in compensating ways.

The average excitation energy of the propane molecule is given by

$$-\langle E^* \rangle = \Delta H_{f_0}^\circ(\text{C}_3\text{H}_8) - \Delta H_{f_0}^\circ(\text{C}_2\text{H}_6) - [\Delta H_{f_0}^\circ(^1\text{CH}_2) + E^*(^1\text{CH}_2)] - E_{\text{th}} \quad (\text{IV})$$

The values for $\Delta H_{f_0}^\circ(\text{C}_3\text{H}_8)$ and $\Delta H_{f_0}^\circ(\text{C}_2\text{H}_6)$ were obtained from ref 20, E_{th} was calculated to be 2.2 kcal/mol, and $[\Delta H_{f_0}^\circ(^1\text{CH}_2) + E^*(^1\text{CH}_2)]$ was taken from reference 15. The values combine to give $\langle E^* \rangle = 119.5$ kcal/mol.

Theoretical Calculations

RRKM theory provides an accurate description of unimolecular decomposition processes.^{7,21-23} The RRKM theory expression for the specific decomposition rate of a molecule at the energy E^* is

$$k_{\epsilon^*} = \frac{d Z_0^\ddagger}{h Z_0^*} \frac{\sum_{\epsilon_{\text{vr}}^\ddagger=0}^{\epsilon^*} P(\epsilon_{\text{vr}}^\ddagger)}{N(\epsilon_{\text{vr}}^*)} \quad (\text{V})$$

where $\sum_{\epsilon_{\text{vr}}^\ddagger=0}^{\epsilon^*} P(\epsilon_{\text{vr}}^\ddagger)$ is the sum of all the active vibrational-internal rotational energy eigenstates of the activated complex up to the energy ϵ^* ; $N(\epsilon_{\text{vr}}^*)$ is the number of eigenstates per unit energy of the active degrees of freedom of the molecule at the energy E^* , h is Planck's constant, d is the reaction path degeneracy, and Z_0^\ddagger/Z_0^* is the ratio of the product of the adiabatic partition functions in the complex to those in the molecule. A more accurate treatment of adiabatic rotations^{21,22} only slightly alters the calculated results from eq V.

For the methylene-ethane system, the distribution function for the chemically activated propane is quite narrow relative to $\langle E^* \rangle$.¹⁵ Thus the experimental rate constant k_3 may be closely approximated by $k_{\langle E^* \rangle}$, the specific rate constant at the average energy $\langle E^* \rangle$. This is the same procedure that was used in determining the quantity $[E^*(^1\text{CH}_2) + \Delta H_{f_0}^\circ(^1\text{CH}_2)]$ and would in effect cancel any errors resulting from equating $k_{\langle E^* \rangle}$ with k_3 . The densities of the vibrational-internal rotational eigenstates and the corresponding sums for the states of the various activated complex structures were calculated using an accurate approximation.^{24,26} The computations were done on an IBM-360 computer.

Arrhenius A factors and activation energies were calculated from absolute rate theory expressions.²⁶ The critical energy was calculated from the C-C bond dissociation energy,^{27,28} and was found to have a value of 82.6 ± 2.0 kcal/mol. The thermodynamic functions were calculated with the aid of oscillator tables,²⁹ and the reduced moments of inertia for the free internal rotors were computed using a technique for unsymmetrical tops.³⁰

Activated Complex Structures. The structure of the

propane molecule was taken from Schachtschneider and Snyder,³¹ along with the two torsional frequencies measured by Weiss and Leroi.³² This structure gave a calculated entropy of propane at 400°K equal to 69.98 eu. The entropy of propane has been experimentally determined to be 70.37 eu.²⁰ This small discrepancy has a negligible effect on these calculations.

Activated complex models were constructed according to a format previously followed for hydrocarbons:^{7,8,12} lengthening of the C-C reaction coordinate and lowering of four frequencies, including methyl rocks, methylene rocks, and a skeletal bend. The propane activated complexes were constructed by lowering two methyl rocks, one methylene rock, and one skeletal bend by a constant factor, until the calculated rate, $k_{\langle E^* \rangle}$, was the same as the experimental decomposition rate (k_3).

The C-C stretch at 924 cm^{-1} was taken as the reaction coordinate. The following is a description of five activated complex models that were used: (I) both torsions treated as free rotors; rupturing C-C bond extended to 2.0 Å; all external rotors adiabatic; (II) same as (I), but the external rotor along the figure axis treated as active in both the complex and the molecule; (III) both torsions treated as free rotors; rupturing C-C bond extended to 3.0 Å; one external rotor active in complex and molecule; (IV) both torsions treated as vibrators; rupturing C-C bond extended to 3.0 Å; one external rotor active in complex and molecule; (III') same as (III), but ϵ_0 raised to 84.6 kcal/mol.

Radical Structures. The methyl radical structure was taken from experimental infrared work.³³

The structure of the ethyl radical has not been determined, but the barrier to internal rotation, although

(20) American Petroleum Institute Research Project No. 44, Carnegie Institute of Technology, Pittsburgh, Pa., 1944-1952.

(21) R. A. Marcus, *J. Chem. Phys.*, **43**, 2658 (1965).

(22) E. V. Waage and B. S. Rabinovitch, *Chem. Rev.*, **70**, 377 (1970).

(23) R. A. Marcus and O. K. Rice, *J. Phys. Colloid. Chem.*, **55**, 894 (1951).

(24) G. Z. Whitten and B. S. Rabinovitch, *J. Chem. Phys.*, **41**, 1883 (1964).

(25) D. C. Tardy, B. S. Rabinovitch, and G. Z. Whitten, *ibid.*, **48**, 1427 (1968).

(26) S. Glasstone, K. J. Laidler, and H. Eyring, "The Theory of Rate Processes," McGraw-Hill, New York, N. Y., 1941.

(27) S. W. Benson, "Thermochemical Kinetics. Methods for the Estimation of Thermochemical Data and Rate Parameters," Wiley, New York, N. Y., 1968.

(28) J. A. Kerr, *Chem. Rev.*, **66**, 465 (1966).

(29) H. L. Johnston, L. Savedoff, and J. Belzer, "Contributions to the Thermodynamic Functions by a Planck-Einstein Oscillator in One Degree of Freedom," Office of Naval Research, Department of the Navy, Washington, D. C., 1949.

(30) D. R. Herschbach, H. S. Johnston, K. S. Pitzer, and R. E. Powell, *J. Chem. Phys.*, **25**, 736 (1956).

(31) J. H. Schachtschneider and R. G. Snyder, *Spectrochim. Acta*, **19**, 117 (1963).

(32) S. Weiss and G. E. Leroi, *ibid.*, Part A, **25**, 1759 (1969).

(33) D. E. Milligan and M. E. Jacox, *J. Chem. Phys.*, **47**, 5146 (1967).

approximately 3.0 kcal/mol in ethane,²⁷ may be rather small.¹² The structural model used was taken from previous studies,³⁴ and consisted of a five-member set of geometrically averaged frequencies based on the vibrational frequencies of the ethane molecule. Since the barrier to internal rotation about the bond adjacent to the unpaired electron is not known, the torsion in the ethyl radical was treated as both a vibrator (289 cm⁻¹, the same as the torsional frequency in ethane) and a free rotor in the CH₃ + C₂H₅ recombination rate calculations.

A complete description of the two radical structures is given in Table III.

Table III: CH₃ + C₂H₅ Radical Recombination Rates

Models ^a			
Methyl radical			
3100 (2)			
2930			
1230 (2)			
611			
	$S^{\circ}_{400} = 49.4$ eu		
	$\ln(Q_T/N) = 20.41$ eu ^b		
Ethyl radical			
2960 (5)			
1155 (2)			
993			
820 (2)			
289 or F.R.			
	Free rotor	289 cm ⁻¹	
	(eu)	(eu)	
	$S^{\circ}_{400} = 62.34$		
	$\ln(Q_T/N)$	26.18	25.67
Rates ^c			
Complex	Torsion as		Torsion as F.R.
	289 cm ⁻¹ vibrator		
I	2.20×10^9		1.34×10^9
II	3.02×10^9		1.84×10^9
III	3.32×10^9		2.01×10^9
IV	6.50×10^8		3.93×10^8
III'	5.82×10^9		3.51×10^9

^a All frequencies are in cm⁻¹. ^b (Q_T/N) is the total partition function. ^c All rates are given in l. mol⁻¹ sec⁻¹ and are calculated by $k_r = (kT/h)(Q_T^{\ddagger}/N)/[Q_T(\text{CH}_3)/N][Q_T(\text{C}_2\text{H}_5)/N]$, where E_0 for recombination was taken to be zero.

Calculational Results

Complex models adjusted to give calculated values for k_{E^*} , in agreement with the experimental decomposition rate (k_3) are presented in Table IV. The torsions in the molecule were treated as free rotors in all the k_{E^*} calculations, since the excitation energy is quite high. In the thermal calculations it was more reasonable to treat these torsions in the molecule as vibrations: 216 cm⁻¹ and 271 cm⁻¹.

The A factors and activation energies for the activated complex are given in Table IV. The A factors for a critical energy of 82.6 kcal/mol range from 5.5×10^{16} to 9.1×10^{16} sec⁻¹, and are approximately twice as large for a critical energy of 84.6 kcal/mol. The pyrolysis of C₃H₈ has been studied, but not exten-

sively;^{2,3} no Arrhenius parameters have been measured. Rabinovitch and Setser calculated a thermal Arrhenius A factor at 873°K of 9.07×10^{17} sec⁻¹ on the basis of a Gorin-type complex model.⁷ Leathard and Purnell estimated the decomposition A factor at 800°K to be 2.14×10^{17} sec⁻¹, allegedly on the basis of a radical recombination rate at 800°K of 2.0×10^{10} l. mol⁻¹ sec⁻¹.^{2a} This estimate is approximately 4 times too small, since it is actually based on an A factor for recombination at 800°K of 2×10^{10} l. mol⁻¹ sec⁻¹, *i.e.*, the Arrhenius activation energy, E_{ar} , for recombination was taken to be exactly zero. An activated complex consistent with these Arrhenius parameters for recombination gives negative values of the critical energy, E_{or} , for recombination. Theoretically, the minimum value of E_{or} is zero. Tsang³⁵ estimated the thermal Arrhenius parameters for propane pyrolysis from shock-tube studies of other hydrocarbons to be $A = 2.5 \times 10^{16}$ sec⁻¹ and $E_a = 81.3$ kcal/mol at 300°K. Trotman-Dickenson had earlier estimated the A factor at 600°K to be 4×10^{17} with an activation energy of 82.0 kcal/mol.³⁶ The Arrhenius parameters estimated by Tsang are slightly lower than our values, while the A factor of Rabinovitch and Setser⁷ is an order of magnitude larger than our values. Trotman-Dickenson's A factor is an estimate, and its absolute value can only be regarded as precise to within an order of magnitude.

Recombination rate calculations of CH₃ + C₂H₅ using the activated complex models derived from this work are given in Table III. Taking an external rotor active, cases II, III, III', and IV, in both the complex and the molecule decreases the calculated rate of decomposition as expected, and the resultant loosened complex gives a 50% larger recombination rate. Thynne³⁷ determined a recombination rate of CH₃ + C₂H₅ to be 5.0×10^{10} l. mol⁻¹ sec⁻¹. Recombination of CH₃ + C₂H₅ can be approximated from $k_{AB} = 2(k_{AA}k_{BB})^{1/2}$,³⁸ where $\log k_{AA} = 10.34$ for CH₃ + CH₃ and $\log k_{BB} = 10.4$ for C₂H₅ + C₂H₅. Thus, $k_{AB} = 4.68 \times 10^{10}$ l. mol⁻¹ sec⁻¹. It is clear from Table III that complex models consistent with the decomposition rate for propane (this work) cannot give a recombination rate for CH₃ + C₂H₅ as large as 4.7×10^{10} l. mol⁻¹ sec⁻¹. The most favorable case gives approximately one-eighth of this magnitude, while more reasonable cases give approximately one-twentieth of this value for the recombination rate. These results clearly demonstrate that no reasonable adjustments will give complexes that correlate the decomposition and recombination rates for the propane system.

(34) W. L. Hase, Ph.D. Dissertation, New Mexico State University, 1970.

(35) W. Tsang, *Int. J. Chem. Kinet.*, **1**, 245 (1969).

(36) A. F. Trotman-Dickenson, "Gas Kinetics," Butterworth, London, England, 1955.

(37) J. C. J. Thynne, *Trans. Faraday Soc.*, **58**, 676 (1962).

(38) H. M. Frey and R. Walsh, *Chem. Rev.*, **69**, 103 (1969).

Table IV: Complex Models

Description of mode	Molecule ^c	Model I	Model II	Model III	Model IV	Model III'
C-C stretch	924 cm ⁻¹
CH ₃ rock	1151	228	200	241	247	203
CH ₃ rock	903	181	163	196	202	162
C-C-C bend	382	77	69	84	86	70
CH ₂ , CH ₃ rock	747	149	135	163	168	135
CH ₃ torsion	F.R. (271)	F.R.	F.R.	F.R.	216	F.R.
CH ₃ torsion	F.R. (216)	F.R.	F.R.	F.R.	76 ^a	F.R.
$I_{r1} \times 10^{40}$, g cm ²		5.02	5.02	5.07	...	5.07
$I_{r2} \times 10^{40}$, g cm ²		4.78	4.78	5.02	...	5.02
$(I_x I_y I_z) \times 10^{116}$, g ³ cm ⁶		4.41	4.41	15.5	15.5	15.5
Thermal A factors, sec ⁻¹ ^b		5.55×10^{16}	8.55×10^{16}	8.36×10^{16}	9.10×10^{16}	1.75×10^{17}
E_0 , kcal/mol		82.6	82.6	82.6	82.6	84.6
E_a , kcal/mol ^b		85.1	85.2	85.1	86.0	87.3

^a Low-frequency torsion of complex IV was taken to be the frequency that would generate an equivalent entropy to that of a free rotor. ^b Arrhenius parameters were calculated at 700°K. ^c The moments of inertia of the propane molecule were taken to be:⁶ $I_x = 1.11 \times 10^{-38}$ g cm²; $I_y = 9.72 \times 10^{-39}$ g cm²; $I_z = 3.01 \times 10^{-39}$ g cm².

The ability of complex III to explain the experimental decomposition rate data for activated propane produced by H atom + isopropyl radical combination was tested. The average rate constant for decomposition, k_a , is defined in terms of the amount of decomposition, D , and the amount of collisional stabilization, S ⁷

$$k_a = \omega \frac{D}{S} = \omega \frac{\int_{\epsilon_0}^{\infty} \frac{k_{\epsilon}}{k_{\epsilon} + \omega} f(\epsilon_{vr}) d\epsilon}{\int_{\epsilon_0}^{\infty} \frac{\omega}{k_{\epsilon} + \omega} f(\epsilon_{vr}) d\epsilon}$$

where ω is the collision frequency, and $f(\epsilon_{vr})$ is a thermal energy distribution function for the associated propane and is of the form⁷

$$f(\epsilon_{vr}) d\epsilon = \frac{k_{\epsilon}' \frac{N^*(\epsilon_{vr})}{Z_{vr}^*} e^{-\epsilon_{vr}/kT} d\epsilon}{\int_{\epsilon_0}' k_{\epsilon}' \frac{N^*(\epsilon_{vr})}{Z_{vr}^*} e^{-\epsilon_{vr}/kT} d\epsilon}$$

where the prime is a symbol for the reverse decomposition process, and Z_{vr}^* is the vibrational-rotational partition function for the active degrees of freedom in the molecule. The structural model used for the isopropyl radical was the same as that of Rabinovitch and Setser.⁷ By taking the minimum energy of the complex to be 9.4 kcal/mol, the average energy of the complex was computed to be 11.7 kcal/mol at 25°, and the average energy of the activated propane to be 94.3 kcal/mol, which are identical with Rabinovitch and Setser's values. These calculations with complex III yield calculated low- and high-pressure rate constants, respectively, of $k_{a_0} = 3.47 \times 10^5$ sec⁻¹ and $k_{a_{\infty}} = 5.49 \times 10^5$ sec⁻¹. For complexes I, II, IV, and

III' these values would be multiplied by factors of 1.24, 1.11, 0.614, and 0.524, respectively. The ratio $k_{a_{\infty}}/k_{a_0} = 1.58$ is rather small, indicating a relatively narrow thermal spread for association of H + isopropyl radical (~10 kcal/mol). Rabinovitch and Setser⁷ calculated values for k_{a_0} and $k_{a_{\infty}}$ which are about 50 times higher than our calculations. Experimentally, Avrahami and Kebarle found $k_a = 6.3 \times 10^6$ at 25°. ³⁹ Heller and Gordon⁴⁰ experimentally found $k_{a_{\infty}}$ to be 3.3×10^6 sec⁻¹ at 85° which compares with our calculated value of 1.05×10^6 sec⁻¹ at 85°. At 25° Falconer, *et al.*,⁴¹ found the decomposition rate constant to be 6.6×10^5 sec⁻¹, and Darwent and Steacie⁴² found 3.6×10^5 sec⁻¹, which was corrected to $\sim 1 \times 10^6$ by Setser and Rabinovitch.⁷ With the exception of Avrahami and Kebarle's value, the agreement between these experimental results and calculations based on the complex models presented here is within experimental error and strongly supports the models.

Reliable unimolecular decomposition data for propane would provide a further means of testing the complex models and activation energies used in this work. The thermal unimolecular specific rate constant, as given by RRKM theory including centrifugal distortion, was calculated.^{21,22,43}

Table V gives values of k_{uni} as a function of pressure at three different temperatures using complex III. Calculation of the Arrhenius parameters from the high-

(39) M. Avrahami and P. Kebarle, *Can. J. Chem.*, **41**, 339 (1963).

(40) C. A. Heller and A. S. Gordon, *J. Phys. Chem.*, **64**, 390 (1960).

(41) W. E. Falconer, B. S. Rabinovitch, and R. J. Cvetanovic, *J. Chem. Phys.*, **39**, 40 (1963).

(42) B. deB. Darwent and E. W. R. Steacie, *ibid.*, **16**, 381 (1948).

(43) E. V. Waage and B. S. Rabinovitch, *ibid.*, **52**, 5581 (1970).

Table V: Thermal Unimolecular Fall-Off Calculations for Propane Decomposition^{a,b}

Temp. °K	Pressure, Torr															Multi- plier
	10 ¹⁰	10 ⁹	10 ⁸	10 ⁷	10 ⁶	10 ⁵	10 ⁴	10 ³	10 ²	10 ¹	10 ⁰	10 ⁻¹	10 ⁻²	10 ⁻³	10 ⁻⁴	
600	8.24	8.24	8.24	8.24	8.24	8.24	8.24	8.24	8.12	7.94	7.51	6.52	4.54	2.28	0.78	10 ⁻¹⁶ sec ⁻¹
700	22.05	22.05	22.05	22.05	22.05	22.05	22.04	21.84	21.62	21.03	18.90	14.43	8.31	3.37	0.95	10 ⁻¹¹ sec ⁻¹
800	46.50	46.50	46.50	46.50	46.50	46.50	46.48	46.10	45.40	42.55	35.16	22.90	10.83	3.64	0.87	10 ⁻⁸ sec ⁻¹

^a The Lennard-Jones collision diameters for propane at 600, 700, and 800°K were calculated to be 5.35, 5.24, and 5.14 Å, respectively.

^b The vibrational frequencies of propane were grouped together: 2925 (8); 1406 (9); 1005 (6); 747; 382; 271; 216.

pressure results at various temperatures gave the same activation energy as absolute rate theory calculations, and an *A* factor that was only 4% lower.

Conclusion

It was shown previously that, by taking extremes of activated complex and radical structures and high critical energies for decomposition, it was barely possible to correlate chemical activation decomposition rates with estimated radical recombination rates for most larger alkanes.^{8,11,12} The correlations were based on RRKM and absolute rate theories. In the present case of chemically activated propane decomposition, where fewer adjustments in complex and radical structure are possible and the CH₃ + C₂H₅ recombination rate can be better estimated (from measurements of

CH₃ + CH₃ and C₂H₅ + C₂H₅), it is shown that the most favorable adjustments cannot satisfactorily correlate the decomposition and recombination rates. Clearly an important dilemma exists here which may have theoretical significance.

A study of chemically activated ethane (¹CH₂ + CH₄), which is in progress, should provide some important information, since in this case there are no reasonable adjustments in complex and radical structures that could improve the correlation of decomposition and recombination rates, and the recombination rate is reliably known. An excellent discussion of some aspects of the ethane problem has appeared recently.⁴⁴

(44) E. V. Waage and B. S. Rabinovitch, *Int. J. Chem. Kinet.*, **3**, 105 (1971).

Journal of Chemical and Engineering Data

JANUARY 1972, Vol. 17, No. 1

TABLE OF CONTENTS

Editorial.	1	Enthalpies of Combustion of Nine Organic Nitrogen Compounds Related to Petroleum. W. D. Good	28	Permeation of Hydrogen and Deuterium Through Palladium-Silver Alloys. F. J. Ackerman and G. J. Koskinas	51
Dipole Moments of Some Diaryl Disulfides. G. C. Pappalardo and S. Pistarà.	2	Phase Studies of Some Nitroalkane Hydrocarbon Mixtures. H. L. Clever, Q. R. Pirkle, Jr., B. J. Allen, Jr., and M. E. Derrick	31	Specific Conductance of Concentrated Solutions of Magnesium Salts in Water-Ethanol System. J. F. Casteel and E. S. Amis	55
Vapor-Liquid Equilibrium of Methane-Propane System at Low Temperatures and High Pressures. Ivan Wichterle and Riki Kobayashi	4	Viscosities of Binary Liquid Mixtures of Nonelectrolytes. R. K. Nigam and M. S. Dhillon	35	Solubility of Propane and Carbon Dioxide in Heptane, Dodecane, and Hexadecane. Walter Hayduk, E. B. Walter, and Philip Simpson	59
Vapor-Liquid Equilibrium of Methane-Ethane System at Low Temperatures and High Pressures. Ivan Wichterle and Riki Kobayashi	9	Temperature Dependence of Solubilities in Water and Heats of Fusion of Solid Aromatic Hydrocarbons. R. D. Wauchope and F. W. Getzen	38	Liquid-Solid Equilibria in Na⁺-HCOO⁻, -CNS⁻, -NO₃⁻ Ternary System. M. A. Berchiesi, A. Cingolani, and G. Berchiesi	61
Vapor-Liquid Equilibrium of Methane - Ethane - Propane System at Low Temperatures and High Pressures. Ivan Wichterle and Riki Kobayashi	13	Some Properties of Binary Systems of Hexane and Normal Chloroalkanes. E. L. Heric and B. M. Coursey	41	Thermal Pressure Coefficients of Di-<i>n</i>-alkyl Ethers. G. R. Driver and A. G. Williamson	65
Thermal Decomposition of Alkali Metal Hexafluorophosphates. T. C. Ehlert and M.-M. Hsia.	18	Diffusion of Some Organic and Inorganic Compounds in Air. R. F. Barr and Harry Watts	45	Solubility of H₂O and D₂O in Carbon Tetrachloride, Toluene, and Cyclohexane at Various Temperatures. P. K. Glasoe and S. D. Shultz	66
Enthalpy of Ruthenium Dioxide to 1200°K by Drop Calorimetry. D. R. Fredrickson and M. G. Chasanov	21	Electromotive Force Studies of Cell Cd₂Hg₂CdSO₄(<i>m</i>)-Hg₂SO₄, Hg in Dioxane-Water Media. Somesh Chakrabarti and Sukumara Aditya	46	Solubility of Carbon Dioxide in Mixed Paraffinic Hydrocarbon Solvents at Cryogenic Temperatures. U. K. Im and Fred Kurata	68
Molecular Weights and Conductivities of Diphenylphosphinic Acid, Diphenylphosphinic Anhydride, and Acetic Diphenylphosphinic Anhydride in Dimethyl Sulfoxide. D. L. Venezky and J. E. Quick	23	Thermodynamics of Solution by Gas Chromatography of Some Heterocyclic Compounds. R. K. Kuchhal and K. L. Mallik	49	Thermodynamic Excess Property Measurements for Acetonitrile-Benzene-<i>n</i>-Heptane System at 45°C. D. A. Palmer and B. D. Smith	71
Thermodynamic Properties of Binary Liquid Mixtures Containing Aromatic and Saturated Hydrocarbons. E. W. Funk, F.-C. Chai, and J. M. Prausnitz	24				

Vapor-Liquid Equilibrium for Binary Systems 2-Butanone with 2-Butanol, 1-Pentanol, and Isoamyl Alcohol. K. J. Miller and H.-S. Huang	77	Low-Temperature Heat Capacity and Entropy of Phosphoryl Triamide. Z. T. Wakefield, B. B. Luff, and J. J. Kohler	94	Chemistry of Sulfur Compounds. Selectivity of Addition of Thiyl Radicals to Terminal Olefins. Kamel Boustany	104
Standard Electromotive Force of Silver-Silver Chloride Electrode and Related Thermodynamic Quantities in <i>tert</i>-Butyl Alcohol-Water Mixtures (2, 6, and 8 Wt %) between 5-45°C. R. N. Roy, William Vernon, Alfred Bothwell, and James Gibbons	79	Enthalpy of Formation of Ammonium Tetrametaphosphate (NH₄PO₃)₄. B. B. Luff, R. B. Reed, and Z. T. Wakefield	96	Gamma-Bromo- and Gamma-Iodoacetoacetanilides. M. I. Ali, M. A. Abou-State, and N. M. Hassan	106
Redetermination of Standard Potential of Silver-Silver Bromide Electrode in Methanol-Water Mixtures at 25°C. K. H. Khoo	82	Vapor-Liquid Equilibrium of System Methyl Isobutylketone-<i>n</i>-Butanol. Ebulliometric Method. P. Dakshinamurty, C. Chiranjivi, and V. Seetharamaswamy	98	Synthesis of Cyclobutanone. J. B. Sieja	108
Diffusion Coefficient of Hexamethylene Tetramine in Concentrated Aqueous Solutions. J. R. Bourne and R. C. Trivedi	85	Adsorption Isotherms at High Pressures. Comment on Data of Stacy et al. P. G. Menon	99	Synthesis of Seven New Phenoxybiphenyls. W. C. Hammann and R. M. Schisla	110
Furfural-Water-Formic Acid System at 25° and 35°C. R. E. Langford and E. L. Heric	87	ORGANIC SECTION			
Flammability Characteristics of Methylene Chloride (Dichloromethane). R. D. Coffee, P. C. Vogel, Jr., and J. J. Wheeler	89	Catalytic Hydrogenation of Polynuclear Hydrocarbons. Products of Partial Hydrogenation of Dibenz(α,j)anthracene, Benzo(ghi)perylene, Dibenz(α,c)anthracene, 3-Methylcholanthrene, 7,12-Dimethylbenz(α)anthracene, and Anthanthrene. W. Lijinsky, G. Advani, L. Keefer, H. Y. Ramahi, and L. Stach	100	Synthesis with 1,1-Diurethanes. Benzylurethanes from Aryl Ethers. G. R. Krow, H. Pannella, and W. Figures	116
				Esterification and Addition Reactions of Perfluoroacryloyl Chloride. L. O. Ross, and M. E. Hill	117
				New Data Compilations.	120

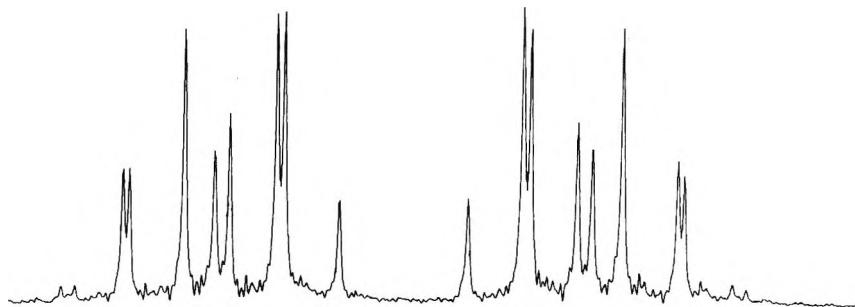
DIGILAB FTS[®]/NMR

WHY BUY A NEW NMR SPECTROMETER?

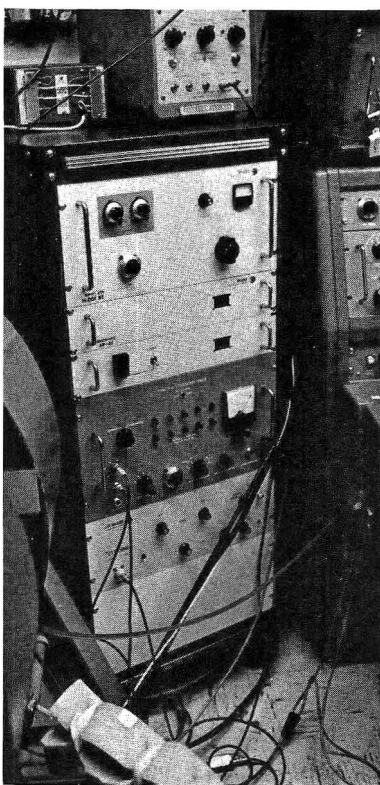
Convert your present c-w system to Fourier transform: You'll get state-of-the-art sensitivity and SAVE UP TO \$100,000!



Versatile NMR-3 Data System with 128K disk memory



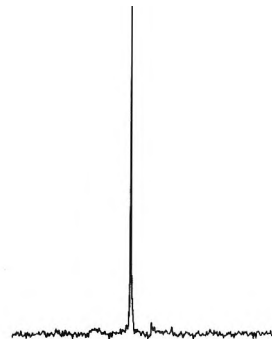
¹H spectrum of ODCB, ¹⁹F lock. **RESOLUTION BETTER THAN 0.3 Hz.**



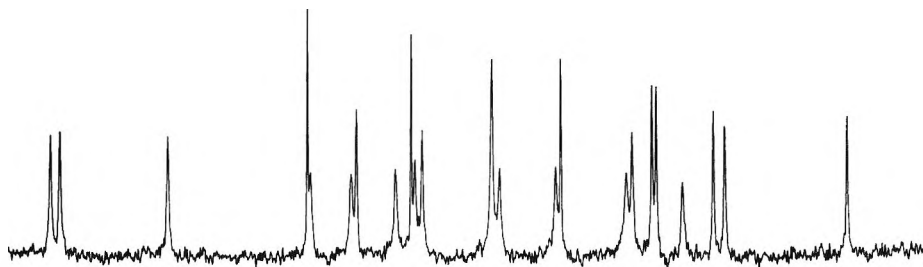
Fourier transform conversion equipment for HA-100 installed at Mount Holyoke College, South Hadley, Mass.



¹H spectrum of Ethylbenzene, ¹⁹F lock. Single pulse. **SIGNAL-TO-NOISE = 106.**



¹³C spectrum of decoupled benzene, ¹⁹F lock. Single pulse. **SIGNAL-TO-NOISE = 83.**



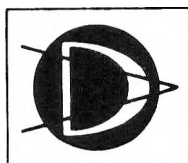
Partial ¹³C spectrum of cholesterol: 2 molar in CHCl₃. A 1.8 mm capillary of C₆F₆ was inserted in the 5 mm probe to obtain the ¹⁹F lock.

All of the above spectra were measured on HA-100 spectrometers modified by Digilab.

Digilab provides complete modification equipment and services for all c-w NMR spectrometers. Complete FTS[®]/NMR systems include: heteronuclear lock, up to 400 watts peak pulse power, advanced design noise decoupler, frequency synthesizer, etc., plus a versatile, fully-softwared data system.

see us at
Booths 618, 620, 622
PITTSBURGH CONFERENCE
Cleveland Convention Center
March 6-10, 1972

TWX 710 320-0821 TELEX 921481



DIGILAB INC

Subsidiary of Block Engineering
237 PUTNAM AVENUE
CAMBRIDGE, MASS 02139

TEL. 617 868-4330

GET INTO ORBIT

ELECTRON SPIN RESONANCE: Elementary Theory and Practical Applications

John E. Wertz, Professor of Physical Chemistry, University of Minnesota and James R. Bolton, Professor of Chemistry, University of Western Ontario 1972, 480 pages, (069454-0), \$22.50
McGraw-Hill Series in Advanced Chemistry

Uniquely self-contained and providing very detailed presentations, this book enables even the reader unfamiliar with the field to analyze and interpret a variety of spectra for himself. An abundance of practical problems—in the text as well as the appendices—lets the reader test his understanding and acquire proficiency in interpretation. A large body of supplementary material on mathematical techniques and elementary quantum mechanics, including angular momentum and spin operators is covered, separated into appendices to make reading continuous for those who do not require it, but readily available for those who do.

If you are looking for a scientific background for systems, then you will be interested in a technical book that introduces you to the physical foundations for all systems—man-made, natural, and social

TOWARD A GENERAL SCIENCE OF VIABLE SYSTEMS

Arthur S. Iberall, Chief Scientist and President of General Technical Services, Inc. 1972, 414 pages, (031672-4), \$14.50

The author, a well-known physicist-cyberneticist, presents a science for systems within a unified framework. Since the 1920's equivalent network analysis has dominated the modeling of processes. Now a methodology is offered for complex hierarchical systems where the variables at one level in the hierarchy cannot be directly coupled to the variables on the next level.

_____Wertz/Bolton, **ELECTRON SPIN RESONANCE** (069454-0)

_____Iberall, **TOWARD A GENERAL SCIENCE OF VIABLE SYSTEMS** (031672-4)

Within 10 (ten) days of receipt of book(s) I will remit for price of book(s) plus postage, handling, and local sales tax.

If you would like to consider the book for classroom adoption, please write to us on your school letterhead and we will send you an examination copy.

Name _____

Address _____

City _____ State _____ Zip _____

Offer good in Continental USA only. Prices subject to change without notice. 62 REV 0107

**Mail to: Norma-Jeanne Bruce
McGraw-Hill Book Company
College Division, 13
330 West 42nd Street, NY NY 10036**

